Allen Hunt
Robert Ewing

LECTURE NOTES IN PHYSICS 771

Percolation Theory for Flow in Porous Media

With Forewords by Robert Horton and John Selker

Second Edition

Springer

Lecture Notes in Physics

The Lecture Notes in Physics

The series Lecture Notes in Physics (LNP), founded in 1969, reports new developments in physics research and teaching – quickly and informally, but with a high quality and the explicit aim to summarize and communicate current knowledge in an accessible way. Books published in this series are conceived as bridging material between advanced graduate textbooks and the forefront of research and to serve three purposes:

- to be a compact and modern up-to-date source of reference on a well-defined topic
- to serve as an accessible introduction to the field to postgraduate students and nonspecialist researchers from related areas
- to be a source of advanced teaching material for specialized seminars, courses and schools

Both monographs and multi-author volumes will be considered for publication. Edited volumes should, however, consist of a very limited number of contributions only. Proceedings will not be considered for LNP.

Volumes published in LNP are disseminated both in print and in electronic formats, the electronic archive being available at springerlink.com. The series content is indexed, abstracted and referenced by many abstracting and information services, bibliographic networks, subscription agencies, library networks, and consortia.

Proposals should be sent to a member of the Editorial Board, or directly to the managing editor at Springer:

Christian Caron
Springer Heidelberg
Physics Editorial Department I
Tiergartenstrasse 17
69121 Heidelberg / Germany
christian.caron@springer.com

A. Hunt
R. Ewing

Percolation Theory for Flow in Porous Media

Springer

Allen Hunt
Wright State University
Dept. of Physics and Geology
Dayton OH 45431
USA
allenghunt@msn.com

Robert Ewing
Iowa State University
Dept. Agronomy
Ames IA 50011-1011
USA
ewing@iastate.edu

Hunt, A., Ewing, R., *Percolation Theory for Flow in Porous Media*, Lect. Notes Phys. 771 (Springer, Berlin Heidelberg 2009), DOI 10.1007/978-3-540-89790-3

ISBN 978-3-540-89789-7 e-ISBN 978-3-540-89790-3

DOI 10.1007/978-3-540-89790-3

Lecture Notes in Physics ISSN 0075-8450 e-ISSN 1616-6361

Library of Congress Control Number: 2008940417

Cover design: Integra Software Services Pvt Ltd.

Printed on acid-free paper

9 8 7 6 5 4 3 2 1

springer.com

Foreword to the Second Edition

Scientists specialize. In attempting to isolate and understand individual processes, we risk losing sight of the whole. In essence, most of us study isolated trees rather than considering the whole forest. This specialization is evident in the science of porous media: most studies focus on just one or a few specific media, with only occasional papers addressing a broad class of media. Thus we have specialists in natural media such as soil, fractured rock, and granular materials, while others focus on powders, foodstuffs, paper and textiles, ceramics, building materials, and so on.

Percolation theory has been touted as providing a general framework for describing generalized transport in all types of media. Can this general framework be applied to a specific class of porous media, with at least as much success as the accumulated insights of decades of more conventional approaches? If the answer is yes, then applying percolation theory to transport processes in porous media will yield great scientific progress.

To illustrate this point, I will briefly consider the porous media that I study. Soils are a growth medium for plants, and so they support most terrestrial life. More than six billion people depend on soils for food, for storing and purifying water, for recycling waste, and for holding us up. This vital layer covering the earth's terrestrial surface is fragile. Often less than a meter thick, soils develop slowly but are easily damaged by accelerated erosion, compaction, tillage, and pollution. Thus knowledge of soils and their wise management is crucial for sustaining civilization.

But soils are tremendously complex and variable. To describe a transport process in the soil, one must first define the time scale and the sample size; only then can the relevant scale(s) of climate, geology, landscape position, vegetation, and management be considered. The interface between air and land, between vegetable and mineral, routinely encounters extremes of heat and cold, wet and dry, growth and decay. Transport is irregular and incessant: heat, water, both as liquid and vapor, organic and inorganic carbon are constantly on the move.

Conceptual and mathematical models describing these transport processes have grown increasingly complex. Attempting to describe a greater range of behaviors, soil scientists have incorporated macropores (wormholes, drying cracks), aggregates, clay flocs and tactoids, and mineral-specific surface chemistry into our models. While our predictions have (on average) improved, the model parameters have become more numerous, more difficult to quantify, and arguably less physically

defensible. Continuous, volume-averaged functions gloss over important details: the ubiquitous nonlinear behaviors appear to be driven by discrete events, discrete pore pathways, and discrete "tipping points."

When I first met Robert (Toby) Ewing about 15 years ago, I invited him to present a guest lecture to students in my graduate-level soil physics course, which covers heat transfer, water flow, chemical transport, and coupled processes. Over the ensuing years I invited Toby to expand his role in the course. His contributions grew in quantity and quality, and now we effectively co-teach the course. I focus on continuous mathematical approaches following Fick, Fourier, Buckingham, Taylor, Richards, and others. Toby focuses on discrete mathematical approaches for flow and transport, including network models, percolation theory, and critical path analysis.

Toby sometimes chides me about being stuck on "old" approaches (playfully using words like ancient and Neanderthal). I respond that the so-called "old" ways are tested and trustworthy, while his "new" approaches lack measurement support and substantive application. However, my defense of the 'old' ways has been weakening since Toby met Allen Hunt about eight years ago. Allen has been at the forefront of applying percolation theory to transport in (mainly geological) porous media. Allen and Toby have developed a fruitful collaboration; this book, rich in insights, is one such fruit. They present examples of percolation theory applied to gas transfer, water retention and flow, electrical conductivity, heat transfer, and dispersion. Over time I have come to appreciate the potential power of their work.

From time to time in science some new concept rings a bell, and scientists rush to engage the new concept. I want to help "ring the bell" for this excellent work of Hunt and Ewing. In soil science we have focused on empirical descriptions of flow and transport. Hunt and Ewing offer percolation theory as a foundational description of how to proceed with a unifying approach. Can percolation theory prove to be a unifying theory in porous media? Perhaps. The theory is sound, but applications of the theory to real porous media will require care and wisdom. The theory is unifying, but like all theories it carries restrictions of simplifying assumptions. Questions of when and when not, how and how not to apply the theory are valid and important questions. Hunt and Ewing provide a foundation, and invite others to engage in the iterative process of applying, evaluating, and advancing the theory.

The foundations of percolation theory presented in this book allow for the study of isolated trees, but Hunt and Ewing also connect the trees to the forest. I encourage the broad range of porous media scientists to study this book. I think the book provides new ways to consider the processes occurring in porous media, and it will inspire new thought, analysis, and exploration of flow in porous media.

Curtiss Distinguished Professor of Agriculture *Robert Horton*
Ames, Iowa, USA
Eve of Thanksgiving (November), 2008

Preface to the Second Edition

Why would we wish to start a 2nd edition of "Percolation theory for flow in porous media" only two years after the first one was finished? There are essentially three reasons:

1) Reviews in the soil physics community have pointed out that the introductory material on percolation theory could have been more accessible. Our additional experience in teaching this material led us to believe that we could improve this aspect of the book. In the context of rewriting the first chapter, however, we also expanded the discussion of Bethe lattices and their relevance for "classical" exponents of percolation theory, thus giving more of a basis for the discussion of the relevance of hyperscaling. This addition, though it will not tend to make the book more accessible to hydrologists, was useful in making it a more complete reference, and these sections have been marked as being possible to omit in a first reading. It also forced a division of the first chapter into two. We hope that physicists without a background in percolation theory will now also find the introductory material somewhat more satisfactory.
2) We have done considerable further work on problems of electrical conductivity, thermal conductivity, and electromechanical coupling. The electrical conductivity may in more complex media than those addressed in the first edition lead to the relevance of nonuniversal exponents of percolation theory, while the thermal conductivity may be strongly affected by complex structures such as capillary bridges or pendular rings between grains. Neither of these subjects in morphology was discussed in detail in the first edition.

   Our additional research into the saturation dependence of the electrical conductivity appeared to confirm the relevance of universal scaling to a much wider range of materials than we knew about at the time of the first edition. However, a related subject long considered important in petroleum engineering is diagenesis, which was handled in some detail in Sahimi's 1993 review. It is possible to make models of rock formation in which the connectivity of the pore space scarcely changes, while the width of the pores diminishes rapidly with diminishing porosity. Such models allow, at least in principle, the possibility of nonuniversal exponents of percolation theory.

   The reason that pendular structures could be relevant, especially to the thermal conductivity of geological porous media, is that the solid fraction generally has

a higher thermal conductivity than the fluid phase (e.g., air or water), while the thermal resistance between neighboring grains may be quite high. Thus, small amounts of fluid at these junctions – pendular structures – may produce a rather large increase in the thermal conductivity, and this increase may have nothing to do with percolation theory as such, since the topology of the connected network might not initially change with increasing fluid content, although critical path analysis may still be useful for this problem. The large increase in material covered in the original Chap. 4 also led to its division into the current Chaps. 5 and 6.

3) We have recently addressed the problem of dispersion in porous media, which brings up the relevance of some additional topological aspects of percolation theory, in particular, the relationship of the tortuosity of the backbone cluster to the distribution of passage times. Because this was not addressed in the first edition, the introductory chapters mentioned the topic only briefly. As a consequence the preface to the first edition is now more dated as dispersion was implied to be a problem that could be omitted. In fact, inclusion of dispersion into the second edition has made a significant advance in the unity of the theoretical approach here.

We also bring in an additional problem (Sect. 11.4) addressing the question of how to generate a realistic prediction in horizontal and vertical K distributions for a topical waste management problem, which uses output parameters from a small-scale upscaling to generate appropriate input parameters in a large-scale upscaling. We hope it is useful to see how difficult practical problems in applying percolation theory at multiple scales might be managed.

In order to give the book a wider relevance, it is useful to embed the discussions of the relevance of universal exponents in a wider context. This is accomplished by looking at a wider range of models of porous media, a wider range of properties, and a wider range of experiments. As a consequence, the introductory review chapters needed to be rewritten in order to accommodate a more widely applicable theory.

Finally, it has been noted that solutions to the problems are not provided. It was our intention, except in the introductory chapters, to suggest mostly problems whose solutions could be published, so these problems have not yet been attempted.

Besides the people acknowledged in the first edition, one of us would like to thank the staff of the library at Wright State University.

Foreword to the First Edition

Though a sledge hammer may be wonderful for breaking rock, it is a poor choice for driving a tack into a picture frame. There is a fundamental, though often subtle, connection between a tool and the application. When Newton and Leibniz developed the Calculus they created a tool of unprecedented power. The standard continuum approach has served admirably in the description of fluid behavior in porous media: the conservation of mass and linear response to energy gradients fit conveniently, and are solid foundations upon which to build. But to solve these equations we must characterize the up-scaled behavior of the medium at the continuum level. The nearly universal approach has been to conceive the medium as a bundle of capillary tubes. Some authors made the tubes porous, so they could fill and drain through their walls; others "broke and reconnected" them so each tube had a range of diameters along its length. In the end it must be admitted that the marriage of tool (capillary tube bundles) and task (to derive the constitutive relations for porous media) has not yet proven to be entirely satisfactory. Lacking in these conceptual models is a framework to describe the fluid-connected networks within the medium which evolve as functions of grain size distribution, porosity, saturation, and contact angle. This is fundamentally a geometry problem: how to concisely describe the particular nature of this evolving, sparse, dendritic, space-filling network.

Recognizing this basic problem, the community flocked to the fractal models as they became better understood in the 1990s. But fractals alone were not enough, as the real problem was to understand not the geometry of the medium, but the geometry of the fluids within the medium, and moreover, to correctly identify the geometry of the locations that control the flow.

I met Allen Hunt in the late 1990s, and over coffee he described his ideas about critical path analysis for the development of constitutive relationships for unsaturated conductivity. I was immediately sold: it was transparent that the geometric model (with the equally important framework for mathematical analysis) was ideally suited to the problem at hand. Since resistance to flow is a function of the fourth power of the pore aperture, clearly the key was to systematize the determination of the "weak link" to compute overall resistance to flow. Paths that had breaks were irrelevant; and paths that contained very small pores provided negligible contribution. The permeability should be proportional to the fourth power of the radius of the smallest pore in the connected path which has the largest small pore. Read that

sentence twice: we are looking for the path of least resistance, and that paths resistance will be a function of the smallest pore in that path. Allen had the tool to identify this path as a function of fluid content. A very useful, appropriately sized, hammer had arrived for our nail. Over the following years Allens work showed the power of using the right tool: he could explain the relationship between the geometry of the medium and liquid content versus permeability, residual fluid content, electrical resistance, diffusion of solutes, and even the thorny issues of the scale of a representative elementary unit. Critical path analysis is not a panacea, but due to the focus on the controlling geometric features, it provides a remarkably concise parameterization of fluidmedium relationships based on physically measurable properties that accurately predict many of the basic ensemble properties.

A fundamental problem in having these results be broadly understood and adopted is sociological. Consider how much time we spend learning calculus to solve the occasional differential equation. Critical path analysis requires calculus, but also understanding of the mathematics of fractals, and the geometric strategy of percolation theory. When Allen started his remarkably productive march into flow through porous media he deftly employed these tools that none of our community had mastered. There is a natural inertia to any discipline since re-tooling requires major investments of time. From this perspective I have long encouraged Allen to help the community make use of this essential set of tools by providing a primer on their application to flow though porous media. In this book Allen has once again moved forward strategically, and with great energy. He has provided an accessible tutorial that not only provides the bridge for the hydrologist to these new tools, but also the physicist a window into the specialized considerations of flow through natural porous media.

Learning new mathematical constructs is much like learning a new language. There is a great deal of investment, and the early effort has few rewards. Ultimately, however, without language there is no communication. Without mathematics, there is no quantitative prediction. If understanding the behavior of liquids in porous media is central to your work, I urge you to make the investment in learning this material. By way of this book Allen provides a direct and efficient avenue in this venture. Your investment will be well beyond repaid.

Corvallis, Oregon *John Selker*
April, 2005

Preface to the First Edition

The focus of research in porous media is largely on phenomena. How do you explain fingering? What causes preferential flow? What "causes" the scale effect on the hydraulic conductivity? Why can the incorporation of 5% of hydrophobic particles into soil make the soil water repellent? Where do long tails in dispersion come from? These are merely a few examples of a very long list of questions addressed. The approach to "solving" problems is frequently to (1) take standard differential equations such as the advection–diffusion equation for solute transport, or Richards' equation for water transport; (2) substitute results for what are called constitutive relations such as the hydraulic conductivity, K, molecular diffusion constants, or air permeability as functions of saturation, and pressure-saturation curves, including hysteresis, etc.; (3) apply various models for the variability and the spatial correlations of these quantities at some scale; and (4) solve the differential equations numerically according to prescribed initial and/or boundary conditions. In spite of continuing improvement in numerical results, this avenue of research has not led to the hoped-for increase in understanding. In fact there has been considerable speculation regarding the reliability of the fundamental differential equations (with some preferring fractional derivatives in the advection–diffusion equation, and some authors questioning the validity of Richards' equation) while others have doubted whether the hydraulic conductivity can be defined at different scales.

Although other quite different approaches have thus been taken, let us consider these "constitutive" relations. The constitutive relationships used traditionally are often preferred because (1) they generate well-behaved functions and make numerical treatments easier; (2) they are flexible. This kind of rationale for using a particular input to a differential equation is not likely to yield the most informative solution. The most serious problem associated with traditional constitutive relations is that researchers use such concepts as connectivity and tortuosity (defined in percolation theory) as means to adjust theory to experimental results. But the appropriate spatial "averaging" scheme is inextricably connected to the evaluation of connectivity. In fact, when percolation theory is used in the form of critical path analysis, it is not the spatial "average" of flow properties which is relevant, but the most resistive elements on the most conductive paths, i.e. the dominant resistances on the paths of least resistance. An additional problem is that usual constitutive relations often cover simultaneous moisture regimes in which the represented physics is not

equilibrium, and thus time-dependent, as well as those moisture regimes where the dominant physics is equilibrium, so that they must be overprescribed (while still not describing temporal effects). Finally, there has been no progress in making the distributions and spatial correlations of, e.g. K, consistent with its values at the core scale, because there is no systematic treatment of the connectivity of the optimally conducting regions of the system. This book shows a framework that can be used to develop a self-consistent and accurate approach to predict these constitutive relationships, their variability, spatial correlations and size dependences, allowing use of standard differential equations in their continuum framework (and, it is hoped, at all spatial scales).

Although applications of percolation theory have been reviewed in the porous media communities (e.g. Sahimi, 1993; Sahimi and Yortsos, 1990) (in fact, percolation theory was invented for treating flow in porous media, Broadbent and Hammersley, 1957) it tends to be regarded as of limited applicability to real systems. This is partly a result of these summaries themselves, which state for example that "Results from percolation theory are based on systems near the percolation threshold and the proximity of real porous rocks to the threshold and the validity of the critical relationships away from the threshold are matters of question," (Berkowitz and Balberg, 1993). However, it is well-known that percolation theory provides the most accurate theoretical results for conduction also, in strongly disordered systems far above the percolation threshold (using critical path analysis). The novelty in this course is the combined use of both scaling and critical path applications of percolation theory to realistic models of porous media; using this combination it is possible to address porous media under general conditions, whether near the percolation threshold or not.

This book will show how to use percolation theory and critical path analysis to find a consistent and accurate description of the saturation dependence of basic flow properties (hydraulic conductivity, air permeability), the electrical conductivity, solute and gas diffusion, as well as the pressure–saturation relationships, including hysteresis and non-equilibrium effects. Using such constitutive relationships, results of individual experiments can be predicted and more complex phenomena can be understood. Within the framework of the cluster statistics of percolation theory it is shown how to calculate the distributions and correlations of K. Using such techniques it becomes easy to understand some of the phenomena listed above, such as the "scale" effect on K, as well.

This work does not exist in a vacuum. In the 1980s physicists and petroleum engineers addressed basic problems by searching for examples of scaling that could be explained by percolation theory, such as Archie's law (Archie, 1942) for the electrical conductivity, or invasion percolation for wetting front behavior, hysteresis, etc. or by using the new fractal models for porous media. The impetus for further research along these lines has dwindled, however, and even the basic understanding of hysteresis in wetting and drainage developed in the 1980s is lacking today, at least if one inquires into the usual literature. In addition, the summaries of the work done during that time suggest that the percolation theoretical treatments are not flexible enough for Archie's law (predict universal exponents), or rely on non-universal

exponents from continuum percolation theory without a verifiable way to link those exponents with the medium and make specific predictions. An identifiable problem has been the inability of researchers to separate connectivity effects from poresize effects. This limitation is addressed here by applying percolation scaling and critical path analysis simultaneously. While there may have been additional problems in the literature of the 1980s (further discussed here in the Chapter on hysteresis), it is still not clear to me why this (to me fruitful) line of research was largely abandoned in the 1990s. This book represents an attempt to get percolation theory for porous media back "on track."

It is interesting that many topics dealt with as a matter of course by hydrologists, but in a rather inexact manner, are explicitly treated in percolation theory. Some examples are:

1. upscaling the hydraulic conductivity = calculating the conductivity from microscopic variability,
2. air entrapment = lack of percolation of the air phase,
3. residual water, oil residuals = critical moisture content for percolation, sum of cluster numbers,
4. grain supported medium = percolation of the solid phase;
5. Representative Elementary Volume = the cube of the correlation length of percolation theory,
6. tortuosity = tortuosity,
7. flow channeling = critical path.

These concepts and quantities are not, in general, treatable as optimization functions or parameters in percolation theory because their dependences are prescribed. Note that in a rigorous perspective for disordered systems, however, one does not "upscale" K. The difficulty here is already contained within the language; what is important are the optimal conducting paths, not the conductivities of certain regions of space. The conductivity of the system as a whole is written in terms of the rate-limiting conductances on the optimal paths and the frequency of occurrence of such paths. Defining the conductivity of the system as a whole in terms of the conductivities of its components is already a tacit assumption of homogeneous transport. Further, some elementary rigorous results of percolation theory are profoundly relevant to understanding flow in porous media. In two-dimensional systems it is not possible for even two phases to percolate simultaneously (in a grainsupported medium there is no flow or diffusion!), while in three dimensions a number of phases can percolate simultaneously. As percolation thresholds are approached, such physical quantities as the correlation length diverge, and these divergences cause systematic dependences of flow and transport properties on system size that can only be analyzed through finite-size scaling. Thus it seems unlikely that treatments not based on percolation theory can be logically generalized from 2D to 3D.

I should mention that a book with a similar title, "Percolation Models for Transport in Porous Media," by Selyakov and Kadet (1996) also noted that percolation theory could have relevance further from the percolation threshold, but overlooked the existing literature on critical path analysis, and never mentioned fractal models

of the media, thereby missing the importance of continuum percolation as well. As a consequence, these authors did not advance in the same direction as this present course.

The organization of this book is as follows. The purpose of Chap. 1 is to provide the kind of introduction to percolation theory for hydrologists which (1) gives all the necessary basic results to solve the problems presented later; and which (2) with some effort on the part of the reader, can lead to a relatively solid foundation in understanding of the theory. The purpose of Chap. 2 is to give physicists an introduction to the hydrological science literature, terminology, experiments and associated uncertainties, and finally at least a summary of the general understanding of the community. This general understanding should not be neglected as, even in the absence of quantitative theories, some important concepts have been developed and tested. Thus these lecture notes are intended to bridge the gap between practicing hydrologists and applied physicists, as well as demonstrate the possibilities to solve additional problems, using summaries of the background material in the first two chapters. Subsequent chapters give examples of critical path analysis for concrete system models Chap. 3; treat the "constitutive relationships for unsaturated flow," including a derivation of Archie's law Chap. 4; hysteresis, non-equilibrium properties and the critical volume fraction for percolation Chap. 5; applications of dimensional analysis and apparent scale effects on K Chap. 6; spatial correlations and the variability of the hydraulic conductivity Chap. 7; and multiscale heterogeneity Chap. 8.

I wish to thank several people for their help in my education in hydrology and soil physics, in particular: Todd Skaggs, whose simulation results have appeared in previous articles and also in this book; John Selker, who showed me the usefulness of the Rieu and Sposito model for the pore space; Glendon Gee, who helped me understand experimental conditions and obtain data from the Hanford site; Eugene Freeman for providing additional Hanford site data; Bill Herkelrath, again for data; Toby Ewing, whose simulations for diffusion were invaluable; Tim Ellsworth for showing me the relevance of the experiments of Per Moldrup; Per Moldrup for giving me permission to republish his figures; Max Hu for providing me with his diffusion data; and Sally Logsdon for her data on soil structure; Alfred Huebler for giving me a forum among physicists to discuss these ideas. I also thank my wife, Beatrix Karthaus-Hunt, for her support.

Dayton *Allen G. Hunt*
April, 2005

Contents

Chapter 1
Percolation Theory: Topology and Structure

1.1 What is Percolation?

Percolation theory describes emergent properties related to the connectivity of large numbers of objects. These objects typically have some spatial extent, and their spatial relationships are relevant and statistically prescribed. Percolation theory is thus related to graph (e.g., [1]) and network (e.g., [2]) theories. All of these exist within the intersection of probability theory and topology. For the present purpose, the chief relevance of percolation theory is its ability to deliver global properties from local specifications. Here the global properties sought describe flow and conduction properties of fluids in porous media. The relationships between local and global properties are not trivial: sometimes the global properties relate to universal topological properties, and sometimes to system-dependent properties.

In percolation theory the topology is customarily referenced to some d-dimensional spatial structure with an existence independent of the probabilistic characteristics of the theory. Examples of such structures include regular grids (known in solid state physics as lattices), consisting of nodes (sites) connected by bonds. In porous media the pore space (filled, e.g., with water or air) corresponds to a random lattice, viewed already in the 1950s ([3]) as a network. The typical twist from percolation theory is to take such a known structure with simple topology, characterized by as few as one or two parameters, and make the presence of, e.g., bonds a probabilistic affair, which generates quite complex topologies.

Percolation theory comes in three basic varieties: bond, site, and continuum, with the first two versions linked by name to the grids mentioned above. We will consider all three varieties. Percolation theory also has some interesting and potentially relevant variants, including bootstrap percolation (an early reference is Chalupa et al. [4]), gradient percolation [5], and invasion percolation [6–8]. Bootstrap and gradient percolations are ignored here, while invasion percolation theory is applied in a few places. Invasion percolation was developed in the context of wetting and drying of porous media, in order to describe phenomena related to, e.g., wetting fronts, where the wetting fluid enters the medium from one side. It should become clear that a great deal of unification was already provided by the basic percolation theory as formulated by Flory [9] and Broadbent and Hammersley [10]. Nevertheless, this

Hunt, A., Ewing, R.: *Percolation Theory: Topology and Structure.* Lect. Notes Phys. **771**, 1–36 (2009)
DOI 10.1007/978-3-540-89790-3_1

book describes some new combinations of uses of percolation theory. In order to understand these combinations it is important to understand clearly the basic applications of percolation theory, particularly to conduction. These applications have some basis in the topology of the system being examined. Our introduction is made more accessible by considering specific physical examples.

A system is said to be at percolation, or to percolate, when a sufficient fraction of the entities in question (sites, bonds, etc.) is connected locally that a global connection emerges. This global connection is a continuous string of locally connected entities which is unbounded in size except as may result from limitations of a finite-sized system. As is often the case in mathematics, percolation theory has some surprises. Here the simplest result, at least conceptually, is that precisely one global connection develops [11–13] exactly at a specific fraction, p_c, of local connections known as the critical fraction. Such a simple result is also profound, and decades elapsed before it was proven.

1.2 Some Examples

A simple bond-percolation problem can be represented by a window screen which maps out a square grid (lattice). Imagine cutting at random a fraction p of the elements of this grid. At some critical fraction $p \equiv p_c$ (which will turn out to be 0.5), the window screen will lose its connectedness and fall apart. Percolation theory addresses directly the question, "at what fraction of cut bonds does the screen fall apart?" (i.e., what is p_c?), and related questions such as, "what is the largest hole in the screen if the cut fraction p is less than p_c," and "what is the structure of such holes?." Percolation theory also readily provides the electrical conductivity of such an incompletely connected network of (conducting) bonds, or what the diffusion coefficient of a network of the same structure would be if the elements were water-filled tubes rather than wires. Answers to the latter questions are given in terms of p, p_c, and the conductivity or diffusivity of the individual bonds.

A simple site-percolation problem can be represented by the random emplacement of equal-sized metallic and plastic spheres in a large container. If two metal spheres touch each other, a current can pass from one to the other. Here the relevant percolation variable is the fraction, p, of spheres that is conducting. If the fraction of metallic spheres exceeds a critical value, a continuous conducting pathway will be formed. The larger the fraction of metallic spheres, the better connected the path will be and the greater the electrical conductivity of the system. Percolation theory generates the electrical conductivity as a function of the fraction of the spheres made of metal. Site and bond percolation problems can be defined on either regular grids, like a square-lattice window screen, or irregular grids like a random sphere pack. They can also be defined on tree structures with constant branching ratios known as Bethe lattices.

A continuum percolation problem receiving attention already in the 1970s is a network of sintered glass and metallic particles. The glass particles may have

different sizes and shapes from the metallic particles (which are typically smaller), while the sintering process tends to change the shapes of the particles, producing a net flow of material into the pore space. The irregularity of the particle shapes can thus be contrasted with the regular geometry of the site percolation problem described above. Such networks have relevance in the xerox industry. In the above continuum percolation problem the relevant percolation variable becomes the volume fraction, p, taken up by the metallic particles. If the detailed structure is known, percolation theory can account for some aspects of the electrical conductivity of these systems as well [14–16]. Other real systems whose electrical properties can be treated in terms of continuum percolation include piezoelectric ceramics [17, 18]. The continuum percolation problem that we will be most interested in here is that of water flowing in variably saturated porous media. Porous media are often far from the percolation threshold whereas piezoelectric ceramics are extremely close to it.

Across these applications of percolation theory, we may see the values of p_c vary widely from system to system. However, the same relationships are still used to determine, e.g., the size of the largest hole in the screen, or the electrical conductivity as a function of $p - p_c$, where p is the fraction of conducting portions, and p_c its critical value for percolation. Relationships that are functions of the difference $p - p_c$ are normally (with isolated exceptions) termed "universal" [19, 20]. Here universal means that the property is independent of the details of the system and depends only on its dimensionality, d. We demonstrate how percolation theory can be used to solve practical problems relating to transport in porous media.

It had earlier been hoped that the universal behavior exhibited by most models near the percolation threshold could be used to guide understanding of real physical systems across the entire range of connectivities (see, for example, [21–24]). But as has been frequently pointed out, it is not clear how close real systems are to the percolation threshold. Thus it is important to emphasize at the outset that this book will explain the use of percolation theory to calculate transport properties not merely near the percolation transition, but also far from it. Far from the percolation transition it is frequently nonuniversal aspects of percolation theory, i.e., the value of p_c and the statistical characteristics of the medium, which control transport; near the percolation threshold it is the universal aspects that dominate. This perspective will be seen to be far more useful than a restriction to either case by itself: it allows calculation of all the transport properties of porous media, as well as their variability and the structure of their spatial correlations.

This first chapter is devoted to the development of basic methods and concepts from percolation theory that refer to the structure of topology of percolation. The material here is drawn from many sources, but most importantly from Stauffer [19], Sahimi [22, 23], Stauffer and Aharony [20], and Bunde and Havlin [25]. Some concepts important for the unification of percolation theory will be treated in some depth for the benefit of those readers with a physics background but without detailed experience in percolation theory. These will be pointed out and can be skipped in an initial reading. The second chapter provides an introduction to transport-related aspects of percolation theory. The third chapter will serve as an introduction to porous media. Subsequent chapters will detail the applications.

1.3 Qualitative Descriptions

Consider a square grid of points, and draw line segments between nearest neighbor points "at random." For very small values of p these segments will only connect pairs of nearest neighbor sites. As p increases more pairs will connect, and gradually clusters of interconnected sites will appear. As p nears p_c many of these clusters will become large, with complex internal structure. What is the occurrence of such clusters as a function of p and their size? We would also like to quantify the structure of the clusters. This structure has been described using various quantities, such as perimeter, density, mass (i.e., number of sites), "chemical path" length, and ramification. The perimeter (the number of sites in the cluster with neighboring sites not in the cluster) has two contributions: one is proportional to the volume [26], while the second, similar to surface area, is proportional to the volume to the $1 - 1/d$ power, where d is the Euclidean dimension [19]. The radius of a large cluster is not given in terms of its volume by the usual relationships valid for Euclidean objects. In fact large clusters at, or near, the percolation threshold are fractal objects, without scale reference except in the small-scale limit when the scale of the grid becomes visible.

As p reaches p_c the largest interconnected cluster just reaches infinite size. For p greater than but still close to p_c, most of the sites on the infinite connected cluster are located on what are called "dead ends." Dead ends are connected to the rest of the infinite cluster by only one bond. If current were to flow across the system through the infinite cluster, these dead ends would carry no current. If the dead ends are "pruned" from the cluster, what remains is called the "backbone," the portion of the infinite cluster that carries current. The backbone has a large number of loops, making it a multiply-connected object. The backbone also has "red" bonds, for which no alternate path exists. If a red bond is cut, the current is interrupted. Red bonds are associated with the largest drops in the potential field, which is why they are designated "red" or "hot." If the length scale viewed is not too large, then large finite clusters just below percolation have the same appearance as the infinite cluster just above percolation. Figure 1.1 shows the "infinite" cluster for $p > p_c$ and bond percolation on a square lattice, and Fig. 1.2 shows its backbone.

The backbone cluster itself has been described using the terms "links," "nodes," and "blobs." A pictorial definition of these terms is given in Fig. 1.3. The characteristic separation of nodes, or the length of a link, will be equivalent to the correlation length, defined in Eq. (1.1) below. A heuristic derivation of the exponent for the vanishing of the conductivity [27] is based on the conceptualization of the infinite cluster depicted in Fig. 1.3. Note that considerable work on nonlinear effects on the electrical conductivity, as well as the usefulness of effective-medium theoretical descriptions is based on this kind of a pictorial concept. This literature will not be discussed here, and if interested, the reader should consult Shklovskii and Efros [28] or Pollak [29] and the references therein.

The clusters, being fractal objects, have many properties which are best characterized using a fractal dimensionality. While the multiplicity of consequent fractal dimensionalities can be confusing, we will concentrate our attention on three of these: (1) the fractal dimension, d_f, associated with the mass distribution of

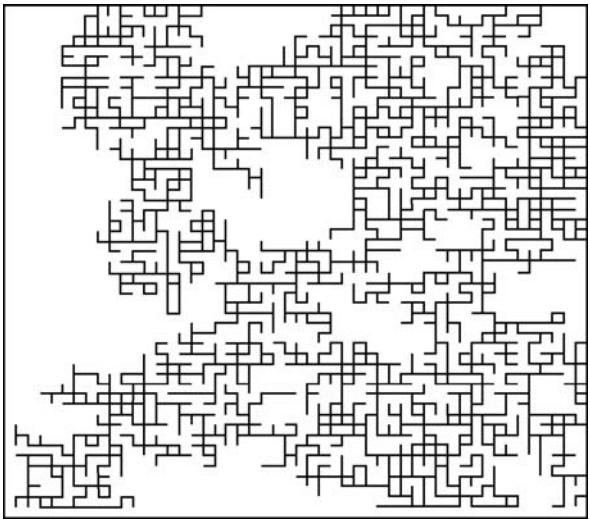

Fig. 1.1 A finite size sample of bond percolation on a square lattice above the percolation threshold

the cluster, (2) the fractal dimension associated with the mass distribution of the backbone, D_b, and (3) the fractal dimension associated with the optimal path length along the backbone, D_{min}. The first is relevant to any understanding of the occurrence of clusters as a function of cluster size, while the second, and perhaps the third,

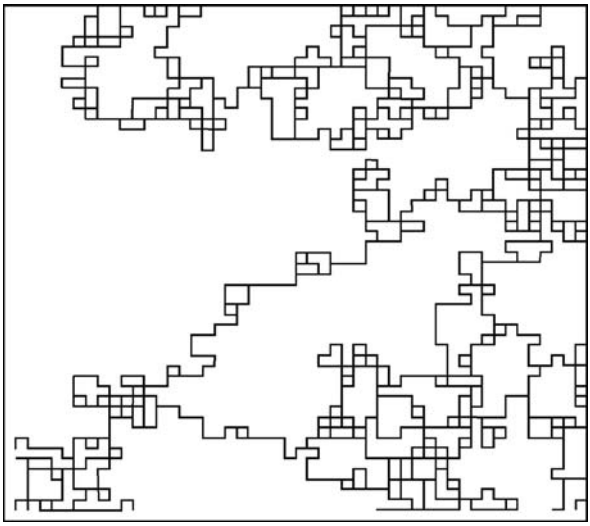

Fig. 1.2 The same system and realization of Fig. 1.1, but for which the dead ends have been removed from the infinite cluster to form the "backbone". Note the existence of many closed loops (Figure from Todd Skaggs, unpublished)

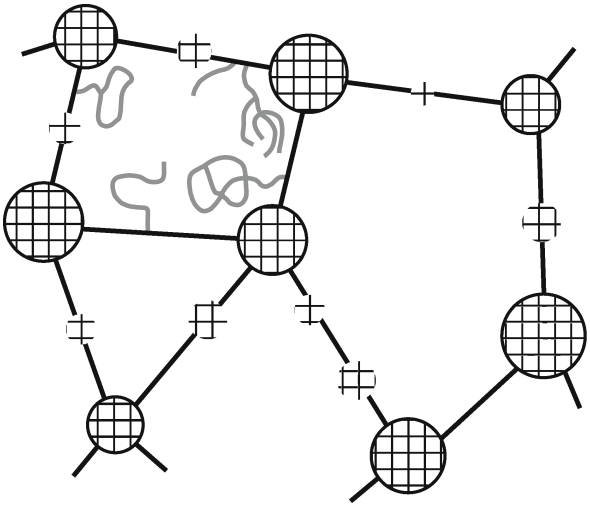

Fig. 1.3 Schematic of a section of the backbone. Links and nodes have conventional meanings from, e.g., Kirchoff's network equations, while blobs are cycles or loops, or collections thereof. Nodes are *hatched circles* with *borders*. Blobs are *hatched circles* without *borders*. Links are the *lines* connecting nodes. *Gray* lines in the upper left hole represent dangling ends. The average link length, χ, is also the average hole size

have relevance to calculations of dispersion through descriptions of solute transport along paths of constant flux through porous media.

1.4 What are the Basic Variables?

The most fundamental variable is p, which for the bond percolation problem is defined to be the fraction of (cut) bonds in the above screen problem, or, equivalently the fraction of bonds emplaced on a background without bonds. In site percolation p normally stands for the fraction of, e.g., the metallic balls mentioned above. It can also stand for the number of lattice (grid) sites marked by some special color, and which "connect" if they happen to be nearest neighbors. (In two dimensions there is little point in distinguishing multiple colors because at most one type of site, bond, or continuum can percolate at one time, but in higher dimensions more than one color can percolate simultaneously.) In continuum percolation, p can stand for a fractional volume, for example, the water content of a soil. The most important value of p is p_c, the critical value at which percolation occurs. In an infinitely large system, p_c is precisely defined: larger values of p guarantee "percolation," the existence of an infinitely large cluster of interconnected sites (bonds or volume), while smaller values of p guarantee that percolation does not occur. For a given finite-sized system this transition may occur at a value of p somewhat greater than or less than p_c. Some authors use this spread in p_c values for finite-sized

systems as a starting point to discuss finite-size effects on percolation properties; here we use the cluster statistics of percolation as a basis for treating such finite-size effects. Percolation theory has sufficient redundancy to make either approach suitable.

Other basic variables are all functions of the difference $p - p_c$. P_∞ is defined to be the fraction of active bonds (or sites) connected to the infinite cluster (if an infinite cluster exists, i.e., for $p > p_c$). χ, known as the correlation length, gives the typical linear extent of the largest cluster for $p < p_c$, and the largest hole for $p > p_c$. n_s is defined to be the volume concentration of clusters of sites or bonds with s interconnected elements, and is a function of s and of the difference $p - p_c$. How to obtain such quantities, and how to use them to calculate realistic and often very accurate values of transport coefficients of disordered porous media, is the point of this book.

1.5 What Is Scale Invariance and Why Is It So Important?

A core concept of percolation theory, central to much of its theoretical development, is that the correlation length, χ, diverges (goes to infinity) in the limit $p \to p_c$. While, for $p \neq p_c$, χ defines a relevant physical scale, this scale disappears precisely at $p = p_c$. The lack of any length scale, known as scale invariance, also implies the relevance of fractal analysis, or self-similarity. Even for $p \neq p_c$, if a percolation system is viewed at length scales less than χ it appears fractal. Only at length scales greater than χ does the geometry become Euclidean [30]. Another physical meaning of a divergent correlation length is that at $p = p_c$, the largest cluster of interconnected bonds, sites, or volume, just reaches infinite size. Thus it can be said that if one examines the system at length scales smaller than the largest self-similar structure, the medium appears to be self-similar. At the percolation threshold, the largest self-similar structure reaches infinite size, and the self-similar appearance of the medium extends to infinite length scales. Of course no physical medium on the earth can precisely obey such a condition.

Before we define the correlation length, we define first the correlation function $g(r)$ as the mean number of sites, at a Euclidean distance r from some arbitrary occupied site, that are also occupied and on the same cluster as that arbitrary site. The sum of $g(r)$ over all values of r will thus yield the total cluster mass. This makes $g(r)$, suitably normalized, a measure of cluster density. Because of the exceedingly complex structure of clusters in higher dimensions, $g(r)$ is cumbersome to construct, except on Bethe lattices and 1D systems.

The correlation length, χ, may be defined as

$$\chi^2 = \frac{\sum_{r=1}^{\infty} r^2 g(r)}{\sum_{r=1}^{\infty} g(r)} \tag{1.1}$$

Thus the correlation length is a root-mean-square (rms) measure of the size of the finite clusters. While Bunde and Havlin [25] take the lower limit of the sum in Eq. (1.1) to be $r = 1$, Stauffer and Aharony ([20], Sect. 2.2) use $r = 0$, a distinction which makes no difference in the behavior of any calculated property in the vicinity of the percolation threshold.

Starting from $p > p_c$, the divergence of the correlation length implies that the largest hole in the infinite connected cluster just reaches infinite size and there is symmetry between $p > p_c$ and $p < p_c$. This symmetry is perfect only in two dimensions, where only one phase, or class, of sites or bonds can percolate simultaneously. The divergence of the correlation length implies that right at percolation there is no finite length scale left in the problem. In reference to the qualitative discussion of Sect. 1.3, this scale invariance shows up also in the shapes and internal structure of the clusters, and is represented through quantities that describe fractal dimensionalities.

What does the lack of a finite length scale at the percolation threshold imply? It requires the use of functions of powers. Powers may appear to have a scale, i.e., under some circumstances the relationship of a conductivity to a length scale, x, can, simply by dimensional analysis, be shown to have a form such as

$$K = K_0 \left(\frac{x}{x_0} \right)^{-(d-1)} \tag{1.2}$$

where the choice of the power $-(d-1)$ is not intended to be anything beyond illustrative, K is a conductivity, K_0 is a particular value of the conductivity, x is a length, and x_0 is a particular value of x. In contrast to an exponential function, x_0 in this case need not identify a particular "scale," though if used in a judicious fashion it may imply a boundary of the validity of the scale invariance (the existence of a lower limit of the validity of scale-invariance in site and bond percolation problems is clearly required by the finite dimensions of the underlying lattice). On the other hand an exponential function, $K = K_0 \exp(-x/x_0)$, must also have an argument x/x_0. But the particular value of x_0 has completely different consequences in the two equations. For example, as long as x is within a range of lengths for which the power law is valid (Eq. (1.2)), for $d = 3$, doubling the system size will always decrease the conductivity by a factor of four, regardless of the actual values of x_0 or K_0. In the case of the exponential function, the conductivity obtained by doubling the system size will depend on the conductivity of the initial system, and thus on the size ratio of the larger system to x_0; this is in no sense a scale-independent relationship. Notice that in physical systems a power law may have upper *and* lower

boundaries. For example, physical objects with fractal characteristics are, strictly speaking, truncated fractals: their fractal nature does not extend to subatomic or galactic length scales. We may therefore give their power-law description an upper and lower bound, but they are still scale-invariant *within those bounds*. More generally, incorporating a particular scale in a power-law equation may provide useful information about one of its bounds without negating its scale invariance within the range under consideration.

The above argument implies that the correlation length must therefore be a power function. The argument of the correlation length is known to be the difference, $p - p_c$, making it simplest to describe the correlation length as in Eq. (1.3),

$$\chi \propto (p - p_c)^{-\nu} \tag{1.3}$$

The negative exponent, $-\nu$, allows χ to diverge at $p = p_c$. The term "universality" can now be understood in a practical way: the form of Eq. (1.3) is the same in all systems and the exponent ν depends only on the dimensionality of the system. The scale invariance—lack of a length scale—also implies the relevance of fractal analysis, or self-similarity. Self-similarity is especially important because it allows the application of the mathematical techniques of renormalization. Application of renormalization will permit us to estimate some important quantities of percolation theory and to employ analogies from the existing framework of the theory of critical phenomena. Renormalization and critical phenomena are treated in many books (e.g., [25, 31–36]). The books by Bunde and Havlin [25] and Sornette [36] address percolation theory, while Sornette [36] specifically links discussion of percolation with critical phenomena, making these references most pertinent here.

In disordered systems that are far above the percolation threshold, it is always possible to define some variable, describing a subset of the system, which is at the percolation threshold. If this variable is defined in such a way as to relate to local transport coefficients, then it will be possible to identify the chief contribution to the transport properties of the medium. Then one has the interesting result that for disordered systems of nearly any structure transport is dominated by connecting paths near the percolation threshold, and the fractal characteristics of percolation can be relevant to transport even in media, which seem to have no resemblance to fractals. The basis for this application, called critical path analysis, is described in the last section of Chapter 2. Many applications of percolation theory to disordered systems (e.g., [21] and [25]) ignore critical path analysis, and so underestimate its value by restricting it to systems near the percolation threshold. The transport property, for which the impact of the fractal structure is greatest, is solute dispersion (Chap. 10).

The fact that percolation variables behave as power laws in $p - p_c$, as in Eq. (1.3) means that they must either diverge or vanish at $p - p_c$, depending on whether the exponent is negative or positive. The term singular behavior (in mathematics) or critical behavior (in physics), however, refers to either divergences or zeros.

It is important to consider some examples of problems that can be solved "exactly," providing a reference point for the more general scaling arguments typically advanced in percolation theory. Most of these exact solutions derive from Essam [37] or Stauffer [30]. We start with one of these, the calculation of the correlation length in one dimension.

1.6 The Correlation Length in One Dimension

It is possible to use the definition (Eq. (1.1)) to make a direct calculation of the correlation length in one dimension. That calculation is described nicely by Bunde and Havlin [25]. The calculation was stated explicitly in terms of site percolation, but is essentially the same for bond percolation. Consider a 1D chain, where each site is occupied randomly with probability p. Clusters of length s consist of chains of s consecutive occupied sites. Since any empty site breaks an infinite chain, the percolation probability in one dimension is $p_c = 1$: every single site must be occupied. Recall that the correlation function, $g(r)$, is the mean number of sites on the same cluster at a distance r from an arbitrary occupied site. In order for another occupied site even to be on the same cluster as the given site, each site in between must be occupied, a situation that occurs with probability p^r in each direction, leading to

$$g(r) = 2p^r \tag{1.4}$$

Substituting Eq. (1.4) in the definition of the correlation length (Eq. (1.1)) leads to

$$\chi^2 = \frac{\sum_{r=1}^{\infty} r^2 g(r)}{\sum_{r=1}^{\infty} g(r)} = \frac{\sum_{r=1}^{\infty} r^2 p^r}{\sum_{r=1}^{\infty} p^r} \tag{1.5}$$

In this expression the sum of p^r is simply a geometric series that yields the well-known result $1/(1-p)$. The factors r^2 may be verified to be generated from the sum over p^r by the (term by term) operation $p(d/dp)(pd/dp)\Sigma p^r$, since each derivative generates from p^r a factor r, but steps the power down by 1, requiring each time the compensating operation of subsequent multiplication by the factor p. The second derivative essentially generates $(1-p)^{-3}$ from $(1-p)^{-1}$, while the simple sum generates $(1-p)^{-1}$ in the denominator, and the result for χ^2 is a quotient of the two [25],

$$\chi^2 = \frac{1+p}{(1-p)^2} \quad \text{or} \quad \chi \propto (p_c - p)^{-1} \tag{1.6}$$

The final result ignores the factor of $1+p$ in the numerator for the purpose of finding the critical exponent (the power of $p - p_c$) for the correlation length. Equation (1.6) thus both confirms the proposed functional form of the correlation length as a divergent power of $p - p_c$ and yields the value $\nu = 1$ in one dimension. In the case of power-law divergences, the choice of a definition of χ is somewhat arbitrary.

See problem 8 for an alternate calculation of χ which leads to the same critical behavior as shown in Eq. (1.6), although the exact result is different. Later we will also find the value of ν by examining the cluster statistics. Percolation allows multiple paths for analysis.

In order to be able to make general application of percolation theory to an arbitrary system of course it is necessary to know the value of such powers under all circumstances. Most of the exponents of percolation theory are the same for all systems in a particular dimension, but differ importantly from dimension to dimension. In other words, for all 3D arrangements of bonds and sites, most of the exponents of percolation theory do not vary, but they do vary depending on whether the system sites are arranged in 3D space, or on a plane, for example.

Note that the correlation length represents an actual distance as measured in the Euclidean space and is thus a measure of a cluster size. The shortest connecting path that links opposite sides of a cluster has a step-by-step length called the chemical distance, r_l [38–40], since this is an actual distance of particle transport.

1.7 The Relationship of Scale Invariance and Renormalization, and the Relationship of the Renormalization Group to Percolation Theory

Renormalization is both a technique and a conceptual foundation for understanding percolation. As a technique it provides many useful results, but its conceptual role is even more important here.

Renormalization as a technique is a rather complex mathematical procedure, corresponding (in real space though not in Fourier space) to a relatively simple physical operation. This operation is a kind of "coarse-graining," caused by the observer drawing back to a greater distance. If the system has true scale invariance, i.e., is exactly at the percolation threshold, it will be impossible to detect a statistical change in the appearance of the system as the scale of observation is increased. A system with an infinite correlation length looks, in a statistical sense, the same at all finite length scales. But if the system is merely near the percolation threshold, so the correlation length is finite, then drawing back to a greater distance will make the correlation length look smaller. Eventually the observation scale will be greater than the correlation length. This (relative) diminution of the correlation length means that at larger length scales the system must appear as though it were further from the percolation threshold. Thus it must also be possible to redefine p simultaneously to be enough closer to p_c so that the appearance of the system does not change. This concept underlies the assertion that it is possible to define 'scaling' variables.

In the operation of renormalization, systems which are precisely at percolation remain at percolation. However, with increasing length scales, systems not at percolation appear to move away from percolation. Considered in terms of the changed p as a function of the scale of observation, repeated renormalization leads to completely different trajectories (trends in p) for systems above and below the

percolation threshold. The trajectory produced by repeated renormalization of a system at the percolation threshold is a point, since no changes can be observed. But the trajectory produced by such repeated applications of renormalization to a system not at percolation will always be away from the percolation threshold. Specifically, if the starting state has $p > p_c$, the trajectory will always be toward $p = 1$, while if the starting state has $p < p_c$, the trajectory will always be toward $p = 0$. If there is a largest cluster or largest hole size, this cluster (or hole) will look smaller every time the renormalization is applied. If the initial p value is either 0 or 1, renormalization will not affect p. Thus $p = 0$, $p = p_c$, and $p = 1$ are all "fixed points" of the renormalization procedure (though $p = 0$ and $p = 1$ are "trivial" fixed points, giving no new information). This same behavior is observed at second-order phase transitions, for which the correlation length also diverges. While the language and understanding of phase transitions has become more complex since the study of percolation theory commenced, the percolation transition does qualify as a second-order phase transition in the traditional definition and the theoretical development for such critical phenomena can be adopted for percolation theory.

1.8 Cluster Statistics of Percolation Theory

Probably the most elegant means to summarize the theory of percolation is to use the scaling theory of percolation clusters [19]. In principle one can formulate most of percolation theory simply in terms of its cluster statistics, and these statistics also allow easy analogies to other phase transitions. The purpose of this section is not to provide a detailed overview; for that the reader is referred to Stauffer's 1979 review [19]. What will be discussed here is sufficient to demonstrate the internal consistency of percolation theory and to provide less-experienced readers with multiple avenues for understanding and application.

The cluster statistics of percolation define the concentration n_s of clusters of volume (number of sites) s as a function of p. Consider initially n_s for $p < p_c$, deferring until later in this section the more complicated case including an infinite cluster. The sum $\sum s n_s$ over all cluster sizes must equal p, since it is by definition the total number of occupied sites per unit volume. Clearly as p increases toward p_c the number of large clusters increases. It turns out that precisely at p_c there can be no volume scale, because there is no length scale: n_s must therefore follow a power law in s. So at percolation n_s must obey [41],

$$n_s\,(p = p_c) \propto s^{-\tau} \tag{1.7}$$

Here τ is an exponent whose value will be discussed later. How does n_s depend on p? For $p \neq p_c$ a length scale exists, and its value is the correlation length χ. Suppose that one increases the observation length scale (reducing χ) and *simultaneously* takes the system closer to p_c (increasing χ); one can recover the original appearance if these operations cancel perfectly. Stauffer [19] states "We assume that the ratio

[...] $n_s(p)/n_s(p_c)$ and similar ratios of other cluster properties are a function of the ratio s/s_χ." Here s_χ is a typical cluster volume at p, which, since cluster sizes follow a power law, is proportional to the *limiting* (or largest) cluster volume at p. Since the linear extent of the largest clusters with $s = s_\chi$ is χ, which diverges as $p \to p_c$, the limiting cluster volume must also diverge in the limit $p \to p_c$. The exponent of $(p - p_c)$ which restricts the largest cluster volume is now denoted $-1/\sigma$, allowing the possibility that it is different from $-\nu$. This exponent must also be negative in order that the largest cluster size diverge at $p = p_c$. Thus $(s/s_\chi)^\sigma = s^\sigma(p - p_c) \equiv z$ is the scaling variable that allows the simultaneous effects of a size change and a change in p to cancel precisely. Consequently the ratio of the cluster numbers at p and at p_c can be written

$$\frac{n_s(p)}{n_s(p_c)} = f(z) = f[s^\sigma(p - p_c)] \tag{1.8}$$

The value of σ is not known a priori. Equation (1.8) may be called semiempirical in that it was designed to: (1) accommodate results of simulations, which revealed that the cluster numbers n_s decay according to a power law (with exponent τ) precisely at the percolation threshold and (2) allow simultaneous rescaling of s and p in such a way that the system looks the same, because the product $(p - p_c)s^\sigma$ remains the same. Approximate values of τ and σ can be found from simulations and/or renormalization procedures. These values will be the same for all systems of a given dimensionality, but have a dependence on spatial dimensionality, d (we will use the notation 1D, 2D, and 3D to denote the dimensionality of the Euclidean space, in which the system is embedded).

Substitution of $p = p_c$ in the left-hand side of Eq. (1.8) forces $f(0) = 1$. The exact form of the function f was uncertain for a long time, with various approximations proposed. In the Stauffer review it was pointed out that a Gaussian form for f could fit a wide range of data. Thus a useful approximation for $n_s(p)$ is [19]

$$n_s(p) \propto s^{-\tau} \exp\left\{-[z - z_0]^2\right\} \approx s^{-\tau} \exp\left\{-[s^\sigma(p - p_c)]^2\right\} \tag{1.9}$$

The approximation made here, which omits z_0, is motivated by the observation that z_0 must have some dependence on the system investigated and thus cannot be universal. Nevertheless the fact that a z_0 exists makes the cluster statistics, in principle, asymmetric about the percolation transition, for which $z = 0$. For bond percolation on a square lattice in two dimensions, however, there is perfect symmetry between connected and unconnected bonds, and the existence of a term z_0 would imply that extrema for the clusters of interconnected bonds would occur at different values of p than for clusters of unconnected bonds. However, it must be kept in mind that the neglect of this detail could lead to small discrepancies. The form of Eq. (1.9) makes it apparent that for $p \neq p_c$ the cluster statistics decay as a power law only up to a certain maximum size $s = s_\chi$, which is proportional to $|p - p_c|^{-1/\sigma}$. This provides an explicit context for the scaling arguments above, because clusters of larger volume rapidly become extremely rare when $|s^\sigma(p - p_c)| >> 1$.

One can use Eq. (1.9) in many ways. As a first application let us use Eq. (1.9) to find the fraction of sites connected to the infinite cluster at $p > p_c$. Note that the summation of sn_s from $s = 1$ to infinity is qualitatively different for $p > p_c$ from its form for $p < p_c$. For $p < p_c$, every occupied site (or bond) must be located on some finite cluster, but for $p > p_c$, some fraction P_∞ of occupied sites is found on the infinite cluster, not included in the summation. Thus every site on the lattice is either (1) empty with probability $1 - p$, (2) occupied and on the infinite cluster with probability pP_∞, or (3) occupied but not on the infinite cluster with probability $p(1 - P_\infty) \equiv \Sigma sn_s$. From these results one finds

$$P_\infty = 1 - \frac{1}{p} \sum_s sn_s \tag{1.10}$$

Stauffer's argument, which has been amply verified, is that it is the "singular" behavior of cluster sums, such as Eq. (1.10), which gives the percolation quantities of interest, such as P_∞, χ, etc. A sum of sn_s with n_s taken from Eq. (1.9) may be approximated by an integral. The functional dependence of such an integral on variables such as $p - p_c$ can be evaluated by transforming the argument of the exponential to dimensionless variables, i.e., z (no dependence on $p - p_c$). The result then contains one or more terms that are products of a power of $p - p_c$, and a definite integral which integrates to some (unimportant) constant. In such cases, singular behavior refers to the lowest nonanalytical power of $p - p_c$. An even easier technique for evaluating the functional dependence of such sums exists, however.

A sum over a power-law distribution of s, truncated at a maximum s value, will typically be dominated by the largest s allowed. At large values of its argument, the exponential function is a much more rapidly diminishing function than a power law, but at small values of its argument it is nearly a constant. Thus the exponential function can be approximated to do nothing except to truncate the sum, or integral, over sn_s at a value of s proportional to $(p - p_c)^{-1/\sigma}$. This argument leads to the following result:

$$\int_1^{(p-p_c)^{\frac{-1}{\sigma}}} ss^{-\tau} ds \propto p \left[1 - (p - p_c)^{\frac{\tau-2}{\sigma}} \right] \tag{1.11}$$

The factor p is included since when $p = p_c$ the integral must yield p. Using Eq. (1.11) in Eq. (1.10) gives

$$P_\infty = \frac{(p - p_c)^{\frac{\tau-2}{\sigma}}}{p} \propto (p - p_c)^\beta \tag{1.12}$$

The exponent β is customarily used for the critical behavior of P_∞. Equation (1.12) relates β to τ and σ via $\beta = (\tau - 2)/\sigma$. If the cluster statistics of percolation theory are known accurately Eq. (1.12) allows direct calculation of β. Otherwise Eq. (1.12) still gives an important scaling relationship.

Since P_∞ must vanish at $p = p_c$, $\beta \geq 0$. Therefore $\tau \geq 2$. In one dimension, because p_c is exactly 1, there is no regime $p > p_c$, and $\beta = 0$ is allowed, but in

all higher dimensions, $\beta > 0$. In systems of practical interest (2D and 3D systems) $0 < \beta < 1$. However, we will only be able to calculate accurately two values of β, 0 in one dimension and 1 in six dimensions or higher (or on Bethe lattices). Though we only show calculations of selected values of the critical exponents of percolation theory, summaries of values given elsewhere are also provided.

One can, in fact, calculate an entire series of integrals similar to Eq. (1.11). In particular, the kth moment of the cluster distribution is given by

$$M_k = \int_1^{(p-p_c)^{\frac{-1}{\sigma}}} s^k s^{-\tau} ds \propto |p - p_c|^{\frac{\tau-1-k}{\sigma}} \tag{1.13}$$

Since the lower moments, M_0, M_1, and M_2, all correspond to important physical properties, the values of $(\tau - 1 - k)/\sigma$ for these cases receive special designations. Thus Eq. (1.13) will provide the basis for three scaling relationships that we will use later. The possibility to organize several scaling relationships into a single Eq. (1.13) makes the cluster statistics formulation of percolation theory so appealing. But further discussion of these scaling relationships is postponed until after we have shown how to calculate n_s in $1 - d$.

1.9 Derivation of 1D Cluster Statistics and Discussion of Fractal Dimensionality

In one dimension the critical bond fraction for percolation, $p_c = 1$. This result is necessary because any break in the chain of elements will prevent the formation of a cluster of infinite size that spreads from negative to positive infinity. A purpose in repeating this fundamental condition is to remind the reader that in 1D systems expressions containing $1 - p$ may be rewritten as $p_c - p$. The next discussion follows Stauffer [19] in its general content. The probability of finding a cluster of s interconnected bonds, all in a row, is

$$n_s = p^s (1 - p)^2 \tag{1.14}$$

where the factor $(1 - p)^2$ truncates the s-cluster on both ends. In the case that $p_c - p << 1$ (p very near p_c), this result can be rewritten to lowest order in $p_c - p$ (noting that $1 - p = p_c - p$) as

$$n_s = s^{-2} [1 - (p_c - p)]^s \left[s^2 (p_c - p)^2 \right] = s^{-2} \exp [-s (p_c - p)] \left[s^2 (p_c - p)^2 \right] \tag{1.15}$$

"Derivation" of Eq. (1.15) from Eq. (1.14) requires also use of the approximation $(1 - x)^s = \exp(-sx)$, valid for $x << 1$. This approximation is used again when the cluster statistics for a Bethe lattice are derived. The cluster statistics of percolation theory can always be written in the following form,

$$n_s = s^{-\tau} f\left[s^{\sigma}(p - p_c)\right] \tag{1.16}$$

Equations (1.15) and (1.16) show that for 1D systems $\tau = 2$ and $\sigma = 1$. Also, consistent with $\sigma = 1$, one sees that there is a cutoff in the occurrence of clusters for sizes $s > s_{max} \approx 1/(p_c - p)$. In $1 - d$ the length of a cluster of s elements is s (times the fundamental bond length), so that the linear dimension of the largest cluster for $p < p_c$ is also $(p_c - p)^{-1}$. This result then defines the correlation length and yields the value $\nu = 1$ in agreement with Eq. (1.6). Note that the fact that $s_{max} \propto (p_c - p)^{-1/\sigma}$ and that $\chi \propto (p_c - p)^{-\nu}$ implies the result that $s_{max} \propto \chi^{1/\sigma\nu} = \chi^1$ where the equality holds in $1 - d$. Any time the total "volume" (s) of an object is proportional to its linear dimension (χ) to an exponent, the implication is that the "dimensionality" of the object is that exponent. As a consequence, the combination of exponents $1/\sigma\nu$ has become known as the fractal dimensionality, d_f, of percolation clusters, i.e., of large clusters near the percolation threshold. This fractal dimensionality has been called a "mass" fractal since it refers to a relationship between volume (proportional to mass) and linear dimension. Since for $d = 1$, $d_f = 1$ as well, in one dimension large clusters near the percolation threshold do not (cannot) have the rough "surface" associated with fractal objects. However, in systems of larger dimensionalities, d_f turns out to be less than d.

1.10 Argument for Dimensionally Dependent Scaling Law, Implications for Critical Exponent, τ, and Applications to Critical Exponents

The scaling form of Eq. (1.8) for the cluster statistics is independent of the dimensionality of the system. The exponents of percolation theory that appear in Eq. (1.8), Eq. (1.12), and similar equations below depend only on the dimensionality of the system. The scaling laws in Eq. (1.13) do not depend explicitly on the dimensionality allowing, in principle at least, the possibility that the values of the exponents are the same in all dimensions. But there is an important scaling law that does depend on dimensionality. The existence of this scaling law forces a variation of the values of the critical exponents with dimensionality, necessitating the tabulation of values given later in this chapter. Here we derive the dimensionally dependent scaling law that relates the various critical exponents from percolation theory.

The dimensionally dependent scaling law relating various critical exponents from percolation theory can be derived starting again from the cluster statistics of percolation, though the cluster statistics are not, by themselves, sufficient for this derivation. We first need to rewrite the cluster statistics of percolation theory in terms of the linear extent of the clusters. A cluster may be defined to have some linear extent N, where N is a number which, when multiplied by a basic length scale (such as a bond length) gives the linear dimension of the cluster. We know that the volume of a cluster of linear extent N is equal to $s = N^{1/\sigma\nu}$, on account of the fractal dimensionality of the clusters. We have derived the form of the cluster statistics in one

dimension, and it has been demonstrated that this form is also appropriate in larger dimensions, though with different values of the exponents [19]. Further, the scale-invariance of the system exactly at percolation requires that the cluster statistics follow a power-law decay, so we can write

$$n_s(p = p_c) = s^{-\tau} \tag{1.17}$$

Now use the probabilistic identity

$$n_s ds = n_N dN \tag{1.18}$$

to obtain

$$n_N = N^{-\frac{(\tau-1-\sigma\nu)}{\sigma\nu}} \tag{1.19}$$

If one integrates this (unnormalized) probability density function over a range of values from, say, N_0 to $2N_0$, which in a power-law discretization scheme (appropriate for self-similar media) would represent one "size class," one obtains

$$P(N_0) = N_0^{-\frac{\tau-1}{\sigma\nu}} \tag{1.20}$$

The significance of Eq. (1.20) becomes clear when it is discussed in the context of the self-similarity of the medium at $p = p_c$. At percolation, typically one cluster of linear extent N_0 should be found in a volume N_0^d (for any value of N_0) in order to be (1) consistent with the idea of percolation, i.e., that one can expect percolation to occur in any size system, all the way to infinite size, and (2) consistent with the concepts of self-similarity, i.e., that all such volumes look alike. Thus the concentration of clusters of size N_0 is proportional to N_0^{-d} so that the product of N_0^d and $N_0^{-d} = 1$. The implication is that

$$\frac{\tau-1}{\sigma\nu} = d \qquad \tau = 1 + \frac{d}{d_f} \tag{1.21}$$

This is the fundamental scaling relationship of percolation theory that cannot be obtained directly from the cluster statistics. It is the only such relationship that involves explicitly the dimensionality of the space, d, in which the percolation problem is embedded. Equation (1.21) relates the fractal dimensionality, $1/\sigma\nu$, to the Euclidean dimensionality, d, in terms of how rapidly cluster numbers decay with increasing size.

It is also straightforward to derive the ratio of the number of connected sites of a large cluster to the total number of occupied sites in the volume spanned by that cluster. Such a ratio is proportional to the mass M of the cluster divided by its volume V, and gives thus the cluster's density, ρ (e.g., [22, 23]). In the context of percolation, a "large" cluster has linear extent approximately equal to the correlation length. The result for ρ is

$$\rho = \frac{M}{V} = \frac{\chi^{d_f}}{\chi^d} = \left[(p-p_c)^{-\nu}\right]^{\frac{1}{\sigma\nu}-d} = (p-p_c)^{d\nu-\frac{1}{\sigma}} \equiv (p-p_c)^{\beta} \tag{1.22}$$

Equation (1.22), just above percolation in the limit of a cluster of infinite extent, also gives the fraction of sites, which is connected to the infinite cluster, justifying the final definition in Eq. (1.22). From Eq. (1.22) we can see that

$$\beta = d\nu - \frac{1}{\sigma} \tag{1.23}$$

or

$$d_{\mathrm{f}} = \frac{1}{\sigma\nu} = d - \frac{\beta}{\nu} \tag{1.24}$$

One can combine Eqs. (1.21) and (1.24) to write

$$\frac{\tau - 2}{\sigma} = \beta \tag{1.25}$$

which is the same result as that derived directly from the cluster statistics. Thus combining the expression for the density of large clusters with the dimensionally dependent scaling relationship yields one of the known cluster-scaling relationships (from Eq. 1.12). The implication of this redundancy is that the density of large clusters is dependent on the probability that an arbitrary site is found on the infinite cluster. Therefore the argument leading to Eq. (1.22) only appears to be new.

The conclusion that $\tau > 2$ (after Eq. (1.12)) can be drawn simply by examining the definition of n_{s}. Consider the integral

$$\int_1^\infty s n_{\mathrm{s}} ds = s^{2-\tau}|_1^\infty \tag{1.26}$$

which represents the total number of connected sites. This integral diverges unless $\tau > 2$. Although in dimensions $d > 1$ this is strictly an inequality, in $d = 1$ the value $\tau = 2$ is allowed. The reason for this is that the percolation probability is identically 1. So there is no regime $p > p_{\mathrm{c}}$ in one dimension. Further, at $p = p_{\mathrm{c}}$ the concentration of clusters of linear size s cannot really follow a power law: all sites are connected, there is only one cluster, and it is infinite in extent. Precisely at p_{c} in one dimension, then, the infinite cluster must be Euclidean, as implied already from the equivalence of d and d_{f}. Equation (1.11), from which the scaling relationship (Eq. (1.12)) for the exponents in n_{s} was derived, yields in 1D fundamentally different results in the limit $p \to 1$ and for $p = 1$. In fact, a sudden increase in P_∞ from 0 to 1 over an infinitesimally small increase in p is consistent with a value of $\beta = 0$. Note that $\beta = 0$ is also obtained by application of the scaling Equations (1.23) or (1.25) consistent with $d = d_{\mathrm{f}}$ or $\tau = 2$. The other immediate implication of the argument from integral 1.26 that $\tau > 2$ is that Eq. (1.21) then requires $d_{\mathrm{f}} < d$.

Finally, the most attractive aspect of the cluster statistics is that it is possible to use the same starting point (Eq. (1.13)) to derive three different scaling relationships. These relationships arise from applying the same techniques to the sums, $\Sigma s^0 n_{\mathrm{s}} \propto (p - p_{\mathrm{c}})^{2-\alpha}$, $\Sigma s^1 n_{\mathrm{s}} \propto (p - p_{\mathrm{c}})^{\beta}$, $\Sigma s^2 n_{\mathrm{s}} \propto (p - p_{\mathrm{c}})^{-\gamma}$. The scaling relationships from the second was already given in Eq. (1.12) (and 1.25); the first and third can be written in the following forms (see problems 1.4, 1.5, and 1.9),

$$2-\alpha=\frac{\tau-1}{\sigma}=d\nu \tag{1.27}$$

$$\frac{\tau-3}{\sigma}=-\gamma \tag{1.28}$$

The three sums also have interesting physical significance; for magnetic systems they correspond to the free energy, the magnetization, and the magnetic susceptibility, respectively. In percolation problems, the first is the mean number of clusters, the second yields the fraction of sites on the infinite cluster, while the third yields the mean mass of the clusters. Each then relates an important exponent from experiment to τ and to σ. Using these three scaling relationships (Eqs. (1.27), (1.28), and (1.12)) and the dimensionally dependent scaling relationship (Eq. (1.21)) it is possible to define all six critical exponents in terms of just two, most simply, for example, τ and σ from the cluster statistics.

1.11 Explicit Calculations of the Second Moment of Cluster Statistics in One Dimension

It will be necessary here to relate the second moment, M_2, of the cluster distribution to a simple sum over $g(r)$. In fact, the sum over $g(r)$ is easy to evaluate; any difficulty comes from the argument of its equivalence to M_2. Together with the results of calculations already shown and the scaling relationships of percolation we will then be able to generate the remaining exponents of percolation theory for the case of 1D systems. We will also generate in subsequent sections the exponents of percolation theory for infinite dimensional systems and then use the information generated from the extreme cases to understand the dimensional dependence of the exponent values.

The mean mass of finite clusters is shown in Bunde and Havlin [25] to be proportional to the second moment of the cluster size distribution. How do they show this? They start with the sum $\Sigma s n_s$ and use the exact expression for n_s in one dimension to show that this sum over finite cluster sizes (the only clusters that exist in one dimension) is exactly p.

The probability that an arbitrary lattice site belongs to an s-cluster is $sp^s(1-p)^2$. The factor s arises from the possibility that such an arbitrary site can be any of the s sites of the cluster. The authors then construct the corresponding probability per cluster site, which is just $p^s(1-p)^2$. Now construct the sum

$$w\equiv\sum_{s=1}^{\infty}sn_s=(1-p)^2\sum_{s=1}^{\infty}sp^s=(1-p)^2\sum_{s=1}^{\infty}p\frac{d}{dp}p^s=\left(1-p^2\right)p\frac{d}{dp}\sum_{s=1}^{\infty}p^s \tag{1.29}$$

The sum is easily performed with the result

$$w=(1-p)^2p\frac{d}{dp}\left(\frac{1}{1-p}-1\right)=(1-p)^2p\left(\frac{1}{1-p}\right)^2=p \tag{1.30}$$

The mean mass of a cluster can be defined as then

$$S = \sum_{s=1}^{\infty} s \left[\frac{sn_s}{\sum_{s=1}^{\infty} sn_s} \right] \tag{1.31}$$

with the factor in brackets generating the probability of an arbitrary site being found on an s-cluster and the product of this factor with s then giving the expected number of sites on s-clusters. Thus the mean mass is seen to be proportional to the second moment of the cluster distribution (s^2 in the sum).

In one dimension, since $g(r)$ gives the expected number of cluster sites at distance r the mean mass of a cluster is given [25] as follows,

$$S \equiv M_2 = 1 + \sum_{r=1}^{\infty} g(r) = \sum_{r=0}^{\infty} p^r = \frac{1}{1-p} = \frac{1}{p_c - p} \tag{1.32}$$

M_2 is traditionally characterized by the exponent γ, i.e., $S \propto (p_c - p)^{-\gamma}$. Thus $\gamma = 1$. From Eq. (1.28) one has $(\tau - 3)/\sigma = -\gamma$, so this result could be used to infer the value of τ, if one already knew σ (which we found using Eq. (1.15) to be 1). Of course in that derivation we also found τ and ν.

Since we have already shown how to obtain four exponents in 1D systems, we can generate the remaining values. In fact $\alpha = [2 - (\tau - 1)/\sigma] = [2 - (2 - 1)/1] = 1$, and $\beta = (\tau - 2)/\sigma = (2 - 2)/1 = 0$. Of course, following Eq. (1.26) we already argued on physical grounds that $\beta = 0$. Thus we have the complete suite of these fundamental exponents for 1D systems.

1.12 Calculation of the Correlation Length on a Bethe Lattice

Sections 1.12 through 1.15 give some exact calculations of exponents of percolation theory for infinite dimensional systems (in particular, Bethe lattices) as well as a mean-field calculation of the exponent β. This mean-field result for β is independent of dimensionality, d. Using these values together with the scaling relationships (Eqs. (1.25), (1.27), and (1.28)) and one physical argument from Bunde and Havlin [25] allows calculation of all the exponents of percolation theory in infinite dimensional systems. The scaling relationships in Eqs. (1.25), (1.27), and (1.28) are consistent with the values of the exponents for infinite-dimensional systems and the mean-field calculation of β. But these values are consistent with the dimensionally dependent scaling relationship (Eq. (1.21)) only for $d = 6$. This will make it possible (in Sect. 1.16) to define the range of dimensionalities for which the complete set of scaling relationships from percolation theory is accurate. Since this range of dimensionalities turns out to be $1 \leq d \leq 6$, the reader, especially those interested only in application of percolation theory to problems of subsurface flow and transport, may assume that the above framework of scaling relationships is accurate

for systems of experimental interest and skip Sects. 1.12 through 1.16 on a first reading. Nevertheless the following material is included here for those readers interested in understanding better the framework of the theoretical results they are encountering. Readers who skip these sections will still encounter five derivations: (1) cluster statistics in one dimension, (2) the correlation length in one dimension, (3) the mean cluster mass in 1D, (4) the correlation length in two dimensions using renormalization techniques, and (5) the relationship between fractal dimensionality and tortuosity. Ability to perform some derivations as well as familiarity with the scaling laws helps cement the understanding of people new to the field of percolation theory.

Percolation problems can be solved rigorously on a Bethe lattice (Cayley tree) as well as in one dimension. In contrast with the 1D system, the Bethe lattice has one advantage: $p_c < 1$ (meaning that it is possible to investigate behavior at $p > p_c$ as well as $p < p_c$). In contrast to all other dimensional systems, Bethe lattices have the following advantage: there are no loops in the structure. In addition, the Bethe lattice actually reduces to a 1D system in a particular limit. It is a relatively simple argument to show that the Bethe lattice is otherwise equivalent to an infinite dimensional structure, so that determination of percolation exponents on Bethe lattice in addition to their values in 1D systems gives these exponents in two extreme cases. A Bethe lattice of coordination number Z has a central site from which Z branches of unit length emanate. The end of each branch is another site, which connects through $Z-1$ branches to new sites. A Bethe lattice with $Z=3$ is like a family tree: at each generation there are twice as many ancestors as in the previous one, and it radiates out from a single point.

The lack of loops in the system means that two sites can be connected by only one path. One can draw (with some difficulty) a Bethe lattice on a 2D surface, but, as we will see, the Bethe lattice is equivalent in several respects to an infinite dimensional object. Clearly a Bethe lattice is a hierarchical structure, and it is convenient (and consistent with a drawing) to refer to each higher order of the hierarchy as a higher order shell. As Bunde and Havlin [25] point out, the Euclidean distance has no meaning on a Bethe lattice; only the chemical distance, r_l, between two sites has any relevance. Thus the correlation length is calculated with respect to a distance measured in shell separations, l. In particular, the chemical distance between the central site and a site in the lth shell is $r_l = l$. The lth shell of the tree consists of $Z(Z-1)^{l-1}$ sites. For the special case of $Z=2$ the lth shell thus contains two sites, as in a 1D chain, but in all other cases the number of sites increases exponentially since the l dependence shows up *in the exponent*. In a d-dimensional lattice, the number of sites at distance l increases as l^{d-1} (the surface area of a sphere of radius r being proportional to r^{3-1}, for example). Exponential functions may be expressed in terms of a Taylor series such as $\Sigma x^n/n!$ As x increases, the power of the dominant term increases as well. As x increases without bound, the dominant term in the series becomes the largest (or infinite) power, meaning that it is consistent to regard a Bethe lattice as an infinite dimensional structure. From the property of universality of the exponents in percolation theory one can thus propose that the exponents derived for the Bethe lattice are the same as for any infinite-dimensional

lattice. Moreover, since Toulouse [42] argues that the upper critical dimensionality for percolation is 6 (which we discuss in Sect. 1.16), it can be argued that the results derived for the exponents for the Bethe lattice are relevant to all systems with $d \geq 6$.

Assume that some fraction p of the sites on a Bethe lattice is occupied. The correlation function $g(l)$ is defined to be the mean number of sites on the same cluster at distance l from an arbitrary occupied site. In order for two sites separated by a distance r_l both to belong to the same cluster, each site in between the two sites must be occupied, bringing in a factor p^{l-1}; thus the probability that the second site is occupied and all the intervening sites as well is p^l. The number of sites on the lth shell is $Z(Z-1)^{l-1}$, making $g(l)$ the product of p^l (the probability that a given site is connected) and $Z(Z-1)^{l-1}$ (the number of possible connected sites). The correlation function, $[p(Z-1)]^l Z/(Z-1)$, being nearly $(p(Z-1))^l$, obviously trends rapidly to zero if the product $p(Z-1) < 1$, while it diverges for $p(Z-1) > 1$. This makes $p_c(Z-1) = 1$ the defining equation for the critical percolation probability, leading to $p_c = 1/(Z-1)$.

Next, the correlation length can be calculated in terms of the variable l as

$$\chi^2 = \frac{\sum_{l=1}^{\infty} l^2 g(l)}{\sum_{l=1}^{\infty} g(l)} \approx \frac{\sum_{l=1}^{\infty} l^2 (Z-1)^l p^l}{\sum_{l=1}^{\infty} (Z-1)^l p^l} \tag{1.33}$$

This sum may be performed by the same techniques as used in the 1D chain, i.e., the geometric sum is now $1/(1-(Z-1)p) = 1/(1-p/p_c) = p_c/(p_c-p)$. The same trick to generate the factor l^2 in 1D lattices works here as well, since differentiation with respect to p leaves the factor $(Z-1)$ alone. Bunde and Havlin [25] then find

$$\chi^2 \propto (p-p_c)^{-2} \tag{1.34}$$

and the correlation exponent equals 1 with respect to the chemical distance, l (in l-space). Since the Euclidean dimension has no meaning on the Bethe lattice, there is no purpose to make a direct calculation of the correlation length as an estimate of the Euclidean dimension of the largest cluster for $p < p_c$. But Bunde and Havlin [25] make the argument that on other lattices of high enough dimension (greater than the critical dimension, 6, as it turns out) any path on a cluster behaves like a random walk (with the number of steps proportional to l), so that $r^2 \propto l$. This argument implies that for $d \geq 6$ (other than Bethe lattices) the correlation length as a function of the Euclidean distance should have exponent $\nu = 1/2$.

1.13 Explicit Calculations of the Second Moment of Cluster Statistics on a Bethe Lattice

The calculation of the mean mass for a Bethe lattice is very similar to its calculation in 1D systems. On a Bethe lattice one has [25]

$$S = 1 + \sum_{l=1}^{\infty} Z\,(Z-1)^{l-1}\,p^l = \left(\frac{Z}{Z-1}\right) \sum_{0}^{\infty} \left[p^l\,(Z-1)^l\right]$$
$$= \left[\frac{p_c}{p_c \big/ (p_c+1)}\right] \frac{1}{1-(Z-1)\,p} = \frac{p_c+1}{1-p/p_c} = \frac{p_c\,(p_c+1)}{p_c-p} \tag{1.35}$$

This result yields once again $\gamma = 1$. On the Bethe lattice this calculation turns out to be quite useful indeed.

The exponent $\beta = 0$ describing the behavior of the infinite cluster in one dimension (and given by the first moment of the cluster statistics) was already inferred in Sect. 1.10. The discussion of the exponent β [25] is slightly more complicated on a Bethe lattice, but the next section gives a derivation valid whenever "mean-field" treatments are appropriate (as it will turn out, for $d \geq 6$, and thus also on the Bethe lattice).

1.14 Mean-Field Treatment of the Probability of Being Connected to the Infinite Cluster

Consider a "mean-field" treatment of the bond percolation problem on a lattice with coordination number (number of nearest neighbors), Z. In mean-field treatments all sites are regarded as equivalent. While all sites were equivalent before the bonds were actually assigned, this equivalence is lost afterwards, and this is a reason why mean-field treatments can fail. Nevertheless, a mean-field treatment does illuminate some important concepts, and we can apply these further.

Assume that an infinite cluster of connected sites exists. Define the probability that some particular site is connected to the infinite cluster as P_∞. Then the probability that it is not connected is $1 - P_\infty$. The probability that the site is connected to one of its nearest neighbors, chosen arbitrarily, is p. According to the mean-field hypothesis, the probability that that neighbor site is connected to the infinite cluster is assumed to have the same value P_∞, with the value independent of whether the two sites are actually connected or not. The probability that the given site is connected to the infinite cluster over this particular nearest neighbor is pP_∞, where the product is used because of the independence of the bond probability and the probability P_∞. The probability that it is not connected to the infinite site over this particular nearest neighbor is $1 - pP_\infty$. The probability that it is not connected to the infinite cluster over any of its nearest neighbors is thus $(1 - pP_\infty)^Z$. Thus we must have

$$1 - P_\infty = (1 - pP_\infty)^Z \tag{1.36}$$

which states that the probability that a site is not connected to the infinite cluster is equal to the probability that it is not connected over any one of its nearest neighbor sites, and that the probability that each of those neighbor sites is not connected to the infinite cluster is identical. Equation (1.36) can be rewritten as

$$(1-P_\infty)^{\frac{1}{Z}} = 1 - pP_\infty \tag{1.37}$$

Note that for $p < 1/Z$, this equation has only one solution, namely, $P_\infty = 0$. If the probability that any arbitrary site is connected to the infinite cluster is 0, there must not be an infinite cluster. If an infinite cluster does not exist, the system must be below the percolation threshold. This indicates that the lowest order $1/Z$ is the percolation threshold. We expand Eq. (1.37) (keeping the first two terms of a Taylor series) in the variable $p - 1/Z = p - p_c$ and assume that $P_\infty << 1$.

$$1 + \frac{1}{Z}(-P_\infty) + \frac{1}{2}(-P_\infty)^2 \left(\frac{1}{Z}\right)\left(\frac{1}{Z} - 1\right) = 1 - \left(\frac{1}{Z} + p - \frac{1}{Z}\right) P_\infty \tag{1.38}$$

Note that the first two terms on each side of the equation are identical and can be subtracted off. Then we have

$$P_\infty = \frac{p - (1/Z)}{1/Z\,[1 - (1/Z)]} = \frac{p - p_c}{p_c\,(1 - p_c)} \tag{1.39}$$

P_∞, like other percolation quantities, is known to be a power of $p - p_c$. Thus the mean-field treatment directly predicts $p_c = 1/Z$ as can be seen from the numerator. Note the implication that $p_c = 1/Z$ has no dependence on d. This is incorrect. However, we are going to assume that the result $p_c \propto 1/Z$ is correct and that the proportionality constant may depend on dimensionality. For our purposes this is the most important result of the application of the mean-field treatment to find P_∞ and we will use it later to deduce some further values of p_c.

Comparison of Eq. (1.39) with $P_\infty = (p - p_c)^\beta$ allows the identification $\beta = 1$. $\beta = 1$ is the mean-field result. Like all such "classical" results, it is independent of d. It will be argued to be relevant for systems with $d \geq 6$. $\beta = 1$ can be derived exactly for a Bethe lattice.

1.15 Cluster Statistics on a Bethe Lattice

In a 1D lattice the cluster statistics were easy to develop. They are almost as easy to develop on a Bethe lattice, but one difference is that it is somewhat more difficult to define the perimeter of an s-cluster, i.e., the number of sites which terminate the cluster. It is, however, relatively easy (for $Z = 3$, at any rate) to convince oneself that a cluster of one site has Z empty sites surrounding it, a cluster of two sites has $Z + Z - 2$ empty sites surrounding it, and a cluster of s sites has $Z - 2$ more empty sites surrounding it than a cluster of $s - 1$ sites. The number of perimeter (empty, bounding) sites can be called u, and u is thus [25]

$$u(s) = Z + (s-1)(Z-2) \tag{1.40}$$

Note that $u(s) = Z$ in the case $Z = 2$, for which the Bethe lattice collapses to a $1-d$ chain. Since an s-cluster again can connect only clusters on shells separated by $l = s$, all sites in between must also be occupied, and

$$n_s = g_s p^s (1-p)^{u(s)} = g_s p^s (1-p)^{Z+(s-1)(Z-2)} \tag{1.41}$$

where g_s is just the number of configurations for an s-site cluster. If $p(1-p)^{Z-2}$ is expanded in a Taylor series around $p_c = 1/(Z-1)$ it is possible to show that [25]

$$n_s \approx n_s(p) f(p) \tag{1.42}$$

where $f(p) = (1 - [(p-p_c)^2/2p_c(1-p_c)])^s$. This expression can be rewritten as $\exp(-s[(p-p_c)^2/2p_c(1-p_c)])$ for p nearly p_c. In order to write this function as a function of the scaling variable $z = (p-p_c)s^\sigma$, one must choose $\sigma = 1/2$ so that the product of the factors $(p-p_c)s^\sigma$ is then squared. Note that the form of the cluster statistics (a Gaussian in $p-p_c$) is the same as the approximate result, Eq. (1.9), from Sect. 1.8.

We now have made calculations of the two exponents γ and σ for the Bethe lattice. We can use one of the scaling relationships to infer the value of τ.

$$\tau = 3 + \sigma\gamma = 3 - 1/2 = 5/2 \tag{1.43}$$

Similarly we can find

$$\alpha = 2 - \left(\frac{\tau - 1}{\sigma}\right) = 2 - \frac{3/2}{1/2} = -1 \tag{1.44}$$

We can thus now find most of the exponents of percolation theory in infinite dimensional systems. The one exponent we do not really know at this point is ν for the correlation length. The dimensionally dependent scaling relationship cannot give it to us. So, practically speaking, we must rely on the argument cited by Bunde and Havlin [25] to find ν.

1.16 Summary of Relationships Between Exponents in One Dimension and in Infinite Dimensions Using Scaling Relationships. Implications for the Validity of Hyperscaling

The term hyperscaling was invented to describe scaling relationships that explicitly involve the dimension, d. The entire compendium of scaling relationships developed in Sects. 1.8 and 1.10 describe exponents with a dimensional dependence provided the dimensionally dependent scaling relationship holds. These scaling relations have been shown to be exact in one and two dimensions and are expected to hold for systems of relatively low dimensionality. The set of exponents derived for Bethe lattices on the other hand, except for $\nu(l)$, has been suggested to be valid for all infinite

dimensional systems. Mean-field theories are believed to describe the behavior of the (classical) exponents of percolation theory in high enough dimensions. If the same set of exponents is used independent of dimensionality for any range of values of d, the dimensionally dependent scaling relationship, Eq. (1.21), cannot generally be true for that set of exponents. However, that set of exponents might be consistent with Eq. (1.21) for one value of d. Thus the set of exponents derived for Bethe lattices may be assumed to be correct in all dimensionalities greater than some maximum (or critical) $d = d_c$, if it is possible to find a $d = d_c$ for which Eq. (1.21) holds for the classical exponents. Without a value of ν, however, this hypothesis cannot be applied. If the suggestion described by Bunde and Havlin [25] regarding the value of $\nu = 1/2$ for infinite lattices is correct (which it is), then we can check to see for which dimension $(\tau - 1)/\sigma\nu = d$ holds for the exponents derived from Bethe lattices. Using these results one finds that $(\tau - 1)/\sigma\nu = 6 \equiv d_c$ meaning that the hyperscaling exponents must be the same as the classical exponents for $d = 6$. This argument was first given by Toulouse [42], and the additional inference is that for systems of dimensionality 6 or greater, the values for percolation exponents found for Bethe lattices are valid. Note that $d_f = 1/\sigma\nu = 4$ holds independently of d for $d \geq d_c$. Thus even in an infinite dimensional system, the percolation cluster can be embedded in a 4D space. This result helps to explain why any path on a cluster behaves like a random walk for $d \geq 6$.

For $d < 6$, where hyperscaling is valid, other means for finding the exponents are required. One of the most productive such means is to apply renormalization group calculations using the so-called epsilon expansion with $\varepsilon = 6 - d$ as an expansion parameter, since the values of the exponents are known in six dimensions when $\varepsilon = 6 - 6 = 0$. $d_c = 6$ then becomes the upper limit of validity of hyperscaling.

1.17 Calculation of the Critical Site Percolation Probability for the 2D Triangular Lattice and of the Critical Exponent for the Correlation Length in Two Dimensions

The following discussion is an exercise in the power, but also imprecision, of spatial renormalization techniques. It requires some subsequent discussion. Although the actual results are not quite right, they appear to be reasonable, are very nearly accurate, and help illustrate an earlier state of thinking.

While the following development is expanded from Stauffer [19], his source was Reynolds et al. [43]. Consider the image of the triangular lattice in Fig. 1.4. The circles represent sites. Each site can potentially be connected to six nearest neighbors. Imagine coloring in a fraction p of the sites. Whenever two colored sites are nearest neighbors they can be considered to connect (as in the case of metallic balls, which could conduct electricity between them if they were in contact). If a colored site is neighbor to an uncolored site, or two uncolored sites are neighbors, then no connection is made. A renormalization process can be developed, which constructs a new lattice out of "supersites," which replace groupings of three sites as shown.

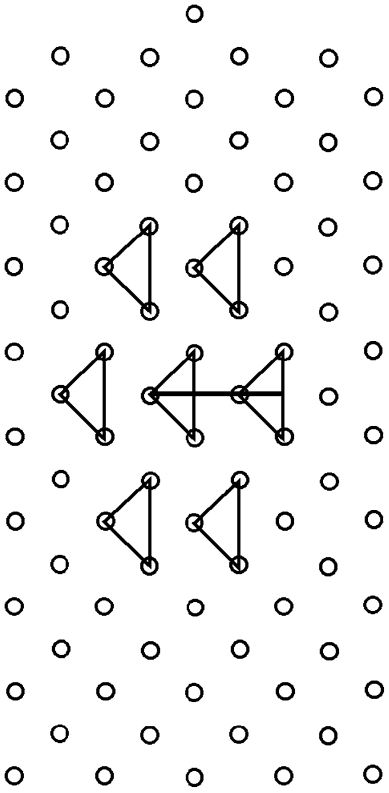

Fig. 1.4 A small portion of a site-percolation problem on a *triangular* lattice. The *circles* are sites. Supersites of a real-space renormalization are located at the centers of the triangles shown. The line drawn in is an aid to measuring distances using 30-60-90 right triangles

A replacement of three sites by a single site must involve a rescaling of the length, or distance between sites, by the factor $3^{1/2}$. That result can be checked directly in Fig 1.4 by examining the geometry of the system; the line separating the new sites forms the bisector of the vertex of the triangles, as shown, thus developing 30-60-90 triangles. The sides of these triangles are in the ratios 1, $3^{1/2}$, 2. The ratio of the separation of supersites to that of the simple sites in the original lattice is $2 \times 3^{1/2}/2$. If one moves just far enough away from the lattice that the new "supersites" are exactly as far away from each other as the old simple sites, then the length scale associated with the separation of sites has been reduced by $1/3^{1/2}$.

Now consider how p changes with such a rescaling of the lattice. The approximation that is used here has been called "majority rule." If either two or three sites on the original lattice are colored in, the new site is colored in. Clearly, if all three sites of the original lattice were colored in, a connection could be made across the triangle in any direction, while if two sites are colored in, often a connection across the triangle can still be made, though not in an arbitrary direction. If one or zero sites are colored in on the original lattice, the new site is not colored in, because no connection across the triangle can be made, and in most cases such a triangle will interrupt the continuity of paths constructed across other nearby triangles. The new

probability, p', of coloring in a site is thus constructed from the old probability, p. The above conceptualization is a very reasonable assumption, and nearly precise. It basically means that if you can get across a given "supersite" from one side to the other, presenting potential connections to new sites on both sides, it should be colored in. Otherwise, it should not be. Mathematically this can be represented as

$$p' = p^3 + 3p^2(1-p) \tag{1.45}$$

The justification for this result is that the probability that all three sites are colored in independently, each with probability p, is p^3. The probability that two particular sites are colored in and the third is not is $p^2(1-p)$. There are three possible locations for the site, which is not colored in, justifying the factor 3. In the case that $p' = p$, the new lattice has precisely the same appearance and statistics as the old, and $p' = p \equiv p_c$. If the substitution $p' = p$ is made in the above equation, it is possible to rewrite the equation as

$$-2p^3 + 3p^2 - p = 0 \tag{1.46}$$

which can be factored as

$$-p(2p-1)(p-1) = 0 \tag{1.47}$$

The three roots of this equation are $p = 0$, $p = 1/2$, and $p = 1$. The existence of the "trivial" roots $p = 0$ and $p = 1$ was predicted in Sect. 1.7 (obviously if all sites or no sites are initially colored in, this condition will persist). The root $p = 1/2$ represents p_c.

The divergence of the correlation length must be according to a power law as discussed. The only reasonable form for this relationship is

$$\chi = \chi_0 |p - p_c|^{-\nu} \tag{1.48}$$

where χ_0 is a scale factor (obviously proportional to the original spacing of the circles marking the fundamental lattice points), which need not concern us here and $\nu > 0$. The value of the critical exponent, ν, can be found through the above renormalization by noting that $-\nu$ is the slope of a graph of the logarithm of χ vs the logarithm of $p - p_c$. Thus also for the above change of scale, take p slightly different, e.g., larger than p_c, $p - p_c = \delta$, where $\delta << 1$, and find the behavior of $p' - p_c$ as a function of δ. This kind of procedure is known as "linearization," because it will define only the lowest order variability in p'. Using Eq. (1.45) without equating p and p' (because if $p > p_c$, then $p' > p$) write p' as

$$p' - p_c = (p_c + \delta)^3 + 3(p_c + \delta)^2(1 - p_c - \delta) - p_c \tag{1.49}$$

and expand the result (again in a Taylor series) to first order in δ. The result (the reader should verify this) is that $p' - p_c = (3/2)\delta$. But since $p - p_c = \delta$ by definition, one finds that

$$\nu = -\frac{\log\left(1/3^{1/2}\right)}{\log(3\delta/2) - \log(\delta)} = \frac{\log\left(3^{1/2}\right)}{\log(3/2)} = 1.355 \tag{1.50}$$

Note that the value of p_c for the site percolation problem on the triangular lattice is precisely 1/2, while the value of ν is $4/3 = 1.333$ and the estimate of Eq. (1.50) is only wrong by 2%.

Consider now also the number of sites on a cluster of linear dimension given by the correlation length. In the renormalization procedure the number of sites on an arbitrary cluster is reduced by the following ratio,

$$\frac{s(p')}{s(p)} = \frac{p'^3 + 3p'^2(1-p')}{3p^3 + 2(3)p^2(1-p) + 3p(1-p^2)} = \frac{1}{3} \tag{1.51}$$

if evaluated right at p_c, i.e., $p = p' = 1/2$. In Eq. (1.51) a standard result for the average number of sites colored in on a given triangle is used, a sum over the product of the probability of occupation and the number of occupied sites. However, if Eq. (1.51) is evaluated at $p = p_c + \delta$, where $\delta << 1$, one finds a ratio of $(1/3)(1 + (5/2)\delta)$, which is slightly larger than 1/3. Equation (1.51) gives a first estimate of the power σ in the cluster statistics, $s_{\max} \propto (p - p_c)^{-1/\sigma}$,

$$\frac{1}{\sigma} = -\frac{\log(1/3)}{\log(3\delta/2) - \log(\delta)} = 2\nu = 2.711 \tag{1.52}$$

Equation (1.52) for σ cannot be quite right. Consider now these rough results in two dimensions, namely $\nu = 1.355$ and $\sigma = 1/2\nu = 1/2.711$ in the context of the scaling relationships. Use $d_f = 1/\sigma\nu$ to find $d_f = d = 2$! If the fractal dimensionality is the same as the Euclidean dimensionality, then, by Eq. (1.24) just as in one dimension, $\beta = 0$. Then Eq. (1.21) gives $\tau = 2$ as well. In fact, however, $\sigma > 1/2\nu$ (and it turns out that $\beta = 0.14$, not 0). While this difference is not great, and $d_f = 1.9$ for $d = 2$ (only slightly smaller than 2), the difference is obviously very important. So, while the approximate renormalization procedure to find ν appeared at least in 1979 to generate some hope that the value was accurate, in fact the result for the exponent σ is sufficient to show that Eq. (1.50) is merely an approximation.

The statement above Eq. (1.52) that σ is slightly larger than $1/2\nu$, while correct, cannot rigorously be based on the argument provided, since that argument does not produce a consistent power, independent of the value of p. It will turn out that the correct value of $1/\sigma$ is $91/36 = 2.53$, or about 7% different from the estimate. While this difference is not large, it is critical.

1.18 Value of p_c for Bond Percolation on the Square Lattice

Consider Fig. 1.5. The small black circles from a square lattice. Imagine that a fraction p of the bonds (thin black lines) has been filled in at random, as shown. Next construct the square lattice denoted by the grey circles, which are placed at the

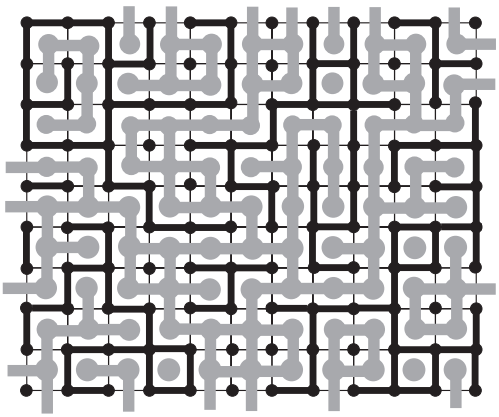

Fig. 1.5 A *square* lattice (*small black circles* and *black lines*) and its dual lattice (*large grey circles* and *grey lines*), which is also a square lattice. Note that the bonds of the dual lattice percolate

centers of individual squares formed by the black circles. Imagine that a total of q of the potential bonds on the grey lattice are connected (grey lines). Each of these square lattices has the same coordination number, $Z = 4$. Further, every potential bond on each lattice intersects (blocks) exactly one bond on the other lattice, which we can call a dual lattice. Thus p for the first lattice is precisely $1 - q$ for the other lattice and $p + q = 1$. Given the 2D nature of the lattices, however, it is not possible that both can "percolate" simultaneously. Either one lattice percolates or the other does. Given the identical natures of the two lattices, however, it does not make sense for $p_c > q_c$, or for $p_c < q_c$. The only alternative is to choose $p_c = q_c = 1/2$. The fact that the square lattice is its own dual lattice means that its percolation probability must be 1/2. The product of Zp_c for this lattice is 2. Miyazima [44] has constructed an analogous argument to find $p_c = 1/2$ for bond percolation on a 4D hypercube (and extended the derivation to $2n$ dimensions).

1.19 Estimations of p_c for Bond Percolation on the Triangular and Honeycomb Lattices

Consider Fig. 1.6. It includes a honeycomb lattice of grey circles $(Z = 3)$ and a triangular lattice of black circles $(Z = 6)$, which are fully complementary (or each other's duals), as were the two square lattices above. Thus every bond that is connected on the triangular lattice would "break" a bond on the honeycomb lattice and vice versa. This means that if no bonds from one lattice are allowed to cross bonds from the other one, the bond probability p on the triangular lattice is $1 - q$, with q the bond probability on the honeycomb lattice and $p = 1 - q$. The black lines represent bonds on the triangular lattice, while the grey lines represent bonds on the honeycomb lattice. As is generally true in two dimensions, either the triangular

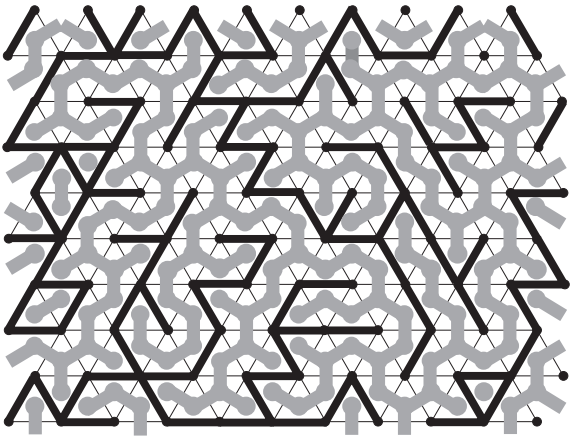

Fig. 1.6 A *triangular* lattice (*small black circles* and *thin black lines*) and its dual lattice (*large grey circles* and *grey bonds*), which is a honeycomb lattice. Here the bonds of the honeycomb lattice percolate

lattice percolates, or the honeycomb lattice percolates, but not both simultaneously. In the figure the triangular lattice percolates. The result $p+q=1$ together with the exclusionary result on the two percolation probabilities implies that $p_c+q_c=1$. But the result from Sect. 1.13 that $p_c \propto 1/Z$ implies that $q_c=2p_c$. ($p_c \propto 1/Z$ implies that the quantity Zp_c is a constant, which turns out to be a good approximation.) Simultaneous solution of these two equations yields $p_c=1/3$, $q_c=2/3$. Note that these estimates for p_c are both consistent with the relationship $Zp_c=2$, but the exact results are $p_c=0.3473$, $q_c=0.6527$, for which values $Zp_c=2.08$ and 1.96, making this product only an approximate invariant. Vyssotsky et al. [45] suggested that the product Zp_c should take on the values $d/(d-1)$, for $d \geq 2$, and such an approximate invariant as this can be quite useful if a system, for which p_c is not known and cannot be readily calculated, is encountered.

1.20 Summary of Values of p_c

In general, in a given lattice, a bond has more nearest neighbors than a site. In the square lattice one bond is connected to six nearest neighbor bonds, while a site has only four nearest neighbor sites. Thus large clusters of bonds can be formed more effectively and a lower concentration of bonds is needed to form a spanning cluster, i.e., p_c for bonds is lower than for sites. For the smallest system possible, four squares, the critical percolation probability is three-fourths for site, but one-half for bond percolation. Here, the ratio of p_c bond to p_c site is exactly $2/3 = Z_{site}/Z_{bond}$. For infinite sized systems the ratio of critical percolation probabilities is not so simply related to the coordination numbers.

Table 1.1 Tabulated values of p_c

Lattice type	Z	p_c bond	Estimated p_c	Zp_c	p_c site (est.)
Honeycomb	3	$1-2\sin(\pi/18)$	2/3	1.96	0.6962
Square	4	$1/2$	1/2	2	0.5927
Triangular	6	$2\sin(\pi/18)$	1/3	2.08	1/2 (1/2)
Diamond	4	0.3886		1.55	0.4299
Simple cubic	6	0.2488		1.49	0.3116
BCC	8	0.1795		1.44	0.2464
FCC	12	0.119		1.43	0.199

The known results for p_c are summarized in Table 1.1. The four cases, for which simple approximations are known and repeated above, are noted. These four cases and those of Miyazima [44].

All the estimated bond p_c values given are exactly consistent with the Vyssotsky et al. [45] relationship above, though, when compared with the most accurate determinations of p_c that relationship gives values that are accurate only to within about 4%.

Some of the references for the above values include Kesten [12] and Essam et al. [46] (triangular bond, honeycomb and triangular site, square bond), Sykes and Wilkinson [47]; Adler et al. [48] (BCC bond, simple cubic bond), Ziff and Sapoval [49] (square site), Stauffer [30] (BCC site, FCC site, FCC bond, honeycomb site), Strenski et al. [50] (simple cubic site).

1.21 More General Relationships for p_c

Some relationships for p_c are mentioned, which may help guide estimations in more complex, but more realistic models.

The lattice structures mentioned so far by no means exhaust the types investigated, and the Vyssotsky relationship is useful only for bond percolation. Galam and Mauger [51] have developed a more general relationship for p_c of the following form, $p_c = p_0[(d-1)(q-1)^{-a}d^b$. For regular lattices, $q = Z$ is the coordination number. For nonperiodic tilings, q is an effective value of Z. The relationship is considered to be valid for anisotropic lattices with nonequivalent nearest neighbors, non-Bravais lattices with two atom unit cells and quasi-crystals. The biggest strength of the relationship, however, may be that it can be applied to both site and bond percolation problems. In the former case, $b = 0$, while in the latter $b = a$. The biggest weakness is probably that the known systems fall into two classes, each with different values of p_0 and a. The first class includes 2D triangle, square, and honeycomb lattices with $a = 0.3601$ and $p_0 = 0.8889$ for site percolation and $a = 0.6897$ and $p_0 = 0.6558$ for bond percolation. 2D Kagome and all (hyper)-cubic lattices in $3 \leq d \leq 6$ constitute the second class with $a = 0.6160$ and $p_0 = 1.2868$ for site

and $a = 0.9346$ and $p_0 = 0.7541$ for bond percolation, respectively. But in order to use these results to predict p_c, one must know to which class of lattice a particular system belongs. Nevertheless it is important here to provide guidance for prediction of p_c in new system geometries.

Finally we come to the result of Scher and Zallen [52] for the critical volume fraction for continuum percolation. Such results have the potential to be of great use in percolation problems in porous media. Scher and Zallen [52] found that for regular lattices the critical occupied volume fraction,

$$V_c = p_c f \tag{1.53}$$

where p_c is the critical bond fraction, and f is the filling factor (the fractional volume covered) of a lattice when each site of the lattice is occupied by a sphere in such a way that two nearest neighboring impenetrable spheres touch one another at one point. For a simple cubic lattice the value of this product is 0.163, and in fact the value of this product for all the lattices considered scarcely differed from 0.17. Note that an analogous model (with different shaped objects) could have direct relevance to porous media with f replaced by the porosity, and there is indeed evidence for the applicability of Eq. (1.53) in this context.

Shante and Kirkpatrick [53] generalized this idea to overlapping spheres, and showed that the average number, B_c, of bonds per site at p_c (equal to the product of Zp_c) is related to the corresponding critical volume fraction by

$$V_c = 1 - \exp\left[\frac{-B_c}{8}\right] \tag{1.54}$$

Note that the choice of $B_c = 1.5$ for three dimensions yields $V_c = 0.17$. This result is generalized to an arbitrary continuum of spheres by choosing B_c to be the limiting value of $p_c Z$ in the limit $Z \to \infty$. Values of V_c on the order of 0.17 have often been suggested to be relevant to real media. Balberg [16] has developed these ideas further, finding,

$$V_c = 1 - \exp\left[\frac{-B_c V}{V_e}\right] \tag{1.55}$$

where V is the volume of the object and V_e is the excluded volume, i.e., the total volume in which the center of a neighboring volume of the same shape cannot be located without overlapping. For spheres this ratio is $(4/3)\pi r^3/(4/3)\pi(2r)^3 = 1/8$, in agreement with the result of Shante and Kirkpatrick [53].

For results for the critical volume fractions for percolation for a number of anisotropic shapes one can also consult the following web page http://ciks.cbt.nist.gov/~garbocz/paper59/node12.html#SECTION00050000000000000000 (geometrical percolation threshold of overlapping ellipsoids, Garboczi, et al. [54]). These values may be of considerable use in geologic applications, at least to guide conceptualization. In particular, the critical volume fraction for percolation has a strong tendency to diminish for increasing shape anisotropy.

Problems

1.1. Show that at arbitrary p the largest clusters have cluster radius $r_s = s^{\sigma\nu}$, and argue then that for arbitrary p and arbitrary s, $r_s = s^{\sigma\nu g}[s^{\sigma}(p - p_c)]$, where g is an unknown function. Does your result for r_s imply an effective dimension of the clusters?

1.2. Derive Eq. (1.50) from Eq. (1.49).

1.3. Derive Eq. (1.42) from Eq. (1.41).

1.4. The critical exponent α is defined through the singular contribution to $\Sigma s^0 n_s \propto (p - p_c)^{2-\alpha}$. Find α in terms of known exponents using the results of development of 1.8 and an analogy to Eq. (1.13).

1.5. The critical exponent γ is defined through the singular contribution $\Sigma s^2 n_s \propto (p - p_c)^{-\gamma}$. Find γ in terms of known exponents.

1.6. Show explicitly that Eq. (1.30) results from Eq. (1.29).

1.7. Verify the scaling relationships for the critical exponents in 1D, 2D, and 6D. Do you expect them to be precisely satisfied in 3D (where the exponents may not ever be represented in terms of rational fractions)?

1.8. Show that, for 1D systems, definition of χ as

$$\chi = \frac{\sum_{r=1}^{\infty} r p^r}{\sum_{r=1}^{\infty} p^r}$$

leads to $\chi = p/(1-p)$ instead of $\chi = (p+1)/(1-p)$ as obtained from Eq. (1.5). How would you characterize the sensitivity of the scaling behavior of the correlation length relative to the details of its definition?

1.9. The sum in problem 1.4 has been argued to describe, for a magnetic system, the free energy, while p (the first moment) corresponds to the magnetization, and the sum in problem 1.5 (the second moment) to the susceptibility. Find an argument for why an increase in the moment of the cluster distribution by one corresponds to a derivative with respect to the applied field.

References

1. Diestel, R., 2000, *Graph Theory*, 3rd edition. Springer-Verlag, Heidelberg, Graduate Texts in Mathematics, Volume 173. 1
2. Du, D.-Z., and F. Hsu, 1995, *Combinatorial Network Theory* (Applied Optimization) Springer, Heidelberg. 1

3. Fatt, I., 1956, The network model of porous media, *Trans. Am. Inst. Min. Metall. Pet. Eng*., **207**: 144–177. 1
4. Chalupa, J., P. L. Leath, and G. R. Reich, 1979, Bootstrap percolation on a Bethe lattice, *J. Phys. C. Solid State Physics* **12**: L31–L35. 1
5. Rosso, M., J. F. Gouyet, B. Sapoval, 1986, Gradient percolation in 3 dimensions and relation to diffusion fronts, *Phys. Rev. Lett*. **57**: 3195–3198. 1
6. Chandler, R., J. Koplik, K. Lerman, and J. F. Willemsen, 1982, Capillary displacement and percolation in porous media, *J. Fluid Mech*., **119**, 249–267. 1
7. Nickel, B., and D. Wilkinson, 1983, *Invasion percolation on the Cayley tree – exact solution of a modified percolation model*, *Phys Rev Lett. 51*(2): 71–74. 1
8. Wilkinson, D., and J. Willemsen, 1983, Invasion percolation: a new form of percolation theory, *J. Phys. A: Math. Gen*. **16**: 3365–3376. 1
9. Flory, P. J., 1941, Molecular size distribution in three dimensional polymers, *J. Am. Chem. Soc*. **63**: 3083–3100. 1
10. Broadbent, S. R. and J. M. Hammersley, 1957, Percolation processes, 1. Crystals and mazes, *Proc. Cambridge Philos. Soc*. **53**: 629–641. 1
11. Gandolfi, A., G. Grimmett, and L. Russo, 1988, On the uniqueness of the infinite cluster in the percolation model, *Commun. Math. Phys*. **114**: 549–552. 2
12. Kesten, H., 1982, *Percolation Theory for Mathematicians*. Progress in Probability and Statistics, vol. 2, Birkhauser, Boston, MA, 423 pp. ISBN 3-7643-3107-0. 2, 32
13. Aizenman M., H. Kesten, and C. M. Newman, 1987, Uniqueness of the infinite cluster and continuity of connectivity functions for short and long-range percolation, *Commun. Math. Phys*. **111**(4): 505–531. 2
14. Pike, G. E., 1978, Conductivity of thick film (cermet) resistors as a function of metallic particle volume fraction, In: *Electrical Transport and Optical Properties of Inhomogeneous Materials*, Ed. J. C.Garland and D. B.Tanner, Vol. 40, AIP, New York, pp. 366–371. 3
15. Kogut, P. M. and J. Straley, 1979, Distribution-induced non-universality of the percolation conductivity exponents, *J. Phys. C. Solid State Phys*. **12**: 2151–2159. 3
16. Balberg, I., 1987, Recent developments in continuum percolation, *Philos. Mag. B* **30**: 991–1003. 3, 33
17. Gaillard-Groleas, G., M. Lagier, and D. Sornette, 1990, Critical behaviour in piezoelectric ceramics, *Phys. Rev. Lett*. **64**, 1577. 3
18. Sornette, D., M. Lagier, S. Roux, and A. Hansen, 1989, Critical piezoelectricity in percolation, *J. Phys. France*, **50**: 2201–2216. 3
19. Stauffer, D., 1979, Scaling theory of percolation clusters, *Phys. Rep*. **54**: 1–74. 3, 4, 12, 13, 15, 17, 26
20. Stauffer, D., and A. Aharony, 1994, *Introduction to Percolation Theory*, 2nd edition, Taylor and Francis, London. 3, 8
21. Berkowitz, B., and I. Balberg, 1993, Percolation theory and its application to groundwater hydrology, *Water Resour. Res*. **29**: 775–794. 3, 9
22. Sahimi, M., 1993, Fractal and superdiffusive transport and hydrodynamic dispersion in heterogeneous porous media, *Transp. Porous Media* **13**: 3–40. 3, 17
23. Sahimi, M., 1993, Flow phenomena in rocks − from continuum models to fractals, percolation, cellular automata, and simulated annealing, *Rev. Mod. Phys*. **65**(4): 1393–1534. 3, 17
24. Sahimi, M., and Y. C. Yortsos, 1990, Applications of fractal geometry to porous media: a review, Paper presented at the 1990 Annual Fall Meeting of the Society of Petroleum Engineers, New Orleans, LA. 3
25. Bunde, A., and S. Havlin, 1996, *Fractals and Disordered Systems*, Springer, Berlin. 3, 8, 9, 10, 19, 20, 21, 22,
26. Kunz, H., and B. Souillard, Essential singularity in percolation model, 1978, *Phys. Rev. Lett*. **40**: 133–135. 4
27. Skal, A. S., and B. I. Shklovskii, 1975, Topology of an infinite cluster in the theory of percolation and its relationship to the theory of hopping conduction, *Sov. Phys. Semicond*. **8**: 1029–1032. 4
28. Shklovskii, B. I., and A. L. Efros, 1984, *Electronic Properties of Doped Semiconductors*, Springer, Heidelberg. 4

29. Pollak, M., 1987, In. *Non-Crystalline Semiconductors*, CRC Press, Boca Raton, FL, Chapter 5ab. 4
30. Stauffer, D., 1985, *Introduction to Percolation Theory*, Taylor and Francis, London. 7, 10, 32
31. Stanley, H. E., 1971, *Introduction to Phase Transitions and Critical Phenomena*, Oxford University Press, New York. 9
32. De 'Bell, K., J. W. Essam, and A. J. Guttman, 1988, *On Two Dimensional Directed Percolation,* University of Melbourne, Dept. of Mathematics, Parkville. 9
33. Benfatto, G., and G. Gallavotti, 1995, *Renormalization Group*, Princeton University Press, Princeton, NJ. 9
34. Domb, C., and J. L. Lebowitz, 1988, *Phase Transitions and Critical Phenomena*, Academic, London. 9
35. Lesne, A., 1998, *Renormalization Methods*, J. Wiley, New York. 9
36. Sornette, D., 2004, *Critical Phenomena in Natural Sciences: Chaos, Fractals, Selforganization and Disorder: Concepts and Tools*, Springer, Heidelberg. 9
37. Essam, J. W., 1980, Percolation theory, *Rep. Prog. Phys*. **43**: 833–912. 10
38. Middlemiss, K. M., S. G. Whittington, and D. C. Gaunt, 1980, Monte-Carlo study of the percolation cluster for the square lattice problem, *J. Phys. A* **13:** 1835–1840. 11
39. Alexandrowizc, Z., 1980, Critically branched chains and percolation clusters, *Phys. Lett. A* **80**: 284–286. 11
40. Pike, R., and H. E. Stanley, 1981, Order propagation near the percolation threshold, *J. Phys. A* **14**: L169–L177. 11
41. Fisher, M. E., Theory of condensation and critial point, 1967, *Physics* **3:** 255. 12
42. Toulouse, G., Perspectives from theory of phase transitions, 1974, *Nuovo Cimento B* **23**: 234–240. 22, 26
43. Reynolds, P. J., W. Klein, and H. E. Stanley, 1977, A real-space renormalization group for site and bond percolation, *J. Phys. C* **10**: L167. 26
44. Miyazima, S., 2005, An exact percolation point for surface filing in a four-dimensional hypercubic lattice, *Prog Theor. Phys*. **113**: 1159–1163. 30
45. Vyssotsky, V. A., S. B. Gordon, H. L. Frisch, and J. M. Hammersley, 1961, Critical percolation probabilities (bond problem), *Phys. Rev*. **123**: 1566–1567. 31, 32
46. Essam, J. W., D. S. Gaunt, and A. J. Guttmann, 1978, Percolation theory at critical dimension, *J. Phys. A* **11**: 1983–1990. 32
47. Sykes, M. F., and M. K. Wilkinson, 1986, Derivation of series expansions for a study of percolation processes, *J. Phys. A* **19**: 3415–3424. 32
48. Adler, J., Y. Meir, A. B. Harris, and A. Aharony, 1989, *Bull Isr. Phys. Soc*. **35**: 102. 32
49. Ziff, R. M., and B. Sapoval, 1987, The efficient determination of the percolation threshold by a frontier-generating walk in a gradient*, J. Phys. A* **19**: L1169-L1172. 32
50. Strenski, P. N., R. M. Bradley, J. M. Debierre, 1991, Scaling behavior of percolation surfaces in three dimensions, *Phys. Rev. Lett*. **66**, 1330–1333. 32
51. Galam, S., and A. Mauger, 1997, A universal formula for percolation thresholds II. Extension to anisotropic and aperiodic lattices, *Phys. Rev E*. **56**: 322. 32
52. Scher, H., and R. Zallen, 1970, Critical density in percolation processes, *J. Chem. Phys*. **53**: 3759. 33
53. Shante, V. K. S., and S. Kirkpatrick, 1971, Introduction to percolation theory, *Adv. Phys*. **20**: 325. 33
54. Garboczi, E. J., K.A. Snyder, J. F. Douglas, and M. F. Thorpe, 1995, Geometrical percolation threshold of overlapping ellipsoids, *Phys. Rev. E* **52**, 819–828. 33

Chapter 2
Properties Relevant for Transport and Transport Applications

This chapter describes aspects of percolation theory that can be used in order to predict transport properties of disordered systems. Topics are selected in order to provide a basis for understanding subsequent applications to porous media and are thus not meant to be exhaustive. Still, there will at times be hints to subjects that may have relevance to problems not yet considered within the present framework.

2.1 Exponents Describing Backbone Structure

The structure of the backbone is important to such issues as distributions of arrival times of passive solutes (simply carried along by fluid flow). The resulting dispersion is an inevitable aspect of transport and is frequently of great practical interest. In the soil physics and hydrology literature it is customary to distinguish between "transport" properties (including conduction) and flow properties. In the physics literature all these properties fall under the category of transport.

A number of related properties of the infinite cluster have been investigated in the context of solute dispersion. The mass fractal dimensionality of the backbone cluster is denoted by D_b. This fractal dimensionality has the same fundamental definition as that of percolation clusters generally, but its value lacks the universality of the percolation cluster. In other words the backbone cluster topology can differ significantly depending on whether the percolation model is invasion or random, site or bond and whether the local site or bond probabilities are correlated with each other. The chemical path [1] is the shortest path length between two sites on a large cluster near percolation. Defining chemical path lengths that incorporate the tortuosity of the backbone cluster makes sense in the context of solute transport through porous media, when such solutes are carried passively through percolation structures. The tortuosity of the backbone cluster has been studied since the 1970s. One of the easiest ways to characterize this tortuosity is to give the length of the shortest path, Λ, along the backbone cluster as a function of p and p_c. Stauffer [2] gives this length as follows:

$$\Lambda \propto |p - p_c|^{-\eta} \tag{2.1}$$

Hunt, A., Ewing, R.: *Properties Relevant for Transport and Transport Applications.* Lect. Notes Phys. **771**, 37–55 (2009)
DOI 10.1007/978-3-540-89790-3_2

with $\eta = 1$ the value of the associated critical exponent (in three dimensions). In fact, the "value" of this exponent has been growing over the last 30 years [3, 4], but any value greater than 0.88 implies that the ratio of the (tortuous) path length to the size of the largest cluster is divergent at $p = p_c$, meaning that the path is infinitely tortuous. Thus the tortuosity, T, may be defined as the ratio Λ/χ, or,

$$T = \left(\frac{\Lambda}{\chi}\right) = |p - p_c|^{\nu-\eta} \tag{2.2}$$

The value of this exponent can be related to the fractal dimensionality, $D_{\min}$, of an optimal chemical path along the backbone by using the defining equation of fractal dimensionality from Mandelbrot [5]. For a path, which is constructed of steps of length ε, the dimensionality is fractal (and larger than 1) if the total length of the path, L, diverges in the limit that ε approaches zero. In particular, $D_{\min}$ is given by

$$L(\varepsilon) = \varepsilon^{1-D_{\min}} \tag{2.3}$$

We can use this expression to relate $D_{\min}$ to η. In percolation of course, as the percolation threshold is approached the correlation length, χ, diverges, whereas the individual step lengths (bond dimensions) are constant, but we can simply rescale the picture by reducing the lengths of the individual steps inversely proportionally to the correlation length. This process maintains the physical size of the cluster but increases the detail at which the cluster is drawn, corresponding to Mandelbrot's definition. Thus $\varepsilon \propto \chi^{-1}$ and

$$T \propto \left(|p - p_c|^{\nu}\right)^{1-D_{\min}} = |p - p_c|^{\nu-\nu D_{\min}} \tag{2.4}$$

which yields $\eta = \nu D_{\min}$.

The mass fractal dimensionality of the backbone cluster D_b [6] appears to be more appropriate in relating the *time of travel* along such a backbone to the linear extent of the cluster. Thus, the time of travel is not simply proportional to the length; it turns out to be even longer than what would be simply predicted by making it proportional to the tortuous length. Further, this time can depend strongly on the type of percolation problem considered.

The argument of Lee et al. [6] follows. For particles entering a backbone cluster at one side of a system, the typical velocity at distance x will scale as $1/n$, where n is the number of bonds at distance x. The number of bonds at distance x is proportional to x^{-1+D_b}. Thus the typical travel time

$$t \propto \int \frac{dx}{v} \propto dx x^{-1+D_b} = x^{D_b} \tag{2.5}$$

Lee et al. [6] do in fact find from simulations in two dimensions that the typical time, t, that a particle takes in traversing a Euclidean distance x scales as the 1.62 power of x, very close to the value of $D_b = 1.6432$ found by Grassberger [7] for the backbone cluster in two dimensions, but nowhere near the value 1.217 for optimal paths (see Table 2.2). Thus a kind of temporal tortuosity factor is given in the

Table 2.1 Fractal dimensionalities associated with chemical path lengths and the backbone percolation cluster in 3D (from Sheppard et al. [4])

Model	$D_{\min}$	D_{b}
Site NTIP	1.37	1.87
Site TIP	1.37	1.86
Bond TIP	1.46	1.46
RP	1.37	1.87
Optimal path	1.43	1.42

Table 2.2 Fractal dimensionalities associated with chemical path lengths and the backbone percolation cluster in 2D (from Sheppard et al. [4])

Model	$D_{\min}$	D_{b}
NTIP	1.1293	1.6422
Site TIP	1.214	1.217
Bond TIP	1.217	1.217
RP	1.1307	1.6432
Optimal paths	1.21	1.21

same form as Eq. (1.59) but with D_{b} substituted for $D_{\min}$. Such a result will have considerable importance for the discussion in Chap. 10.

Sheppard et al. [4] give values for the mass fractal dimensionality of the sample-spanning cluster and the backbone, D_{b}, as well as the fractal dimensionality of the optimal path, $D_{\min}$, in various percolation models. Presenting the basic information from their summary (Tables 2.1 and 2.2) requires defining their acronyms: IP = invasion percolation, TIP = trapping invasion percolation, NTIP = nontrapping invasion percolation, RP = random percolation (the focus here). The difference between trapping invasion percolation and nontrapping invasion percolation is that in the former case the "defending" fluid (defending against the "invading" fluid) is incompressible, meaning that it can be trapped (in finite clusters). In the latter case, the defending fluid can always escape, even if it does not percolate, since it can be compressed to zero volume.

In the present case for our dispersion calculations (Chap. 10) we have used several values of the exponent D_{b}. These values for the fractal dimensionality each lead to distinct values for the exponent η.

2.2 Exponents for Conduction Properties

Consider the site percolation problem introduced in Sect. 1.2 and stipulate for simplicity that all the metallic balls are of the same size and composition. Allow them to be placed on a simple cubic lattice. We have not calculated p_{c} for this lattice

but numerical simulations give the result $p_c = 0.3116$. Thus, in an infinite lattice, if fewer than 31.16% of the balls emplaced are conducting and the remainder are insulators, the system will not conduct at all. If $p > p_c$, the system will conduct. Clearly the conductivity of the system must follow a functional form, which vanishes (rather than diverge) at $p = p_c = 0.3116$. The result of percolation theory is that the functional form must be a power law (and the arguments given here justify that), so that what we need to be able to do is predict the exponent.

The most important aspects of this problem treated by percolation theory are probably the connectivity and the tortuosity of the conducting paths; certainly these concepts have been independently (but inconsistently) developed in the porous media communities. Discussions of this topic have occupied a great deal of literature but, as will be seen, the original discussion of Skal and Shklovskii [8] is the simplest introduction, although it does not lead to the most widely accepted result. The following is consistent with the general results of that work.

The electrical conductivity of a system is defined as the ratio of the current per unit area and the applied electrical field. If this ratio is independent of the field (as is normally the case at small field strengths), the system obeys Ohm's law. The current per unit area in the present case involves the current per path and the number of connected paths per unit area. The simplest assumption is that the current for each connected path is identical. Then the number of connected paths per unit cross-sectional area (in three dimensions) is proportional to

$$\chi^{-2} \propto (p - p_c)^{2\nu} \tag{2.6}$$

Since in three dimensions, $\nu = 0.88$, the lowest order estimate of the conductivity is that it should vanish as the $2\nu = 1.76$ power of the difference, $p - p_c$. This suggestion is actually fairly close to observation. But, as we know, the structure of large clusters near the percolation threshold, and by extension also the infinite cluster just above the percolation threshold, is fractal for distances below the correlation length (which of course diverges right at percolation). This fractality produces a tortuosity in the current-carrying path as well. The distance along a connected path, Λ, over a separation equal to the correlation length is actually longer than the correlation length. Λ diverges at the percolation threshold according to [2]

$$\Lambda \propto (p - p_c)^{-\nu D_{\min}} \tag{2.7}$$

Thus, assuming that the resistance of the current-carrying path is just the sum of the resistances of all the metal balls encountered, this resistance per unit system length must actually increase as the percolation threshold is approached, and the increase must be given by the ratio of Λ to χ. This ratio is proportional to $(p - p_c)^{\nu - \nu D_{\min}} = (p - p_c)^{-0.33}$. Here we have used the value for $D_{\min}$ for random percolation given in Table 2.1. Such an increase in resistance produces an alteration of the results for the conductivity to

$$\sigma \propto (p - p_c)^{2\nu + (D_{\min}\nu - \nu)} = (p - p_c)^{2.09} \equiv (p - p_c)^{\mu} \tag{2.8}$$

Here the first contribution to the exponent is essentially a result of the connectivity, or separation of the paths along which current can flow, while the second contribution is due to the tortuosity of these paths. The combined exponent is thus the sum of two contributions, $1.76 + 0.33 = 2.09 = \mu$. At the time of the original estimate by Skal and Shklovskii [8], it was thought that $\eta = 1$, which leads to $\mu = 1.88$. Nowadays, μ is known at least as accurately as are the constituents that distinguish μ from 2ν, and more modern publications [9, 10] give $\mu = 2$. As pointed out already by Berkowitz and Balberg [11] the explanation for the discrepancy $\mu = 2$ instead of $\mu = 2.09$ is quite simple. The discussion up until now has omitted the effects on μ of the "blobs," or finite-length parallel paths. But the fact that such blobs become increasingly complex and more numerous in the limit of $p \to p_c$ leads to a reduction in the resistance of the backbone cluster, meaning that μ is reduced from 2.09. The presentation of this argument is meant more to provide extra qualitative understanding than to imply a quantitative inference on the effects of these "blobs" on conductivity.

In two dimensions the Skal and Shklovskii [8] argument would start with $\mu \approx \nu$ rather than 2ν since the relevant current density is defined relative to a perpendicular length (χ) rather than a cross-sectional area (χ^2). Then complications due to a tortuosity would be added. But the exponent μ appears to be smaller in magnitude than ν, making the argument of Skal and Shklovskii [8] more difficult to apply. As Berkowitz and Balberg [11] explain, the structure of the backbone cluster in 2D is different enough to make blobs a more important modification to μ than the tortuosity. As a first approximation to μ one can simply use the exponent for the correlation length, $\nu = 1.33$. Derrida and Vannimenus [12] find that the value of μ in two dimensions is 1.28 and Jerauld et al. [13] find $\mu = 1.27$, while Normand and Herrmann [14] find $\mu = 1.30$. Note that all of these values for μ in two dimensions are not greatly different from the 2D value for ν. Establishing values for μ will have relevance to discussions of Archie's law for the electrical conductivity of porous media. This is why it is important to find the best values for these exponents as well as to determine the conditions under which one expects to observe them. The value for μ in two dimensions (three dimensions) will be assumed here to be 1.3 (2).

In one dimension, the conductivity is either zero (if there are any nonconducting elements at all) or a finite value, implying $\mu = 0$. But μ is, in general, nonuniversal for 1D systems, meaning that, in principle any value of μ can be generated. If there is a variation in the conduction properties of the individual elements (not all resistance values identical), the result $p_c = 1$ implies that the total resistance may be dominated by the resistance of the most resistive element in 1D systems. In that case the conductivity is calculated using extreme value statistics. The choice of the extreme value statistics is determined by the statistics of the individual resistances, making 1D systems highly nonuniversal.

Note that although the concept of conductivity and the discussion of the value of μ were introduced using the example of electrical conduction, the arguments are perfectly general, and the results could be applied to, e.g., the hydraulic conductivity or to air flow as well. What will turn out to differ among these properties is the conditions under which arguments to invoke Eq. (2.8) actually apply.

Berkowitz and Balberg [15] in fact explicitly demonstrated that models of hydraulic conduction yield Eq. (2.8) for the hydraulic conductivity near the percolation threshold, and found values of the exponents compatible with $\mu = 2$ in 3D and $\mu = 1.3$ in 2D, respectively, although they also found results compatible with nonuniversal exponents [16, 17] in certain 3D systems.

One can also use the Einstein relationship [18, 19] between diffusion, D, and conductivity, σ,

$$\sigma = nD \tag{2.9}$$

where n is the number of charge carriers, which is normally assumed to be given by the fraction of sites connected to the infinite cluster, to find

$$D \propto (p - p_c)^{\mu-\beta} \tag{2.10}$$

Interestingly enough, as we will find, although other relationships given here are verified, Eq. (2.10) may give inaccurate predictions for solute and gas diffusion in porous media. In fact these two properties are not identical and, although these results may not yet be completely understood, the main discrepancy appears to be due to the ability of solutes to diffuse over thin water films present in otherwise dry pores, while there is ordinarily no equivalent possibility for gases to diffuse through water. It is curious that a simple effective-medium theoretical result [20] yields $D \propto (p - p_c)^1$, which is exactly what is observed [21], although it is almost certain that it would be for the wrong reasons. On account of this coincidence, however, and because of the rather close correspondence between effective-medium and percolation theories, the essence of this derivation is repeated here.

The lowest order effective medium approximation for the mean diffusivity, D_m, can be obtained via physical arguments [22, 23] or via lattice Green functions [24] as [20]

$$\int_0^\infty \frac{D_m - D}{[(Z/2) - 1]D_m + D} f(D)\, dD = 0 \tag{2.11}$$

Keffer et al. [20] use as a distribution of diffusivities (to describe ultimately the diffusion in zeolites)

$$f(D) = p\delta(D - D_b) + (1 - p)\,\delta(D - D_0) \tag{2.12}$$

where D_b is a very small value and D_0 is relatively large, and for which these authors define $f \equiv D_b/D_0$. Note that, in an unusual choice, these authors chose to use the symbol p for the low diffusion elements! The solution of Eq. (2.11) using Eq. (2.12) for $f(D)$ is

$$\frac{D_m}{D_0} = \frac{1}{2}\left\{A + \left[A^2 + \frac{4f}{(Z/2) - 1}\right]^{\frac{1}{2}}\right\} \tag{2.13}$$

and

$$A = 1 - p + fp - \frac{f + p - fp}{(Z/2) - 1} \tag{2.14}$$

For $f = 0$ Eq. (2.14) yields

$$\frac{D_m}{D_0} = \frac{[(Z/2)-1]-(Z/2)\,p}{[(Z/2)-1]} = \frac{(1-p)-(2/Z)}{1-(2/Z)} \tag{2.15}$$

which would seem to yield $p_c = 1-2/Z$ and a critical exponent of 1. But given that these authors exchanged the roles of p and $1-p$, the actual result obtained for p_c is $Zp_c = 2$, which would be in agreement with the results of percolation theory except that the constant, 2, is more appropriate for 2D, rather than the 3D configurations considered. Note also the conclusion that the critical exponent 1 is unaffected by the transposition of p and $1-p$.

2.3 Summary of Derived Values of Critical Exponents

While most of the entries in Table 2.3 refer to quantities discussed in Chap. 1, it is not presented there because of its inclusion of the conductivity exponent, μ.

Table 2.3

Exponent	$D = 1$	$d = 2$	$d = 3$	$d \geq 6$
α	**1**	$-2/3$	-0.62	-1
β	**0**	5/36	0.41	**1**
γ	**1**	43/18	1.82	**1**
σ	**1**	$36/91 = 0.396$ **(0.369)**	0.45	**1/2**
τ	**2**	187/91	2.18	**5/2**
ν	**1**	4/3 **(1.355)**	0.88	1/2
μ	Not universal	1.3 **(1.355)**	2.0 (**1.88**)	3

This table was constructed synthesizing the tabulated values for these exponents from Sahimi [18, 19] and Stauffer [2], but using $\mu = 2.0$ in three dimensions [9, 10] and $\mu = 1.3$ in two dimensions [14]. Known values, for which the derivations were described here, are underlined and in bold; if the values obtained here are different from the known values, they are given in parentheses.

2.4 Finite-Size Scaling and Fractal Characteristics

Numerical simulations are a common means to generate values of p_c *as well as of critical exponents in percolation theory. But simulations can be performed* only for finite-sized systems. While it is possible to try to extract limiting behavior in the infinite system limit as a means to generate such quantities, a better approach is to generate dependences of, e.g., the conductivity on the system size and use a known transformation to yield the associated dependences on percolation variables. This technique is used often for treating transport problems. For example, quantities like the conductivity, which vanish at the percolation threshold, will diminish with increasing system size until the linear dimension of the system exceeds the correlation

length. At larger length scales the system is known to be Euclidean, meaning that the property in question becomes independent of system size. The exception of course is right at the percolation threshold, for which the correlation length is infinite and the scale dependence continues to infinite system size.

Originally it was Fisher [25] who showed how to relate percolation quantities for finite-sized systems to their behavior as a function of $p - p_c$ in the limit of infinite-sized systems. In particular for a system of finite size L, a percolation quantity, ψ, which obeys an arbitrary power law, $(p - p_c)^{q_0}$, will behave as follows:

$$\psi \propto L^{-\frac{q_0}{\nu}} h\left[\left(\frac{L}{\chi}\right)^{\frac{1}{\nu}}\right] = L^{-\frac{q_0}{\nu}} h\left[L^{\frac{1}{\nu}}(p - p_c)\right] \tag{2.16}$$

with h an unknown nonsingular function. Substitute $L = \chi$ into Eq. (2.16) to obtain

$$\psi \propto (p - p_c)^{-\nu\frac{-q_0}{\nu}} h[1] = (p - p_c)^{q_0} \tag{2.17}$$

Note the similarity of Eq. (2.16) with Eq. (1.8) for the cluster statistics. In particular, the ratio of L to the correlation length enters here because of the fact that systems near the percolation threshold obey fractal geometry (with, e.g., fractal cluster dimensions) only for length scales smaller than the correlation length, χ. For length scales larger than χ the system follows Euclidean geometry. For example, if a system with $p > p_c$ is smaller than the correlation length, the above finite-size scaling results hold and such transport quantities as a diffusion constant or the conductivity will trend to zero with increasing system size up to a length scale equal to the correlation length. But at larger system sizes, the transport coefficient will not change for any further increase in system size. Only precisely at p_c will the behavior of the transport coefficient continue to diminish indefinitely with increasing system size. But on the way to $p = p_c$, the transport coefficient has taken on values at each size, which were equal to the transport coefficient at that value of the correlation length. Therefore the first factor in Eq. (2.16) gives the behavior of the variable ψ for the condition $L = \chi$, since the second factor does not change with L for L constrained to equal χ. Thus any such exponent obtained from finite-size simulations (and presented as a function of system size, L) must be multiplied by $-\nu$ to find the value predicted by percolation theory. The similarity of Eq. (2.16) with Eq. (1.8) is a consequence of the relevance to percolation scaling of homogeneous functions, a topic not further considered here, but treated in some detail in the standard references mentioned earlier in the chapter.

2.5 Critical Path Analysis

Although an entire chapter is devoted to critical path analysis (CPA), its introduction here serves to familiarize the reader with its basic concepts. This introduction addresses more general issues, such as effects of the dimensionality of the system,

the connectivity of the medium, and the width of a distribution of local conductances, while Chap. 3 treats detailed applications of CPA to systems of experimental relevance.

CPA uses percolation theory to calculate effective conduction properties of a disordered medium. CPA was developed [26–28] to find the limiting resistance value in a random medium with a wide range of local resistances. The initial work was meant to address the electrical conduction problems of impurity conduction systems in crystalline semiconductors as well as amorphous semiconductors, and so topological disorder was included. The present introduction, however, concentrates on lattice models. Because the connectivity of the more highly conductive regions is a critical input into the calculation of effective properties, the fundamental theory of connectivity is an obvious tool to be employed for such a calculation. Then it is not necessary to add connectivity as an afterthought, or to develop alternative methods to quantify connectivity, such as the Euler number [29]. While the latter has an advantage in that it can be used to identify a percolation transition [29], i.e., when the Euler number changes sign the system crosses p_c, its disadvantage is that there is no known relationship between the Euler number and p. Thus there is no way to express $(p - p_c)$ in terms of Euler numbers, making it impossible to use the Euler number to predict any properties given in percolation theory. Two additional advantages of CPA are that it can be applied to any conductance (or conductivity) distribution and that it yields results, which are most accurate (exact) in the limit of large disorder rather than in the limit of a homogeneous system (although in many cases CPA can be formulated to be exact in both limits).

The gist of CPA is that it defines that interconnected network of conductances which has the largest possible value of the smallest, or bottleneck, conductance. This value is called the critical conductance and is found by setting an integral over the conductance distribution equal to the critical percolation probability, p_c. The lower limit of this integral is the critical conductance, and the upper limit is the largest conductance. The analysis can be formulated equivalently in terms of a resistance distribution, for which p_c fixes the upper limit of integration while the lower limit is the smallest resistance in the distribution. In CPA p_c is thus the most important parameter, rather than the critical exponents. The critical percolation probability can vary significantly from system to system. Thus there might be important differences in applying CPA in different systems. Important differences do exist in applying CPA in different dimensions.

2.5.1 Relation of CPA to Extreme Value Statistics in 1D Systems

Consider first the case of 1D systems. In infinite 1D systems the conductivity can always be calculated exactly using what is often called the harmonic mean value of the conductance distribution. This value is related simply to the inverse of the sum of the resistance values since the effective resistance of resistances in series is their sum. For uniform size characteristics (all bonds the same length, for example) the

resistance distribution is a perfect proxy for the resistivity distribution as the resistance of any bond is a given constant times its resistivity. For a wide distribution of resistance values, the harmonic mean is dominated by the largest resistance in the system. For a truncated power-law distribution of resistances, $W(R)$ (or equivalently conductances), the harmonic mean conductivity is in fact proportional to the largest resistance value, at least as long as $RW(R)$ is a power of R that is greater than -1. This is simply a property of power-law distributions and may easily be verified by integration (Problem 2.4). Since $p_c = 1$ in one dimension, CPA requires that the lower limit of integration on the conductance distribution be the smallest conductance in the system (or the largest resistance). In other words it is not possible to connect an infinite path which avoids even the smallest conductance. A single missing element will break the path. Thus CPA quickly reaffirms the relevance of the largest resistance to the system conductivity. For a power-law resistance distribution that extends to infinite resistance the conductivity is zero. In general the conductivity in 1D is given by $\sigma = l/R$, with l the system length and R its total resistance.

In finite-length 1D systems, the problem is more interesting. Again, since in 1D $p_c = 1$, the critical conductance g_c is now the smallest actual conductance in the system, rather than the smallest allowed by the distribution. Since it is impossible to avoid even the largest resistance on the path, but this largest resistance can vary from realization to realization, extreme value statistics are implicated in the procedure to find both an ensemble mean conductivity of the system and a distribution of conductivity values as a function of the system length. To find an ensemble mean conductivity it is necessary first to find the dependence on x of the largest expected resistance value, $R_{\max}(x)$ in a system of length x. If $R_{\max}(x)$ is a power of x, then evaluation of the limit of $x/R_{\max}(x)$ for x approaching infinity gives the scaling of the conductivity as a function of length, x. In such cases, the limiting value of $x/R_{\max}(x)$ as x approaches infinity will typically be zero so that an infinite system does not conduct at all. This is the case in the spatially random hopping conduction system considered below. Whenever the system has a nonzero minimum conductance value, however, the typical resistance of a system of length x is proportional to x and the system conductivity is nonzero and well-defined.

The following specific system, r-percolation, is discussed in considerably more detail in Sect. 4.1. Here we only give the briefest summary sufficient to actually perform the calculations. Consider a 1D system with resistances connecting every pair of sites, i and $i+1$, where i denotes the position of a site on a linear chain. Let the separation of the sites $r_{i,i+1}$ be a random variable with uniform probability density, $1/b$, where b is the typical separation of sites. Let the resistance $R_{i,i+1} = R_0 \exp[2r_{i,i+1}/a]$, where $a << b$ and R_0 are constants with units length and resistance, respectively. While the probability of finding an arbitrary site a distance r (within dr) from site i is dr/b, the probability that that site is the nearest neighbor is $(dr/b)\exp(-r/b)$. This probability is normalized over the interval $[0,\infty]$; the nearest neighbor must be somewhere. Now what is the largest likely value of the nearest neighbor distance in a chain of length x? First, the expected number of sites on such a chain is x/b. Thus the number of possible realizations of the nearest neighbor distance is proportional to x/b. This means that the total area under the curve

$\exp(-r/b)/b$ would typically be divided into x/b roughly equal areas, meaning that the largest expected resistance value, $R_{\max} = R_0 \exp[2r_{\max}/a]$, would be found by setting the area under the extreme value distribution between $r_{\max}$ and infinity proportional to b/x,

$$\frac{b}{x} \propto \int_{r_{\max}}^{\infty} \frac{dr}{b} \exp\left[\frac{-r}{b}\right] \tag{2.18}$$

Solution of this integration for $r_{\max}$ in terms of x leads to

$$r_{\max} \propto b \ln\left(\frac{x}{b}\right) \tag{2.19}$$

Substitution into $R_{\max} = R_0 \exp[2r_{\max}/a]$ leads to

$$R_{\max} \propto R_0 \left[\frac{x}{b}\right]^{\frac{2b}{a}} \tag{2.20}$$

with the result that

$$\sigma(x) \propto x^{1-\frac{2b}{a}} \tag{2.21}$$

Equation (2.21), since $b >> a$, leads to a conductivity [30, 31] which is a negative power of the system length and which vanishes in the limit of an infinite chain. In condensed matter applications, where individual resistance values are typically exponential functions of random variables, the only easy way to generate a power-law behavior of the conductivity with system size is to invoke extreme value statistics. The only systems, in which mean-value statistics appear to be relevant, are 1D systems, because of the fact that $p_c = 1$. Thus 1D systems make a very poor starting point for understanding percolation behavior generally. We will find out in the next chapter that, for other reasons, 2D systems make very poor models of 3D porous media.

2.5.2 CPA in Two Dimensions

Next we apply CPA to an idealized conductance distribution on a 2D lattice. An attractive point about 2D systems is the direct relationship there between critical conductance and system conductivity. Consider the elementary relationship between the resistance R and the resistivity ρ for a homogeneous system of length l and cross-sectional area A, in particular $R = \rho l/A$. In two dimensions the analogous relationship is $R = \rho l/z$, where z is the system dimension perpendicular to flow. The particular case of two dimensions, where the sample-dependent property R is equal to the ratio of two lengths times the material property, ρ, is interpreted [32] for the case of disordered systems to imply the equivalence of ρ and R, and thus between the conductance, g, and the conductivity, σ, as well. This makes the system conductivity equal to the critical conductance.

For the bond percolation problem we need the probability density function (pdf) for finding a conductance between two arbitrary nearest neighbor sites with value between g and $g + dg$, called $W(g)$. Normalization of this pdf requires

$$\int_0^\infty W(g)\, dg = 1 \tag{2.22}$$

Consider the case that $W(g)$ is a log uniform distribution of (electrical or hydraulic) resistance values with width 10 orders of magnitude, e.g., from 10^0 to 10^{10} in arbitrary units. Place each conductance at random between two arbitrary nearest neighbor sites on a square lattice. Each site has four nearest neighbors, $z = 4$, and $p_c = 0.5$. The conductivity of this arrangement is the median conductance value $g = 10^5$ because it is known that emplacement of a fraction 0.5 of the bonds of this lattice guarantees that the system is at the percolation threshold. The median conductance on this lattice is then the smallest conductance value that cannot be avoided by the current, a value which is more generally known as the critical conductance, g_c. g_c is found from

$$\int_{g_c}^\infty W(g)\, dg = p_c = 0.5 \tag{2.23}$$

For an infinite square lattice, placement of half the conductances into lattice positions at random guarantees existence of a cluster of interconnected conductances, which just reaches infinite size; choosing that half of the conductance distribution with the largest conductances yields the path of least resistance. If, in a corresponding physical system all bonds have not only the same length, but also the same cross-sectional area, the median conductance value would correspond rigorously to the median conductivity in a distribution of conductivities. Such a picture applies also to media in which the currents are represented numerically in terms of finite difference equations, as long as the medium is divided up into subregions of identical squares. Since the effective conductivity of the medium is known in porous media communities as the upscaled conductivity, then under fairly common conditions we can identify the median of a conductivity distribution with the upscaled conductivity in two dimensions. If the logarithm of K is symmetrically distributed, then the median of the conductivity is also the geometric mean. But the same results do not apply for all 2D systems.

If the same conductances are placed on a triangular lattice, where each point has six nearest neighbors ($Z = 6$), the dominant conductance value from the distribution is $10^{6.55}$ because p_c is 0.345 and the current avoids the slowest two-thirds of the connections. If the same conductances are placed on a honeycomb lattice, with $z = 3$, the dominant conductance is $g_c = 10^{3.45}$ because $p_c = 0.655$ and the current avoids only the slowest one-third of the connections. The corresponding values of the rate-limiting conductances and associated conductivities extend over more than three orders of magnitude in the simplest 2D lattices! In Fig. 2.1 we represent these results pictorially and include as well the range

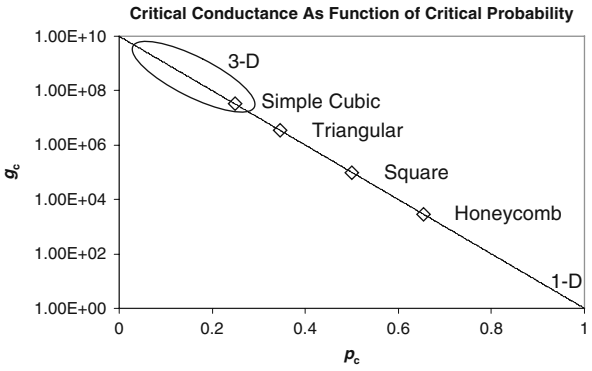

Fig. 2.1 For a log-uniform distribution of conductances the critical (percolating) rate-limiting conductance, g_c, as a function of the critical percolation probability, p_c. Note the rapid diminution of p_c and increase of g_c with increasing dimensionality. Further, if the geometric mean of the distribution is held constant, but the width is increased, all systems to the left of the square lattice will have an increase in K, while all those to the right will experience a decrease

of likely values for g_c in 3D lattices ($p_c \leq 0.2488$) as well as on a 1D chain (where $p_c = 1$). In 3D the relationship between g_c and system conductivity is more complex, and only in 2D systems can g_c in Fig. 2.1 be interpreted also as the conductivity.

2.5.3 CPA in 3D

In 3D we need to be able to write expressions for the conductivity as well. If only enough resistors are placed on the lattice to guarantee the existence of an infinite cluster ($p = p_c$), then there will be only a single connected path in, say, the x direction over a distance χ in both the y and the z directions. But χ diverges right at the percolation threshold. While this path has the largest rate-limiting conductance value possible for a given network topology and conductance distribution, construction of such a critical path does not optimize the conductivity since the conductivity due to a single conducting path in an infinite cross-sectional area (or perpendicular distance in two dimensions) is zero. However, emplacement of a few smaller conductances into their positions in the network reduces χ rapidly while scarcely diminishing the rate-limiting conductance, allowing the possibility of a general optimization procedure. Such an optimization procedure for a 3D lattice, $d = 3$, is given below. The optimization procedure results in the determination of an optimal value of the conductance, g_{opt}, which is useful as long as g_{opt} is close enough to g_c so that the topology of the conducting paths is described by percolation theory. Nevertheless, the tendency for p_c to be much smaller in 3D than in 2D tends to make the conductivity of 3D systems much higher than in 2D, and we discuss first general tendencies for the conductivity in terms of the dimension of the medium.

2.5.4 Dimensional Dependence and Similarity to Matheron Conjecture

In Fig. 2.1 the dimensional dependence of g_c for the proposed log-uniform distribution of conductance values is clear and strong. In 2D square lattices the critical conductance, 10^5, yields the conductivity and is the geometric mean of the distribution $[(10^0)(10^{10})]^{1/2}$. For 1D systems g_c is the smallest g in the system, while in 3D systems, it is near the large end of the distribution. This dimensional dependence is reminiscent of that in a classical conjecture of Matheron [33]. The relevance of the geometric mean of a conductivity distribution to the 2D upscaled conductivity is not restricted to a log-uniform distribution, but is repeated for log-normal distributions and power law distributions as well, making it possible to compare the result from CPA to a completely different formulation for upscaling K in heterogeneous media. Assume that the logarithm of the hydraulic conductivity is normally distributed,

$$W(K) \propto \exp\left\{-\left[\frac{(\ln(K)-\ln(K_0))^2}{2Var(\ln(K))}\right]\right\} \tag{2.24}$$

where $Var[\ln(K)]$ is the variance of the distribution of $\ln[K]$. Then the lowest order approximation to the hydraulic (or electrical) conductivity is [34]

$$K = K_{gm}\exp\left[\left(\frac{1}{2}-\frac{1}{d}\right)Var(\ln(K))\right] = K_0\exp\left[\left(\frac{1}{2}-\frac{1}{d}\right)Var(\ln(K))\right] \tag{2.25}$$

where K_{gm}, the geometric mean of K, is here equal to K_0, the most likely value of K. In fact, De Wit [34] explains that Eq. (2.25) is essentially a perturbation expansion in the (small parameter) $Var(\ln(K))$. Equation (2.25) also implies that the upscaled conductivity in 2D is equal to the geometric mean or to the median value. Further, the hydraulic conductivity increases with increasing variance in 3D and diminishes with increasing variance in 1D, just as in Fig. 2.1. Since all methods generate the hydraulic conductivity in 1D systems using the inverse of the sum of the resistance values, the two results coincide in 1D as well as in 2D, at least under some circumstances. But in 3D there are some fundamental differences.

In 3D Eq. (2.25) suggests that the conductivity is independent of the properties of the connectivity of the medium as long as $\ln(K)$ is a normally distributed random field. It is known, however, that the connectivity of such fields plays an important role in the upscaling [35–38]. As can be seen from CPA, the tendency for K to increase with diminishing p_c is not restricted to the effects of increasing dimensionality, but includes effects of larger coordination number, Z, as well. Thus increasing the local connectivity reduces p_c and increases K. Further, Eq. (2.25) implies that the conductivity can be represented in terms of the mean value and some parameter describing the variation about the mean. However, it should be apparent from critical path arguments that the important conductance may be far in the tail of the distribution. As mentioned, Eq. (2.25) is not complete: it is believed that

in fact Eq. (2.25) represents only the first term in a series [34] of terms proportional to powers of the variance of $\ln(K)$. Thus the validity of Eq. (2.25) is subject to an important condition on the magnitude of $Var(\ln(K))$, which must be small. Similarly, even using all the terms in the series is insufficient if the series does not converge, which will be the case for large $Var(\ln(K))$.

2.5.5 *Optimization of the Percolation Network: Contrast Between 2D and 3D*

The idea of CPA is actually not best expressed as an upscaling of the conductivity. In particular, in CPA, one seeks an optimization of an expression for the conductivity, which is based on selection of paths with very small values of the maximum resistance and the separation of those paths. Thus we find the dominant conducting paths, the current (or flow) on those paths, and how many such paths per unit area intersect a plane perpendicular to the flow. We cannot restrict our attention precisely to the paths with the smallest possible values of the maximum resistance, since these paths would be precisely at the percolation threshold and then have infinite separation (leading to a zero conductivity). Incorporating some larger resistances reduces the conductances of these paths, but increases their areal density rapidly from zero. The typical separation of these paths is given in terms of the correlation length, χ. The areal density of the relevant paths is thus χ^{-2}. We will then invert an elementary relationship for the resistance of a homogeneous wire $R = \rho l/A$, with $\rho \equiv \sigma^{-1}$ the resistivity, l the length and A the cross-sectional area, to obtain the conductivity from R, l, and A, i.e., $\sigma = l/RA$. A will thus be the square of the correlation length, and l will be the typical separation of maximal resistances on the path. In that expression for the conductivity, however, all the functions must be written in terms of the maximally valued resistance (or minimum conductance) in order to perform an optimization.

The correlation length is defined in terms of $(p - p_c)$; thus we must have a general expression for $(p - p_c)$, which is written in terms of the resistance distribution itself, in order to apply the optimization procedure.

Define

$$F(R) \equiv \int_0^R W\left(R'\right) dR' = p \tag{2.26}$$

Then

$$F(R_c) = \int_0^{R_c} W\left(R'\right) dR' = p_c \tag{2.27}$$

Equations (2.26) and (2.27) can be solved in parallel for $p - p_c$. Define a conductance $g \equiv R^{-1}$ and define l to be the typical separation of the rate-limiting resistances, R. It is then possible to write a relatively simple expression for the

conductivity of a 3D network, on which a fraction, p, of bonds with the smallest R values possible, is placed at random,

$$\sigma = \frac{l\left[F\left(g^{-1}\right) - F\left(g_c^{-1}\right)\right]^{2\nu}}{\chi_0^2} g \tag{2.28}$$

In Eq. (2.28) $\chi_0^2[F(g^{-1}) - F(g_c^{-1})]^{-2\nu}$ is the square of the correlation length as a function of the smallest conductance included, g. l is actually the separation of rate-limiting resistances on the dominant, current-carrying path and, as such, would seem to involve only the statistics of the resistance values. If the resistance distribution is discretized in steps of the fundamental constant $e = 2.718$, then one could write for l,

$$l \approx \chi_0 \left\{ \frac{\int_0^R W(R)\, dR}{\int_{-R/e^{1/2}}^{e^{1/2}R} W(R)\, dR} \right\}^{-\frac{1}{3}} \tag{2.29}$$

in three dimensions. Equation (2.29) has a very simple basis actually. Note that the ratio on the right-hand side is just the inverse of the fraction, f, of emplaced resistances which is in the largest discretization class, so that $l^3 f \approx 1$. In this formulation, the distribution of resistances on the percolating cluster is the same as in the medium generally, so that the volume concentration of the largest resistances is easy to obtain from the appropriate bulk distribution, $W(R)$. Note that l in Eq. (2.28) is thus only a very slowly varying function of p, and not a function of $p - p_c$ at all. For this reason optimization of Eq. (2.28) is not complicated by consideration of l. Result Eq. (2.28), however, is not generally agreed on. Several authors identify l with the correlation length $\chi = \chi_0[F(g^{-1}) - F(g_c^{-1})]^{-\nu}$, by arguing that the separation of rate-limiting resistances is topologically constrained, rather than a function of the frequency of occurrence of such resistances. The physical basis for this argument is that, in the vicinity of p_c at least, most of the largest resistances are shorted by alternate paths with smaller dominant resistance values, but that, for self-consistency l cannot be larger than χ, otherwise the value of p would have to be changed. This important problem is still not completely settled, with several different perspectives taken in the literature.

If in Eq. (1.83) R is an exponential function of a random variable, such as a site separation ($R \propto \exp(2r/a)$ with a a constant length), then $F(R) - F(R_c) \propto \ln(R/R_c) = \ln(g_c/g)$, but if R is a power of, e.g., a tube radius (for hydraulic conduction), then $F(R) - F(R_c) \propto (R - R_c)$ or $g - g_c$ (see the assigned problems). Using Eq. (2.29) for l and optimizing Eq. (2.28) leads to, in the first case,

$$\frac{d\sigma}{dg} = \frac{d}{dg}\left[\frac{l\left[F\left(g^{-1}\right) - F\left(g_c^{-1}\right)\right]^{2\nu}}{\chi_0^2} g\right] = \left[\ln\left(\frac{g_c}{g}\right)\right]^{2\nu} - 2\nu\left[\ln\left(\frac{g_c}{g}\right)\right]^{2\nu-1} = 0 \tag{2.30}$$

Solution of Eq. (2.30) leads immediately to $\ln(g_c/g) = 2\nu$, or $g = g_c \exp(-2\nu)$. Thus the controlling conductance, g, is closely related to the critical value, g_c, and this value of g can also be substituted into $\chi = \chi_0[F(g^{-1}) - F(g_c^{-1})]^{-\nu})$ to generate an expression for σ in Eq. (2.28). Note that choice above of $l \propto \chi$ would yield $g = g_c \exp(-\nu)$, because the exponent 2ν would be replaced by ν. In two dimensions, the factor χ^2 in the denominator is replaced by χ. If l is taken to be proportional to χ, the 2D case becomes special because l/χ has no dependence on the percolation variables, with the conductivity a universal numerical factor (of order unity) times the critical value of the conductance, g_c. This result does appear to be verified [32], and our own simulations agree [39]. Specific results from CPA will be discussed in Chap. 4 and elsewhere.

Note, however, that in many cases it may be possible to apply CPA without using the above optimization if it is desired only to find the ratio of the critical resistance value at two different values of a changing external parameter such as the moisture content, and under the assumption that far from the percolation threshold the topological aspects affecting the optimization will change only slowly with such external parameters. Such cases will also be considered in the chapters on applications.

In hydrogeology one of the most important problems is to be able to predict the effective (hydraulic) conductivity, K_{eff}, of a medium from information regarding the variability of K within the medium. This problem is known as "upscaling the hydraulic conductivity." It is often stated that K_{eff} is bounded by its harmonic and arithmetic mean values. The harmonic mean of a collection of resistance values is the value obtained by configuring them all in series. The arithmetic mean of a collection of resistors is the equivalent resistance value when they are all configured in parallel. Geologists often assert that physicists do not comprehend the complexity of geologic material, which is true, but such an upscaling scheme was obviously developed from the geologic perspective of a subsurface stratified in horizontal geologic units, where horizontal conduction is governed by the arithmetic mean and vertical conduction by the harmonic mean.

Upscaling K in three dimensions as though all resistances were configured in parallel (series) is consistent with assuming that $p_c = 0 (p_c = 1)$. The latter is valid for 1D systems. Thus regarding the bounds of K as being its harmonic and its arithmetic means corresponds to assuming that the critical bond (or volume) fraction for percolation is between 1 and 0, valid for one- and infinite-dimensional systems, respectively. This means that typical guidelines for upscaling state only that the critical percolation probability is a probability, or that conduction takes place in a dimension between one and infinity. In this context we can see what potential improvement in theory exists when a perspective based on percolation theory is adopted. The value of p_c for a given system defines what fraction of the (smallest) individual resistances, which must be considered as connected in series, with the remaining $1 - p_c$ fraction of larger resistances connected in parallel. Any information on connectivity should help to estimate the appropriate value of p_c for a system, guiding the upscaling.

Problems

2.1. Provide the details of the derivation of Eqs. (2.13) and (2.14) for solute diffusion.

2.2. Verify that $p - p_c \propto \ln(g_c/g)$ if $R \propto \exp(2r/a)$, whereas $p - p_c \propto (g - g_c)$ if $R \propto r^{-4}$. Are there any conditions or restrictions on $W(R)$ for the validity of this derivation? Can you name any systems for which these resistance values are appropriate?

2.3. Repeat the optimization procedure for the conductivity if $R \propto r^4$ and $p - p_c \propto g_c - g$. Note that the optimization procedure described in the text (for the exponential case) is unchanged if the conductivity is represented in terms of R rather than in terms of g. However, the optimization procedure in terms of R fails for the case of the power-law dependence of R. Show this explicitly. What does this failure imply?

2.4. Verify that if $W(R) \propto R^{-\alpha}$ between $R_{\min}$ and $R_{\max}$, such that $-2 < \alpha < -1$, the effective resistance of a 1D chain for this choice of $W(R)$ is proportional to $R_{\max}$.

References

1. Pike, R., and H. E. Stanley, 1981, Order propagation near the percolation threshold, *J. Phys. A 14:* L169–L177. 37
2. Stauffer, D., 1979, Scaling theory of percolation clusters, *Phys. Rep. 54*: 1–74. 37, 40, 43
3. Herrmann, H. J., and H. E. Stanley, 1988, The fractal dimension of the minimum path in two-dimensional and three-dimensional percolation, *J. Phys. A 21:* L829–L833. 38
4. Sheppard, A. P., M. A. Knackstedt, W. V. Pinczewski, and M. Sahimi, 1999, Invasion percolation: new algorithms and universality classes, *J. Phys. A: Math. Gen*. **32**: L521–L529. 38, 39
5. Mandelbrot, B. B., 1983, *The Fractal Geometry of Nature*, W. H. Freeman, San Francisco. 38
6. Lee, Y, J. S. Andrade, S. V. Buldyrev, N. V. Dokholoyan, S. Havlin, P. R. King, G. Paul, and H. E. Stanley, 1999, Traveling time and traveling length in critical percolation clusters, *Phys. Rev. E 60*(3): 3425–3428. 38
7. Grassberger, P., 1999, Conductivity exponent and backbone dimension in 2-d percolation, *Physica A 262*: 251–263. 38
8. Skal, A. S., and B. I. Shklovskii, 1975, Topology of an infinite cluster in the theory of percolation and its relationship to the theory of hopping conduction, *Sov. Phys. Semicond*. **8**: 1029–1032. 40, 41
9. Gingold, D. B., and C. J. Lobb, 1990, Percolative conduction in three dimensions. *Phys. Rev. B 42*(13): 8220–8224. 41, 43
10. Clerc, J. P., V. A. Podolskiy, and A. K. Sarychev, 2000, Precise determination of the conductivity exponent of 3D percolation using exact numerical renormalization. *Eur. Phys. J. B* **15**: 507–516. 41, 43
11. Berkowitz, B., and I. Balberg, 1993, Percolation theory and its application to groundwater hydrology, *Water Resour. Res*. **29**: 775–794. 41
12. Derrida, B., and J. Vannimenus, 1982, A transfer matrix approach to random resistor networks, *J. Phys. A: Math. Gen*. **13**: L557–L564. 41
13. Jerauld, G. R., J. C. Hatfield, L. E. Scriven, and H. T. Davis, 1984, Percolation and conduction on Voronoi and triangular networks: a case study in topological disorder, *J. Phys. C 17*: 1519–1529. 41

14. Normand, J.-M., and H. J. Herrmann, 1990, Precise numerical determination of the superconducting exponent of percolation in three dimensions, *Int. J. Mod. Phys. C* **1**: 207–214. 41, 43
15. Berkowitz, B., and I. Balberg, 1992, Percolation approach to the problem of hydraulic conductivity in porous media, *Transp. Porous Media 9*: 275–286. 42
16. Sen, P. N., J. N. Roberts, and B. I. Halperin, 1985, Non-universal critical exponents for transport in percolating systems with a distribution of bond strengths, *Phys. Rev. B 32*: 3306–3308. 42
17. Feng, S., B. I. Halperin, and P. N. Sen, 1987, Transport properties of continuum systems near the percolation threshold, *Phys. Rev. B*, **35**: 197. 42
18. Sahimi, M., 1993, Fractal and superdiffusive transport and hydrodynamic dispersion in heterogeneous porous media, *Transp. Porous Media 13*: 3–40. 42, 43
19. Sahimi, M., 1993, Flow phenomena in rocks – from continuum models to fractals, percolation, cellular automata, and simulated annealing, *Rev. Mod. Phys. 65*(4): 1393–1534. 42, 43
20. Keffer, D., A. V. McCormick, and H. T. Davis, 1996, Diffusion and percolation on zeolite sorption lattices, *J. Phys. Chem. US 100*: 967–973. 42
21. Moldrup, P., T. Oleson, T. Komatsu, P. Schjønning, and D. E. Rolston, 2001, Tortuosity, diffusivity, and permeability in the soil liquid and gaseous phases. *Soil Sci. Soc. Am. J.* **65**: 613–623. 42
22. Kirkpatrick, S., 1971, Classical transport in disordered media, scaling and effective medium theories, *Phys. Rev. Lett*., **27**: 1722. 42
23. Kirkpatrick, S., 1973, Percolation and conduction, *Rev. Mod. Phys*. **45**: 574. 42
24. Sahimi, M., B. D. Hughes, L. E. Scriven, and H. T. Davis, 1983, Real-space renormalization and effective-medium approximation to the percolation conduction problem, *Phys. Rev. B 28*: 307–311. 42
25. Fisher, M. E., 1971, in *Critical Phenomena*, Enrico Fermi Summer School, ed. M. S. Green, Academic Press, New York, p. 1. 44
26. Ambegaokar, V. N., B. I. Halperin, and J. S. Langer, 1971, Hopping conductivity in disordered systems. *Phys. Rev. B 4*: 2612–2621. 45
27. Pollak, M., 1972, A percolation treatment of dc hopping conduction. *J. Non-Cryst. Solids 11*: 1–24. 45
28. Friedman, L., and M. Pollak, 1981, The hall effect in the variable-range hopping system, *Philos. Mag. B 44*: 487–507. 45
29. Neuweiler, I., and H.-J. Vogel, 2007, Upscaling for unsaturated flow for non-Gaussian heterogeneous porous media, *Water Resour. Res*. **43**: W03443. 45
30. Bernasconi, J., and W. R. Schneider, 1981, Classical hopping conduction in random one-dimensional systems – non-universal limit-theorems and quasi-localization effects, *Phys. Rev. Lett*. **47**: 1643–1647. 47
31. Hunt, A. 1991, Transport in ionic conducting glasses, *J Phys Condens Matter 3(*40**):** 7831–7842. 47
32. Stauffer, D., and A. Aharony, 1994, *Introduction to Ppercolation Ttheory*, 2nd edition, Taylor and Francis, London. 47, 53
33. Matheron, G., 1967 *Elements pour une Theorie des Milieux Poreux*, Masson et Cie, Paris. 50
34. De Wit, A., 1995, Correlation structure dependence of the effective permeability of heterogeneous porous media, *Phys. Fluids 7*(11): 2553–2662. 50, 51
35. Batchelor G. K., 1974, Transport properties of two-phase materials with stochastic structure. *Ann Rev Fluid Mech*. **6**:227–255. doi:10.1146/annurev.fl.06.010174.001303. 50
36. Sanchez-Villa, X., J. Carrera, and J. P. Girardi, 1996, Scale effects in transmissivity, *J Hydrol 183*: 1–22. 50
37. Torquato, S., 2002, *Random Heterogeneous Materials*, Springer-Verlag, Berlin. 50
38. Knudby, C., J. Carrera, J. D. Bumgardner, and G. E. Fogg, 2006, Binary upscaling – the role of connectivity and a new formula, *Adv. Water Resour, 29:* 590–604. 50
39. Hunt, A. G., 2001, Applications of percolation theory to porous media with distributed local conductances, *Adv. Water Resour.* **24(**3,4**):** 279–307. 53

Chapter 3
Porous Media Primer for Physicists

3.1 Introduction and Background

The study of soils and rocks is the province of many different disciplines. These disciplines have historically focused on applications rather than understanding, and this pragmatic approach has led to some cutting of corners. Furthermore, the different disciplines have different goals, so they have developed their own peculiar vocabulary, insights, and biases. For example, petroleum engineers generally work with consolidated rock, so the concept of a particle size distribution is not as central to their thinking as it is to a soil scientist. Meanwhile, soil scientists working with just two fluids – air and water – can frequently get away with assuming that air is infinitely compressible (and has density and viscosity of zero); petroleum engineers working with multiple flowing gases and liquids must consider all fluid phases in concert. Insofar as the structure of the medium is concerned, the material presented here tends to be centered on soil physics, but we have attempted to make contact with other disciplines in important cases.

The literature on porous media is vast. Two particularly useful reference books are Bear's [1] classic *Dynamics of fluids in porous media*; and Dullien's [2] *Porous media: Fluid transport and pore structure*. Others include Warrick [3]; Marshall et al. [4]; Hillel [5]; Sahimi [6], and Surkov and Tanaka [7]. In general, however, we find that the biases of researchers in each field tend to be reflected in weaknesses in their corresponding books: for example, soil physicists tend not to understand basic concepts of the physics of transport in disordered systems, while engineers (and physicists) tend to difficulties in understanding the basic patterns of the morphology of soils. This book is no exception: it cannot serve as a substitute for any of the standard texts on soil physics.

During the 1980s physicists (and some geophysicists) devoted considerable efforts to understanding the physical (meaning here not hydraulic) properties of sandstones [8–14]. These investigations were largely driven by curiosity about novel materials such as fractal media, and by the prospect of finding novel behavior, such as nonuniversal scaling of transport properties associated with continuum percolation theory. Much of the remaining physics research was driven by the needs of the petroleum industry and its desire to understand the dynamics of multiphase flow. But a great deal of information can now be gleaned from the soil physics community,

Hunt, A., Ewing, R.: *Porous Media Primer for Physicists.* Lect. Notes Phys. **771**, 57–96 (2009)
DOI 10.1007/978-3-540-89790-3_3

which could not be incorporated into the standard physics journals of that period. In fact several soil scientists [15–23] have addressed the question of whether natural porous media can be treated practically and consistently using fractal models. Some of these results call into question aspects of the fractal treatments of the 1980s' physics community.

In contrast to its treatment of soil morphology and structure, the soil science literature is quite inadequate when it comes to treating flow and transport. Models are based on detailed treatments of single pores, but then averages are performed over a pore-size distribution without considering the effects of connectivity [24–37]. More complicated averaging schemes exist, such as Burdine's [38], which uses a joint probability distribution rather than a single probability, thus diminishing the connectivity of the largest pores. Following the averaging, connectivity (and tortuosity) may be added in later, almost as an afterthought, in order to make theory agree with experiment.

When an arithmetic mean of transport properties is performed, the assumption of perfect connectivity has tacitly been made. That is, choice of a conductivity averaging scheme (and there is no space here to describe all those used in this community) independently from the connectivity is inherently contradictory. An internally inconsistent phenomenology can produce any result, including wrong ones. But this community has come to value flexible formulations of flow and transport above predictive ones: somewhere a combination of parameters must exist that makes "correct" predictions. And in fact, with the most flexible formulations [27], there may be a large number of such combinations, so a common concern of the community regards the "uniqueness" of parameter determinations. Another advantage of flexible formulations is that experimental error, which is often appreciable, can be readily accommodated. Usually the resulting relationships are recognized in the soil science and hydrology community as being phenomenological only. But the point of a physics-based treatment must be to derive relationships that are both predictive and physically sound, even in the face of complexity.

The fundamental physics of porous media is classical Newtonian mechanics, even though many natural porous media are not strictly Euclidean. The physics of porous media does not use concepts that are foreign to physicists, although discussions (particularly in the soil science community) may seem opaque to physicists. The purpose of this chapter is to introduce physicists to the web of subsurface hydrological science, to give an overview of the conceptual basis of the literature. As such it will show both the internal inconsistencies and the successes of this literature.

Probably the most striking aspects of natural porous media are their complexity and variability. To narrow the variability somewhat, these notes will be limited to soils and rocks, largely ignoring complications due to organic matter in the medium. We also exclude synthetic porous media and, except for one minor digression, living organisms, further reducing the variability.

The fundamental difficulty in estimating transport properties of geological porous media is obtaining a useful yet valid description of the pore space in three dimensions. The dimensionality of the description is crucial for many reasons. In fact systematic errors result for fractal media if 2D images are used to estimate the porosity.

But it is difficult to image a 3D volume of great complexity embedded in an opaque medium. Attempts to isolate a sample of a natural medium generally cause some rearrangement of the particles; this also changes the pore space, so accurate descriptions of media in their natural setting are seldom available by direct measurement. Another part of the uncertainty in treating geological porous media arises from the lack of consensus as to what information is actually required. While new imaging methods may help define the pore space, the danger also exists that these new methods will produce mainly superfluous data. If porous media are indeed fractal (within limits, of course), then the information required for models may be distilled to a few parameters.

The soil science community generally distinguishes between soil *physical* properties (comprehensive descriptions of the pore and particle space as well as mechanical properties), soil *hydraulic* properties (describing the flow of fluids through the medium), and soil *transport* properties (diffusion, electrical conductivity, dispersion, and advection of both sorbing and nonsorbing solutes). Such distinction between flow and transport tends to muddle the fact that all conductivities, whether thermal, electrical, or hydraulic, are proportionality coefficients in the same equation in which a flux, J, is proportional to the negative of a potential gradient, $-\nabla\Psi$. While the general problem of fluid flow in porous media is described by the Navier–Stokes equation, at the usual low Reynolds number flows encountered this equation also reduces to $J \propto -\nabla\Psi$, with the hydraulic conductivity as the proportionality constant. But a major goal of soil science has been to predict hydraulic properties from physical properties, then to predict transport properties from the physical and hydraulic properties. So a physicist needs to understand this distinction. Most treatments (pedo-transfer functions) have been based either primarily on empiricism or on numerical simulations. These notes show an alternative path to making predictions of flow and transport properties.

3.2 Relevant Soil Physics

3.2.1 Porosity and Moisture Content

The most basic information regarding the pore space of a porous medium is its porosity, the volume fraction of the pore space. The porosity, denoted ϕ, is thus a fraction less than 1. Rock porosity values range from less than 1% in many crystalline rocks such as granite, through 5–15% in sandstones, to well over 60% in pumice. Because soils are particulate rather than rigid, the requirement of mechanical stability restricts soil porosity values to a smaller range. Most mineral soils (as opposed to, e.g., peat) have porosities between about 30 and 60%, with 40–50% being a common value near the surface.

In a natural setting, a geological porous medium's pore space is generally completely occupied by air and/or water. The volume fraction of the water is usually denoted θ, and the air-filled porosity ε. Assuming a constant volume, $\phi = \theta + \varepsilon$.

But the assumption of a constant volume requires no movement or rearrangement of the particles, and something as simple as a change in water content can affect the particles' arrangement. Specifically, clay minerals can adsorb water onto their surfaces, causing clayey soils to swell with increasing moisture content. While this issue is clearly important for the field of soil science, it is not fundamental to the present discussion, and would force the development of more complicated, nonlinear techniques.

An aspect of porous media that will surprise physicists is the manner of measurements, and the implied systematic and random errors. For example, the concept of porosity is certainly simple, but typically the most reliable means of estimating that porosity is by measuring dry bulk (sample) density and *assuming* the particle density. While the density of individual soil particles may easily vary by up to 15%, the mean density of a collection of particles will not vary greatly from $2.65\,\mathrm{g\,cm^{-3}}$ (the density of quartz); typical errors in these porosity estimates are thus only a few percent. The following discussion combines information from Warrick [3], Ewing [39], and Marshall et al. [4].

The dry bulk density of a soil is readily obtained by weighing a predetermined volume, but the processes of sample removal, transport, and drying can change the volume. Biologically active soils, having some large pores between the soil clods or aggregates, are particularly vulnerable to compaction. However, the porosity of such pores (called "structural;" see below) is rarely more than 5% of the total porosity, so errors resulting from such repacking may be restricted by this value. Another means of obtaining the porosity is from measuring the loss of mass of an initially saturated soil ($\theta = \phi$) during long-term oven drying at 105°C. This method requires that the volume of pore space not change with addition or removal of water, not necessarily a reasonable assumption for soils with significant clay content. It also requires that the soil start completely saturated, but it takes good experimental technique to guarantee water contents greater than about $\theta = 0.9\phi$. For example, estimates of saturated moisture contents taken on the same soils by different Department of Energy laboratories vary by as much as 20%. Faced with such issues, a physicist must evaluate whether his/her notions of experimental tolerance are realistic.

Alternative indirect methods of estimating bulk density or porosity include gamma ray attenuation [4] and gas pycnometry [40] with dry samples. These methods also are subject to changes in volume during sampling and transport.

Imaging techniques involving X-ray tomography can also be used to determine the porosity of a medium, as well as to distinguish between different kinds of pore space. Considerable effort has been expended in developing algorithms to distinguish pores and particles in 3D images of porous media. We list some recent references [41–43] in order to point interested readers in a useful direction. These publications describe procedures to solve practical issues: thresholding or segmenting, skeletonizing via medial axis transformation or deformation retract, and using various algorithms to identify and classify pore space components. Naturally each of these steps introduces some error, with a key consideration being the scales of the voxels relative to the characteristic grains or pores.

A sample's water volume fraction is easily calculated by mass loss during drying, but frequently one wants to obtain repeated in situ measurements. One widely used method uses the medium's electrical properties. A standard equation from the physics of *homogeneous* media is used in what is called time-domain reflectometry, relating the speed of an electromagnetic signal to the dielectric permittivity of the medium. However, the usual means to relate the dielectric constant of disordered media to their water contents are insupportable and must be reevaluated; at present this method requires extensive calibration for each new soil. Another common method to measure the water content uses the fact that hydrogen atoms, having small mass, are the most efficient at slowing fast neutrons. The neutrons are emitted from (typically) a mixture of ^{241} Am and Be, and a nearby detector measures the flux of thermalized neutrons. Nevertheless the analysis is rather grossly simplified, so again the inferences for water content involve soil-specific calibrations. It is asserted that the highest precision available by such methods is 0.5%, but one should assume that typical precisions are much lower.

3.2.2 Classification of the Pore Space

Suppose we have a high-resolution 3D image of a medium, for example, obtained from X-ray microtomography (e.g., [44, 45]). After distinguishing between pore space and solid, it is useful to classify portions of the pore space as either pore bodies or pore throats. This difference is believed (correctly) to be fundamental to differences between wetting and drying of porous media. Pore bodies are larger voids, generally having one or more pore throats leading from them. The constricted porespace connecting neighboring porespaces referred to as pore throat or neck. The distinction between pore bodies and pore throats was not earlier made rigorous, but recent research by Glantz and Hilpert [46] has utilized dual graph theory in an attempt to accomplish this. Their work appears to be a generalization of usual solid-state techniques for constructing dual lattices. But other arbitrary definitions exist as well: what is the cutoff for the smallest pore, and what precisely is a pore [47]?

To better visualize these porous media descriptions, consider spherical particles that are hexagonal close-packed Fig. 3.1) [[48], web pages] or cubic close-packed (similar to Fig. 3.1, but with the difference that the third layer of spheres eclipses the holes in both the first two layers, rather than merely repeating the first layer). The emphasis in porous media on the spaces between the particles is complementary to the usual emphasis in, e.g., condensed matter physics. The interstitial volumes are found within two quite different solid structures, one of which is tetrahedral (Fig. 3.2) and the other octahedral (Fig. 3.3) (http://www.kings.edu/∼chemlab/vrml/clospack.html). The tetrahedral structure is found between three spheres in one layer, and one sphere in the next layer placed over the center of these three spheres; these four spheres form a tetrahedron. At the center of mass of these particles is a void, which would be classified as a pore body. This void is everywhere negatively curved on account of the positive curvature of the spheres. Leading out through the

Fig. 3.1 Hexagonal close-packed packing of spheres. (From Weisstein [48])

center of each face of the tetrahedron is a constriction in the void space, which would be called a pore neck or throat. Similarly, each octahedral pore body is connected to eight other pore bodies by constrictions, each passing through the center of a face of the octahedron. One-third of the pore bodies have eightfold coordination ($Z = 8$), and the remainder have fourfold coordination. In general, increased coordination between pores enhances the transport properties of the medium. In addition to the regular sphere packs, useful for basic concepts, random sphere packs have also been intensively studied (e.g., [49]). Random sphere packs of equal-size spheres have average sphere coordination around 6 (like a simple cubic lattice), and average pore coordination in the range 4.7–5.5 [50], depending on how dense the packing is, and on precisely how a pore is defined.

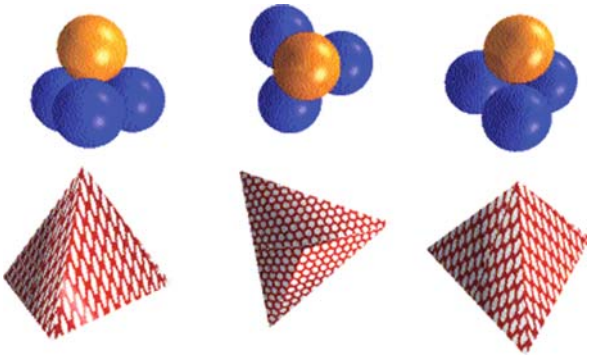

Fig. 3.2 The tetrahedral structures in the hexagonal close-packed system. From http://www.kings.edu/∼chemlab/vrml/clospack.html

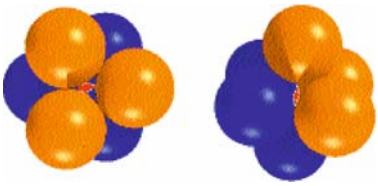

Fig. 3.3 The octahedral structures in the hexagonal close-packed system. From http://www.kings.edu/∼chemlab/vrml/clospack.html

If the radii of all the spheres in a sphere pack were varied proportionately and simultaneously, the porosity would not change: porosity is independent of particle size. Additionally, the pore radii would remain a constant fraction of the sphere radii. Also preserved is this aspect of the Scher and Zallen [51] relation, that the critical volume fraction is a constant fraction of the porosity, though in this case the relation would have to be appropriately defined to refer to the interstitial space. Theoretical treatments of the hydraulic and electrical conductivities based on such pictures of porous media lead to scaling formulations (e.g., [52]) that may not hold in natural porous media.

To the extent that the distinction between pore bodies and throats is relevant to a given medium, the storage properties of the medium relate most closely to the pore bodies while the flow properties relate most closely to the pore necks. Pore-scale network models (e.g., [53]) generally make use of this distinction. But storage capacity alone is not the whole picture: differences in water storage during drainage and wetting can be introduced by the presence of both pore bodies and pore necks. Drainage of a single pore body (air displacing water, or more generally, a non-wetting fluid displacing a wetting fluid) necessitates air entering the pore body through a narrow pore throat, while filling a pore body with water requires the air/water meniscus to expand from throat-sized to body-size (the importance of this will be more evident in Chap. 7). This distinction, at the scale of the individual pore, is generally recognized in the soils and hydrology community, where it is called the "ink-bottle effect." However, it is less widely appreciated that this difference also manifests itself macroscopically, due to wetting and drying being history-dependent processes; this also is further addressed in Chap. 7.

Further classification of the pore space can be useful in some natural media. For example, in a granular medium at very low water saturation, most of the water may be in the form of pendular rings (also called capillary bridges) surrounding the contact point of two particles. Also at low water saturation, a significant portion of the water may be sorbed to rough or fractal solid surfaces. While various investigators have addressed the effects of fractal surfaces on water storage and flow properties, we will show that storage effects are often masked by lack of equilibration, while flow effects may not be seen at all.

The flow of fluids through porous media is strongly affected by pore sizes, shapes, and connections. In order to generate a detailed representation of the pore space, a number of imaging techniques have been used, beyond the X-ray imaging

mentioned above (in connection with the difficulties of converting the 3D image to information on the pore space). These include laser diffraction/scattering (e.g., Eshel et al. [54]), neutron radiographic imaging (e.g., [55]), confocal miscroscopy (e.g., [56]), and filling a porous medium with a fluid which hardens (for example, a resin), then dissolving the solid particles [57]. Methods that use penetrating radiation are limited by attenuation, which leads to a loss of information in the third dimension (sometimes within a millimeter or less). On the other hand, because one cannot choose the chemistry of the natural medium being investigated, there may be no suitable choice of a resin that can withstand the caustic agent used to dissolve the porous solid. While synchrotron X-ray radiation is currently one of the best 3D imaging options, with a resolution of, e.g., 5 μm in a 5-mm sample [58], this method may not yield the local connectivity.

The focus on an exact reproduction of the pore space reflects the modern tendency to try to model at the pore scale the hydraulic properties of the porous medium using the "exact" Navier–Stokes equation, or a simplification such as lattice Boltzmann techniques. Such an approach requires vast quantities of data, yet presumably much of the data is irrelevant. Moreover, even the simpler lattice Boltzmann technique is insufficient to allow modeling more than a few hundred pores on a side. Use of such a technique for treating multiple scales of heterogeneity simultaneously is likely to be prohibitively difficult for the near future. This is especially relevant if the medium is fractal over a couple of orders of magnitude. Finally, particularly in the case of soils, these imaging methods have simply not been applied, and the available data are derived from particle size and related textural information (described below).

Biologically active soils (e.g., prairie, forest, and agricultural soils) and soils with significant clay content tend to be "structured." By structured is meant two things: first, some pores are larger than the largest grains, and second, a network of large pores may percolate even though it constitutes only a small fraction of the total porosity, typically less than the critical fraction for percolation for the "nonstructural" pores. The effects of soil structure on hydraulic properties in biologically active soils are considered in Chap. 11. In the case of swelling clays, these larger "pores" are mud cracks, and such media are not further considered here.

For a physically sound prediction of transport properties, the most important information would describe the entire range of pore sizes, including their connectivities. Such information is rarely available, and when obtained its value may not be recognized.

3.2.3 Particle Sizes and Pore Sizes

Most of the available soil physical information in the USA is collected by the US Department of Agriculture (USDA). In the relevant databases, the information most widely available is the texture of a soil. Texture, a USDA classification scheme having 12 classes, is related to the particle size distribution via the volume fractions

of sand, silt, and clay particles graphed on a ternary plot. But in order to make a quantitative prediction of the transport properties of the medium, it is the pore size distribution that must be known. (The situation is similar in some rocks, where the classification sandstone merely means that most of the particles are of sand size.) We make the common assumption that the particle size distribution is related in some fashion to the pore size distribution. The exact relationship is mediated somewhat by the porosity. Where soil porosity information is not given, the organic matter fraction may be available; knowing the organic fraction and texture constrains our estimate of the porosity. Since percolation theoretical techniques refer directly to the pore sizes, poor inferences of pore sizes from particle sizes will degrade its performance.

Soil textural information is given in terms of the fractions of sand- (maximum diameter 2 mm), silt- (maximum diameter 50 μm), and clay-sized (maximum diameter 2 μm) particles in the soil. This classification scheme was developed primarily for its relevance to agricultural soils, which need simultaneously to optimize water retention (small pore sizes) and flow (large pore sizes). It has long been recognized that soils with a wide range of particle sizes, incorporating sands, silts, and clays, are ideally suited to agriculture. Such soils are classed as loams, with subclasses silt loams, sandy loams, etc. For predicting the hydraulic properties of soils, however, this information is essentially useless, especially since these diagnoses are often made by crumbling the soil between the fingers [4], and it is known that in at least 50% of the cases such analyses fail to classify soils correctly.

In the usual absence of detailed knowledge of the pore space, the most detailed information that can be obtained derives from particle-size measurements for soils, or optical measurements of features related to the particles for rocks. One then tries to relate this information to useful descriptions of the pore space. Even if the particle size distribution is known accurately, it is a customary practice to report the soil textural information as well because typical experimental difficulties vary with texture and the community in general is put on guard.

Particle sizes, if not shapes, are presumed to give indirect information on pore sizes, and it is often assumed that pore sizes are some typical fraction of particle sizes [16, 59, 60]. Particle-size data yield the cumulative mass as a function of a discretized distribution of particle sizes. This discretization, fortuitously for investigators with an investment in fractals, is defined with respect to a geometric sequence: each size class is bounded by particle diameters that are in the ratio of 2:1. This Udden-Wentworth scale developed by geologists extends over many orders of magnitude, from clay through silt and sand all the way to boulders. Sizes larger than sand, called gravel or cobbles by soil scientists, are excluded from soil texture by definition; the existence of such large particles is not correlated with pores of a similar size. The 2-mm cutoff for inclusion in "soil" is based on moist soils being cohesive; at sizes above this cutoff, cohesive forces between particles are negligible.

Particle size measurements have traditionally been made by sieving, that is, vibrating a stack of sieves (with the largest diameter opening on top) and collecting the *mass* fraction in each sieve. It is not trivial to relate the mass fraction of particles

that fit through a square opening of some given size, but not through an opening half that size, to the fractional volume of particles of some appropriate intermediate diameter (probably best considered the geometric mean of the two opening sizes). To complicate matters, this sieving can be done either wet or dry. In the former case, cohesive forces from water must be overcome in order to separate particles; in the latter case, it is quite possible to miss the modifications on the pore size distribution provided by soil "aggregates," assemblages of soil particles glued together by organic materials and the tendency of individual grains to clump together if they are small enough. The latter tendency is especially strong in particles of clay mineralogy, which tend to have high surface area and charge imbalances. Thus, if complete information on the pore size distribution is desired, including the "structural" pores that can be found along the boundaries of soil aggregates, then the apparently riskier method of wet-sieving may be preferred [61].

A limitation on sieving is that the smallest particle size trapped by conventional sieves is about 0.05 mm. Particle size data for smaller particles, i.e., silt and clay sizes, must be obtained by other methods. The traditional means to determine the weight fractions for smaller sizes is called hydrometry and amounts to Stokes settling. In settling measurements, density corrections are asserted to be less than 5%. A significant problem arises here: data obtained by these two different methods are no longer constrained. The result is that frequently the total weight fraction does not equal 1, so that the cumulative size distribution graph may not accumulate to 1, or there may be regions with apparent negative slope. Since both these results are unphysical, a protocol must be developed for accepting or rejecting data, or making consistent adjustments to provide a reasonable synthesis.

To state the obvious, any measurement technique which isolates the particles also destroys the pore space. For unconsolidated systems it is usually assumed that recombining the soil particles – putting the dried, ground, and sieved particles back into a sample container – reconstructs some semblance of the original soil texture, though ordinarily not the soil structure. Clearly the use of such an option for rocks misses entirely the role of cementation in the properties of the medium.

If the usual assumptions are made, then a distribution of particle sizes may be transformed to a distribution of pore sizes by assuming that pores of size $\alpha d (\alpha < 1)$ are represented at the same frequency as particles of size d. In unstructured soils, this may reasonably approximate the entire range of pore sizes that exists. Typical estimates of the numerical value of α run about 0.3, though this value is notoriously variable in terms of the typical particle size; finer soils tend to have a larger proportionality constant than coarser ones. Obviously compaction of a given soil, resulting in a smaller porosity, would reduce α. Further, the proportionality between particle and pore sizes may hold over part of the range of particle sizes measured and not over the entire range. Especially if the larger pores are "structural" in nature a simple relationship between particle and pore sizes is unlikely to exist. If the larger pores are structural in nature, a different means of measuring them should be used as well: because, e.g., optical measurements may give a pore dimension rather than a

particle dimension, even if a consistent relationship between particle and pore sizes existed, it would not be discovered.

3.2.4 Parallel Tube, Network, and Fractal Models

In addition to sphere packings considered above, there are also models of porous media based on parallel capillary tubes, networks, and fractal concepts. Additionally, while we discussed sphere packings primarily to introduce concepts and terminology, they are also useful as descriptions of artificial porous media such as formed by glass beads. Whether such artificial media prove to be useful for understanding hydraulic properties of natural porous media is a question to which we return in Sect. 5.4. We will not further treat bundles of capillary tube models. Because each of the tubes implicitly spans the entire medium, the "pores" have infinite coordination and zero percolation threshold. The capillary bundle is therefore a misleading and physically incorrect model, though it has a use in teaching basic concepts. It also serves as a limiting case of perfect connectivity between pores of any given size, but zero connectivity between pores of different sizes. Because this book is a study of how connectivity affects flow and transport in natural media, we will not pursue constructs as artificial as capillary tube models, popular though they may be.

Network models of porous media began with Fatt [62] and have undergone tremendous evolution in the past three decades. Where Fatt's networks were tubes meeting at a dimensionless point, a "ball-and-tube" configuration soon became common, reflecting the distinction made earlier between storage in pore bodies, and flow through pore throats. More recent pore throat models have a polygonal rather than a circular cross section [63–65] and/or a converging/diverging geometry (e.g., biconically shaped throats; [66, 67]) rather than a constant cross section. Early networks were almost all 2D, while modern networks are almost all 3D, a critical distinction. In a 2D medium percolation of only one phase is possible. Thus not only is simultaneous flow of air and water impossible, but if all the grains are in contact with each other (necessary for mechanical stability) no flow is possible at all. Early networks used regular lattices, with pore radii assigned at random to the bodies and throats, and individual throats pruned (eliminated) at random to yield the desired mean coordination. In contrast, modern treatments often use irregular networks [68], with pore radii spatially correlated [69] and pore coordination positively correlated with pore size [41]. Network models were used as conceptual tools in petroleum engineering for two decades before their relationship to percolation processes was recognized [70, 71].

The increasing capability of computers, combined with the increasing sophistication of network models, has made it possible to perform numerical flow simulations of rather realistic media, if on a small scale. However, we seek an analytical framework for prediction. The ability of fractal models to represent highly complex

natural media with a paucity of relevant parameters is therefore a strong factor in their favor.

Suppose we want to model a natural fractal porous medium. Even if the range of fractal properties is restricted to one order of magnitude, the medium cannot be mapped to a regular network because the network has a fundamental scale and associated regularity. The question is how are natural porous media best modeled? Does the distinction between pore body and pore throat still hold in real media, even if they are fractal? A natural porous medium has a random arrangement of unequal size and irregular shaped particles, complicating the precise identification of pore bodies and throats. For some real media it has been suggested that a topological definition using, e.g., dual graph theory [46] will yield a consistent distinction. The application of dual graph theory is related to the construction in condensed matter theory for finding the dual of a lattice, in this case for a random medium. Does the distinction hold for fractal media? We assumed implicitly that it does, but what inaccuracies may result from not having a rigorous classification for such a fractal model?

Other practical questions arise. If one uses fractal models to interpret real media, is there a tendency for the fractal dimensionalities to cluster around a single value [72]? Should one use different fractal characteristics in the different ranges of pore sizes corresponding to sand, silt, and clay particles [18], or even a multifractal analysis [73]? Many early network models of porous media used log-normal pore size distributions instead of power-law distributions. Which distribution is more common in nature, and does the existence of a power-law pore-size distribution really imply the relevance of a fractal model? Does it make sense to use a power-law pore-radius distribution on a regular grid?

Of course these practical details beg the question: How should one formulate flow and transport theories in such problems? If one starts with a percolation theoretical basis, which form of percolation theory should one choose? Since treatment of fractal media using regular network models would be ill-advised, we chose continuum over site or bond percolation theory, a choice with significant consequences. As regards the question of whether to use fractal models, or more complicated treatments, we have consistently followed an approach of allowing the available data to guide us.

3.2.5 Representative Elementary Volume and the Concept of "Upscaling"

An important concept in porous media goes by the name of Representative Elementary Volume, or REV for short. The concept of the REV was developed in recognition of the variability of natural porous media at small scales, and has been interpreted to be the minimum volume for which statistical treatments of properties should apply. Statistical treatments in the porous media community are generally interpreted in terms of mean values. Insofar as physical properties are concerned,

such as density, this interpretation is valid, as is an ensemble mean value for entire samples of a given size and shape. But when applied to transport properties, the definition of the statistical treatment as a mean (or geometric or harmonic mean) of values taken at a smaller scale is inaccurate. Nevertheless, percolation theory gives a consistent and accurate interpretation of an REV.

The derivation of an expression for an effective hydraulic or electrical conductivity at a larger scale, in terms of the variability it exhibits at smaller (e.g., pore) scales, is termed "upscaling" in the porous media community. However, we make no distinction between upscaling at the pore scale and upscaling at larger scales, such as field scales in soils, or formation scales in rocks. The particular strategy may change with scale, but percolation theory must in principle be relevant at all scales. Interestingly, the porous media communities view these two cases quite differently.

3.2.6 Porosity and Fractal Media

The fractal fragmentation model of Turcotte [11] added legitimacy to the study of fractal models of porous media, particularly soils, because it developed a mechanism by which scale-independent fracture properties could form a fractal distribution of particles. Rieu and Sposito [17] then developed a model, called from here on the Rieu and Sposito (RS) model, of a fractal pore space linked to a fractal particle model. Several sets of investigators have shown that it is possible to predict pressure–saturation curves from particle-size data using the RS model [21, 74, 75]. In the RS notation, d_0 denotes the largest pore size, and d_m the smallest. The reason for their choice is that they can use an index i, representing the iteration of the fractal process, which runs from 0 to m. This convention will be reversed here, because it is more intuitive to consider r_0 to be a minimum radius and r_m a maximum, and since one of us has used this convention consistently elsewhere.

For simplicity, consider that pores exist only at discretized diameters, d_i. V_i represents the total volume in all pore sizes greater than d_m and less than or equal to d_i. There is a constant ratio N of the number of pores of diameter $d_{i+1} = qd_i$ to the number of pores of diameter d_i. q is the ratio of pore diameters in successive classes, and is less than 1. Define the partial volume $P_i \equiv V_i - V_{i+1}$, the total volume as V_0, and the volume of the solid material as V_m. Then one can write

$$V_0 = \sum_{i=0}^{m} P_i + V_m \tag{3.1}$$

Self-similarity requires

$$V_i = NV_{i+1} + P_i \tag{3.2}$$

This result allows Eq. (3.1) to be rewritten as

$$V_0 = \sum_{i=0}^{m-1} N^i P_i + N^m V_m = P_0 \sum_{i=0}^{m-1} \left(Nq^3\right)^i + \left(Nq^3\right)^m V_0 \tag{3.3}$$

Here, as in the original treatment of Rieu and Sposito, the solid volume is now reinterpreted as $N^m V_m$. One way to think of this is that pores smaller than d_m can be ignored; that is, if we could resolve smaller pores, the iteration would proceed further. The total pore volume, V_p, can be written as

$$V_\mathrm{p} = P_0 \left[1 + Nq^3 + \left(Nq^3\right)^2 + \ldots + \left(Nq^3\right)^{m-1}\right] = P_0 \frac{1 - \left(Nq^3\right)^m}{1 - Nq^3} \tag{3.4}$$

Now one can express the porosity as

$$\phi = \frac{P_0 \left\{\left[1 - \left(Nq^3\right)^m\right] / \left(1 - Nq^3\right)\right\}}{P_0 \left\{\left[1 - (Nq^3)^m\right] / (1 - Nq^3)\right\} + N^m V_m} \tag{3.5}$$

One can solve Eq. (3.3) for P_0 in terms of V_0 to find

$$P_0 = V_0 \left(1 - Nq^3\right) \tag{3.6}$$

Using the same substitution in Eq. (3.5) for $N^m V_m$ as in Eq. (3.3), and substituting Eq. (3.6) for P_0, one finds

$$\phi = 1 - \left(Nq^3\right)^m \tag{3.7}$$

Consider the definition of the fractal dimensionality [76, Chap. 13, 77, Chap. 3]:

$$D = \log(N) / \log(1/q) \tag{3.8}$$

Combine this definition with Eq. (3.7) to obtain

$$D = 3 - \frac{\log(1 - \phi)}{\log(q^\mathrm{m})} \tag{3.9}$$

The numerical factor q^m, however, is nothing more than the ratio of the smallest pore diameter to the largest, d_m/d_0, so that

$$D = 3 - \frac{\log(1 - \phi)}{\log(d_\mathrm{m}/d_0)} \tag{3.10}$$

Equation (3.10) may be rewritten as

$$\phi = 1 - \left(\frac{d_\mathrm{m}}{d_0}\right)^{3-D} \tag{3.11}$$

Equation (3.11) establishes the RS result for the porosity. This result is very simple, being for example independent of shape parameters and the choices of N and q. Equation (3.11) can also be used to show that

$$\left(Nq^3\right)^m = \left(q^m\right)^{3-D} \tag{3.12}$$

which simplifies to $N = q^{-D}$. What sort of a distribution of pore sizes does the above analysis lead to? For the partial volume $P(i)$ of pores of size class i, we can write

$$P(i) \propto N^i = q^{-iD} = \left(\frac{d_i}{d_0}\right)^{-D} \tag{3.13}$$

where the last expression uses the relationship between the pore radius r_i and the fractal iteration i: $r_i = q^i r_0$. Equation (3.13) for $P(i)$ could be written as $P(i)\Delta i$ without change, since i is an integral index and $\Delta i = 1$. Then the probability $W(d)$ that a pore's diameter is within dd of d is found by using the transformation, $W(i)\mathrm{d}i = W(d)\mathrm{d}d$,

$$W(r) \propto \frac{(d/d_0)^{-D}}{d\ln(q)} \propto d^{-D-1} \tag{3.14}$$

One can develop a normalized form for a pdf for pore radii, $W(r)$, which generates the same result for the porosity as Eq. (3.11):

$$W(r) = \frac{3-D_\mathrm{p}}{r_m^{3-D_\mathrm{p}}} r^{-1-D_\mathrm{p}} \quad r_0 \le r \le r_m \tag{3.15}$$

In this expression we have substituted D_p for D to indicate that the fractal dimensionality concerned applies to the pore space. The result for the total porosity derived from Eq. (3.15) is [74]

$$\phi = \frac{3-D_\mathrm{p}}{r_\mathrm{m}^{3-D_\mathrm{p}}} \int_{r_0}^{r_\mathrm{m}} r^3 r^{-1-D_\mathrm{p}} dr = 1 - \left(\frac{r_0}{r_\mathrm{m}}\right)^{3-D_\mathrm{p}} \tag{3.16}$$

exactly as in RS. Equation (3.16), as written, is compatible with a volume r^3 for a pore of radius r. If a particular geometry for the pore shape is envisioned, it is possible to change the normalization factor to maintain the result for the porosity, and also maintain the correspondence to RS. This is an important restriction and is applied because ϕ in the RS treatment is independent of geometry. Integration of $W(r)r^3$ over the continuous pore size distribution between pr and r, where $p < 1$ is an arbitrary factor, yields the contribution to the porosity from each size class obtained by RS. Integration of $W(r)$ over the same size range yields the probability that an arbitrary pore has a radius of r that is in agreement with the direct calculation of RS. Thus the present model is just a continuous version of the discrete RS model. The power law distribution of pore sizes is bounded by a maximum radius r_m, and truncated at the minimum radius r_0. Note that knowledge of ϕ, r_0, and r_m is sufficient to give D explicitly. ϕ is typically obtained through density measurements, and r_0 and r_m are obtained from particle size measurements. Several examples of the determination of r_0 and r_m are given in Figs. 3.4, 3.5 and 3.6. We show below that the RS model yields predictions for the water retention characteristics that have been verified in experiment.

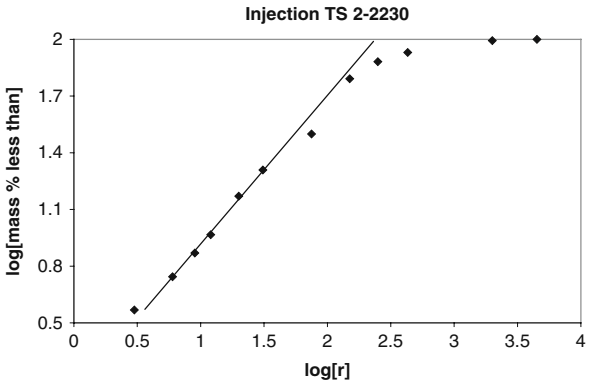

Fig. 3.4 The cumulative particle-size distribution data from the Injection Test Site 2-2230 soil at the US Department of Energy Hanford site. Data from Freeman [22]. The horizontal scale is in logarithm base 10. The maximum particle radius is very nearly two orders of magnitude larger than the minimum value (Log[2.5]–Log[0.5])

Using the substitutions $\phi \rightarrow 1 - \phi$ and $D_\mathrm{p} \rightarrow D_\mathrm{s}$ (where D_s refers to the fractal dimensionality of the solid portion of the medium), the result is obtained [74]

$$\phi = \left(\frac{r_0}{r_\mathrm{m}} \right)^{3-D_\mathrm{p}} \tag{3.17}$$

As a reminder, in Eq. (3.16) r_0 and r_m refer explicitly to the minimum and maximum *pore* sizes, and in Eq. (3.17) to the minimum and maximum *particle* sizes. Here we have made the common assumption [15, 59, 60] that pore and particle radii are proportional to each other. Under this assumption, the ratio r_0/r_m is the same for both particles and pores.

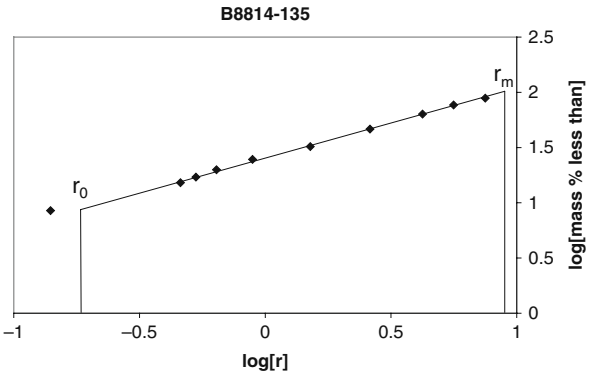

Fig. 3.5 The cumulative particle-size distribution from the B8814-135 soil at the US Department of Energy Hanford site

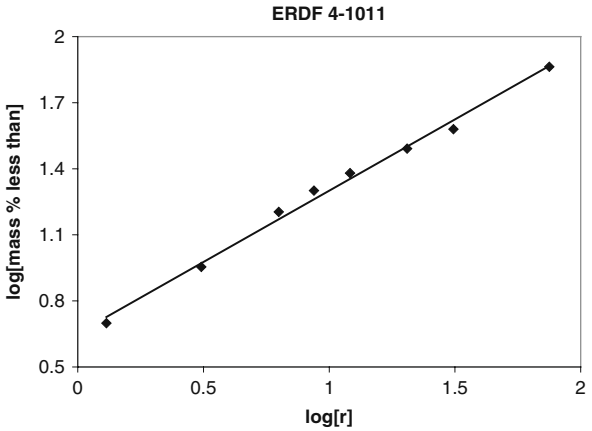

Fig. 3.6 The cumulative particle-size data from the ERDF 4-1011 soil at the US Department of Energy Hanford site

Katz and Thompson [10] used optical measurements to detect the range of sizes in the particle space corresponding to the range from r_0 to r_m. They assumed a lower cutoff of $r_0 \approx 1\,\text{nm}$, and determined values of r_m of up to $100\,\mu\text{m}$. Then they used Eq. (3.17) (as did [78]) to relate the porosity, the ratio r_m/r_0, and the fractal dimensionality of the solid volume, D_s. But their statement, "successful prediction of the porosities from the fractal parameters verifies the assumption that the pore surface and volume are fractals with the same dimension," does not follow, because Eqs. (3.16) and (3.17) are complementary [79]. Given Eq. (3.16), which relates the fractal dimensionality of the pore space to the porosity, and their assumed values $r_m/r_0 \approx 10^4$, their fractal dimensionality range from 2.57 to 2.87 would imply porosities between 95 and 73%, rather than the values between 5 and 27% that they calculated and measured. The real question, presumably, is whether one trusts the Rieu and Sposito fractal model. We have provided two derivations of their result for the porosity above. Further, in addition to our tests on ca. 40 Hanford site soils, which demonstrated that the Rieu and Sposito model can be used to predict water retention curves, at least two other groups of researchers [19, 21] have also demonstrated that the RS model is predictive in this way.

Where does the typical asymmetry between particles and pores come from? A reasonable hypothesis is that it chiefly arises from the tendency for particles to be positively curved and for the pores to be negatively curved (note the exception of such materials as pumice, which can be formed when air bubbles percolate, and for which values of ϕ are probably largest of geological porous media). Such a contrast in curvature would tend to produce $\phi < 0.5$. According to Eqs. (3.16) and (3.17), $\phi < 0.5$ is consistent with pore space having a greater fractal dimensionality than that of the particles, a tendency noted also by Rieu and Sposito [17]. In soils, mechanical strength tends to limit porosity as well, a consideration of less importance in rocks on account of cementation, although the mean porosity of rocks is less

than that of soils. This discussion is not meant to justify a rule, but only to explain tendencies.

3.3 Soil Water Potential and Water Retention

The study of unsaturated media today is strongly influenced by the ideas of Edgar Buckingham, particularly his 1907 publication. Most of his ideas were actually quantitatively incorrect, though useful for a qualitative understanding (or, as the case may be, for a deeper understanding of the resistance of members of the soil physics community to new ideas). T. V. Narasimhan at the University of California at Berkeley has made a study of the influence of these ideas on subsequent researchers, and we quote his recent paper [80] liberally:

> The concept of a capillary potential, first conceived by Buckingham a century ago, continues to play a fundamental role in modern theory of soil-moisture movement.
>
> Buckingham recognized that to satisfy the needs of an equation of motion, a potential must be a conservative quantity in that its integral must identically vanish over a closed path in space. Accordingly, Buckingham assumed that capillary potential, defined as work done against the water-solid attractive forces, was a reversible process.
>
> Buckingham made an important assumption that the work involved in pulling a given mass of water away from a moist soil is fully reversible in order that capillary potential may be conservative. This assumption was shown to be unrealistic for natural soils in an important contribution by Haines [81], who experimentally established hysteresis in the soil-moisture retention curve. In explaining hysteresis, Haines contributed the fundamental insight: "[t]he mode of moisture distribution in soil does not give reversible conditions but leads to two main values of capillary pull. The case of falling moisture tends to be governed by a higher value of pressure deficiency as determined by the narrower section of the pores, while conditions of wetting or increasing moisture tend to be governed by a lower value depending on the wider sections of the pores. In other words it is found that a granular system, of which soil is typical, will in general offer a greater capillary pull against the extraction of water from its pores than it can engender when absorbing water into them" (Haines [81], p. 98).

We will return to this subject later, because it turns out that, at least under realistic experimental conditions, percolation theory gives a second reason for the difference between wetting and drying soils.

Water is held in porous media by adsorption at surfaces of particles, particularly noticeable in clay minerals (which have high surface area) and presenting as capillarity in pores. Capillarity in pores is thus a result of the tendency of water to wet the mineral surfaces, together with the tendency of surface layers of water to be attracted to the interior, i.e., the source of interfacial tension [82]. The basic understanding of water in a pore space relates the physics concept of capillary rise in a tube to a water potential in the soil. Suppose that a tube (manometer) is connected through a porous cup to a porous medium at a position above the water surface or water table, as in Fig. 3.7. The height of water in the manometer (which will be negative) relative to the point in the soil is $-h$ (say, -10 cm), and the water pressure is less than the atmospheric pressure P_a at the air/water interface by $P = -\rho g h$ (for ρ the density of water, and g the acceleration due to gravity). h is thus a pressure

per unit weight (in a given volume) and is also called pressure head, matric head, or just head.

Consider the case that the water is pure H_2O. The quantity $-h$ is also a specific and simple example of the soil water potential (also called matric potential), $\psi = -h$, which is defined as a work per unit weight that must be done on an infinitesimally small amount of pure water to bring it into the soil at the same elevation. The stipulation "small amount" is a necessary condition so as to prevent the change in water content from changing the condition of the soil. A similar stipulation applies in electrodynamics, where a field is to be detected with an arbitrarily small test charge.

In general the soil water potential may depend on many variables and include many effects, such as osmotic pressures, overburdens, pneumatic pressures [39], but the subject of the present discussion is limited to capillarity. $h = -\psi$ is the height above the water surface that water will rise at this negative pressure; it is also the capillary rise of water in a tube of radius r, from the surface tension acting on the meniscus with contact angle α, i.e.,

$$F = 2\pi r\gamma\cos(\alpha) = \pi r^2\rho hg \tag{3.18}$$

This equation equates the vertical component ($\cos\alpha$) of the force due to interfacial tension γ on a surface of area $2\pi rh$, to the gravitational force (product of density

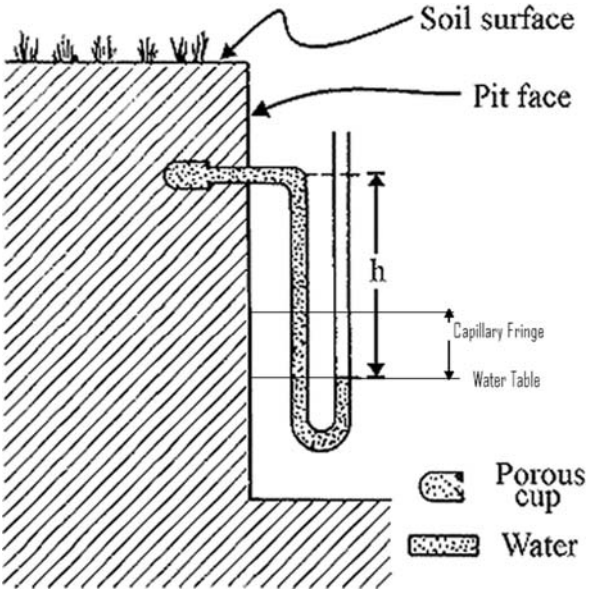

Fig. 3.7 After University of Florida web page, http://edis.ifas.ufl.edu/SS109. The capillary fringe is discussed after Eq. (3.21) and has vertical thickness inversely proportional to the largest pore size. This region has negative matric potential (pressure), but the tension is insufficient to drain the largest pore

ρ, volume $\pi r^2 h$ and gravitational acceleration g) on the volume between that surface and the water table. The result, $h \propto \gamma/r$, can be generalized by replacing $1/r$ by $1/2r_1 + 1/2r_2$ for irregular solid surfaces with two (or more) different radii of curvature [3]. But usually the result is written simply as $h = A/r$, with A in general unknown and r a *characteristic* radius for a given pore size. An analogous argument leads to the general relationship that, for an arbitrary pressure difference (per unit weight) between air and water, $P/\rho g = h$ (leading to the use of h as an equivalent pressure), and at equilibrium, only those pores with radius $r < A/h$ will contain water. The basis of this argument is in the radius of curvature of the air–water interface, which must be as large as a pore radius in order for water to fill the pore. Then analysis of $d\theta/dh$ (within experimental uncertainty) over the full range of h yields, in principle, the pdf for the pore-size distribution.

To illustrate, assume spherical pores, equilibrium conditions, and a pore radius pdf equal to $W(r)$. Then the total water content in the medium may be written

$$\theta = \int_{r_0}^{A/h} W(r) \left(\frac{4}{3} \pi r^3 \right) dr \tag{3.19}$$

where A is a numerical coefficient (known for spherical pores, but unknown in a natural medium where the shapes of pores are typically unknown). Even in media with nonideal pores, as long as pore lengths and radii are correlated, the factor r^3 in the integrand is appropriate. One then finds $d\theta/dh \propto W(r) r^3 h^{-2} \propto W(h)(dh/dr) h^{-5} \propto W(h) h^{-3}$, so that to find $W(h)$ (within numerical factors), one simply takes the product of h^3 and the derivative of the water content with respect to h at the given h.

$W(h)$ determined in this way typically contains a region at intermediate saturations which is consistent with power-law behavior and fractal models, but deviates at the wet and dry ends of the moisture spectrum. The deviations give $W(h)$ (and $W(r)$) sigmoidal shapes, with regions of pronounced curvature at the wet and dry ends. Such deviations have led some to conclude that (1) the appropriate distribution of pore volumes is not fractal but, e.g., log-normal, and (2) water content changes at the wet end result from the wetting or drying of larger, "structural" pores, and at the dry end from the volume of thin films of water. van Genuchten has developed a special phenomenological relationship (discussed below) which matches the sigmoidal shape by construction. Of course, some deviation from the predictions of fractal models must be expected at both ends, since continuity of the constituent phases is interrupted. Such discrepancies are not by themselves sufficient to accept or reject a fractal model. Further, to the extent that such deviations arise from fluid properties and percolation, they may be time-dependent (as discussed in Chap. 7). Incorporation of both time-dependent and time-independent phenomena into a single time-independent phenomenology is by definition inconsistent.

We contend that the RS fractal model is accurate and appropriate for a large number of natural porous media. Certainly it is not sensible to assume this of all media. It will be seen below that for some media, the equilibrium water content predicted by the RS model deviates from experiment at both the wet and the dry

ends of the spectrum. These observed deviations helped to spur the collection of more detailed (and possibly superfluous) information, because they may represent defects of the fractal models. But in fact they may represent strengths of the model, because they are typically due to complications demanded by percolation theory.

For an RS fractal medium in equilibrium, the water content is

$$\theta = \frac{3-D}{r_{\mathrm{m}}^{3-D}} \int_{r_0}^{A/h} r^{2-D} dr \tag{3.20}$$

where A/h in the range $r_0 \leq A/h \leq r_{\mathrm{m}}$ determines the largest pore that contains water. For values of h outside this range (A/h larger than r_{m} or smaller than r_0), $\theta = \phi$ or $\theta = 0$. At a particular value of h denoted h_{A} (called the air entry pressure), air could just enter the largest pore if that pore were located at the edge of the sample. Thus, $A/h_{\mathrm{A}} = r_{\mathrm{m}}$. h_{A} can then be related to the porosity:

$$\phi = \frac{3-D}{r_{\mathrm{m}}^{3-D}} \int_{r_0}^{A/h_A} r^{2-D} dr \tag{3.21}$$

Note that for any given soil, there must be some maximum pore size. For $h < h_{\mathrm{A}}$ corresponding to that largest pore, the soil may be saturated. There is a saturated region *above* the water table (i.e., $h > 0$) known as the capillary fringe; the height of this region approaches zero in the limit that the largest pore size approaches infinity.

It is easy to combine Eqs. (3.20) and (3.21) to produce

$$S \equiv \frac{\theta}{\phi} = 1 - \frac{1}{\phi}\left[1 - \left(\frac{h_A}{h}\right)^{3-D}\right] \tag{3.22}$$

for the relative saturation S, a relationship also obtained by Rieu and Sposito [17] using their discrete version of this model. Equation (3.22) may be (very roughly) approximated as $S = (h_{\mathrm{A}}/h)^{3-D}$, which is precisely the form of the phenomenological relationship proposed by Brooks and Corey [30]. The water content of natural porous media most closely resembles the result of Eq. (3.22) during drainage. The $\theta(h)$ or $S(h)$ relationship during drying is referred to as a water retention curve. In Figs. 3.8, 3.9 and 3.10 the results of Eq. (3.22) are compared with water retention data from the same media as for Figs. 3.4, 3.5 and 3.6. The value of the fractal dimensionality was found from analysis of the particle size data (i.e., r_0 and r_{m}) according to Figs. 3.4, 3.5 and 3.6, and knowledge of the porosity (Eq. (3.16)). Note that the predicted water retention curve agrees with observation in the middle of the range of saturations, where both the water and the air phase percolate simultaneously, but does not predict the curvature at the wet and dry ends, where complications would be expected due to lack of percolation.

The complicating behavior at the wet and dry ends of the water retention curve need not be due only to percolation behavior. Some pore size distributions may

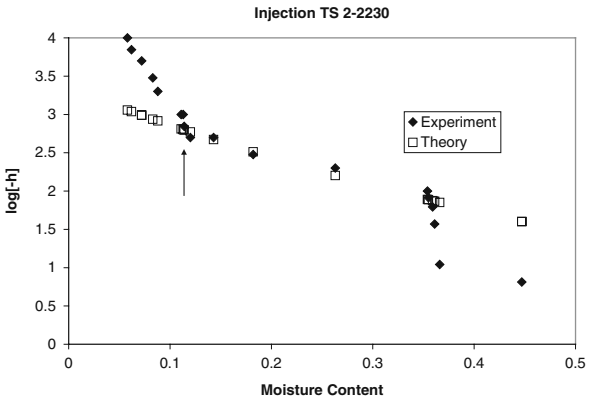

Fig. 3.8 The water retention data for the Injection Test Site 2-2230 soil at the US Department of Energy Hanford site. The prediction of the fractal scaling in the open squares is taken from the value of D_p determined from the particle-size data in Fig. 3.4, and one parameter, h_A, which fixes the vertical scale, was chosen to optimize the fit. The *arrow* denotes the dry-end moisture content at which experiment begins to deviate from the fractal model

indeed be log-normal. At the wet end, structural pores often *do* complicate the analysis. At the dry end, water present in surface films *may* complicate matters. It is important to keep these uncertainties in mind during analysis, although other than percolation effects, only those effects due to structural pores will be considered here, and those only in the final chapter. Before useful conclusions can be drawn from any discrepancies in predictions from the fractal model, however, effects due to percolation must be excluded. Otherwise inferences will be nonsense.

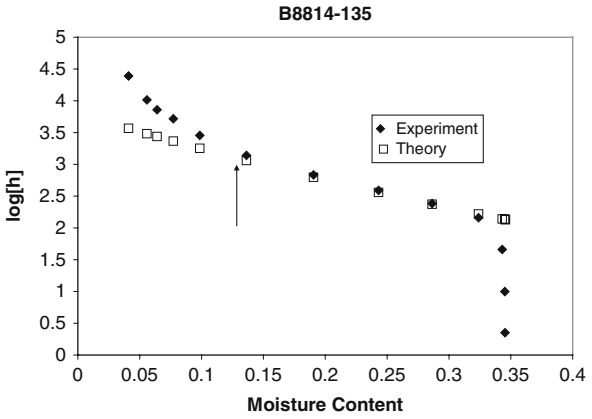

Fig. 3.9 The water-retention data for the B8814-135 soil at the US Department of Energy Hanford site. The prediction was made analogously to Fig. 3.8

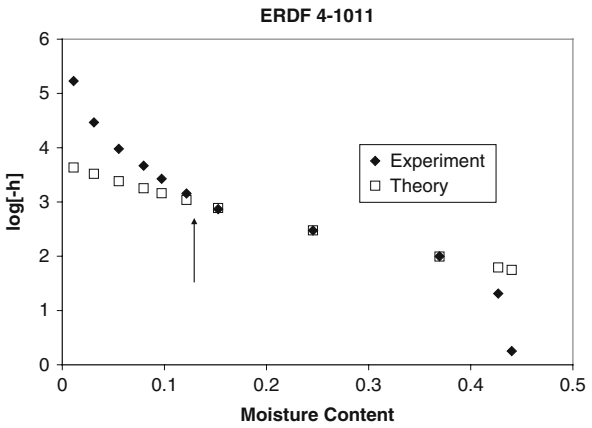

Fig. 3.10 The water-retention data for the ERDF 4-1011 soil at the US Department of Energy Hanford site. The prediction was again made analogously to Fig. 3.8

As mentioned, a phenomenological relationship for the water retention curves of porous media was developed by van Genuchten, having the form [36]

$$\Theta = \left[\frac{1}{1+(h/h_A)^n}\right]^m \tag{3.23}$$

In this expression $\Theta \equiv (\theta - \theta_r)/(\phi - \theta_r)$, where the subscript r means the moisture content remaining in the soil after it becomes difficult to remove further moisture. m and n are powers. The use of multiple powers in such a phenomenology is typical in the porous media community [and is common in the field of dielectric relaxation as well – physicists and soil physicists familiar with that literature may consider Cole-Cole [83] and Havriliak-Negami [84] forms for the dielectric relaxation], but is not justifiable on the basis of theory. A van Genuchten water retention curve is given in Fig. 3.11, where it is seen that a smooth sigmoidal curve is generated. Many soil scientists and hydrologists favor this phenomenology because both h and $dh/d\theta$ are continuous over the entire range of saturations. This makes its substitution into partial differential equations governing larger scale transport properties less troublesome, since the numerical solutions are then well-behaved. However, numerical convenience and stability are not sufficient reason to prefer a particular phenomenology.

Although this chapter is not an introduction to geologic processes, the context of unsaturated properties in hydrology matches the unsaturated zone in geology. This zone, above the water table and below the earth's surface, is also called the vadose zone.

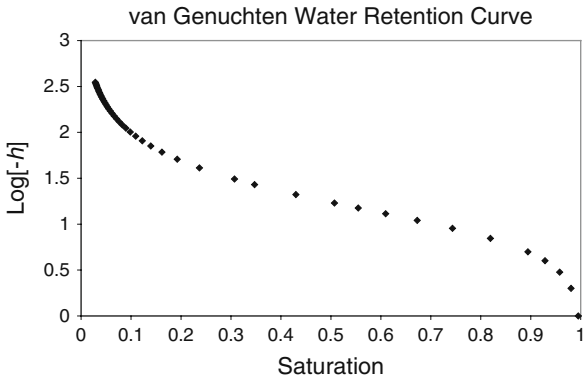

Fig. 3.11 The van Genuchten water-retention function. Note that both the water-retention function and its derivative are continuous

3.4 Hysteresis and Time Dependence in Pressure–Saturation Relationships

Hysteresis in wetting and drying is quite complex, making it necessary first to introduce some terms. This terminology will be presented with respect to the specific three-phase system of water/air/solid, but it applies equally to the general system wetting/nonwetting/solid.

Drainage (drying) refers to air displacing water, or more generally, to a nonwetting phase displacing a wetting phase. Imbibition (wetting) is the opposite: the displacement of air by water. We likewise distinguish between allowable and accessible pores. A pore is allowable if the current pressure is sufficiently high (low) that the capillary rise Eq. (3.18) predicts that it will drain (imbibe). A pore is water-accessible if it is on the infinite water cluster, and air-accessible if it is on the infinite air cluster. If drainage develops from completely saturated initial conditions, it is called "primary" drainage. If wetting occurs from perfectly dry initial conditions, it is the primary wetting curve. Starting from any intermediate point gives a secondary curve. This discussion focuses on the primary wetting and drainage curves. The drying curve (water retention curve) and wetting curve together constitute the pressure–saturation relationship.

There is one clearly symmetrical aspect of complete wetting and drying. In both cases, two distinct phase transitions occur: the first when the displacing fluid first percolates, the second when the displaced phase ceases to percolate [85]. However, there is an intrinsic asymmetry in the connectivity of water and air: if the air-filled pore space percolates but the water-filled pore space does not, the water phase may nevertheless connect through thin films, providing an alternate means to transport water through the pore space. The opposite situation (thin films of air connecting otherwise disconnected air-filled pores) does not exist, because air is not wetting. So a pore must be allowable, air-accessible, *and* water-accessible to fill with water, but it can fill with air if it is merely allowable and air-accessible. In principle, one

could invoke water film flow [86, 87] to eliminate all issues of connectivity from hysteresis. But while this alternate path for water flow exists in principle, it may not be important in a given situation, because the hydraulic conductance of thin films is orders of magnitude lower than that of water-filled pores. Under conditions where thin film flow is too slow to be relevant, the percolation theoretical issues are symmetrical with respect to drainage and imbibition.

A second important structural asymmetry is that drainage is controlled by the pore necks, while imbibition is controlled by the pore bodies. Specifically, for a pore to be allowed to drain, the meniscus' radius of curvature must be less than the pore throat's radius, while for a pore to be allowed to imbibe, the meniscus radius must be greater than the pore body's radius. Consequently, the water content for a given tension (meniscus curvature) is always higher during drainage than during imbibition, resulting in a hysteresis loop. This particular effect is not eliminated by film flow. This aspect of structural hysteresis is called the ink-bottle effect.

The discussion so far has treated only structural hysteresis, which largely consists of two contributions: connectivity-related limitations (discussed in Chap. 7) and the ink-bottle effect. Another contributor to (apparent) hysteresis is the experimental artifact of transport-limited equilibration. To illustrate: if water must leave the soil at a given pressure in order for the soil to attain equilibrium, but the hydraulic conductivity is too low (e.g., less than 10^{-8} cm/s), then experimenters will not have time to observe an equilibrium water content. Such conditions certainly occur as the percolation threshold is approached, but they may also occur whenever the controlling (bottleneck) pore radius is sufficiently small, i.e., when the saturated value of the hydraulic conductivity is very low. Topp et al. [88] developed a nomogram (a graphical extrapolation tool) for estimating the equilibrium water content of a medium when the equilibration time is prohibitively long. Unfortunately, the nomogram has an insufficient basis in the relevant physics.

Hysteresis in the pressure–saturation relationship is accompanied by a major hysteresis in the hydraulic conductivity, which can be expressed as either a function of the pressure ($K(h)$) or the saturation ($K(\theta)$). Hysteresis in $K(h)$ can be significant, because at a given h the moisture contents in drainage and imbibition can be quite different. The hysteresis in $K(\theta)$, however, is much smaller, since at a given saturation (ignoring connectivity complications) the same pore sizes are filled with water in both drainage and imbibition. Experimental data generally support this reasoning, showing much greater hysteresis in $K(h)$ than in $K(\theta)$.

The transport-limited equilibration that causes apparent hysteresis in the pressure–saturation relationship also has implications for experimentally measured hydraulic conductivity. At a given imposed tension, if equilibration has not been attained because the hydraulic conductivity is too low, then the moisture content is too high. The estimated hydraulic conductivity $K(h)$ is associated with the higher moisture content. So paradoxically, just when the hydraulic conductivity is dropping rapidly, equilibrium is not attained, with the result that the "measured" K is too high. Because the water content is also too high, the (apparent) $K(\theta)$ function is much less affected than the function $K(h)$. $K(\theta)$ drops approximately as it should,

simply because the errors partially compensate for each other, but $K(h)$ may be too small to measure accurately.

Finally, we consider the issue that, in principle, it is possible for water-filled pores to be unable to drain when they are allowable and air-accessible, but not water-accessible. That is, if they have become disconnected from the infinite cluster during drainage, they may be unable to drain when thermodynamically appropriate. Qualitative analysis led Hunt [89] to conclude that such a situation should have two measurable effects: (1) for a given h value the moisture content is too high, and (2) the excess moisture, being cutoff from the infinite cluster, cannot contribute to K, so that the measured K is lower than the equilibrium value. Because the excess moisture does not contribute to K, $K(h)$ is approximately its equilibrium value while $K(\theta)$ is too small; thus a greater hysteresis would be observed in $K(\theta)$ than in $K(h)$. Because these tendencies are the opposite from what is observed in experiment, this scenario cannot be correct. To explain this discrepancy, Hunt [89] suggested that film flow could be responsible. That argument hinges on an analysis of the total distance that water would have to flow through films. It was shown that, above the percolation threshold, this distance is only a few pore lengths because this distance is not a function of the variable $p - p_c$ ($\theta - \theta_t$ in continuum percolation). Below the percolation threshold this distance can be represented as the system size x, minus the correlation length χ, and it increases rapidly with diminishing θ. But above the percolation threshold, the microscopic distances required, and the lack of a critical dependence, tend to mitigate the low value of film flow. Thus the disconnected pores *can* drain, though with some delay which is weakly dependent on the moisture content. This argument can break down, however, if too little time is allowed. In fact, under those conditions a reversal of the usual tendencies does occur: time-dependent effects are larger in $K(\theta)$ than in $K(h)$, and $K(\theta)$ for a given θ diminishes progressively with increasing drainage rates [90].

3.5 Hydraulic and Transport Properties

The basic science of fluid flow in porous media is based on the Navier–Stokes equation, although the treatment might be more accurate if interactions between the water and the particles were included. Nevertheless, for our purposes it is not necessary to consider the full Navier–Stokes equation, because when velocity advection is not important (low Reynolds numbers, laminar flow) the Navier–Stokes equation is equivalent to linear response. In the porous media community, this linear response – the flow is proportional to the pressure gradient – is known as Darcy's law. In the case that Darcy's law is valid, the hydraulic conductivity K is defined to be the total volume of water transported per unit time, divided by the product of the cross-sectional area of the flow and the pressure gradient. If the pressure is expressed as an *equivalent* capillary rise, $h \equiv P/\rho g$, then the pressure gradient is unitless and K is a volume of flow per unit cross-sectional area per unit time, which has units of length per time. Expressing the units of K as $\mathrm{cm\,s^{-1}}$ gives a measure

of how fast water with a given depth can "infiltrate" into the soil, and also gives an estimate of the pore-scale water velocity. Conveniently, gravity flow in a column of arbitrary height, with no water ponded on the surface, produces what is called a unit gradient, i.e., a pressure gradient $h/h = 1$.

It is often objected that Darcy's law cannot be applied at the pore scale (Darcy's experiments used meter-scale samples), but the validity of linear response is not scale-dependent. Such comments probably arise from the general failure of "upscaling" techniques for the hydraulic conductivity. But it is also well known that the flow at the pore scale follows a kind of generalized Poiseuille behavior, that is,

$$Q \propto \Delta P \frac{r^4}{\mu l} \tag{3.24}$$

In this expression Q is the total fluid flow (in volume per second), ΔP is the pressure difference across the pore, μ is the viscosity, r is the effective radius, and l the effective length of the pore. For right circular cylinders the numerical coefficients are well known, and r and l can be treated as the actual radius and length of the cylinder. In this case the hydraulic *conductivity* of the pore is $K \propto r^2$, but the hydraulic *conductance* of the pore is proportional to r^4/l, a critical difference in perspective. In the general case the numerical values can be obtained by modeling the flow using the Navier–Stokes equation, and such flow is typically called Poiseuille flow. The key point is that for a given pore shape, the numerical coefficients do not depend on the size of the pore, as long as the linear regime (low Reynolds number) is maintained. Considering typical pore radii in the micron to millimeter range, and typical flow velocities less than $10^{-3}\,\mathrm{cm\,s^{-1}}$, one finds Reynolds numbers as low as 10^{-5}, and the linear approximation is seldom in jeopardy [1].

When one desires a flow function which is purely a property of the medium, one can multiply K by the viscosity and divide by the density, eliminating specific properties of the fluid. The resulting function is called the permeability and has units of length squared.

If the same pore is filled with a fluid of electrical conductivity σ_0, and a potential difference ΔV is applied, the total current passing through such a pore is

$$I \propto \Delta V \sigma_0 \frac{r^2}{l} \tag{3.25}$$

Thus the conductance of the pore is proportional to $\sigma_0 r^2/l$. The correct means to "upscale" the hydraulic and electrical conductivities are discussed in the next two chapters; here we describe the general state of upscaling in the porous media literature.

Consider the simplified regular porous medium from the beginning of this chapter. Some fundamental relationships for the hydraulic conductivity and the electrical conductivity of such idealized media can be readily obtained by scaling. The electrical conductivity must be independent of the sphere size, because the conductance of each pore is proportional to its radius r, while the number of connected paths is proportional to r^{-2} and the number of pores along each identical path is proportional to

$1/r$. Thus the resistivity $\rho \propto r^2/(r)(r)$ is independent of r. On the other hand, the hydraulic conductivity of this medium would be proportional to r^2, since the hydraulic conductance of each pore is proportional to r^3 and the other quantities have the same behavior as for the electrical conductivity. This conclusion for the hydraulic conductivity is sometimes referred to as Miller–Miller similitude [52]. In general, formulations for the saturated hydraulic conductivity, K_S, conform to this conclusion: K_S is ordinarily stated to be proportional to the square of the radius of some "characteristic" pore [even in the Katz and Thompson [110] critical path analysis], consistent with permeability having units of length squared. Theoretical approaches differ mainly in what particular pore size is "characteristic" of the medium. It is typically assumed in the porous media community that, by analogy, the ratio of the unsaturated to the saturated hydraulic conductivity should also be the square of the ratio of the relevant characteristic pore sizes, but this is not the case.

Many treatments of the electrical and hydraulic conductivity have been based on "bundle of capillary tubes" model discussed in Sect. 3.2.4. In its simplest form, this model represents the medium as a collection of right circular cylinders, all of the same length, and occurring with a frequency that gives the same volume pdf as the medium. Pressure–saturation relationships are derived by assuming that all tubes with radius $r < A/h$ are filled with water (regardless of height!), while larger tubes are empty: allowability is considered but accessibility is not. Hysteresis is related to the history-dependence of the water–solid contact angle in a long straight tube, which has negligible impact on hysteresis in real soils. The hydraulic conductivity is then calculated as the arithmetic mean conductivity of all the tubes (both air- and water-filled), an indefensible scheme. Additional "physics" may be added in the form of misalignment of tubes, variable tube radii to generate the inkbottle effect, tortuosity, etc. The culmination of this model is probably the generalized Kozeny–Carman equation of Wyllie and Gardner [27], which "implicitly contained twelve adjustable parameters" [12]. Most authors admit that the bundle of capillary tubes model can tell them nothing about transverse dispersion (spreading of contaminants in a direction perpendicular to the water flow), but attempts have been made to relate the longitudinal dispersion to the distribution of velocities in the various tubes. Because the distribution of velocities in a real medium must relate to distributions of paths of varying capacity, each of which passes through some range of pore sizes, the bundle of capillary tubes model cannot predict longitudinal dispersion with any validity. And yet, a recent publication [91] endorsed by the National Research Council of Canada recommended abandoning models that are over 100 years old, turning instead to the modern science of models based on the bundle of capillary tubes.

The general understanding of "upscaling the hydraulic conductivity" from the pore scale is that, given a pore size distribution transformed into a bundle of capillary tubes, an arithmetic mean is appropriate for averaging. "Cut and rejoin" modifications, which connect two different radii with a single tube, change the weighting function in the averaging to a joint probability distribution (e.g., [28, 92]). Upscaling procedures for geologic scales have been proposed and followed with no apparent physical basis and no demonstrable correspondence to reality. Rather, these procedures follow from the observation that a collection of resistors in parallel produces an arithmetic mean conductance, while a collection of resistors in series is

equivalent to a harmonic mean. The first case corresponds conceptually to a critical percolation probability of zero (as in a bundle of tubes model, each individual element of the medium may be regarded as connecting both sides), while the second corresponds directly to a critical percolation probability of one. The arithmetic mean conductance of a collection of conductances is

$$< g_a >= \left[(1/N)\sum (g_i)^1\right]^1 \tag{3.26}$$

while the harmonic mean is

$$< g_h >= \left[(1/N)\sum (g_i)^{-1}\right]^{-1} \tag{3.27}$$

Scheibe and Yabusaki [93] argued that the upscaled hydraulic conductivity must lie somewhere between the harmonic and the arithmetic mean, and that the appropriate upscaling condition would be consistent with power-law averaging [94, 95],

$$< g >= \left[(1/N)\sum (g_i)^{-z}\right]^{z} \tag{3.28}$$

choosing some exponent z in $-1 < z < 1$. They then used extensive modeling to try to identify trends of the exponent z. It is true that for any specific case, some value of z in Eq. (3.28) must yield the appropriate value of $< g >$. However, their conclusion does not follow, as there is no particular reason why the averaging must follow any power law. We will return to this point below.

Here are two results of capillary bundle models, presented without the details of the derivations [[91, 96] respectively].

$$K = C\frac{g}{\nu_{\mathrm{w}}}\left(\frac{e}{A/V}\right)^2 \phi \quad \text{or} \quad K = \frac{D_{\mathrm{r}}^2 \phi^3}{72\tau(1-\phi)^2} \tag{3.29}$$

In the second expression, D_{r} is the diameter of a "characteristic" pore, and τ is a tortuosity (ratio of path length to Euclidean or straight-line distance). In the first expression, g is the acceleration due to gravity, e is the void ratio ($e \equiv \phi/(1-\phi)$), ν_{w} is the kinematic viscosity, and A/V is the specific surface area of the solid component. The inverse of A/V is proportional to a pore size and arises from consideration of a "wetted radius," while e is a measure of porosity. Both expressions therefore contain both a pore size squared and a porosity cubed, features common to relationships in the Kozeny–Carman tradition [24, 26].

Given the current understanding of the permeability (or hydraulic conductivity) of porous media, there are no exact results for media with an arbitrary microstructure. As a consequence there has been some interest in developing upper and lower bounds of the hydraulic conductivity and exact solutions of simplified problems. A summary of such results is given by Sahimi [97, 98]. These results include slow fluid flow through a dilute cubic array of non-permeable spheres by the Stokes equation [99]; an extension of this result to all three types of cubic lattices [100]; the

same problem using a transformation to a set of Fredholm's integral equations of the first kind [101]; harmonic expansions in spherical coordinates for cubic packings [102]; and treatments of [103–105] (corrected by [106]). Other results are for mixtures in which both components are permeable, including solutions for upper and lower bounds of the hydraulic conductivity [107–109]. Sahimi comments, "in all cases that have been discussed so far [several more than those mentioned here], the Kozeny–Carman empirical formula falls within 15% of the results for at least one of the three types of periodic packings if [the porosity is less than half]" (1993). On the other hand, in disordered media the Kozeny–Carman prediction of K came in dead last when compared with treatments by Katz and Thompson [110] , Johnson and Schwartz [111], and Bernabe and Revil [112], missing the numerically verified result by orders of magnitude [113].

We mention here the upper bound, k_0, on the permeability of a collection of solid spheres [114], given as

$$k_0 = \frac{2}{9}\frac{< r^3 >^2}{(1-\phi) < r >^2} \approx \frac{2}{9}\left(\frac{5-D_s}{6-D_s}\right)^2 \left[1+2\left(\frac{r_0}{r_m}\right)^{5-D} - 2\left(\frac{r_0}{r_m}\right)^{6-D}\right] \frac{r_m^2}{1-\phi} \tag{3.30}$$

Here r refers to the particles, i.e., the solid space. The expression is written explicitly for the Rieu and Sposito model, and the result for k_0 is, asymptotically in the "polydisperse limit" (large range of sizes), a constant factor of the square of the largest particle size, r_m. r_m will typically be proportional to the maximum pore radius, with the proportionality constant a diminishing function of the porosity; however, neither ϕ nor $(1-\phi)$ to a negative power is such a function. Clearly Eq. (3.30) is larger than Kozeny–Carman treatments, consistent with its being an upper bound. The Stokes dilute-limit permeability follows the same general form Torquato and Lu [114], with slightly different second and third terms in the square brackets. These dilute-limit results do not apply in the limit of small porosity, where the permeability must vanish. But k_0, as in the various theoretical approaches summarized in Bernabe and Bruderer [113], is proportional to the square of a maximum radius. This kind of result is generated by critical path analyses as well [110, 115]. It is interesting that Eq. (3.30) as well as Eq. (3.29) tend to produce factors of $1-\phi$ in the denominator, but Eq. (3.30), unlike Eq. (3.29), does not produce a proportionality to ϕ in the numerator.

In strongly disordered media, the weighting function that is applied to local conductivities to generate the system conductivity is not monotonic in the conductivity. The weighting function thus cannot be consistent with a power-law averaging. This has been verified both in solid state applications (see [116, 117]) and for fluid flow in porous media [113]. This nonmonotonicity occurs because the quasi-1D paths, along which the optimal conduction occurs, are dominated by the largest resistances on these paths. Smaller resistances in series are so much smaller that they do not contribute substantially to the total resistance; larger resistances in parallel are never encountered. As stated by Bernabe and Bruderer, the pressure field for strongly disordered media is controlled by a few large potential drops due to the

critical elements (bottlenecks), making stochastic (small-disorder = homogeneous in the mean) treatments unappealing. Only approaches that are based on percolation theory are consistent with this observation.

Many empirical relationships for unsaturated hydraulic conductivity have also been proposed. The widely used phenomenology due to van Genuchten [34–36] is

$$\frac{K(\theta)}{K_S} = \left(\frac{\theta - \theta_r}{\phi - \theta_r}\right)^{1/2} \left[1 - \left(1 - \left[\frac{\theta - \theta_r}{\phi - \theta_r}\right]^{1/m}\right)^m\right]^2 \tag{3.31}$$

θ_r is intended to represent the lowest moisture content reached. Here the square on the outer brackets is intended to be consistent with the contention that the hydraulic conductivity should be proportional to the square of the "characteristic" pore radius, as in the above discussion of the saturated hydraulic conductivity K_S. In the van Genuchten phenomenology one can also represent K as a function of h:

$$\frac{K(h)}{K_S} = \left[\frac{1}{1 + \left(h/h_A\right)^n}\right]^{\frac{m}{2}} \left[1 - \left(\frac{1}{1 + \left(h/h_A\right)^n}\right)^m\right]^2 \tag{3.32}$$

A graphical comparison of Eq. (3.31) with the results for K from critical path analysis (next chapter) is given in Fig. 3.12. The van Genuchten equation produces a sigmoidal curve, as is typically observed for the (logarithm of the) hydraulic conductivity as a function of saturation. It is often assumed that $m = 1 - 1/n$; this relationship was applied in Fig. 3.12. These parameters are known to have some relationship with the pore size distribution, but the community has been unable to discover the form of the relationship. The relationship between m and n relates the

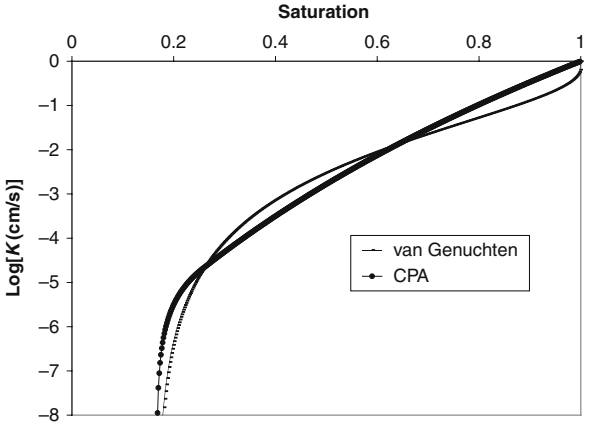

Fig. 3.12 A comparison of the hydraulic conductivity as a function of saturation by percolation theoretical means and using the van Genuchten empirical function. Note that the van Genuchten function tends to a vertical slope at complete saturation, in contrast to the result from percolation theory (critical path analysis). This will accommodate, as will be seen, the tendency for soil structure to enhance K strongly right near saturation

curvatures at large and small saturations. We show later that these curvatures must be related, because percolation constraints on the air (water) phase must affect the limits at large (small) saturations. The air and water critical volume fractions appear to be equal for coarse soils, but not for soils with high clay content.

A number of problems exist with the van Genuchten relationship (Eq. (3.31)). The argument of the first factor, known as the tortuosity/connectivity factor, has a dependence on the moisture content consistent with percolation theory, but the power of 1/2 is far from the appropriate value of 2 [118, 119]. Meanwhile, the second factor is obtained through a simple arithmetic averaging procedure, which as noted is only appropriate with perfect connectivity. Perfect connectivity requires a critical volume fraction of zero, which should be reflected in the first (connectivity) factor. But zero critical volume is inconsistent with an adjustable residual moisture content [120]. These inconsistencies make the phenomenology capable of matching almost any experimental result. The cherished flexibility has been obtained at the cost of predictive science.

The porous media community broadly recognizes that there is a relationship between the slope of the pressure–saturation curve $\mathrm{d}\theta/\mathrm{d}h$, and that of the hydraulic conductivity as a function of saturation $\mathrm{d}K(\theta)/\mathrm{d}\theta$. On the other hand, the community is also devoting considerable effort to relating the air flow as a function of saturation to the pore size distribution. Both theory and experiments demonstrate that this dependence is weak at best, but this has not become common knowledge.

3.6 Some Notes on Experimental Procedures

We start with an extended quote from a description [121] of an experiment to measure $K(h)$ and $h(\theta)$.

> The experimental setup [...] includes a constant-head [h] water supply, a flow cell, tensiometers [devices to measure the tension, h], and a constant-head outflow system. In general typical flow cells for the samples are ≈ 10.2 cm in diameter and 15.7 cm in length. The system governing the constant-head water supply to the inlet is a Mariotte flask (influent reservoir). The outlet tubing is put through a rubber stopper at the top of a 50-mL burette to maintain the head at a constant level by fixing the location of the drip point on the outflow end. The flow cell contains end caps, fitted with porous ceramic plates, sealing the ends of the container (using rings) with inlet/outlet valves in each cap. Built into the sides of the flow cell are two tensiometer ports used to house tensiometer-transducer systems. Approximately 15 cm of tubing is attached to the small bleed ports on each end of the flow cell. During operation, water is forced through the bleed ports across the ceramic plates and out the inflow/outflow ports to remove air from between the porous plate and the plastic end cap. The heights of the Mariotte bottle and lower burette are adjusted to create a uniform pressure head within the sample. At pressure heads of -100 cm or more, a vacuum system [...] is used. Starting at near saturation, a series of unit gradient flows are established at progressively decreasing (i.e., more negative) pressure heads in the soil. At each flow the pressure heads in the tensiometers and the volumetric flow rate through the sample are measured. The procedure is repeated until the most negative value of the desired pressure head is reached. Depending on individual samples, experimental run times varied from $\approx$ 2–6 weeks; the average being ≈ 5 weeks per sample.

While details of this discussion may be obscure for physicists, some fundamental issues are clear. First, when flow must proceed through both the sample and the ceramic end plates, the flux of water through the system can in principle be limited by either the hydraulic conductivity of the sample or that of the plates. If, in addition, the time is limited for the equilibration of the sample at a new value of h, a limitation is, in principle, being set on the minimum hydraulic conductivity measurable. This combination can generate a situation where measured values of the moisture content and K are both too high for a given h: the moisture does not have time to leave, and K is an increasing function of the moisture content. Finally, the porous media community does not generally trust statements that the pressure head is uniform within the sample. The tendency is therefore to invest effort into generating volume models where $h = h(z)$ (z = height), while using the above phenomenological relations to describe local water rearrangements. It will turn out (Chap. 7) that use of percolation theory on models without a z-dependence (effectively 0D models) describes the limitations of the experiments due to lack of equilibration, much better than the usual column models with the inaccurate phenomenologies in common use. This is perhaps not surprising, as it has already been demonstrated [122] that increasing the sophistication of percolation theory to treat spatial gradients of p (invasion and gradient percolation) does not lead to significantly better treatments of wetting fronts and hysteresis than ordinary percolation theory.

3.7 One Example from Living Organisms

A recent publication [123] illustrates that the concepts of physical porous media translate directly to biological media, in particular, apples and pears. While we had not intended to discuss such media, Verboven et al. [123], address the influences of the same fundamental characteristics (porosity, pore size, connectivity) on flow and diffusion properties as are recognized in, e.g., soils. These physical properties are currently being investigated with synchrotron radiation X-ray tomography, just as physical porous media. Further, the diffusion differences in apples and pears produce the well-known contrasts in spoilage, bringing out a broader relevance. Delivery of oxygen to internal cells through water-free intercellular voids is essential to prevent spoilage. Apples may be stored a long time, while pears have a very short shelf life. Figure 3.13 shows the contrast between the pore space in apples and pears, and is included partly because of its visual similarity with such images in physical media. We quote from Verboven et al. [123]:

> Our understanding of the gas exchange mechanisms in plant organs critically depends on insights in the three-dimensional structural arrangement of cells and voids. Using synchrotron X-ray tomography, we obtained for the first time high-contrast 3-D absorption images of in vivo fruit tissues of high moisture content at 1.4 μm resolution.

Note that the resolution quoted is also very similar to 5 μm, as given in Sect. 3.2.2.

> Voids between apple parenchyma form an incompletely connected network (Fig. 3.14a) confirming previous results [124] but now with much better contrast and resolution. Void

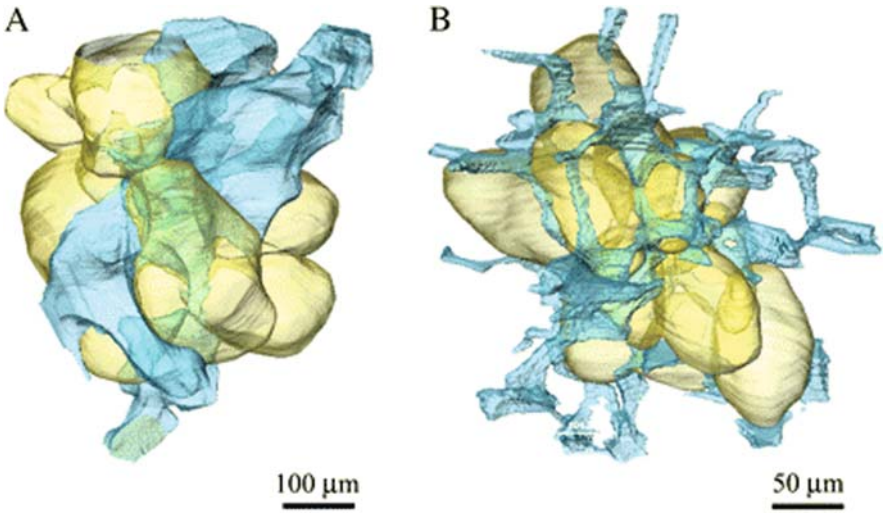

Fig. 3.13 (Reprinted with permission from Verboven et al. [123]) Void space of an apple (**A**) and pear (**B**). Note the difference in appearance, with the pear pores being long and thin. In color, the pore space is *blue*

spaces can be long and may stretch over several hundreds of micrometers in the tissue. These voids do not connect or split, but are surrounded by smaller individual voids without preferential direction. On the equator of the apple fruit where the samples were taken, the axes of the long voids in the cortex tissue are preferentially oriented in the radial direction into the fruit. In contrast, although the void fraction of pear is very small, the pores form a complete network throughout the cortex sample without preferential direction (Fig. 3.14b).

The most significant difference between apples and pears is in the "void fraction" (porosity) and the values given are 5.1% for pear cortex and 23.0% for apple. Since Verboven et al. [123] look for a linear dependence of diffusion on porosity, they

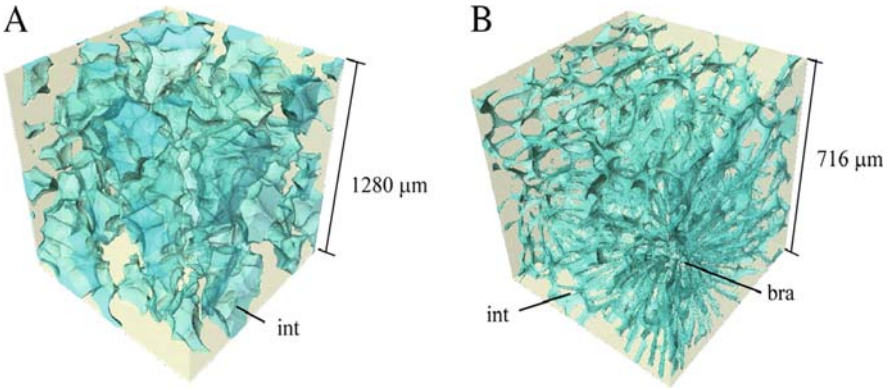

Fig. 3.14 (Reprinted with permission from Verboven et al. [123]). Void space in an apple (**A**) and a pear (**B**)

interpret the large difference in oxygen diffusion rates in terms of the other differences between pears and apples, that is, connectivity and pore sizes. In fact, as we will see in Chap. 6, it may be possible that the differences in gas diffusion between apples and pears can be understood solely in terms of the differences in porosity.

Problems

3.1. Remember that pumice (specific gravity of the solid portion typically about 2.65) may float on water. Does this mean that the holes in pumice cannot be connected? Use the Scher and Zallen results (Chap. 1) to set an upper limit on the porosity of a regular pumice, for which all the "holes" are the same size. Assume that the holes are spherical. What lattice would you choose for this calculation?

3.2. Assuming a solid material density of 2.65, calculate the minimum porosity required for the condition that pumice float. Is the Scher and Zallen result useful as a predictor? In a fractal model the porosity of a medium may approach 1. Do you expect that the holes in pumice (due to gas bubbles) are of uniform size, or highly variable?

3.3. If the holes in pumice are due to gas bubbles, did the gas escape? How? Can the relevant porosities for these questions be the porosity not accessible to an infinite cluster instead of the bulk porosity?

3.4. Suppose that the pumice was formed in a violent explosion that resulted when the gas bubbles "percolated." What sort of size distribution of pieces of pumice would you expect to find?

References

1. Bear, J., 1972, *Dynamics of Fluids in Porous Media*, American Elsevier Publishing Co. Inc., New York. 57, 83
2. Dullien, F.A.L. 1992. *Porous Media, Fluid Transport and Pore Structure*. Academic, London. 57
3. Warrick, A. A., 2002, *Soil Physics Companion*, CRC Press, Boca Raton. 57, 60, 76
4. Marshall, T. J., J. W. Holmes, and C. W. Rose, 1996, *Soil Physics*, 3rd edition, 469 pages ISBN:0521451515 | ISBN13:9780521451512. 57, 60, 65
5. Hillel, D., 1998, *Environmental Soil Physics*, Academic Press. (Elsevier?), San Diego, CA 57
6. Sahimi, M., 1995, *Flow and Transport in Porous Media and Fractured Rock from Classical Methods to Modern Approaches*, Wiley VCH Weinheim, Germany, 500 pp. 57
7. Surkov, V. V., and H. Tanaka, 2005, Electrokinetic effect in fractal pore media as seismoelectric phenomena, in: *Fractal Behavior of the Earth System*, Ed. V. P. Dimri, Springer, Heidelberg. 57
8. Sen, P. N., C. Scala, and M. H. Cohen, 1981, A self-similar model for sedimentary rocks with application to the dielectric constant of fused glass beads, *Geophysics* **46**: 781–795. 57
9. Krohn, C. E., and A. H. Thompson, 1986, Fractal sandstone pores: automated measurements using scanning-electron-microscope images, *Phys. Rev. B* **33**: 6366–6374. 57
10. Katz, A. J., and A. H. Thompson, 1985, Fractal sandstone pores: implications for conductivity and pore formation, *Phys. Rev. Lett*. **54**: 1325–1328. 57, 73

11. Turcotte, D. L., 1986, Fractals and fragmentation. *J. Geophys. Res*. **91**: 1921–1926. 57, 69
12. Thompson, A. H., A. J. Katz, and C. E. Krohn, 1987, Microgeometry and transport in sedimentary rock, *Adv. Phys*. **36:** 625. 57, 84
13. Balberg, I., 1987, Recent developments in continuum percolation, *Philos. Mag. B* **30**: 991–1003. 57
14. de Gennes, P. G., 1985, *Phys. of Disordered Materials*, Adler, D., H. Fritzsche, and S. R. Ovshinsky (eds.) Plenum Press, New York. 57
15. Tyler, S. W., and S. W. Wheatcraft, 1990, Fractal processes in soil water retention. *Water Resour. Res*. **26**: 1045–1054. 58, 72
16. Tyler S. W., and S. W. Wheatcraft, 1992, Fractal scaling of soil particle-size distributions – analysis and limitations, *Soil Sci. Soc. Am. J*. **56**: 362–369. 58, 65
17. Rieu, M., and G. Sposito, 1991, Fractal fragmentation, soil porosity, and soil water properties I. Theory, *Soil Sci. Soc. Am. J*. **55**: 1231. 58, 69, 73, 77
18. Bittelli, M., G. S. Campbell, and M. Flury, 1999, Characterization of particle-size distribution in soils with a fragmentation model. *Soil Sci. Soc. Am. J*. **63**: 782–788. 58, 68
19. Bird, N. R. A., E. Perrier, and M. Rieu, 2000, The water retention function for a model of soil structure with pore and solid fractal distributions, *Eur. J. Soil Sci*., **51**: 55–63. 58, 73
20. Gimenez, D., E. Perfect, W. J. Rawls, and Ya A. Pachepsky, 1997, Fractal models for predicting soil hydraulic properties: a review, *Eng. Geol*., **48**: 161–183. 58
21. Filgueira, R. R., Ya. A. Pachepsky, L. L. Fournier, G. O. Sarli, and A. Aragon, 1999, Comparison of fractal dimensions estimated from aggregate mass-size distribution and water retention scaling, *Soil Sci*. **164**: 217–223. 58, 69, 73
22. Freeman, E. J., 1995. *Fractal Geometries Applied to Particle Size Distributions and Related Moisture Retention Measurements at Hanford, Washington*, M. A. Thesis, University of Idaho, Moscow. 58, 72
23. Baveye, P., J.-Y. Parlange, and B. A. Stewart (ed.), 1998, *Fractals in Soil Science*, CRC Press, Boca Raton, FL. 58
24. Kozeny, J., 1927, Ueber Kapillare Leitung des Wasssers im Boden, *Sitzungsber. Adak. Wiss. Wien*, **136**: 271–306. 58, 85
25. Childs, E. C., and N. Collis-George, 1950, The permeability of porous materials, *Proc. Royal Soc. London, Ser. A* **201**: 392–405. 58
26. Carman, P. C. 1956, *Flow of Gases Through Porous Media*, Butterworths, London. 58, 85
27. Wyllie, M. R. J., and G. H. F. Gardner, 1958, World Oil (March and April Issues), p. 2. 58, 84
28. Millington, R. J., and J. P. Quirk, 1959, Permeability of porous media. *Nature* (London) **183**: 387–388. 58, 84
29. Millington, R. J., and J. P. Quirk, 1961, Permeability of porous media, *Trans. Faraday Soc*. **57**: 1200–1208. 58
30. Brooks, R. H., and A. T. Corey, 1964, Hydraulic properties of porous media, Colorado State Univ. Hydrology Paper 3. 58, 77
31. Mualem, Y., 1976, A new model for predicting the hydraulic conductivity of unsaturated porous media, *Water Resour. Res*. **12**: 513–522. 58, 113
32. Mualem, Y., 1976. A catalogue of the hydraulic properties of unsaturated soils, Res. Proj. No. 442, Technion, Israel Institute of Technology, Haifa. 58, 113
33. Mualem,Y., and G. Dagan, 1978, Hydraulic conductivity of soils: unified approach to the statistical models, *Soil Sci. Soc. Am. J*. **42**: 392–395. 58, 113
34. van Genuchten, M. T., 1980, A closed form equation for predicting the hydraulic conductivity of unsaturated soils, *Soil Sci. Am. J*., **44**: 892–898. 58, 87
35. Luckner, L., M. Th. van Genuchten, and D. R. Nielsen, 1989, A consistent set of parametric models for the two-phase flow of immiscible fluids in the subsurface, *Water Resour. Res*. **25**: 2187–2193. 58, 87
36. van Genuchten, M. Th., F. J. Leij, and S. R. Yates, 1991, The RETC code for quantifying the hydraulic functions of unsaturated soils, US EPA 000/091/000, ADA OK, 83 pp. 58, 79, 87
37. Hassanizadeh, S. M., and W. G. Gray, 1993, Toward an improved description of two-phase flow, *Adv. Water Res*. **16**: 53–67. 58

38. Burdine, N. T., 1953, Relative permeability calculations from pore-size distribution data. *Petrol. Trans. Am Inst. Min. Eng*. **198**: 71–77. 58
39. Ewing, R. P., 2004, Soil water potential (I), *Soil Physics Lecture Notes*, http://www.agron.iastate.edu/soilphysics/a577pot1.html 60, 75
40. Danielson, R. E. and P. L. Sutherland, 1986, Porosity, pp. 443–461 in A. Klute (ed.), Methods of Soil Analysis. Part 1. Agron. Monogr. 9 (2nd ed.), ASA and SSSA, Madison, WI. 60
41. Lindquist, W. B., 2002, Network flow model studies and 3D pore structure, *Contemp. Math*. **295:** 355–366. 60, 67
42. Vogel, H.-J., 2002, Topological characterization of porous media. *In* K. R. Mecke and D. Stoyan (eds.), *Lecture Notes in Physics 600*, pp. 75–92, Springer-Verlag, Berlin. 60
43. Silin, D., and T. Patzek, 2006, Pore space morphology analysis using maximal inscribed spheres, *Physica A*. **371**: 336–360. 60
44. Ham, K., H. Jin, R. Al-Raoush, X. G. Xie, C. S. Willson, G. R. Byerly, L. S. Simeral, M. L. Rivers, R. L. Kurtz, and L. G. Butler, 2004, Three-dimensional chemical analysis with synchrotron tomography at multiple x-ray energies: brominated aromatic flame retardant and antimony oxide in polystyerene, *Chem. Mater*. **16**: 4032–4042. 61
45. Lehmann, P., P. Wyss, A. Flisch, P. Vontobel, M. Krafczyk, A. Kaestner, F. Beckmann, A Gvgi, and H. Fluhler, 2006, Tomographical imaging and mathematical description of porous media used for the prediction of fluid distribution, *Vadose Zone J*. **5**: 80–97. 61
46. Glantz, R., and M. Hilpert, 2007, Dual models of pore spaces, *Adv. Water Resour*. **30**(2): 227–248. 61, 68
47. Mohanty, K. K, H. T. Davis, and L. E. Scriven, 1987, Physics of oil entrapment in water-wet rock. *SPE Reserv. Eng*. **2:** 113–128. 61
48. Weisstein. E. W., 2003, Hexagonal Close Packing. From *MathWorld*–A Wolfram Web Resource. http://mathworld.wolfram.com/HexagonalClosePacking.html 61, 62
49. Finney, J. L., 1970, Random packings and the structure of simple liquids I. The geometry of random close packing. *Proc. Roy. Soc. London A* **319**: 479–494. 62
50. Al-Raoush R., K. Thompson, and C. S. Willson, 2003, Comparison of network generation techniques for unconsolidated porous media, *Soil Sci. Soc. Am. J*. **67**: 1687–1700. 62
51. Scher, H., and R. Zallen, 1970, Critical density in percolation processes, *J. Chem. Phys*. **53:** 3759. 63
52. Miller, E. E., and R. W. Miller, 1956, Physical theory for capillary flow phenomena, *J. Appl. Phys*., **27**: 324–332. 63, 84
53. Fatt, I., 1956, The network model of porous media, *Trans. Am. Inst. Min. Metall. Pet. Eng*., **207**: 144–177. 63
54. Eshel, G., G. J. Levy, U. Mingelgrin and M. J. Singer, 2004, Critical evaluation of the use of laser diffraction for particle-size distribution analysis, *Soil Sci. Soc. Am. J*. **68**:736–743. 64
55. Raine, D. A., and J. S. Brenizer, 1997, The analysis and correction of neutron scattering effects in neutron imaging, *Mater. Eval*. **55**: 1174–1178. 64
56. Tija, J. S., and P. V. Moghe, 1998, Analysis of 3-D microstructure of porous poly(lactide-glycolide) matrices using confocal microscopy, *J. Biomed. Mater. Res*. **43**: 291–299. 64
57. MacDonald, I. F., G. D. Yadav, I. Chatzis, amd F. A. L. Dullien, 1988, 2-phase flow in porous media – obtaining sharp digitized images of serial sections for subsequent quantitative analysis, *J. Microscopy – Oxford*, **150**: 191–198. 64
58. Peth, S., R. Horn, F. Beckman, T. Donath, J. Fischer, and A. J. M. Smucker, 2008, Three-dimensional quantification of intra-aggregate pore-space features using synchrotron radiation-based microtomography, *Soil Sci. Soc. Am. J*. **72**: 897–907. 64
59. Arya, L. M., and J. F. Paris, 1981, A physicoempirical model to predict the soil moisture characteristic from particle size distribution and bulk density data, *Soil Sci. Soc. Am. J*. **45**: 1023–1080. 65, 72
60. Gvirtzman, H., and P. V. Roberts, 1991, Pore scale spatial analysis of two immiscible fluids in porous media. *Water Resour. Res*. **27**: 1167. 65, 72
61. Gee, G. W., and J. W. Bauder, 1986, Particle-size analysis, pp. 383–411. *In* A. Klute. (ed.) *Methods of Soil Analysis. Part 1*. 2nd ed. Agron. Monogr. 9. ASA and SSSA, Madison, WI. 66

62. Fatt, I., 1956, The network model of porous media. *Petrol. Trans. AIME* **207**: 144–181. 67
63. Lago, M., and M. Araujo, 2001, Threshold pressure in capillaries with polygonal cross-section, *J. Colloid Interface Sci*. **243**: 219–226. 67
64. Camassel, B., N. Sghaier, M. Prat, and S. Ben-Nasrallah, 2005, Evaporation in a capillary tube of square cross-section: application to ion transport, *Chem Eng Sci. 60*: 815–826. 67
65. Lindquist, W. B., 2006, The geometry of primary drainage, *J. Colloid and Interface Science*, **296**: 655–668. 67
66. Toledo, P. G., L. E. Scriven, and H. T. Davis, 1989, Pore space statistics and capillary pressure curves from volume controlled porosimetry, *Paper SPE 19618, 64th Ann. Tech. Conf. and Exhib. of the SPE*, Oct. 8–11, San Antonio, Texas. 67
67. Hilpert, M., C. T. Miller, and W. G. Gray, 2003, Stability of a fluid-fluid interface in a biconical pore segment, *J. Colloid Interface Sci* **267**: 397–407. 67
68. Bakke, S., and P-E. Øren, 1997, 3-D pore-scale modelling of sandstones and flow simulations in the pore networks, *SPE J*. **2**: 136–149. 67
69. Knackstedt, M. A., A. P. Sheppard, and M. Sahimi, 2001, Pore network modelling of two-phase flow in porous rock: the effect of correlated heterogeneity, *Adv. Water Res*. **24:** 257–277. 67
70. Chatzis, I. and F. A. L. Dullien, 1977, Modelling pore structures by 2-D and 3-D networks with application to sandstones, *Can. J. Petrol. Tech*. **16**: 97–108. 67
71. Levine, S., P. Reed, G. Shutts, and G. Neale, 1977, Some aspects of wetting/dewetting of a porous medium, *Powder Tech*. **17:** 163–181. 67
72. Wu, Q., M. Borkovec, and H. Sticher, 1993, On particle-size distributions in soils, *Soil Sci. Soc. Am. J*. **57**: 883–890. 68
73. Posadas, A. N. D., D. Gimenez, M. Bittelli, C. M. P. Vaz, and M. Flury, 2001, Multifractal characterization of soil particle-size distributions. *Soil Sci. Soc. Am. J*. **6**5: 1361–1367. 68
74. Hunt, A. G., and G. W. Gee, 2002, Water retention of fractal soil models using continuum percolation theory: tests of Hanford site soils, *Vadose Zone J*, **1:** 252–260. 69, 71, 72
75. Bird, N. R. A., E. Perrier, and M. Rieu, 2003, The water retention function for a model of soil structure with pore and solid fractal distributions. *Eur. J. Soil Sci*. **51**: 55–63. 69
76. Mandelbrot, B. B., 1983, *The Fractal Geometry of Nature*, W. H. Freeman, San Francisco. 70
77. Jullien, R. and R. Botet, 1987, *Aggregation and Fractal Aggregates*, World Scientific, Singapore. 70
78. Nigmatullin, R. R., L. A. Dissado, and N. N. Soutougin, 1992, A fractal pore model for Archie's law in sedimentary rocks, *J. Phys. D. Appl. Phys*. **25**: 32–37. 73
79. Hunt, A. G., 2007, Comments on "Fractal Fragmentation, Soil Porosity, and Soil Water Properties: I. Theory", *Soil Sci. Soc. Am. J*. **71**:1418–1419. 73
80. Narasimhan, T. N., 2007, Central ideas of Buckingham, 1906: a century later, *Vadose Zone J*. **6**: 687–693. 74
81. Haines, W. B., 1930, Studies in the physical properties of soil: V. The hysteresis effect in capillary properties, and the modes of moisture distribution associated therewith. *J. Agric. Sci*. **20**: 97–116. 74
82. Sears, F. W., and G. L. Salinger, 1975, *Thermodynamics, Kinetic Theory, and Statistical Thermodynamics*, 3rd edition, Addison-Wesley, Reading, MA. 74
83. Cole, K. S., 1941, Dispersion and absorption in dielectrics I. Alternating current characteristics, *J. Chem. Phys*. **9**: 341. 79
84. Havriliak, S., and S. Negami, 1966, Analysis of α-dispersion in some polymer systems by the complex variables method, *J. Polymer Science* (C) **14**, 99–117. 79
85. Wilkinson, D., 1986, Percolation effects in immiscible displacement, *Phys. Rev. A* **34**: 1380–1391. 80
86. Blunt, M. J., and H. Scher, 1995, Pore-level model of wetting, *Phys. Rev. E*, **52**: 6387–403. 81
87. Tokunaga, T., and J. Wan, 1997, Water film flow along fracture surfaces of porous rock, *Water Resour. Res*. **33**: 1287–1295. 81

88. Topp, G. C., A. Klute, and D. B. Peters, 1967, Comparison of water content-pressure head data obtained by equilibrium, steady-state and unsteady state methods. *Soil Sci. Soc. Am. Proc*. **31**: 312–314. 81
89. Hunt, A. G., 2004, Continuum percolation theory for water retention and hydraulic conductivity of fractal soils: 2. Extension to non-equilibrium, *Adv. Water Resour*. **27**: 245–257. 82
90. Wildenschild, D., and J. W. Hopmans, 1999, Flow rate dependence of hydraulic properties of unsaturated porous media, in: *Characterization and Measurement of the Hydraulic Properties of Unsaturated Porous Media*, ed. M. Th. van Genuchten, F. J. Leij, and L. Wu, U.S. Salinity Laboratory, Agricultural Research Service, U.S. Department of Agriculture, Riverside, CA, pp. 893–904. 82
91. Hansen, D., 2004, Discussion of "On the use of the Kozeny-Carman equation to predict the hydraulic conductivity of soils", NRC Research Press Web site at http://cgj.nrc.ca (Appears in *Can. Geotech. J*. **40**: 616–628). 84, 85
92. Marshall, T.J., 1958, A relation between permeability and size distribution of pores, *J. Soil Sci*. **9:** 1–8. 84
93. Scheibe, T., and S. Yabusaki, 1998, Scaling of flow and transport behavior in heterogeneous groundwater systems, *Adv. Water Resour*. **22**: 223–238. 85
94. Deutsch, C. V., 1989, Calculating effective absolute permeability in sandstone/shale sequences, *SPE Form Eval*, **4(3)**: 343–348. 85
95. Desbarats, A., 1992, Spatial averaging of hydraulic conductivity in 3-dimensional heterogeneous porous-media. *Math Geol*. **24**(3): 249–267. 85
96. Amyx, J. W., D. M. Bass, and R. L. Whiting, 1960, *Petroleum Reservoir Engineering. Physical Properties*, McGraw-Hill Book C., New York. 85
97. Sahimi, M., 1993, Fractal and superdiffusive transport and hydrodynamic dispersion in heterogeneous porous media, *Transp. Porous Media* **13**: 3–40. 85
98. Sahimi, M., 1993, Flow phenomena in rocks – from continuum models to fractals, percolation, cellular automata, and simulated annealing, *Rev. Mod. Phys. 65*(4): 1393–1534. 85
99. Hasimoto, H., 1959, On the periodic fundamental solutions of the Stokes equations and their applications to viscous flow past a cubic array of cylinders, *J. Fluid Mech*. **5**(2): 317–328. 85
100. Sangani, A. S., and A. Acrivos, 1983, The effective conductivity of a periodic array of spheres, *Proc. R. Lond. A* **386**: 263–275. 85
101. Zick, A. A. and G. M. Homsy, 1982, Stokes flow through periodic arrays of spheres, pp. 13–26. *J. Fluid Mech*. **115**: 13. 86
102. Larson, R. E., and J. J. L. Higdon, 1989, A periodic grain consolidation model of porous media, pp. 38–46. *Phys. Fluids A* **1**: 38. 86
103. Childress, S., 1972, Viscous flow past a random array of spheres, pp. 2527–2539. *J. Chem. Phys*., **56**: 2527. 86
104. Howells, I. D., 1974, Drag due to the motion of a Newtonian fluid through a sparse random array of small fixed rigid objects, pp. 449–476. *J. Fluid Mech*. **64**: 449. 86
105. Hinch, E. J., 1977, An averaged-equation approach to particle interactions in a fluid suspension, Ref. **83**(4): 695–720. *J. Fluid Mech*., **83**: 695. 86
106. Kim, S., and W. B. Russell, 1985, Modelling of porous media by renormalization of the Stokes equations, pp. 269–286. *J. Fluid Mech*. **154**: 269. 86
107. Prager, S., 1961, Viscous flow through porous media, pp. 1477–1482. *Phys. Fluids* **4**: 1477. 86
108. Weissberg, H. L., and S. Prager, 1962, Viscous flow through porous media. II. Approximate three-point correlation function, pp. 1390–1392. *Phys. Fluids*, **5**: 1390. 86
109. Berryman, J. G., and G. W. Milton, 1985, Normalization constraint for variational bounds on fluid permeability, pp. 754–760. *J. Chem. Phys*. **83**: 745. 86
110. Katz, A. J., and A. H. Thompson, 1986, Quantitative prediction of permeability in porous rock, *Phys. Rev*. *B* **34**: 8179–8181. 84, 86
111. Johnson, D. L., and L. M. Schwartz, 1989, Unified theory of geometric effects in transport properties of porous media. In Paper presented at SPWLA, 30th Annual Logging Symposium, Soc. of Prof. Well Log. Anal. Houston, TX. 86

112. Bernabe, Y., and A. Revil, 1995, Pore-scale heterogeneity, energy dissipation and the transport properties of rocks, *Geophys. Res. Lett*. **22**: 1529–1532. 86
113. Bernabe, Y., and C. Bruderer, 1998, Effect of the variance of pore size distribution on the transport properties of heterogeneous networks, *J. Geophys. Res*., **103**: 513. 86
114. Torquato, S., and B. Lu, 1990, Rigorous bounds on the fluid permeability: effect of polydispersivity in grain size, *Phys. Fluids A* **2**: 487–490. 86
115. Hunt, A. G., and G. W. Gee, 2002, Application of critical path analysis to fractal porous media: comparison with examples from the Hanford site, *Adv. Water Resour.*, **25**: 129–146. 86
116. Pollak, M., 1987, In. *Non-Crystalline Semiconductors*, CRC Press, Boca Raton, FL, Chapter 5ab. 86
117. Mallory, K., 1993, Active subclusters in percolative hopping transport, *Phys. Rev. B* **47**: 7819–7826. 86
118. Gingold, D. B., and C. J. Lobb, 1990, Percolative conduction in three dimensions. *Phys. Rev. B* **42**(13): 8220–8224. 88
119. Clerc, J. P., V. A. Podolskiy, and A. K. Sarychev, 2000, Precise determination of the conductivity exponent of 3D percolation using exact numerical renormalization. *Eur. Phys. J. B* **15**: 507–516. 88
120. Hunt, A. G., 2004, A note comparing van Genuchten and percolation theoretical formulations of the hydraulic properties of unsaturated media, *Vadose Zone J.* **3**: 1483–1488. 88
121. Khaleel, R., and J. F. Relyea, 2001. Variability of Gardner's alpha for coarse-textured sediments. *Water Resour. Res*. **37**: 1567–1575. 88
122. Sahimi, M., and Y. C. Yortsos, 1990, Applications of fractal geometry to porous media: a review, Paper presented at the 1990 Annual Fall Meeting of the Society of Petroleum Engineers, New Orleans, LA. 89
123. Verboven, P., G. Kerkhofs, H. K. Mebatsion, Q. T. Ho, K. Temst, M. Wevers, P. Cloetens, and B. M. Nicolaï, 2008, Three-dimensional gas exchange pathways in pome fruit characterized by synchrotron X-ray computed tomography, *Plant Physiol*. **147**: 518–527. 89, 90
124. Mendoza, F., P. Verboven, H. K. Mebatsion, G. Kerckhofs, M. Wevers, and B. Nicolaï, 2007, Three-dimensional pore space quantification of apple tissue using X-ray computed microtomography, *Planta* **226**: 559–570. 89

Chapter 4
Specific Examples of Critical Path Analysis

At the end of Chap. 2 the general technique of critical path analysis was introduced within the framework of the electrical conductivity of disordered systems. In many systems the charges that move between these sites are electrons, but in some cases they may be ions, or even protons. Critical path analysis will actually form the basis of much of the remainder of this book. However, there are some subtleties to the technique, and its application cannot be so easily generalized as sometimes assumed. To some extent every case or system must be evaluated separately. In typical solid-state applications conductances are connected between sites, which are located randomly in space (why?[1]) meaning that the critical bond fractions from the lattice models of Chap. 1 are not directly applicable. Nevertheless, when transport is locally defined according to the probability per unit time that, say, an electron moves from one clearly defined site to another, then it is clear that the appropriate form of percolation theory to apply is bond percolation, even though one may not know from the results of Chap. 1 what an appropriate bond percolation threshold is. But in porous media it is not initially obvious even which form of percolation theory, bond, site, or continuum, should be used. While network models, which distinguish carefully between pore bodies and pore throats, and for which it is known that the chief limitation to flow comes through the pore throats, clearly require a bond percolation approach, it has been the contention of one of us that use of a continuous random fractal model requires application of continuum percolation theory. If continuum percolation is not used, one can make a good case for treating the wetting of a porous medium as a site percolation problem and the drying of the same medium as a bond percolation problem [1, 2]. In each of these cases, for which an important random component of the model is already linked with the topology of the connections, the critical percolation probability becomes a major issue, especially when the distribution of local flow (or transport) rates is very wide, and particularly since one of the basic components of the analysis is supposed to be the determination of the critical path.

In the electrical conductivity in condensed matter systems described below (and, if our interpretation is correct, also in humid clay minerals, Sect. 6.4), transport occurs by the "hopping" of charges from site to site. The term "hopping" means that

[1] In solid-state physics applications, electronic transport is wavelike in ordered systems. Localization of electrons and hopping transport occur primarily in the presence of disorder.

Hunt, A., Ewing, R.: *Specific Examples of Critical Path Analysis.* Lect. Notes Phys. **771**, 97–122 (2009)
DOI 10.1007/978-3-540-89790-3_4

charges that are located on specific sites most of the time jump to another site in a much shorter time period. "Hopping" can be a classical process, by which a particle jumps over an energy barrier to another site, or it can be a quantum mechanical process, whereby the particle tunnels through an energy barrier. Consider first the classical process. While the typical time taken to jump to another site is essentially zero, the time a charge spends "waiting" to jump is typically an exponential function of the energy barrier, E, between the sites, that is, $\tau = \upsilon_{\text{ph}}^{-1} \exp(E/kT)$. Here the quantity υ_{ph} is a vibrational, or "attempt" frequency and kT is the product of the Boltzmann constant and the temperature. The subscript, ph, refers to a phonon, a quantized lattice vibration. The exponential dependence on energy E ultimately derives from the probability that the energy to transport the particle over the barrier can be absorbed by the particle from thermal fluctuations in the surroundings, and the probability that such thermal fluctuations, or "phonons," may be found is proportional to the Boltzmann factor, $\exp(-E/kT)$. This "waiting" time may also be loosely referred to as a relaxation time, or a hopping time. In disordered systems, such energy barriers can vary widely from place to place and the total time required to transport charges through the material (related to an effective velocity, or current) depends on all the waiting times along the particular path followed. For dc conduction in macroscopic natural systems there is usually enough time, enough individual charges, and sufficient local heterogeneity that the dominant transport paths can be identified as those with the "least resistance," or with smallest transport times, that is, smallest activation energies.

In the quantum process, the transition rates are related through Fermi's "golden rule" (any fundamental text on quantum mechanics) to the square of overlap matrix elements calculated between localized "hydrogenic" wave functions. The electrons are localized on sites due to disorder and occasionally tunnel from site to site. This tunneling introduces an exponential factor with argument proportional to twice (from the operation of squaring the matrix element) the separation of sites.

4.1 *r*-Percolation

The first system investigated in terms of critical path analysis [3] was a slightly idealized representation of impurity conduction in crystalline semiconductors. This system is represented schematically in two dimensions in Fig. 4.1 and can be described as follows. Sites, i, are located randomly in 3D space (their individual positions are uncorrelated) with a mean concentration, N_0. Resistances, R_{ij}, are connected between each pair of sites, i, j, and have the values [4]

$$R_{ij}^{-1} = \frac{e^2 \nu_{\text{ph}}}{k_{\text{B}} T} \exp\left[-\frac{E_0}{k_{\text{B}} T}\right] \exp\left[-\frac{2r_{ij}}{a}\right] \equiv R_0^{-1} \exp\left[-\frac{2r_{ij}}{a}\right] \tag{4.1}$$

In this expression for R_{ij} the only variable quantity is r_{ij}, which is equal to the spatial separation between sites i and j. The other quantities are the electronic

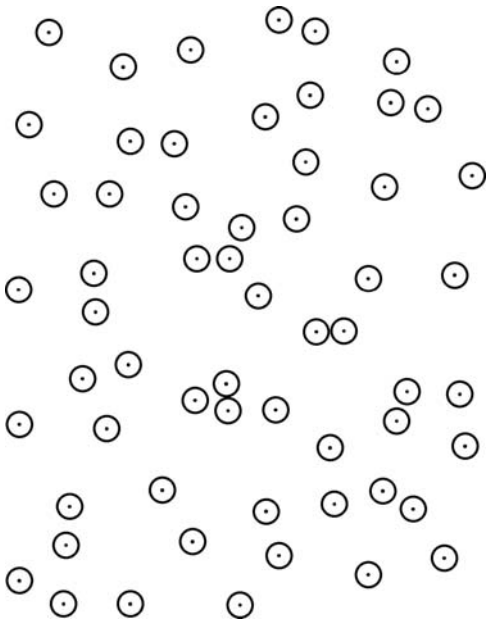

Fig. 4.1 A schematic (and 2D) representation of the Ambegaokar site percolation treatment of *r*-percolation. If one draws spheres of a given radius, *r*, about every site on the network, when the radius of these spheres reaches r_c, an interconnected network of spheres of infinite size will appear. This r_c is the critical radius for percolation and defines the minimum possible value of the maximum resistance encountered by the current

charge, *e*, a fundamental vibrational frequency, $\nu_{ph} \approx 10^{12}$ Hz, the Boltzmann constant k_B, the temperature *T*, a uniform activation energy, E_0, and a fundamental length scale, *a*. The magnitude of *a* is a few nanometers and its origin is in its description of the radius of the hydrogenic wave function. Typical site separations, r_{ij}, may be 5–15 times larger. Equation (4.1) actually arises from consideration of equilibrium transition rates, w_{ij}, that describe the probability per unit time that an electron will jump from site *i* to site *j*. When $r_{ij}/a >> 1$, w_{ij} is very small, and it is very difficult, and thus unlikely, for an electron on site *i* to jump to site *j* in a short time. In Sect. 6.4 we will revisit this subject when we consider a time-dependent (or frequency-dependent) electrical field.

Since in Eq. (4.1) all the quantities except r_{ij} are constant, it is convenient to express the individual resistances in terms of a constant prefactor R_0 and the random variable r_{ij}. The resistances actually represent averages over local stochastic processes involving the sudden motion of electrons from, e.g., site *i* to site *j*, a type of electronic transport termed *hopping*. Because the only variable in the resistances is the site separation, *r*, this system is also called *r*-percolation. Note that the origin of the exponential function in r_{ij}/a most simply relates to an overlap in electronic (hydrogenic) wave functions on sites *i* and *j*, and represents a tunneling probability. In the more complicated $r-E$ percolation discussed in the following subsection the physical interpretation of this function remains the same.

$$W(r)\,dr = 4\pi r^2 N_0 dr \tag{4.2}$$

The mean number, $< N >$, of sites j within a distance r of i is then

$$< N >= \frac{4}{3}\pi r^3 N_0 \tag{4.3}$$

When r is chosen so that $< N >= 1$, r must be the typical site separation, b, i.e., $(4/3)\pi b^3 N_0 = 1$. A typical value of $r_{ij}/a = b/a$ may be 10 or larger, so a site which is twice as far from a given site as the typical nearest neighbor distance, b, will be connected to it with a resistance, which is $e^{10} \approx 20^8$ larger than the typical value. Thus if one starts to connect appropriate resistors between neighboring sites in Fig. 4.1 the resistance values may be spread over 10–20 orders of magnitude or more. This exponential dependence of R_{ij} on the random variable r_{ij} makes the spread of R_{ij} values enormous and promotes the value of percolation theory for finding the macroscopic transport coefficients.

We make use again of the probabilistic identity $W(r)dr = W(R)dR$, which should be familiar from substitution of variables in integration, to transform Eq. (4.3) to

$$W(R) = \frac{\pi a^3 N_0}{2R} \ln^2\left(\frac{R}{R_0}\right) = \frac{3a^3}{8b^3 R} \ln^2\left(\frac{R}{R_0}\right) \tag{4.4}$$

Note the appearance of the factor R^{-1}, which is a result of the fact that the R_{ij} are exponential functions of the random variable, r_{ij}. Insofar as the R_{ij} are exponential functions of random variables, this power of -1 is universal. For ill-condensed matter (impurity conduction systems, glasses, disordered ceramics, supercooled liquids, etc.), this type of local transport (quantum mechanical tunneling and/or thermally activated hopping) is the rule rather than the exception and the factor R^{-1} leads to a number of universal results, although these results are not discussed here. For most applications in porous media, however, local resistances (either electrical or hydraulic) will not be of this form, but are actually powers of random variables and this will lead to fundamental differences between the two systems. The logarithmic factor in Eq. (4.3) is also a product of the functional form of the resistances, but its specific form, $\ln^2(R/R_0)$, requires also that the pdf of the site separations, Eq. (4.2), be a power law with power 2. If the pdf of the site separations were an exponential function of the distance (as is the case for nearest neighbor separations in a 1D analogue to the present system), then the logarithmic factor would be replaced with a power. That power, in contrast to R^{-1}, is not universal, but depends on the specifics of the system, such as the ratio b/a.

Now that we have the expressions for the local resistance values in terms of site separations as well as the pdf for the site separations, it is, in principle, a straightforward process to find the critical resistance of the system. What is missing is a reference to percolation. Clearly the problem under discussion is most fundamentally related to bond percolation, but in Chap. 1 there is no critical bond fraction given for a random lattice. In fact computer simulations [5] for such random systems have shown that the percolation threshold is defined in terms of the average

number of bonds, α, connected to an arbitrary site. When $\alpha \geq 2.7 \equiv \alpha_c$, then the network of interconnected bonds percolates. The percolation condition can now be satisfied by setting the average number of sites within a distance r_c of an arbitrary site equal to the critical value, α_c,

$$\alpha_c = \int_0^{r_c} 4\pi r^2 N_0 dr = \int_0^{r_c} 3\frac{r^2}{b^3} dr \tag{4.5}$$

The meaning of Eq. (4.5) is that on the average α_c bonds with lengths that do not exceed r_c can be connected to such an arbitrary site. That result implies that it is possible to connect an infinitely large network of connected bonds that do not individually exceed r_c in length. This means that the largest resistance in such a network is given by $R_c = R_0 \exp(2r_c/a)$. The solution of Eq. (4.5) is

$$r_c = \alpha_c^{1/3} b \tag{4.6}$$

The critical resistance, R_c, is then

$$R_c = R_0 \exp\left[\frac{2\alpha_c^{1/3} b}{a}\right] \tag{4.7}$$

and is not obtainable by any procedure based on averaging. Furthermore, with $\alpha_c^{1/3} \approx 1.4$ and $b/a \approx 10$, $R_c \approx R_0 \exp(28) \approx R_0 10^{12}$, two things are apparent: (1) paths, which allow a space between sites even twice the critical separation have resistances 12 orders of magnitude larger, and (2) using a typical separation $2b/a$ in place of the critical separation underestimates the controlling resistance by four orders of magnitude. These are the reasons why predictions of transport processes that are not based on percolation theory will fail. Note that Eq. (4.7) can just as easily be derived if one considers the dimensionless variable, $\xi \equiv 2r/a$, such that $R = R_0 \exp \xi$. The integrand is then modified by the extra factor $(a/2)^3$ and the variable of integration becomes ξ instead of r, but the functional dependence is still ξ^2. Thus one finds $\xi_c = (2/a)\alpha_c^{1/3} b$ leaving the result that $R_c = R_0 \exp[(2/a)\alpha_c^{1/3} b]$ unchanged. For r-percolation such a change of variables seems needlessly complicated, but application of such a technique using a dimensionless variable to $r - E$ percolation proves to be very useful indeed.

We can find the typical separations, d, of all resistances $R < R_c$ as follows:

$$\frac{(4\pi/3)\, d^3}{(4\pi/3)\, b^3} \left[\int_0^{r_c} 4\pi r^2 N_0 dr\right] = 1 \tag{4.8}$$

The solution of Eq. (4.8) is

$$d = \alpha_c^{-1/3} b \tag{4.9}$$

Result Eq. (4.9) allows the percolation condition to be expressed in a nice geometric form

$$r_c = \alpha_c^{2/3} d \tag{4.10}$$

i.e., that the typical length of bonds with $r = r_c$, is proportional to their typical separation, d, with a proportionality constant $\alpha_c^{2/3}$. The interpretation is thus clear that a larger value of α_c requires that the typical bond length be a larger fraction of the typical bond separation making it increasingly difficult to connect up the bonds into a percolating network.

Although we have treated the impurity conduction problem as a bond percolation problem it can be easily represented in terms of site percolation through a geometrical construction. Ambegaokar et al. [3] presented this problem initially in terms of overlapping spheres (see the circles in Fig. 4.1). In particular their idea was that one could construct spheres of an arbitrary but uniform radius, r, about each site i, and increase r until at $r = r_c$ a path of touching or overlapping spheres could be found. Imagining these spheres to be metallic and not bothering about the physical problems of their overlap allows an obvious site percolation interpretation in terms of a connected conducting path. The largest resistances on that path, where the spheres just touch, is R_c, and this value (Eq. (4.7)) dominates current.

To proceed further with critical path analysis we need to find a useful expression for $p - p_c$, in terms of which all other percolation variables are expressed. We have not expressed R_c in terms of a critical bond probability, however, but in terms of a number of connected bonds, α_c. However, $p - p_c$ must be proportional to $\alpha - \alpha_c$. Thus the first step must be to express an arbitrary R, (which, for $R < R_c$ gives the maximum resistance on finite-sized clusters of interconnected resistors, and for $R > R_c$ gives the maximum resistance of the infinite cluster), in terms of an arbitrary α. This is done as follows:

$$\alpha = \int_0^r 3\frac{y^2}{b^3} dy \tag{4.11}$$

using y as a dummy (spatial) variable. Combining Eqs. (4.5) and (4.8) gives

$$\alpha - \alpha_c = \frac{r^3 - r_c^3}{b^3} = \left(\frac{a}{2b}\right)^3 \left[\ln^3\left(\frac{R}{R_0}\right) - \ln^3\left(\frac{R_c}{R_0}\right)\right] \tag{4.12}$$

This expression is somewhat complicated. We factor $r^3 - r_c^3$ in keeping with the spirit of percolation theory, in which quantities are expanded to lowest order in $p - p_c$; thus $(r - r_c)(r^2 + r r_c + r_c^2) \approx (r - r_c) 3 r_c^2$. In the second factor, which contains only sums, r may be approximated as r_c. This result is identical to the first term in a Taylor series expansion of $r^3 - r_c^3$ evaluated at the point r_c. Then

$$p - p_c \propto \alpha - \alpha_c = \frac{r^3 - r_c^3}{b^3} \approx \frac{3r_c^2}{b^3}(r - r_c) = \left(\frac{3a\alpha_c^{2/3}}{2b}\right) \ln\left(\frac{R}{R_c}\right) \tag{4.13}$$

From Chap. 2 we can write for the conductivity of a subnetwork defined by a maximal resistance R,

$$\sigma = \frac{l}{R\chi^{2\nu}} \tag{4.14}$$

where l is the typical separation of resistances R and χ is the correlation length evaluated at a value of p corresponding to the choice R. The point will be to optimize the right-hand side of Eq. (4.14) in terms of system and percolation parameters. We can write χ as

$$\chi \propto (p - p_c)^{-\nu} \propto \ln^{-\nu}\left(\frac{R}{R_c}\right) \tag{4.15}$$

To address the separation of the largest resistances in the subnetwork we must use a discretized distribution of resistance values rather than a continuous distribution, since it is otherwise impossible to define "the largest" resistance values. Since the resistances considered are exponential functions of a random variable it makes sense to discretize the distribution in steps of the natural constant $e = 2.718$, i.e., $R = R_0 \exp(j)$, where j is an integer. Such a unit of resistance corresponds to an increment in r of magnitude $a/2$. Then it is possible to write the separation of the largest resistances, with length r, in terms of the separation, d, of all resistors with $R \leq R_c$,

$$l = d\left[\frac{\int_{r-a/2}^{r+a/2} 4\pi r^2 N_0 dr}{\int_0^r 4\pi r^2 N_0 dr}\right]^{-\frac{1}{3}} = d\left[\frac{3r}{a}\right]^{\frac{1}{3}} = b\left[\frac{3r}{\alpha_c a}\right]^{\frac{1}{3}} \tag{4.16}$$

Whether this value of l has any relationship with the typical separation of maximally valued resistances along the current-carrying paths on the infinite cluster is not yet clear, however. While the distribution of resistance values on the infinite cluster may be approximated as being the same as in the bulk, except terminated at R, it is clear that the dominant current-carrying path might avoid most of the larger resistances. Two widely different perspectives can be formulated for this problem. Stauffer (and others) use the "links-nodes-blobs" model to argue $l \propto \chi$. Certainly it makes no sense to choose $l > \chi$, because one would then be basing the calculation of l on a value of the controlling resistance smaller than the value used in Eq. (4.14). Hunt [6] has used Eq. (4.16), which can lead to $l << \chi$. While simulations clearly show that $l \propto L$ in two dimensions, comparison of analogous results with experiments on variable-range hopping systems in three dimensions [7, 8] has proved at least ambiguous [6]. Below we give a self-consistent argument for using Eq. (4.16) or slight modifications thereof.

l from Eq. (4.16) is not a function of the variable $p - p_c(r - r_c)$, and its dependence on $r \propto \ln(R)$ is weak. So for the purpose of optimizing Eq. (4.14) the dependence of l on r may be neglected. Then one can write,

$$\sigma \propto \frac{1}{R}\ln^{2\nu}\left(\frac{R}{R_c}\right) \tag{4.17}$$

It is easy to optimize such an expression for the dependence of σ on R with respect to the arbitrary parameter R to find the optimal value of the limiting

resistance, R_{opt}. Note also that it is immaterial whether the optimization is formulated in terms of R_c or $g_c \equiv R_c^{-1}$. This equivalence is not preserved in typical problems in porous media, as will be seen. The result of optimizing Eq. (4.17) is

$$R_{\text{opt}} = R_c \exp(2\nu) \tag{4.18}$$

a result which is independent of the details of the system. Note that if the Stauffer argument is used the power of 2ν on the logarithm is reduced to ν, and $R_{\text{opt}} = R_c \exp(\nu)$. In two dimensions the power of the logarithm is reduced by ν in either perspective, so that the Stauffer argument yields $R_{\text{opt}} = R_c$, while a treatment analogous to Eq. (4.16) would yield $R_{\text{opt}} = R_c \exp(\nu)$. $R_{\text{opt}} = R_c$ appears to be confirmed in 2D simulations [6, 9].

How does one proceed further? The question which needs to be evaluated is what fraction of the largest resistors on the connected path is shortened by smaller resistances? If $l \propto \chi$, the implication is that in the limit $p \to p_c$ all the largest resistances are shortened. This argument appears to be inconsistent, especially in the context of the optimization procedure, which, in three dimensions leads to $R_{\text{opt}} > R_c$ in either procedure [either $R_c \exp(\nu)$ or $R_c \exp(2\nu)$], and suggests that it is only the inclusion of resistances larger than the optimal value, R_{opt}, which does not change the conductivity. Such a result is consistent with the physical result that 100% of the largest resistances are shortened only for the choice $R \geq R_{\text{opt}}$. If $R_{\text{opt}} > R_c$, then it is not logical to choose l as a singular function at R_c. If l is not singular at R_c, then l may be approximated as slowly varying in the immediate vicinity of R_c, and the result (in three dimensions) follows that $R_{\text{opt}} = R_c \exp(2\nu)$ generating the self-consistent result that the fraction of shortened maximal resistors is only 1 at this larger value of R. However, such an argument leaves a loophole in 2D. If l is assumed to be a singular function of $p - p_c (l \propto \xi)$ in 2D, then the optimization procedure does not lead to $R_{\text{opt}} > R_c$, because of the cancellation of l/χ (in contrast to l/χ^2 in 3D). Of course one could also make the argument that l is not singular at R_c, and that result would also be self-consistent. If both possibilities, which are mutually exclusive, are self-consistent in 2D, it may imply that 2D systems allow different solutions depending on the details of the problem. It certainly appears likely that the optimization is fundamentally different in 2D than in 3D since only the argument that l is not singular at p_c is self-consistent there. So we continue to use Eq. (4.16) (and the appropriate analogue for variable-range hopping systems) for l in 3D systems. Skaggs [10] and references cited therein discuss this subject in a detail beyond the scope of this book.

An especially important physical result is an evaluation of the correlation length at R_{opt}. To find this value of χ simply substitute $R = R_c \exp(2\nu)$ in the expression (Eq. (4.13)) for $p - p_c$, and raise to the $-\nu$ power. The result is

$$\chi\left(R_{\text{opt}}\right) = \left[\frac{b}{3a\nu\alpha_c^{2/3}}\right]^{\nu} \equiv L \tag{4.19}$$

This value, denoted with L, is particularly important because it gives (to within a numerical constant) the structure of the optimal current-carrying paths. Thus the

largest holes in the current-carrying paths are of approximate radius L, percolation calculations of all transport quantities require that the system size be considerably greater than L, or the effects of fluctuations will be large, etc. In the language of hydrology, L^3 would be the REV. Note that Berkowitz and Balberg [11] already pointed out that in the neighborhood of the percolation threshold χ^3 gives the REV, and this result for critical path analysis is in conformance with their analysis. Also analogous calculations of l and L for the hydraulic conductivity of network models of porous media were verified [6] to give the right dependence on system and distribution parameters, although the values from the simulations were typically 30–40% smaller than predicted.

Figure 4.2 gives a comparison of the backbone cluster for the largest $R = R_c$ with the corresponding cluster for the largest $R = R_{max}$.

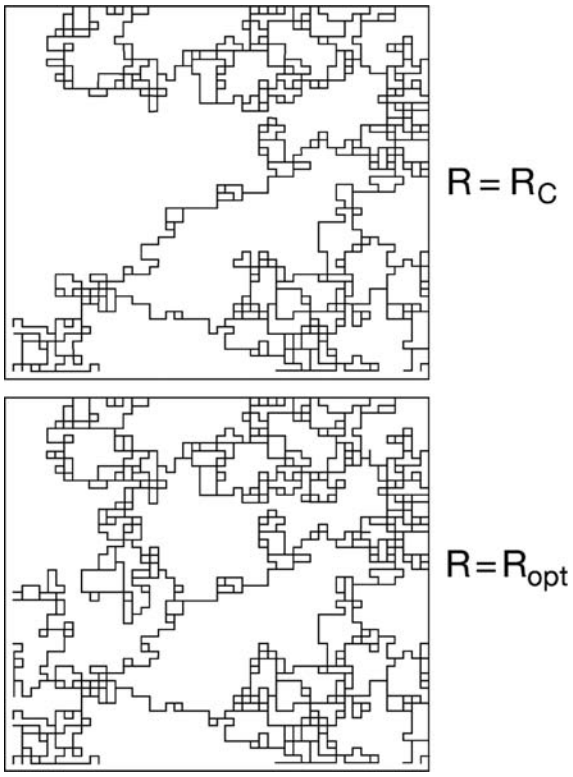

Fig. 4.2 A comparison of the backbone clusters for maximum R values R_c and R_{opt}. Note that in the first case the correlation length is infinite and there is only one connected path across the (finite-sized) system. In an infinitely large system there would still be only one connected path. But for R_{opt} there are several connected paths (from Todd Skaggs, unpublished)

4.2 r – E-Percolation (Variable-Range Hopping)

Amorphous semiconductors represent the classic case for the application of critical path analysis. Here the energy is also a random variable, meaning that electrons can

have a variety of energy values. At zero temperature, T, the electrons occupy the lowest energy states and essentially do not move. At higher temperatures they can move and there is a nonzero electrical conductivity. The Fermi energy at $T = 0$ divides states occupied by electrons (with $E < E_{\rm f}$) from those without electrons (with $E > E_{\rm f}$). Since we will consider only continuous energy distributions, $E_{\rm f}$ is then the highest energy of any state occupied by electrons. In such systems, called $r-E$-percolation, the resistances between individual sites are functions of two random variables, energy and distance, as follows:

$$R_{ij}^{-1} = \left(\frac{e^2 \nu_{\rm ph}}{k_{\rm B}T}\right) \exp\left[-\frac{E_{ij}}{k_{\rm B}T} - \frac{2r_{ij}}{a}\right] \tag{4.20}$$

T is the absolute temperature. The random energy, E_{ij}, is either the difference in energy from the initial, E_i, to the final, E_j, state (if this difference is positive and the sites are on opposite sides of the Fermi energy) or it is the larger of the absolute values of the two energies (measured with respect to the Fermi energy, E_f). The reason for this peculiar definition of E_{ij} is that the resistance is inversely proportional to the probability per unit time that an electron jumps from site i to site j. This probability is composed of the product of the conditional probability that an electron could jump from site i to site j, if it were on site i to begin with and site j were empty, with the probabilities that an electron resides on site i and that no electron resides on site j. The first probability brings in a factor of $\exp[-(E_j - E_i)/k_B T]$, if $E_j > E_i$, because of the necessity to find a phonon to deliver this energy to the electron. The second probability is the product of the Fermi function, $f(E_i)$, for electron occupation of a site at energy E_i and $1 - f(E_j)$ for no electron occupation of site j. $f(E_i)$, for example, is often approximated by a Boltzmann factor in the energy difference $E_i - E_f$. So the energy term in the exponent represents a composite of effects of site occupation and energy conservation.

The energies of the individual sites are considered to be distributed uniformly between $-W_0/2$ and $W_0/2$, so that the probability that a site has energy within dE of any given energy in that range is

$$W(E)dE = \frac{dE}{W_0} \tag{4.21}$$

One can now write for the density of states (per unit energy per unit volume) at the Fermi energy, E_f,

$$N(E_{\rm f}) = \frac{1}{W_0 b^3} \tag{4.22}$$

where b is again the typical separation of sites. With two random variables, and with local correlations introduced by the fact that neighboring bonds share one common site (and its energy value), the application of critical path analysis is considerably more complex. In analogy to Eq. (4.5) one would have to integrate over three spatial coordinates and one energy coordinate. This was done [12] and the result obtained that

$$\sigma_{\mathrm{dc}} \propto \exp\left[-\left(\frac{T_0}{T}\right)^{\frac{1}{4}}\right] \tag{4.23}$$

with

$$k_{\mathrm{B}} T_0 \propto W_0 \left(\frac{b}{a}\right)^3 \tag{4.24}$$

The same result was obtained earlier by Mott [13] who, however, used an optimization procedure for individual resistances. In this procedure electrons can hop greater distances to relieve the energy increase, since there are more sites to attempt at larger distances. The competition between energy and distance tends to shift slowly toward a greater relevance of energy at lower temperatures (because of the ratio of $-E/k_B T$ in the exponential function) so hops become longer and stay at energies nearer the Fermi energy with diminishing temperature. While Mott's procedure is not strictly valid, since it does not guarantee that the individual optimal resistances connect up to form a continuous path for current flow, it is cited more often because of its simplicity. Here a percolation argument, which is equally simple, is presented. The argument is based on a generalization of Eq. (4.10). If the maximum hopping energy allowed is E_{m} (when $r_{ij} = 0$) and the maximum hopping distance is r_{m} (when $E_{ij} = 0$), then we must have

$$\frac{E_{\mathrm{m}}}{kT} = \frac{2r_{\mathrm{m}}}{a} \tag{4.25}$$

This equation guarantees the existence of a maximum resistance, $R_{\mathrm{c}} = R_0 \exp E_{\mathrm{m}}/k_B T = R_0 \exp 2r_{\mathrm{m}}/a$. Connectivity is guaranteed if we relate the typical separation of the sites utilized for the transport equal to the appropriate fraction of the length of the individual resistors. To lowest order the typical resistance length is

$$< r >= \frac{\int_0^{r_{\mathrm{m}}} r\left(4\pi r^2\right) dr}{\int_0^{r_{\mathrm{m}}} \left(4\pi r^2\right) dr} = \left(\frac{3}{4}\right) r_{\mathrm{m}} \tag{4.26}$$

If one takes into account the fact that the occurrence of large hopping distances must be suppressed because the energy range of sites must be increasingly restricted with increasing r, the numerical coefficient (3/4) would be altered, so this factor cannot be considered accurate[2]. Choosing 1 for the numerical coefficient is therefore equally justified, though slightly less accurate, and it is best simply not to attach any importance to the factor (3/4). The typical separation between sites with low-enough energies (less than E_{m}) is

$$d = b\left(\frac{3}{4\pi}\right)^{\frac{1}{3}} \left[\frac{W_0}{E_{\mathrm{m}}}\right]^{\frac{1}{3}} = \left(\frac{3}{4\pi}\right)^{\frac{1}{3}} \left[\frac{1}{N\left(E_{\mathrm{f}}\right) E_{\mathrm{m}}}\right]^{\frac{1}{3}} \tag{4.27}$$

[2] Getting that particular number was the motivation, in fact, for going beyond the particular calculation here to generate a fully consistent percolation calculation (Pollak, personal communication, 2005).

Inserting the results of Eqs. (4.26) and (4.27) into Eq. (4.10) and solving simultaneously with Eq. (4.25) yields

$$r_{\mathrm{m}} = a\left(\frac{\alpha_{\mathrm{c}}^2}{9\pi}\right)^{\frac{1}{4}}\left[\frac{1}{k_{\mathrm{B}}TN(E_{\mathrm{f}})a^3}\right]^{\frac{1}{4}} \propto a\left[\frac{k_{\mathrm{B}}T_0}{k_{\mathrm{B}}T}\right]^{\frac{1}{4}} \propto a\left[\frac{W_0\,(b/a)^3}{k_{\mathrm{B}}T}\right]^{\frac{1}{4}} \tag{4.28}$$

This result is compatible with the prior results of Pollak [12] and Mott [13] since $r_{\mathrm{m}}/a = (T_0/T)^{1/4}$, but it yields a slightly different numerical constant compared with each of those derivations. The numerical constants given here are not correct. Since, in order to connect sites with smaller energies, the hopping distance thus increases with diminishing temperature this type of transport has become known as variable-range hopping. If the combination of variables $2r/a + E/k_BT$ is defined to be ξ, then one can represent the effects of the full percolation calculation in a form analogous to Eq. (4.5):

$$4\alpha_{\mathrm{c}}\frac{T}{T_0}\int_0^{\xi_{\mathrm{c}}}\xi^3 d\xi = \alpha_{\mathrm{c}} \tag{4.29}$$

Instead of integrating over $\xi^2 d\xi$, as in r-percolation, one must integrate over $\xi^3 d\xi$ here because of the existence of three spatial dimensions (random variables) and one energy dimension (random variable). Clearly the result of the integral is $\xi_{\mathrm{c}} = (T_0/T)^{1/4}$. The integral thus expresses that the resistance values required for percolation are spread through the interior of a 4D volume. One can calculate the typical spatial separation of the resistances with the largest values in a similar way as for r-percolation, by noting that the largest resistance values are spread out over the surface of this 4D volume

$$l = a\left(\frac{T_0}{T}\right)^{\frac{1}{4}}\left[\frac{\int_{\xi_{\mathrm{c}}-1}^{\xi_{\mathrm{c}}+1}\xi^3 d\xi}{\int_0^{\xi_{\mathrm{c}}}\xi^3 d\xi}\right]^{-\frac{1}{3}} = a\left(\frac{T_0}{T}\right)^{\frac{1}{3}} \tag{4.30}$$

Thus the largest resistances are located with a unit variation in ξ from the surface, or percolating value, ξ_{c}. It is also possible to calculate the correlation length, which describes the dc conduction. To calculate the correlation length it is necessary first to find the fundamental length scale of the resistances. In the case of $r-E$-percolation only a fraction of the sites actually take part in the conduction process and their typical separation is $a(T_0/T)^{1/4}$, so that this fundamental scale is $a(T_0/T)^{1/4}$. Then we have

$$\chi \propto a\left(\frac{T_0}{T}\right)^{\frac{1}{4}}(p-p_{\mathrm{c}})^{-\nu} = a\left(\frac{T_0}{T}\right)^{\frac{1}{4}}\left[k_BT\left(\xi^4-\xi_{\mathrm{c}}^4\right)\right]^{-\nu} \tag{4.31}$$

The substitution giving the second form on the right-hand side was obtained by writing Eq. (4.29) also for an arbitrary ξ (and α) and making p and p_{c} proportional to α and α_{c}. Linearization allows $\xi^4 - \xi_{\mathrm{c}}^4$ to be expressed as roughly $\xi_{\mathrm{c}}^3(\xi - \xi_{\mathrm{c}})$, and one finds

$$\chi \propto a\left(\frac{T_0}{T}\right)^{\frac{1}{4}}\left[\left(\frac{T_0}{T}\right)^{\frac{1}{4}}\ln\left(\frac{R}{R_c}\right)\right]^{\nu} = a\left(\frac{T_0}{T}\right)^{(1+\nu)\left(\frac{1}{4}\right)}\ln^{\nu}\left(\frac{R}{R_c}\right) \tag{4.32}$$

Evaluated at $R = R_c \exp(2\nu)$, just as for r-percolation, this expression yields

$$\chi(R_{opt}) \equiv L \propto a\left(\frac{T_0}{T}\right)^{\left(\frac{1+\nu}{4}\right)} \tag{4.33}$$

One can now write for the electrical conductivity,

$$\sigma = \frac{l}{L^2 R_{opt}} = \frac{a\,(T_0/T)^{1/3}}{\left[a\,(T_0/T)^{((1+\nu)/4)}\right]^2 R_0 \exp\,(T_0/T)^{1/4}} \tag{4.34}$$

Note that in the case of either r-percolation or $r-E$-percolation systems the uncertainty in the calculation of l has no effect on the exponent ($2\alpha_c^{1/3}\ b/a$ or $(T_0/T)^{1/4}$, respectively). The effect is thus on the preexponential, which is only a power of the temperature. Since the exponential function is a much more rapidly varying function of system parameters and, in the case of variable range hopping, of the temperature, it was possible to use the percolation theoretical argument to predict the electrical conductivity over as much as 14 orders of magnitude of the conductivity with minimal discrepancy with experiment [though not in a-Si, [7] rather with a-Si:H:Au [8]]. While such accuracy is clearly a selling point in the theory it does not, except perhaps in the latter case, help to distinguish between theoretical treatments of l. The only reason why, in the latter case, it was possible to make any judgment as to the accuracy of a particular result for l was that experimental data were reported in the form of the ratio of the ac to the dc conductivity (which eliminated the exponential T dependence), but a detailed treatment of the ac conductivity is a topic beyond the present scope. In the case of the hydraulic conductivity, which has no equivalent separation of exponential and nonexponential contributions, this uncertainty in theory has reduced confidence somewhat in the validity of the percolation-based treatment and introduced some confusion.

An important point of this exercise is to demonstrate from basic physics how to calculate relevant length scales. The numerical values of these length scales are not well-defined, but their dependence on system parameters has been approximately verified in comparison with both experiment [6] and numerical simulations [14]. As problems of hydrology are addressed, it will be important to have prior guidance for calculating these quantities.

4.3 Saturated Hydraulic Conductivity

One difference between hydrological and solid-state applications of critical path analysis is that in the former case the sites take up a nonnegligible volume. In

addition, in spite of the approximation of (probabilistic) fractal modeling, the coordination number of large pores is likely larger, on average, than of small pores. Besides, there is no possibility to put pores on a regular grid if their lengths (as well as widths) vary over more than an order of magnitude. For all of these reasons it is a better idea to base the critical path analysis on continuum percolation theory than to use the bond or site versions. In continuum percolation accurate application of critical path analysis requires an expression for the critical volume fraction for percolation, which we will call V_c. In contrast to the solid-state problems discussed above, this value is not known from simulations, but we will show in Chaps. 6 and 7 that it is known empirically from experiments on solute diffusion in unsaturated media [15]. Balberg [16] (inspired by earlier work of Kogut and Straley [17]) already gave a detailed discussion of continuum percolation problems in porous media. In particular he demonstrated that in continuum percolation transport exponents may be nonuniversal, but this topic is postponed until the next chapter. Finally, the local transport law (Poiseuille flow) is a power law in geometric quantities such as the pore radius and the pore length, rather than an exponential function. This difference will be important too, and the implications of this difference have not been completely appreciated [18–20] in existing critical path applications to the saturated hydraulic conductivity.

Let us assume low Reynolds number flows, meaning that for any given geometry the dependence of the flow through a pore can be written in terms of an effective pore length and pore radius. The appropriate way to relate these radii and lengths to physical lengths requires pore-scale treatments of the Navier–Stokes equation. For calculating the ratio of the hydraulic conductivity at an arbitrary saturation to its value at full saturation such complications are unimportant, as long as the fractal model of the pore space is accurate, since these geometrical factors do not change with pore size. However, to calculate the hydraulic conductivity at full saturation, such a complication is important and can only be resolved exactly by detailed imaging and careful numerical work at the single pore scale, subjects not addressed in this book. Note that the proposed activity of calculating the hydraulic conductivity is called "upscaling" (at the pore scale) in the hydrology literature, but would be called a calculation of an effective macroscopic transport parameter from its microscopic variability in the physics literature.

Poiseuille flow implies that pores of radius r and length l have a hydraulic conductance

$$g^{\mathrm{h}} \propto \frac{r^4}{\mu l} \tag{4.35}$$

with μ the viscosity of the fluid, here assumed to be water. The reason for the form of Eq. (4.35) is that in the linear regime (assumed here) the total flow through such a pore is proportional simultaneously to g^{h} and the pressure difference across the pore, ΔP. The numerical constants are suppressed. If the medium is assumed to be fractal, the aspect ratio (shape) of pores is, on the average, independent of their size, meaning that l must be taken as proportional to r. In this case then,

$$g^h \propto r^3 \tag{4.36}$$

To calculate the hydraulic conductivity accurately under conditions of saturation one needs to find a critical value of a conductance, g_c, from critical path analysis, then find expressions for l and χ, and finally optimize the result. The easy part is to find g_c.

Under saturated conditions, r_c is given through [21]

$$\frac{3-D_p}{r_m^{3-D_p}} \int_{r_c}^{r_m} r^3 r^{-1-D_p} dr = V_c \tag{4.37}$$

with the critical volume content for percolation, V_c. Solution of this equation yields,

$$r_c = r_m (1-V_c)^{\frac{1}{3-D_p}} \tag{4.38}$$

Note that we can write for an arbitrary r,

$$r = r_m (1-V)^{\frac{1}{3-D_p}} \tag{4.39}$$

The critical conductance, g_c^h must be of the form

$$g_c^h \propto r_m^3 (1-V_c)^{\frac{3}{3-D_p}} = r_c^3 \tag{4.40}$$

We assumed [21], as in Stauffer and Aharony [9] (as well as Katz and Thompson [20], Banavar and Johnson [19], and Le Doussal [18]) that both l and χ are proportional to r_c so that the saturated hydraulic conductivity, K_S, is represented by

$$K_S \propto r_c^2 \tag{4.41}$$

How does this arise?

First we linearize the difference $V - V_c$,

$$V - V_c = \left(3 - D_p\right) \left(\frac{r_c}{r_m}\right)^{3-D_p} \left(\frac{r - r_c}{r_c}\right) \tag{4.42}$$

Then for the case that $g_c \propto r_c^3$ we can write $V - V_c$ in terms of the conductance difference,

$$V - V_c = \left(\frac{3-D}{3}\right) \left(\frac{r_c}{r_m}\right)^{3-D_p} \left(\frac{g - g_c}{g_c}\right) \tag{4.43}$$

For the optimization procedure the material result is that $V - V_c \propto g - g_c$. The optimization

$$\frac{d}{dg}\left[g\left(g_c - g\right)^{2\nu}\right] = 0 \tag{4.44}$$

yields

$$g_{\text{opt}} = \frac{g_c}{1+2\nu} \tag{4.45}$$

The factor $1+2\nu$ could be written (if ν were very small) as $\exp(2\nu)$. The reader may verify that repeating the procedure with respect to the resistance yields $R_{\text{opt}} = R_c/(1-2\nu)$ which, again if ν were very small, would yield $R_{\text{opt}} = R_c \exp(-2\nu)$ and the two methods would be consistent (as in the exponential case above). But ν is 0.88, which is not small, and the optimization procedure with respect to the resistance yields a value, which is outside the range of physical values. This means either that it is preferable to use the optimization procedure with respect to the conductance rather than the resistance, or that the optimization procedure is not reliable in the present context. Our choice is to consider the optimization procedure with respect to the conductance as reasonable, but to interpret the results with caution. There is a physical reason behind these results.

In the case where g is an exponential function of random variables (e.g., impurity conduction systems), a small change in g is associated with a very small change in p because of the logarithmic dependence of p on g. When g is a power of a random variable as here, the result is that a small change in g makes a change of roughly the same magnitude in V (corresponding to p), which sweeps χ right out of the range where percolation theory gives an accurate estimation of the separation of dominant current-carrying paths. This means that for g very near g_c the separation of current-carrying paths can be very small, i.e., on the order of the separation of pores, which is the same order as r_c, and the same order as the separation of controlling resistances along the dominant paths. For a pictorial example of such a contrast between current-carrying paths for exponential and power-law functions of random variables refer to Fig. 4.3. Note that the exponential case is the same as in Fig. 4.2.

For these reasons we [21] decided to formulate K_S as proportional to

$$K_S \propto \frac{l r_c^3}{\chi^2} = \frac{r_c r_c^3}{r_c^2} = r_c^2 \tag{4.46}$$

However, it should be kept in mind that l and L could have been written as other pore length scales with different numerical constants, meaning that in some sense a proportionality to r_c^2 is a matter of convenience. Note that K_S proportional to the square of a pore radius is a result obtained by many other authors, including Katz and Thompson [20] [also Kozeny [22]-Carman [23], Johnson and Schwartz [24], Bernabe and Revil, 1995 [25]; Torquato and Lu [26] who did not use critical path analysis, but Banavar and Johnson [19] and Le Doussal [18], who did] who also used the critical radius, r_c, and whose critical path analysis yielded as well the same sort of result for the critical radius, r_c. However, there is some fairly considerable uncertainty in the numerical prefactors, probably reflecting the choice to make other pore length scales proportional to ${r_c}^2$. Nevertheless, loosely at least, the Katz and Thompson [20] and the Hunt and Gee [21] treatments of K_S are equivalent. The focus here is not on K_S, for which one really needs additional information (pore shape, in particular). But it is essential to present the basic discussion of K_S. Also, although we anticipate that both percolation-based treatments could be improved, in

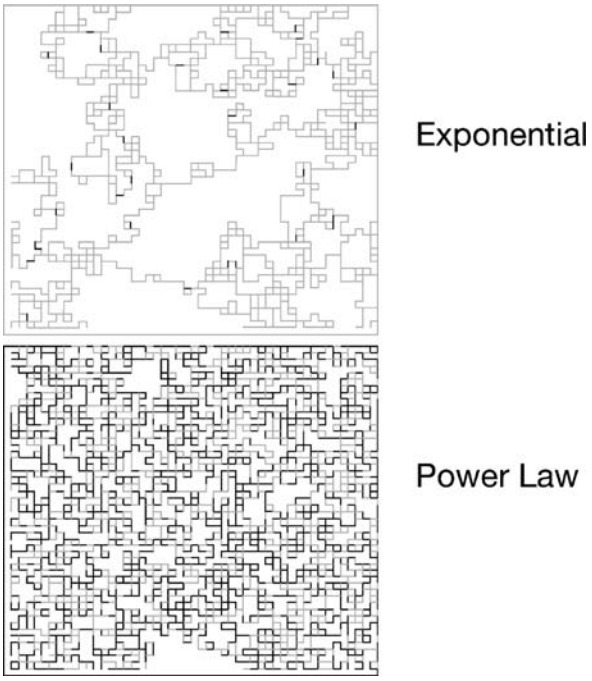

Fig. 4.3 A comparison of the backbone clusters for maximum $R = R_{\text{opt}}$ for (**a**) the case that the resistances of the bonds follow Eqs. (4.1) or (4.20), and (**b**) that the bond resistances follow Eq. (4.35), i.e., exponential vs. power law functions (from Todd Skaggs, unpublished)

a controlled test [27] of four methods to calculate K [Kozeny-Carman, a "stochastic" pore-scale model due to Bernabe and Revil (1995) and the Johnson and Schwartz [24] treatment being the other three] the Katz and Thompson [20] result came out on top. Notably, in the case of large variance the Kozeny-Carman results came in a distant last place, although all four results were equally accurate in the limit of low variance.

4.4 Unsaturated Hydraulic Conductivity

Typical formulations ([28–31], the various references to Mualem ([31–33] in Chap. 3)) of the unsaturated hydraulic conductivity are in the form of a ratio with K_{S}. The reasons for this have already been discussed in the previous chapter, but chiefly this is due to the typical lack of direct information regarding the pore space and the difficulty of formulating an accurate calculation of K_{S} without explicit information about pore sizes and shapes. However, in fractal systems, the particular pore shapes are the same for all radii, and thus this geometric factor cancels out in the ratio of $K(S)/K_{\text{S}}$. The formulation of the hydraulic conductivity in this ratio will also simplify the application of critical path analysis greatly.

The effects of partial saturation are treated using the premise that film flow permits, Blunt and Scher [32], Tokunaga and Wan [33], the porous medium to adjust to removal of water by evacuating *all* pores with radii larger than some equilibrium value, which we call, $r_>$. Thus neither hysteresis nor effects of nonequilibrium are considered yet. The following is taken from Hunt and Gee [21]. The relative saturation is the quotient of the pore-space volume in pores with $r < r_>$ and the total pore volume,

$$S = \left(\frac{1}{\phi}\right)\left(\frac{3-D_\mathrm{p}}{r_\mathrm{m}^{3-D_\mathrm{p}}}\right)\int_{r_0}^{r_>} dr r^{2-D_\mathrm{p}} = \frac{1}{\phi}\frac{\left[r_>^{3-D_\mathrm{p}} - r_0^{3-D_\mathrm{p}}\right]}{r_\mathrm{m}^{3-D_\mathrm{p}}} \tag{4.47}$$

Remember from Chap. 3 that r_0 and r_m are the lower and upper bounds of validity of the fractal description of the pore space. When $r_> = r_\mathrm{m}$, Eq. (4.47) yields $S = 1$. Next, the percolation condition relating the smallest (or critical) pore size needed to be traversed, to the critical volume fraction, V_c, when the largest pore filled with water has $r = r_>$, is,

$$V_\mathrm{c} = \left(\frac{3-D_\mathrm{p}}{r_\mathrm{m}^{3-D_\mathrm{p}}}\right)\int_{r_\mathrm{c}(\theta)}^{r_>} dr r^{2-D_\mathrm{p}} = \left(\frac{r_>}{r_\mathrm{m}}\right)^{3-D_\mathrm{p}} - \left(\frac{r_\mathrm{c}(\theta)}{r_\mathrm{m}}\right)^{3-D_\mathrm{p}} \tag{4.48}$$

Equation (4.48) has the same form as Eq. (4.47), but the upper limit has been reduced from r_m to $r_>$, producing a related reduction in $r_\mathrm{c}(\theta)$ (and requiring its representation as a function of θ) consistent with the effects of partial saturation. Since our goal here is to calculate the hydraulic conductivity as a function of moisture content we should consider using a threshold moisture content, θ_t, in place of the critical volume fraction, V_c. This turns out to be a good plan, since solute diffusion experiments demonstrate a linear vanishing of the diffusion constant at such a moisture content, θ_t. Together, Eqs. (4.37), (4.47), and (4.48) (and using θ_t in place of V_c) allow r_c for unsaturated conditions to be expressed in terms of r_c for saturated conditions,

$$r_\mathrm{c}(\theta) = r_\mathrm{c}(\theta = \phi)\left[\frac{1-\phi+(\theta-\theta_\mathrm{t})}{1-\theta_\mathrm{t}}\right]^{\frac{1}{3-D_\mathrm{p}}} \tag{4.49}$$

The critical hydraulic conductance as a function of moisture content is now,

$$g_\mathrm{c}(\theta) = g_\mathrm{c}(\theta = \phi)\left[1 - \phi\frac{1-S}{1-\theta_\mathrm{t}}\right]^{\frac{3}{3-D_\mathrm{p}}} \tag{4.50}$$

Equation (4.50) implies a scaling of the same form for the ratio of $K(S)/K_\mathrm{S}$. The hydraulic conductivity of the medium is controlled by the hydraulic *conductance* of the rate-limiting pore throat, which is proportional to the *cube* of the critical radius. How does the vanishing of the correlation length (and therefore the minimum path separation) at the percolation threshold affect the critical path results for $K(S)/K_\mathrm{S}$? The answer is, not at all, at least to a very good approximation (over a fairly wide range of moisture contents). Why? The answer has two parts: (1) such topological

complications only have a strong effect in the vicinity of the percolation threshold and (2) the calculation of K_S takes into explicit account the competition between the effects of finding the minimum value of the blocking or bottleneck resistance and the infinite path separation. Thus in the calculation of $K(S) = K_S(K(S)/K_S)$ the effects of the path separation are already included at saturation, and as long as the percolation threshold is not approached too closely, there is very little change in these effects. However, this perspective must be reevaluated for moisture contents that are low enough that the percolation threshold is near [34]. Thus we can now write for the unsaturated hydraulic conductivity,

$$K(S) = K_S \left[1 - \phi \frac{1 - S}{1 - \theta_t}\right]^{\frac{3}{3-D_p}} \tag{4.51}$$

a result which can also be written as

$$K(S) = K_S \left[\frac{1 - \phi + (\theta - \theta_t)}{1 - \theta_t}\right]^{\frac{3}{3-D_p}} \tag{4.52}$$

While the present evidence is that Eq. (4.52) is accurate for typical porous media over a wide range of moisture contents, it cannot be accurate [34] in the limit $\theta \to \theta_t$. In that limit Eq. (4.52) yields

$$K(\theta_t) = K_S \left[\frac{1 - \phi}{1 - \theta_t}\right]^{\frac{3}{3-D}} \tag{4.53}$$

$K(\theta_t)$ from Eq. (4.53) is not zero, in fact it is the hydraulic conductivity associated with the limiting conductance of the smallest pore in the system. However, it is an absolute requirement from percolation theory that the hydraulic conductivity vanish at the percolation threshold. In fact, in this limit, the hydraulic conductivity (like the electrical conductivity) must vanish according to the following result:

$$K(\theta) = K_1 (\theta - \theta_t)^{\mu} \tag{4.54}$$

How these results are to be reconciled is the subject of the next chapter; the reconciliation illuminates the difference between the electrical and the hydraulic conductivities of porous media, and also clarifies the role of some exact results for nonuniversal scaling of transport properties derived by Balberg [16].

4.5 Hydraulic Conductivity for Geologic Media: Parallel vs. Series

In this section we present a general result, which may be utilized to "upscale" the hydraulic conductivity in geologic media, that is to calculate an effective hydraulic

conductivity, K_{eff}, when a wide distribution of individual K values exists. In the beginning of this chapter we have, of course, argued that one should carefully address the difficulties of each medium individually. Further, we argued elsewhere that the appropriate conceptual view of this problem is not even upscaling the *conductivity*, per se. One should characterize the dominant conduction paths in terms of their blocking resistance value and then find the frequency of occurrence of such paths. A discussion in terms of the hydraulic conductivity implies already that the individual portions of the medium have uniform conduction properties. Nevertheless, as witnessed by the large number of such results for upscaling in use, there is a need to write down a general result, which can be applied as a simple algorithm. We write down such a result here. It is clearly a conceptual advance over the results currently in use.

It is a typical argument in geology to consider a horizontally layered system and contrast the vertical flow properties with the horizontal flow properties. The effective hydraulic (or electric) conductivities under such conditions are given through the average resistance and average conductance values, respectively, since the respective configurations of the resistance values are in series and in parallel. We cast this discussion in the language of percolation theory and then seek the appropriate generalizations.

In 1D systems water (or current) must flow through every element of the system. In the thermodynamic limit of infinite system size, this means that every element of a distribution of resistance values must be present with its occurrence described by the relevant pdf of resistance values, $W(R)$. The equivalent resistance of such a 1D system is given by the series combination of the individual resistances, which is the arithmetic sum of the resistance values. The conductivity, hydraulic or electrical, must be inversely proportional to the total resistance of the system, R_{tot}, which can be simply calculated as

$$R_{\text{tot}} \propto < R > = \int_0^\infty RW(R)dR \quad \text{or} \quad R_{\text{tot}} = \sum_i R_i \tag{4.55}$$

Thus,

$$K_{\text{eff}} \propto \left[\sum_i R_i\right]^{-1} \propto \left[\sum_i K_i^{-1}\right]^{-1} \tag{4.56}$$

If the individual elements are geometrically identical, then K_{eff} is equal to the second sum. Such a particular operation is often referred to as obtaining the harmonic mean of the conductivities. For the two versions of Eq. (4.56) to be equivalent, it is necessary that all the individual elements have the same size and shape; otherwise the only valid sum is over the resistances, R_i.

The opposite extreme to the combination of all the resistances in series, as in a 1D system, is the combination of all the resistances in parallel. In the case of a parallel combination the total conductance is the sum of the individual conductances, and the upscaled hydraulic conductivity, K_{eff}, is then given through

$$K_{\text{eff}} \propto \left[\sum_i K_i^1\right]^1 \tag{4.57}$$

The same geometric restriction applies here, namely that the individual elements all be congruent (have the same size and shape); otherwise it will be necessary to include geometrical factors to transform the elements of the series to conductances. When the factors are all identical, approximate Eq. (4.57) becomes an equality. As a consequence of the validity of these two extremes, Scheibe and Yabusaki [35] proposed the following formula:

$$K \propto \left[\sum_i K_i^z\right]^z \quad -1 \le z \le 1 \tag{4.58}$$

The problem with such power-law averaging [36, 37] is that it is conceptually incorrect. Comparison of percolation theoretical calculations with simulations [5, 27] demonstrate consistently that the importance of individual resistances to an effective resistance of a medium is not a monotonically increasing or decreasing function of resistance. In fact, this importance is peaked. In particular, the peak of importance of resistance values occurs at the critical resistance, R_c. Smaller resistances on the percolation path behave very much like shorts. Larger resistances are avoided. These critical resistances control the field of potential drops in the entire medium [27].

In a low order approximation (used as well by Balberg [16]) one can calculate the hydraulic conductivity of a medium, to which critical path analysis is to be applied, by including all the resistance values smaller than R_c on a 1D path, and ignoring the remainder of the resistance distribution. While this is not completely accurate, it is an improvement over Eq. (4.58), and in more or less the same spirit, as will shortly become clear.

The two cases, parallel and series combinations or resistances, correspond in critical path analysis, to the percolation probabilities, $p_c = 0$ and $p_c = 1$, respectively (Why?). The answer is because, in the first case, it is possible to find a path through the medium, which utilizes a vanishingly small part of the resistance distribution, while in the second case it is impossible to find a path through the medium that excludes any portion of the resistance distribution. In the first case, an arbitrarily small fraction of the resistance distribution means that each resistor out of the entire distribution can span from one side of the system to the other, consistent with a parallel configuration of the resistors. Such a topology is, in fact, precisely what is imagined in pore-scale models that rely on bundles of capillary tube approximations. Thus, out of a continuum of possible values, the bundle of capillary tubes model chooses one end point, meaning that the conditions for which it is valid never occur. The second case is, as already discussed, equivalent to a series configuration. The latter can be obtained in a 1D system, while the former is a necessary result only of an infinite dimensional system [using the Vyssotsky et al. [38] formula, $Zp_c = d(d-1)$]. What we present here is a procedure which maintains the fundamental

perspective of critical path analysis, but also reduces to the proper results in the limit of $p_c = 0$ and $p_c = 1$, respectively.

$$K_{\text{eff}} = < K > \left[\frac{\int_{K_c}^{K_{\max}} W(K) K^{-1}}{K_{\max}^{-1}} \right]^{-1} \tag{4.59}$$

In this expression the pdf, $W(K)$, must be proportional to the distribution of K values in bulk, but normalized so that $\int dK W(K)$ between the limits K_c and $K_{\max}$ is 1. Further, we require the same geometric constraints as in Eqs. (4.56) and (4.57). Note that when $p_c = 0$, Eq. (4.59) yields $< K >$, since $K_c = K_{\max}$, $W(K)$ becomes a delta function, $\delta(K - K_{\max})$, and the integral then yields $K_{\max}^{-1}$, which cancels with the denominator. However, when $p_c = 1$, the integral yields the harmonic mean conductivity, while the denominator $(K_{\max}^{-1})^{-1}$ approximately cancels $< K >$, since for a wide distribution of hydraulic conductivity values, $W(K)$, the arithmetic mean is dominated by the largest K value.

It is important here that Eq. (4.59) essentially represents an averaging procedure where the importance of K values is strongly peaked right at the critical conductivity, K_c. For $p_c = 0$, this peak moves to $K_{\max}$, while for $p_c = 1$, the peak moves to $K_{\min}$. Thus, in these two cases, Eq. (4.59) corresponds to the parallel and series combinations, and the importance of individual conductivity values is either monotonically increasing or monotonically decreasing. But in any other case (much more realistic values of p_c) this procedure yields an averaging procedure peaked at K_c. We should bring up, however, that Eq. (4.59) performs rather disappointingly when it is applied to a bimodal distribution [39]. In such a case the effective conductivity as a function of the volume fraction of the medium in the upper mode of the distribution has a sigmoidal shape with a point of inflection at the percolation threshold. Such a bimodal distribution can be appropriate for geological media composed of sands and muds. In particular, when the upper mode of the distribution (say sand fraction) is below the percolation threshold, Eq. (4.59) drastically underestimates K, although it otherwise does quite well. Further, Eq. (4.59) does generate a rapid increase in K when the upper mode just exceeds the percolation threshold, and percolation theoretical results are generally in accord with the sigmoidal shape of $\log[K]$ vs. sand fraction [39]. Power-law averaging performs most poorly, never generating a point of inflection for any value z [39].

The implication of this discussion is that the tendency of water (or electrical current) to follow the path of least resistance means that such a path is configured in parallel with other paths, whose resistances are much higher (and can be ignored), while the resistances on such an optimal path are configured in series. Power-law averaging configures all the resistors equivalently, somewhere between series and parallel. While power-law averaging does yield any value for K_{eff} between the two limits, and thus any value that experiment can develop, the logic of cause and effect is missing and the parameter μ has neither predictive value nor experimental significance. This defect shows up clearly in the case of the bimodal distribution where its results are only useful in the limits that the medium is either 0% or 100% sand.

4.6 Summary

Several examples of the application of critical path analysis were given. The most difficult issue in these examples is the relationship between a critical, or rate-limiting, conductance and the effective electrical or hydraulic conductivity. In the first four calculations of the effective conductivity, we have chosen to apply a general technique of Friedman and Pollak [40] in making this transition. This technique develops the result in terms of the following length scales: (1) the separation of controlling resistances along a path and (2) the separation of dominant paths. In the fifth calculation we developed an algorithmic procedure that offers greater simplicity, if not greater accuracy.

In 3D well-connected systems with local conductances exponential functions of random variables, the typical separation of controlling resistances appears not to be a critical function of percolation variables, but the opposite is likely in 2D systems. In 3D systems critical path analysis requires an optimization of topological (current-carrying path separations) and geometrical (resistance magnitude), but in 2D systems a simpler scaling argument becomes possible with the conductivity given merely by the critical conductance. If, however, local conductances are power functions of random variables, such as is the case in porous media, then even in the 3D case it is difficult to separate the effects of topology and geometry, since both show up in factors relating to length scales of similar magnitudes. Nevertheless the calculations of the hydraulic conductivity at full saturation with the highest degree of accuracy are based on precisely this form of critical path analysis. Finally, it is possible even in the kind of messier problem that is prevalent in porous media to formulate conductivity ratios, which are given purely in terms of the geometry (though we will find that this formulation will generally break down as the percolation threshold is approached). When the relevant problem is formulated as a ratio of conductivities at two different saturations, even 3D problems are equally tractable. But for the case of porous media we will find (next chapter) that not all conductivities are equivalent, and that specifically the electrical conductivity and thermal of porous media behave quite differently as a function of, e.g., saturation, from the hydraulic conductivity. Nevertheless, we also presented at the end of this chapter an upscaling result that should apply on geologic scales equally to the electrical and to the hydraulic conductivities.

Problems

4.1. Show that integration of Eq. (4.4) to find R_c directly yields the same value as Eq. (4.7) derived through the procedure of Eqs. (4.5) and (4.6). This provides the link between the probabilistic identity $W(r)dr = W(R)dR$ and substitution of variables in integration.

4.2. Repeat the analysis of Eqs. (4.35), (4.36), (4.37), (4.38), (4.39), (4.40) and (4.41) for a log-normal distribution of pore radii. What additional assumptions must

be made in order to complete the analysis? Constrain the pore-size distributions for the log-normal and the fractal case to be in some sense similar (define the similarity or equivalence) and then compare the results for the hydraulic conductivity. Give graphical representations of both the comparison between the two pore-size distributions and the two results for the hydraulic conductivity.

4.3. Repeat the analysis of Eqs. (4.42), (4.43), (4.44) and (4.45) for a log-uniform distribution of pore radii. Compare your results with those for *r*-percolation.

4.4. Assume for simplicity that, as *r*-percolation involves an integral over a 3D spherical region of space, $r-E$-percolation involves an integral over the analogue to a sphere in 4D space. In such a picture write an analogue to Eq. (4.16) for l. What length replaces d as the first factor? What is the dependence of l on T?

4.5. Find the temperature dependence of the correlation length for $R = R_{\text{opt}}$ in $r-E$-percolation.

4.6. Show that variable-range hopping in d dimensions leads to the result

$$\sigma \propto \exp\left[-\left(\frac{T_0}{T}\right)^{\frac{1}{d+1}}\right]$$

4.7. Let the density of states, $N(E)$, be proportional to E^{n}. Show that VRH in d dimensions now leads to

$$\sigma \propto \exp\left[-\left(\frac{T_0}{T}\right)^{\frac{n+1}{n+d+1}}\right]$$

4.8. Suppose that a VRH system is long in two of its dimensions [41], y, but short in the third, x, i.e., $y >> x$. Consider moreover that x may be shorter than the correlation length found in problem 4.5, and that a potential difference is set up across one of the long axes of the system (longitudinal, rather than transverse, conduction). In this case the conduction path cannot develop fully in the third dimension and conduction follows some intermediate dimensionality between 2 and 3. It is possible to constrain the conduction path to stay within the system by the trick of allowing conduction to proceed through larger resistances, and using a larger effective critical resistance, i.e.,

$$\chi = \chi_0 (p - p_{\text{c}})^{-\nu} \leq x$$

Let the exponent $2r_{ij}/a + E_{ij}/kT = \xi$. First solve this equation for the correlation length for p and then substitute this new value of p into a linearized version of the following equation (relating $\xi - \xi_{\text{c}}$ to $p - p_{\text{c}}$),

$$\xi_{\text{c}}^4 \left[\frac{T}{T_0}\right] = 1$$

to find

$$\sigma \propto \exp\left[-\left(\frac{T_0}{T}\right)^{\frac{1}{4}}\right] \exp\left[-\left(\frac{T_0}{T}\right)^{\frac{1}{4}}\left(\frac{\chi_0}{x}\right)^{\frac{1}{\nu}}\right]$$

Actually a more accurate calculation would replace χ_0 with the correlation length for the dc conductivity in 3D VRH (from problem 4.5), but this is sufficiently accurate for the present purposes, and provides a preparation for material in Chap. 8.

References

1. Sahimi, M., 1993, Fractal and superdiffusive transport and hydrodynamic dispersion in heterogeneous porous media, *Transp. Porous Media 13*: 3–40. 97
2. Sahimi, M., 1993, Flow phenomena in rocks – from continuum models to fractals, percolation, cellular automata, and simulated annealing, *Rev. Mod. Phys. 65*(4): 1393–1534. 97
3. Ambegaokar, V. N., B. I. Halperin, and J. S. Langer, 1971, Hopping conductivity in disordered systems. *Phys. Rev. B 4*: 2612–2621. 98, 102
4. Miller, A., and E. Abrahams, 1960, Impurity conduction at low concentrations, *Phys. Rev*. **120**: 745. 98
5. Seager, C. H., and G. E., Pike, 1974, Percolation and conductivity: a computer study II, *Phys. Rev. B* **10**: 1435–1446. 100, 117
6. Hunt, A. G., 2001, AC hopping conduction: perspective from percolation theory, *Philos. Mag. B 81:* 875–913. 103, 104, 105, 109
7. Long, A. R., J. McMillen, N. Balkan, and S. Summerfield, 1988, The application of the extended pair approximation to hopping conduction in rf sputtered amorphous silicon, *Phil. Mag*. B **58**: 153–169. 103, 109
8. Long, A. R., and L. Hansmann, 1990, *Hopping and Related Phenomena*, ed. M. Pollak and H. Fritzsche, World Scientific, Singapore, p. 309. 103, 109
9. Stauffer, D., and A. Aharony, 1994, *Introduction to Percolation Theory*, 2nd edition, Taylor and Francis, London. 104
10. Skaggs, T. H., 2003, Effects of finite system size and finite heterogeneity on the conductivity of broadly distributed resistor networks, *Physica B*, **338:** 266–269. 104
11. Berkowitz, B., and I. Balberg, 1993, Percolation theory and its application to groundwater hydrology, *Water Resour. Res*. **29**: 775–794. 105
12. Pollak, M., 1972, A percolation treatment of dc hopping conduction. *J. Non-Cryst. Solids* **11**: 1–24. 106, 108
13. Mott, N. F., 1969, Conduction in non-crystalline materials 3. Localized states in a pseudo gap and near extremities of conduction and valence bands, *Phil. Mag*. **19:** 835. 107, 108
14. Hunt, A. G., 2001, Applications of percolation theory to porous media with distributed local conductances, *Adv. Water Resour.* **24**(3,4)**:** 279–307. 109
15. Moldrup, P., T. Oleson, T. Komatsu, P. Schjønning, and D. E. Rolston, 2001, Tortuosity, diffusivity, and permeability in the soil liquid and gaseous phases. *Soil Sci. Soc. Am. J*. **65**: 613–623. 110
16. Balberg, I., 1987, Recent developments in continuum percolation, *Philos. Mag. B* **30**: 991–1003. 110, 115, 117
17. Kogut, P. M. and J. Straley, 1979, Distribution-induced non-universality of the percolation conductivity exponents, *J. Phys. C. Solid State Phys.* **12**: 2151–2159. 110
18. Le Doussal, P., 1989, Permeability versus conductivity for porous media with wide distribution of pore sizes, *Phys. Rev*. B **39**: 4816–19. 110, 111, 112
19. Banavar, J. R., and D. L. Johnson, 1987, Characteristic pore sizes and transport in porous media, *Phys. Rev. B* **35**: 7283–7286. 110, 111, 112

20. Katz, A. J., and A. H. Thompson, 1986, Quantitative prediction of permeability in porous rock, *Phys. Rev. B* **34**: 8179–8181. 110, 111, 112, 113
21. Hunt, A. G., and G. W. Gee, 2002, Application of critical path analysis to fractal porous media: comparison with examples from the Hanford site, *Adv. Water Resour.*, **25**: 129–146. 111, 112, 114
22. Kozeny, J., 1927, Ueber Kapillare Leitung des Wasssers im Boden, *Sitzungsber. Adak. Wiss. Wien*, **136**: 271–306. 112
23. Carman, P. C. 1956, *Flow of Gases Through Porous Media*, Butterworths, London. 112
24. Johnson, D. L., and L. M. Schwartz, 1989, Unified theory of geometric effects in transport properties of porous media. In Paper presented at SPWLA, 30th Annual Logging Symposium, Soc. of Prof. Well Log. Anal. Houston, TX. 112, 113
25. Bernabe, Y., and A. Revil, 1995, Pore-scale heterogeneity, energy dissipation and the transport properties of rocks, *Geophys. Res. Lett.* **22**: 1529–32. 112
26. Torquato, S., and B. Lu, 1990, Rigorous bounds on the fluid permeability: effect of polydispersivity in grain size, *Phys. Fluids A* **2**: 487–490. 112
27. Bernabe, Y., and C. Bruderer, 1998, Effect of the variance of pore size distribution on the transport properties of heterogeneous networks, *J. Geophys. Res.*, **103**: 513. 113, 117
28. van Genuchten, M. T., 1980, A closed form equation for predicting the hydraulic conductivity of unsaturated soils, *Soil Sci. Am. J.*, **44**: 892–898. 113
29. Millington, R. J., and J. P. Quirk, 1959, Permeability of porous media. *Nature* (London) **183**: 387–388. 113
30. Millington, R. J., and J. P. Quirk, 1961, Permeability of porous media, *Trans. Faraday Soc.* **57**: 1200–1208. 113
31. Childs, E. C., and N. Collis-George, 1950, The permeability of porous materials, *Proc. Royal Soc. London, Ser. A* **201**: 392–405. 113
32. Blunt, M. J., and H. Scher, 1995, Pore-level model of wetting, *Phys. Rev. E*, **52**: 6387–403. 114
33. Tokunaga, T., and J. Wan, 1997, Water film flow along fracture surfaces of porous rock, *Water Resour. Res.* **33**: 1287–1295. 114
34. Hunt, A. G., 2004, Percolative transport and fractal porous media, *Chaos Solitons Fractals* **19***:* 309–325. 115
35. Scheibe, T., and S. Yabusaki, 1998, Scaling of flow and transport behavior in heterogeneous groundwater systems, *Adv. Water Resour.* **22**: 223–238. 117
36. Deutsch, C. V., 1989, Calculating effective absolute permeability in sandstone/shale sequences, *SPE Form Eval*, **4(3)**: 343–348. 117
37. Desbarats, A., 1992, Spatial averaging of hydraulic conductivity in 3-dimensional heterogeneous porous-media. *Math Geol*. **24**(3): 249–267. 117
38. Vyssotsky, V. A., S. B. Gordon, H. L. Frisch, and J. M. Hammersley, 1961, Critical percolation probabilities (bond problem), *Phys. Rev*. **123**: 1566–1567. 117
39. Hunt, A. G., and B. Idriss, 2009, Percolation-based effective conductivity calculations for bimodal distributions of local conductances, *Phil. Mag*. in press. 118
40. Friedman, L., and M. Pollak, 1981, The hall effect in the variable-range hopping system, *Philos. Mag. B* **44**: 487–507. 119
41. Shklovskii, B. I., and A. L. Efros, 1984, *Electronic Properties of Doped Semiconductors*, Springer, Heidelberg. 120

Chapter 5
Hydraulic and Electrical Conductivity: Conductivity Exponents and Critical Path Analysis

This chapter describes how to estimate hydraulic and electrical conductivity. Electrokinetic currents, because of their very close relationship with electrical and hydraulic conductivity, are discussed here too. Other properties, such as air permeability, solute and gas diffusion, and thermal conductivity are discussed in Chap. 6. The results are valid for generating sample-scale properties from pore-scale variability. The theoretical development and the parameters obtained are consistent across the various properties, and the results predict experimentally measured values. The primary focus is on the saturation dependence of such properties, though sometimes we also consider the saturated values of these properties, and their dependences on porosity.

Several authors have considered whether the universal scaling of percolation transport coefficients should be seen in basic properties such as hydraulic or electrical conductivity [1–7]. An alternative perspective has also been proposed, namely that conduction processes may follow nonuniversal power laws: the conductivity exponent μ may take different values in different systems. Both models and data exist [2, 8, 9] supporting a nonuniversal scaling of electrical or hydraulic conductivity for specific cases in continuum percolation. Feng et al. [9] obtained the then "universal" value $\mu = 1.88$ for a conducting matrix from which equal-sized, overlapping spherical voids are removed. This so-called random void or Swiss cheese model is functionally equivalent to a conducting fluid with insulating spherical inclusions, e.g., a brine-saturated sandstone, and its low percolation threshold and universal exponent support a percolation basis for Archie's law (discussed below). In their (1987) model the width of the conducting necks remaining between spherical voids was denoted δ, and its values were argued to be uniformly distributed. For the inverse case, that of overlapping spherical conductors in an insulating matrix (the inverted random void or cannonball rock model), Feng et al. [9] obtained the nonuniversal value $\mu^* = \mu + 0.5 = 2.38$ (where the superscript * denotes a nonuniversal value). Because this latter case is the negative of a typical particulate geological medium, its nonuniversal exponent need not imply nonuniversal behavior in rock and soil. Further, the role of the overlapping volume (whether void or solid) is very prominent in generating the nonuniversal exponents, but the construction of solid overlaps is not obviously related to a physically based formation of geological media.

Hunt, A., Ewing, R.: *Hydraulic and Electrical Conductivity: Conductivity Exponents and Critical Path Analysis.* Lect. Notes Phys. **771**, 123–167 (2009)
DOI 10.1007/978-3-540-89790-3_5

We do not deny that there may be cases where such exotic power laws are appropriate, but we find both theoretical rationale and experimental evidence that universal scaling is far more common than the nonuniversal exponents. Further, we show that CPA (critical path analysis, the subject of Chap. **??**) can yield known nonuniversal scaling results under mathematical conditions which extend its validity to the percolation threshold. While the derivation of a nonuniversal exponent in this case requires using an unphysical limit of a reasonable model, our derivation demonstrates clearly that treating geometrical conditions with CPA provides an appropriate mathematical framework to generate nonuniversal exponents of percolation theory.

A common example of universal scaling is Archie's law [10] for the saturation dependence of the electrical conductivity. Archie's law has often been expressed in a form, in which both the saturation dependence and the dependence of the electrical conductivity on porosity are represented as (possibly different) powers. Examining the basis for Archie's law has occupied many researchers, including (among others) Adler et al. [11], Bigalke [12], Binley et al. [13–15], Thompson et al. [16], Kuentz et al. [17], Lemaitre et al. [18], Johnson and Schwartz [19], Le Ravalec et al. [20], Mattisson and Knackstedt [21], Ruffet et al. [22], Wong et al. [23], and Montaron [24]. While Archie's data are often cited to demonstrate the occurrence of different values of such powers, we found [25] that each of his distinct data sets supports universal scaling precisely. Moreover, all other experimental studies we found relating to saturation dependence were compatible with the universal scaling. Thus we concluded that universal scaling is the most commonly observed result, if not the only result found.

When we address the question of how percolation theory should be applied to predicting conduction properties, we have to adapt our analyses to the medium in question. This process, as suggested in Chap. 3, may be very different for artificial and natural media, and may also differ depending on whether the medium is a product of aggregation or of fragmentation processes. The analysis presented will be tailored to media formed chiefly through fragmentation processes, such as soils, but the results appear to be valid for many other media as well. The particular analysis is based on the Rieu and Sposito [26] random fractal model presented in Chap. 3. Certainly a large amount of data do seem to be in accord with that model, so it is at least widely applicable. In case the RS model does not describe the pore space, an analogous treatment should be used; the basic procedure is outlined in Sect. 5.3. It is of general importance to consider the limitations of our methods, and in what kinds of systems we might expect them to be incomplete. For example, one can imagine scenarios in which Archie's law follows universal scaling for saturation dependence but not for porosity dependence, consistent with typical phenomenological representations of Archie's law. While such a result is not generated specifically by the methods described here, that does not mean that it is generally incompatible with percolation theory.

What is novel in this method, and, in this book, new in this chapter, is the development of tests to distinguish when geometry (the pore-size distribution) is important to the conductivity: this technique combines critical path analysis (chiefly geometry) and percolation scaling (chiefly topology). As a result of such tests, we

find that universal percolation scaling should explain a wide range of data; we can also predict under what conditions nonuniversal results may apply, and what form they should take, whether nonuniversal power laws or otherwise.

We also can now better identify complications from experiment. In particular, when analysis leads us to expect universal scaling from percolation theory, but observations indicate otherwise, we find that factors other than nonuniversal exponents of percolation frequently influence experimental results. For example, we have seen evidence for experimental issues such as contact resistance, nonzero conductivity of the solid phase, misjudging the value of a critical moisture content, and dissolution of precipitated ions; these issues complicate the analysis and may, if not accounted for, appear to support nonuniversal exponents. We analyze over 80 data sets for electrical conduction or diffusion (and summarize prior analysis of another 50 data sets), all of which appear consistent with universal scaling. Some of these data sets (e.g., Archie [10]) had been interpreted differently in the past to support the relevance of nonuniversal exponents.

5.1 Hydraulic and Electrical Conductivities, and Electrokinetic Coupling: Universal and Nonuniversal Exponents

The scaling difference between electrical and hydraulic conduction, though only a matter of the specific power of a pore radius, produces a huge difference in measurable properties. We start by contrasting electrical and hydraulic conductivity, with each expressed as a function of moisture content, and for completeness include electrokinetic effects as well.

From Chap. 4 we had that the hydraulic conductance of a (roughly cylindrical) pore of radius r and length l filled with fluid of viscosity η is

$$g^{\mathrm{h}} \propto \frac{r^4}{\eta l} \tag{5.1}$$

The electrical conductance of the same pore is

$$g^{\mathrm{e}} \propto \sigma_{\mathrm{b}} \frac{r^2}{l} \tag{5.2}$$

where σ_{b} is the electrical conductivity of the water or brine filling the pore; σ_{b} is therefore proportional to the concentration of charge carriers. Equation (5.2) is equivalent to stating that the resistance of a homogeneous wire of resistivity $\rho \equiv 1/\sigma$, length l, and cross-sectional area A is $\rho l/A$, a result familiar from elementary physics. Equation (5.2) implicitly assumes that conduction is uniform within a given pore and would be relevant for the thermal conductivity as well, if it were not for the fact that the solid medium typically has a higher thermal conductivity than the fluid-filled pore space. Because electrokinetic effects (as opposed to thermal conduction) also relate chiefly to the water-filled pore space, we include them in

this discussion. In this case in a cylindrical pore, so that the total charge transport is confined to a cylindrical shell of length $2\pi r$ and thickness Δr, rather than a cylinder of cross-sectional area πr^2. Therefore the conductance g^{ek} (the coefficient of proportionality between electrokinetic current, J^{ek}, and the gradient of pore pressure) takes the form [27].

$$g^{ek} \propto \frac{r}{l} \tag{5.3}$$

In finding the controlling conductance in an infinitely large system, critical path analysis will yield the same critical radius r_c for electrical as for the hydraulic conductivity [28], and for that matter also for the electrokinetic current, since in all three cases a pore's conductance is a monotonically increasing function of r. Using a network model on a cubic grid, Friedman and Seaton [28] showed that the relationship between the saturated electrical conductivity σ_S and the saturated hydraulic conductivity K_S is $K_S \propto r_c^2 \sigma_S$. Extending the relationship to include an electrokinetic conductance, g^{ek} would yield $g_c^e \propto r_c g_c^{ek}$. The proportionality constant r_c^2 between K_S and σ_S is therefore system dependent rather than universal, even when both properties are determined by critical path analysis. We will see that the connection between the two properties is even less straightforward, and that there is little hope of deriving a rigorously predictive relationship between the two quantities – without knowing much more about the medium than one is likely to know if one's aim is simply to obtain K_S from σ_S.

Consider the implications of treating a self-similar medium. If a medium is fractal, it is not possible to distinguish the size of a pore on the basis of its aspect ratio l/r. More generally, while all pore shapes of a given size need not be identical, self-similarity still requires that the distribution of pore shapes be independent of pore radius. Thus self-similarity implies $r \propto l$ in the mean.

In a medium in which the pore space is self-similar, we can summarize the scaling of various pore-scale conductances with r

$$g^h \propto r^3 \tag{5.4}$$

$$g^e \propto r^1 \tag{5.5}$$

and

$$g^{ek} \propto r^0 \tag{5.6}$$

Of course the porous medium may be simulated using a network model with a fixed grid, such that all pore lengths are identical even while the pore radii vary. In such a case it would be necessary to increase by 1 the powers of r in Eqs. (5.4) through (5.6), giving the original values of 4, 2, and 1, respectively. The particular results derived below would then no longer hold, but analogues to these results are treated in the problem sets.

Assume the RS model as a case consistent with $l \propto r$. Consider that if a pore has radius r with probability $W(r)$, it must have volume r^3, making the chance that a

small volume chosen arbitrarily belongs to a pore of radius r proportional to $r^3W(r)$. Thus, since $W(r) \propto r^{-1-D_\mathrm{p}}$, we must have the probability of "landing on" a pore of radius r be $r^3W(r) \propto r^{2-D_\mathrm{p}}$. Combine Eqs. (5.4) and (5.5) with the relationship

$$W(r)\,dr = W(g)\,dg \tag{5.7}$$

as well as $r^3W(r) \propto r^{2-D_\mathrm{p}}$ and the results

$$W\left(g^\mathrm{h}\right) \propto \left(g^\mathrm{h}\right)^{-\frac{D_\mathrm{p}}{3}} \tag{5.8}$$

and

$$W\left(g^\mathrm{e}\right) \propto \left(g^\mathrm{e}\right)^{2-D_\mathrm{p}} \tag{5.9}$$

follow. In Eq. (5.8) it is almost always true that $0 < D_\mathrm{p}/3 < 1$, while in Eq. (5.9) $-1 < 2 - D_\mathrm{p} < 0$ as long as $2 < D_\mathrm{p} < 3$, which is typically the case. Thus, under usual circumstances, the distributions of both the electrical and the hydraulic conductances are power laws with exponents $-\alpha$ such that $0 < \alpha < 1$. But Balberg [2] determined that if

$$W(g) \propto g^{-\alpha} \quad 0 < \alpha < 1 \tag{5.10}$$

for a distribution that continued to $g = 0$, then the conductivity described by that distribution must obey

$$\sigma \propto (p - p_\mathrm{c})^{\frac{\alpha}{1-\alpha}} \tag{5.11}$$

Thus Eqs. (5.8) and (5.9) give results that correspond to those treated by Balberg[2] (1987) as generating nonuniversal exponents of percolation theory, except that, as we will see, they cannot be extended to $g = 0$ as required for that derivation. On the other hand, the distribution of electrokinetic conductances follows the form

$$W\left(g^\mathrm{ek}\right) \propto \delta(g - g_0) \tag{5.12}$$

(where δ is the Dirac delta function): all conductances have the same value, which we designate g_0. In a system with heterogeneous mineralogy, Eq. (5.12) would no longer hold, because the streaming potential, which we do not discuss (see, e.g., Bernabe [29]), would also vary. However, even in a heterogeneous network there could be no correlation between saturation and the conductance distribution, so arguments that conduction (as a function of saturation) is governed by nonuniversal exponents would not apply.

A network in which all conductances have the same value cannot generate a nonuniversal exponent for the conductivity. Further, application of critical path analysis to such a network cannot yield a saturation dependence of the electrokinetic current J^ek, since the critical conductance value will have no dependence on saturation. Thus the only saturation dependence available for J^ek is topologically based, and must be given by the universal scaling of percolation theory (also given in Surkov and Tanaka [30]). When the pore-size distribution is irrelevant to conductance, the universal exponents of percolation theory describe the behavior of the

saturation dependence of the conductivity over the full range of saturations and J^{ek} must depend on saturation as

$$J^{ek} \propto (\theta - \theta_t)^{\mu} \tag{5.13}$$

Normalization for $\phi = 1$ of such a property that depends only on surface properties is subtler than we wish to address, so this concludes our discussion of electrokinetic currents and we return to the electrical and hydraulic conductivities, whose dependences on saturation and porosity have not yet been completely described.

From Chap. 4 the ratio of the (unsaturated) hydraulic conductivity $K(\theta)$ and its value K_S at saturation is

$$K(\theta) = K_S \left[\frac{(1-\phi) + (\theta - \theta_t)}{1 - \theta_t} \right]^{\frac{3}{3-D_p}} \tag{5.14}$$

Equation (5.14) was developed in critical path analysis as the cube of the ratio of the corresponding critical radii. In analogy with Eq. (5.14) for hydraulic conductivity, we can write for electrical conductivity [31]

$$\sigma(\theta) = \sigma_S \left[\frac{(1-\phi) + (\theta - \theta_t)}{1 - \theta_t} \right]^{\frac{1}{3-D_p}} \tag{5.15}$$

The only difference between the forms of Eqs. (5.14) and (5.15) is that the power $3/(3-D_p)$ in Eq. (5.14) is replaced by $1/(3-D_p)$ in Eq. (5.15); this is done because the power of r for hydraulic conductivity (3 in Eq. (5.4)) is replaced by its power for electrical conductivity (1 in Eq. (5.5)).

Combination of Eq. (5.14) with Eq. (3.22) for moisture content as a function of hydraulic head h gives the following result for $K(h)$:

$$K(h) = K_S \left[1 - \frac{1 - (h_A/h)^{3-D_p}}{1 - \theta_t} \right]^{\frac{3}{3-D_p}} \tag{5.16}$$

In the case $\theta_t \to 0$, Eq. (5.16) reduces to $K(h) = K_S (h_A/h)^3$ independent of pore-size distribution. Usual soil physics treatments imply the dependence h^{-2}. But for $\theta_t > 0$, $K(h)$ in Eq. (5.16) follows an approximate rather than an exact power law, and the approximate power is greater than 3. See the discussion following Eq. (5.19) for further details.

5.1.1 Balberg Nonuniversality

Balberg [2] demonstrated explicitly that distributions such as Eqs. (5.8) or (5.9), if continued to $g = 0$ (which represents no mathematical problem, i.e., the distribution is normalizable), lead to nonuniversal exponents for conduction. That is, the

conductivity vanishes according to some nonuniversal power of the difference between a volume fraction and its critical value. If we adapt Eq. (5.11) for continuum variable p to the case that the fractional volume is a water content we find

$$\sigma \propto (\theta - \theta_t)^{\frac{\alpha}{1-\alpha}} \tag{5.17}$$

Substituting the exponent from Eq. (5.8) [Eq. (5.9)] in Eq. (5.11) would yield the nonuniversal exponent $D_p/(3-D_p)[(D_p-2)/(3-D_p)]$. However, the distributions given in Eqs. (5.8) and (5.9) are truncated, both at a maximum g corresponding to r_m, and at a minimum g corresponding to r_0. The cutoff at the minimum g is required by physical constraints, not mathematical conditions: a fractal medium with $r_0 = 0$ would have porosity $\phi = 1$, zero solid volume, and infinite solid surface area in a finite volume (see Chap. 7). Because these are clearly unphysical results, we do not expect Balberg's prediction of nonuniversal exponents to be observed in the saturation dependence of hydraulic or electrical conductivity through water-filled pore space. On the other hand, the Balberg derivation will be seen below to be useful in the present analysis, because his results follow from Eqs. (5.18) and (5.19) below in the limit $\phi \to 1$. This provides a mathematical check on the present results. In principle the Balberg result also provides a functional envelope that constrains the actual behavior. But it appears that for experimental results to resemble the nonuniversal scaling results, the porosity must be on the order of 90%, an unusual condition for geological materials.

In this discussion we have identified the scaling of the bottleneck resistance as a function of moisture content with the scaling of the conductivity. In order to clarify the correspondence with the results of Balberg [2], we make the same assumption that was made there – that conduction on these paths is basically 1D in character – then calculate the average resistance of the resulting paths. To do this, one integrates over the bulk resistance distribution cutoff at g_c^{-1}, with the result that $< g^{-1} >^{-1}$ is given in each case by $g_c^{-\alpha}$. Applied to Eqs. (5.14) and (5.15), the results are [32]

$$K(\theta) = K_S \left[\frac{(1-\phi) + (\theta - \theta_t)}{1 - \theta_t} \right]^{\frac{D_p}{3-D_p}} \tag{5.18}$$

and

$$\sigma(\theta) = \sigma_S \left[\frac{(1-\phi) + (\theta - \theta_t)}{1 - \theta_t} \right]^{\frac{D_p-2}{3-D_p}} \tag{5.19}$$

differing from Eqs. (5.14) and (5.15) solely in the substitution of D_p for 3 in the numerator of the exponent. While these exponents are exactly $\alpha/(1-\alpha)$, as required by Balberg [2], the arguments of the powers in Eqs. (5.18) and (5.19) are not simply $\theta - \theta_t$, as in his result. While it is already clear that Eqs. (5.18) and (5.19) yield Eq. (5.17) (with $p - p_c \to \theta - \theta_t$) in the case $\phi = 1$, we still need to demonstrate under what range of moisture contents Eqs. (5.18) and (5.19) are generally valid, before we apply the condition $\phi = 1$.

While Eqs. (5.18) and (5.19) were derived to allow comparison with those of Balberg[2] (1987), they may have significance beyond that comparison. For example, derivation of Eq. (5.18) implies that Eq. (5.16) in the case $\theta_t = 0$ would reduce to the nonuniversal result $K(h) \propto h^{-D_p}$, rather than h^{-3}. Note that the observed scaling of K with h is usually according to a power between 2 and 3: typically closer to 3 than to 2, but not to precisely either 2 or 3 (Sposito, personal communication, 2002). Furthermore, $K(h)$ tends to drop more rapidly for coarser soils than for finer soils [33]. Such a result cannot be understood in terms of Eq. (5.16), which has no pore-size information beyond h_A. But if D_p tends to be larger for sandy soils than for clayey soils [34], such a result is indicated, and is consistent with Eq. (5.18). Without analyzing a large number of additional media, these comments need not be conclusive to the typical physicist reading this passage, but they should have considerable significance to the typical soil physicist. If these considerations are indeed relevant, then the Balberg [2] treatment, *which uses the average resistance* along the critical path *rather than the largest resistance*, is a significant refinement to the simpler critical path treatment.

For typical values of the fractal dimensionality of soils (say 2.8; [35]), the difference between D_p and 3 in the numerator of the exponent (Eq. (5.14) vs. (Eq. (5.18)) and Eq. (5.15) vs. Eq. (5.19)), while small, may be detectable. However, there is some theory-based uncertainty as to whether using D_p is really more accurate than 3: as Mallory [36] pointed out, the distribution of resistances on the backbone clusters is not the same as in the bulk. Larger resistors are shorted more often than smaller ones, so integration over the bulk distribution, even with the cutoff, is not strictly justifiable. Our comparisons with experiment have thus far used Eq. (5.14) rather than Eq. (5.18), and we continue to use that equation here for evaluation, but we emphasize that the issue of which exponent is more appropriate and accurate remains unresolved.

In order to complete our comparison with Balberg's [2] results, we need to discuss the relationship between critical path analysis and percolation scaling. This analysis leads to inferences regarding Kozeny–Carman phenomenology and Archie's law as well.

5.1.2 Transition from Critical Path Analysis to Percolation Scaling

Regardless of whether the exponent's numerator contains 3 (Eqs. (5.14) and (5.15)) or D_p (Eqs. (5.18) and (5.19)), the critical path equations imply that when the moisture content $\theta \to \theta_t$, the conductivity (whether hydraulic or electrical) is governed by the smallest pore in the system. But this contradicts percolation scaling, according to which K and σ must both go to zero in the limit $\theta \to \theta_t$, even if the smallest pore $r_0 > 0$. In fact, if $r_0 > 0$, then one expects universal scaling to hold and

$$\frac{K(\theta)}{K_0} = \frac{\sigma(\theta)}{\sigma_0} \propto (\theta - \theta_t)^{\mu} \tag{5.20}$$

with the constants K_0 and σ_0 having appropriate units and physical foundations. So we must address the issue of these two distinct dependences of $K(\theta)$ and $\sigma(\theta)$ in the limit $\theta \to \theta_t$, first considering hydraulic conductivity.

When θ is near θ_t, Eq. (5.20), which results from topology and percolation scaling, must replace Eq. (5.14), which describes $K(\theta)$ based on the size (geometry) of the bottleneck pore. Denote by θ_{xK} the moisture content at that cross-over or replacement point. The value of θ_{xK} can be determined [37] by setting equal the two dependences of $K(\theta)$, and also setting equal their derivatives, at some moisture content $\theta = \theta_{xK}$. The use of these two conditions, requiring continuity of both K and $dK/d\theta$, yields both θ_{xK} and the constant prefactor K_0 in Eq. (5.20). Notice that we must have $\theta_t \leq \theta_{xK}$.

The practical consequence of the analysis for the crossover moisture content is that for any θ, the appropriate equation for K is the one that gives the larger value of $|dK/d\theta|$. That is, the form to choose is the one most sensitive to changes in moisture content at the current moisture content. Equivalently, the less-sensitive dependence is set equal to a constant. This procedure also permits us to find K_0, the prefactor of the hydraulic conductivity in the range of moisture contents where K is given by universal percolation scaling [37](Hunt, 2004c). This is a valuable capability, as earlier recognized by Berkowitz and Balberg [5](1993): "One might suggest that, since the hydraulic conductivity can vary by orders of magnitude among rocks of the same porosity, the coefficients of equality in the power law relationship may be of greater significance than the critical exponent."

For short-hand reference, Eq. (5.20) will be referred to as percolation scaling of K, while Eq. (5.14), derived from critical path analysis, will be referred to as fractal scaling. Although both ultimately derive from percolation theory, in Eq. (5.14) it is the fractal characteristics, through the power-law pore-size distribution, which make the dominant impact on K and show up in the exponent.

The result from the above analysis for θ_{xK} is [37]

$$\theta_{xK} = \theta_t + \left[\frac{\mu\,(1-\phi)}{3/(3-D_p)-\mu}\right] \tag{5.21}$$

Note that if consistency with the Balberg result for nonuniversal scaling is required, $3/(3-D_p)$ must be replaced by $D_p/(3-D_p)$. For $\mu = 2$ and typical values of $\phi = 0.4$ and $D_p = 2.8$ [35], Eq. (5.21) leads to $\theta_{xK} - \theta_t \approx 0.09$, about 22% of the range of moisture contents. Figure 5.1 demonstrates an example of this crossover for the values of D_p, ϕ, and θ_t from the McGee Ranch soil [32, 39], along with experimentally measured values of K. $D_p \approx 2.81$ was obtained from porosity and particle size data via Eq. (3.16), while θ_t was obtained by comparison with studies examining percolation scaling of the diffusion constant [38]. Note that the data for Fig. 5.1 [40] were obtained in a field experiment (unsteady drainage), and stops at a moisture content approximately equal to θ_{xK}. Lower moisture contents are associated with very small values of K and require much longer drainage times than attainable in experiment. Thus the question of equilibration becomes very important at moisture contents below θ_{xK}, a topic which is discussed in detail in Chap. 7.

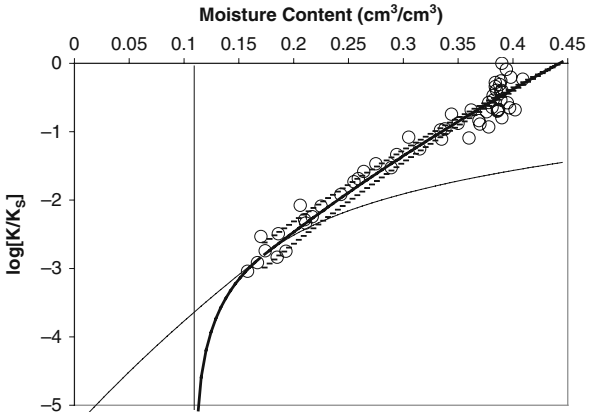

Fig. 5.1 The hydraulic conductivity of the McGee Ranch soil as a function of moisture content. Data from Rockhold et al. [40]. The *circles* are the experimental values. The *bold line* is the combined prediction of critical path analysis (Eq. (5.14)) and universal scaling near the percolation threshold (Eq. (5.20)). The *light line* for $\theta > 0.15$ is Eq. (5.20), for $\theta < 0.15$, Eq. (5.14). The *dashed lines* on either side of the *bold line* represent the approximate uncertainty in the prediction due to the variability (9 samples) in the measured values of r_0 and r_m and the consequent uncertainty in D_p. The critical moisture content, 0.107, for percolation was obtained from the regression of Hanford site soils on the Moldrup relationship for the threshold moisture content for diffusion (Chap. 7), and is shown by the vertical line. K_S was chosen to be the largest K value measured. The porosity was 0.444. Note that the unsteady drainage (field) experiment did not attain lower moisture contents than approximately θ_{xK}, where K begins to drop precipitously

For completeness, Fig. 5.2 shows predicted and observed $K(\theta)$ for a multi-modal pore-size distribution, treated analytically by assuming that each mode of the distribution follows a power law. An interesting aspect of a multi-modal pore-size distribution is its effect on the representation of $K(h)$. While $K(h)$ tends to follow a power law in hydraulic head (either h^{-3} or h^{-D_p}) in the case of a simple power-law pore-size distribution (with a positive curvature on a log[K] vs. h plot), when the distribution is bimodal this universal tendency is lost. Consider a case when the largest

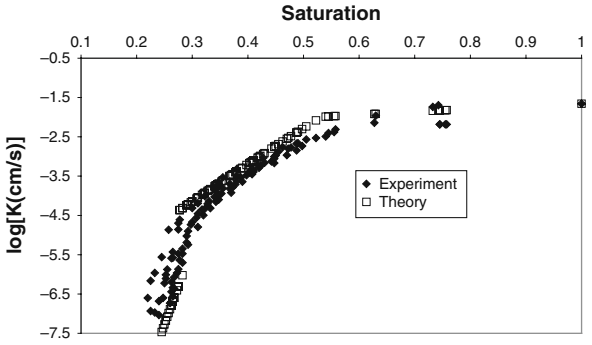

Fig. 5.2 The hydraulic conductivity of the North Caisson soil. The North Caisson soil had a multimodal particle-size distribution. Like the McGee Ranch soil the theoretical comparison involves no uncertain parameters. Data from Rockhold et al. [40]

water-filled pore is in the upper mode of the pore-size distribution (say, with dimension D_u), but the critical pore radius is in the lower mode (say, D_l). Then the two powers $3-D_u$ and $3/(3-D_l)$ will not combine to form 3, because the two values of D are not the same. (Use of the Balberg technique is a bit more complex here, but does not change the conclusions qualitatively.) If the lower mode of the distribution has a very small associated porosity, such as a small silt fraction in a sandy soil, then the usual fractal analysis will generate a value of D_l very close to 3, and $K(h)$ will have a cusp associated with a crossover to a much more rapid drop in K with increasing h. Experimental data near the cusp may appear to have a negative curvature on the typical plot because of the experimental uncertainty, but it is actually positively curved everywhere except at the crossover. Interestingly, the variability in K values increases rapidly below the crossover, since there is typically considerable relative variability in the concentration of fine soil particles when the medium is rather coarse. So if (for example) silt and clay compose on average 5% of a given soil, one is likely to encounter samples with concentrations from 2 to 10%; this variability can easily produce a variability in $1/(3-D_l)$ of 50–15, respectively [39].

Repeating for electrical conductivity the analysis that led to the hydraulic conductivity crossover θ_{xK} from fractal to percolation scaling yields [31]

$$\theta_{x\sigma} = \theta_t + \left[\frac{\mu(1-\phi)}{1/(3-D_p)-\mu}\right] \tag{5.22}$$

[or, using Balberg's approach, $(D_p-2)/(3-D_p)$ rather than $1/(3-D_p)$ in the denominator]. If the same values for $\theta_t = 0.04$, $\mu = 2$, $D_p = 2.8$, and $\phi = 0.4$ are substituted into Eq. (5.22) as into Eq. (5.21), one finds $\theta_{x_\sigma} - \theta_t \approx 0.4$ for the electrical conductivity, rather than the value 0.09 found for the hydraulic conductivity. That is, in the case of electrical conductivity, it is percolation scaling which dominates over the entire range of water contents. Thus the saturation dependence of the electrical conductivity, in contrast to that of the hydraulic conductivity, may to a good approximation be written in the form of percolation scaling all the way to full saturation where $\theta = \phi$ [31]:

$$\sigma = \sigma_0(\phi - \theta_t)^{\mu} \tag{5.23}$$

K at saturation is typically determined through r_c, but σ is not. When K at saturation contains information from the entire distribution of pore sizes, but σ at saturation is independent of the pore-size distribution, there is no possibility to infer the hydraulic conductivity from the electrical conductivity.

Further, Eq. (5.23), in its simplicity, should recall Archie's law, in which the conductivity is written as a power of the porosity.

5.1.3 Return to Balberg Nonuniversality

Equations (5.21) and (5.22) allow us to set a limit on the applicability of Balberg's results for nonuniversal scaling. Consider the limit $r_0 \to 0$, i.e., that fractal

fragmentation has proceeded indefinitely (and the limit that the power law of the conductance distribution continues to zero conductance). From Eq. (3.27) it is seen that $\phi \to 1$. If $\phi = 1$, Eq. (5.18) yields

$$K = K_S \left(\frac{\theta - \theta_t}{\phi - \theta_t} \right)^{\frac{D_p}{3-D_p}} \tag{5.24}$$

and Eq. (5.19) yields

$$\sigma = \sigma_S \left(\frac{\theta - \theta_t}{\phi - \theta_t} \right)^{\frac{D_p-2}{3-D_p}} \tag{5.25}$$

Further, Eqs. (5.21) and (5.22) both yield

$$\theta_x = \theta_t \tag{5.26}$$

Thus in the limit $r_0 \to 0$, the percolation scaling regime disappears, while the fractal scaling regime develops a dependence on the moisture content $(\theta - \theta_t)$ to a power, where the value of the exponent is related to the specific characteristics of the fractal structure, and is thus nonuniversal [32]. The predicted powers are in exact agreement with the results of Balberg if the average pathway resistance (rather than the critical resistance) is used. In a formal sense, extending the Rieu and Sposito fractal pore space model to pores of zero radius is consistent with continuing the power law conductance distribution to zero conductance, which allows direct comparison of Eqs. (5.24) and (5.25) with results of Balberg [2]. While Eqs. (5.24) and (5.25) predict that the nonuniversal behavior is valid for the entire range of (conducting) moisture contents, i.e., $\theta_t < \theta < \phi$, the universal contribution to the power from μ should also be added on at least in the vicinity of θ_t. Although we have been treating universal scaling effects separately, in the limit $\phi = 1$ the nonuniversal scaling results dominate over the entire range of moisture contents, and the additional contribution from universal scaling ($\mu = 2$) may simply be added on in the vicinity of the percolation threshold at θ_t. Note that for typical values of $D_p \approx 2.8$ in soils [35], the nonuniversal contributions to the power of Eqs. (5.18) and (5.19) are 14 and 4, respectively, i.e., much larger than 2. However, such soils also typically have $\phi \approx 0.4$, and the argument of the power $(1 - \phi) + \theta - \theta_t$ then becomes approximately $0.6 + \theta - \theta_t$. Such a function does not present as a power law when graphed logarithmically.

5.1.4 Inferences on Porosity Dependences at Full Saturation: Archie's Law

Result Eq. (5.23) also allows further discussion of the electrical conductivity under saturated conditions. It has been shown [41] that for natural media with insignificant clay content, $\theta_t = p_c \phi$, with p_c a numerical constant independent of porosity.

While the motivation of that derivation was theoretical, it was also shown that experimental data provided additional confirmation. The basis for this proportionality is easily understood in terms of a network of identical tubes: when a fraction p_c of the tubes is filled with water, the water-filled tubes percolate and the moisture content is $p_c\phi$, the result can be generalized heuristically to an arbitrary network with unknown p_c. Such an argument is really in the spirit of the first continuum percolation calculation of a critical volume fraction [42]. Combining this proportionality with the experimentally obtained approximation $p_c \approx 0.1$ (further discussion in Chap. 7), Eq. (5.23) may be rewritten [31] as

$$\sigma \propto (\phi - 0.1\phi)^{\mu} = (0.9)^{\mu}\,\phi^{\mu} \tag{5.27}$$

Equation (5.27) is in the form of Archie's law, and the result implies that the observed power μ of the porosity should be 1.3 in 2D systems and 2.0 in 3D systems. Berkowitz and Balberg [5] suggested that Archie's law might be a consequence of a critical moisture content that is zero, but did not mention the possibility that it would arise as a consequence of a proportionality of θ_t to ϕ. In fact we find experimental evidence for both cases.

Although we do not expect that nonuniversal scaling will apply to the saturation dependence of conduction properties, there is nevertheless a possible relevance of nonuniversal scaling to the *porosity*-dependence of the conductivity (hydraulic or electrical) of saturated media. Such a topic relates to a wider range of models of porous media than those we have concentrated on so far, including diagenesis. Nonuniversal exponents can, however, also result from pore-size distribution effects, and sometimes be implied by inappropriate analysis of experimental data.

Diagenesis is a physico-chemical process by which rock is altered at the grain scale. For example, after burial, sediments may be exposed to thermal, chemical, and pressure gradients that drive dissolution and precipitation of minerals. One can envision a precipitation process by which sand grains grow concentrically, except where they are already in contact with other grains. Such simplified models of diagenesis are discussed by Sahimi [43, 44] and bear some resemblance to the Swiss cheese and cannonball rock models for generation of nonuniversal exponents of conduction. Certainly the progression to systems with smaller porosity is geometrically distinct from, e.g., drying of a fractal medium. In the former case, pore shapes change continuously as the particles dilate, but in the latter, pore shapes must be independent of pore size; thus in the latter case both the largest water-filled pore and the critical pore radius have shapes independent of moisture content and both the connectivity of the water-filled medium and the sizes of the water-filled pores change with saturation, but not the porosity. In diagenesis, however, as the pore sizes are reduced, the connectivity of the medium remains constant (at early stages), but the porosity changes.

An important component of models for diagenesis is that they allow different dependences of the electrical conductivity on saturation and on porosity. Because the pore necks may diminish rapidly with diminishing porosity, it becomes possible to develop a nonuniversal dependence of the conductivity on porosity. This allows a more general phenomenological representation of Archie's law:

$$\sigma = \sigma_0 (S - S_c)^{\mu} \phi^n \tag{5.28}$$

with μ and n being different powers. We still expect μ to be 2.0 in 3D and 1.3 in 2D. However, n could respond to different influences, and variation in values of n could have different interpretations. What many models of diagenesis have in common (and also with the models of Feng et al. [9], 1987) are (1) reliance on a specific pore geometry and (2) dependence of the relevant pore radii on porosity. While this research direction is not incompatible with percolation theory (indeed, many of its papers have been developed within the framework of percolation theory and examination of nonuniversal exponents), it is not a necessary development of percolation theory. Even though an extensive literature exists on this subject, since we have found that in many cases more mundane explanations exist for results that at first glance might appear to imply nonuniversal exponents, we will not explore the literature on diagenesis. For a good early review on diagenesis, the reader is referred to Sahimi [43, 44]. But we will continue using μ for both powers (and μ^* for, e.g., pore-size induced deviations from 2) as well as the logical development of this subsection.

5.1.5 Universal Exponents Masquerading as Nonuniversal

Even as far as the porosity dependence of the electrical conductivity is concerned, we find a great deal of evidence to support the relevance of universal exponents of percolation theory. For simulations of 2D conduction, Kuentz et al. [17] effectively found $\mu = 1.28 \pm 0.07$ (Table 5.1), while experiments on 3D systems compiled by Krohn and Thompson [45] yield $\mu = 1.86 \pm 0.19$. Thompson et al. [16] give more than 40 values (Table 5.2), also with μ around 1.8. Balberg [2] and Krohn and Thompson [45] have two different perspectives on the wider range of μ values reported in the literature at that time; by constraining their results to systems that were consistent with each other, Krohn and Thompson [45] produced a much smaller variation in μ values. Nevertheless, the measured porosity exponent in Archie's law need not be precisely 2.0. We have already mentioned the potential relevance of diagenesis to series of related rocks with decreasing porosity. There exist also possible influences of pore-size variability. Data analysis may also include effects of

Table 5.1 Archie's law exponents from 2D simulations [17]

System	m
Random	1.22
Random	1.21
Triangle grains	1.26
Triangle pores	1.35
Diamond grains	1.24
Diamond pores	1.38

Table 5.2 Archie's law exponents from 3D rocks (mainly sandstones, from Thompson et al. [16]). The minimum l value was a theoretical estimation of Thompson et al. [16]. They determined the maximum l from mercury porosimetry. The D_p value calculated for the pore space is from Eq. (2.16)

Price river (depth)	D calculated	Porosity	Min l	Max l	m
67.5	2.975881	0.0828	0.02	0.72	1.78
93.8	2.975627	0.1265	0.02	5.14	1.81
93.2	2.975393	0.116	0.02	3	1.77
111.3	2.977919	0.1165	0.02	5.46	1.84
115	2.97452	0.1485	0.02	10.99	1.83
117	2.972552	0.1586	0.02	10.8	1.94
122.6		0.1282	0.02		1.84
125.4	2.976145	0.1192	0.02	4.09	1.87
128.1	2.977859	0.1275	0.02	9.47	1.88
130.3	2.974817	0.1095	0.02	2	1.85
132	2.974178	0.1242	0.02	3.4	1.9
137.3	2.974131	0.12	0.02	2.8	1.89
139.9	2.976272	0.1196	0.02	4.29	1.88
148.4	2.973592	0.1247	0.02	3.1	1.89
160.2	2.979283	0.1071	0.02	4.74	1.85
161.7	2.974569	0.1517	0.02	12.9	1.66
164.3	2.973942	0.1508	0.02	10.6	1.49
169.3	2.975546	0.1427	0.02	10.85	1.84
178.4	2.97544	0.1287	0.02	5.46	1.81
178.2	2.978037	0.1056	0.02	3.22	1.79
178.1	2.978725	0.0991	0.02	2.7	1.74
183.4	2.972752	0.1223	0.02	2.4	1.92
181.8	2.964996	0.123	0.02	0.85	1.88
189.1	2.974282	0.0922	0.02	0.86	1.77
197.1	2.971668	0.1044	0.02	0.98	1.77
199.7	2.979947	0.0848	0.02	1.66	1.78
203.8	2.977885	0.0656	0.02	0.43	1.69
210	2.981212	0.0359	0.02	0.14	1.57
224.8	2.971516	0.0751	0.02	0.31	1.78
233.1	2.972501	0.0726	0.02	0.31	1.79
265.8	2.978607	0.0526	0.02	0.25	1.77
607.3	2.97957	0.0943	0.02	2.55	1.81
626.2	2.984087	0.0691	0.02	1.8	1.72
637.8	2.984759	0.0658	0.02	1.74	2.24
652.9	2.981554	0.068	0.02	0.91	1.81
652.9	2.986981	0.042	0.02	0.54	1.66
Boise Table 1	2.948788	0.35	0.02	90	2.12
Boise Marsing 1	2.961246	0.239	0.02	23	2.1
Boise Silver 1	2.98126	0.097	0.02	4.63	2.37
Berea	2.96568	0.205	0.02	16	1.76
Navajo	2.973338	0.178	0.02	31.18	1.71
Coconino	2.975293	0.099	0.02	1.36	1.86
Nugget	2.981648	0.109	0.02	10.77	1.87
St Peters	2.983855	0.093	0.02	8.45	1.73
Tennessee	2.978262	0.062	0.02	0.38	1.67
Red Navajo	2.963027	0.23	0.02	23.5	1.8
Layered Navajo	2.964098	0.2295	0.02	28.5	1.76
White Navajo	2.96259	0.2676	0.02	82.5	1.5
Carmel	2.969541	0.1161	0.02	1.15	1.66
Austin Chalk	2.934058	0.2881	0.02	3.46	2.22

incorrect estimations of a relevant critical volume fraction, in the case that θ_t is not zero. We will later see that such effects can be detected already in the saturation dependence of σ.

While the effects of connectivity and tortuosity (represented by percolation scaling) appear to have the dominant effect on μ for electrical conductivity, the pore-size distribution may introduce some variability. In particular, if $\theta_{x_\sigma} < \phi$ (the crossover for the electrical conductivity is less than the porosity) then the pore-size distribution will modify somewhat the value of μ expected from experiment. In such a case, the electrical conductivity at saturation should be larger than the value predicted from Eq. (5.20) by a factor F:

$$F = \left[1 - \left(\frac{\phi - \theta_{x\sigma}}{\phi - \theta_t}\right)\right]^{\mu} \left[\frac{1}{1 - (\phi - \theta_{x\sigma})/(1 - \theta_t)}\right]^{(D_p - 2)/(3 - D_p)} \tag{5.29}$$

Because $F \geq 1$, one might think that representing the electrical conductivity as a power of the porosity would always yield a power $\mu^* \geq 2$ in a fully 3D medium. Accordingly, one might then also assume that since the exponent $(D_p - 2)/(3 - D_p)$ for the electrical conductivity would be replaced by $D_p/(3 - D_p)$ for the hydraulic conductivity, approximate powers for K should tend to be larger than for the electrical conductivity. These conclusions cannot be generally confirmed, however, since the actual result for the power of the porosity depends on the precise sequence of media considered. The value of a particular model is that one can directly analyze different sequences of media.

Consider If one holds the ratio r_m/r_0 constant while changing the porosity, then D_p is a *diminishing* function of the porosity, making high-porosity media more nearly commensurate with universal scaling than lower-porosity media, and thus tending to produce a porosity exponent less than 2, not greater. If, on the other hand, one holds D_p constant (forcing an increase in r_m/r_0 with increasing ϕ), then there is a tendency for an effective μ^* to exceed 2 and to be larger for larger values of D_p. These tendencies can be shown graphically as well (exercise 5.4). In this case larger values of D_p correspond to larger disorder (larger ratio r_m/r_0). For example, for $\phi = 0.4$, the effective (and approximate) μ^* rises rapidly from 2.3 to 8.3 as D_p increases from 2.9 to 2.97.

It would be nice to use a comparison with experimental data to make further tests of the present concepts. Because of the tendency for the exponents to be clustered near $\mu = 2$, the best data set for such comparison might appear to be that of Thompson et al. [16]. But in order to make a comparison with the data compiled by Thompson et al. [16] it would be necessary to use values for D_p calculated from Eq. (3.16) in contradiction to the result used by Thompson et al. [16]: Eq. (3.17). Such a calculation is rendered unreliable since Thompson et al. [16] did not actually measure r_0; rather they assumed that r_0 was the same for all of their media. Because the comparison (presented in the first edition of this book) was only suggestive, not conclusive, and we have in the meantime many additional data sets to analyze, we omit from the present edition the investigation of such variability of μ^* as may result from pore-size distributions and note only that the typically observed discrepancies of 10–15% would not be unusual.

We now pose the question: Which porous media have the appropriate structure to make the simple scaling result Eq. (5.20) a valid predictor of the hydraulic or electrical conductivity under conditions of full saturation? Models for the hydraulic conductivity along these lines are known as Kozeny–Carman as they are known as Archie's law for the electrical conductivity. The analysis will be appropriate for porous media which are well described by fractal models, but it may be approximately valid for other media to the extent that they can be approximated by the fractal model. Also it is assumed that the conduction in these systems is 3D; a simple alteration extends the derivation to 2D.

5.1.6 Regions of Applicability

Of the three parameters (r_m/r_0, D_p, and ϕ) which describe a fractal pore space in the RS model, only two are independent, so we represent the entire range of accessible parameters in a 2D parameter space of porosity and fractal dimensionality. If Eqs. (5.21) and (5.22) are solved for $\theta_x = \phi(1-0.1)$, each solution represents a distinct curve in this space (we used 0.1, mainly because field soils rarely saturate above 90%, and we remind the reader of the quote from Suleiman and Swartzendruber [46] cited in Sect. 3.2.1). Two sets of curves (Fig. 5.3) divide the parameter space into three regions. For the leftmost region both the hydraulic and the electrical conductivities can be represented as proportional to ϕ^2, and they are thus proportional to each other. While this region is large, it represents relatively ordered media,

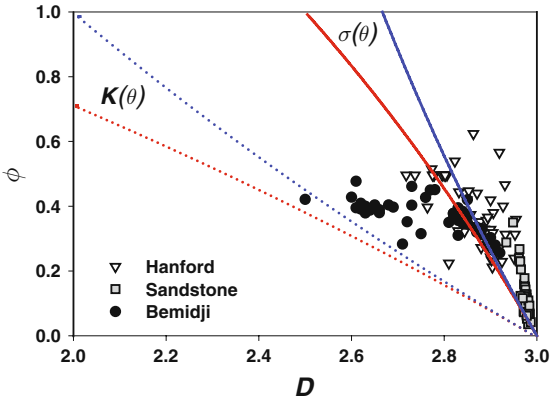

Fig. 5.3 Plot of the $\phi - D_p$ (porosity–fractal dimension) plane showing regions of validity for percolation scaling. Below the electrical conductivity lines scaling is valid for electrical conductivity; below the hydraulic conductivity lines, scaling is valid for the hydraulic conductivity. The *upper lines* represent solutions of Eqs. (5.21) and (5.22) under the conditions that θ_{xK} and θ_{x_σ}, respectively, are equal to 0.9ϕ. The *lower lines* represent the solutions of the equivalent equations generated by the Balberg [2] theoretical framework Bemidji data are from W. Herkelrath (unpublished), sandstone data are from [16], and Hanford data are from [37]

and few natural media are found there (though many artificial media are because of their near uniformity). *This represents a crucial difference between natural and artificial media, and means that conclusions reached by studying artificial media will typically be unsuitable for natural media.* In the middle region it is still reasonable to represent the electrical conductivity in the simple scaling form, but the hydraulic conductivity develops a more complicated dependence on ϕ, so there is no simple relationship between the two. In the rightmost region, neither property is a simple power of ϕ and $K \propto \sigma r_c^2$, just as in Friedman and Seaton [28] (the reader should check that this conclusion is independent of the assumption of self-similarity). But, if the fundamental parameters of a porous medium are not known, it will not be possible to predict which of the three regions a system will be found in, nor would it be possible to determine r_c^2, if it could be guessed that the rightmost region were appropriate.

For porosities just above the relevant crossover, each conductivity may be approximated as a nonuniversal power of ϕ, with $\mu^* > 2$ for the case that D_p is held constant. An equivalent result is obtained by holding the porosity constant and increasing D_p past its crossover. So crossing the parameter space from bottom to top or, equivalently, from left to right, each conductivity solution moves from the universal scaling region, through a region in which the conductivity can be approximated by a nonuniversal scaling power, before entering a region where it is clearly inappropriate to use simple scaling results. This process sets on at smaller values of D_p in the hydraulic conductivity than in the electrical conductivity. Note also that smaller values of D_p for a given ϕ are associated with narrower pore-size distributions, supporting (and allowing testing of) the common assumption that larger values of the power of the saturation dependence of the electrical conductivity arise from wider distributions.

In Fig. 5.3, the Hanford site soils (Table 5.3) are well out of the regime of validity of Eq. (5.20) for K, but tend to cluster about the boundary for the validity of Eq. (5.20) for σ. For small porosities, such as in rock, the region of validity of Eq. (5.20) for K may approach actual conditions. Thus there appears to be a greater justification for representing K as a power of ϕ in rocks than in soils, though even in rocks the power is likely to be larger than 2. This is why we plot the sandstone data from Thompson et al. [16] on the same figure. Interestingly, if the correct expression relating porosity and the fractal dimensionality (Eq. (3.16)) is used, the data compiled by Thompson et al. [16] follow the same trend as the Hanford Site soils, near the margin of the validity of Archie's law for the electrical conductivity, meaning that their exponents might well differ slightly from 2, as they indeed do. But if the Thompson et al. [16] result for D_p is used, the rock samples fall along a curve connecting the origin to the lowest porosity value of the Hanford site soils, clearly a quite different tendency. This supports our contention that the Thompson et al. [16] calculation of D_p is incorrect. It also suggests an intriguing possible connection between transport and structure: some aspect of transport during depositional processes may prevent too large a value of the fractal dimensionality, i.e., too great a disorder.

Table 5.3 (from Hunt and Gee [38]). Physical characteristics of Hanford site soils. Except for the soil texture and K_S (from Khaleel and Freeman [78]), all the primary data came from Freeman [79]

Soil	D_p	D_s	ϕ	θ_d	Texture	K_S	h_A
VOC 3-0647	2.773	2.8	0.515	0.134	Loamy sand	0.0002	85
VOC 3-0649	2.823	2.898	0.539	<0.12	Loam	**ng**	530
VOC 3-0650	2.863	2.917	0.624	0.37§	Sandy loam	2.6E-07	51.5
VOC 3-0651	2.857?	2.87	0.374	0.126	Loamy sand	0.0094	25
VOC 3-0652	2.878	2.56	0.352	0.11	Sand	0.00037	58
VOC 3-0653	2.9?	2.874	0.419	0.12	Sandy loam	5.8E-06	55
VOC 3-0654	2.931	2.916	0.466	<0.18	Sandy gravel	0.00027	40
VOC 3-0654-2	2.849		0.419	0.11	Sandy gravel	0.0136	3
VOC 3-0655	2.927		0.4	<0.15	Silty, sandy gravel	0.000158	13
VOC 3-0657	2.955		0.359	<0.1	Gravelly sand	0.0136	30
ERDF 4-1011	2.871	2.816	0.44	0.125	Loamy sand	0.00001	56
ERDF 4-0644	2.906	2.81	0.38	0.115	Loamy sand	5.7E-06	100.5
B8814-135	2.891	2.727	0.356	0.14	Silty sand	1.36E-06	135
B8814-130B	2.886	2.682	0.329	0.11	Loamy sand	4.1E-07	46
FLTF D02-10	2.778	2.776	0.496	0.2	Silt loam	0.00012	100
FLTF D02-16	2.718	2.71	0.496	0.18	Silt loam	0.00012	150
FLTF D04-04	2.806	2.804	0.496	0.2	Silt loam	0.00012	100
FLTF D04-10	2.778	2.773	0.496	0.19	Loam	0.00024	100
FLTF D05-03	2.737	2.735	0.496	0.205	Loam	0.00029	130
FLTF D07-04	2.796	2.791	0.496	0.198	Silt loam	0.00012	98
FLTF D09-05	2.8	2.83	0.496	0.19	Loam	0.00029	72
FLTF D10-04	2.775	2.769	0.496	0.21	Silt loam	0.00012	90
FLTF D11-06	2.803	2.798	0.496	0.2	Silt loam	0.00012	76
FLTF D11-08	2.802	2.797	0.496	0.22	Silt loam	0.00012	80
Inj. Test Site 1-1417	2.919	2.876	0.566	0.088	Sand	0.00014	35
Inj. Test Site 1-1418	2.953	2.762	0.313	0.08	Gravelly sand	0.00014	2
Inj. Test Site 2-1417	2.9	2.719	0.328	0.033	Sand	0.00014	20
Inj. Test Site 2-1637	2.932	2.708	0.313	0.07	Sand	0.0042	11
Inj. Test Site 2-1639	2.951	2.654	0.239	0.06	Sand	0.0012	5
Inj. Test Site 2-2225	2.844	2.548	0.322	0.06	Sand	0.0055	15
Inj. Test Site 2-2226	2.925	2.573	0.229	0.06	Sand	0.015	7
Inj. Test Site 2-2227	2.919	2.666	0.271	0.056	Sand	0.0087	5.4
Inj. Test Site 2-2228	2.904	2.376	0.212	0.047	Sand	0.021	10
Inj. Test Site 2-2229	2.902	2.465	0.234	0.069	Sand	0.0064	11
Inj. Test Site 2-2230	2.853	2.8	0.447	0.11	Sand	0.00023	40
Inj. Test Site 2-2231	2.905	2.716	0.318	0.13	Gravelly sand	0.0075	70
Inj. Test Site 2-2232	2.88	2.508	0.272	0.08	Sand	0.041	14
Inj. Test Site 2-2233	2.9	2.492	0.243	0.075	Sand	0.017	11
Inj. Test Site 2-2234	2.81	<2	0.224	0.025	Sand	0.021	80
US Ecology MW10-45	2.859	2.634	0.34	0.066	Sand	0.00531	15.2
US Ecology MW10-86	2.764	2.569	0.397	0.069	Sand	0.0197	20
US Ecology MW10-165	2.8299	2.511	0.324	0.058	Sand	0.00663	22
218 W-5-0005	2.894	2.765	0.366	0.12	Sandy loam	0.000067	35
North Caisson	2.806			0.08	Sand	0.02	5
McGee Ranch	2.832			0.107	Silt loam	0.001	45

We note in conclusion some potentially relevant work based on the effective-medium approximation (EMA) and a related paper using percolation theory. Sahimi [43, 44] gave a derivation of the EMA to produce Archie's law. The exponent he used, $\mu^* = z/(z-2)$, is appropriate for spherical particles but should be larger for flatter particles, such as clay grains [47]. Bussian [48] generalized the self-similar EMA to include finite rock conductivity. He found $\mu^* > 3/2$ in almost all cases, arguing that it was due to the finite rock conductivity resulting from clay particles. Hilfer [3] also used percolation theory to find $\mu^* \geq \mu$. Sahimi [43, 44] criticized this result on the basis of its quasi-universality (and his understanding of the larger variability of μ^*). Clearly there is some variability in the exponent, but not a great deal, and it appears that Hilfer's result is more general and more relevant than Sahimi indicated. In any case, Hilfer's work is related to the present treatment.

5.2 Electrical Conductivity as a Function of Saturation: Trends and Potential Complications in Experimental Data

If the percolation interpretation of Archie's law is correct at full saturation, then the electrical conductivity must follow Eq. (5.20) as a function of saturation. In this section, we examine data relating to electrical conductivity as a function of saturation.

Electrical conductivity is frequently analyzed in terms of a "formation factor." We avoid this analysis because it is rooted in assumptions (which we have shown to be unjustified) regarding a universal relationship between the electrical and the hydraulic conductivities. We will continue use of the concept of tortuosity, despite some uncertainty in its definition far from the percolation threshold, and despite possible confounding influence of other factors, such as a nonzero critical volume fraction for percolation.

We performed extensive analysis of 11 data sets for the electrical conductivity as a function of saturation $\sigma(\theta)$ (Ewing and Hunt, 2006). This analysis (1) showed that the typical formula used in the soil physics community for the saturation dependence of the electrical conductivity is inferior in description of the data to percolation scaling, even for the data set it was originally developed for (and has a less satisfying physical basis), (2) identified several errors in analysis, which could lead to a false estimate for the actual experimental power on $\sigma(\theta)$, and (3) identified several physical complications which can make experimental data appear to have a lower degree of universality than implied by percolation scaling. One such complication involves overlooking effects of contact resistance, which can prevent the data from obeying a power law even though the data approach the appropriate power law asymptotically in the large resistance (low moisture content) limit. Another complication is overlooking effects of "residual" salinity, i.e., cases where the salinity of the injected fluid is less than the salinity in situ. This can arise from dissolution of ions in the solid medium, and is most important in the case where the injected fluid has low conductivity. Such an influence introduces an additional saturation dependence, though it is easily modeled.

In both petroleum engineering and soil science, it is frequently assumed that the electrical conductivity has contributions from both the solid and the liquid phases [49–51]. A widely used relationship in soil science is

$$\sigma(\theta) = \sigma_s + \sigma_b \theta (a\theta + b) \tag{5.30}$$

where the σ_s term denotes a "surface" or "solid" term [50, 51]. Interpreted as the contribution of hydrated clay minerals, this term is considered independent of moisture content except under very dry conditions (discussed in Sect. 6.4). The second term, attributed to conducting fluid in the pore space, is the product of the conductivity of the liquid phase, the water content, and a "transmission coefficient" (a fudge factor) which is itself a linear function of the water content [51]. Over a limited range of moisture values, $\theta(a\theta + b)$ can present as $(\theta - \theta_c)^\mu$ for $\mu = 2.0$ (as can be seen in Fig. 5.4), so this traditional phenomenology may mask a universal dependence compatible with Archie's law.

Because the solid phase is always well above the percolation threshold, a "surface" or "solid" conductivity term might be taken to be independent of saturation. In Sect. 6.4 we discuss data that show a pronounced dependence of the clay conductivity on water contents; at sufficiently low water contents it may be necessary to expand the analysis, depending on the mineralogy of the medium. The solid phase conductivity becomes more important as the water content is reduced [52, 53], approaching the (water) percolation threshold from above. So while surface conductivity is typically neglected, it may dominate the system conductivity if the solution electrical conductivity is low, the medium has low porosity or a low degree of saturation, and/or the medium has a high specific surface [54].

Universal formulations of the electrical conductivity were derived for a conductivity ratio σ_b/σ_s that is very large or infinite. Complications arise if this ratio is small. In a number of the media we analyzed, there is evidence of a significant

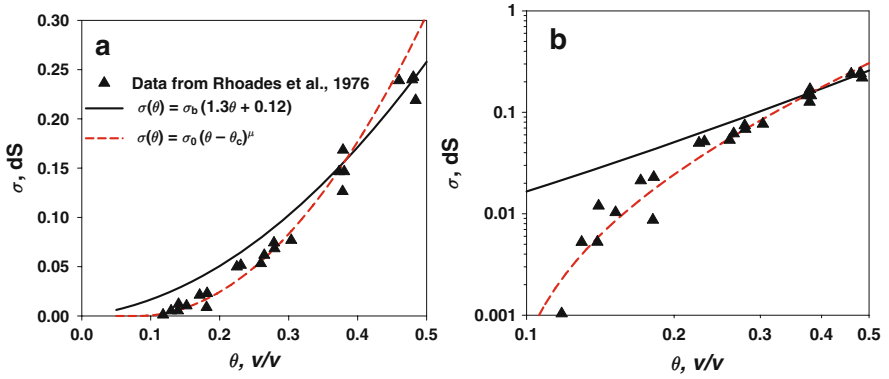

Fig. 5.4 Analysis of data by Rhoades et al. [51], data for the saturation dependence of the electrical conductivity. The percolation scaling result (Eq. (5.31)) is compared with the phenomenology (Eq. (5.30)) of Rhoades et al. [51]. Figure 5.4a, linear plot, Fig. 5.4b, logarithmic representation. Note that Fig. 5.4b clearly shows the superiority of Eq. (5.31)

contribution of the solid medium to the electrical conductivity, implying that the conductivity ratio is not particularly large. In such cases, individual conducting pathways will tend to include both phases. We see therefore three approximations in order of increasing complexity:

1. The solid phase is assumed to have zero conductivity, so current flows through the liquid phase only (Eq. (5.20)).
2. The solid and liquid phases are assumed to conduct strictly in parallel, and so a constant solid phase conductivity σ_s is added to Eq. (5.20):

$$\sigma(\theta) = \sigma_s + a\sigma_b(\theta - \theta_t)^{\mu} \tag{5.31}$$

   This parallel approach is quite common, and yet it is most appropriate for $\sigma_s \ll \sigma_b$ in which only a negligible quantity of current flows from one phase to another.
3. If the solid and fluid conductivities do not have a large contrast, then an optimized path of conduction will sometimes go through the solid phase in order to bypass a more tortuous path through the liquid, and sometimes through liquid to bypass a higher resistance solid path. In other words, the two phases will not conduct strictly in parallel; in fact, the degree of interaction in the conducting pathways will vary with the relative conductivities of the two phases, as well as with the liquid content. There is no universally agreed-upon mathematical formulation for this interaction, which has been an active area of research for decades. We conjecture that such a phenomenon would reduce the value of μ by the tortuosity contribution to the conductivity exponent [55]. This could reduce the exponent on χ to $2\nu = 1.76$ when there is little contrast between solid and liquid conductivities.

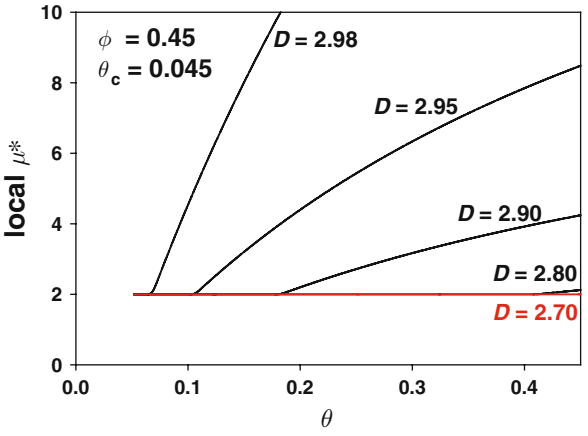

Fig. 5.5 Values of the apparent conductivity exponent (logarithmic derivative) μ^* calculated across a moving range of water contents $\Delta\theta = 0.01$ for the given porosity and several values of D_p. Data following some of these curves could be interpreted as having a nonuniversal value of the conductivity exponent

When D_p increases slightly past the limit of validity of Eq. (4.20), electrical conductivity is under-predicted by percolation scaling [31]; with further increases in D_p, percolation scaling is no longer a useful framework for analysis. For some combinations of ϕ and D_p the difference is subtle (Fig. 5.5), and data may indicate percolation scaling (Eq. (5.20)) with an exponent $\mu^* > \mu$. We do not analyze data to test this suggestion, however.

When data are within the range of validity of percolation scaling, and yet indicate a nonuniversal value μ^*, caution is still advisable. For example, incorrect estimates of θ_t can produce apparently nonuniversal values for μ^*. Hence simultaneous fitting for both θ_t and μ has built-in pitfalls: under-estimation of θ_t can result in apparent values of $\mu^* > \mu$, while over-estimation of θ_t can produce values of $\mu^* < \mu$ (Fig. 5.6). As a practical matter, it is best to start with the assumption that universality is observed, and only resort to nonuniversal exponents when other, more mundane explanations have been exhausted. We try to minimize effects of incorrect estimations of θ_t, including exclusion of the possibility of its existence, probably contributing to our tendency to generate universal scaling where others have not.

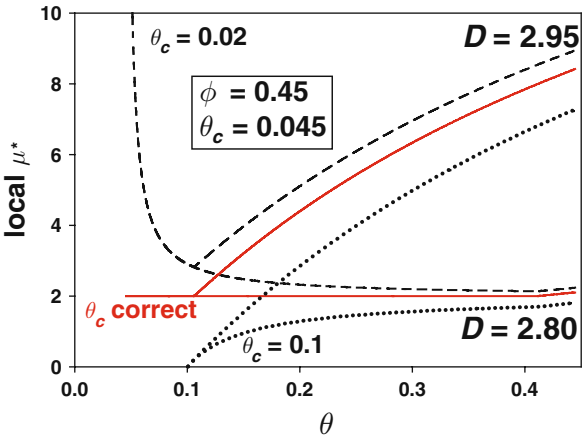

Fig. 5.6 Values of the apparent conductivity exponent (logarithmic derivative) μ^* calculated across a moving range of water contents $\Delta\theta = 0.01$ for the given porosity and two values of D_p for cases where the critical water content is underestimated, correct, and overestimated

5.2.1 Comparison with Experiment

Here we apply the percolation scaling framework to analysis of experimental data. To the best of our knowledge, all of these data are from water-wet media, and hysteresis (if present) is ignored. The data sets examined (Table 5.4) represent both coarse and fine soils, and both igneous and clastic sedimentary rock. We discuss some of these data sets, with the presentation proceeding from simpler to more

complex cases. The complex cases illustrate how a sound theoretical footing can help handle potentially confounding issues.

The data of Rhoades et al. [51] (Fig. 5.4) were originally plotted in a form that subtracted out any surface or solid conductivity σ_s, so our analysis simply involved fitting values for a and θ_t. Our Eq. (5.31) yields the same R^2 as Rhoades et al.'s Eq. (6), but where their a and b are meaningless fitting parameters, our parameters a and θ_t have physical significance: a gives the medium's tortuosity at saturation,

Table 5.4 Sources of electrical conductivity data examined. All data except Ren's (1999) were obtained by digitizing published figures

Source	Medium	Parameters fit*	Slope	Intercept	R^2	Comments
Archie, *Trans. AIME* [10]	Gulf coast sandstones	$\phi_c = 0.020$, $a = 1.591$	1.000	0.0023	0.746	No units given in figure
	Nacatoch sand	$\phi_c = 0.010$, $a = 1.067$	1.000	0.0019	0.852	
Rhoades et al., *Soil Sci. Soc. Am. Proc.* [51]	Indio vfsl	$\theta_c = 0.073$, $a = 1.232$	1.000	−0.0053	0.982	Surface contribution (if any) removed in figure
Abu-Hassanein et al., *J. Geotech. Eng.* [59]	Soil A: 7% S, 40% c	$\theta_c = 0.011$, $\sigma_r = 0.725$	0.991	0.0011	0.973	Each soil tested at three bulk densities; all densities lumped together in our analysis
	Soil B: 7% S, 53% c	$\theta_c = 0.064$, $\sigma_r = 0.787$	0.843	0.0210	0.823	
	Soil C: 38% S, 40% c	$\theta_c = 0.020$, $\sigma_r = 0.112$	0.919	0.0023	0.880	
	Soil D: 35% S, 20% c	$\theta_c = 0.000$, $\sigma_r = 0.239$	0.900	0.0038	0.865	
Roberts and Lin, *Water Resour. Res.* [64]	Tuff: distilled water	$\theta_c = 0.0024$, $\sigma_r = 0.0039$ (both)	0.715	0.0000	0.962	$\sigma_b = 0.0$ (DW),
	J-13 water		1.215	−0.0000	0.916	$\sigma_b = 0.0256$ (J-13)†
Tusheng Ren, unpublished data, 1999	Silica sand	$\theta_c = 0.066$, $a = 2.703$ ($\sigma_s = 0.396$)	0.972	0.0143	0.948	Conductive solid phase, six solution concentrations†
Binley et al. [13–15]	Sandstone	($\theta_c = 0.000$) $a\sigma_b = 0.1466$, $\sigma_s = 0.0020$	1.000	−0.0004	0.965	Cassiani et al. [56] give $a\sigma_b = 0.143$, $\sigma_s = 0.0156$
Rinaldi and Cuestas, *J. Geotech. Geoenv. Eng.* [58]	Loess, 16% clay	$\theta_c = 0.040$, $a = 2.132$, $\sigma_r = 0.085$	1.028	−0.0032	0.980	4 solution concentrations

Table 5.4 (continued)

Kechavarzi and Soga, *Geotech. Test. J.* [62]	Clean sand	$\theta_c = 0.000$, $a\sigma_b = 20.67$, and $c\rho_c = 0.792$ (Test 1), 0.705 (Test 2), and 0.702 (Test 3)	0.980	0.0114	0.980	Three replications‡. Miniature resistivity probe appears to have contact resistance
Mori et al., *Vadose Zone J.* [60]	Tottori dune sand	$\theta_c = 0.000$, $a = 1.417$	1.060	−0.0739	0.982	Three solution concentrations
Tuli and Hopmans, *Eur. J. Soil Sci.* [61]	Oso flaco fine sand	$\theta_c = 0.065$, $a = 1.637$, $\sigma_r = 0.384$ ($\sigma_s = 0.0725$)	1.002	−0.0011	0.984	σ_s value given. Four solution concentrations

*Values in parentheses were given rather than fit. Units omitted from table for simplicity; see corresponding figures for actual units. †Where different solution concentrations were used, only σ_b varied: other parameters were held constant across all concentrations. ‡Fitting allowed a different value of ρ_c for each replication, but kept other parameters constant across all replications.

while θ_t is the critical volume for percolation. For the Indio soil represented here, we have a tortuosity at saturation of 1.232, and a critical volume fraction $\theta_t = 0.073$. Plotting the same data in logarithmic coordinates (Fig. 5.4b) highlights the percolation scaling formulation's superiority at low water contents.

Archie's [10] seminal paper presented electrical resistivity data for a number of saturated consolidated Gulf Coast sandstones, and for samples of saturated unconsolidated Nacatoch sand. Fitting Eq. (5.23) to his sandstone and sand data, we obtain correlation slopes of almost precisely one and intercepts near zero, in contrast to his slopes of 0.66 (sandstone) and 1.55 (sand) (Table 5.4). As expected, tortuosity is lower in sand than in sandstone. The critical volume for percolation in the sand is just 1% of porosity; that in the sandstone (2% of porosity) would probably be higher if the sandstones were strongly cemented.

Binley et al. [13] use their data to make inferences regarding moisture content and are content with a simple calibration to Archie's law. A second set of data from the same sandstone ($\phi = 9.3\%$) was published in 2002. Cassiani et al. [56] tested their own model using the data from Binley et al. [13] and found a constant solid contribution to the electrical conductivity of $\sigma_s = 0.00143\,\mathrm{S\,m^{-1}}$ added to the $0.0156\,\mathrm{S\,m^{-1}}$ electrical conductivity of the fully saturated pore space. However, the Cassiani et al. [56] analysis implies a relatively weak θ-dependent contribution (Fig. 5.7). Using Cassiani et al.'s numerical values, and the common assumption that at typical experimental frequencies the solid and solution conductions operate in parallel, we have $\sigma(\theta) = 0.00143 + 0.0156(\theta - \theta_t)^{2.0}\,\mathrm{S\,m^{-1}}$ as a specific instance of Eq. (5.31). We have no independent basis upon which to choose a value of θ_t in these sandstones. We could assume $\theta_t = 0.1\phi$, but $\theta_t = 0$ is more likely in a medium with significant solid conductivity. As in the case of conducting spheres with pendular bridges (see Sect. 6.2), any water at all should increase conductivity. Using the numerical values from Cassiani et al. [56] and assuming $\theta_t = 0$ gives a no-parameter fit that is

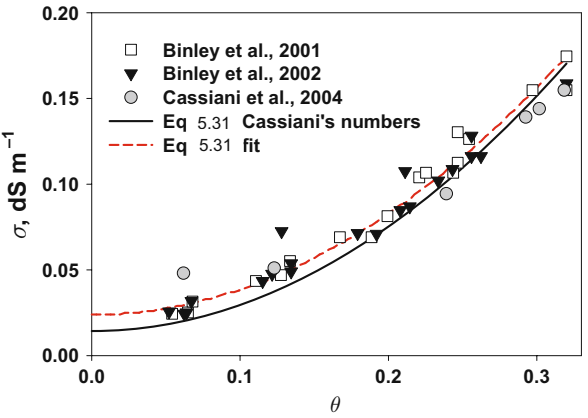

Fig. 5.7 Comparison of data for electrical conductivity, σ, as a function of water content, θ from Binley et al. [13–15] with Eq. (5.31) and model results of Cassiani et al. [56]

clearly superior to Cassiani et al.'s [56] fit (Fig. 5.7). Fitting gives values slightly different from Cassiani et al.'s [56] and yields a slope of 1.00 and an intercept of -0.0004 for regressing predicted against observed values. Notice that if the solid contribution (σ_s in Eq. (5.31)) had been underestimated, the prefactor $\sigma_b = 0.0156$ would be overestimated. That is, if we had optimized for θ_t alone, our value would be dependent on the accuracy of the estimated σ_s.

Our predicted values compare well with Binley et al.'s [13–15] observations (Fig. 5.7 and Fig. 5.8). For both data sets (2001 and 2002), individually as well as combined, Eq. (5.31) with $\theta_t = 0$ matches the data with slope near one, intercept near zero, and a high correlation coefficient (Table 5.4). In support of our conjecture about the exponent μ taking on smaller values for conducting solids, we find $\mu^* = 1.88$ fits the data just as well as $\mu = 2.0$.

A greater solid phase conductivity is seen (Fig. 5.9) in silica sand data (personal communication; described in Ren et al. [57]). Here it is clear that the solid phase makes a constant contribution to the overall conductivity – again suggesting $\theta_t = 0$ – with the remaining conductivity varying with the conductivity and volume fraction of the solution. When we subtract the solid contribution, estimated as the mean conductivity for the $\sigma_b = 0$ solution, the data fall on lines of $\mu = 2$ in logarithmic space (Fig. 5.10). Because each datum is from a separate packed core, the data as a whole are somewhat noisy, but the figure shows reasonable prediction of total conductivity from only the known values σ_b and θ, the assumed $\theta_t = 0$, and the estimated value of σ_s. A slight improvement is given by optimizing for a and θ_t. The lower slopes at low water contents, as suggested by the data, are consistent with our conjecture that a somewhat smaller value of μ may be more appropriate for media with similar solid- and liquid-phase conductivities. Thus, at low saturations, the current does not have to avoid the solid phase and the topology of the current path is not coincident with the topology near the percolation threshold, so that the conductivity does not quite follow the percolation prediction.

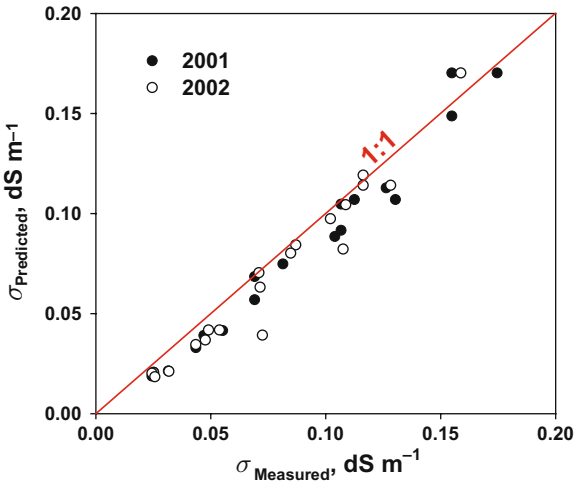

Fig. 5.8 Direct comparison of measured and predicted electrical conductivity values for the data of Fig. 5.7

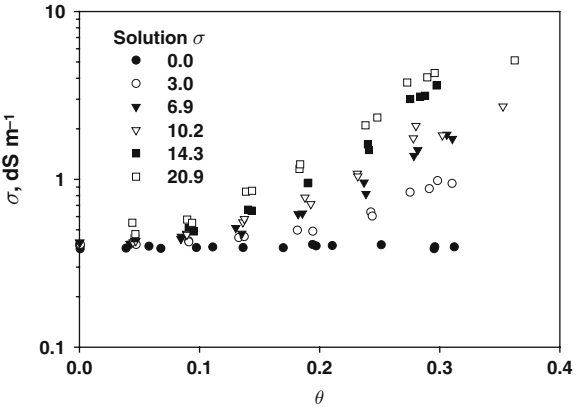

Fig. 5.9 Electrical conductivity of unsaturated silica sand at different solution contents and conductivities. Data from Ren et al. [57]

Residual salt in soil, whether precipitated or in the form of exchangeable cations, may contribute a significant fraction of the liquid-phase conductivity. Making the assumption that any residual salinity dissolves completely at any nonzero water content, we adapted Eq. (5.31) to account for residual salinity:

$$\sigma(\theta) = \frac{a(\sigma_b\theta + \sigma_r)}{\theta(1-\theta_t)^{\mu}}(\theta - \theta_t)^{\mu} \tag{5.32}$$

where σ_r is the residual salinity's contribution to electrical conductivity. The factor $(\sigma_b\theta + \sigma_r)/\theta$ therefore accounts for both solution and residual salinity con-

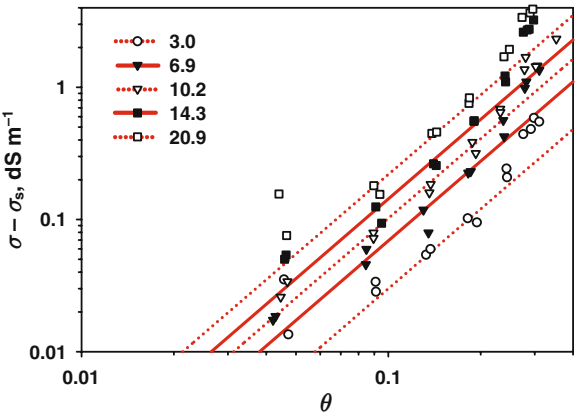

Fig. 5.10 Comparison of data with zero-parameter predictions of electrical conductivity of silica sand after subtracting the solid-phase electrical conductivity (Data from Fig. 5.9)

tributions. Note that Eq. (5.32) is consistent with an apparent $\mu^* = \mu - \sigma_r(\theta - \theta_t)/[(\sigma_b\theta + \sigma_r)\theta)]$ and approaches μ if either $\theta \to \theta_t$ or $\sigma_r \to 0$. We apply the analysis of Eq. (5.32) to the data of Rinaldi and Cuestas [58], who packed loess soils with known volume fractions of NaCl solution, and measured electrical conductivity at different water contents (their Fig. 12). In the zero-electrolyte treatment, the increase in electrical conductivity with water content can reasonably be attributed to residual salts in the soil. Fitting Eq. (5.32) to their data provides an excellent fit (Fig. 5.11), with $R^2 = 0.98$. The optimized value for the residual salt equivalent conductivity is $0.085\,\mathrm{S\,m^{-1}}$. If the relative concentration of the various cations were known, their absolute concentrations could also be determined.

The data of Abu-Hassanein et al. [59] provide another example of the importance of accounting for residual salt. They present data on four soils differing in texture and clay mineralogy; each soil was also tested at three different degrees of compaction. Tap water ($\sigma_b = 9.5 \times 10^{-3}\,\mathrm{S\,m^{-1}}$) was used throughout. Because we did not know a priori whether any given soil will have residual salt- and/or solid-phase conductivity, we added a solid-phase conductivity to Eq. (5.32). As it turned out, the solid contribution was zero for all but soil D, which had a negligible value of $\sigma_s = 6.6 \times 10^{-5}\,\mathrm{S\,m^{-1}}$, so this was dropped from the analysis. Fitting each soil in turn, we obtain R^2 between 0.82 and 0.97 (Fig. 5.12). Residual salt accounts for 92–99% of the saturated conductivity. Note that in Fig. 5.15, when all data sets for $\sigma(\theta)$ are plotted simultaneously, these data lie conspicuously above the universal line. Consistent with expectations, higher clay soils had higher percentages of their conductivity contributed by residual salinity and also had higher critical volumes for percolation.

The data sets from Mori et al. [60] and Tuli and Hopmans [61] are somewhat similar, so we present them together (Fig. 5.13). We obtain $R^2 = 0.98$ fitting Eq. (5.31) to Mori et al.'s data, slightly lower than their 0.99 using the Rhoades equation (Eq. (5.30)), but we learn that $\theta_c = 0.0$ and $a = 1.417$. Tuli and Hopmans [61] give $\sigma_s = 0.0725\,\mathrm{dS\,m^{-1}}$ for Oso Flaco sand; this is the only medium we encoun-

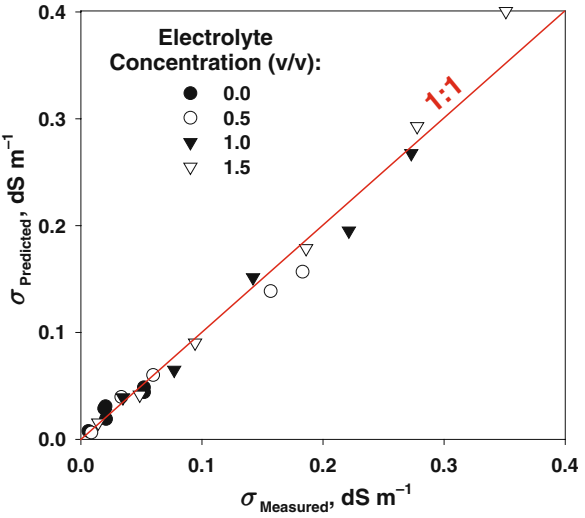

Fig. 5.11 Comparison of predicted (Eq. (5.32)) with measured electrical conductivity in loessial soils [data from Rinaldi and Cuestas [58]]

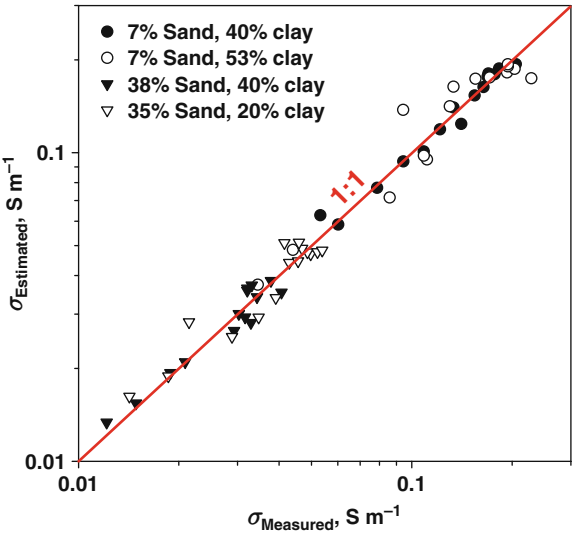

Fig. 5.12 Comparison of predicted (Eq. (5.32)) with measured electrical conductivity in four soils [data from Abu-Hassanein et al. [59]]

tered that combined nonnegligible solid conductivity with a nonzero critical volume for percolation. Our fit yields a mean absolute residual of only 0.02, compared with their value of 0.08.

Last, we examine an unexpected complication in the data published by Kechavarzi and Soga [62]. They present triplicate calibration curves for their minia-

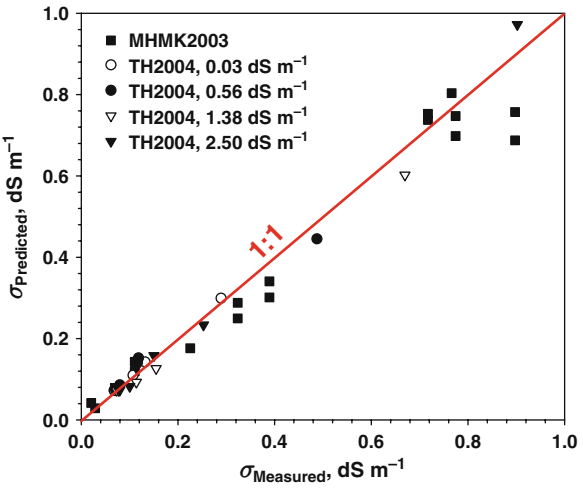

Fig. 5.13 Comparison of predicted and measured electrical conductivity in soils presented by Mori et al. [60] labeled as MHMK2003 and Tuli and Hopmans [61], labeled as TH2004

ture resistivity probes, and report that fitting Archie's law to the data gives $R^2 = 0.91$, a disappointing value for a calibration curve. A plot of the raw data (Fig. 5.14) shows a marked decrease in the slope of the $\sigma(\theta)$ curve; this, combined with the unknown characteristics of the miniature probe, raised the possibility that there was some contact resistance in their experimental setup. The washed sand was unlikely to have residual salinity, and solid conductivity would curve the slope up rather than down. We accordingly allowed for contact resistance ρ_c in the $\sigma(\theta)$ relationship

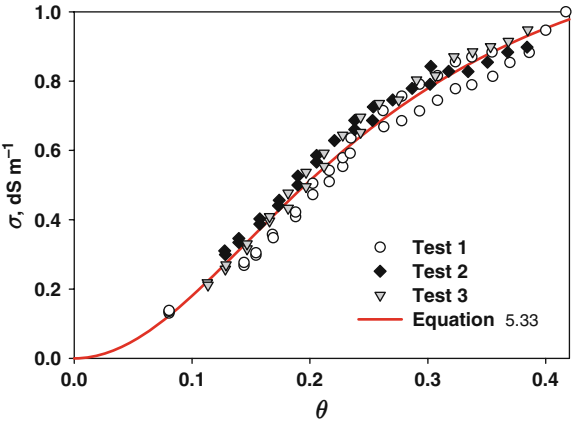

Fig. 5.14 Comparison of electrical conductivity as a function of water content with Eq. (5.33), including effects of a contact resistance that is independent of water content [Data from Kechavarzi and Soga [62]].

through a modification of Eq. (5.28), giving

$$\sigma(\theta) = \frac{1}{c\rho_c + \left[1/a\sigma_b(\theta - \theta_t)^{\mu}\right]} \tag{5.33}$$

where the constant c corrects for geometric factors specific to their experimental setup. Equation (5.33) yields $\mu^* = \mu/[1 + a\sigma_b c\rho_c(\theta - \theta_t)]$, which coincides with μ if any of the constants are 0 as well as in the limit $\theta \to \theta_t$. This new equation fits the data quite well (Fig. 5.14), with $R^2 = 0.97$.

The analyses of the saturation dependence of the electrical conductivity are summarized in Table 5.4. Our examination of the data sets discussed above found critical volume fractions for percolation ranging from 0.0 to 0.073, reasonably in line with Hunt's [63] observed range. Values of a, which we interpret as the electrical tortuosity at saturation, ranged from 1.07 to 2.73, a relatively small variation. In two cases brine conductivity σ_b was not given, forcing us to lump $a\sigma_b$ into a single parameter; when this is done, the value of the lumped parameter cannot yield useful information about its component parts. Conductivity attributable to residual salinity was encountered in tuff and several of the soils, but in only one sand and none of the sandstones. In Fig. 5.15 we represent all the saturation-dependent electrical conductivity from Table 5.4 together. As predicted, all the data indicate an exponent $\mu = 2.0$ (Fig. 5.15), with deviations below the line indicating contact resistance (e.g., Kechavarzi and Soga [62]) and deviations above the line indicating the effect of residual salinity (e.g., Roberts and Lin [64]; Abu-Hassanein et al., [59]). Deviations attributable to residual salinity are most pronounced for low-conductivity

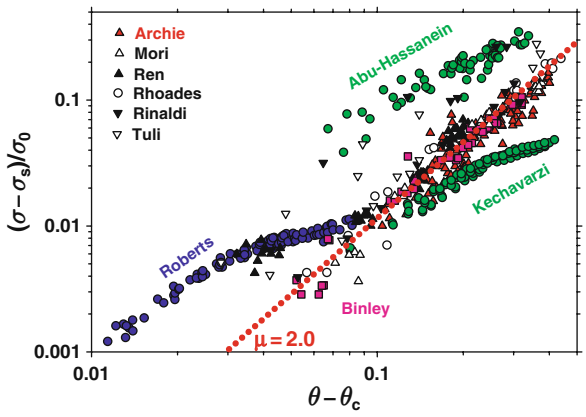

Fig. 5.15 Summary plot of all the data sets presented in Table 5.4 showing constant adherence to the predicted universal behavior. For all data sets, the water content was normalized by subtracting the critical value, and the electrical conductivity was normalized by subtracting the solid phase contribution, then dividing by the brine conductivity value. Data are parallel to the line given by the universal conductivity exponent, $\mu = 2$. Those data sets that lie above the universal line were analyzed as having residual salinity, those that curved downward away from the universal line, as having a contact resistance

solutions and/or low water contents (e.g. Ren et al., [65]). Further, as predicted, the apparent power μ^* increases to 2 in the limit $\theta \to \theta_t$ for data sets with either contact resistance (e.g., Kechavarzi and Soga [62]) or residual salinity (e.g., Abu-Hassanein et al. [59])

In subsequent analysis, we plotted critical volume fractions versus porosity to examine the possibility that a linear relationship between them exists. The result (Fig. 5.16) is consistent with our conjecture that $\theta_t \propto \phi$, and finds a similar coefficient (0.12 rather than 0.1). In this analysis the regression line was forced through the origin, and we did not include cases for which $\theta_t = 0$. Note that almost all cases with $\theta_t = 0$ had large solid conductivities; in such cases the simple percolation argument that $\theta_t = p_c\phi$ will not hold. However, plotting $1/a$ against $(1 - \theta_t)^2$ shows no relationship as might have been expected from arguments leading to Eq. (5.27). This indicates that a may indeed be best interpreted as the tortuosity of the conducting pathways in the limit of full saturation.

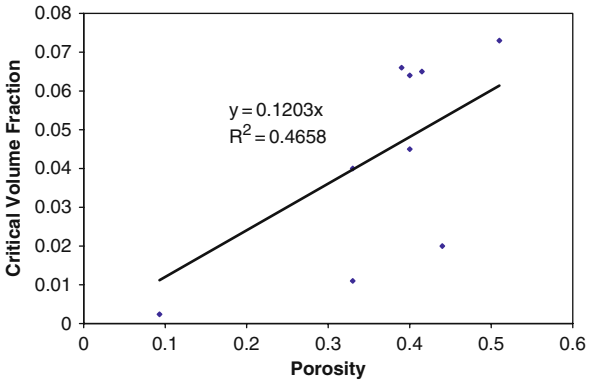

Fig. 5.16 Excel plot of the (nonzero) critical volume fractions from Fig. 5.15 vs. porosity. Although the plot is quite noisy, it generates $\theta_t \propto \phi$, with a proportionality constant of approximately 1/8 (fit constrained to pass through origin)

5.3 Effects of Arbitrary Pore-Size Distributions

This calculation of $K(\theta)$ follows the same procedure as in Chap. 4, but here we assume no particular form for the pore-size distribution. However, we do assume that there are minimum and maximum pore sizes, so the pdf for $W(r)$ should still be valid between the limits r_0 and r_m. Thus the same integral provides the basis for all the calculations of equilibrium quantities, regardless of the actual form of $W(r)$ appropriate for a given soil:

$$\int_{r_1}^{r_2} r^3 W(r)\, dr \tag{5.34}$$

When $r_2 = r_m$ and $r_1 = r_0$ – when we are integrating from the smallest to the largest pore in the system – Eq. (5.34) yields a numerical constant of order unity times the porosity ϕ. As we saw in the fractal treatment it is possible to define a suitable normalization constant to generate precisely the porosity; here this is also of no real concern since we will be using proxy data from the cumulative soil particle size distribution. Such a choice guarantees normalization as well. When $r_2 = A/h$ (as long as this value is less than r_m) and $r_1 = r_0$, Eq. (5.34) defines the moisture content θ. When $r_2 = r_m$ and $r_1 = r_c$, Eq. (5.34) yields the critical moisture content for percolation θ_t; if θ_t is known we can thereby deduce the bottleneck pore radius r_c under saturated conditions. When $r_2 = A/h$ and $r_1 = r_c$, Eq. (5.34) again yields θ_t and can be used to deduce the bottleneck pore radius $r_c(\theta)$ for any moisture content $\theta > \theta_t$. If one assumes that distributions of pore aspect ratios are independent of pore size, the ratio $[r_c(\theta)/r_c|_{\theta=\phi}]^3$ again yields $K(\theta)/K_S$, as long as $\theta > \theta_{xK}$. Building in this assumption deprives the procedure of some generality, but the assumption is not unreasonable for many natural media, and allows the procedure to generate the known appropriate $K(\theta)/K_S$ when the medium is well described by a fractal model. Thus the present formulation allows comparison of the present prediction with analytical results for media presumed compatible with the fractal model.

The crossover moisture content θ_{xK} is found as follows. Instead of using Eq. (5.14) as the functional form for the hydraulic conductivity (a result specific to fractal geometry), K is set to the unspecified (and thus general) form $K(\theta)$. Combining this K with Eq. (5.20), and setting $K(\theta)$ and $dK/d\theta$ equal for each equation when $\theta = \theta_{xK}$ yields

$$\theta_{xK} = \theta_t + \frac{2K(\theta_{xK})}{\frac{dK}{d\theta}|_{\theta=\theta_{xK}}} \tag{5.35}$$

This is the fundamental analytical result employed by Blank et al. [66] to make comparisons between theoretical and experimental results for $K(\theta)$. The factor $2 = \mu$.

The pore-size distribution for field samples is seldom, if ever, known. But one often has access to the cumulative particle-size distribution, which can be used as a proxy for the cumulative pore-size distribution (with the usual uncertainties relating pore and particle sizes). Evaluating Eq. (5.34) between any two limits is thus equivalent to taking differences in the cumulative particle size distribution evaluated at two corresponding limits. Comparison with experiment is shown in Fig. 5.17a, b. The comparisons are drawn from the same soils as in Fig. 5.1, but here no assumptions have been made regarding the form of the pore-size distribution. Given results from both experiment and an analytical model of flow on a random fractal, the numerical procedure could serve as a test of the validity of the fractal model. But note that in the present case there were 11 different particle size distributions to choose from (all taken at the surface) while the hydraulic conductivity was determined at 5 different depths. We have chosen the two comparisons with the lowest R^2 values. We believe that this means that the two particle size distributions chosen were the least suitable for the hydraulic conductivity shown, though this is not the only possible interpretation. Thus, if we chose to fit the fractal model to the same particle

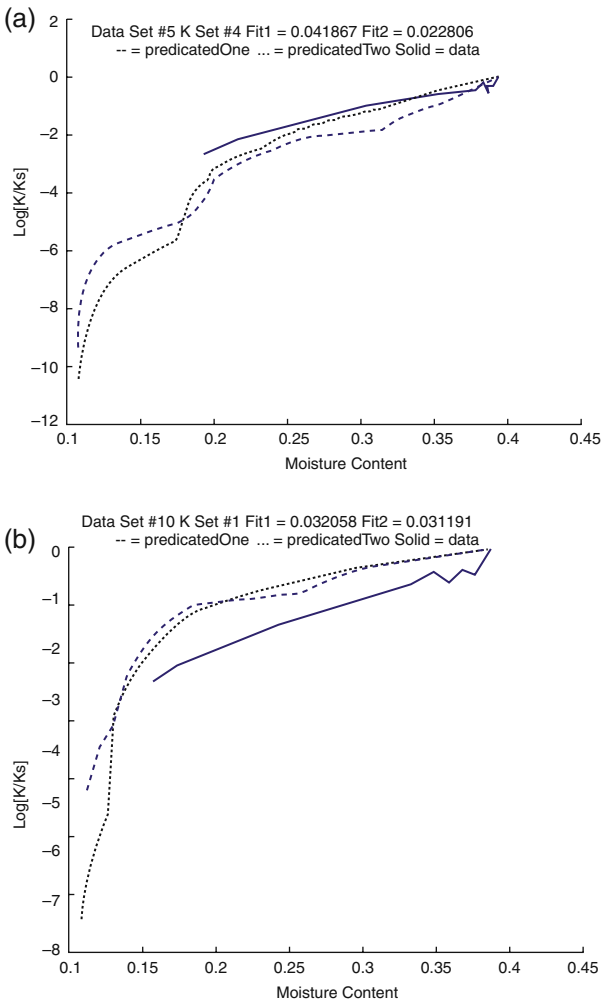

Fig. 5.17 (**a**, **b**) Use of numerical model to predict K for arbitrary soil pore space distribution and comparison with saturation dependence of K for McGee Ranch soils (used in Fig. 5.1). Note that there were 11 different particle size distributions taken from surface soils from which to generate a pore size distribution, and that K was measured at 5 different depths. This leaves as many as 55 possible comparisons, of which we present 2. Note that these two presented had the lowest R^2 values of all 55 comparisons. This may have happened because the particle size data chosen was not representative of the pore-size distribution at the particular depth. In any case comparing a numerical result with an analytical result for a fractal model and experimental data can clarify the relevance of the fractal model

size distributions and use those to predict the same two hydraulic conductivity functions, we would also presumably have similar discrepancies. The meaning of the discrepancies would indeed be that the model was not appropriate for the data, but we think that in such a case the message would simply be that the parameters were inappropriate, not the choice of model. Figure 5.1 did indicate that for this particular suite of soils the fractal model was appropriate.

5.4 Water Film Issues

As saturation is reduced and pathways through water-filled pore space lose connectivity, other modes of water transport become more prominent. Two such modes are film flow and vapor phase flow. Film flow will be governed by the roughness of grain surfaces, with surface fractal dimension D_s. It has been argued [67, 68] that such conduction will follow

$$K \propto S^{\frac{3}{m(3-D_s)}} \tag{5.36}$$

For discussion of the physical interpretation of the parameter m, see the original articles. Equation (5.36) is reminiscent of Eq. (5.14), and clearly has a similar origin. But in natural porous media, especially those in which the pore-size distribution covers at least two orders of magnitude, we do not expect to see Eq. (5.36) easily verified. In such media the pore-size distribution itself is sufficient to cause a variation in K of six or more orders of magnitude; then for $\theta < \theta_{xK}$ the percolation scaling will cause a further drop before film flow can prevent K from disappearing altogether. For example, if $K_S = 10^{-2}\,\mathrm{cm\,s^{-1}}$, then values well below $10^{-8}\,\mathrm{cm\,s^{-1}}$ would still be dominated by capillary flow through water-filled pores. Values of K much lower than $10^{-8}\,\mathrm{cm\,s^{-1}}$ are seldom measured, because experiments under typical conditions would have to last several years. However, monosized sphere packs (e.g., glass beads) may have a ratio of the maximum to the minimum pore size as small as 2, so their hydraulic conductivity may vary by as little as $2^4 = 16$ before other flow mechanisms become more important.

To see more clearly how an alternate means to transport water might show up in experimental data, consider Fig. 5.18, which shows data for $K(S)$ from Dr. M. Ioannidis (personal communication, 2006) for a medium of nearly monodisperse glass beads. The porosity of the medium is 0.3, noticeably smaller than appropriate for a cubic packing, and more nearly appropriate for a random close-packed structure. To a first approximation, one can consider the experimental medium to have no variability in pore size (Ioannidis, personal communication, 2007). The theoretical formulation of this chapter would therefore require that the hydraulic conductivity should exactly follow the universal scaling of Eq. (5.21). Clearly it does not, at least not over the full range of saturations.

Our single-fit parameter is a critical volume fraction (or moisture content) for percolation. The value obtained is $\theta_t = 0.049$. This corresponds to a critical fraction

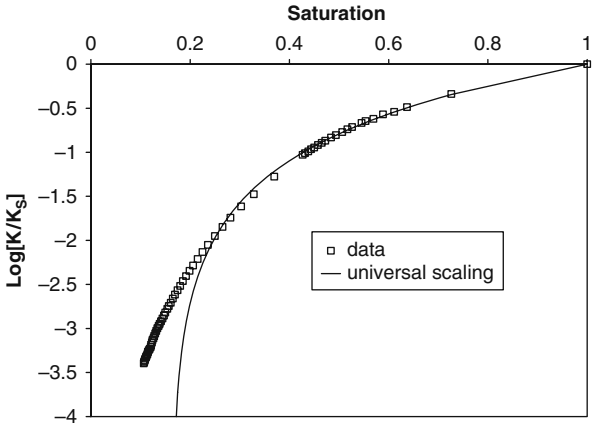

Fig. 5.18 Semi-log comparison of universal scaling with data from Dr. Ioannidis on the saturation dependence of the hydraulic conductivity of comparatively ordered granular media. The media should be considered to have pore radii that vary over less than a factor 2

of the porosity of 0.049/0.3, about 16%, a very common result for continuum percolation noted first by Scher and Zallen [42]. Over almost two orders of magnitude, K via Eq. (5.21) is in good agreement with the experimental data; only at lower saturations do the experimental data exceed the prediction. This discrepancy has two obvious interpretations. One possibility is that a different mechanism for water transport becomes important as the saturation nears 20%. The second is that universal scaling of the hydraulic conductivity is not valid, and that both the exponent μ^* and the critical volume fraction θ_t should be considered fitting parameters. This possibility is shown in Fig. 5.19; then in Fig. 5.21 we show that $\log(K)$ vs. $\log(\theta)$ is rather well described as a nonuniversal power with $\mu^* = 2.81$ and $\theta_t = 0.0145$, rather than $\mu = 2.0$ and $\theta_t = 0.049$.

How should one interpret these results? We will consider this problem from two perspectives. First we revisit Buckingham's [69] paper of a century ago and its continuing influence. Consider Fig. 5.20, Buckingham's schematic understanding of the dependence of hydraulic conductivity (denoted by Buckingham as λ) as a function of moisture content. As reported by Narasimhan [70], "Buckingham was led to the conclusion 'that the capillary conductivity, λ, will be a strong function of water content, θ, in a soil.' He conjectured that the relation would have the shape indicated schematically in Fig. 5.20. Between A and B, flow occurs dominantly through saturated capillaries. Between B and C, capillary and film flow coexist. Between C and D flow is exclusively through films. Between D and F films progressively break up."

Based on our quantitative theory of K, we broadly agree with this interpretation of Fig 5.20. Capillary flow will dominate from A to B, but also for much of the range from B to C, where the steep slope is related to the approach to the percolation threshold for the water-filled pores. Although film flow will become important well before C, it is not film flow in parallel that is so important (and seemingly implied by Narasimhan [70]), but film flow in series with capillary flow, preventing the

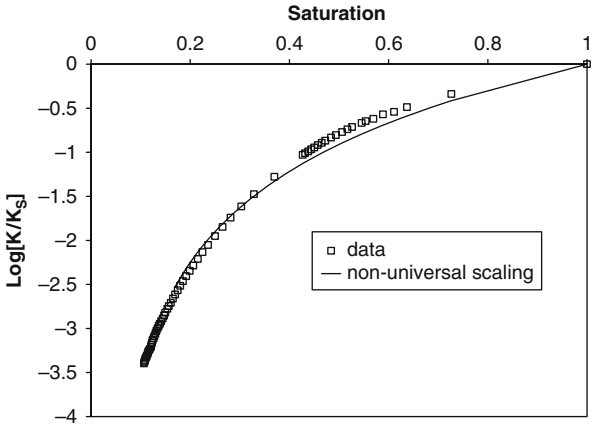

Fig. 5.19 Semi-log comparison of nonuniversal scaling with the same data as in Fig. 5.18 and with choice of an optimal value of the exponent, μ^*

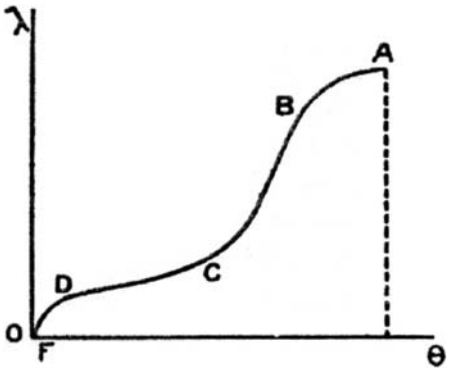

Fig. 5.20 Buckingham's (1907) schematic interpretation of the various regimes of hydraulic conductivity

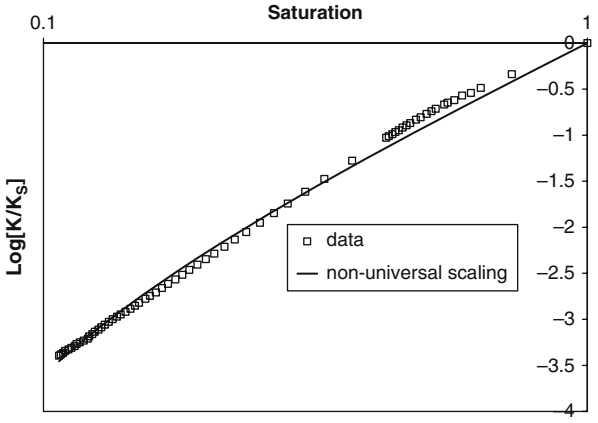

Fig. 5.21 The same comparison as in Fig. 5.19, except represented on a log-log plot

mean separation of water flow paths from diverging as the percolation threshold is approached. Even as the percolation threshold is approached, water need flow only a microscopic distance through thin films to incorporate finite-sized clusters into the flow and thus avoid divergence in flow path separation [71]. From C onward we generally agree with Buckingham: film flow can maintain higher values of K than predicted by theory as the percolation threshold is approached. As the saturation drops further, in the vicinity of C, Fig. 5.20) shows qualitatively what one would expect if an alternate mode of conduction were to act in parallel to the mechanism of capillary flow treated theoretically. Narasimhan [70] continues, "Voluminous soil hydraulic conductivity data now exist not only confirming Buckingham's conjecture of the form of the functional dependence but also showing that the λ vs. θ relation is strongly hysteretic [72–74]." Linear plots of the universal curve, together with $K(\theta)$ from Ioannidis as a function of moisture content (Fig. 5.22), are in general accord with Buckingham's sketch (Fig. 5.20). Buckingham's proposed mechanism appears generally consistent with the discrepancy between data and universal scaling of percolation theory.

Secondly, we consider the actual values of the fitting parameter θ_t. To estimate the critical volume fraction in Ioannidis' glass bead medium, one can apply the Vyssotsky et al. [76] bond percolation result. In a hexagonal close-packed system (similar to random close-packed) there are two types of sites (see Sect. 3.2.2): one

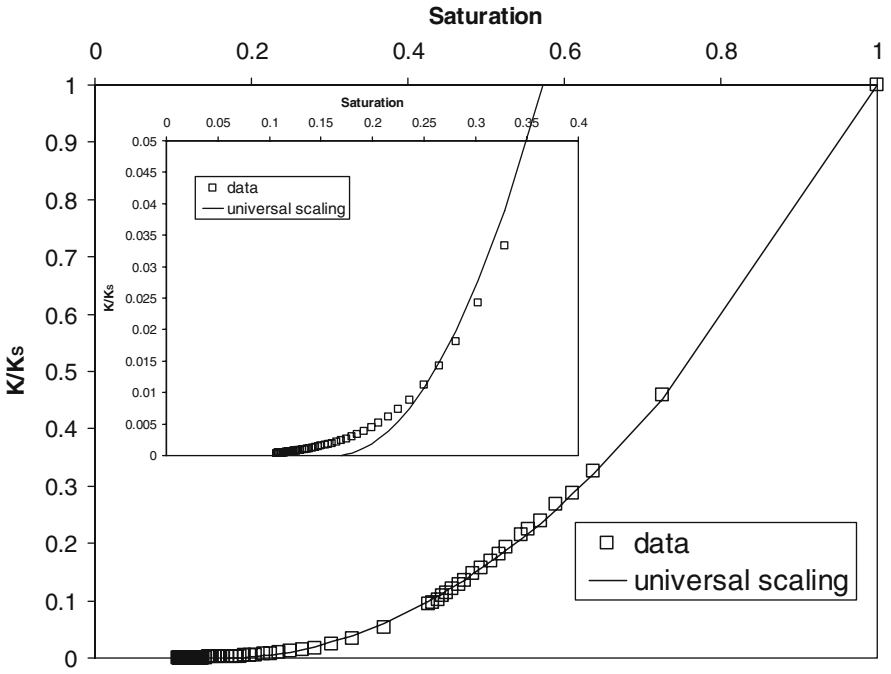

Fig. 5.22 The same comparison as in Fig. 5.18, but shown on a linear plot to make a graphical correspondence with the schematic drawing of Buckingham (1906)

with coordination number 4, the other with coordination number 8. The mean of these two values is 6, which would correspond to a bond percolation probability $p_c \approx 0.25$. But in hexagonal packing there are two tetrahedra for every octahedron; the mean is therefore ~ 5.3. This would increase p_c to 0.283. If half of the pore space is found in the bonds, then a water volume fraction $\theta = (0.5)(0.28)\phi = 0.0425$ should suffice for percolation. The critical volume fraction found using the universal value $\mu = 2.0(\theta_t = 0.049)$ is considerably closer to $\theta_t = 0.0425$ than is the value $\theta_t = 0.0149$ fitted using a nonuniversal exponent. The critical volume fraction fitted using a nonuniversal exponent requires closer to one-sixth of the pore space to be in the bonds. Moreover, $\theta_t = 0.049$ is consistent with the critical volume fractions extracted from a wide range of experiments (Ewing and Hunt, 2006; Hunt, 2004e).

We conclude that the discrepancy between universal scaling and experiment shown in Fig. 5.18 does not imply relevance of a nonuniform conductivity exponent. It more likely represents a crossover from K dominated by flow through water-filled pores, to the less-conductive film flow. At higher saturations, film flow operates in parallel with capillary flow but is negligible in comparison; when the continuity of capillary flow is interrupted, film flow operates in series with capillary flow through finite clusters.

How do the data from Ioannidis fit in with the themes of this chapter? Practically speaking, Buckingham's conclusions are most relevant for granular media with narrow grain size distributions. Even in Ioannidis' artificial medium, we detect only the onset of film flow. In natural media with much broader pore-size distributions, the hydraulic conductivity variation attributable to the pore-size variability is already several orders of magnitude; effects of percolation scaling extend a couple of orders of magnitude below that. Thus, if the saturated hydraulic conductivity is $10^{-2}\,\mathrm{cm\,s^{-1}}$, our percolation approach may account for values down from $10^{-7}\,\mathrm{cm\,s^{-1}}$ to $10^{-11}\,\mathrm{cm\,s^{-1}}$, and values in this range are rarely measured. So while Buckingham's thesis has supposedly been amply verified [70], we doubt that it has been verified often. Recall that the difference between two nearly equal values may easily vary over several orders of magnitude. Rigorous comparisons between theory and experiment for this capillary/film flow crossover issue therefore require exacting methods, and may still be inconclusive. Nonetheless, we believe our interpretation of alternate water transport modes operating in concert with capillary flow is consistent with both theory and observations.

The above discussion simultaneously addresses two common but apparently unrelated questions: (1) What properties or mechanisms could result in a nonuniversal conductivity exponent? and (2) Why is the critical volume fraction so small? As seen here, both questions may be resolved by considering a parallel conduction mechanism.

How would Narasimhan view our above approach? We assume that he would be skeptical, in view of the following quotes from the same paper [70]:

> Philosophically, Buckingham's skepticism raises the issue of the role of mathematics in the earth sciences. Milton Whitney, who led the Bureau of Soils and who had the vision to bring in talented physicists such as Briggs and Buckingham, believed that soil physics problems were so complex that they should not be handled strictly mathematically [76].

> It is appropriate to conclude with a thoughtful remark attributed to Ansel Adams, the renowned landscape photographer and conservationist: "There is nothing more disturbing than a sharp image of a fuzzy concept."

It is our belief, however, that with improvements in both the resolution and quantitative analysis of experiments, fuzzy concepts lose their validity if they do not become clearer.

5.5 Electrical Conductivity for $\theta < \theta_t$

We now present a suggestion for the means to calculate the electrical conductivity for $\theta < \theta_t$. Below the percolation threshold, electrical conduction must utilize a portion of the medium with a smaller electrical conductivity, σ_s, than whatever conducting fluid (with $\sigma = \sigma_0$) is filling the pore space. Clearly, however, the system conductivity is maximized by minimizing the path length in the lower conducting medium.

The present calculations simply seek an optimal path length. An optimal path will utilize many finite clusters in addition to the infinite cluster. Such a path was shown [71] to scale with $p - p_c$ exactly as the correlation length χ. This was the basis of our earlier argument regarding liquid-phase diffusion: the total distance that water must flow through liquid films above the percolation threshold is not a critical function of percolation: both the separations between the connected water-carrying paths and the total distance through the disconnected finite clusters scale the same way, and the distance through film flow is the difference between the two. Of course it is not necessary that the difference between two divergent quantities cancel; only that their ratio do so. However, if it is the optimal path that is sought, then the difference should be as small as possible, and thus not diverge. Thus the total distance that the electrical current travels through the liquid should scale as the correlation length for $\theta < \theta_t$, and the distance through the solid medium must be the size of the system, x, less the correlation length χ. This suggests that the conductivity should have the form

$$\sigma(\theta) = \frac{x}{(\chi/\sigma_0) + (x-\chi)/\sigma_s} = \frac{x}{\left[\chi_0 (\theta_t - \theta)^{-0.88}/\sigma_0\right] + \left[x - \chi_0 (\theta_t - \theta)^{-0.88}/\sigma_s\right]} \tag{5.37}$$

proportional to the inverse of the sum of the resistances along 1D paths which minimize the total resistance. Such a power law rapidly reduces the conductivity below the percolation threshold to the solid or surface conductivity. A similar decomposition may be applied to solute diffusion through water-filled pores and pores with only films of water.

The above calculation can equally apply to finding an optimal flow path (and associated K) through a system of muds and sands for which the sand portion does not

percolate. The Stanley group has long addressed the problem of finding distributions of such path lengths and transit times; see, for example, Lopez et al. [77].

Because Chaps. 5 and 6 are very closely related, a summary of Chap. 5 is combined with the summary of Chap. 6 and given at the end of Chap. 6.

Problems

5.1. Prove that r_c is the same for electrical and hydraulic conductivities and draw an analogy to problem 1 in Chap. 3, which asked to show that the value obtained for R_c was independent of whether one obtained r_c first and substituted into the equation for $R(r)$, or whether one integrated over R directly.

5.2. The experimental results, Fig. 6.7, for $D_{pm}/D_w\theta$ (where D_{pm} is the diffusion constant of an arbitrary solute in a porous medium and D_w is the corresponding diffusion constant in water) appear to show very straight lines over a wide range of moisture contents, which intersect the θ axis at distinct points, θ_t. Thus one can write (Sect. 6.3) an empirical relationship $D_{pm}/D_w = \theta(\theta - \theta_t)$. In analogy with Sect. 5.5 derive a relationship to predict D_{pm}/D_w for moisture contents less than θ_t.

5.3. Consider a log-normal distribution of pore sizes, but assume as in a fractal model that all pores have the same shapes (this is a necessary assumption in a fractal model, but only an assumption of convenience, otherwise). Derive equivalent expressions for the saturation dependence of the hydraulic and electrical conductivities using critical path analysis and find the moisture contents at which the critical path analysis must be replaced by percolation scaling. These exercises may be performed numerically. Compare the ranges of parameter space (D_p, ϕ), for which Archie's law may be reasonably derived from percolation theory determined from the log-normal and the power-law distributions. Does a log-normal distribution tend to make Archie's law more or less widely applicable than is the case for a power-law distribution of pore sizes?

5.4. Graphically represent the apparent power $\mu^*(\phi)$ of the porosity in Archie's law when the pore-size distribution modifies its value from 2 in the cases that a) the ratio r_0/r_m is held constant and b) the fractal dimensionality is held constant. You will need to keep in mind that in either case μ^* is $d\ln(\sigma)/d\ln(\phi) = ((/\sigma)d\sigma/d\phi$.

References

1. Jerauld, G. R., J. C. Hatfield, L. E. Scriven, and H. T. Davis, 1984, Percolation and conduction on Voronoi and triangular networks: a case study in topological disorder, *J. Phys. C 17*: 1519–1529. 123

2. Balberg, I., 1987, Recent developments in continuum percolation, *Philos. Mag. B 30*: 991–1003. 123, 127, 128, 129, 130, 134, 136, 139
3. Hilfer, R., 1991, Geometric and dielectric characterization of porous media, *Phys. Rev*. **44**: 60. 123, 142
4. Berkowitz, B., and I. Balberg, 1992, Percolation approach to the problem of hydraulic conductivity in porous media, *Transp. Porous Media 9*: 275–286. 123
5. Berkowitz, B., and I. Balberg, 1993, Percolation theory and its application to groundwater hydrology, *Water Resour. Res*. **29**: 775–794. 123, 131, 135
6. Golden, K. M., S. F. Ackley, and V. I. Lytle, 1998, The percolation phase transition in sea ice, *Science 282*: 2238–2241. 123
7. Golden, K. M., 2001, Brine percolation and the transport properties of sea ice. *Ann. Glaciology 33*: 28–36. 123
8. Kogut, P. M. and J. Straley, 1979, Distribution-induced non-universality of the percolation conductivity exponents, *J. Phys. C. Solid State Phys. 12*: 2151–2159. 123
9. Feng, S., B. I. Halperin, and P. N. Sen, 1987, Transport properties of continuum systems near the percolation threshold, *Phys. Rev. B*, **35**: 197. 123, 136
10. Archie, G. E., 1942, The electrical resistivity log as an aid in determining some reservoir characteristics. *Trans. Am. Inst. Mech. Eng*. **146**: 54–61. 124, 125, 146, 147
11. Adler, P. M., C. G. Jacquin, and J. F. Thovert, 1992, The formation factor of reconstructed porous media. *Water Resour Res*. **28**: 1571–1576. 124
12. Bigalke, J., 2000, A study concerning the conductivity of porous rock, *Phys. Chem. Earth 25*: 189–194. 124
13. Binley, A., P. Winship, R. Middleton, M. Pokar, and J. L. West, 2001, Observation of seasonal dynamics in the vadose zone using borehole radar and resistivity. In Proceedings of the Symposium on the Application of Geophysics to Environmental and Engineering Problems, SAGEEP, March 4–7, 2001. 124, 146, 147, 148
14. Binley, A., P. Winship, L. J. West, M. Pokar, and R. Middleton, 2002, Seasonal variation of moisture content in unsaturated sandstone inferred for borehole radar and resistivity profiles, *J. Hydrol. 267*: 160–172. 124, 146, 148
15. Binley, A., C. Cassiani, R. Middleton, and P. Winship, 2002, Vadose zone model parameterization using cross-borehole radar and resistivity imaging, *J. Hydrol*. **267**: 147–159. 124, 146, 148
16. Thompson, A. H., A. J. Katz, and C. E. Krohn, 1987, Microgeometry and transport in sedimentary rock, *Adv. Phys*. **36:** 625. 124, 136, 137, 138, 139, 140
17. Kuentz, M., J. C. Mareschal, and P. Lavallee, 2000, Numerical estimation of electrical conductivity in saturated porous media with a 2-D lattice gas, *Geophysics 65*: 766–772. 124, 136
18. Lemaitre., J., J. P. Roadec, D. Bideau, A. Gervois, and E. Bougault, 1988, The formation factor of the pore space of binary mixtures of spheres, *J. Phys. D: Appl. Phys*. **21**: 1589–1592. 124
19. Johnson, D. L., and L. M. Schwartz, 1989, Unified theory of geometric effects in transport properties of porous media. In Paper presented at SPWLA, 30th Annual Logging Symposium, Soc. of Prof. Well Log. Anal. Houston, TX. 124
20. Le Ravalec, M., M. Darot, T. Reuschle, and Y. Gueguen, 1996, Transport properties and microstructural characgteristics of a thermally cracked mylonite, *Pure Appl Geoph*. **146**: 207–227. 124
21. Mattisson, C., and M. A. Knackstedt, 1987, Transport in fractured porous solids, *Geophys. Res. Lett*. **24**: 495–498. 124
22. Ruffet, C., Y. Gueguen, and M. Darot, 1991, Complex conductivity and fractal microstructures, *Geophysics 56*: 758–768. 124
23. Wong, P., J. Koplik, and J. P. Tomanic, 1984, Conductivity and permeability of rocks, *Phys. Rev. B 30*: 6606–6614. 124
24. Montaron, B., 2005, Fractals, percolation theory, and the stability of Archie's m exponent, SPWLA topical conference on "Low Resistivity Pay in Carbonates" in Abu-Dhabi, UAE, 2005. 124
25. Ewing, R. P., and A. G. Hunt, 2006, Dependence of the electrical conductivity on saturation in real porous media, *Vadose Zone J*. **5**(2): 731–741. 124

26. Rieu, M., and G. Sposito, 1991, Fractal fragmentation, soil porosity, and soil water properties I. Theory, *Soil Sci. Soc. Am. J*. **55**: 1231. 124
27. Hunt, A., N. Gershenzon, and G. Bambakidis, 2007, Pre-seismic electromagnetic phenomena in the framework of percolation and fractal theories, *Tectonophysics* **431**: 23–32. 126
28. Friedman, S. P., and N. A. Seaton, 1998, Critical path analysis of the relationship between permeability and electrical conductivity of three-dimensional pore networks, *Water Resour Res*. **34**: 1703. 126, 140
29. Bernabe, Y., 1998. Streaming potential in heterogeneous network. *J. Geophys. Res*., **103**: 20827–20841. 127
30. Surkov, V. V., and H. Tanaka, 2005, Electrokinetic effect in fractal pore media as seismo-electric phenomena, in: *Fractal Behavior of the Earth System*, Ed. V. P. Dimri, Springer, Heidelberg. 127
31. Hunt, A. G., 2004e, Continuum percolation theory and Archie's law, *Geophys Res* Lett. **31**(19): Art. No. L19503. 128, 133, 135, 145
32. Hunt, A. G., 2005, Continuum percolation theory for transport properties in porous media, *Phil. Mag*. **85**: 3409–3434. 129, 131, 134
33. Hillel, D., 1998, *Environmental Soil Physics*, Academic Press. (Elsevier?), San Diego, CA 130
34. Bittelli, M., G. S. Campbell, and M. Flury, 1999, Characterization of particle-size distribution in soils with a fragmentation model. *Soil Sci. Soc. Am. J*. **63**: 782–788. 130
35. Wu, Q., M. Borkovec, and H. Sticher, 1993, On particle-size distributions in soils, *Soil Sci. Soc. Am. J*. **57**: 883–890. 130, 131, 134
36. Mallory, K., 1993, Active subclusters in percolative hopping transport, *Phys. Rev. B 47*: 7819–7826. 130
37. Hunt, A. G., 2004, Percolative transport and fractal porous media, *Chaos Solitons Fractals 19:* 309–325. 131, 139
38. Hunt, A. G., and G. W. Gee, 2002, Water retention of fractal soil models using continuum percolation theory: tests of Hanford site soils, *Vadose Zone J*, **1:** 252–260. 131, 141
39. Hunt, A. G., and G. W. Gee, 2002, Application of critical path analysis to fractal porous media: comparison with examples from the Hanford site, *Adv. Water Resour.*, **25**: 129–146. 131, 133
40. Rockhold, M. L., M. J. Fayer, and G. W. Gee, 1988, Characterization of unsaturated hydraulic conductivity at the Hanford site, *PNL 6488* Pacific Northwest National Laboratory, Richland, WA 99352. 131, 132
41. Hunt, A. G., 2004, Continuum percolation theory for water retention and hydraulic conductivity of fractal soils: 1. Estimation of the critical volume fraction for percolation, *Adv. Water Resour. 27:* 175–183. 134
42. Scher, H., and R. Zallen, 1970, Critical density in percolation processes, *J. Chem. Phys*. **53:** 3759. 135, 158
43. Sahimi, M., 1993, Fractal and superdiffusive transport and hydrodynamic dispersion in heterogeneous porous media, *Transp. Porous Media 13*: 3–40. 135, 136, 142
44. Sahimi, M., 1993, Flow phenomena in rocks – from continuum models to fractals, percolation, cellular automata, and simulated annealing, *Rev. Mod. Phys. 65*(4): 1393–1534. 135, 136, 142
45. Krohn, C. E., and A. H. Thompson, 1986, Fractal sandstone pores: automated measurements using scanning-electron-microscope images, *Phys. Rev. B 33*: 6366–6374. 136
46. Suleiman, K. A., and D. Swartzendruber, 2003, Measurement of sated hydraulic conductivity of surface soil in the field with a small-plot sprinkling infiltrometer, *J Hydrology 272*: 203–212. 139
47. Mendelson, K. S., and M. H. Cohen, 1982, The effect of grain anisotropy on the electrical properties of sedimentary rocks, *Geophysics 47*: 257. 142
48. Bussian, A. E., 1983, Electrical Conductance in a porous medium, *Geophysics 48*, 1258. 142
49. Patnode, H. W., and M. R. J. Wyllie, 1950, The presence of conductive solids in reservoir rocks as a factor in electric log interpretation. *Trans. AIME 189*: 47–52. 143
50. Cremers, A. and H. Laudelout. 1965. Note on the "isoconductivity value" of clay gels. *Soil Sci. 100*: 298–299. 143

51. Rhoades, J. D., P. A. C. Raats, and R. J. Prather, 1976, Effects of liquid-phase electric conductivity, water content, and surface conductivity on bulk soil electrical conductivity, *Soil Sci. Soc. Am. J*. **40**: 651–655. 143, 146
52. Letey, J., and A. Klute, 1960, Apparent mobility of potassium and chloride ions in soil and clay pastes, *Soil Sci*. **90**: 259–265. 143
53. Cremers, A., J. van Loon, and H. Laudelout, 1966, Geometry effects for specific electrical conductance in clays and soils. Proc. Internat. Conf. Clays Clay Miner. 14th Ghent, Belgium, pp 149–162. 143
54. Klein, K. A., and J. C. Santamarina, 2003, Electrical conductivity in soils: underlying phenomena, *J. Envir. Eng. Geophys*. **8**: 263–273. 143
55. Stauffer, D., 1979, Scaling theory of percolation clusters, *Phys. Rep. 54*: 1–74. 144
56. Cassiani, G., E. Dalla, A. Brovelli, and D. Pitea, 2004, Pore-scale modeling of electrical conductivity in unsaturated sandstones, Computational Methods in Water Resources: Proceedings of the XVth International Conference, June 13–17, Chapel Hill, NC, USA, 235–246. 146, 147, 148
57. Ren, T., K. Noborio, and R. Horton, 1999, Measuring soil water content, electrical conductivity, and thermal properties with a thermo-time domain reflectometry probe, *Soil Sci. Soc. Am. J*. **63**: 450–457. 148, 149
58. Rinaldi, V. A., and G. A. Cuestas, 2002, Ohmic conductivity of a compacted silty clay. *J. Geotech. Geoenvir. Eng*. **128**: 824–835. 146, 150, 151
59. Abu-Hassanein, Z. S., C. H. Benson, and L. R. Blotz, 1996, Electrical resistivity of compacted clays, *J. Geotech. Eng*. **122**: 397–406. 146, 150, 151, 153, 154
60. Mori, Y., J. W. Hopmans, A. P. Mortensen, and G. J. Kluitenberg. 2003. Multi-functional heat pulse probe for the simultaneous measurement of soil water content, solute concentration, and heat transport parameters. *Vadose Zone J*. **2**: 561–571. 147, 150, 152
61. Tuli, A., and J. W. Hopmans, 2004, Effect of degree of saturation on transport coefficients in disturbed soils, *Eur. J. Soil Sci*. **55**: 147–164. 147, 150, 152
62. Kechavarzi, C., and K. Soga, 2002, Determination of water saturation using miniature resistivity probes during intermediate scale and centrifuge multiphase flow laboratory experiments. *Geotech. Test. J*. **25**: 95–103. 147, 151, 152, 153, 154
63. Hunt, A. G., 2004, A note comparing van Genuchten and percolation theoretical formulations of the hydraulic properties of unsaturated media, *Vadose Zone J*. **3**: 1483–1488. 153
64. Roberts, J. J., and W. N. Lin, 1997, Electrical properties of partially saturated Topopah Spring tuff. Water distribution as a function of saturation, *Water Resour. Res*. **33**: 577–587. 146, 153
65. Ren, T., K. Noborio, and R. Horton, 1999, Measuring soil water content, electrical conductivity, and thermal properties with a thermo-time domain reflectometry probe, Soil Sci. Sco. *Am. J*. **63**: 450–457. 154
66. Blank, L. A., A. G. Hunt, and T. E. Skinner, 2008, A numerical procedure to calculate hydraulic conductivity for an arbitrary pore size distribution, *Vadose Zone J. 7*: 461–472. 155
67. Davis, H. T., R. A., Novy, L. E. Scriven and P. G. Toledo, 1990, Fluid distribution and transport in porous media at low wetting phase saturations, *J. Phys. CM 2*: SA 457–SA 464. 157
68. Toledo, P. G., R. A. Novy, H. T. Davis, and L. E. Scriven, 1992, On the transport properties of porous media at low water content, in: *Indirect Methods for Estimating the Hydraulic Properties of Unsaturated Soil*s, ed. M. Th. Van Genuchten, F. J. Leij, L. J. Lund, University of California, Riverside, CA 92521. 157
69. Buckingham, E., 1907, Studies on the movement of soil moisture, Bul. No. 38, Bureau of Soils, USDA, Washington, D. C. 158
70. Narasimhan, T. N., 2007, Central ideas of Buckingham, 1906: a century later, *Vadose Zone J. 6*: 687–693. 158, 160, 161
71. Hunt, A. G., 2004, Continuum percolation theory for water retention and hydraulic conductivity of fractal soils: 2. Extension to non-equilibrium, *Adv. Water Resour. 27:* 245–257. 160, 162
72. Mualem, Y., 1976, A new model for predicting the hydraulic conductivity of unsaturated porous media, *Water Resour. Res*. **12**: 513–522. 160
73. Mualem, Y., 1976. A catalogue of the hydraulic properties of unsaturated soils, Res. Proj. No. 442, Technion, Israel Institute of Technology, Haifa. 160

74. Mualem, Y. 1976, Hysteretical models for prediction of hydraulic conductivity in unsaturated porous media, *Water Resour. Res*. **12**: 1248–1254. 160
76. Vyssotsky, V. A., Gordon, S. B., Frisch, H.L. and Hammersley, J. M. 1961, Critical percolation probabilities (bond problem) *Phys. Rev.* **123**: 1566–1567. 160, 187
76. Landa, E. R., and J. R. Nimmo, 2003, The life and scientific contributions of Lyman J. Briggs, *Soil Sci. Soc. Am. J*. **67**: 681–693. 161
77. Lopez, E., S. V. Buldyrev, N. V. Dokholyan, L. Goldmakher, S. Havlin, P. R. King, and H. E. Stanley, 2003, Postbreakthrough behavior in flow through porous media, *Phys. Rev. E 67:* 056314: 1–16. 163
78. Khaleel, R., and E. J. Freeman, 1995. Variability and scaling of hydraulic properties for 200 area soils, Hanford site, Westinghouse Hanford Company Report WHC-EP-0883. 141
79. Freeman, E. J., 1995. *Fractal Geometries Applied to Particle Size Distributions and Related Moisture Retention Measurements at Hanford, Washington*, M. A. Thesis, University of Idaho, Moscow. 141

Chapter 6
Other Transport Properties of Porous Media

In this chapter we discuss the air permeability, the thermal conductivity, as well as solute and gas diffusion. Some interesting limitations and complications of the percolation-based approach are illuminated in the context of the saturation dependence of thermal conductivity. Then we summarize a treatment of the frequency-dependent electrical conductivity in hydrated smectite clay minerals. We interpret these experimental results using critical path analysis for interacting hopping charges (a topic of Chap. 4) through surface water between and on the outside surfaces of sheet silicates, which also brings in the subject of the continuity of water paths. We also briefly present potential applications to electroseismic phenomena and give a summary of Chaps. 5 and 6.

By contrasting the predicted behaviors of the various properties, and comparing those predictions with experiment, we generate a deeper understanding of the relative roles of geometry (pore size) and topology (pore connectivity). These relative roles are different for different properties. We also discover which property is most sensitive to the particular way water is apportioned in the pore space (thermal conductivity).

6.1 Air Permeability

Unlike the electrical and hydraulic conductivities, the air permeability k_a as a function of the air-filled porosity ε is relatively simple to predict. Recall that if water and air are the only two fluids, they must occupy the entire void volume: $\varepsilon + \theta = \phi$. For an arbitrary fluid the permeability is obtained from the conductivity by multiplying by the kinematic viscosity. This adjustment allows simple comparison between permeabilities of different fluids, as long as their critical volume fractions for percolation are the same.

First we consider the assumption that the critical volume fractions ε_t for air percolation has the same value as θ_t for water percolation. A key difference between air and water in soil is that water is a wetting fluid, while air is not. This difference is accentuated by clay minerals, which have high specific surface area and whose surfaces are often electrostatically charged; both these properties cause clay to adsorb water. Water sorbed to a clay surface has higher viscosity than the bulk water

Hunt, A., Ewing, R.: *Other Transport Properties of Porous Media.* Lect. Notes Phys. **771**, 169–206 (2009)
DOI 10.1007/978-3-540-89790-3_6

(Sect. 6.4), so we could consider sorbed water (say, the first 4 molecular layers) to be part of the solid phase. This would effectively decrease the size of the pores with respect to water, but not with respect to air. A clayey soil therefore has $\varepsilon_t < \theta_t$. However, when the medium in question has low clay content, water sorption can be neglected, and we expect $\varepsilon_t \approx \theta_t$; in such cases ε_t should also be on the order of 0.1ϕ. To the extent that the critical volume fraction for percolation (ε_t for air and θ_t for water) is independent of the fluid, the air permeability of a completely dry porous medium equals the water permeability of the same medium when water saturated.

Consider now the saturation dependence of the air permeability. Because water is the wetting fluid, at any intermediate water content $0 < \theta < \phi$ the water occupies the smaller pores, while air occupies the larger. Consequently, adding water to a dry medium does not change the bottleneck radius r_c for air flow, even while it increases the r_c for water flow. This holds for all air-filled porosity values $\varepsilon \geq \varepsilon_t$. Because there are no geometrical effects via a bottleneck pore radius, topological effects must control permeability. With these topological effects accounted for by universal percolation scaling, air-filled permeability $k_a(\varepsilon)$ must follow

$$k_a(\varepsilon) = k_a\big|_{\varepsilon=\phi} (\varepsilon - \varepsilon_t)^{\mu} \tag{6.1}$$

over the entire range of air-filled porosity values [1]. This result, as all percolation results, becomes approximate far from the percolation threshold because percolation theory is approximate far from the threshold, but clearly there is virtually no additional dependence related to the pore-size distribution. The analysis of Hazlett and Furr [2] is essentially equivalent to this result.

Again we have the complication that for 2D systems the exponent μ should be 1.3, instead of 2.0 in 3D. For experiments which were essentially 2D in nature (one dimension transverse to flow smaller by a factor of ca. 1000 than the other two dimensions), Steriotis et al. [3] reported the nonwetting phase relative permeability shown in Fig. 6.1. These experimental results are compared with the prediction of Eq. (6.1), using the 2D value $\mu = 1.3$ [1]. This comparison required one adjustable parameter, $\varepsilon_t = 0.16$.

Experiments on volcanic ash soils yielded a power relationship for air permeability similar to Eq. (6.1), with the exponent given as 1.84 ± 0.54 [4]. There is no simple relationship discernible using percolation theory between the fractal dimensionality of a soil and its air permeability, though these authors report a slight dependence on pore-size distribution (as well as a great deal of scatter). Soil structure may have a large impact on k_a at $\varepsilon = \phi$ (Chap. 11), so it is possible that the results were affected by structure. While the range of powers reported may be unacceptably wide, most of the soils yielded an exponent slightly smaller than 2, while those with high clay contents (which can produce a 2D structured soil) yielded an exponent somewhat larger than 1 (Moldrup, personal communication, 2004).

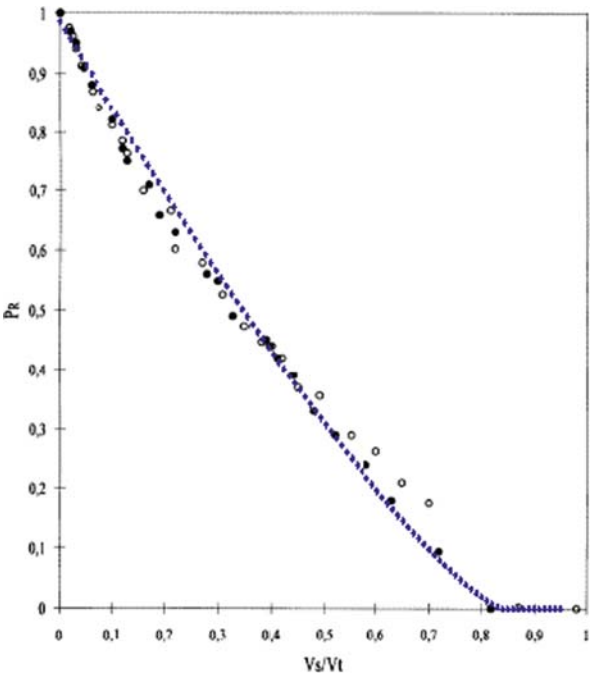

Fig. 6.1 Plots of the air-phase permeability as a function of wetting phase saturation. The solid dots are actual measurements with two phases present; the open circles are measurements of single phase flow. Data from Steriotis et al. [3]. The experimental conditions were appropriate for 2D flow. The exponent, m, was thus chosen to be 1.27 (not updated to 1.3). The theoretical prediction (dashed curve) from Eq. (6.1) uses one parameter, the critical air fraction for percolation, equal to 0.16. Note that only the solid circles represent a direct measurement, while the open circles are from a proxy, and that Steriotis et al. [3] wished to show that the open circles were a reasonable approximation to the actual values

Unsal et al. [5] present data for air permeability which compare well with universal scaling (Eq. (6.1)), as seen in Figs. 6.2 and 6.3. An additional data set from Tuli et al. [6] is rather noisy. The Tuli et al. [6] data comprise 13 soils, while the data of Unsal is from a single system. For the Unsal et al. [5] system we find $\varepsilon_t = 0.017 \approx \phi/22$. With this value of the critical volume fraction we can choose a prefactor as a second fit parameter and generate the following linear fit (Fig. 6.3): $y = x + 0.0004$ with $R^2 = 0.9977$. In order to analyze the data set of Tuli et al. [6] we fitted a critical volume fraction and a prefactor to each soil, making each a two parameter fit. When we plot predicted vs. observed values for all the systems of Tuli et al. [6] together (Fig. 6.4) we find a 3% discrepancy in slope and an R^2 of 0.95. Two of the thirteen soils had fit parameters $\varepsilon_t = 0.0$. When those are excluded and we plot for the remaining soils ε_t against ϕ, the linear regression yields $\varepsilon_t = 0.09\phi + 0.01$, but with very small $R^2 = 0.05$. The average of the eleven nonzero values of ε_t is 0.032, or just under 8% of the average porosity 0.45, not greatly different from the 9% obtained in the regression. The critical air fraction for percolation

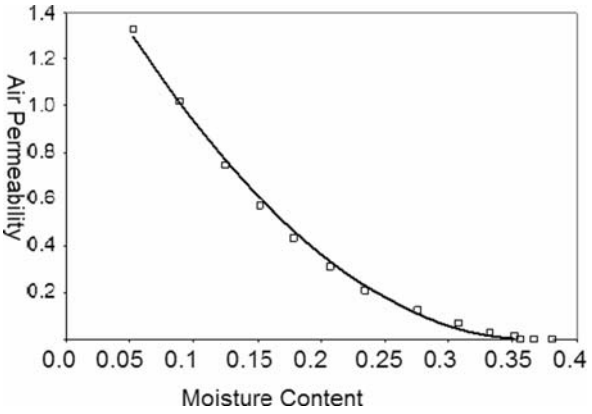

Fig. 6.2 Comparison of air permeability with universal percolation scaling (Eq. (6.1)). Data from Unsal et al. [5]

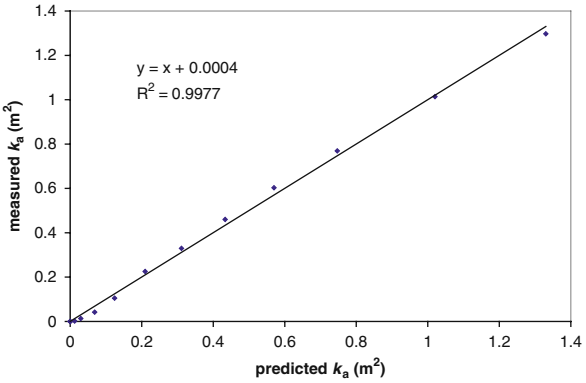

Fig. 6.3 Direct comparison of predicted and observed values of the air permeability (data from Fig. 6.2). Note that the slope is 1, $R^2 = 0.998$, and the value of the intercept is about 1/1000 of the typical permeability values

is much smaller in 3D than in 2D (compare the Unsal et al. and Tuli et al. values of 0.017 and 0.032 with those of Stereotis et al. 0.16), generally consistent with other 3D versus 2D comparisons shown in Table 1.1 (percolation thresholds for various lattices). Interestingly, Unsal et al. [5] had asserted that the air permeability function $k_a(\varepsilon)$ can be used to obtain information about the pore-size distribution, at odds with our analysis, as a two-parameter fit from a universal result predicts the data with a slope of 1, an intercept of 1/1000 of the mean measured value and an R^2 value of 0.998.

The three data sets investigated are at least compatible with universal scaling, as predicted. Two of these data sets can be predicted extremely accurately with the universal result from percolation theory.

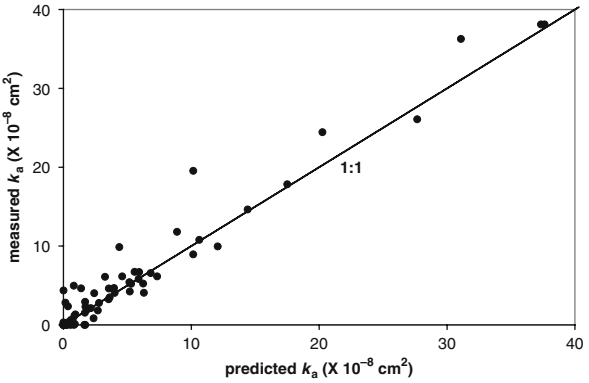

Fig. 6.4 Comparison of predicted and observed values of the air permeability [data from Tuli et al. [6]]

6.2 Thermal Conductivity

6.2.1 General Comments on the Saturation Dependence of the Thermal Conductivity

The saturation dependence of the thermal conductivity $\lambda(\theta)$ is difficult to analyze within the context of percolation theory. First, all three phases in a typical unsaturated geological medium (water, air, solid) have nonzero thermal conductivities, though the thermal conductivity of air λ_a is typically sufficiently small to ignore. Second, the thermal conductivity of the water and solid phases is not a simple or universal ratio. The solid-phase conductivity λ_s may be only half that of water λ_w (organic soils), or as much as 15 times greater (high quartz soil), with more typical ratios (5–10) depending on mineralogy; other ratios will be obtained in artificial media. Third, the ratio of the thermal conductivity of a saturated soil to its value in the same soil under perfectly dry conditions is seldom much over 10. This implies that the kind of critical path analysis arguments that we have been employing, which can easily contain uncertainty regarding factors of 2, for example (in order to get tendencies of many orders of magnitude correct), will tend to contain too high a level of uncertainty. Unfortunately, because of the typically higher conductivity of the solid phase, even under dry conditions the medium is not near the percolation threshold. This introduces considerable uncertainty into percolation-scaling arguments. In fact, when the medium becomes saturated, the equivalent volume fraction incorporated by conducting material is 1 (while a critical volume fraction may be zero), as far from the percolation threshold as it is possible to get, and the worst possible conditions for percolation theory. An additional complication arises from the physical arrangement of the solids. While water at both smaller and larger saturations has the tendency to enhance the global connectivity of the pathways, in granular media at fairly low saturations, the most important effect of water is to

enhance the conduction between individual grains. A simultaneous solution, rather than a separation, of all these issues is required because the total range of thermal conductivity values from dry conditions to saturation is seldom much more than an order of magnitude, mixing all these effects together. This places a high degree of importance on an accurate description of the geometry (a very difficult problem) for a property that does not really exhibit a wide range of values. Under such conditions it may be difficult to find sufficient motivation for attacking the problem logically and quantitatively. Still, it is important to attempt to develop a unified picture of all conduction and transport properties in one place.

6.2.2 Theoretical Construction

In this discussion we come at the problem, so to speak, from two directions. First we look at geometrical influences under ideal conditions to make geometry dominant, then we look at percolation scaling under ideal conditions to make scaling simple. Then we combine the two approaches to see whether the resulting expression is compatible with experiment over all saturations and mineralogies, i.e., including all possible nonideal conditions.

Consider a medium composed of solid spheres. Ignoring deformation, contact between two spheres is simply a point, leading to an infinite contact resistance between each pair of spheres. When water enters such a medium it tends to form pendular (ring) structures at the contact points [7]. Because the pendular structures are much wider than they are long, for a small increase in water content one gains a large increase in conductivity. This geometrical problem has never been solved analytically. However, for a cubic lattice of spheres with all water being in pendular rings, the conductivity is given approximately by [8]

$$\lambda(\theta) \approx \lambda|_{\theta=0} + a\theta^b \tag{6.2}$$

with $a \approx (\lambda_s/\lambda_w)^{3/2}$ and $b \approx 0.1 + 1.75(\lambda_w/\lambda_s)$. Commonly b appears to take on a value near 1/4. This approximate power-law form of $\lambda(\theta)$, with a sublinear power at typical values of λ_s/λ_w, is consistent with measurements of $\lambda(\theta)$ in granular media at low water contents [9]. The form of Eq. (6.2) also holds for deformed spheres [8], so the behavior (if not the actual value of the exponent) applies beyond perfect spheres in a cubic lattice. Equation (6.2) also holds, under some rather restrictive assumptions (needed for calculation), for spherical particles with a range of sizes, though the expressions for the parameters are not identical [8]. At higher water contents, as menisci coalesce and fill pores, resistance to heat flow is mainly due to air inclusions, probably well described by simplistic treatments of tortuosity. In the wet regime $\lambda(\theta)$ is often predicted by a simple linear mixing model.

What would percolation theory have to say about the thermal conductivity? We have constructed the following percolation theoretical argument for the thermal conductivity of natural porous media under the conditions that $\lambda_a = 0$, and $\lambda_w = \lambda_s$ and

that geometrical effects of pendular structures can be ignored. Under such conditions, ignoring everything except the bulk fraction of the medium which is either solid or water, one can represent thermal conductivity via universal scaling as

$$\lambda(\theta) \propto (1-\phi+\theta)^2 \tag{6.3}$$

Note that, even in the case $\phi \to 1$, the solid portion of the medium percolates by construction as any medium must be "grain-supported," otherwise it would collapse, and the porosity would change. Thus there should be no need to include a critical solid fraction for percolation.

Such an expression as Eq. (6.3) cannot be quantitatively accurate, because the percolation threshold is never approached, not even for $\theta = 0$. Further, in the limit $\theta \to \phi$ (effectively $p - p_c = 1$) it predicts $d\lambda/d\theta = 2$, instead of 0. On the other hand, Eq. (6.3) does reproduce an observed proportionality of the thermal conductivity of dry soils ($\theta = 0$) to a nonlinear power of the density $(1-\phi)^n$ [10, 11], with Campbell [12] choosing precisely 2. In fact, Campbell's result for the thermal conductivity of dry soils, considered by some (including Campbell) to be predictive, is $\lambda = 0.03 + 0.7(1-\phi)^2$. This relationship given in Campbell is in fact closely related to Archie's law. To investigate further, we have digitized 168 data points for thermal conductivity of dry rocks and soils from Cóté and Konrad [13] and present $\log[\lambda]$ vs. $\log[1-\phi]$ (investigating Eq. (6.3) in the limit $\theta \to 0$). Allowing Excel to choose a power leads to a slope of 2.017, less than 1% different from the predicted value, but considerable curvature exists (Fig. 6.5). Note that analysis of rocks separately leads to a larger slope (2.47) and soils separately to a smaller slope (1.43), while each of those individual graphs also contains noticeable curvature (not shown). Including 18 additional soil data points from Lu et al. [14] would make no visible change in the curvature, but would reduce the power to 1.98. Given that the thermal conductivity of dry soils/rocks is sensitive to the exact mineralogy, our preliminary comparison, lumping all types together is only suggestive, not conclusive.

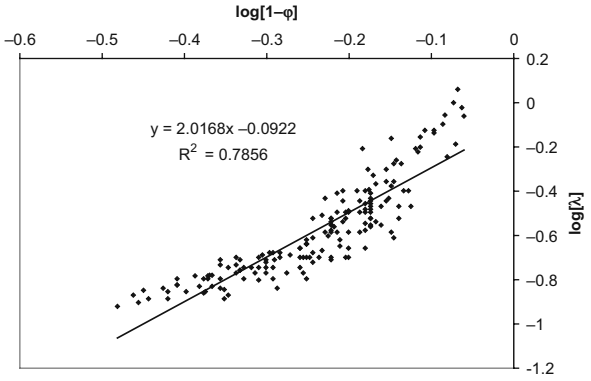

Fig. 6.5 Comparison of Eq. (6.3) for $\theta = 0$ (dry soils) with all the relevant data collected by Cote and Konrad [13]. While considerable curvature exists, the slope picked by Excel on a logarithmic plot is 2.017, less than 1% different from the percolation theoretical slope

By itself Eq. (6.3) bears little resemblance to experimental results for the saturation dependence of the thermal conductivity. So we return to the approximate result (Eq. (6.2)) of Ewing and Horton [8] and the fact that it appears to have relevance also in media with a wider range of particle sizes. This allows an interpretation of Eq. (6.2) in terms of critical path analysis, namely that it generates the appropriate expression for the dependence of the critical (most highly resistive) pendular ring on a percolating path. If this is true, then we could postulate the following formula for the thermal conductivity,

$$\lambda(\theta) \propto (1+\theta-\phi)^2 \left(a + c\theta^{\frac{1}{4}}\right) \tag{6.4}$$

which includes simultaneously effects of the saturation dependence of the connectivity, or topology, of the connected network (the first factor) and the resistance of the most resistive elements (the second factor). These factors affect the thermal conductivity simultaneously (think back on the elementary physics formula, $R = \rho l/A$, discussed in Sect. 2.5) and thus should appear in a product. Of course in the limit $\theta \to \phi$ topology and percolation scaling can no longer have a significant effect and the contribution from Eq. (6.3) should be replaced by a function that asymptotically approaches a constant value. Further, the resistance of the critical conductance only begins to fall after a volume of water roughly equal to the surface film contribution to θ_t – see Chap. 7 – has been adsorbed. Finally, at higher saturations menisci start to coalesce, water begins to fill pores, and the pendular rings cease to grow as individual structures [8]. Thus, c in Eq. (6.4) must be zero for very small saturations and jump to a geometrically dependent nonzero value at some saturation. At the moisture content at which pendular structures cease to grow, the term $c\theta^{1/4}$ should remain constant. Finally, note that, according to the interpretation, the term a in Eq. (6.4) ultimately represents the contact area in the absence of water. Together, this generates four parameters.

In the context of this book, however, Eq. (6.4) is rather disappointing. It has, in fact, more parameters and less simplicity than corresponding equations for the hydraulic and electrical conductivities. Further, as we will see, it only describes data for the thermal conductivity up to a certain point; at higher moisture contents Eq. (6.4) uniformly overestimates λ; in the case of sandy soils, seriously so. The reason for this is, of course, that the topological description near the percolation threshold cannot hold in the vicinity of $p = 1$. Once the correlation length diminishes to a typical grid spacing, it cannot diminish further, and the conductivity cannot rise further, although Eq. (6.4) does describe *almost* the entire saturation dependence of λ for some clay-rich soils (Fig. 6.6a). So, from an analytical perspective, one would simply have to stop at Eq. (6.4) and ignore near-saturated conditions. Such a course, however, is not satisfying to a hydrologist.

It turns out that a very small modification of Eq. (6.4) makes it perform very well indeed over the entire range of saturations for all soils investigated. These include thermal conductivity data of Lu et al. [14] and the saturation-dependent phenomenology of Campbell [15], for which the dry limit was mentioned below Eq. (6.3). It should be noted that the latter represents a smoothing of experimental

error, and is not as reliable a comparison, though it simultaneously implies a much wider relevance of the present results. The specific modification of Eq. (6.4) is to reduce the power of the factor $(1 - \phi + \theta)$ from 2 to 1 (making it a linear function). Such a change is indefensible (and ruins the approximate correlation of the thermal conductivity under purely dry conditions with the square of the density as well). But the result describes the thermal conductivity well (Fig. 6.6), and the parameters extracted mostly make as much sense as those extracted from a comparison with

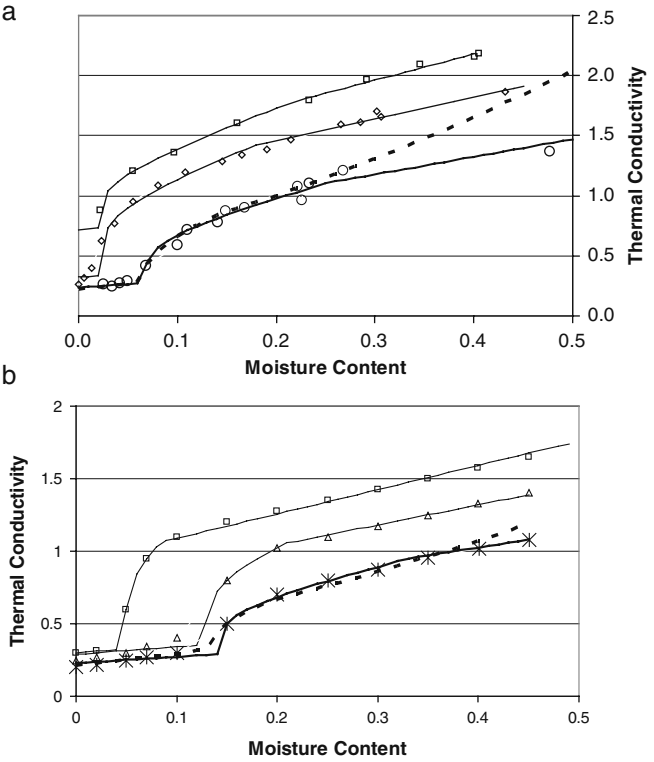

Fig. 6.6 (**a**) Comparison of experimental data for the thermal conductivity from Lu et al. [14] with predictions from Eq. (6.4) and its modification. Experimental data are the various symbols, while Eq. (6.4) is the *dashed line*, and Eq. (6.4) with a substitution of the linear power is represented by the *solid lines*. Note that in the particular soil with contrasting theoretical expressions, the superiority of the linear model is confined to a single data point, but typically the divergence between experiment and Eq. (6.4) becomes clear for data above $\theta = 0.25$, or even $\theta = 0.2$. Soils with higher thermal conductivity have higher sand contents (**b**) Comparison of phenomenological data (equation from Campbell plotted by Bristow) with theoretical predictions from Eq. (6.4) and its modification. Different symbols were chosen for different soil types: squares for a sand, triangles for a silt loam, and crosses for a clay loam. Again the discrepancy between experiment and Eq. (6.4) is smallest in the finest soil and it is this case that is compared with both Eq. (6.4) (*dashed line*) and the modification with a linear power (*solid line*). In the other two cases, Eq. (6.4) would become inaccurate already by $\theta = 0.20$ and $\theta = 0.35$, respectively

Table 6.1 Thermal conductivity parameters and statistical quantities

	cl (Bristow)	sl (Bristow)	Sand (Bristow)	scl (Lu)	sl (Lu)	Sand (Lu)
Eq. (6.4)						
Dry soil conductivity	0.21	0.25	0.3	0.25	0.221	
Pendular contribution	0.305	0.5	1.02	0.42	0.56	
Threshold	0.14	0.12	0.04	0.06	0.068	
Pendular water fraction	0.06	0.07	0.03	0.03	0.07	
Slope	1.1	1.19	1.5	1.2	1.19	
Intercept	−0.03	−0.09	−0.27	−0.12	−0.09	
R^2	0.993	0.97	0.92	0.91	0.924	
Modified Eq. (6.4)						
Dry soil conductivity	0.13	0.16	0.16	0.144	0.12	0.43
Pendular contribution	0.3	0.49	0.79	0.29	0.38	0.54
Threshold	0.14	0.13	0.049	0.11	0.068	0.02
Pendular water fraction	0.19	0.077	0.036	0.18	0.18	0.2
Slope	0.994	0.992	1.007	0.998	0.988	0.998
Intercept	0.004	0.007	−0.009	0	0.008	0.004
R^2	0.997	0.997	0.999	0.989	0.985	0.998
Ratio linear/quadratic						
Dry soil conductivity	0.61904762	0.64	0.533333333	0.576	0.542986	
Pendular contribution	0.98360656	0.98	0.774509804	0.6904762	0.678571	
Threshold	1	1.0833333	1.225	1.8333333	1	
Pendular water fraction	3.16666667	1.1	1.2	6	2.571429	

cl = clay loam, sl = silt loam, scl = silty clay loam.

Eq. (6.4) (Table 6.1). The one exception is the total amount of water in pendular structures which typically yields about 10% of the porosity or less. But in the case that the quadratic dependence is replaced by the linear dependence, this parameter on some occasions takes on much larger values, up to 40% of the porosity. However, this may not be as serious as it seems; the 1/4 power factor from the pendular structures rises very rapidly at first and more slowly at higher moisture contents, making its contribution nearly constant. Thus the fit does not depend sensitively on the value of θ chosen at which the pendular structures no longer increase in size, making it possible to increase the agreement with experiment rather minimally at the cost of

a significant increase in pendular water. In other cases the ratios of the parameters are consistent and not too different from Eq. (6.4) (Table 6.1). The threshold water fraction is likely largely stored in films. The sum of the threshold water fraction and the amount in pendular structures is 0.09 (silty clay loam) and 0.14 (silt loam) in the fits of the data of Ren using Eq. (6.4). These values are similar to the critical volume fraction, 0.11, in a silt loam in the Hanford site as well as to characteristic values for the threshold for diffusion in silt loams of 0.12 [16]. The linear fit leads to 0.29 and 0.25 for the water fractions of the silty clay loam and the silt loam, respectively. These values are upwards of 50% of the porosity. Nevertheless, the statistical comparisons always favor the linear version of the topological factor, because the quadratic version overestimates λ as saturation is approached.

The theoretical problem is that using a linear power of the percolation argument makes that factor similar to a mixing model result, which is supposed to derive ultimately from effects of volume averaging in heterogeneous media for which distinct constituents have differing conductivities. But we are already isolating the chief effect of the saturation dependence of the individual conductances when we concentrate on the effects of the critical pendular structures. We are allowed to take a product of topological and geometrical effects on conductivity (Eq. (6.4)), as long as they are independent. The product of two geometrical effects could only make sense in a 1D system where conductances add reciprocally. We conclude that so much of the regime of interest in the thermal conductivity is so far from the percolation threshold that the asymptotic results from percolation theory cannot be applied over a large range of moisture contents. This is in contrast to the electrical conductivity. Practically speaking, however, the effective power of the percolation argument drops from 2 toward 0 as $p = 1$ is approached, and it is accurate enough over the majority of the range of values to apply an effective $\mu = 1$.

If we ignore the saturation dependence of the thermal conductivity and concentrate on its value in dry soils, we note that it has an interesting relationship with the electrical conductivity of saturated soils (main contribution from fluid phase). Both are (apparently) proportional to the square of the relevant volume fraction. While Eq. (6.4) is much less accurate than corresponding equations for the electrical conductivity in terms of saturation, in order to generate the corresponding property dependence under dry conditions, it must be evaluated in a limit that is as close to the percolation threshold as it is possible to reach, and under conditions that make its chief defects negligible. Equation (5.20) for the electrical conductivity, on the other hand, while much more accurate, must be evaluated at the limit furthest from the percolation threshold, and there appears to be similar uncertainties in both these examples.

Since the percolation-scaling result (Eq. (6.3)) requires a near coincidence of solid and wetting phase conductivities, cannot be extended to wet conditions, and neglects possible effects of pendular structures, while reliability of the sublinear power result (Eq. (6.2)) requires existence of particles that can at least be represented as deformed spheres, there would appear to be no simple and general analysis of the thermal conductivity that would be useful for prediction. But the remarkable coincidence of the modification of Eq. (6.4) with experiment over the entire range of

saturations and the mostly logical and consistent values of the extracted parameters makes us hesitant to "throw in the towel." For contrast, the theoretically more defensible result (Eq. (6.4)) often leads, as expected, to unacceptably large discrepancies when values of $p - p_c$ exceed about 0.75 (typically half the range of accessible saturation values), and even its apparently successful prediction of the porosity dependence of the thermal conductivity in dry soils leaves unanswered questions. Thus we leave this topic with the hopes that our discussions can help to guide further investigations (and maybe suggest a useful phenomenology) together with the belief that the limitations of percolation theoretical descriptions of this property will help the reader to gain better perspective regarding its successes elsewhere.

6.3 Solute and Gas Diffusion

Experimental results for solute and gas diffusion as functions of moisture content obey simple percolation-scaling relationships, though these relationships are not trivially compatible with the discussion in Chap. 2. The present discussion is largely based on numerical simulations of Ewing and Horton [17], plus some unpublished simulations. All simulations were based on a (simple cubic) network model, and were developed originally for saturated conditions with a variable pore connectivity. Pruning (cutting) bonds also reduced the porosity. The diffusion coefficient was found through particle tracking: random walkers were released on one side of a system of linear dimension x, and removed upon arrival at the other side, with their time of passage recorded. For any given porosity the effective diffusion coefficient was measured as a function of length. The authors expressed the diffusion coefficient D_{pm} of an inert conservative solute in the porous medium in terms of its value D_w in water

$$\frac{D_{pm}}{D_w \phi} \equiv \Gamma^{-1} \tag{6.5}$$

and used the simulations to evaluate the quotient Γ^{-1}, known in the porous media community as the tortuosity. The authors found that the tortuosity had length dependence

$$\Gamma \propto x^{1.11} \tag{6.6}$$

Hunt and Ewing [18] then used the physical arguments from Sect. 2.4 to deduce that

$$\Gamma \propto (p - p_c)^{-1.11\nu} \tag{6.7}$$

which is the result that would obtain from finite-size scaling. For continuum percolation problems which use moisture content θ rather than p as the fundamental variable, make the substitution $(p - p_c) \rightarrow (\theta - \theta_t)$.

Consider the factor ϕ in the denominator of the left-hand side of Eq. (6.5). Hunt and Ewing [18] argued that, for unsaturated problems, ϕ should be replaced by θ. The choice of θ, as opposed to the *accessible* water-filled porosity $\theta(\theta - \theta_c)^{\beta}$, was justified as follows. When a medium is being drained but still has $\theta > \theta_t$, clusters of

water-filled pores may lose their (water-filled pore) connection to the infinite cluster of water-filled pores, but they are still connected through water films. The distance that a molecule would travel along film pathways between a disconnected cluster and the infinite cluster need not be a critical function of percolation variables [19], so it must be a function of the moisture content. That is, the slower diffusion through thin water films does introduce a delay factor, but that delay factor is not a power function of $(\theta - \theta_t)$. This is an important argument, which we will revisit below in the context of gas diffusion at partial saturations. With these substitutions, one has

$$\frac{D_{pm}}{D_w} = \theta\,(\theta - \theta_t)^{0.98} \tag{6.8}$$

Experiments yield essentially this result (Fig. 6.7), except that the reported power is 1 instead of 0.98, and a numerical prefactor of 1.1 was given. We sought no numerical prefactor in our analysis, so difference of 10% in magnitude is merely fortuitous. Note that what Ewing and Horton [17] called tortuosity is called "impedance factor" by Moldrup et al. [16], from which paper Fig. 6.7 was obtained. Several other experiments [20–23] are summarized in Fig. 6.8, taken from Hu et al. [24]. Note that for $\theta >> \theta_t$, Eq. (6.8) approaches $D_{pm}/D_w = \theta^2$; this asymptotic dependence is consistent with data near saturation. Additionally, some data sets diminish much more rapidly than θ^2 at small values of θ, consistent with the critical behavior of Eq. (6.8) near θ_t. Figure 6.9 shows a set of data reported in Hu and Wang [25]. These data do not show evidence of a nonzero θ_t, but are clearly consistent with θ^2 as the asymptotic dependence on the moisture content. Figure 6.10 [which includes data from Hu and Wang [25] not published in Fig. 6.9] allows a simple power-law fit of the data from nearly 50 years of experiments (excluding only those experiments

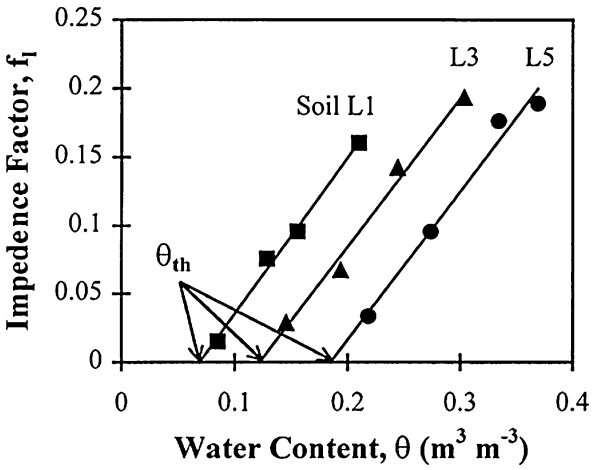

Fig. 6.7 Reprinted by permission from Moldrup et al. [16]. The ratio $D_{pm}/D_w\theta$ is plotted as a function of moisture content. Note from the experimental results for different soils that this ratio gives parallel lines of slope 1; the intercepts yield the critical moisture content for percolation, θ_t

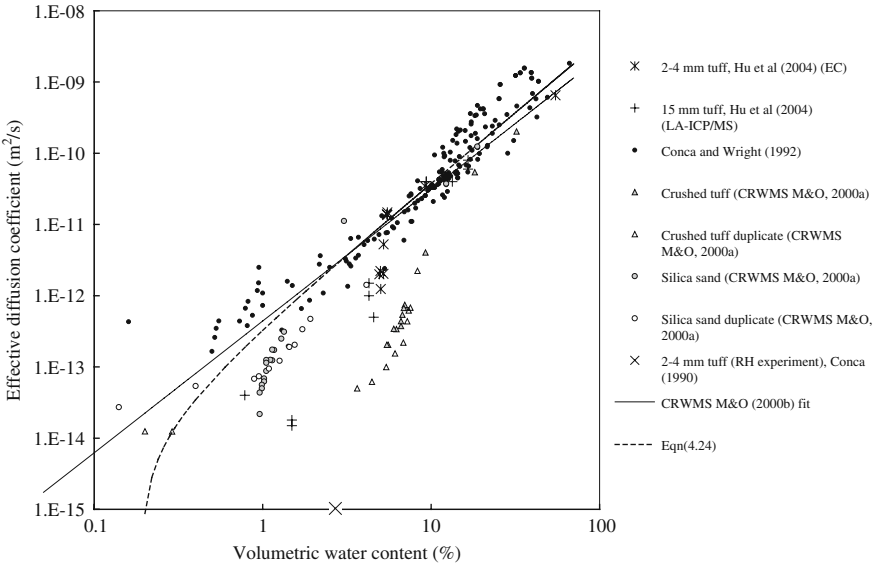

Fig. 6.8 After Hu et al. [24]. The first two data sets are from that work. Note that several of the data sets drop rapidly between 1 and 10% saturation, consistent with a critical saturation in that range of values. For large θ, Eq. (6.8) yields the asymptotic limit $\theta^{1.98} \approx \theta^2$. The CRWMS fit has a slope of 1.9. CRWMS refers to the Civilian Radioactive Waste Management System of the U.S. Department of Energy

which show an apparent nonzero θ_t), giving an exponent value of 1.97 compared with Hunt and Ewing's [18] value of 1.98. Again this near coincidence (rather than an exponent of, say, 2) is clearly fortuitous, but it does suggest the validity of the overall approach.

The agreement between theory and experiment is heartening, but also disturbing. By neglecting the factor regarding accessible porosity, the exponent here for solute diffusion is reduced from about 1.4 to about 1. However, it was precisely by inclusion of this effect (Chap. 2) that the prediction of the exponent for diffusion is reduced by about 0.4 from the exponent for conduction. Thus some future work is required to reconcile these results and determine why the percolation arguments from Chap. 2 seem to break down. On the other hand, for $\theta_t = 0$ the moisture content dependence is nearly θ^2, identical to the power in the conductivity, although we should probably expect $\theta^{\mu-\beta}$. This raises the possibility that the tendency of investigators to generate diffusion and electrical conductivity results from each other (e.g., Schofield and Dakshinamurthi [26]; Klinkenberg [27]; Snyder [28]; Garrouch et al., [29]) actually makes Fig. 6.10 more of an additional verification of universal scaling for the conductivity than it is a result for diffusion.

Interestingly the effective-medium treatment from Sect. 2.2 predicts the experimentally observed power (1) for the vanishing of the diffusion constant precisely. However, that also appears to be fortuitous; if the contrast between the experimental results for gas and solute diffusions is based on the asymmetrical characteristics

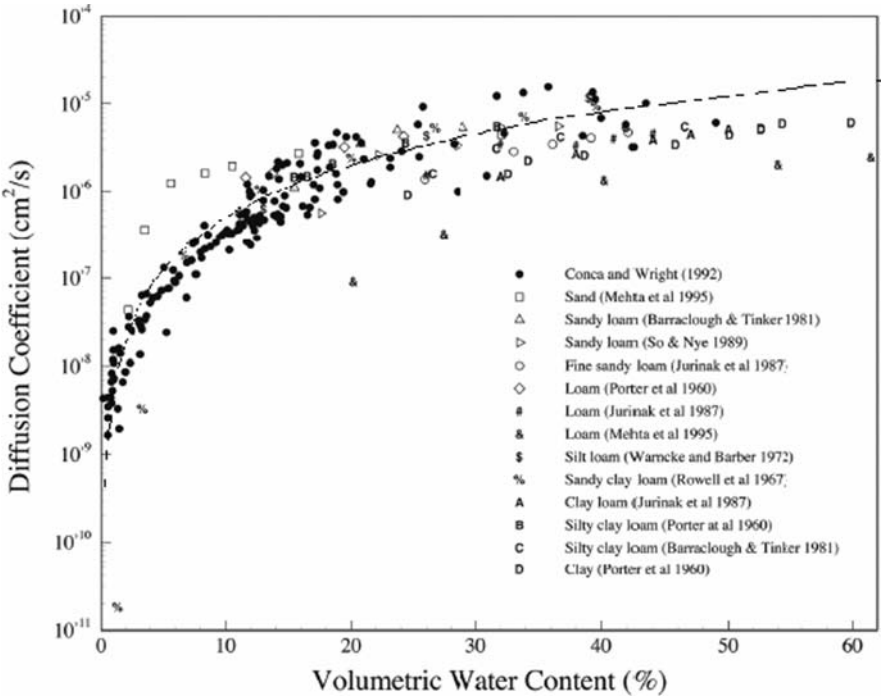

Fig. 6.9 After Hu and Wang [25]. Here the comparison with Eq. (6.8) (the *dashed line*) is given under the assumption that $\theta_t = 0$

from wetting (water) and nonwetting (air) fluids, then the effective-medium treatment was not even constructed with this physics in mind. Also, the effective-medium treatments do not predict a proportionality to θ^2 in the event that a critical moisture content is zero.

Hunt and Ewing [18] adapted the same simulations to gas diffusion. A naïve development would be to replace θ by ε, the air-filled porosity. Then one would have for the analogous ratio, $D_{\mathrm{pm}}/D_{\mathrm{g}}$ (with the subscript g implying diffusion in gas),

$$\frac{D_{\mathrm{pm}}}{D_{\mathrm{g}}} = \varepsilon\,(\varepsilon - \varepsilon_{\mathrm{t}}) \tag{6.9}$$

But when gas-filled pores become cut off from the infinite cluster, water-filled pores block gas diffusion much more effectively than water films block solute diffusion. The reason for this is that, in addition to diffusing through water-filled pores, the gas must be dissolved and exsolved at the boundaries of the water-filled regions. Additionally, for a given molecule, liquid-phase diffusion is generally several orders of magnitude lower than gas-phase diffusion. To lowest order and for many cases, water-filled pores may be considered to block gas diffusion perfectly. This means that the factor ε should be replaced by $\varepsilon[(\varepsilon - \varepsilon_{\mathrm{t}})/(\phi - \varepsilon_{\mathrm{t}})]^{0.4}$, and

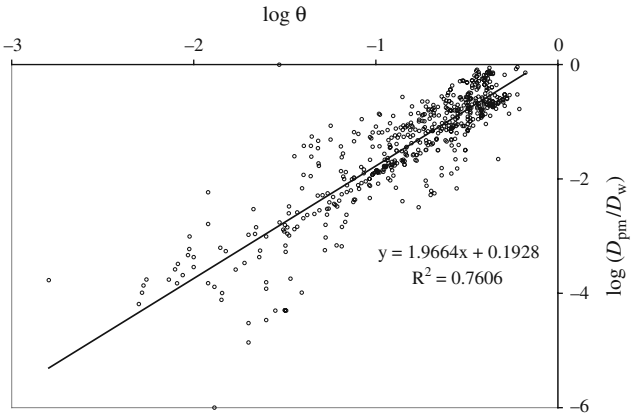

Fig. 6.10 Compilation of data (including sources not published in Figs. 6.7 and 6.8) from Hu and Wang [25] and Hu et al. [24]. Excel fitted slope of 1.97 compares to 1.98 predicted by Eq. (6.8) with $\theta_t = 0$. The data from Conca and Wright [21] were not given in a form normalized to water, so their data were graphically extrapolated to 100% water content with the intercept fitted by Excel, which was then used to normalize that data. Then the normalized data from Conca and Wright [22] were incorporated with the following sets [20, 79–94]. The CRWMS and Hu data sets are not included because they show signs of nonzero θ_t (see Fig. 6.7) as well as not being normalized to diffusion in water

$$\frac{D_{pm}}{D_g} = \frac{\varepsilon\,(\varepsilon - \varepsilon_t)^{1.4}}{(\phi - \varepsilon_t)^{0.4}} \tag{6.10}$$

It turns out that ε_t for many systems is much smaller than θ_t (which is expected to be $\approx 0.1\phi$). Moldrup et al. [4, 16] also note that the air permeability may actually vanish at $\varepsilon = 0.02$, about half the value given by $\varepsilon_t = 0.1\phi$. Supposing that $\varepsilon_t \to 0$, the product of the two factors in ε may be approximated by $\varepsilon^{2.4}$, and $\phi - \varepsilon_t$ by ϕ, yielding

$$\frac{D_{pm}}{D_g} = \frac{\varepsilon^{2.4}}{\phi^{0.4}} \tag{6.11}$$

The only difference between Eq. (6.11) and results summarized by experiment [30] is that the reported powers are 2.5 and -1, respectively, instead of 2.4 and -0.4. In fact, for consistency between the two relationships for solute and gas diffusions one might argue that the apparent experimental proportionality to ϕ^{-1} should be $\phi^{-0.5}$, so that in both gas and solute diffusions the right-hand side of the equation is proportional to a composite factor, which is the square of some combination of porosities. This assertion receives a little support from gas diffusion data in apples and pears, but is somewhat at variance with the data described next.

Werner et al. [31] analyzed 81 published measurements of gas-phase diffusion, both in situ and laboratory measurements, for which the air-filled porosity and the total porosity were available. The data were compared with the usual formulations in the literature, including Millington and Quirk [32], Currie [33], Sallam et al. [34], and Moldrup et al. [30], using standard root mean square error (RMSE). Werner

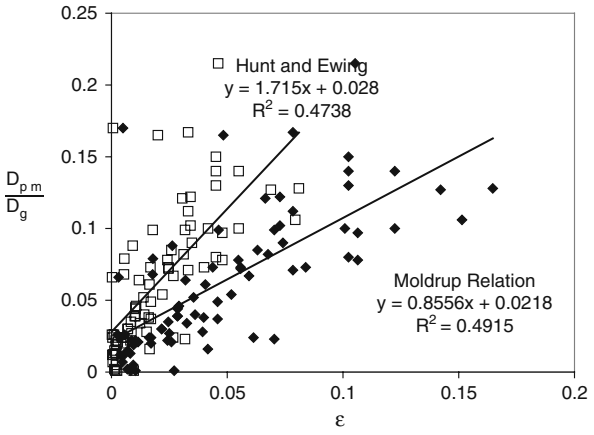

Fig. 6.11 Data from Werner et al. [31] for gas diffusion under field conditions compared with Eq. (6.11) and with the Moldrup relation. Since the relationships are akin, there is little difference in the comparison, but the Moldrup relationship has a slightly higher R^2 (0.49 instead of 0.47) and a slightly smaller intercept (0.022 rather than 0.028), both points in its favor

et al. [31] state, "The Moldrup relationship, $D_{\rm pm}/D_{\rm g} = \varepsilon^{2.5}/\phi$, originally proposed for sieved and repacked soils, gave the best predictions of several porosity-based relationships, but the relative deviation between observed and predicted $D_{\rm pm}$ can be substantial." "The data suggest that the air-filled and the total porosity of a soil are not always sufficient descriptors for the prediction of $D_{\rm pm}$." In Fig. 6.11 we compare 80 of their compiled measurements (all of Table 6.2, excluding one measurement) with both Eq. (6.11) above and the similar Moldrup relationship mentioned. In comparison with Eq. (6.11) there is no independent estimation of $\varepsilon_{\rm t}$ possible, so we have simply used $\varepsilon_{\rm t} = \phi/10$. Note that both relationships underestimate $D_{\rm pm}$ somewhat, and both produce an R^2 of slightly less than 0.5. While this is the poorest comparison of percolation-based predictions (except, in this edition, the thermal conductivity) with experiment among the basic properties considered here, it still appears to be "the best [...] of several porosity-based relationships." If, as we argue, the percolation theoretical treatment is best suited to describe such properties, then it is logical to assume that the fundamental information missing in this data set is $\varepsilon_{\rm t}$, and that knowledge of the variability of $\varepsilon_{\rm t}$ would allow a much more accurate prediction of $D_{\rm pm}$. It should also be mentioned that the derivation here, and the Moldrup phenomenology, were both intended for use with disturbed or weakly structured soils. Although soil structure can have a large impact on the air permeability (as shown in Chap. 11, it may increase the air permeability by a factor of 1000), its impact will be much less on air diffusion, since with air diffusion the actual pore radius should not be relevant, only the total porosity. Further research should examine whether the Moldrup relationship works best on soils which are least likely to be structured (e.g., sands).

Figure 6.12 shows the original comparison with experiment on six repacked soils of the Moldrup relationship [30] for gas diffusion.

Table 6.2 Compilation of effective diffusion coefficients measured directly in the subsurface. Data from Werner et al. [31]

Soil type	D_{pm}/D_a	ε	ϕ
Rolston et al. [72]			
na	0.005	0.12	0.53
na	0.007	0.09	0.51
na	0.021	0.13	0.53
na	0.035	0.18	0.56
na	0.030	0.17	0.55
na	0.030	0.17	0.55
na	0.052	0.21	0.57
na	0.034	0.20	0.55
na	0.038	0.22	0.57
na	0.078	0.25	0.57
na	0.067	0.26	0.58
na	0.046	0.19	0.54
na	0.039	0.19	0.55
na	0.044	0.19	0.55
na	0.061	0.22	0.56
na	0.040	0.21	0.56
na	0.027	0.18	0.55
na	0.045	0.19	0.55
na	0.102	0.28	0.57
na	0.121	0.27	0.57
na	0.090	0.28	0.56
na	0.073	0.25	0.56
na	0.082	0.27	0.56
na	0.072	0.25	0.56
na	0.122	0.28	0.57
van Bochove et al. [73]			
Sandy loam	0.088	0.16	0.39
Ball et al. [74]			
Sandy loam	0.001	0.17	0.44
Sandy loam	0.023	0.26	0.49
Sandy loam	0.024	0.24	0.46
Sandy loam	0.016	0.20	0.43
Clay loam	0.001	0.12	0.48
Clay loam	0.001	0.11	0.48
Clay loam	0.170	0.09	0.49
Clay loam	0.002	0.10	0.46
Loam/clay loam	0.068	0.15	0.49
Loam/clay loam	0.021	0.17	0.46
Loam/clay loam	0.013	0.10	0.39
Washington et al. [75]			
na	0.099	0.26	0.49
na	0.054	0.23	0.49
na	0.024	0.08	0.45
na	0.012	0.08	0.47

Table 6.2 (continued)

Soil type	D_{pm}/D_a	ε	ϕ
Werner and Höhener [76]			
na	0.024	0.14	0.45
na	0.015	0.10	0.45
na	0.022	0.11	0.46
na	0.106	0.37	0.55
na	0.073	0.29	0.54
na	0.064	0.18	0.43
na	0.079	0.14	0.41
na	0.012	0.09	0.45
na	0.020	0.14	0.43
na	0.024	0.14	0.43
na	0.019	0.11	0.42
na	0.509	0.28	0.50
na	0.165	0.22	0.47
na	0.066	0.07	0.42
na	0.026	0.06	0.34
na	0.026	0.08	0.32
na	0.028	0.19	0.40
na	0.099	0.19	0.34
Sand	0.100	0.25	0.31
Sand	0.140	0.29	0.37
Sand	0.100	0.29	0.37
Sand	0.140	0.27	0.37
Sand	0.080	0.27	0.37
Sand	0.130	0.27	0.37
Sand	0.150	0.27	0.37
Hers et al. [77]			
Sand	0.167	0.24	0.36
Sand	0.215	0.27	0.36
Sand	0.085	0.22	0.36
Sand	0.073	0.19	0.36
Sand	0.039	0.16	0.36
Sand	0.112	0.24	0.36
Nicot and Bennett [78]			
Clay	0.022	0.15	0.36
Clay	0.071	0.24	0.36
Silty sand	0.127	0.33	0.44
Silty sand	0.128	0.35	0.44
Silty sand	0.097	0.28	0.39
Silty sand	0.078	0.28	0.39
Clayey sand	0.037	0.18	0.30
Clayey sand	0.049	0.18	0.30

na, not available.

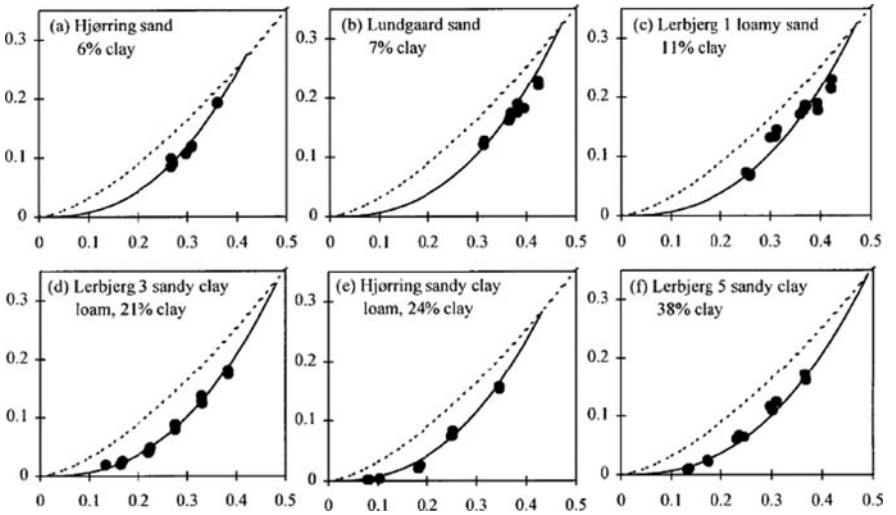

Fig. 6.12 Reprinted by permission from Moldrup et al. [30]. Gas diffusion coefficients for six repacked soils compared with the Moldrup relation (*solid curve*) and with another popular phenomenology

Equation (6.11) implies the same dependence of gas diffusion of dry media on porosity as the dependence of solute diffusion in saturated media from Eq. (6.8), namely a proportionality to the porosity squared. Verboven et al. [35] report results for the mean gas diffusion constants of apples and pears as well as their mean porosities. These data are generally compatible with a quadratic dependence of the gas diffusion constant on porosity. It is not really significant to determine the exact behavior from the published data because they consist only of mean values and standard deviations of porosity and diffusion constants. We have tried to analyze the unpublished data (thanks to Dr. Verboven for sharing it), but we reached no definite conclusions. Apparently the samples from which the porosity values were extracted are not generally the same samples as those on which the diffusion constant was measured. So there is no unique relationship between porosity and diffusion. Nevertheless we tried two different schemes to associate the porosity values with the diffusion data: scheme (1) generated a power-law relationship of $D_g \propto \phi^{2.05}$, while scheme (2) generated $D_g \propto \phi^{2.26}$, both with R^2 values of about 0.85. Thus there is a tantalizing suggestion that the same simple scaling behavior for diffusion describes gas diffusion data from living organisms as well as solute diffusion data from soils.

6.4 Electrical Conductivity of Hydrated Clay Minerals

This section applies the techniques of critical path analysis for hopping conduction to the electrical conductivity σ of hydrated clay minerals. Most publica-

tions on the subject treat only the dc conductivity; experimental measurements of that quantity are made at frequencies ω that are assumed low enough to exclude ac conduction processes. This assumption may not be valid in practice. The ac conduction processes are also typically considered to have a different source from the dc conduction, another assumption that appears to be invalid in light of the evidence presented in Hunt et al. [36]. The following discussion aims to clarify these topics.

The dc electrical conductivity of a porous medium is usually considered related to its water content through two terms; although Eq. (5.30) is the form traditionally used in soil science, we will use Eq. (5.31), because of its superior physical interpretation. The first term gives a surface or solid contribution, and the second term represents the contribution of water in the pore space. The solid contribution may dominate the medium's bulk electrical conductivity at low water contents [37, 38]. The solid contribution arises especially from water associated with clay surfaces, and the specific physical processes giving rise to this electrical conductivity are an interesting and long-standing problem. There is as yet no consensus even as to what charge carriers give rise to the conductivity, even though it is clear that the conduction proceeds through the near-surface water phase. Both ionic conduction and proton transfer have been suggested. Conductivity diminishes with increasing cation charge, suggesting that the conducting entities are actually protons [36], because the greater Coulomb repulsion impedes the charge transport more. This argument would be qualitatively similar even if the moving charges were the ions, but the coupling of the charge and the applied field would have the opposite tendency because larger charges lead to larger changes in electric field potential energy, and thus larger currents. Nevertheless, the increase in conductivity due to the coupling with the field is linear in the charge, whereas the linear increase in Coulomb repulsion energy appears in an exponential (as an activation energy), so it is not a priori obvious whether ionic transport should yield a conductivity which increases with ionic charge.

The electrical conductivity of clay minerals is frequency-dependent down to rather low frequencies. This frequency dependence suggests the important role of disorder: the electrical conductivity of an ordered system is frequency-independent at frequencies as high as 10^{12} Hz and as low as 10^{-2} Hz or lower. The subject of the ac conductivity of noncrystalline materials, however, is part of a much broader discussion, in which critical path analysis is also represented.

In the 1970s Andrew Jonscher wrote several articles (e.g., Jonscher [39]) pointing out the quasi-universal behavior of the ac electrical conductivity $\sigma(\omega)$ of noncrystalline solids. The substances included β-alumina, amorphous semiconductors, cellulose, humidified clays, and many others. In most of these systems, $\sigma(\omega)$ appeared to follow a sublinear power law $\sigma(\omega) \propto \omega^s$ (with $0 < s < 1$) over many decades of frequency. The existence of so many such similar power laws triggered many investigations. Some key questions were asked: Is the behavior truly universal? If so, how is it best described? What could cause the same behavior to be observed in so many different systems? If the behavior is not universal, what underlying physical

tendencies producing similar behavior could be found in so many systems? The discussion continues today with no sign of a consensus emerging.

For convenience, we separate physical treatments of ac conduction in noncrystalline solids into three classes: (1) effects of energy and spatial disorder on hopping conduction, (2) effects of "dynamic" Coulomb interactions on hopping conduction, and (3) hopping conduction on fractal structures. The first class is treated using critical path analysis or effective medium theories, and the third is often related to percolation scaling ideas. The second class will not be treated here, as its integration into the present discussion would require considerable background not yet presented here. We will concentrate on the first class, because it seems implausible that fractal structures are causative in so many cases, especially as most systems do not appear to be near a structural percolation threshold. Moreover, in Chap. 4 we showed how to calculate the dc conductivity of disordered systems using critical path analysis, and calculations of the ac conductivity have an analogous basis. Finally, one of us (AGH) has recently published on the ac conductivity of clay minerals, including a rather detailed analysis in terms of percolation theory in the form of critical path analysis [36].

Even within the first class (effects of energy and spatial disorder on hopping conduction), there is still uncertainty. The effects of Coulomb interactions between hopping charges cannot be completely neglected in the model we developed. Although theory is relatively mature for "noninteracting" systems, controversy remains in cases where the hopping motions of the individual charge carriers are strongly correlated [39, 40]. In Hunt et al. [36], indeed, such interactions were treated in a somewhat heuristic way. Also, while the dependence of $\sigma(\omega)$ on frequency ω is classical percolation [41, 42], the amplitude of the variability is only about 2 orders of magnitude. This smaller amplitude means that analysis in terms of effective medium theories or even mixing theories could also be useful, at least for the typical temperatures investigated.

The ac conductivity is related to the time dependence of the time derivative of the electrical polarization of a system. This is because a temporally changing dipole moment (such as produced by a spatial rotation) is equivalent to charge transport. However, charge transport in a capacitive medium (hopping conduction) over sufficiently small time and space intervals is considerably enhanced over steady-state current: thus ac conductivity is distinct from dc. The polarizability of a medium is described using the frequency-dependent dielectric permittivity $\varepsilon(\omega)$. As a consequence of the physical relationship between a time-changing polarization and the electrical current, $\sigma(\omega)$ in Fourier space is given by the sum of $i\omega\varepsilon(\omega)$ (where $i = \sqrt{-1}$) and the dc conductivity $\sigma(0)$. Thus the ac conductivity relates to a quantity, the polarization, which may be nonzero even in the absence of mobile charges. This explains the claim of many researchers (e.g., Sposito and Prost [43]) that the only process which can produce a nonvanishing ac conductivity is the rotation of a molecular dipole. But this is not the only such physical process! In fact, charges hopping through a disordered landscape (either r-percolation, E-percolation, or $r-E$-percolation, discussed in Chap. 4) produce a time-dependent polarization, yielding the kind of $\sigma(\omega)$ behavior that is actually observed.

Before addressing the physics, we caution the reader that many phenomenological approaches have been used to fit the data, and arguments continue over which is the most nearly appropriate. The most commonly used phenomenology for ac conductivity is a power law. For dielectric relaxation one finds a large number of phenomenologies (Cole–Cole, Cole–Davidson, Havriliak–Negami, Kohlrausch–Williams–Watts, see references at Cole [44]; Davidson [45]; Havriliak [46]; Kohlrausch [47]; Williams [48]), but none of these works for the entire frequency range (as wide as 10^{-2}–10^{12} Hz) in any material (e.g., Dixon et al. [49]), so perhaps it is not productive to try to derive such a "universal" result anyway. We suggest that it is more important to derive a result which produces something similar to the apparent power-law behavior observed [39] as well as the dc conductivity and a characteristic time scale.

6.4.1 r-Percolation and E-Percolation

Hunt [50] derived a result for the ac conductivity of disordered materials, using what could be called *E*-percolation in analogy with the terminology of Chap. 4. Here the energy barriers between sites are random variables, but there is no relevant disorder in site separation: either the sites have equal separation or the equivalent resistances between sites have insignificant dependence on that variable:

$$\sigma(\omega) - \sigma(0) \approx \sigma(0)\left[\frac{\omega}{\omega_c}\right]^s \quad \omega > \omega_c \tag{6.12}$$

where

$$\sigma(0) \propto \omega_c \propto \exp\left[-\frac{E_a}{k_B T}\right] \quad \text{and} \quad 1 - s \propto \frac{k_B T}{E_a} \tag{6.13}$$

In these equations k_B is the Boltzmann constant, T is the absolute temperature, $\sigma(0)$ is the electrical conductivity at zero frequency (i.e., the dc conductivity), $\omega_c = \nu_{ph} \exp(-E_a/k_B T)$ is the critical frequency, (where ν_{ph}, called the phonon frequency, is a vibrational frequency), and E_a is an activation energy. Specifically, E_a is the smallest possible value of the largest activation energy on the transport path, the highest unavoidable activation energy barrier [51]; it thus plays the part of a bottleneck resistance. General features of Eqs. (6.12) and (6.13) have been verified in a wide variety of systems.

The dc conductivity given by Eq. (6.13) varies widely with T. According to theory, as T diminishes the dc conductivity diminishes exponentially, but the high-frequency ac conductivity scarcely changes. The relationship $1–s \propto k_B T/E_a$ (Eq. (6.13)) arises from the requirement that in the high-frequency limit, the results for different temperatures must approach the same limiting conductivity value (Fig. 6.13). The same results are obtained for increasing E_a at a constant temperature, which is compatible with the physical experiments on smectite clays that were performed on systems with diminishing water content. Such curves are shown for Mg-otay smectite clay in Fig. 6.14 [52, 53]. Similar frequency-dependent

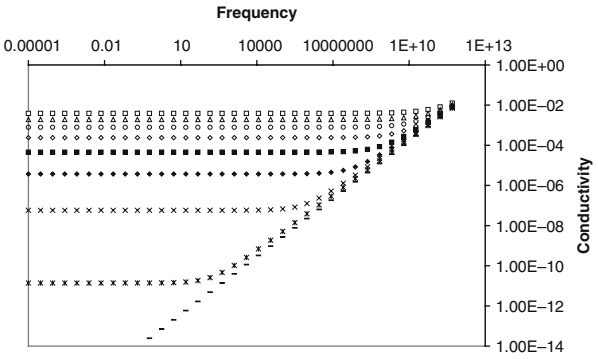

Fig. 6.13 Percolation theoretical calculations of ac electrical conductivity for disordered media at 9 different temperatures. Note that (1) the dc conductivity is a strong function of temperature, (2) the high frequency ac conductivity is nearly independent of temperature, (3) the ac conductivity is approximately a sublinear power of the frequency

conductivity was also seen in Ca-, Mg-, K-, and Na-saturated hectorite, otay, SPV, and IMV smectites [52, 53], and also in Na- and Li-saturated smectites [54], so the results of Fig. 6.14 are rather general. Notice the strong similarity between Figs. 6.13 and 6.14.

Here we discuss the general physics behind Eqs. (6.12) and (6.13), though without deriving them. We also present experimental data supporting the validity of these equations. We see that E_a calculated from critical path analysis appears reasonable for most of the systems investigated.

To better understand ac conduction, consider the *r*-percolation system described in Sect. 4.1. This *r*-percolation is analogous to the *E*-percolation described above. Electrons sit at sites which all have the same energy, but are separated by varying

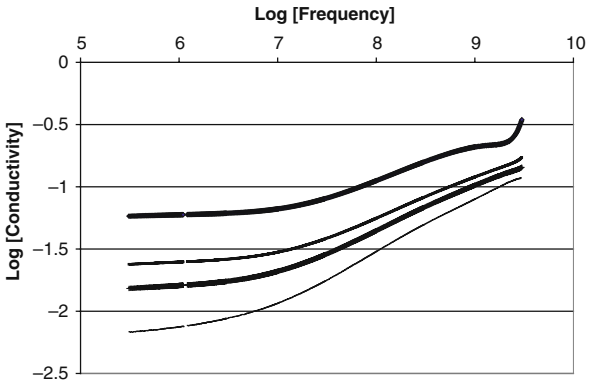

Fig. 6.14 AC conductivity of Mg-otay smectite. In this figure, the dc conductivity increases more rapidly with increasing water content than does the high-frequency ac conductivity [Data from Logsdon and Laird [52, 53]]

distances. Even in the absence of an electric field, electrons occasionally hop from one site to another. The rate at which an electron may hop from site i to site j is $\Gamma_{ij} = \nu_{\mathrm{ph}} \exp[-2r_{ij}/\mathrm{a}] \approx \tau_{ij}^{-1}$, where the relaxation time representation, τ_{ij}, makes explicit contact with Chap. 4 notation, and a is the size of the wave function. Here the phonon frequency, ν_{ph}, is often around 10^{12} Hz, but closer to 10^8 Hz in smectites; this rate expression is a chief input into the resistance value R_{ij} given in Chaps. 2 and 4. Now impose an electric field in (say) the positive x direction. Electrons will now tend to hop more frequently in the negative x direction than in any other direction, because that reduces their electrical potential energy. As long as the electric field is small, that tendency is slight, and the system is said to be in the Ohmic regime: the response to the field is linearly proportional to the strength of the field. But suppose that the electric field has been in this orientation only a very short time $t \propto \nu_{\mathrm{ph}}^{-1} = \omega^{-1}$: Which electrons will respond? Clearly those for which the typical hopping time (the inverse of the transition rate) is not greater than the time that the electric field has been in its new orientation (making $r_{ij} \approx$ a). Causality (the fundamental precept that causes precede effects) allows a proof that in fact the electrons that contribute to the in phase (real part of the complex conductivity) have response times approximately equal to the inverse of the frequency of the applied field, while those that respond much more rapidly contribute chiefly to the imaginary part. The electrons responding in phase with the field will have a velocity $v = a/t$, or $v = a\nu_{\mathrm{ph}}$. This velocity value is independent of the temperature, and because electrical conductivity is $nqev/\Xi$ (for n the volume concentration of mobile charges, qe their charge, v their velocity, and Ξ the electric field), this velocity tends to fix the ac conductivity in the high-frequency limit.

Now consider the ac conductivity as a function of frequency, ω. A direct analogy exists between ω and the percolation probability p; there is also a critical frequency ω_{c} analogous to p_{c}. In particular, changing the frequency can effectively sweep a system through a percolation transition.

Since electron jumps with characteristic times t approximately equal to the time the electrical field has been in place dominate, however, $t \approx \omega^{-1}$ and $v \approx r_{ij}\omega$. The exponential dependence of Γ_{ij} on r_{ij} makes the dependence of r_{ij} on ω logarithmic, justifying the statement that the typical distance r_{ij} only increases slightly with diminishing frequency. Thus the velocity of the hopping charges becomes, in r-percolation, a sublinear function of the frequency. While the hopping distances vary only slightly with frequency in r-percolation they do not vary at all in E-percolation, and in this case $v = < r > \omega$, where $< r >$ is a typical hopping distance. However, the number of electrons that can respond in time with the field is almost always a diminishing function of frequency, making the conductivity a sublinear function of the frequency. Meanwhile, because it is based on dividing the complex conductivity by i, it is the imaginary (out of phase) part of the dielectric permittivity at frequency ω which is dominantly influenced by hopping transitions with that characteristic rate. This completes an understanding that is based on the treatment of individual electrons, independent of each other [55, 56].

For high frequencies, only the fastest responding electrons can adjust their positions (and thus their potential energies with respect to the external field) fast enough

to hop. As the frequency decreases, more electrons can respond, and the responding electrons begin to cover overlapping paths. When the frequency is dropped sufficiently that the overlapping paths percolate, the ac conductivity is dominated by the same resistive process that controls the dc conductivity: no connections are through pairs with slower rates than this particular Γ. The critical frequency, $\omega_c = \nu_{ph} \exp[-E_{ac}/k_B T]$, is proportional to the critical rate Γ_c, and the critical resistance is proportional to the inverse of this critical rate. As a result, the ac conductivity at a frequency proportional to the dc conductivity is approximately equal to the dc conductivity. This argument is based on the relevance of critical path analysis to hopping conduction in a disordered system. If the ac conductivity can be approximated by a power law in frequency, Eqs. (6.12) and (6.13) must follow. In the case of hopping conduction in clay minerals, critical path analysis implies that both the dc and the ac conductivities should be controlled by the same rate-limiting process; thus $\sigma(0) \propto \omega_c$ and both these quantities have the same activation energy E_a. In fact this is what is observed, *and it is incompatible with conduction via rotating dipoles*: there is no reason why the hopping conduction energy barriers (if they were associated with rotational motion) would have the same value as those encountered by particles in translational motion.

6.4.2 Percolation Calculation of E_a

Here we show that a percolation calculation of E_a leads to realistic results without use of adjustable parameters.

Hunt et al. [36] used percolation theory at the molecular level to find the principal energy barrier limiting charge transport, and hence the dc conductivity in humified monoionic smectite clays. The activation energy was assumed due to Coulomb energy barriers from counterions in the vicinity of the path of the hopping charges, themselves believed to be protons. The measured electrical conductivities were consistent with proton hopping in a maximum interlayer spacing above a threshold water content, plus a constant term apparently due to hopping along external clay surfaces. The basic physical interpretations were that (1) a minimum water layer thickness is required for protons hopping along internal surfaces to effectively avoid the vicinity of such counterions, and (2) it takes considerably less water along external surfaces than along internal surfaces for protons to avoid the clay counterions. This interpretation is consistent with previous conclusions of Laird [57] that water along external surfaces tends to be concentrated in the vicinity of counterions.

Consider the possible charge pathways through the humified smectite clay (Fig. 6.15). Assume that proton hopping is the mechanism by which water transfers charge. This may initially seem implausible, because in neutral water at chemical equilibrium the concentration of protons (H^+ ions) is 10^{-7} M, too small to produce the conductivity observed. But chemical equilibrium can be compatible with a high conductivity if individual proton hops are highly correlated, such that as one proton vacates a given site, another proton moves into the now-vacant position. This

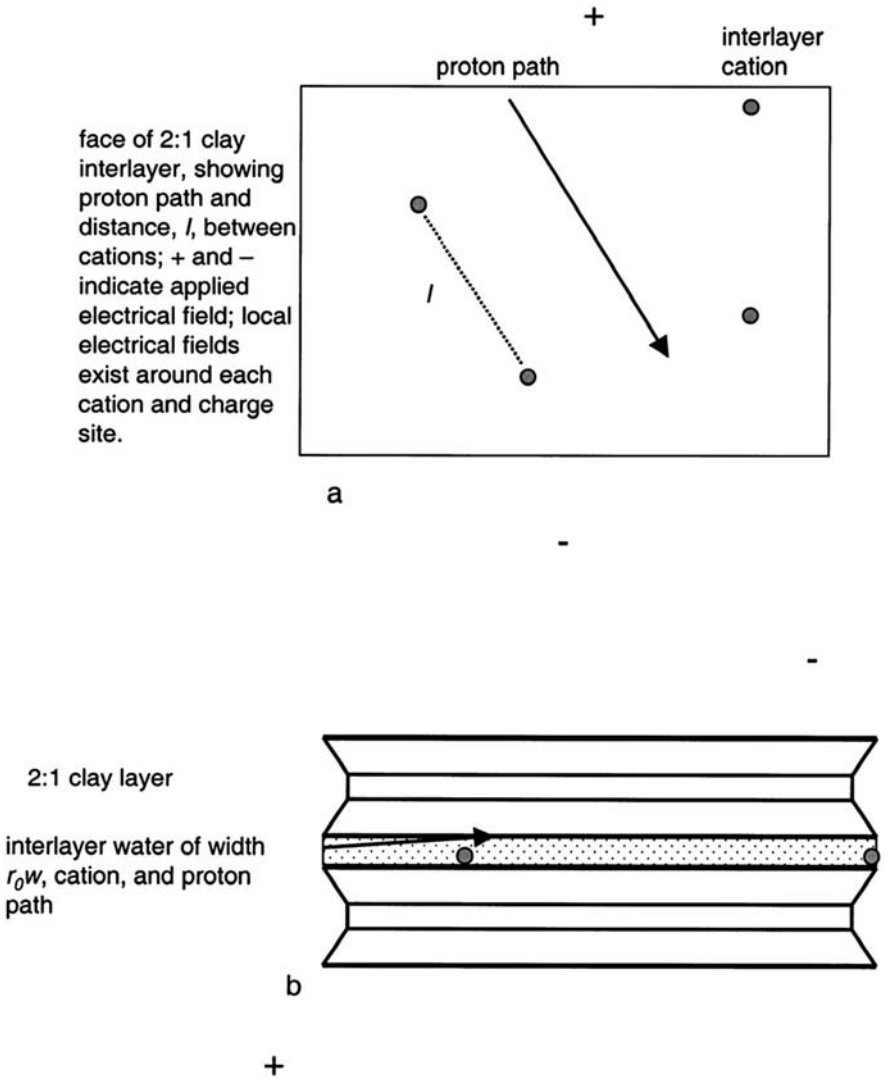

Fig. 6.15 Possible pathways for charge transport in smectite clay minerals [from Hunt et al. [36]]

interpretation allows transport to involve more protons than are actually free at any given moment, and applies equally to water in smectite clays. In such an interpretation the reduction in conductivity with decreasing number of the water layers relates to the presence of Coulombic energy barriers produced by counterions near the interior clay surfaces. These counterions produce a rough electrical potential with fluctuations that diminish with increasing distance from the surface. Closer to the surface, the higher potential energy barriers generate a greater resistance to proton hopping.

We thus have a problem of correlated proton hopping in a relatively slowly varying Coulombic potential (because the typical charge separation is greater than the separation of the water molecules). But the rate-limiting location on any given path is the one which is slowest (i.e., has the highest energy barrier [58]), while the most important pathways are those with the fastest effective hopping rate – that is, the pathways along which the greatest energy barrier is small.

Dyre [58] expressed the idea of a limiting barrier height in terms of an effective-medium theoretical description, but the concept was formulated in the context of percolation theory. Start with the activation energy of the dc conductivity. Assume that the negative charge on the basal surfaces of 2:1 phyllosilicates (e.g., smectite) is located in basal oxygen atoms that are proximal to sites of isomorphic substitution. The counter-positive charges are associated with the exchangeable cations in the interlayers. Although these exchangeable cations are mobile, at any given instant they tend to be located as close as possible to the negative surface charge sites, and as far as possible from each other. Thus the spatial distribution of the interlayer cations is determined by the distribution of negative surface charge. The charge of the cations is qe (for q the valance of an individual cation, and e the protonic charge). The charge sites due to interlayer cations are separated on the clay layer surface by some typical distance, denoted l (see Fig. 6.15). Within the water, the potential due to a single cation is not a "naked" potential; it is reduced through the dielectric properties of the water. The energy of interaction of a charge e (the protonic charge) and a single cation charge qe, separated by a distance r, is then

$$E = \frac{e^2 q}{4\pi\varepsilon_0\varepsilon_w r} \tag{6.14}$$

where ε_o is the permittivity of free space, and ε_w is the permittivity of water.

This energy of interaction is related to the activation energy of the hopping conduction, E_a, as will be shown. Consider a problem in two dimensions (2D) with no significant water thickness (Fig. 6.15a). A hopping charge must normally be brought within a distance $d = l/2$ of a cation of charge qe in order to find a path through the system. In three dimensions (represented in cross-sections in Fig. 6.15a, b), with water thickness wr_0 (w is the number of water layers, and $r_0 \approx 0.25$ nm is the thickness of one water layer), this distance becomes $d = [(l/2)^2 + w^2 r_0^2]^{1/2}$. However, for smectites dominated by octahedral charges at high water contents, the distance may become $d = [(l/2)^2 + 1/4(w^2 r_0^2)]^{1/2}$, especially around divalent cations. We ignore this alternative, which would result in an increasing (rather than decreasing) activation energy with increasing water content. In a neutral medium with some disorder in the position of the charges, the average interaction energy of a charge is zero. If, on average, a proton starts at zero energy, then at its closest approach to a counterion its total energy has increased by an amount

$$E_{ac} = \frac{qe^2}{4\pi\varepsilon_0\varepsilon_w\sqrt{(l^2/4) + w^2 r_0^2}} \tag{6.15}$$

At this point we must consider how l depends on the concentration of cation charges, N. In a 3D system we have $l \propto N^{-1/3}$; the 2D result ($l \propto N^{-1/2}$) may be more appropriate in platy systems, but it turns out that the choice does not matter. Here we ignore orientation of the clay plates, which introduces a numerical factor 1/3 for random orientations. Now,

$$E_{\mathrm{ac}} = \frac{2qe^2 N^{\frac{1}{3}}}{4\pi\varepsilon_0\varepsilon_{\mathrm{w}}\sqrt{1+4N^{\frac{2}{3}}w^2r_0^2}} \tag{6.16}$$

This E_{ac} was our first estimate of the activation energy for the dc conductivity due to the Coulombic repulsion of the counterions. Comparison with experimental data (not shown), which show a strong dependence of charge mobility on water layer thickness, indicated that Eq. (6.16) was incorrect. A Taylor series expansion in the quantity $N^{2/3}r_0^2w^2$ of Eq. (6.16) shows why the calculated E_{ac} is almost independent of r_0w for $r_0w < l$, producing a conductivity independent of water content. For agreement with experiment it was necessary to modify Eq. (6.16) by dropping the first term in the square root. Apparently (if the proposed mechanism of transport is correct) the hopping protons cannot avoid the counterions in the plate parallel direction, but they can in the perpendicular direction. Then we have

$$\exp\left[\frac{-E_{\mathrm{ac}}}{k_{\mathrm{B}}T}\right] = \exp\left[\frac{-qe^2}{4\pi\varepsilon_0\varepsilon_{\mathrm{w}}wr_0k_{\mathrm{B}}T}\right] = \exp\left[\frac{-0.707q}{w}\right] \tag{6.17}$$

This last expression was written in anticipation of comparison with experiments conducted at $T = 298$ K. Although using $\varepsilon_{\mathrm{w}} = 80$ may underestimate E_{ac}, consider the case for $w = 1$. The proposed mechanism of highly correlated hopping motions would be unlikely, during any individual hop, to change the number of protons on the water molecule nearest the counterion. One proton would simply replace another at a given location. But the conduction process would require a proton to jump between that site and a neighboring site. This means that, for the purpose of calculating a barrier height, the nearest distance of approach would be somewhat larger than wr_0, and the energy somewhat smaller. To estimate this effect, consider that the highest energy that the proton experiences (including the Coulombic attraction to the water molecules) is likely to occur at about half the water molecule spacing. At this distance, the Coulombic effects due to the counterion will be reduced to somewhere between $(4/5)^{1/2}$ and 2/3 (by 11–33%) depending on orientation. This numerical uncertainty is the same magnitude that would arise from using a dielectric permittivity of (say) 50 rather than 80, which would increase the Coulomb interaction strength by 38%. As a consequence we ignore these complications and use the numerical factor of Eq. (6.17).

The preexponential for the conductivity was estimated from the perspective of a 3D random resistor network (disordered medium). In such a network, the dc conductivity $\sigma(0)$ is given by [41, 42, 59]

$$\sigma(0) = \frac{l_0}{L^2 R_c} \tag{6.18}$$

where $R_c = [(e^2/k_B T)\nu_{ph} \exp(-E_{ac}/k_B T)]^{-1}$, l_0 is the linear separation of critical (bottleneck) resistances on a critical path, and L is the linear separation of such paths. This makes L^{-2} the number of current-carrying paths per given cross-sectional area; in d dimensions L^{-2} is replaced by $L^{-(d-1)}$. Right at critical percolation $L \to \infty$ [60], but when critical path analysis [59] is used to develop σ_{dc}, the bottleneck resistance value is slightly larger than the critical value, and the value of L is more nearly the molecular separation, as found by the optimization procedure discussed in detail in Chap. 4. Thus L can be taken to be r_0 times some numerical constant; Hunt [42] found values between 5 and 15. In our problem, however, these

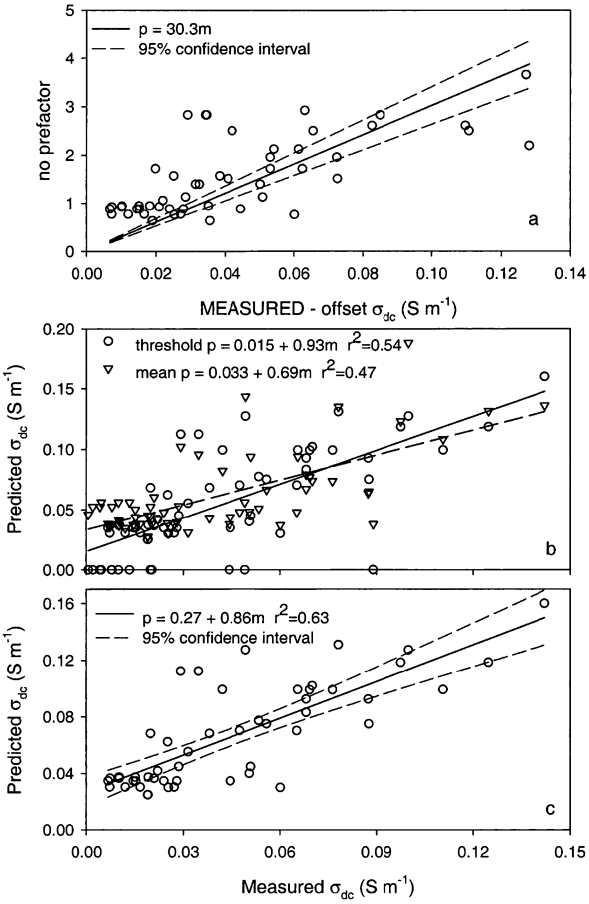

Fig. 6.16 Comparison of predicted and observed dc conductivity of smectite clay minerals. The various data correspond to 4 different mineralogies, 4 different cations, and 4 different moisture contents [from Hunt et al. [36]]

considerations do not strictly apply. The L^2 is related to the dimensionality of the optimization procedure, and would be replaced by L if the optimization were performed in 2D. This is consistent with structural constraints for the 3D in the clay, for example, a distance between proton-carrying paths of $(4+w)r_0$, where $4+w$ is the thickness (in units of water molecule size) of a simple clay sheet. It may be that in the plate parallel direction (Fig. 6.15) the path separation is structurally controlled, and is approximately equal to l. The largest resistance values, however, will be separated by $l_0 = l$, when protons come into the vicinity of a counterion. Thus the length scales in the preexponential are all multiples of r_0 with numerical values greater than 1. Altogether we have

$$\sigma_{\mathrm{dc}} = \frac{e^2 l \nu_{\mathrm{ph}}}{k_{\mathrm{B}} T L r_0 (4+w)} \exp\left[\frac{-E_{\mathrm{ac}}}{k_{\mathrm{B}} T}\right] \propto \frac{e^2 \nu_{\mathrm{ph}}}{k_{\mathrm{B}} T r_0 (4+w)} \exp\left[\frac{-E_{\mathrm{ac}}}{k_{\mathrm{B}} T}\right] \tag{6.19}$$

The factor $\exp[-E_{\mathrm{ac}}/(k_{\mathrm{B}}T)]$ is given in Eq. (6.18). The predicted dc conductivity is compared with experimental values in Fig. 6.16.

In predicting the dc conductivity $\sigma(0)$, we did not assume a continuous increase in water thickness w with θ. Rather, we assumed that the equivalent thickness of the water layer increased by r_0 every time the water content increased by a given fraction. This is in the spirit of continuum percolation theory: until there is sufficient water in a given layer, it does not form a continuous layer. This discretized thickness means that protons in a given water layer cannot avoid the layer below (with its greater proximity to counterions) until the given water layer is continuous. Since the water tends to collect preferentially in the vicinity of counterions, the apparent inability of protons to avoid counterions in a given water layer seems reasonable.

A major subject of the analysis in Hunt et al. [36] relates to ac conductivity $\sigma(\omega)$ measurements performed by Logsdon and Laird. The advantage here is that the frequency-dependent analysis provides a second means to check that the pre-

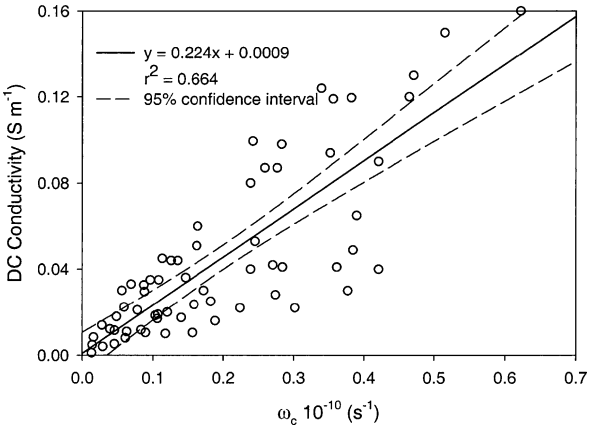

Fig. 6.17 Comparison of dc conductivity and critical frequency for the same systems as in Fig. 6.14 [from Hunt et al. [36]]

dicted exponential dependence of $\sigma(0)$ on temperature is obeyed. We tried fitting Eqs. (6.12) and (6.13) to the experimental data by using s, ω_c, and $\sigma(0)$ as fitting parameters. Figure 6.17 shows a comparison of $\sigma(0)$ and ω_c, with the result that these two quantities appear to have the same temperature dependence. Further analysis also allowed a better check on the actual value of the phonon frequency, ν_{ph}. We found that $\nu_{ph} \approx 10^8$ Hz in contrast to the usual assumption of 10^{12} Hz. Since $\nu_{ph} \approx (k/m)^{1/2}$, with k an atomic (or molecular) spring constant and m a corresponding mass, this result implies that the binding in hydrated clay minerals is about 8 orders of magnitude weaker than in, say, quartz, which seems to be too large a contrast.

6.5 Geophysical Applications

We now address two geophysical applications relating to seismic precursors in seismoelectric phenomena. These applications do not address whether seismic precursors could be used to predict earthquakes. Rather, our incursion into the realm of geophysics examines the implications that specific processes could explain data which has been argued to be related to seismic processes. In each case, the ultimate question is whether the magnitude of the apparent precursors can be explained in a manner consistent with theory. These examples thus hint at further possible ramifications of the present work.

Merzer and Klemperer [61] examine the sudden increase in the low-frequency contribution to the magnetic field 7 km from the Loma Prieta epicenter, three hours before the earthquake. This increase was superimposed upon other changes in the low-frequency magnetic field during the previous weeks. The authors suggest that a plausible explanation for the increase in the magnetic field strength could be a 15-fold increase in the electrical conductivity under saturated conditions. They give three possible mechanisms for such an increase: (1) an increase in the salinity of the fluids occupying the fault zone, (2) an increase in the porosity, and (3) the exponent m of Archie's law ($\sigma(\phi) \propto \phi^m$ [62]) changing from 2 to 1. In the context of percolation theory, it may be possible to find a physical basis for the third mechanism. In fact, a change in Archie's exponent from 2 to 1.3 would be expected if the random connectivity of the pore space were to change from 3D to 2D [63]. Such a change would be consistent with the development of an interconnected network of microfractures along or parallel to the fault plane. It is difficult to say by how long the development of such an interconnected network could precede an actual earthquake, but one would expect that an earthquake would follow relatively quickly thereafter (e.g., Gao and Crampin [64]). The general mechanism proposed (Merzer and Klemperer) has been criticized on the basis that the mutual inductance between the fault zone and the crust may mitigate the effects of the increased conductivity [65].

Another potential application regards the ability of the electrokinetic effect to generate sufficient charge separation to produce a measurable electric field. The question ultimately relates to the ability of the separated charge to recombine under the influence of the induced electric field. In a homogeneous medium the means to generate an electric field are not present, but the earth's crust is extremely

heterogeneous. Here we consider partially saturated conditions. It is relatively easy to show that any electric field produced will be on the order of J^{ek}/J^{e}, where J^{e} is the electric current (proportional to the electrical conductivity). Note that (as shown in Sect. 5.1) J^{e} and J^{ek} are expected to have the same dependence on the moisture content (universal scaling), meaning that no electric field can be generated when both the electrokinetic and the return current are generated in the same medium, even if it is not homogeneous. However, if the electrokinetic current is generated in the vicinity of a fault, a large portion of the return current, which generally requires the entire medium, might need to flow in a different medium – for example, on the opposite side of the fault plane. The first medium had a moisture content above the percolation threshold but the second was below the threshold; the possibility may exist to generate a large electric field.

The question of whether charges can percolate before crack networks do, which may be relevant for the possible existence of electromagnetic precursors to earthquakes [66, 67], has been addressed as long ago as 1983 [68]. In that article "Microcrack connectivity in rocks: a renormalization group approach to the critical phenomena of conduction and failure in crystalline rocks," Madden argues that percolation of charge is easier in general than of cracks. This argument was made independently in the context of the glass transition by Hunt [69], who explained, using critical path analysis-type arguments, that the macroscopic transport of charge was easier (lower activation energy and smaller p_c) in viscous liquids than mechanical response. This argument was based on the dimensionality of the transport process: steady-state electrical transport requires only the connection of a quasi-1D path, whereas viscosity experiments measure the transport of one entire surface relative to another. Miyazima [70] and Miyazima and Yamamoto [71] are currently putting this concept on a sounder footing. In any case (from Freund and Sornette [66]), "We conjecture that the intermittent and erratic occurrences of EM signals are a consequence of the progressive build-up of the battery charges (from plastic deformations of peroxy bonds in silicates) in the Earth crust and of their release when crack networks percolate through the stressed rock volumes."

Note that the relative ease of percolation of charge carriers relative to that of cracks is cited in both the change of Archie's law exponent from 2 to 1.3 (when the crack network finally percolates, a higher degree of continuity of charge pathways increases the electrical conductivity) and the explicit arguments quoted in the previous paragraph, although the detailed arguments are distinct in the two cases.

The point of this discussion is less to address the question of whether earthquake precursors may or may not exist, but rather to show that a solid theoretical development of the fundamental conduction processes may inform the discussion of the potential relevance of earthquake precursors.

6.6 Summary

This summary incorporates results from both Chaps. 5 and 6.

Combining percolation theory with a random fractal model of porous media, we can assess which transport properties are predominantly governed by the pore-size distribution, and which are more tied to topology. We find that the saturation dependence of the air permeability is influenced only by topological effects described in percolation theory. However, we note that both the air permeability of dry soils and the hydraulic conductivity of saturated soils must be calculated by essentially the same optimization procedure that combines effects of topology (percolation scaling) and pore-size distribution (using critical path analysis from percolation theory). We find that $K(\theta)$ is determined primarily by the pore-size distribution, while $\sigma(\theta)$ may be partially influenced by the pore-size distribution. In each of these properties, however, the influence of pore sizes increases as one moves away from the percolation threshold. In the case of the hydraulic conductivity, in particular, it is advantageous to separate out pore-size distribution contributions (using critical path analysis) from topological influences described in percolation scaling, and thus divide possible saturations into two separate regimes. A similar division is useful for the electrical conductivity, though in the case that the pore-size distribution is not too wide, the critical path analysis is never needed and the percolation scaling extends through the entire range of saturations, justifying the application of a restricted form of Archie's law. If there is virtually no distribution of pore sizes (in artificial media), one may see effects of film flow, and if the solid phase also has a large conductivity, those of pendular structures. In the case of the thermal conductivity, the pore-size distribution is not particularly relevant, as the thermal conductivity of each fluid in the pore space is typically much less than that of the solid portion of the medium. In the thermal conductivity it is more useful to combine topological effects from percolation scaling with the geometrical effects from the conductances of pendular structures between the grains. The percolation scaling leads to an analogue to Archie's law in the thermal conductivity, λ, of dry soils, namely that $\lambda \propto \rho^2$, where ρ is the bulk density of the soil. In the absence of soil structure, the saturation dependence of diffusion in both liquid and gas phases, as well as air permeability, are essentially unaffected by pore-size distribution.

Table 6.3 Dominant influences on various conduction or flow properties, describable using percolation theory, depending on saturation. *Topology* means that universal percolation scaling applies, *geometry* means that a bottleneck pore (or pendular structure) radius is relevant as found in critical path analysis, and *competition* implies that a combined method, in which both influences are important, is required (described in Chap. 4). The difference between "small" and "large" values of S depends on the property considered, so is not quantitatively defined. No entry means either that the property cannot realistically be calculated using percolation theory, or that it is zero

Property	$S = 0$	Small S	Large S	$S = 1$
K		Topology	Geometry	Competition
k_a	Competition	Topology	Topology	
σ_e		Topology	Topology	Competition
σ_{ek}		Topology	Topology	Topology
λ	Topology	Geometry		

These and related results are summarized above in Table 6.3. Evaluations in the Table were made using specific models and circumstances. For the first four properties, the random fractal model was used; for thermal conductivity it is assumed that solid and liquid phases have similar thermal conductivities. Under other conditions not all the table entries need be identical, but the general tendencies should be observed.

References

1. Hunt, A. G., 2005, Continuum percolation theory for transport properties in porous media, *Phil. Mag*. **85**: 3409–3434. 170
2. Hazlett, R. D., and M. J. Furr. 2000. Percolation model for permeability reduction in porous media by continuous-gas foams, *Ind. Eng. Chem. Res*. **39**: 2709–2716. 170
3. Steriotis, T. A., F. K. Katsaros, A. K. Stubos, A. Ch. Mitropoulos, and N. K Kanellopoulos, 1997, A novel experimental technique for the measurement of the single-phase gas relative permeability of porous solids, *Meas. Sc. Technol*. **8**: 168–173. 170, 171
4. Moldrup, P., S. Yoshikawa, T. Oleson, T. Komatsu, and D. E. Rolston, 2003, Air permeability in undisturbed volcanic ash soils: predictive model test and soil structure fingerprint, *Soil Sci. Soc. Am. J*. **67**: 32–40. 170, 184
5. Unsal, E., J. H. Dane, G. V. Dozier, 2005, A genetic algorithm for predicting pore geometry based on air permeability measurements, *Vadose Zone J*. **4**: 389–397. 171, 172
6. Tuli, A., J. W. Hopmans, D. E. Rolston, and P. Moldrup, 2005, Comparison of air and water permeability between disturbed and undisturbed soils, *Soil Sci. Soc. Am. J*. **69**: 1361–1371. 171, 173
7. Rose, W., 1958. Volumes and surface areas of pendular rings. *J. Appl. Phys*. **29(4)**: 687–691. 174
8. Ewing, R. P., and R. Horton, 2007, Thermal conductivity of a cubic lattice of spheres with capillary bridges, *J Phys* D – *Appl Phys*. **40**: 4959–4965. 174, 176
9. Géminard, J.-C., and H. Gayvallet, 2001, Thermal conductivity of a partially wet granular material. *Phys. Rev. E* **64**. DOI: 10.1103/PhysRevE.64.041301. 174
10. Chaudhary, D. R., and R. C. Bhandari, 1969, Thermal conductivity of two-phase porous materials: dry soils, *Brit. J. Appl. Phys.* (*J. Phys. D*) **2**: 609–610. 175
11. Farouki, O. T., 1986, *Thermal properties of soils* (Series on Rock and Soil Mechanics vol. 11) Trans Tech Publications, Clausthal-Zellerfeld, Germany. 175
12. Campbell, G.S., 1985, *Soil physics with BASIC*. Elsevier, New York, NY 175
13. Cóté, J., and J.-M. Konrad, 2005, A generalized thermal conductivity model for soils and construction materials, *Can. Geotech. J*. **42**: 443–458. 175
14. Lu, S., T. Ren, Y. Gong, and R. Horton, 2007, An improved model for predicting soil thermal conductivity from water content at room temperature, *Soil Sci. Soc. Am. J*. **71**: 8–14. 175, 176, 177
15. Bristow, K. L., 2002, Thermal conductivity, in *Methods of Soil Analysis*. Part 4: Physical Methods, ed. J. H. Dane and C. Topp, Soil Science Society of America 5 1209–1232. 176
16. Moldrup, P., T. Oleson, T. Komatsu, P. Schjønning, and D. E. Rolston, 2001, Tortuosity, diffusivity, and permeability in the soil liquid and gaseous phases. *Soil Sci. Soc. Am. J*. **65**: 613–623. 179, 181, 184
17. Ewing, R. P., and R. Horton, 2003, Scaling in diffusive transport. In: *Scaling Methods in Soil Physics* (Ya. Pachepsky, ed.). CRC Press, Boca Raton. 180, 181
18. Hunt, A. G., and R. P. Ewing, 2003, On the vanishing of solute diffusion in porous media at a threshold moisture content, *Soil Sci Soc Am J*. **67**: 1701–1702. 180, 182, 183
19. Hunt, A. G., 2004, Continuum percolation theory for water retention and hydraulic conductivity of fractal soils: 2. Extension to non-equilibrium, *Adv. Water Resour.***27**: 245–257. 181
20. Conca, J. L., 1990, Diffusion barrier transport properties of unsaturated Paintbrush tuff rubble backfill, p. 394-401. In Proceedings of the First International High-Level Radioactive Waste Management Conference. ASCE and American Nuclear Society, Las Vegas, NV. 181, 184

21. Conca, J. L., and J. Wright, 1992, Diffusion and flow in gravel, soil, and whole rock, *Appl. Hydrogeol*. **1**: 5–24. 181, 184
22. Civilian Radioactive Waste Management System Management and Operating Contractor (CRWMS M&O), 2000, The determination of diffusion coefficient of invert materials. TDR-EBS-MD-000002 REV 00.CRWMS M&O Las Vegas, NV. 181, 184
23. Civilian Radioactive Waste Management System Management and Operating Contractor (CRWMS M&O), 2000, Invert diffusion properties model. ANL-EBS-MD-000031 REV 01.CRWMS M&O Las Vegas, NV. 181
24. Hu, Q., T. J. Kneafsey, J. J. Roberts, L. Tomutsa, and J. S. Y. Wang, 2004, Characterizing unsaturated diffusion in porous tuff gravel, *Vadose Zone J*. **3**: 1425–1438. 181, 182, 184
25. Hu, Q., and J. Wang, 2003, Aqueous phase diffusion in unsaturated geologic media: a review, *Crit. Rev. Environ. Sci. Tech*. **33**: 275–297. 181, 183, 184
26. Schofield, R. K., and C. Dakshinamurthi, 1948, Ionic diffusion and electrical conductivity in sands and clays. *Disc. Farad. Soc*. **3**: 56–61. 182
27. Klinkenberg, L. J., 1951, Analogy between diffusion and electrical conductivity in porous rocks. *Bull. Geol. Soc. Am*. **62**: 559–564. 182
28. Snyder, K. A., 2001, The relationship between the formation factor and the diffusion coefficient of porous materials saturated with concentrated electrolytes: theoretical and experimental considerations. *Concrete Sci. Eng*. **3**: 216–224. 182
29. Garrouch, A. A., L. Ali, and F. Qasem, 2001, Using diffusion and electrical measurements to assess tortuosity of porous media. *Ind. Eng. Chem. Res*. **40**: 4363–4369. 182
30. Moldrup, P., T. Olesen, J. Gamst, P. Schjønning, T. Yamaguchi, and D.E. Rolston, 2000, Predicting the gas diffusion coefficient in repacked soil: water-induced linear reduction model, *Soil Sci. Soc. Am. J*. **64**: 1588–1594. 184, 185, 188
31. Werner, D., P. Grathwohl, and P. Hoehener, 2004, Review of field methods for the determination of the tortuosity and effective gas-phase diffusivity in the vadose zone, *Vadose Zone J*. **3**: 1240–1248. 184, 185, 186
32. Millington, R. J., and J. P. Quirk, 1961, Permeability of porous media, *Trans. Faraday Soc*. **57**: 1200–1208. 184
33. Currie, J. A., 1970, *Movement of Gases in Soil Respiration. Sorption and Transport Processes in Soils*. Rothamsted Exp. Stn., Harpenden, England. 184
34. Sallam, A., W. A. Jury, and J. Letey, 1984, Measurement of gas diffusion coefficient under relatively low air-filled porosity, *Soil Sci. Soc. Am. J*. **48**: 3–6. 184
35. Verboven, P., G. Kerkhofs, H. K. Mebatsion, Q. T. Ho, K. Temst, M. Wevers, P. Cloetens, and B. M. Nicolaï, 2008, Three-dimensional gas exchange pathways in pome fruit characterized by synchrotron X-ray computed tomography, *Plant Physiol*. **147**: 518–527. 188
36. Hunt, A. G., S. D. Logsdon, and D. A. Laird, 2006, Percolation treatment of charge transfer in humidified smectite clays, *Soil Sci. Soc. Am. J*. **70**: 14–23. 189, 190, 194, 195, 198, 199
37. Letey, J., and A. Klute, 1960, Apparent mobility of potassium and chloride ions in soil and clay pastes, *Soil Sci*. **90**: 259–265. 189
38. Cremers, A., J. van Loon, and H. Laudelout, 1966, Geometry effects for specific electrical conductance in clays and soils. Proc. Internat. Conf. Clays Clay Miner. 14th Ghent, Belgium, pp 149–162. 189
39. Jonscher, A. K., 1977, The "universal" dielectric response, *Nature (London) 267*: 673–679. 189, 190, 191
40. Funke, K., 1991, Ion transport and relaxation studied by high frequency conductivity and quasi-elastic neutron scattering, *Philos. Mag. A* **64**: 1025–1034. 190
41. Hunt, A. G., 2001, AC hopping conduction: perspective from percolation theory, *Philos. Mag. B* **81**: 875–913. 190, 197
42. Hunt, A. G., 2001, Applications of percolation theory to porous media with distributed local conductances, *Adv. Water Resour*. **24**(3,4): 279–307. 190, 197, 198
43. Sposito, G., and R. Prost, 1982, Structure of water adsorbed on smectites, *Chem. Rev*. **82**: 553–573. 190
44. Cole, K. S., 1941, Dispersion and absorption in dielectrics I. Alternating current characteristics, *J. Chem. Phys*.**9**: 341. 191

45. Davidson, D. W., 1951, Dielectric relaxation in glycerol, propylene glycol, and normal-propanol, *J. Chem. Phys*. **19** : 1484 191
46. Havriliak, S., and S Negami, 1966, Analysis of α-dispersion in some polymer systems by the complex variables method. *J. Polymer Sci.* (C) **14:** 99–117. 191
47. Kohlrausch, R., 1854, Theorie des elektrischen Rückstandes in der Leidner Flasche, Pogg. *Ann. Phys. Chem*. **91**: 179–213. 191
48. Williams, G., 1970, Non-symmetrical dielectric relaxation behaviour arising from a simple empirical decay function, *Trans. Faraday Soc*. **66**: 80. 191
49. Dixon, P. K., L. Wu, S. R. Nagel, B. D. Williams, and J. P. Carini, 1990, Scaling in the relaxation of super-cooled liquids, *Phys. Rev. Lett*. **65**: 1108. 191
50. Hunt, A. 1991, Transport in ionic conducting glasses, *J Phys Condens Matter* **3**(40): 7831–7842. 191
51. Dyre, J. C. and T. B. Schroeder, 2000, Universality of ac conduction in disordered solids, *Rev. Mod. Phys*. **72**: 873–892. 191
52. Logsdon, S. D., and D. A. Laird, 2004, Electrical conductivity spectra of smectites as influenced by saturating cation and humidity, *Clays Clay Miner*. **52**: 411–420. 191, 192
53. Logsdon, S. D., and D. A. Laird, 2004, Cation and water content effects on dipole rotation activation energy of smectites, *Soil Sci. Soc. Am. J*. **68**: 1586–1591. 191, 192
54. Bidadi, H., P. A. Schroeder, and T. J. Pinnavaia, 1988, Dielectric properties of montmorillonite clay films. Effects of water and layer charge reduction, *J. Phys. Chem. Solids* **49**: 1435–1440. 192
55. Pollak, M., and T. H. Geballe, 1961, Low-frequency conductivity due to hopping process in silicon, *Phys. Rev*. **122:** 1742–1753. 193
56. Pollak, M., and G. E. Pike, 1972, ac conductivity of glasses, *Phys. Rev. Lett*. **28**: 1449–1451 193
57. Laird, D. A., 1999, Layer charge influences on the hydration of expandable 2:1 phyllosilicates, *Clays Clay Miner*. **47**: 630–636. 194
58. Dyre, J. C. , 1991, Some remarks on ac conduction in disordered solids, *J. Non-Cryst. Solids* **135**: 219. 196
59. Friedman, L., and M. Pollak, 1981, The hall effect in the variable-range hopping system, *Philos. Mag. B* **44**: 487–507. 197, 198
60. Stauffer, D., 1979, Scaling theory of percolation clusters, *Phys. Rep*. **54**: 1–74. 198
61. Merzer, M., and S. L. Klemperer, 1997, Modeling low-frequency magnetic-field precursors to the Loma Prieta earthquake with a precursory increase in fault-zone conductivity, *Pure Appl. Geophys*. **150**: 217–248. 200
62. Archie, G. E., 1942, The electrical resistivity log as an aid in determining some reservoir characteristics. *Trans. Am. Inst. Mech. Eng*. **146**: 54–61. 200
63. Hunt, A. G., 2004, Comment on "Modeling low-frequency magnetic-field precursors to the Loma Prieta Earthquake with a precursory increase in fault-zone conductivity," by M. Merzer and S. L. Klemperer, *Pure and Applied Geophysics*, DOI: 10.1007/s00024-005-2776-6. 200
64. Gao, Y. and S. Crampin (2004), Observations of stress relaxation before earthquakes, *Geophys. J. Int 'l*. **157**(2): 578–582. 200
65. Egbert, G. D., 2002, On the generation of ULF magnetic variations by conductivity fluctuations in a fault zone, *Pure Appl. Geophys*. **159**: 1205–1227. 200
66. Freund, F., and D. Sornette, 2007, Electromagnetic earthquake bursts and critical rupture of peroxy bond networks in rocks, *Tectonophysics*, **431**: 33–47. 201
67. Hunt, A., N. Gershenzon, and G. Bambakidis, 2007, Pre-seismic electromagnetic phenomena in the framework of percolation and fractal theories, *Tectonophysics* **431**: 23–32. 201
68. Madden, T. R., 1983, Microcrack connectivity in rocks: a renormalization group approach to the critical phenomena of conduction and failure in crystalline rocks, *J. Geophys. Res*. **88**: 585–592. 201
69. Hunt, A., 1992, Dielectric and mechanical relaxation in liquids and glasses: transition from effective medium to percolation theories, *Solid State Commun*. **84**(7): 701–704. 201
70. Miyazima, S., 2005, An exact percolation point for surface filing in a four-dimensional hypercubic lattice, *Prog Theor. Phys*. **113**: 1159–1163. 201

71. Miyazima, S., and Yamamoto, K., 2006, Site and bond percolation problem for construction of a macroscopic surface in a cubic lattice, *J. Res. Inst. Sci. Tech.* **18**: 101–106. 201
72. Rolston, D. E., R. D. Glauz, G. L. Grundmann, and D. T. Louie, 1991, Evaluation of an in situ method for measurement of gas diffusivity in surface soils, *Soil Sci. Soc. Am. J*. **55**: 1536–1542. 186
73. van Bochove, E., N. Bertrand, and J. Caron. 1998. In situ estimation of the gaseous nitrous oxide diffusion coefficient in a sandy loam soil. *Soil Sci. Soc. Am. J*. **62**: 1178–1184. 186
74. Ball, B. C., C. A. Glasbey, and E. A. G. Robertson, 1994, Measurement of soil-gas diffusivity in-situ, *Eur. J. Soil Sci*. **45**: 3–13. 186
75. Washington, J. W., A. W. Rose, E. J. Ciolkosz, and R. R. Dobos, 1994, Gaseous diffusion and permeability in four soil profiles in central Pennsylvania, *Soil Sci*. **157**: 65–76. 186
76. Werner, D., and P. Höhener, 2003, In situ method to measure effective and sorption-affected gas-phase diffusion coefficients in soils, *Environ. Sec. Technol.* **37**(11): 2502–2510. 160, 187
77. Hers, I., J. Atwater, L. Li, and R. Zapf-Gilje, 2000, Evaluation of vadose zone biodegradation of BTX vapors. *J. Contam. Hydrol*. **46**: 233–264. 187
78. Nicot, J. P., and P. C. Bennett, 1998, Shallow subsurface characterization of gas transport in a Playa wetland. *J. Environ. Eng*. **124**: 1038–1046. 187
79. Patil, A. S., K. M. King, and M. H. Miller, 1963, Self-diffusion of rubidium as influenced by soil moisture tension, *Can. Soil Sci*., **43**: 44. 184
80. Graham-Bryce, I. J., 1963, Effect of moisture content and soil type on self diffusion of ^{86}Rubidium in soils, *J. Agric. Sci*. **60**: 239. 184
81. Romkens, M. J. M, and R. R. Bruce, 1964, Nitrate diffusivity in relation to moisture content of non-adsorbing porous media, *Soil Sci*. **98**: 332. 184
82. Warncke, D. D., and S. A. Barber, 1972, Diffusion of zinc in soil I. The influence of soil moisture, *Soil Sci. Soc. Am. J*. **36**: 39. 184
83. Sadeghi, A. M., D. E. Kissel, and M. L. Cabrerra, 1989, Esitmating molecular diffusion coefficients of urea in unsaturated soil, *Soil Sci. Soc. Am. J*. **53**: 15. 184
84. Barraclough, D., and P. H. Nye, 1979, The effect of molecular size on diffusion characteristics in soil, *J. Soil Sci*. **30**: 29. 184
85. Mehta, B. K., S. Shiozawa, and M. Nakano, 1995, Measurement of molecular diffusion of salt in unsaturated soils, *Soil Sci*. **159**: 115. 184
86. Barraclough, D., and P. B. Tinker, 1981, The determination of ionic diffusion coefficients in field soils. I. Diffusion coefficients in sieved soils in relation to water content and bulk density, *J. Soil Sci*. **32**: 225. 184
87. Porter, L. K., W. D, Kemper, R. D. Jackson, and B. A. Stewart, 1960, Chloride diffusion in soils as influenced by moisture content, *Soil Sci. Soc. Am. Proc*. **24**: 460. 184
88. Jurinak, J. J., S. S. Sandhu, and L. M. Dudley, 1987, Ionic diffusion coefficients as predicted by conductometric techniques, *Soil Sci. Soc. Am. Proc*. **51**: 626. 184
89. Rowell, D. L., M. W. Martin, and P. H. Nye, 1967, The measurement and mechanism of ion diffusion in soil, III. The effect of moisture content and soil solution concentration on the self-diffusion of ions in soils, *J. Soil Sci*. **18**: 204. 184
90. So, H. B., and P. H. Nye, 1989, The effect of bulk density, water content and soil type on the diffusion of chloride in soil, *J. Soil Sci*. **40**: 743. 184
91. Olesen, S. R., and W. D. Kemper, 1968, Movement of nutrients to plant roots, *Advances in Agronomy*, Academic Press, Inc., San Diego CA, Vol. 30, pp. 91. 184
92. Moldrup, P., T.G. Poulsen, P. Schjønning, T. Olesen, and T. Yamaguchi, 1998, Gas permeability in undisturbed soils: Measurements and predictive models, *Soil Sci.* **163**(3): 180–189. 184
93. Schaefer, C. E., R. R. Arands, H. A. van der Sloot, and D. S. Kosson, 1995, Prediction and experimental validation of liquid-phase diffusion resistance in unsaturated soils, *J. Contam. Hydrol*. **20**: 145. 184
94. Klute, A., and J. Letey, 1958, The dependence of ionic diffusion on the moisture content of nonsorbing porous media, *Soil Sci. Soc. Am. Proc*., **22**: 213. 184

Chapter 7
Pressure–Saturation Curves and the Critical Volume Fraction for Percolation: Accessibility Function of Percolation Theory

The pressure–saturation $(h(\theta))$ curves of porous media give fundamental information about the pore space. In equilibrium, ignoring effects due to hysteresis and pore accessibility, it should be possible to extract a pore-size distribution from $(h(\theta))$ data, as described in Chap. 3. However, a number of percolation effects complicate the analysis and make such a simple inference impossible. The pressure–saturation relation is affected by both the lack of continuity of the air phase near saturation and by a similar lack of continuity of the water phase near the dry end. Given that these effects are due to phase transitions (in the percolation sense), small changes in experimental conditions can produce major (and sometimes puzzling) changes in the results. Further, since the correlation length diverges near these transitions, numerical simulations under both wet and dry conditions are amenable to finite-size scaling analysis. Since the critical volume fractions for percolation of air and water are central to the discussion, experimental evidence regarding these values is presented toward the end of this chapter.

When a porous medium is dried from near saturation, the wetting phase becomes discontinuous below the percolation transition. While the soil science community has only rarely adopted percolation theoretical methods, they have used some of its core concepts in their own language. For example, "The use of residual saturations is [...] appropriate when a fluid phase becomes incoherently distributed, in which case the fluid does not move anymore as a connected phase" (Luckner et al., 1989). When the water phase is disconnected, water can move only by film flow or as a vapor. These new modes of transport could be safely ignored at high moisture contents, because they involve coefficients that are orders of magnitude lower than typical hydraulic conductivities from capillary flow. But if these new modes are not effective in a given situation, it will prove difficult to reduce θ to values less than the critical volume fraction θ_t for percolation. In fact, just reducing θ to θ_t is difficult because the hydraulic conductivity value for capillary flow vanishes rapidly as θ_t is approached. A related possibility, that even above the critical moisture content some water-filled pores could lose access to the infinite cluster and fail to drain, was discussed qualitatively in Chap. 3. This scenario will not be further discussed here, particularly since it seems to be relevant only in a fairly small subset of experiments involving rapid drainage.

Hunt, A., Ewing, R.: *Pressure Saturation Curves and the Critical Volume Fraction for Percolation: Accessibility Function of Percolation Theory.* Lect. Notes Phys. **771**, 207–231 (2009)
DOI 10.1007/978-3-540-89790-3_7

7.1 Structural Hysteresis

The role of percolation in hysteresis in wetting and drying of porous media has been appreciated in the physics community for over two decades [1], but much less so in the porous media community. A basic consideration of hysteresis in wetting and drying should suggest that changes in the water content will be limited by the continuity of the air phase near saturation, and by continuity of the water phase at the dry end. That is, a porous medium that wets and dries will typically pass through two distinct percolation transitions. What this means is that, neglecting edge effects, water (air) may be trapped in isolated clusters during drying (wetting), while water (air) cannot enter in arbitrarily small quantities [less than the critical volume fraction] during wetting (drying). In a 2D medium these two phase transitions would occur at the same moisture content, but in 3D media they are generally separated by a wide range of moisture contents where both phases percolate. As Gist et al. [2] point out: "The subset of pores occupied by mercury at the [percolation] threshold diameter has been directly visualized by injecting a porous medium with molten metal, then solidifying the metal. Examined optically, the resulting structure has the fractal dimension expected from percolation theory" [3].

A second important contributor to hysteresis, the so-called ink-bottle effect, is well known to the porous media community [4, 5]. According to the Young–Laplace relationship, when an air–water–solid system is at equilibrium, a given pore can be filled with water only if its radius is less than some value proportional to the air/water interfacial tension γ and inversely proportional to the pressure: $r < A\gamma/h$. Water is "allowed" in these pores. But according to the pore-body, pore-throat picture of porous media, the tension required to remove water from such a pore is higher than that which allows water in: in the removal process (drainage) the meniscus must "fit" through a pore throat, while in the filling process (imbibition) the meniscus must span the pore body. This fundamental asymmetry in the wetting and drying processes means that, at a given water content, the pressure in a drying curve should be higher than in a wetting curve. This factor relates to the geometry of an individual pore, but in a system with self-similar properties it relates to every pore.

Consider imbibition under a high tension (negative water pressure) into an initially dry medium. Water cannot access most pores that are allowed, because the paths to those pores pass through other pores that are not small enough to allow water [6]. This problem is obviously related to percolation theory, but it was originally thought that traditional percolation theory was not adequate to treat this problem. In the 1980s considerable literature arose in the physics community regarding a special form of percolation theory called "invasion" percolation [7]. From our standpoint, invasion percolation deals with the movement of the wetting or drying front, and therefore (in principle) with spatial gradients of percolation quantities. By the end of the 1980s it was accepted that, at least with respect to hysteresis, the difference between traditional percolation theory (discussed here) and invasion percolation was minimal [8] – though at least one key investigation [1] had a significant inconsistency which will be revisited below.

In traditional percolation theory, the fraction of accessible sites is that fraction P that is part of the infinite cluster. During drying, if we allow for drainage by water films, then all of the water-allowed sites are accessible to water. But in wetting the

fraction of water-allowed sites that are also accessible to water is reduced by P. P is known to behave in 3D as

$$P \propto (p - p_c)^{\beta} = (\theta - \theta_t)^{0.4} \tag{7.1}$$

where the equality follows from the application to continuum percolation with the moisture content playing the role of p. An obvious problem in applying this concept is that our expression for P is a proportionality, not an equality. Clearly P should be constrained to equal 1 at or above some moisture content; a reasonable choice is to require $P = 1$ at $\theta = \phi$. For this case we can write [9]

$$P = \left(\frac{\theta - \theta_t}{\phi - \theta_t} \right)^{0.4} \tag{7.2}$$

The implication of this particular normalization factor is that, during wetting, it is certain only at saturation that all water-allowable pores are also water-accessible. For practical purposes the condition $P = 1$ is likely reached at somewhat lower water contents.

It is possible to express the actual moisture content as the product $\theta \cdot P(\theta)$, as long as θ in this product refers to the *equilibrium* moisture content, that is, the volume of the allowable pore space. This notational complication can be easily removed by expressing both factors in terms of the tension h. Referring water content to pressure requires reference of the critical water content to a critical pressure h_c, which can be defined via [9]

$$\theta_t = \left[\frac{3 - D}{r_m^{3-D}} \right] \int_{r_0}^{A/h_c} r^{2-D} dr \tag{7.3}$$

Thus, starting from dry conditions with a very large value of $h \geq A/r_0$, reduction of h produces an increasing fraction of water-allowable pore space (but, ignoring edge effects, no increase in water-accessible pores or water content) until, at the value $h = h_c$, the water-allowable pore space percolates. Proceeding from this point we have [9]

$$\theta(h) = \frac{3 - D}{r_m^{3-D}} \left[\frac{(A/h)^{3-D} - (A/h_c)^{3-D}}{(A/h_A)^{3-D} - (A/h_c)^{3-D}} \right]^{0.4} \int_{r_0}^{A/h} r^{2-D} dr \tag{7.4}$$

where (as discussed in Chap. 3) h_A is the air entry pressure.

We emphasize again that this approach neglects the effects of finite clusters of water-allowed pores which are accessible from the edges of the system. The effects of such pores can be incorporated into the treatment via finite-size scaling, but we will not do that here. The present approach also neglects water that would fill "pores" on rough (fractal) surfaces of individual grains, at least insofar as this contribution to the pore space is described by a separate surface fractal dimensionality. Such a contribution could theoretically lead to a change in slope of the pressure–saturation curves at low moisture contents.

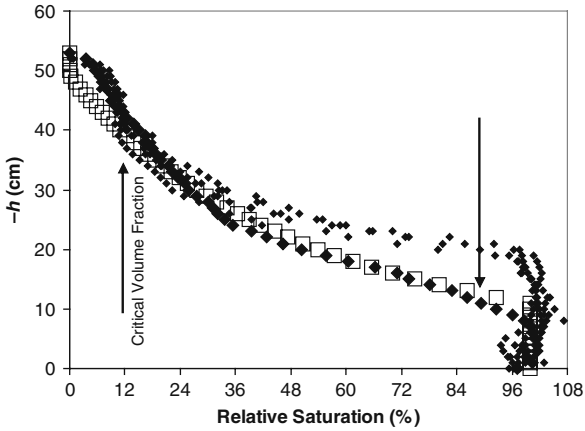

Fig. 7.1 Drainage data from Bauters et al. [10] for a collection of sands with differing fractions (the *smaller diamonds*) of hydrophobic particles, with the fraction being zero for the large diamonds. The theoretical curve (open squares) was obtained by using the particle-size data to find the fractal dimensionality of the pore space while the air entry pressure, h_A, was used as an adjustable parameter. The critical moisture content for percolation (0.048) is designated by the arrows; in a soil with only sand particles these values are assumed identical for air and water

With these caveats we compare Eq. (7.4) with experimental measurements (Fig. 7.1) of the drying of blasting sand with various fractions of particles treated to be water-repellent [10]. Each different fraction of water-repellent particles gave a different curve, but displaying them all together shows that the critical moisture content for percolation is the same in each case. As in earlier chapters, particle-size data were used to find the ratio r_0/r_m, after which ϕ and the ratio r_0/r_m are combined to give D. A single air-entry pressure h_A was adjusted to produce the best fit with experiment over the range of intermediate saturations. The value of the critical volume fraction for percolation, $\theta_t = 0.048$, was chosen as the point below which theory and experiment deviated (due to nonequilibrium, discussed below).

It is clear from the data that the appropriate value of the characteristic pressure for imbibition could not be the same as for drainage. This is due to the "ink-bottle" effect mentioned earlier in this chapter. Lenhard [5] and coworkers [4] investigated this effect for a number of soils and found that the typical ratio of characteristic pressures for drainage and imbibition is 2, indicating that pore bodies characteristically have radii twice that of pore throats. Using Eq. (3.22) (derived for drainage) for imbibition, but with the characteristic pressure reduced by a factor 2 as per Lenhard et al. [4], does not suffice to transform a drainage curve into an imbibition curve [9]: the curve intersects reality only near saturation (Fig. 7.2). But when the accessibility effects of percolation are included by using Eq. (7.4) (without additional unknown parameters), the match between experiment and theory is quite good. Figure 7.2 provides an additional check on the estimate of the critical volume fraction: deviations from prediction set in at a moisture content $\phi - \theta_t$ (still with $\theta_t = 0.048$). These deviations arise from "entrapped" air, and become apparent as the volume of air-filled pore space reaches the percolation threshold.

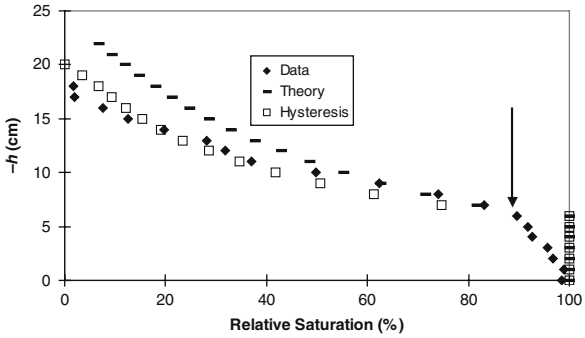

Fig. 7.2 The imbibition curve for the hydrophilic sand of Fig. 7.1. "Theory" uses Eq. (3.22) with a characteristic pressure half of h_A in Fig. 7.1. "Hysteresis" uses the prediction of Eq. (7.4). There are no other adjustable parameters here; the critical volume fraction comes from Fig. 7.1, and the fractal dimensionality from the particle size distribution. Here the critical air content for percolation is clearly also very close to 0.05

The general idea of allowable vs. accessible pores in the context of percolation theory was introduced by Heiba et al. [6] in a publication treating a Bethe lattice model. Publications of Wilkinson (e.g., 1986) later in the 1980s developed this framework further, accounting for the connectivity of water films during drying, and their absence during wetting. This led to different treatments for air entrapment during wetting (residual air) and residual water during drying. In that respect his treatment was more careful and general than the present treatment. However, Wilkinson treated the pressure as the fundamental percolation variable – which was reasonable for the bond percolation problem he was addressing with a network model – and then expressed the moisture content in terms of a *sublinear* power of h, rather than using the moisture content as the fundamental variable (in continuum percolation) and expressing the pressure as a *superlinear* power of θ. This reversal of the roles of the variables calls his conclusions into question, because those conclusions depend on the *sublinearity* of the powers.[1] In addition, his comparison with experiment was schematic, without specific data; a detailed comparison between his analysis and experimental data (for example, the results given here) has yet to be made. Wilkinson also did not consider various experimental difficulties, which include lack of equilibration due to low values of the hydraulic conductivity (or rapid drainage), nor the differences in media, some of which may be structured. Any one of these factors can influence the shape of the drainage and imbibition curves. The first of these questions will be treated next; effects of the structure of a medium will be addressed in the final chapter.

[1] In particular, Wilkinson addressed the curvature of the pressure saturation curve, $\log[-h]$ vs. θ, at large moisture contents and determined that the typically observed negative curvature was appropriate from percolation theory. However, we find that a positive curvature is appropriate (and indeed observed for sandy media), while we are forced to attribute a negative curvature, commonly observed in finer media, to the existence of structural pores. See Sect. 7.4 for additional quantitative evidence supporting our interpretation.

7.2 Hydraulic Conductivity-Limited Equilibration, and Dry-End Deviations from Fractal Scaling

Chapter 5 discussed the limits of validity of an equation for hydraulic conductivity,

$$K_{\mathrm{f}}(\theta) = K_{\mathrm{S}}\left[1 - \phi + (\theta - \theta_{\mathrm{t}})\right]^{\frac{3}{3-D_{\mathrm{p}}}} \tag{7.5}$$

and the fact that it must be replaced by

$$K_{\mathrm{p}}(\theta) \propto (\theta - \theta_{\mathrm{t}})^2 \tag{7.6}$$

in the vicinity of θ_{t}. For the sake of clarity, K calculated by Eq. (7.5) is fractal scaling, denoted K_{f}, while K according to Eq. (7.6) is percolation scaling, denoted K_{p}.

Standard methods of producing pressure–saturation curves use drainage across a porous ceramic plate. A positive air pressure is applied to the sample, and its effect on pore water allowability is assumed equivalent to that of an equivalent tension applied to the water phase. These measurements typically require long equilibration times, because at low water contents, hydraulic conductivity values can be extremely low. For example, suppose we have a partially drained 10-cm high column of soil with porosity $\phi = 0.5$, and we subject it to a pressure $h = 1\,\mathrm{m}$. If $K(\theta) = 10^{-8}\,\mathrm{cm\,s^{-1}}$ (a reasonable value), then removing water equivalent to a 1-mm thick layer, i.e., decreasing θ by 0.02, will take over 500 days. As long as measured values of K diminish in a regular way according to Eq. (7.5), one can extrapolate the equilibration time for the next step of an experiment. But the two relationships for K (K_{p} in Eq. (7.5) and K_{f} in Eq. (7.6)) raise a new complication: if θ drops below the crossover moisture content $\theta_{K\mathrm{x}}$, then K decreases much more rapidly (see Fig. 7.3)). The equilibration times required by Eq. (7.6) are therefore

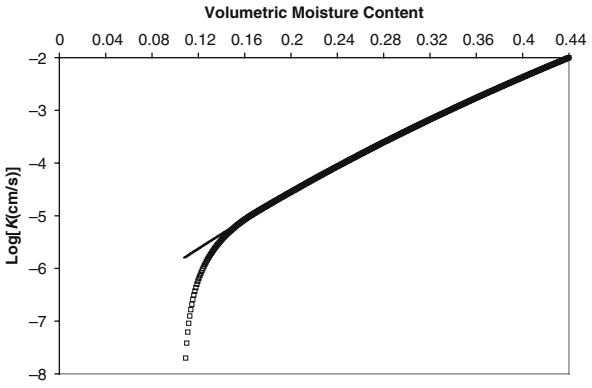

Fig. 7.3 A generic hydraulic conductivity as a function of saturation, but similar to that of the McGee Ranch soil (Fig. 5.1). This figure shows the deviation from fractal scaling of the conductivity at low moisture contents associated with the crossover to percolation scaling

much greater [11]. If this marked increase in equilibration time is not anticipated, then the ratio of the allowed time to the required time would equal the ratio K_p/K_f; the observed reduction in water content would likewise be too small on the order of K_p/K_f. Specifically, on a fractal soil which at pressure h_i equilibrates to a moisture content $\theta = \theta_{xK}$, then when the pressure is increased to h_{i+1} the water content will be reduced by only

$$\Delta\theta = \frac{K_p}{K_f}\phi\left[\left(\frac{h_A}{h_{i+1}}\right)^{3-D} - \left(\frac{h_A}{h_i}\right)^{3-D}\right] \tag{7.7}$$

within the allowed time: with too little drainage time, the moisture content will not drop as rapidly as predicted by the fractal model.

We have developed an algorithm for predicting the nonequilibrium moisture content of a medium. The algorithm is based on Eq. (7.7); that is, it assumes that the allowed drainage time at any given tension is calculated by extrapolating K_f (Eq. (7.5)) to ever-drier conditions. The algorithm assumes differentially small changes in tension and relates a geometrical water loss to an actual water loss:

$$d\theta_a = \left[\frac{K_p(\theta_a)}{K_f(\theta_a)}\right] d\theta \tag{7.8}$$

where the subscript a denotes actual. Now integrate (over the dummy variable, θ') to obtain

$$\int_{\theta_{xK}}^{\theta} d\theta' = \int_{\theta_{xK}}^{\theta_a} d\theta' \frac{K_f(\theta')}{K_p(\theta')} \tag{7.9}$$

The right-hand integral is given in terms of the Gauss hypergeometric function ${}_2F_1$. By defining

$$G(x) \equiv \frac{K_S}{(1-t)K_0}\left[\frac{1-\phi}{1-\theta_t}\right]^{\frac{3}{3-D}}(x-\theta_t)^{1-t}\,{}_2F_1\left[1-t, \frac{3}{3-D}, 2-t, \frac{\theta_t - x}{1-\phi}\right] \tag{7.10}$$

we can write an implicit relationship for θ_a:

$$\theta - \theta_{xK} = G(\theta_a) - G(\theta_{xK}) \tag{7.11}$$

that maps $\theta_t \le \theta_a \le \theta_{xK}$ to $0 \le \theta \le \theta_{xK}$. The original, or presumed water-retention function, $h(\theta)$, is then mapped to $h(G(\theta_a))$. Note that since K vanishes at θ_t, the moisture content θ_t is never reached with this procedure. Figure 7.4 shows the effects of incomplete equilibration on the apparent water-retention curve, as predicted by this algorithm, for the same system shown in Fig. 7.3. Although the algorithm is simple, the results are robust. The procedure was also performed algorithmically for finite pressure steps Δh. Over the relatively wide range of Δh values investigated, the resulting nonequilibrium portion of the water-retention curve (not shown) was identical to that predicted by Eq. (7.11), generated by changing the pressure in

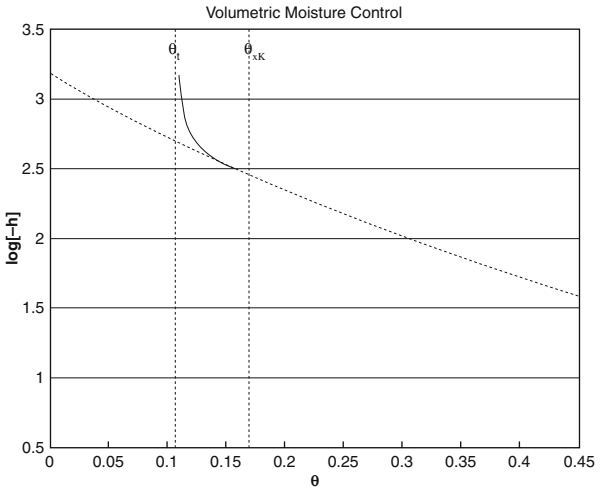

Fig. 7.4 The nonequilibrium water-retention curve expected for the medium with K represented in Fig. 7.3. Here the threshold water content is given as θ_t, while the crossover moisture content is given as θ_{xK} [changed from Hunt and Skinner [11]]. Equations (7.10) and (7.11) were used to make this figure

infinitesimal steps. An interesting aspect of these results is the quasi-universality of the shape of the water-retention curve in the vicinity of θ_t.

The above is a somewhat oversimplified picture as well as an oversimplified calculation: both the actual value of K and its extrapolated value change over the time the water is draining. Nonetheless, it gives accurate predictions of experimental data, as shown in Figs. 7.5, 7.6, 7.7, 7.8, 7.9, 7.10 and 7.11 (from Hunt and Skinner [11]). To generate these predictions, particle-size data were used to find the ratio r_0/r_m, the porosity ϕ and ratio r_0/r_m were combined to give D_p, then h_A was used as an adjustable parameter to generate the equilibrium moisture contents. θ_t was taken as the lowest water content obtained in the experiment, and θ_{xK} was calculated from Eq. (5.21); then for all values of h corresponding to $\theta < \theta_{xK}$, the magnitude of $\Delta\theta$ was reduced by the ratio K_p/K_f as in Eq. (7.7). However, this procedure still yielded a predicted moisture content lower than the observed value. In order to match the observed moisture contents, it was necessary to take the ratio of the actual value of K and the value of K assumed to be accurate for a moisture content *two time steps prior*. This suggests that the value of K from a previous measurement was used as a guide for a subsequent measurement, which would imply that the authors of the study were not anticipating any reduction in K, even according to a result compatible with Eq. (7.5). Applying this connection to K two measurements earlier is equivalent to using an adjustable parameter; on the other hand the same value of this parameter was used for all seven of the cases investigated and presented here. Given this restriction on flexibility, the predictions appear to be quite accurate.

The results presented here suggest that widely observed deviations from fractal scaling of pressure–saturation curves at low saturations are not a defect of the fractal model itself. On the contrary, because parameters derived from the use of fractal

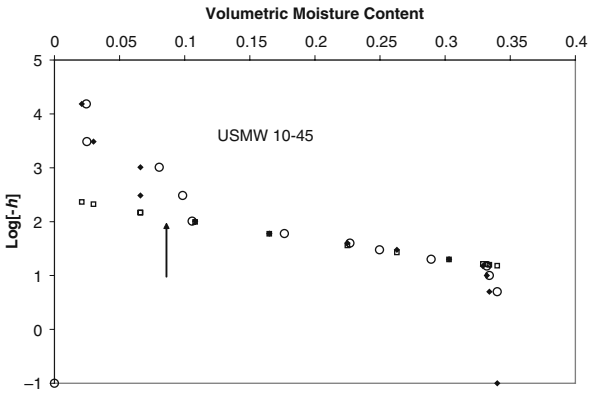

Fig. 7.5 A reevaluation of the deviation of experimental water-retention curves from the fractal scaling (Eq. (3.22) at low moisture contents. The *solid diamonds* are experimental data for the USMW 10-45 soil from the Hanford site [29], while the open squares are the predictions from Eq. (3.22). The *open circles* are obtained from the algorithm described in the text, which reduces the actual moisture lost by the ratio of Eqs. (7.6) to (7.5). This algorithm is only appropriate for $\theta < \theta_x$, which was obtained using Eq. (7.12) and the lowest moisture content attained by experiment for θ_t

models (in particular, θ_t) can then be used to predict hysteresis in drainage and imbibition, or the shape of the water-retention curve in the vicinity of the percolation threshold, the case for fractal treatments is actually strengthened. It is not unreasonable to speculate that a large number of natural soils may be best described by the Rieu and Sposito [12] fractal model.

In addition to the 12 soils analyzed for dry-end deviations caused by nonequilibration (of which 7 are shown in this chapter), we have also analyzed soils for which neither the particle-size data nor the water-retention curves is consistent with the relatively simple Rieu and Sposito model [13]. Rather, in these soils there is considerable complexity at relatively high water contents. These results are described in Chap. 11 in another context.

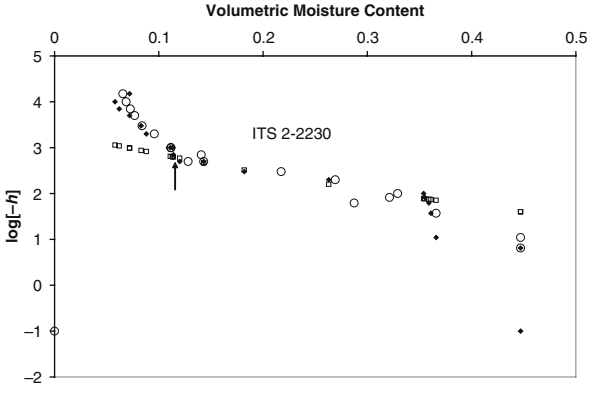

Fig. 7.6 Deviation of experimental water-retention curves from the fractal scaling (Eq. 3.22) at low water contents. Solid diamonds are experimental data from Hanford site soils [29], open squares are predictions from Eq. 3.22, and open circles are from the deviation algorithm [11].

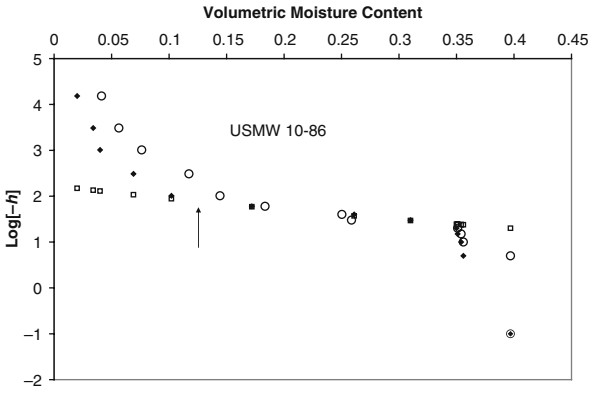

Fig. 7.7

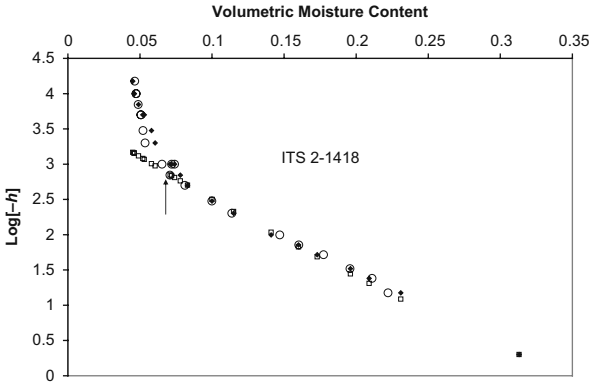

Fig. 7.8

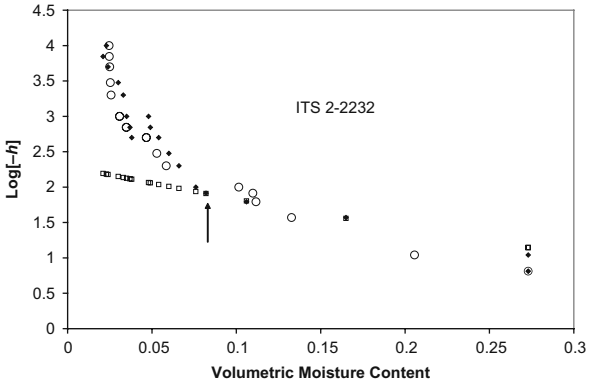

Fig. 7.9

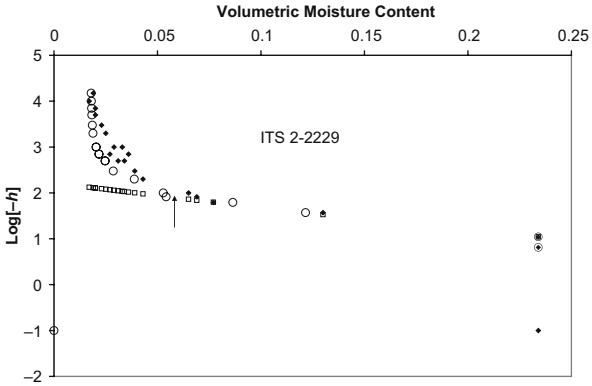

Fig. 7.10

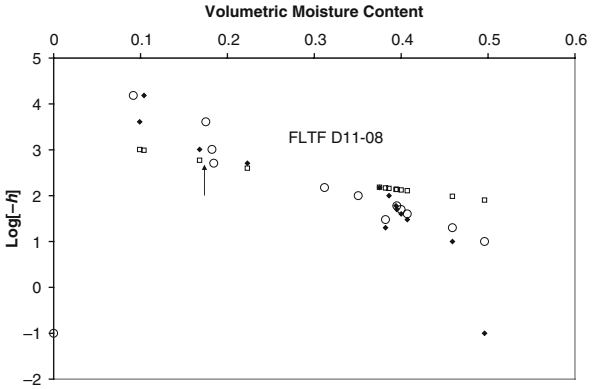

Fig. 7.11

We (Dr. Skinner and Dr. Hunt) are currently engaged in a project (NSF Grant No. EAR-0609884) which reverses the procedure described here. Rather than predicting the (nonequilibrium) water-retention curve from a given pore-size distribution, we estimate the actual pore size distribution from the (nonequilibrium) water-retention curve. The procedure involves inverting Eq. (7.8), solving for $0 < \theta < \theta_{xK}$ in terms of $\theta_t < \theta_a < \theta_{xK}$. For a fractal model then, the equilibrium water loss would be given by multiplying the nonequilibrium water loss by K_f/K_p. In the general case, K_f is replaced by a general result from critical path analysis. The inverse problem is made more complex as a consequence of the lack of sufficient pore-size data to apply critical path analysis for all values of $\theta < \theta_{xK} + \theta_t$. Any solution must then be tested for self-consistency. We estimated first θ_t as the lowest moisture content reached. We estimated θ_{xK} as the point where the water-retention curve appears to develop a positive deviation (in h). If θ_t was chosen to be too large, we generated negative moisture contents and chose a smaller value for θ_t. In order to constrain the values of θ_{xK} we required the ratio of conductivities to be a monotonically increasing function.

We found that using critical path analysis to generate an extrapolation of the numerical results for K to moisture contents $\theta < \theta_{xK} + \theta_t$ gives a good trial solution; when $K(\theta)$ so obtained is substituted in Eq. (5.35), we found that, for the case shown, our initial estimate of θ_{xK} was within 1% of the solution from Eq. (5.35), which we considered to be acceptable. The results of our procedure are shown in Fig. 7.12. Such final results could then be used to recalculate any properties that were estimated originally from the pore-size distribution implied by the water-retention curve. If the results of Fig. 7.12 prove reliable, they will indicate that a much larger fraction than is typically assumed is contained in water-filled pores and that the amount of water on surfaces or in pits of grains is relatively small (<5%). Note that this conclusion is generally compatible with other results that imply small critical moisture contents for percolation, and small water contents in pendular structures (thermal conductivity). But for the present this transformation to an equilibrium pore-size distribution is still mostly untested.

This discussion ultimately leads to the question: which is more useful in determining the pore size distribution: the water-retention curve, or the particle-size distribution? The reader will have to answer that question for him- or herself, but our contention is that, due to complications from phase continuity of the fluids (residual water, air entrapment, inaccessible allowed pores) and from fluid flow properties (nonequilibration), the water-retention curve is quite inadequate by itself. Of course the particle-size distribution is also inadequate, lacking direct information on pore

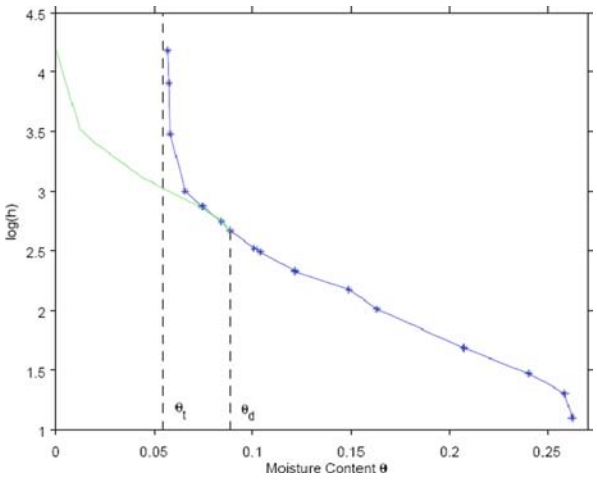

Fig. 7.12 The *crosses* and the associated curve show initial water-retention data [from Schaap et al. (2003)]. The critical moisture content for percolation, θ_t, and the point at which the water-retention curve begins to deviate from the equilibrium pore-size statistics, $\theta_d = \theta_{xK}$, are clearly indicated. Our procedure generated the curve without crosses as the equilibrium water-retention curve, implying that a pore-size distribution extracted from the raw data would put a great deal more water into smaller pores than is justified. This result, if verified generally, would imply that many conclusions based on the importance of surface water and water in pits or fractures of individual particles have been overstated

sizes as well as pore structure. From a pragmatic perspective, one uses the information that is available, and particle-size data are far more widely available than water-retention data. We hope that future work will allow us to make use of both together, such that each can overcome deficiencies in the other.

7.3 Analysis of Water-Retention Curves in Terms of the Critical Moisture Content for Percolation

The possibility that the dry-end percolation transition might somehow produce deviations from the fractal scaling prediction motivated an earlier investigation into dry-end deviations in water-retention curves [14]. While it was suspected that the lack of phase continuity could interfere with the removal of water, we did not think that the small magnitude of the hydraulic conductivity would produce the effect directly. Thus the values that were compiled were simply the moisture contents,[2] θ_d, at which the deviation from scaling set on. These moisture contents were then compared with the critical volume fractions for percolation from the solute diffusion experiments of Moldrup et al. [15].

The procedure followed was to use the particle size information from each of Freeman's soils [29] to find r_0/r_m, and thus determine the fractal dimensionality of the pore space from Eq. (3.16). Particle size data from seven of the soils are shown in Fig. 7.13. h_A was then adjusted to produce the best visual fit with the

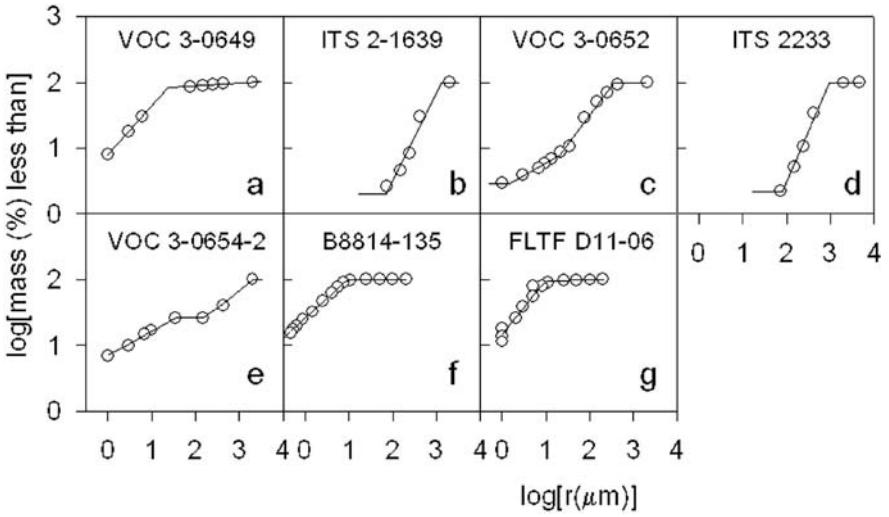

Fig. 7.13 Particle-size data for 7 Hanford site soils, all different from Figs. 7.3, 7.4, 7.5, 7.6, 7.7, 7.8 and 7.9 (from Hunt and Gee [19]). The flat portions of the curve intersect the fractal scaling region at the radii r_0 and r_m

[2] Although it became clear that the experimentally determined θ_d could be identified with the theoretical θ_{xK}, it is useful to continue referring to θ_d in the context of these experiments.

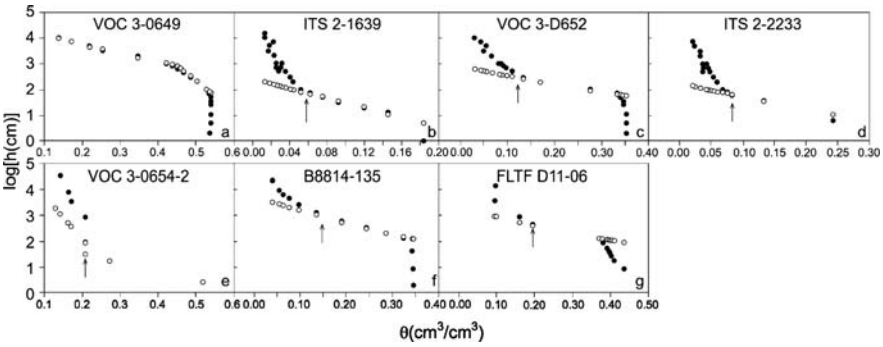

Fig. 7.14 The predicted and observed water-retention curves for the same 7 Hanford site soils as in Fig. 7.13 [from Hunt and Gee [19]]. h_A was again used as an adjustable parameter. In each case the arrow shows the value chosen for θ_d

experimental data for the water-retention relationship (Eq. (3.22)), concentrating on the middle range of saturations. The value of θ_d was then determined by inspection (Fig. 7.14). Meanwhile, θ_t was also predicted using the relationship of Moldrup et al. [15], $\theta_t = 0.039(A/V)^{0.52}$, where A/V is the specific surface area. Application of this relationship normally relies on experimentally determined values of A/V, but that information was not available for Hanford site soils. The alternative was to calculate the dependence of the surface area on such quantities as r_0/r_m, and the fractal dimensionality of the solid medium, D_s, obtained from Eq. (3.17). We estimated A/V using the ratio implied by the RS model,

$$\frac{A}{V} \propto \frac{\int_{r_0}^{r_m} r^2 \left(r^{-1-D_s}\right) dr}{\int_{r_0}^{r_m} r^3 \left(r^{-1-D_s}\right) dr} \tag{7.12}$$

implicitly assuming that the geometrical factors relating particle volume and particle surface area were both scale-invariant, and also the same for all of our soils. This last (necessary) assumption is clearly incorrect, and introduced some random error into the comparison.

We could now compare the measured θ_d with the value of θ_t from the Moldrup relationship. There was clearly a proportionality constant that we had not estimated, but the important result [14] was that $\theta_d = C\theta_t + 0.06$ for some numerical constant C [Fig. 7.15; meanings of the abbreviations for the various soils are given in Hunt and Gee [14]]. The value of R^2 for the regression was 0.83. At the time of the study the result that there was a positive intercept was not understood since the further development of the theoretical description [16] to include the crossover from Eqs. (7.5) to (7.6) had not been made. Thus several attempts were made to try to find some complicating factor in the analysis.

In the most important analysis, a subset of soils was excluded from consideration because in these soils the hydraulic conductivity could be deduced to fall to very low values at moisture contents well above θ_t on account of either small K_S values or D_p values near 3. For values of the hydraulic conductivity less than approximately

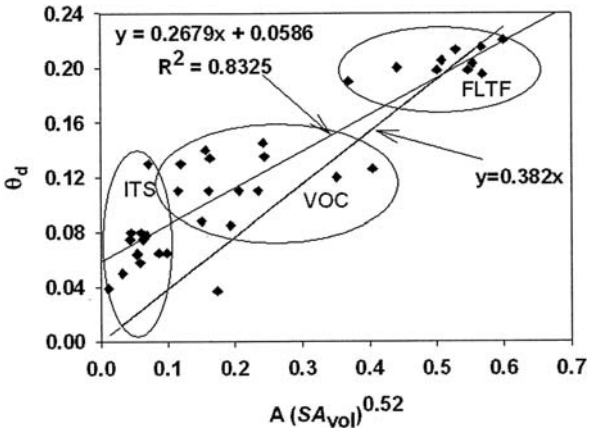

Fig. 7.15 Regression of θ_d on calculated θ_t, using the Moldrup relation for θ_t. in terms of the specific surface area and using the Moldrup notation, SA_{vol} for A/V [from Hunt and Gee [19]]

$5 \times 10^{-8}\,\mathrm{cm\,s^{-1}}$, the experimental procedure described at the end of Chap. 3 (which was the one used to gather the data, Khaleel and Relyea [17]) could be shown using Eq. (7.15) to be inadequate to drain the soils to equilibrium on account of their experimental time limit of six weeks. The prediction was based on the use of Eq. (7.5) to calculate $K(\theta)$ from porosity, fractal dimensionality, and the saturated value of the hydraulic conductivity [18]. Figure 7.16 shows the values of K at θ_d from this calculation for soils of various areas on the Hanford site. Note that the lowest K values were obtained for the volatile organic carbon (VOC) soils, and it is apparent from

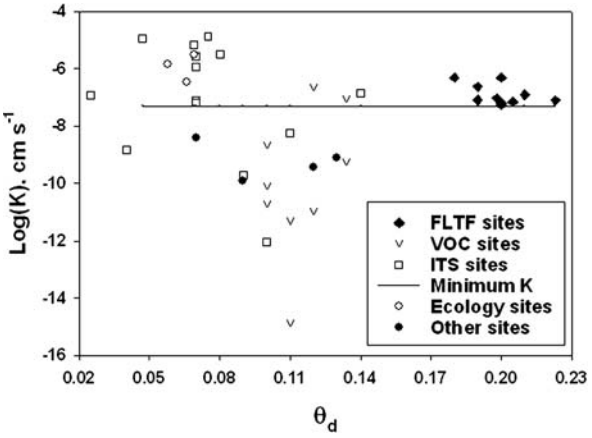

Fig. 7.16 From Hunt and Gee [19]. Representation of $\log(K)$ at θ_d vs. θ_d for 40 Hanford site soils. The horizontal line depicts the minimum value of $K = 5 \times 10^{-8}\,\mathrm{cm\,s^{-1}}$ (Hunt and Gee [19]), for which equilibrium moisture contents were measurable under the stated experimental conditions [17]. The 15 soils with $K(\theta_d) < 5 \times 10^{-8}\,\mathrm{cm\,s^{-1}}$ were excluded from subsequent analysis in terms of percolation theory; their deviation from fractal scaling was determined by other factors (see text)

Fig. 7.15 that these soils also exhibited the largest values of θ_d relative to the regression equation. Although R^2 for the correlation between θ_d and θ_t rose to 0.94 after soils with low K values were excluded from the analysis, for reasons other than the proximity to the percolation transition, the intercept remained unchanged at 0.06. After the development of Eq. (5.21) for the relationship between θ_{xK} and θ_t [9] we could interpret θ_d as θ_{xK}. Indeed it turns out that if the mean values $D_p = 2.857$ and $\phi = 0.394$ for the Hanford site soils are inserted into Eq. (5.21), one finds $\theta_{xK} - \theta_t = 0.06$ [16]. The equivalence of these two numerical values implies that the conclusions for the subset of soils investigated in Sect. 7.2 would likely apply to most of the data set of 43 soils.

The implication of the study as a whole was that *all of the deviations from fractal scaling* of the water-retention curve could be attributed to lack of equilibration, i.e., values of $K(\theta)$ which were too low to allow the equilibrium change in water content actually to occur. Not all soils had low values of $K(\theta)$ for the same reason, but for a large number of the soils the cause was the approach to the percolation transition. This question is further discussed in the last portion of this chapter.

The development of this regression of θ_d on θ_t had an added benefit. It was now possible to calculate A/V from Eq. (7.12) for the McGee Ranch soil and North Caisson soils [16], and to use the same regression to predict their values of θ_t. Using the values of θ_t it became possible to predict the hydraulic properties of those two soils without use of adjustable parameters (Figs. 5.1 and 5.2). Of course the same regression could have been used for any of the individual soils in this study for the same purpose (and was), but there was a limited use for those predictions since the data for the hydraulic conductivity as a function of saturation for the remaining 43 soils was not made available to us. Nevertheless, those calculations were then used to predict $K(\theta_d)$ as shown above, and to exclude from analysis those soils for which $K(\theta_d) < 5 \times 10^{-8}\,\mathrm{cm\,s^{-1}}$.

Some important additional comments need to be made. The fact that the critical moisture content for percolation of the Hanford site soils (usually small clay contents) correlated quite well with the value from the Danish soils [15], and their often rather high clay contents will have several consequences for further analysis of the predictability of θ_t. It may be important, however, that the Hanford site soils often had 3–5% clay-sized particles and only in rare cases up to 10% or so.

7.4 Wet-End Deviations from Fractal Scaling of Water-Retention Curves, and Discussion of the Critical Volume Fraction for Percolation

In most cases the fractal predictions of water-retention curves also deviate from experiment at water contents near saturation. These deviations involve predictions of the water content that can be either too high (Fig. 7.17) or too low (Fig. 7.18). Understanding of these deviations is at present inferior to that of the deviations at low moisture contents, although it appears that on the whole such discrepancies relate

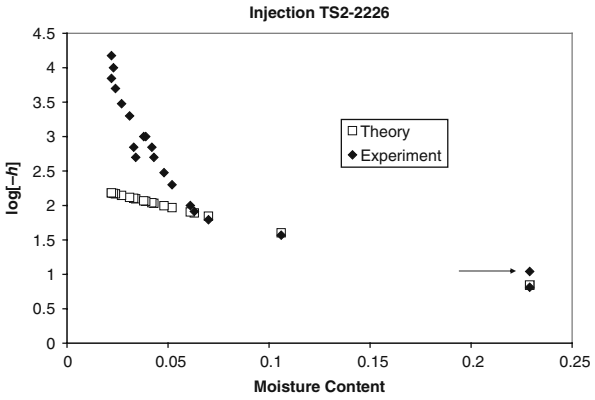

Fig. 7.17 An example of a wet-end deviation to higher moisture contents than predicted from fractal scaling. The solid diamonds are again data from Freeman [29], while the open squares are from Eq. (3.22). This deviation is predicted by percolation theory from the inability of air to enter the system until the air-allowable pore space percolates

to lack of percolation of the air phase. In Fig. 7.19 the determination of the wet-end moisture contents, θ_w, at which deviations from fractal scaling occurred, is shown. Hunt and Gee [19] showed that, for a suite of approximately 40 Hanford site soils θ_t was the same as, or slightly larger than, $\phi - \theta_w$, though perhaps slightly larger (Fig. 7.20). The case where a higher tension must be reached than h_A before air actually begins to enter the soil, with consequent upward curvature of the water-retention curve exceeding the prediction from fractal scaling, could be reasonably

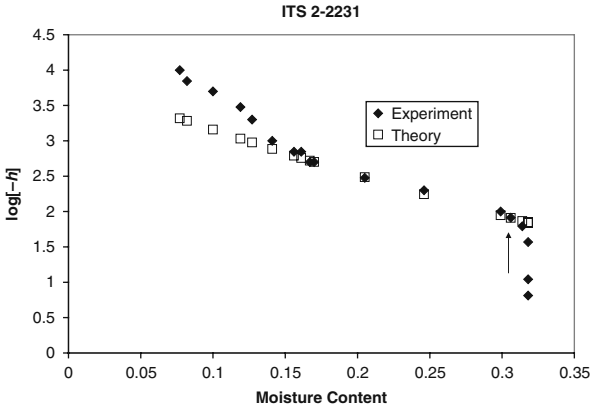

Fig. 7.18 An example of a wet-end deviation to lower moisture contents than predicted from fractal scaling. This deviation could be explained by the existence of soil structure, since it would allow air into the air-allowable textural pores and since some of the pore space would be structural pores, not accounted for by the particle size data. But the Hanford site soils, with low clay content and extremely low organic content, are not known for exhibiting structure

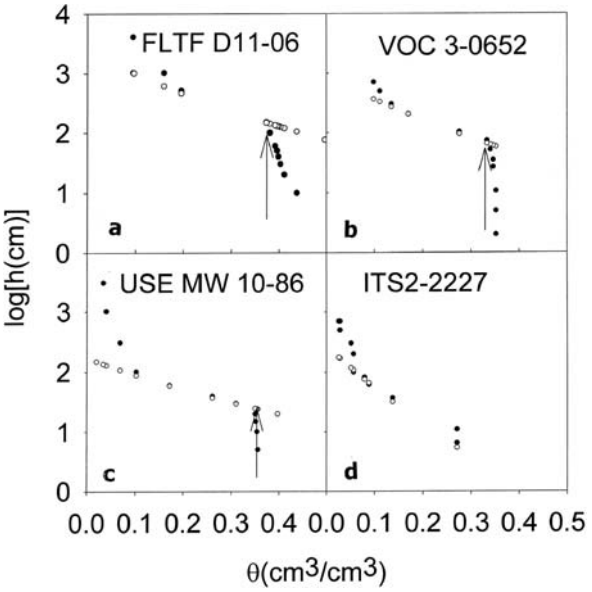

Fig. 7.19 From Hunt and Gee [19]. Determinations of wet-end moisture contents θ_w at which deviation from fractal scaling of water retention occurs for four soils. The *open circles* are theory (from Eq. (3.22)), the solid circles experiment. The fractal dimensionality for the pore space was determined in Hunt and Gee [14] from the particle-size distribution and the porosity, and the air-entry head (h_A) was used as an adjustable parameter. The wet-end deviations from fractal scaling are indicated with *arrows*. Two soils from Hunt and Gee [14] are used for which the wet-end deviation could clearly be seen, FLTF D11-06 (Fig. 7.19a) and VOC 3-0652 (Fig. 7.19b). For a number of the ITS soils, such as 2-2227 shown here, θ_w was better determined from the bubbling pressure by the method of problem 1.1

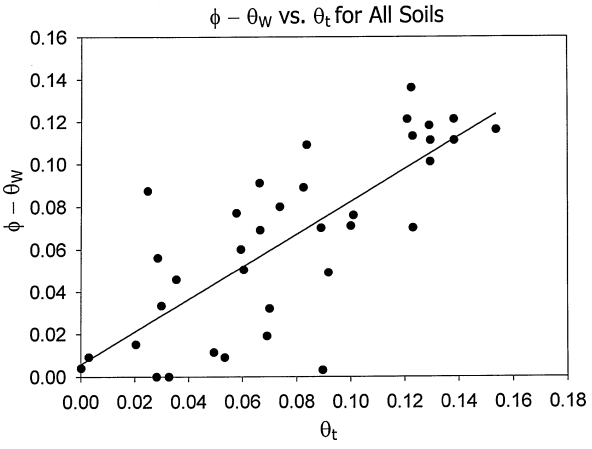

Fig. 7.20 Comparison for the Hanford site soils of θ_t, determined from θ_d using Eq. (5.21) with $\phi - \theta_w$, the wet end deviation from fractal scaling. θ_w determined as in Fig. 5.16

interpreted using percolation concepts. In some of these soils the actual value of θ_w could not be determined directly but was calculated by the method presented in problem 1.1. But the case where air entered at lower tensions than expected was less easy to interpret. Finite size effects allow some air to enter from the sides of the system, but this merely reduces the excess upward curvature described above. Soil structure, i.e., the existence of large pores unrelated to the particle dimensions, is frequently considered to be a cause of air entering at lower tensions than expected, and the logic is correct. However, such structure is normally associated with agricultural soils, which contain higher clay contents than the typical Hanford site soils, and almost certainly higher organic contents. Arid land soils like the Hanford site soils are not normally considered good candidates for soil structure, and this explanation may not be applicable. As mentioned above, a reanalysis of Wilkinson's arguments using continuum percolation theory and in the context of the possibility of the existence of structural pores would be advantageous here.

The result that $\phi - \theta_w$ for the Hanford site soils is very nearly the same as θ_t raises the question of whether one should actually expect the critical volume fraction to have the same value for air as for water. If the effects of wetting of surfaces are neglected then it is possible for the two critical volume fractions to be the same. But this is not a sufficient condition for equality. One must also have that the critical moisture content for percolation be independent of the moisture content. While this is not by any means guaranteed by theory, experiment appears to confirm that θ_t is a constant, independent of moisture content (see the results for solute diffusion in Chap. 6). The effects of water adsorbed to surfaces would be minimized when the surface area to volume ratio of the soil is minimized, which would be the case for porous media composed mainly of large particles. Clay minerals, due to their lack of charge neutrality, are known to adsorb an especially large amount of water. Practically speaking, media with very low or zero clay content (sand and silt only) have relatively small surface area to volume ratios, and in these media the fraction of the water adsorbed on surfaces can be neglected. So the result that θ_w for the Hanford site soils is very nearly the same as $\phi - \theta_t$ is consistent for media with low clay content, but the results of Moldrup et al. [15] for θ_t are interpreted in terms of the adsorption of water on clay mineral surfaces, providing an apparent conflict. An explanation for this puzzle may be given by a combination of the following argument for θ_t and the results that R^2 varied between 0.6 and 0.8 for the various correlations (and the fact that the Hanford sites do contain some clay).

How would one estimate the critical volume fraction for percolation in a porous medium with insignificant adsorption of water to solid surfaces? Consider first a network of tubes of uniform diameter and length placed on a lattice. The space between the tubes can be considered the solid portion of the medium. In such a case one can immediately deduce that the critical volume fraction for percolation must be

$$V_c = p_c \phi \tag{7.13}$$

and the critical volume fraction for percolation is a fraction of the porosity. Experimentally obtained values for very coarse soils [20] suggest that p_c in three dimensions is typically on the order of 0.1, and one finds $V_c = \theta_t \approx 0.1\phi$. For the proportionality constant to be so small requires a rather large coordination number for the pores, and it is also important that the pore space itself be well connected. There is some evidence of this; Manwart et al. [21] report that 97.2% of the pore space in the Berea sandstone and 99.4% in the Fountainebleau sandstone belong to the percolating cluster. In soils we expect these values to be higher. With increasing clay content, however, a simple proportionality between V_c and ϕ becomes inadequate [20]; either the proportionality constant p_c tends to increase, or another contribution to V_c must exist. Continued use of Eq. (7.13) with an increasing value of V_c is not preferred for several reasons [20]. A second contribution to V_c comes from water adsorbed on the surface of particles; this is a water content, which will be present, but which does not contribute to capillary flow. It is this contribution to $V_c (= \theta_t)$, which appears to have been detected in the diffusion experiments that established the relationship $D_{pm}/(D_w(\theta)) = 1.1(\theta - \theta_t)$. Analysis of the experimental relationship $\theta_t = 0.039(A/V)^{0.52}$ showed [20] that this could be interpreted as a surface water contribution on clay minerals as long as $3 - D \approx 0.5$. $D = 2.5$ is a rather small value from the present perspective, although it has been stated [22] that D values for clayey soils are typically in the range $2.5 - 2.6$ (in contrast to coarser soils).

On the basis of the above analysis it was concluded that a general expression for θ_t should probably contain both contributions and look something like

$$\theta_t - 0.1\phi \propto \left(\frac{A}{V}\right)^{3-D} \tag{7.14}$$

Theoretical development does not really permit an accurate estimation of the proportionality constant at present; one can also not use the experimental value from Moldrup et al. [15] since that experimental regression did not include a term independent of surface area. Thus it is best to leave the result (7.14) in terms of a proportionality. It is worthy of note that it is common in the porous media community to speak of a "residual" water content, present after normal drainage of a soil. Quoting Luckner et al. [23] by way of van Genuchten et al. (1991), based on Luckner et al., 1989, stated "The residual water content, θ_r, specifies the maximum amount of water in a soil that will not contribute to liquid flow because of blockage from the flow paths or strong adsorption onto the solid phase." Equation (7.14), with further developing and testing to clarify the values of the constants, should prove a general means to estimate both contributions to θ_t. It is very important, however, that only the term $p_c\phi$ would contribute to the critical air fraction for percolation, since air is not wetting and does not adsorb to the surface of any particles. Thus, except for very coarse soils, one should expect that the critical air fraction for percolation should be much smaller than the critical moisture content. But for coarse soils these two values should usually be very similar if not identical, as appears to be the case in Fig. 7.20.

Such a small value of $p_c \approx 0.1$ for a lattice model in three dimensions would imply that the effective coordination number, Z, is 15 [using $Zp_c = d/(d-1)$; Vyssotsky et al., 1961]. Even a face-centered cubic system has a value of Z of only 12, so this large value of Z suggests either that the typical coordination number is unexpectedly large or that there is a variation in coordination number with pore size. The latter possibility certainly seems logical; the largest pores must connect to more small pores than do small pores with large pores. Such a picture, however, has some defects. If the local Z value were a decreasing function of pore size, then θ_t might be expected to develop a dependence on moisture content. Also, it is not really consistent with a fractal picture. If one takes the fractal picture seriously, then Z should be independent of pore size, and we will present an argument in the final chapter as to why a self-similar medium should produce V_c independent of scale, but it is not clear that this argument also applies to the present case.

7.5 General Formulation for Equilibrium and Analogy to Ideal Glass Transition

Sections 7.2 and 7.3 demonstrate that reduction of the moisture content to values near the threshold moisture content for percolation can easily cause experiments involving changes in moisture content in porous media to fall out of equilibrium. This process can also be called a kinetic transition, because on one side of the transition, the system obeys the ergodic hypothesis, but on the other side it does not, whereas the transition point is not precisely defined on account of its dependence on the rate of change of system parameters, and thus on experimental conditions. A similar situation exists in the case of the glass transition in viscous liquids. As the temperature of viscous liquids is reduced, the temperature-dependent transport properties slow down so much that it may be impossible for the liquids to attain equilibrium with further reduction in temperature (on experimental time scales). All geologists are probably familiar with the argument that window glass will flow if given enough time (although the examples cited may not actually be evidence of this). Many investigators have sought to relate the glass transition in viscous liquids to a phase transition. What can be gained from a comparison between these systems and concepts?

In an ideal glass transition a kinetic transition is underlain by a structural phase transition, but the structural phase transition is never directly observed because the system falls out of equilibrium first. Since the result is never directly observed, one cannot measure directly a transport quantity that is approaching zero. Thus people look for some length scale, which seems to be diverging in the vicinity (but slightly below) the kinetic transition. Exactly this kind of result (Sect. 2.2) and the accompanying physics of a diverging correlation length, has now been obtained for porous media, and the accompanying predictions regarding lack of equilibration apparently verified. Although similar evidence has been sought regarding the glass transition in viscous liquids, it has never been found, and so it must be concluded that the

glass transition in viscous liquids is not an example of an ideal glass transition [24]. Nevertheless there is some benefit in a comparison, particularly in the matter of the calculation of such a kinetic transition point. The transition point corresponds to a temperature in the case of the glass transition, and a moisture content for porous media.

The "kinetic" transition in viscous liquids is basically a case where the system falls out of equilibrium and the ergodic hypothesis fails. The kinetic transition has been defined to result when the time for mechanical relaxation exceeds 100 s [24]. This is an imprecise definition and cannot be appropriate for all experiments. The mechanical relaxation time is an exponential function of the temperature, and relaxation times can thus increase very rapidly when the temperature is lowered, if it is low relative to the fundamental scale of the exponential function to begin with. In fact such an exponential dependence of the mechanical relaxation time on temperature allows for a definition of the transition temperature.

In experiments on the glass transition the system is cooled at a constant rate, and at a given temperature, called the glass transition temperature, T_g, there is a sudden drop in the heat capacity of the system. For the calculation of T_g [25–27] a constant cooling rate was represented as a staircase function with finite changes in temperature ΔT in times Δt. The average slope $\Delta T/\Delta t$ was constrained to equal the actual dT/dt. The glass temperature was found by relating the temperature steps ΔT to the time steps Δt through the condition that the relaxation time of the system increases by Δt over the temperature range ΔT. The solution of this equation could be obtained by numerical methods if the dependence of the relaxation time (α-relaxation peak) on the temperature was known. The result could be verified to give the correct dependence of T_g on the cooling rate, even though this dependence was very weak (logarithmic). Thus, even in the absence of an assumption of a special value of T, for which motion was essentially frozen, the rapid slowing down of systems represented by the exponential function was sufficient to define a kinetic transition temperature, T_g.

In the actual calculation of the transition moisture content we approximate a discontinuous function, the discrete changes, Δh, in tension over discrete time intervals, Δt, by a continuous function [9], exactly the reverse of the situation for the glass transition. This approximation allows a simple application of the chain rule to relate theoretical and experimental quantities. Consider an experiment on a column of height z. If the required value of $d\theta/dt$ is larger than the ratio of $K(h)$ to z ((cm/s)/cm), the column moisture content cannot change rapidly enough to adjust. But the required value of $d\theta/dt$ is related to experimental quantities as follows [9]:

$$\frac{d\theta}{dt} = \frac{dh/dt}{dh/d\theta} \equiv \frac{\Delta h/\Delta t}{dh/d\theta} = \frac{K(h)}{z} \tag{7.15}$$

If, through a procedure during which the tension h is increased episodically by Δh and a subsequent time interval Δt is allowed for drainage, $K(h)$ has finally diminished to the extent that the right-hand side can no longer exceed the left-hand side of Eq. (7.15), then the time scale of the experiment must be increased, or the system will fall out of equilibrium. Equation (7.15) can easily be solved for the time

interval, Δt, as a function of $K(h)$, z, and the derivative $dh/d\theta$ while $dh/d\theta$ can be obtained from the appropriate equilibrium water-retention function.

It may be of interest that while the glass transition in viscous liquids is apparently not an example of an ideal glass transition, the drying of porous media is.

7.6 Oil Residuals

In the early 1980s Chandler et al. [28] produced a very nice analysis of 2D simulations of residual oil ganglia remaining after flooding with water. The total oil remaining was a function of the width, y, of the channel flooded. We believe that it is a valuable exercise to bring up these results again and discuss them from a different perspective. The total oil remaining must, in two dimensions, be present only in finite clusters of sites, since it is not possible for both the water and the oil phase to percolate simultaneously. If one sums all the finite cluster contributions (of size less than $y = r_s = s^{\sigma\nu}$) to the oil volume one finds

$$V_{\text{oil}} \propto \int_1^{y^{\frac{1}{\sigma\nu}}} s^1 s^{-\tau} ds = 1 - y^{\frac{2-\tau}{\sigma\nu}} \tag{7.16}$$

Using Eq. (1.25), $(\tau - 2)/\sigma = \beta$ one finds that the remaining oil volume must scale as $V_c - y^{-\beta/\nu}$, in agreement with the scaling results of Chandler et al. [28] and with finite-size scaling. Consider that the fraction of sites connected to the infinite cluster is $(p - p_c)^\beta$, which implies a scaling with system size, $y^{-\beta/\nu}$. But the sites not connected to the infinite cluster are those (oil-filled) sites left, $\propto V_c - y^{-\beta/\nu}$.

Problems

7.1. Calculate the "bubbling pressure" for a fractal model. Assume that air does not begin to enter (bubble) until the air-allowable volume is a large-enough fraction of the porosity to percolate.

7.2. It is a common practice in the porous media community to assume that the interfacial tension is a more fundamental variable than the moisture content. Find a reason why people might assume this. Hint: use the bubbling pressure result from problem 1.1 and then calculate the pressure at which the water phase would become discontinuous. Assume that both critical volume fractions are 0.1ϕ. You should obtain a ratio for the two pressures of $[(1-0.9\phi)/(1-0.1\phi)]^{1(/3-D)} \approx (1-\phi)^{1/(3-D)}$. For typical soils $(D = 2.8, \phi = 0.4)$ this ratio is 1/7.6 (the approximation yields 1/12.9). Of course this ratio is smaller than the ratio of the smallest to the largest

pore size, and thus typical pressure saturation curves do not, in the intermediate saturation regime, contain the full range of pore sizes present.

7.3. Reevaluate the Wilkinson [1] treatment of hysteresis using moisture content as the fundamental percolation variable rather than the pressure. Do his conclusions still hold? What physics could be responsible for the discrepancies between the modified theory and the experiment?

7.4. Compare the present derivation of oil residuals with the treatment of Chandler et al. [28]. What does the comparison say about scaling arguments from percolation theory?

References

1. Wilkinson, D., 1986, Percolation effects in immiscible displacement, *Phys. Rev. A* **34**: 1380–1391. 208, 230
2. Gist, G. A., A. H. Thompson, A. J. Katz, and R. L. Higgins, 1990, Hydrodynamic dispersion and pore geometry in consolidated rock. *Phys. Fluids A*. **2**: 1533–1544. 208
3. Clement, E., C. Baudet, and J. Hulin, 1985, Multiple scale structure of non wetting fluid invasion fronts in 3d model porous-media. *J. Phy. Lett.* **46**(24): 1163–1171. 208
4. Lenhard, R. J., J. C. Parker, and J. J. Kaluarachchi, 1991, Comparing simulated and experimental hysteretic 2-phase transient fluid-flow phenomena. *Water Resour. Res*. **27**: 2113–2124. 208, 210
5. Lenhard, R. J., 1992, Measurement and modeling of 3-phase saturation pressure hysteresis, *J. Contam. Hydrol*. **9**: 243–169. 208, 210
6. Heiba, A. A., M. Sahimi, L. E. Scriven and H. T. Davis, 1982, Percolation theory of two-phase relative permeability, *SPE Reservoir Eng*. **7**: 123–132. 208, 211
7. Wilkinson, D., and J. Willemsen, 1983, Invasion percolation: a new form of percolation theory, *J. Phys. A: Math. Gen*. **16**: 3365–3376. 208
8. Sahimi, M., and Y. C. Yortsos, 1990, Applications of fractal geometry to porous media: a review, Paper presented at the 1990 Annual Fall Meeting of the Society of Petroleum Engineers, New Orleans, LA. 208
9. Hunt, A. G., 2004, Continuum percolation theory for water retention and hydraulic conductivity of fractal soils: 2. Extension to non-equilibrium, *Adv. Water Resour.* **27**: 245–257. 209, 210, 222, 228
10. Bauters, T. W. J., D. A. DiCarlo, T. S., Steenhuis, and J.-Y. Parlange, 1998, Preferential flow in water-repellent sands, *Soil Sci. Soc. Am. J*. **62**: 1185–1190. 210
11. Hunt, A. G., and T. E. Skinner, 2005, Hydraulic conductivity limited equilibration: effect on water-retention characteristics, *Vadose Zone J.* **4**: 145–150. 213, 214, 215
12. Rieu, M., and G. Sposito, 1991, Fractal fragmentation, soil porosity, and soil water properties I. Theory, *Soil Sci. Soc. Am. J*. **55**: 1231. 215
13. Blank, L. A., A. G. Hunt, and T. E. Skinner, 2008, A numerical procedure to calculate hydraulic conductivity for an arbitrary pore size distribution, *Vadose Zone J.* **7**: 461–472. 215
14. Hunt, A. G., and G. W. Gee, 2002, Water retention of fractal soil models using continuum percolation theory: tests of Hanford site soils, *Vadose Zone J*, **1:** 252–260. 219, 220, 224
15. Moldrup, P., T. Oleson, T. Komatsu, P. Schjønning, and D. E. Rolston, 2001, Tortuosity, diffusivity, and permeability in the soil liquid and gaseous phases. *Soil Sci. Soc. Am. J*. **65**: 613–623. 219, 220, 222, 2
16. Hunt, A. G., 2004, Percolative transport and fractal porous media, *Chaos Solitons Fractals* **19**: 309–325. 220, 222
17. Khaleel, R., and J. F. Relyea, 2001. Variability of Gardner's alpha for coarse-textured sediments. *Water Resour. Res.* **37**: 1567–1575. 221

18. Khaleel, R., and E. J. Freeman, 1995. Variability and scaling of hydraulic properties for 200 area soils, Hanford site, Westinghouse Hanford Company Report WHC-EP-0883. 221
19. Hunt, A. G., and G. W. Gee, 2003, Wet-end deviations from scaling of the water retention characteristics of fractal porous media, *Vadose Zone J.* **2**: 759–765. 219, 220, 221, 223, 224
20. Hunt, A. G., 2004, Continuum percolation theory for water retention and hydraulic conductivity of fractal soils: 1. Estimation of the critical volume fraction for percolation, *Adv. Water Resour.* **27**: 175–183. 226
21. Manwart, C., S. Torquato, and R. Hilfer, 2000, Stochastic reconstruction of sandstones. *Phys. Rev. E* **62**: 893–899. 226
22. Bittelli, M., G. S. Campbell, and M. Flury, 1999, Characterization of particle-size distribution in soils with a fragmentation model. *Soil Sci. Soc. Am. J*. **63**: 782–788. 226
23. Luckner, L., M. Th. van Genuchten, and D. R. Nielsen, 1989, A consistent set of parametric models for the two-phase flow of immiscible fluids in the subsurface, *Water Resour. Res*. **25**: 2187–2193. 226
24. Hunt, A., 1993, A general treatment of 1-dimensional hopping conduction, *Sol. State Commun*. **86**: 765–768. 228
25. Hunt, A. 1991, Transport in ionic conducting glasses, *J Phys Condens Matter* **3**(40): 7831–7842. 228
26. Hunt, A., 1991, The calorimetric glass transition: a simple model, *Phil. Mag. B* **64**, 563–567. 228
27. Hunt, A., 1991, One-dimensional hopping conductivity calculations, *Phil. Mag. B* **64**: 327–334. 228
28. Chandler, R., J. Koplik, K. Lerman, and J. F. Willemsen, 1982, Capillary displacement and percolation in porous media, *J. Fluid Mech*., **119**, 249–267. 229, 230
29. Freeman, E. J., 1995. *Fractal Geometries Applied to Particle Size Distributions and Related Moisture Retention Measurements at Hanford, Washington*, M. A. Thesis, University of Idaho, Moscow. 215, 219, 223

Chapter 8
Applications of the Correlation Length: Scale Effects on Flow

Even in the absence of geologic correlations, sedimentary deposits near the percolation threshold will exhibit correlations in medium type. One of the important arguments of the works that this chapter is based on has been that, under common circumstances, a relevant correlation length may be constructed as the product of a geologic factor and a statistical factor from percolation theory. In particular, the correlation length in percolation theory is proportional to a (negative) power of $|p - p_c|$ and a prefactor which, in a bond percolation problem, is proportional to the length of a bond. In a geologic medium described in continuum percolation theory, however, this quantity corresponding to a bond length is actually a geologic correlation length. How these two factors can be separated is discussed below.

The correlation length is the system-dependent parameter, which defines the structure of the dominant current-carrying (electric or fluid) paths. Refer back to Fig. 1.3. The typical separation of the nodes is represented in this figure, and this separation is equal to the correlation length, χ. The physical reason for this is that χ describes the size of the largest holes above the percolation threshold. Furthermore, the tortuosity of the backbone of the largest clusters below the percolation threshold is the same as the tortuosity of the links above the percolation threshold. The influence of the blobs in calculating the conductivity is rather secondary since the most resistive elements that cannot be avoided tend to be found in the portions of links without blobs – by definition there is no alternative to the paths through these (except, in the case of critical path analysis, to go to more resistive elements). In fact, as just suggested, χ can be used to describe the structure of such paths in two different contexts: (1) near the percolation transition it gives a characteristic separation of the only possible paths of interconnected medium, which can be used to transport, e.g., air, water, or electrical current, (2) *far from the percolation threshold*, application of critical path analysis involves an optimization which leads to a calculation of the separation of the paths along which the *dominant* transport occurs. In either case, χ^3 is effectively the REV, because in each case χ defines the length scale of the heterogeneity relevant for transport. In earlier chapters critical path analysis was used to generate explicit expressions for the correlation length. As long as the numerical coefficient in the proportionality from percolation theory is not available, however, calculations using the correlation length cannot reliably yield precise numerical coefficients for specific systems so the results are given only in terms of

Hunt, A., Ewing, R.: *Applications of the Correlation Length: Scale Effects on Flow.* Lect. Notes Phys. **771**, 233–246 (2009)
DOI 10.1007/978-3-540-89790-3_8

system parameters. In this chapter some systems are treated for which there is little or no information regarding "microscopic" variability, and the expressions derived contain further unknown constants. Thus the development here is only diagnostic and not predictive. In Chap. 4 an example of this type of argument (originally due to Shklovskii and Efros [1]) is given in the problems with an at least semiquantitative prediction.

8.1 Isolation of Geologic and Percolation Effects on a Correlation Length

We propose that the percolation and geologic effects on a correlation length can be isolated as follows. The research ideas presented in this section have been developed in parallel with Dr. Robert Ritzi and coworkers, and citations to their relevant articles are given.

Consider first a medium which contains a small fraction of sands ($< 25\%$, say) and for which the remainder is composed of finer materials, such as muds. Even though $p < 0.25$ it is nevertheless not unlikely that the sand fraction of the medium is near the percolation threshold. Percolation thresholds tend to be lowered in strongly correlated systems [2, 3]. Geologically correlated systems are typically characterized by anisotropy while local correlations tend to make the system smaller in a statistical sense. Both anisotropy [4] and small system size [5, 6] tend to reduce p_c.

Discretize a representation of a natural medium in cubic grid blocks. Choose each grid as sand or mud, associating the label chosen with the dominant volume fraction in each block. In one dimension, the percolation probability is one so that in a 1D transect the sand fraction is far below the percolation threshold, and even the mud fraction is not close. Suppose then that one considers the statistics of 1D transects through such a medium. The correlations of the individual grid cells will be at most minimally affected by the percolation variables, so that any correlations are geologic in nature. If the geologic correlation structure is appropriate (for example, exponential rather than power law in form), these correlations will be described by a typical length scale [7, 8], which we can call here, χ_0, and which has insignificant influence from percolation. The composite correlation length in the 3D medium will then be given by the product of a geological factor, χ_0, and a percolation function, $|p - p_c|^{-\nu}$.

8.2 Effects of Dimensional Crossovers on Conductivity

A great deal of debate surrounds the issue of whether the hydraulic conductivity can increase with the scale of the measurement. Given the fact that experiment has repeatedly given such results, it seems obvious that the answer is yes. But this does not seem to be the answer from percolation theory. To some this is the

major unsolved problem in subsurface hydrology. A few of the examples often quoted are Bradbury and Muldoon [9], Schad and Teutsch [10]; Shouse et al. [11]; Rovey and Cherkauer [12]; Sanchez-Villa et al. [13]; Schulze-Makuch [14]; Tidwell and Wilson [15, 16]; Schulze Makuch and Cherkauer [17]; Samper-Calvete and Garcia-Vera [18]; Schulze-Makuch et al. [19]; Davy et al. [20], Paleologos et al. [21]; Di Federico and Neuman [22, 23], Di Federico et al. [24]; Hunt [25, 26]; Chen et al. [27], Martinez-Landa et al. [28]; Zhang et al. [29]; Zlotnik et al. [30]; Hyun et al. [31]; Neuman and Di Federico [32]. Of the above, all publications except that of Shouse et al. [11] deal with geologic scales. Some authors have contested some of the individual experiments (e.g., Butler and Healey [33]) and some authors have certainly reported theoretical descriptions for which K diminishes with increasing scale [21]. In Chap. 9 it is shown that the cluster statistics of percolation theory are clearly compatible only with a diminishing value of K with increasing measurement scale. Nevertheless we feel that it is necessary to discover why measurements of the hydraulic conductivity can increase with increasing scale.

Of the above works, Davy et al. [20] and Neuman and coworkers look for theoretical reasons to generate an increase in K with the scale of measurement. The works of Neuman and coworkers are largely based on information from variograms, considered in Chapter 9, and a concrete comparison between those works and percolation theoretical works does not yet exist. Davy et al. [20] propose an increase in connectivity with increasing scale, but their model appears to generate a porosity which increases according to a power of the measurement scale x. There is nothing wrong per se with a porosity which increases with scale; the Rieu and Sposito [34] fractal model would allow an increase of the form $1-(r_0/x)^{3-D_p}$, if the largest pore radius, r_m, could be proportional to the system size, x. However, a power-law form for the porosity can exceed 1, while the Rieu and Sposito [34] model is limited by $\phi = 1$. This matter becomes partly semantic; it makes some sense to declare that a sample which falls entirely within a given pore (or fracture) does not belong to the medium when the property of interest is the porosity. But it makes no sense to exclude such a region from the hydraulic conductivity. Why? A region of air that surrounded an instrument would not be considered part of a solid medium, but the hydraulic properties of that medium are defined exclusively by the pore space and to leave out the largest pores at the smallest scales is to introduce a scale-dependent bias into the measurement.

There are other reasons for an apparent increase in K with scale x that can be easily discovered within the framework of percolation theory (and one example is given below), but it turns out that such results are not indicative of a scale effect per se. Although the relevance of percolation theory to geologic scales has sometimes been called into question, the same general difficulties to describe the flow and transport in such media exist, e.g., flow channeling [35], which Shah and Yortsos [36] demonstrate is also best treatable in a framework such as that of Katz and Thompson's [37] critical path analysis.

The fact that critical values of the percolation probability, p_c, are such strong functions of dimensionality, together with the fact that for strongly disordered media the "upscaled" value of a conduction or flow property depends so sensitively on p_c means that a crossover in the dimensionality of conduction can produce a very large

effect in the effective transport (or flow) parameter. Thus it is of great importance to be able to identify what physical constraints on conduction lead to dimensional constraints. The important quantity to determine relates, as one might expect, to an REV, or in the language of percolation theory, to the correlation length.

When conduction is isotropic, the analysis is relatively simple and unsurprising. Consider first a cylindrical system, such as a heterogeneous wire. How thick can such a wire be before conduction along it is not 1D? The maximum thickness can be obtained by considering an infinitely large and equidimensional system of such material, calculating the correlation length (according to either problem above) and comparing χ with the diameter of the wire, d. If $d > \chi$, the system is not strictly 1D and increasing d values will eventually make the conduction of the system 3D. If $d < \chi$, however, for large lengths, the cylinder exhibits strictly 1D conduction. As an alternative, consider an infiltration experiment, in which a grid is mapped out and metallic plates each some specific length, such as 1 m, are inserted into the soil to divide it into a simple square grid [11]. How small can the separation of these plates be made while maintaining 3D conduction in the vertical direction? Again the answer is based on the comparison of the separation of the dividing plates with the correlation length. However, the depth of insertion of the plates is also an important input. Even if the separation of the plates is smaller than the correlation length, if the depth is equally small (for isotropic conduction), the problem involves only finite-size effects, not dimensionality effects. Such a simple picture is complicated by anisotropy, but it is nevertheless possible to take a number of anisotropic systems and transform the medium to isotropic form [38]. Such a coordinate transformation affects the volumes of existing or proposed experiments as well, however, and then the problem is to analyze the transformed experimental volumes in terms of the correlation length.

In fact, any of the sort of problems dealt with in this chapter in terms of the correlation length can also be treated in greater depth using the cluster statistics of percolation in subsequent chapters. Nevertheless, when it is possible to make a simple calculation based on the correlation length, the labor saved may be well worth the choice.

For conduction through a rectangular solid to be truly 3D, all dimensions of the solid must be larger than the correlation length, χ. For solid-state physics treatments of the dimensionality of conduction in terms of the correlation length see Shklovskii and Efros [1] and Raikh and Ruzin [39]. In three dimensions χ behaves as

$$\chi = \chi_0 (p - p_c)^{-\nu} \tag{8.1}$$

where $\nu = 0.88$ [40]. Here χ_0 is a fundamental length, which we take here as being a typical length of a single resistor. An appropriately shaped volume, which is in principle compatible with experiments for treating upscaling in isotropic 3D systems, is a cube. As Tartakovsky and Neuman [38] point out, the axes of anisotropic systems can be rescaled to give equal conductances in each direction. The appropriately shaped upscaling volume for an anisotropic system with, e.g., K values 1000 times larger in the horizontal directions is a rectangular solid with equal horizontal

dimensions, but a vertical dimension $1000^{1/2} \approx 31$ smaller [41]. The cross-sectional area on the sides is diminished by a factor $1000^{1/2}$, reducing its conductance accordingly, while the length of the vertical dimension is diminished by the same factor, increasing its conductance by the same factor. This leaves equal conductances in each dimension. The reason why such a "flattened cube" is the appropriate system shape for upscaling is that the fundamental relationships of the system dimensions to the details of the conduction process cannot change differently in different directions as the scale of the problem is increased. Use of, e.g., a cubic volume for the purposes of scaling up the hydraulic conductivity in the presence of such anisotropy would be equivalent, in the isotropic case, to using a prism with long (vertical) axis 31 times as long as the horizontal axes (Fig. 8.1 from Hunt [41]). In such a case it is easily possible for the correlation length to be shorter than the vertical dimension and larger than the horizontal dimensions. This means that for vertical transport, the optimal flow would not be constrained to narrow volume. Constraining the flow to remain within the volume is a dimensional constraint. If all axes are subsequently lengthened by, say, a factor 31, certainly all dimensions will be larger than the correlation length, whereupon the flow would be 3D, with K as calculated for a 3D medium. This constitutes a change in dimensionality, from 1 to 3, that occurs as a result of the increase in scale, but is not a scale effect per se, since it could be eliminated by choosing the appropriate experimental volume shape.

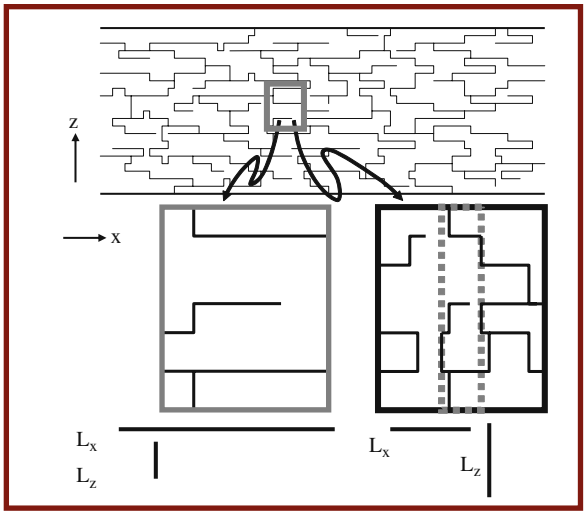

Fig. 8.1 A schematic depiction of a medium with much higher horizontal connectivity than vertical connectivity and the correlation lengths in each direction. A rescaling of length in the horizontal coordinates transforms the system to an isotropic system, but also shrinks the horizontal dimensions of the experimental volume. Now the correlation length is the same in each direction, but it is larger than the horizontal dimension of the experimental volume and smaller than the vertical dimension, providing for 1D conduction

Instead of considering the equidimensional anisotropic case, consider for clarity the transformed medium with elongated volume and isotropic K (Fig. 8.1). Rather than considering flow along the vertical axis to go through a qualitatively defined crossover from 1D flow to 3D, the method constructed here for solution of this problem is to choose a maximum R, such that the value of the correlation length, χ, is always constrained to be smaller than or equal to the horizontal dimensions of the system. If χ is smaller than the horizontal dimensions, it is certainly smaller than the vertical dimension. This gives a continuous dependence of the effective value of the critical volume fraction and thus of the value of the limiting resistance on the size of the system. In the limit that the system size goes to infinity, this constraint becomes inconsequential and the result must conform to the 3D value of K. In the limit of small system size, p_c must approach 1 and the result for K must conform to the value for 1D flow. χ is constrained to be smaller than the dimensions of the system by the simple matter of making an effective p_c larger than the 3D value, exactly as expected from restricted dimensionality. In such a case the flow paths may appear to be 3D at all scales, but the changing value of p_c is a result of the dimensional crossover. So now let $\chi = x = V^{1/3}$, the original system size, and calculate how much larger p would have to be than p_c for a given x. The result is [41].

$$p = p_c + \left(\frac{\chi_0}{x}\right)^{\frac{1}{\nu}}; \qquad V = V_c + \left(\frac{\chi_0}{x}\right)^{\frac{1}{\nu}} \tag{8.2}$$

where the second form of the equation is the equivalent form for a continuum with volume fraction, V, replacing p (and V_c replacing p_c). The reason why the second form of the equality can be used by analogy is that the correlation length, χ, is expressed in terms of V and V_c for continuum percolation in the same way that it is expressed in terms of p and p_c for bond percolation. Equation (8.2) obviously gives $V = V_c$ for a system of infinite size, $x \to \infty$. For calculations of finite size corrections, Eq. (8.2) implies $p > 1$ in the limit of $x < \chi_0$, an unphysical limit, which can be approximately corrected by a small change in Eq. (8.2) to [41]

$$V = V_c + \left(\frac{\chi_0}{\chi_x + x}\right)^{\frac{1}{\nu}} \tag{8.3}$$

The basis for this modification is the physical requirement that χ be less than $x + \chi_0$, rather than merely x, compensating for the finite separation of resistances arising from their own intrinsic length, χ_0. Such a modification is clearly unnecessary for large x, but, in order for the formulation to make sense at small x it must be added. Equation (8.3), while still approximate, leads to no significant problem with p exceeding 1 as long as $p_c(\alpha_c)$ is very small, as can be the case in highly correlated systems [2, 3], and is assumed to hold here. The limiting value, $p_c = 1$, for small system sizes is a characteristic of strictly 1D conduction, and means that the most resistive element in the system can no longer be avoided. Use of a formulation such as Eq. (8.3) to find the change in V_c for small system sizes has the potential defect that the proportionality for the correlation length is being used in a range where it need not be accurate, far from percolation.

We can apply Eq. (8.3) to the continuum percolation calculation of Rieu and Sposito [34]. The Rieu and Sposito [34] model has been variously applied to soil porosity and to fracture systems. The Rieu and Sposito [34] fractal fragmentation model for soils expresses the total porosity as $\phi = 1 - (r_0/r_m)^{3-D}$ in terms of the fractal dimensionality, D, and the minimum and maximum radii, r_0 and r_m, over which the fractal description holds. This model can also be used for fracture networks, but in this case r_0 and r_m refer to the smallest and largest fracture apertures, respectively. To calculate the rate-limiting resistance on the critical path one needs an expression for the fractional pore (or fracture) volume, $W(r)$, with pore radius (or fracture aperture) between r and $r+dr$, i.e., the pore volume probability density function. This expression is $W(r) = ((3-D)/r_m^{3-D})r^{2-D}$ [42], which yields the known porosity, assumed to be the same for the fracture application. In the fully 3D case, under saturated conditions, the Rieu and Sposito model yields for the smallest aperture, r_c, on the optimal system-traversing path,

$$V_c = \frac{3-D}{r_m^{3-D}} \int_{r_c}^{r_m} dr r^{2-D}; \qquad r_c = r_m (1 - V_c)^{1/(3-D)} \tag{8.4}$$

Note that in the limit $V_c \to 0$, $r_c \to r_m$, meaning that with a critical volume fraction of zero, percolation is possible just using the largest fractures. Applied to fracture networks, in which the solid medium is ignored, Eq. (8.4) is best rewritten [41],

$$V_c = \left[\frac{1}{1 - \left(r_0/r_m\right)^{3-D}}\right] \left[\frac{3-D}{r_m^{3-D}}\right] \int_{r_c}^{r_m} dr r^{2-D} \tag{8.5}$$

where a fraction V_c of the total fracture volume, $1 - (r_0/r_m)^{3-D}$ (rather than a fraction of the total system volume), is sufficient to guarantee percolation through the fractures.

In order to find out how the smallest pore size changes as the critical volume fraction approaches 1 (the fully 1D limit), substitute Eq. (8.3) in Eq. (8.5) with the new $V > V_c$ taking the place of V_c, and letting (for convenience and simplicity) the original $V_c \to 0$ for infinite system size,

$$\left(\frac{1}{1 - \left(r_0/r_m\right)^{3-D}}\right) \left(\frac{3-D}{r_m^{3-D}}\right) \int_{r_c}^{r_m} dr r^{2-D} = \left(\frac{\chi_0}{\chi_0 + x}\right)^{\frac{1}{v}} \tag{8.6}$$

Eq. (8.6) yields

$$r_c = r_m \left[1 - \left(1 - \left[\frac{1}{R}\right]^{3-D}\right) \left(\frac{\chi_0}{\chi_0 + x}\right)^{1/v}\right]^{\frac{1}{3-D}} \tag{8.7}$$

with $R \equiv r_m/r_0$. Using (for 3D saturated media) $K \propto r_c^2$, consistent with Hunt and Gee [42] (and Katz and Thompson [37], and in fact all the methods summarized by

Bernabe and Bruderer [43]), and expressing $K(x)$ in terms of the value $K(3D)$ for $x \to \infty$, valid in 3D one finds [41],

$$\frac{K(x)}{K(3D)} = \left[1 - \left(1 - \left[\frac{1}{R}\right]^{3-D}\right)\left(\frac{\chi_0}{\chi_x + x}\right)^{1/\nu}\right]^{\frac{2}{3-D}} \tag{8.8}$$

Because Eq. (8.8) is expressed as a ratio of $K(x)/K(3D)$, the complications arising from the fact that even in an infinite system p is slightly larger than p_c can be neglected, just as these same complications were neglected in the calculation of the ratio of the unsaturated to the saturated hydraulic conductivity.

It should be noted that the general framework of the calculation given here would not change if the values of the hydraulic conductivity in the vertical and horizontal dimensions were the same, but the correlations of the hydraulic conductivity in the horizontal direction were much larger than the vertical direction. Use of a correlation length-based treatment of a dimensional crossover would still be appropriate. Now the correlation length from percolation theory would be larger in the horizontal direction than in the vertical because the random selection of a highly conductive element in the horizontal direction would more likely (in comparison with the vertical direction) be associated with other highly conductive elements in the same direction too, not simply because most connections in that direction were larger. Such conditions could be consistent with horizontal layering of sedimentary facies.

Field data from Schulze-Makuch and Cherkauer [17] as well as some other sources [12] are nominally consistent with hydraulic conductivity proportional to power laws of the support volume, $K \propto V^m$, over 5–6 orders of magnitude of volume V and 3–5 orders of magnitude of K. Reported powers, m, range from 0.5 to nearly 1. Represented as $\log(K)$ vs. $\log(V)$, the data appear to curve toward the horizontal at very small V, and also flatten at large V. Fits with data have simply employed power laws with the above values of m for small V and a horizontal line representing a constant K at large V.

8.3 Comparison with Field Data

In Fig. 8.2 *all* scale-dependent data for K from Schulze-Makuch [14] are plotted as $\log K$ vs. $\log V$, where V is a water volume, assumed here to be proportional to the solid volume. The data from Schulze-Makuch [14] certainly incorporated fracture flow, at least at larger support volumes. To fit these data, $R = 2500$, $D = 2.98$, and $K(3D) = 0.007\,\mathrm{m\,s^{-1}}$ were chosen. This combination of R and D is consistent with a "fracture" porosity of $\phi = 0.14$. However, the result is quite insensitive to the chosen D, and values of 2.97 and 2.95 fit the data equally well. These are consistent with fracture porosity values of $\phi = 0.21$ and 0.32, respectively, meaning that the theory is not particularly sensitive to the value of the porosity chosen. The values of "vuggy" porosity for small *cores* quoted in Schulze-Makuch [14] are 9% or lower,

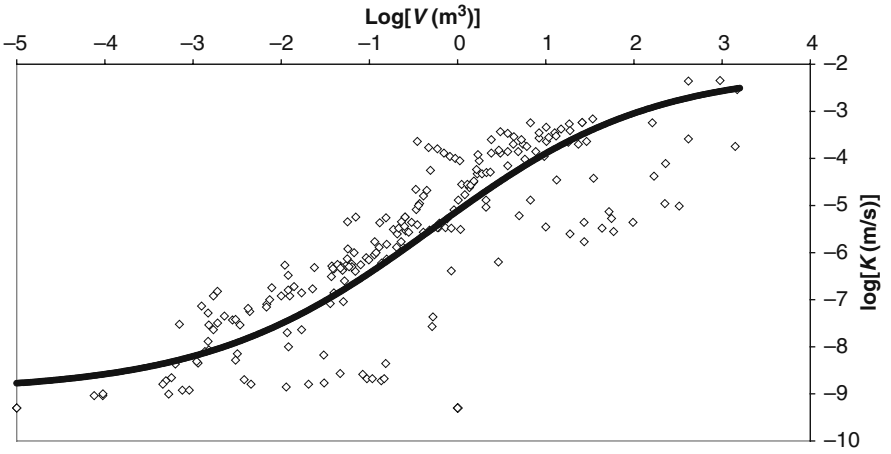

Fig. 8.2 Comparison of the prediction of Eq. (8.8) with the experimental data of Schulze-Makuch [14] for fracture networks in a carbonate aquifer. The experimental data are given by the open triangles. The parameters are $D = 2.98$ and $r_m/r_0 = 2,500$

though these values may account for 90% of the total core porosity in some cases. A "fracture" porosity is mentioned, but no values are given. The selected value of R implies that if the smallest fracture has an aperture of, e.g., 40 μm, the largest has an aperture of 10 cm. While this is certainly a large range, dissolution of fractured carbonates can produce fractures over a wide size range. Although most of the data do appear to fit the same trend, the comparison made here, which uses all the data simultaneously, may not be appropriate. If individual facies were analyzed separately, the range of K values, and thus ratios of r_m to r_0, would be smaller, consistent with smaller porosities.

The horizontal asymptotes in these graphs correspond to ensemble averages for pure 1D ($\alpha_c = 1$) and 3D (with vanishing critical volume fraction) conduction, respectively. The ratio of the values of K in these two asymptotes is, by construction, R^2. If a more realistic finite, but small, value of α_c were chosen, the ratio of the values of K at the asymptotes would be reduced somewhat, since $r_c(3D) < r_m$ in that case.

It is also possible to compare the values of these parameters with parameters from soils, to which the Rieu and Sposito [34] has been applied. Note that while $D = 2.95$ is larger than typical values quoted (closer to 2.8 for soils, Bittelli et al., 1999) [44], values as high as 2.95 have been reported in Hanford soils [45]. The associated porosity (with one exception) of the 45 Hanford soils ranged from $\phi = 0.24$ to $\phi = 0.54$, with the smaller ϕ values associated with the larger D values. Further, although $R = 5000$ is large, ratios of maximum to minimum pore sizes as high as 250 were described within centimeter-sized core samples for Hanford soils. A related implication is that the same physical mechanism as described here could generate a scale effect on K of over 4 orders of magnitude (up to 250×250) in Hanford soils with significant clay layers as well. See Sect. 11.4 for a treatment of such anisotropy in the Hanford subsurface.

If the present theoretical description forms the basis for the observed scale dependence of K in anisotropic porous media, then it is possible, *in principle*, to conduct experiments in the same media, which do not show a scale effect. The means to do this is to use experimental volumes with shapes elongated appropriately (by the square root of the ratio of K values) in the direction(s) of highest K values. Such experimental constructions are mathematically equivalent to isotropic media investigated with equidimensional support volumes, for which K diminishes with increasing size. The reason why K diminishes in that case is that the dimensional crossover with increasing system size described here is eliminated. This is a fundamental argument for associating the increase in K with the dimensional crossover rather than the increase in scale [41].

8.4 Effects of Hydrophobicity on Water Uptake of Porous Media

It has been regarded as puzzling that the existence of a few hydrophobic particles (ca. 5%) in a porous medium could prevent water uptake at negative pressures (thus preventing spontaneous uptake of water). The puzzle likely arises from an incorrect perspective. It is true that it does not seem reasonable that a fraction of hydrophobic particles as small as 3–5% could make an entire medium hydrophobic, but this perspective ignores the need to get the water into the medium. The water follows flow paths, whose separations are governed by the correlation length from percolation theory. *The fact that the pressure at which water normally enters the porous medium corresponds to the percolation transition* means that it is possible that a very small change in conditions can have a large effect on the flow paths.

Consider the following experimental arrangement [46]. From a large quantity of blasting sand a fraction was treated with cyclo-octanol, a chemical with extreme hydrophobic tendencies. This portion was then mixed in at various fractions from 1 to 8%. If the concentration of hydrophobic particles is N, and the typical diameter of the particles is d, then the typical separation of such particles must be approximately $(d)N^{-1/3}$. When water enters the medium the separation of the paths of water flow is equal to χ, which must be proportional to $d(\theta - \theta_t)^{-0.88}$. Use of the factor d acknowledges that a fundamental length scale proportional to the particle sizes must exist. Clearly water cannot access the major portion of the medium unless $\chi < (d)N^{-1/3}$, because otherwise it would be impossible to get the water between the hydrophobic particles. But such a small value of the correlation length can only be obtained when the moisture content (or allowed moisture content in the present case) is much larger than the critical moisture content for percolation.

Consider the following thought experiment. Start with a dry medium without hydrophobic particles and begin to decrease the tension, h. When h reaches h_c, defined in the previous chapter, water will begin to enter the medium. However, at this tension the infiltration paths are infinitely far apart. With a slight reduction in h, the path separation drops to, say, somewhere between one and ten per sample. If even a small fraction of the normal sand grains had been replaced by hydrophobic grains,

then these paths would have been interrupted and it would not be possible to bring water to the interior of the medium without running into hydrophobic grains. Water can be forced past hydrophobic grains at sufficiently large positive pressures, but in our case the pressure is still negative. So a further slight reduction in the magnitude of the pressure has little or no effect on the interaction of water with the hydrophobic grains, but it has a large effect on the separation of the infiltration paths, which becomes much smaller. This effect is very large because the value h_c corresponds to the percolation phase transition. If the value for the correlation length is equated to the separation of the hydrophobic particles one can calculate the smallest value of the effective moisture content, for which the infiltration path separation is small enough to wet the interior. If the value of the moisture content needed is as large as the porosity, then it would be impossible to wet the interior of the system without forcing water past individual hydrophobic grains, which requires a positive pressure. Thus

$$N^{-\frac{1}{3}} d \approx d\,(\phi - \theta_t)^{-0.88} \tag{8.9}$$

Solution of Eq. (8.9) for N (and using $\theta_t \approx \phi/10$) yields

$$N = (0.9\phi)^{2.64} \tag{8.10}$$

[47], which for typical porosities of about 0.4 yields about 0.067. In fact the Bauters et al. [46] sand from the previous section has porosity 0.4 and critical volume fraction 0.048, which would yield a slightly smaller value for N (0.063). Nevertheless one would expect that at a concentration of roughly 6% hydrophobic particles a typical soil would already become water repellent. Experiment shows that water repellency for the relevant soil from Bauters et al. [46] already sets on at a concentration of about 5.5% in a soil with porosity 0.4 and critical volume fraction approximately 0.04. Such a close agreement with experiment may be at this stage merely fortuitous, since all numerical constants in Eq. (8.9) have been suppressed. However, it is important that the predicted result, because of the 2.64 power, is much smaller than 1, and is more nearly on the order of 1–10%. Solution of the problem below should help to convince students that the theoretical description is indeed accurate.

Problem

8.1. Suppose you know experimentally the water imbibition curve for a hydrophilic medium (0% hydrophobic particles). Using the calculation above for the modification to the effective critical moisture content for percolation (and water uptake) due to the presence of hydrophobic particles, describe a technique, which would allow you to predict the imbibition curve for your system (with a prescribed fraction of hydrophobic particles). Use the results from Chap. 7 to predict the imbibition curve of any arbitrary medium (without hydrophobic particles) and then apply the procedure you just described to get a family of imbibition curves with varying fractions of hydrophobic particles. Compare your results with Fig. 7.2.

References

1. Shklovskii, B. I., and A. L. Efros, 1984, *Electronic Properties of Doped Semiconductors*, Springer, Heidelberg. 234, 236
2. Ioannidis, M. A., and I. Chatzis, 1993, The effect of spatial correlations on the accessibility characteristics of three-dimensional cubic networks as related to drainage displacements in porous media, *Water Resour. Res*. **27**: 1777. 234, 238
3. Prakash, S, S. Havlin, M. Schwartz, and H. E. Stanley, 1992, Structural and dynamical properties of long-range correlated percolation, *Phys. Rev*. B **46**: R1724. 234, 238
4. Garboczi, E. J., K.A. Snyder, J. F. Douglas, and M. F. Thorpe, 1995, Geometrical percolation threshold of overlapping ellipsoids, *Phys. Rev. E 52*, 819–828. 234
5. Sahimi, M., 1993, Fractal and superdiffusive transport and hydrodynamic dispersion in heterogeneous porous media, *Transp. Porous Media 13*: 3–40. 234
6. Sahimi, M., 1993, Flow phenomena in rocks – from continuum models to fractals, percolation, cellular automata, and simulated annealing, *Rev. Mod. Phys.* **65**(4): 1393–1534. 234
7. Proce C. J., R. W. Ritzi, D. F. Dominic, and Z. X. Dai, 2004, Modeling multiscale heterogeneity and aquifer interconnectivity, *Ground Water* **42**: 658–670 234
8. Guin, A., and R. W. Ritzi, 2008, Studying the effect of correlation and finite-domain size on spatial continuity of permeable sediments, *Geophys. Res. Lett*. **35**: Article Number L10402. 234
9. Bradbury, K. R., and M. A. Muldoon, 1990, Hydraulic conductivity determinations in unlithified glacial and fluvial materials, In Nielson, D. M. and A. I. Johnson, eds., *Ground Water and Vadose Zone Monitoring*, ASTM STP 1053, 138–151 235
10. Schad, H., and G. Teutsch, 1994, Effects of the investigation scale on pumping test results in heterogeneous porous aquifers, *J Hydrology* **159**: 61–77. 235
11. Shouse, P. J., Ellsworth, T. R., and Jobes, J. A., 1994, Steady-State infiltration as a function of measurement scale, *Soil Sci*. **157**: 129–136. 235, 236
12. Rovey II, C. W., and D. S. Cherkauer, 1995, Scale dependency of hydraulic conductivity measurements, *Ground Water* **33**: 769–780. 235, 240
13. Sanchez-Villa, X., J. Carrera, and J. P. Girardi, 1996, Scale effects in transmissivity, *J Hydrol* **183**: 1–22. 235
14. Schulze-Makuch, D., 1996, Dissertation, Facies dependent scale behavior of hydraulic conductivity and longitudinal dispersivity in the carbonate aquifer of southeastern Wisconsin, University of Wisconsin, Milwaukee. 235, 240, 241
15. Tidwell, V. C., and J. L. Wilson, 1997, Laboratory method for investigating permeability upscaling, *Water Resour. Res*. **33**: 1067–1616. 235
16. Tidwell, V. C., and J. L. Wilson, 2000, Heterogeneity, permeability patterns, and permeability upscaling: physical characterization of a block of Massillon sandstone exhibiting nested scales of heterogeneity, *SPE Reserv Eval Eng.* **3**: 283–291. 235
17. Schulze-Makuch, D., and D. S. Cherkauer, 1998, Variations in hydraulic conductivity with scale of measurement during aquifer tests in heterogeneous, porous, carbonate rocks, *Hydrogeology J.* **6**: 204–215. 235, 240
18. Samper-Calvete, F. J., and M. A. Garcia-Vera, 1998, Inverse modeling of groundwater flow in the semiarid evaporitic closed basin of Los Monegros, Spain, *Hydrogeology J.* **6**: 33–49. 235
19. Schulze-Makuch, D., D. A. Carlson, D. S. Cherkauer, and P. Malik, 1999, Scale dependency of hydraulic conductivity in heterogeneous media, *Ground Water* **37**: 904–919. 235
20. Davy, P., O. Bour, C. Darcel, and J. De Dreuzy, 2002, Permeability of 2D multi-scale fracture networks, *Eos, Trans. AGU Abstract* H71B-0822, **83**(47). 235
21. Paleologos, E. K., S. P. Neuman, and D. M. Tartakovsky 1996, Effective hydraulic conductivity of bounded strongly heterogeneous porous media, *Water Resour. Res.*, **32**: 1333–1341. 235
22. Di Federico, V. and S. P. Neuman, 1997, Scaling of random fields by means of truncated power variograms and associated spectra, *Water Resour. Res*. **33**: 1075–1085. 235
23. Di Federico, V., and S. P. Neuman, 1998, Flow in multiscale log conductivity fields with truncated power variograms, *Water Resour. Res.*, **34**: 975–987. 235

24. Di Federico, V., Neuman, S. P., and Tartakovsky, D. M., 1999, Anisotropy, lacunarity, and upscaled conductivity and its autocovariance in multiscale random fields with truncated power variograms, *Water Resour Res* **35**: 2891–2908. 235
25. Hunt, A. G., 1998, Upscaling in subsurface transport using cluster statistics of percolation, *Transp. Porous Media* **30**(2): 177–198. 235
26. Hunt, A. G., 2003, Some comments on the scale dependence of the hydraulic conductivity in the presence of nested heterogeneity, *Adv. Water Resour.*, **26**: 71–77. 235
27. Chen, G., W. A. Illman, D. L. Thompson, V. V. Vesselinov, and S. P. Neuman, 2002, Geostatistical, type curve and inverse analyses of pneumatic injection tests in unsaturated fractured tuffs at the Apache Leap Research Site near Superior Arizona, 73–98, in Dynamics of Fluids in Fractured Rocks, edited by B. Faybishenko et al., Geophysical Monograph 122, AGU, Washington, DC. 235
28. Martinez-Landa, L., J. Carrera, J. Guimera, E. Vasquez-Suñe, L. Vives and P. Meier, 2000, Methodology for the hydraulic characterization of a granitic block, 340-345, in *Calibration and Reliability in Groundwater Modeling: Coping with Uncertainty*, ModelCARE 99, edited by F. Stauffer, W. Kinzelbach, K. Kovar and E. Hoem, IAHS Publication 265, IAHS Press, Wallingford, Oxfordshire, UK. 235
29. Zhang, D., R. Zhang, S. Chen, and W. E. Soll, 2000, Pore scale study of flow in porous media: Scale dependency, REV, and statistical REV, *Geophys. Res. Lett*., **27**: 1195–1198. 235
30. Zlotnik, V. A., B. R. Zurbuchen, T. Ptak, and G. Teutsch, 2000, Support volume and scale effect in hydraulic conductivity: experimental aspects, in: D. Zhang and C. L. Winter, eds., *Theory Modeling, and Field Investigation in Hydrogeology: A Special Volume in Honor of Shlomo P. Neuman's 60th Birthday*, Boulder, Colorado, Geological Society of America Special Paper 348, 191–213. 235
31. Hyun, Y., S. P. Neuman, V. V. Vesselinov, W. A. Illman, D. M. Tartakovsky, and V. DiFederico, 2002, Theoretical interpretation of a pronounced permeability scale-effect in unsaturated fractured tuff, *Water Resour. Res*. **38**: Article No. 1092. 235
32. Neuman, S. P., and V. Di Federico, 2003, Multifaceted nature of hydrogeologic scaling and its interpretation, *Rev. Geophys*. **41**: Art. No. 1014. 235
33. Butler, J. J., and J. M. Healey, 1998, Relationship between pumping-test and slug-test parameters: scale effect or artifact? *Ground Water* **36**: 305–313. 235
34. Rieu, M., and G. Sposito, 1991, Fractal fragmentation, soil porosity, and soil water properties I. Theory, *Soil Sci. Soc. Am. J*. **55**: 1231. 235, 239, 241
35. Moreno, L., and C. F. Tsang, 1994, Flow channeling in strongly heterogeneous porous media: A numerical study, *Water Resour. Res*. **30**: 1421. 235
36. Shah, C. B., and Yortsos, Y, C., 1996, The permeability of strongly disordered systems, *Phys. Fluids* **8**: 280–282. 235
37. Katz, A. J., and A. H. Thompson, 1986, Quantitative prediction of permeability in porous rock, *Phys. Rev*. *B* **34**: 8179–8181. 235, 239
38. Tartakovsky, D. M., and Neuman, S. P., 1998, Transient effective hydraulic conductivity under slowly and rapidly varying mean gradients in bounded three-dimensional random media, *Water Resour. Res*. **34**: 21–32. 236
39. Raikh, M. E., and I. P. Ruzin, 1990, Size effect of the longitudinal hopping conduction of a narrow 2-dimensional channel, *Phys. Rev. B* **42**: 11203–11207. 236
40. Stauffer, D., and A. Aharony, 1994, *Introduction to Percolation Theory*, 2nd edition, Taylor and Francis, London. 236
41. Hunt, A. (2006). Scale-dependent hydraulic conductivity in anisotropic media from dimensional cross-over. *Hydrogeology J*., **14**(4): 499–507. 237, 238, 239, 240, 242
42. Hunt, A. G., and G. W. Gee, 2002, Application of critical path analysis to fractal porous media: comparison with examples from the Hanford site, *Adv. Water Resour.*, **25**: 129–146. 239
43. Bernabe, Y., and C. Bruderer, 1998, Effect of the variance of pore size distribution on the transport properties of heterogeneous networks, *J. Geophys. Res*., **103**: 513. 240
44. Bittelli, M., G. S. Campbell, and M. Flury, 1999, Characterization of particle-size distribution in soils with a fragmentation model. *Soil Sci. Soc. Am. J.* **63**: 782–788. 241

45. Hunt, A. G., and G. W. Gee, 2002, Water retention of fractal soil models using continuum percolation theory: tests of Hanford site soils, *Vadose Zone J*, **1**: 252–260. 241
46. Bauters, T. W. J., D. A. DiCarlo, T. S., Steenhuis, and J.-Y. Parlange, 1998, Preferential flow in water-repellent sands, *Soil Sci. Soc. Am. J*. **62**: 1185-1190. 242, 243
47. Steenhuis, T., A. G. Hunt, J.-Y., Parlange, and R. P. Ewing, 2005, Assessment of the application of percolation theory to water-repellent soils, *Aust. J Soil Res*. **43**: 357–360. 243

Chapter 9
Applications of the Cluster Statistics

9.1 Spatial Statistics and Variability of K from Cluster Statistics of Percolation Theory

This chapter presents a conceptually straightforward treatment of spatial correlations of "random" heterogeneous media, but does not intend to capture at this point even a majority of the actual behavior. A great deal of work still needs to be done since what has been accomplished so far neglects the expected geological complications due to patterns of deposition (on a wide range of scales), dewatering, alteration, deformation, and fracture. A fundamental point of this chapter will be that, even if a medium itself does not exhibit correlations, the transport properties of this medium will be correlated over distances which can be very large. In fact a simple physical result emerges, namely that the length scale of correlations in the measurement of a conduction process is directly proportional to the size of the volume of measurement (Hunt [1], given in Sect. 9.3 here), known in the hydrologic community as the "support" volume. This result is observed over 3–4 orders of magnitude of length, i.e., over 10+ orders of magnitude of the volume [2]. Although there is no proof yet that the percolation theoretical prediction is at the root of this experimental result, it is certainly a viable candidate.

The concepts here will be developed first, however, for simple models of solid-state problems, for which initial calculations have already been presented, and for which relatively reliable microscopic models exist. The general approach will combine cluster statistics of percolation theory with critical path analysis. However, the results, which are given in terms of certain length scales (whose calculations were described in Chap. 4), can be easily generalized to hydrologic systems. The purpose of the first section will be to calculate the distribution of electrical conductivity values for a system of cubic shape and linear dimension x.

The critical subnetwork, which just percolates, is defined by the association of all resistors with resistance values less than or equal to R_c. If another subnetwork is picked by choice of an arbitrary maximum R value such that the maximum $R < R_c$, the largest cluster of interconnected resistors cannot reach infinite size. But it can be large if R is not much less than R_c. Cluster statistics of percolation theory give the occurrence of such clusters. It is necessary for us only to use these statistics to

Hunt, A., Ewing, R.: *Applications of the Cluster Statistics.* Lect. Notes Phys. **771**, 247–264 (2009)
DOI 10.1007/978-3-540-89790-3_9

calculate how often such clusters with a given governing R value can occur, and thus how often a finite measurement device or technique will measure the conductivity from a finite cluster with R different from R_c. But in converting the cluster statistics to a form useful for these calculations it is necessary to review some basic scaling arguments and to recall some definitions and values of several length scales.

Take $r-E$-percolation. In Chap. 4, Eq. (4.28) shows that r_m, proportional to the typical hopping distance, is

$$r_m = a\left(\frac{\alpha_c^2}{9\pi}\right)^{\frac{1}{d+1}}\left[\frac{1}{k_B T N(E_f)a^3}\right]^{\frac{1}{d+1}} = a\left[\frac{T_0}{T}\right]^{\frac{1}{d+1}} \tag{9.1}$$

while Eq. (4.25)

$$\frac{E_m}{kT} = \frac{2r_m}{a} \tag{9.2}$$

demonstrates that the range of available hopping energies is proportional to

$$E_m \propto kT\left[\frac{T_0}{T}\right]^{\frac{1}{d+1}} \tag{9.3}$$

Note that the numerical factors of these quantities are not reliable, since important correlations have been excluded from the calculations. In Chap. 4 the bulk separation of maximally valued resistances for $r-E$-percolation was calculated to be

$$l = a\left(\frac{T_0}{T}\right)^{\frac{1}{d}} \tag{9.4}$$

Below it will be shown how this calculation can be improved in steps. The correlation length evaluated at the optimal resistance for conduction, which will now be denoted as L, was found to be

$$L = a\left(\frac{T_0}{T}\right)^{\frac{1+\nu}{d+1}} \tag{9.5}$$

Consider a cluster of s elements (volume s) at bond probability p. The purpose here is to relate s to a system length, x, and to relate p to R. Then it will be possible to find the probability that in a system of length x a continuous path can be found with no resistance greater than R, which connects both sides of the system.

It is known [3] that the radius of (distance across) such a cluster is $r_s \propto s^{\sigma\nu}h(z)$, where $z = s^{\sigma}(p - p_c)$. The proportionality constant must include the factor $a(T_0/T)^{1/4}$, because both the resistance length and the resistance separation are equal to this value. Therefore the relationship must have the following form:

$$r_s = a\left(\frac{T_0}{T}\right)^{\frac{1}{d+1}} s^{\sigma\nu}h(z) \tag{9.6}$$

The function $h(z)$ is not well known, so that it will be neglected henceforth. Consider the Euclidean distance between maximally valued resistances on such a cluster to be l, then the distance across such a cluster, ignoring tortuosity, can be written as Nl, where N is the number of such resistances in a Euclidean length r_s. Therefore,

$$Nl = a\left(\frac{T}{T_0}\right)^{\frac{1}{4}} s^{\sigma\nu} \tag{9.7}$$

The total distance across the cluster is thus the product of a grid scale factor and a percolation function. The following ratio expresses the assumption that the statistical occurrence of critical resistance values on the backbone of the cluster is the same as in the bulk,

$$\frac{N^{\frac{1}{\sigma\nu}}}{s} = \left(\frac{T_0}{T}\right)^{\frac{1}{d+1}} \tag{9.8}$$

since $N^{1/\sigma\nu} = N^{\mathrm{df}}$ is proportional to the number of critical bonds on the cluster. In accord with the discussion in Chap. 4, the factor on the right-hand side of Eq. (9.8) represents $\xi_c^3/\xi_c^4 \propto \xi_c^{-1}$, which is the ratio of a 3D surface area to its enclosed 4D volume, where ξ_c gives the linear dimension of the volume. Simultaneous solution of Eqs. (9.7) and (9.8) yields

$$l = a\left(\frac{T_0}{T}\right)^{\frac{1+\sigma\nu}{1+d}} \tag{9.9}$$

While the ratio above seems quite different from that in Eq. (9.4), note that $\sigma\nu = 1/d_f$; replacement of $1/d_f$ by $1/d$ would lead to the same result as in Eq. (9.4). One can as a final measure account for the tortuosity of the backbone cluster as well. Remember that the length, Λ, of the tortuous path along the backbone is described by a different exponent than that of the correlation length, $\Lambda \propto (p - p_c)^{-\eta}$, with $\eta = \nu D_{\min}$. This modification includes substituting $(s^{\sigma\nu})^{D_{\min}}$ for $s^{\sigma\nu}$ on the right-hand side of Eq. (9.7)

$$Nl = a\left(\frac{T_0}{T}\right)^{\frac{1}{d+1}} (s^{\sigma\nu})^{D_{\min}} \tag{9.10}$$

where N is no longer the Euclidean separation between critical resistances, but the actual number of such resistances along the percolation backbone and l is now their separation in steps along the backbone. One must then also make a corresponding change to Eq. (9.8) so as to make the left-hand side the ratio of $N^{d_f/D_{\min}}$. The result that one obtains is

$$l = a\left(\frac{T_0}{T}\right)^{\frac{1+D_{\min}/d_f}{1+d}} \tag{9.11}$$

This result was also found in Hunt [4], though it was expressed as

$$l = a\left(\frac{T_0}{T}\right)^{\frac{1+1/\nu d_f}{1+d}} \tag{9.12}$$

as a result of using the exponent $\eta = 1$ (from Stauffer [3]) without taking advantage of the intervening advances in knowledge of tortuosity (see Sect. 2.1). Numerically the values of the exponent on (T_0/T) for l do not differ greatly, with Eq. (9.4) yielding 0.33, Eq. (9.9) 0.35, and Eq. (9.11) 0.388, although Eq. (9.12) was used [4] to produce an exponent of 0.365. All four of these values would scarcely be distinguishable in experiment. Note, however, that Eq. (9.5) for L yields an exponent of 0.47, and experiment might distinguish between any of the above values of l and the choice $l = L$. Further, the larger the value of the exponent, owing to the large value of (T_0/T), the larger is the length scale. This makes $L > l$.

Now turn to the cluster statistics

$$n_s = Ks^{-\tau} \exp\left\{-[s^{\sigma}|(p - p_c)|]^q\right\} \tag{9.13}$$

K is a (dimensionally-dependent) constant, but the value is of no consequence, since the result will ultimately have to be normalized. Here the absolute value signs are meant to allow the cluster statistics to be applicable on either side of p_c. For the Gaussian form, $q = 2$, such a manipulation is not necessary. No solid conclusions with respect to the value of the exponent p are given in Stauffer [3]. The Fisher droplet model gave $q = 1$, but large numerical simulations were very well approximated by $q = 2$ (for which the result was correct on both sides of the percolation threshold), even though theory indicated that the Gaussian form could not be correct (Stauffer). Since the Gaussian form works extremely well, we will use it when making predictions, but when we wish to generate analytic results we use $q = 1$ on account of its simpler manipulation. It is understood, however, that those calculations could probably be modified to yield more accurate results by choice of the Gaussian form. Later in this chapter we show that it is also possible to approximate the cluster statistics by a simple power law with an abrupt cut off.

Although it is possible that ultimately predictions of distributions of the values of the conductivity will require a more precise form for the cluster statistics than either choice mentioned, another aspect of the calculation, which has been left out entirely is that the cluster statistics of Eq. (9.13) do not really apply far from percolation. Thus one ought to combine treatments near and far from percolation. The use of any cross over in functional form would greatly complicate normalization. Here, our development is meant mainly to demonstrate concepts and can use more simplified cluster statistics; nevertheless the calculations of ensemble means appear to generate verifiable results.

Equation (9.8) implies that $s^{\sigma\nu} \propto N$, but Eq. (9.10), including tortuosity, gives $s^{D_{\min}/d_f} \propto N$. Generating two such expressions derives from two different necessities. In Chap. 4 we spent considerable time treating the optimization of the dc conductivity in an infinite system. In such a case the actual values of the lengths l and L could play key roles, and in that context we needed a separation of resistances on the tortuous path. The decisive point is that if one should find by the argument of Eq. (9.10) that $l > L$, one would better use percolation scaling concepts to replace l with L. It is probably a contradiction to declare that the correlation length determines the structure of the dc current-carrying cluster and then to allow the separation of

the critical resistances to exceed that of the nodes. In such a case, the links are made similar to blobs. However, we found that $l < L$ by virtue of its smaller exponent on the temperature-dependent factor. Thus our derivation here provides additional support for our arguments of Chap. 4 that l is not a critical function of $(p - p_c)$. However, in the context of application of cluster statistics, we are more interested in an expression regarding the Euclidean dimension of a cluster. This interest comes from the necessity to compare the actual size of a cluster with a finite system; Is the cluster large enough to span the system in question? Thus for transformations of the cluster statistics to useful forms we need the kind of procedure associated with Eq. (9.8).

Now transform $s^{-\tau}$ using Eq. (9.7), $n_s ds = n_N dN$, and the dimensionally dependent scaling relationship (Eq. (1.21)) to N^{-d+1}. Then use $s^\sigma = N^{1/\nu}(T_0/T)^{\sigma/(d+1)}$ (from Eq. (9.8)) and the relationship for $p - p_c = k_B T(\xi_c^{d+1} - \xi^{d+1}) \approx (T/T_0)^{1/(d+1)}$ (from Eq. (4.31)) to transform the argument of the exponent in Eq. (9.13) and obtain [4],

$$n_N \propto \frac{1}{N^{d+1} l^d} \exp\left\{ -\left[\left(N^{\frac{1}{\nu}} \right) \left(\frac{T_0}{T} \right)^{\frac{\sigma\nu - \nu}{(d+1)\nu}} \ln\left(\frac{R}{R_c} \right) \right]^2 \right\}$$
$$= \frac{1}{N^{d+1} l^d} \exp\left\{ -\left[\left(\frac{Nl}{L} \right)^{\frac{1}{\nu}} \ln\left(\frac{R}{R_c} \right) \right]^2 \right\} \tag{9.14}$$

The combination of exponents on the ratio of the temperatures is also generated by the ratio l/L, if we use the value for l referred to the Euclidean distance, as argued above. Note that χ is given as proportional to $\chi_0(p - p_c)^{-\nu}$, making it always possible to replace Nl/L with Nl/χ_0 and some numerical constant which, in the case of porous media with their largely unknown distributions, is not likely to be known anyway.

If one expresses $R = R_c \exp(j)$, i.e., one quantizes resistance values in steps of $e = 2.718\ldots$, the following form for $W(N, j)$ results [4],

$$W(N, j) = \frac{1}{N^{d+1} l^d} \exp\left\{ -\left[\left(\frac{Nl}{L} \right)^{\frac{1}{\nu}} j \right]^q \right\} \tag{9.15}$$

In the form of Eq. (9.15) contributions to the conductivity may be summed over the index j. Later representation in the form of an integral over R requires the transformation $dj \rightarrow dR/R$. Using the cluster statistics in a form like Eq. (9.14) or Eq. (9.15) it is possible to answer a large number of problems.

A cubic volume, $x^3 > L^3$, selected at random, will include some clusters of resistors with, e.g., maximal resistance values less than the critical resistance, which extend from one side of that cube to the other. Such clusters can be defined at all resistance values. Some cubes will contain additional paths [compared with the expected value, $(x/L)^2$] with maximal resistors of the critical resistance value. Other

cubes will not contain paths with maximal resistance value R less than or equal to R_c at all. Such cubes will have a finite probability of being spanned by clusters with $R > R_c$, which are not connected to the critical cluster. The cluster statistics near critical percolation can be used to describe the statistical occurrence of such clusters defined by $R > R_c$ as well.

The calculation of the distribution of resistance values for a given cube of dimension x requires summing the statistical occurrence of all cluster sizes, for a given R value, whose lengths exceed x according to the probability that such clusters "fall" on the volume x^3. The condition

$$N_m l = x \tag{9.16}$$

states explicitly that $N_m l$ is the minimal cluster length which can contribute. The probability that a given cube has conductivity l/Rx^2, where l is the separation of the resistances with the particular value of R chosen, and x^2 is the area normal to the current, is equal to the probability that a cluster with $N > x/l$ is found at the volume x^3. In the following it will be necessary to assume that $x > L$, otherwise the desired statistics for resistance distributions are strongly dependent on the distribution of individual resistances, and thus unrelated to universal cluster statistics. In fact, one way to recognize the value of L from simulations is that the skewness of a distribution of system conductivity values, which is a very rapidly falling function of x for $x < L$, becomes nearly constant for $x > L$.

The probability that a given volume x^3 will intersect a cluster with linear dimension larger than x (providing the current carrying path) is proportional to the volume, $(Nl)^3$, because it does not matter whether the center of the volume x^3 actually falls on the backbone cluster. It is sufficient that the volume "cut" the cluster. Thus the probability that a given cubical volume, x^3, is characterized by a maximal resistance, R, is proportional to

$$J = \int_{x/l}^{\infty} \frac{dN}{N} \exp\left\{ -\left[\left(\frac{Nl}{L} \right)^{\frac{1}{\nu}} \ln\left(\frac{R}{R_c} \right) \right]^q \right\} \tag{9.17}$$

The factor dN/N arises from $(Nl)^3/N^4 l^3$, the numerator resulting from the volume argument above and the denominator from the cluster statistics. In Hunt [4] an additional factor $1 - K$ was included to represent the probability that there was no cluster with a smaller R value, which also spanned the volume, but this factor was later argued to be negligible.

Integral (9.17) could be performed relatively easily only in the case that $q = 1$. Since the purposes here are still largely illustrative, this case will be used. Then integral (9.17) yields

$$J = -\mathrm{Ei}\left\{ -\left[\left(\frac{Nl}{L} \right)^{\frac{1}{\nu}} \ln\left(\frac{R_c}{R} \right) \right] \right\} \tag{9.18}$$

where $\mathrm{Ei}(x)$ is the exponential integral of x. Equation (9.18) is in a form, which is not particularly illustrative. But for relatively large values of its argument, $-\mathrm{Ei}(x) \to \exp(-x)/x$ and [4]

$$J = \frac{(L/x)^{1/\nu} \left(R/R_c\right)^{(x/L)^{1/\nu}}}{\ln\left(R_c/R\right)}, \qquad R < R_c \tag{9.19a}$$

$$J = \frac{(L/x)^{1/\nu} \left(R_c/R\right)^{(x/L)^{1/\nu}}}{\ln\left(R/R_c\right)}, \quad R > R_c \tag{9.19b}$$

$J(R)$ represents an unnormalized distribution of resistance values, but it is possible to find the variance from Eq. (9.19) to be $R_c^2(L/x)^2$ (under the condition that $x > 3L$, and approximating $1/\nu$ as 1). Using this unnormalized distribution it is also possible to calculate approximately the mean value of the conductivity of cubes of dimension x. The conductivity of a cube of dimension x with a dominant conducting path of length Nl and resistance NR is

$$\sigma = \frac{Nl}{NR}\frac{1}{x^2} \tag{9.20}$$

The mean conductivity of an ensemble of such cubes is an integral over all cubes according to the frequency of their occurrence. The integral over R was split into two parts, $R \le R_c/\mathrm{e}$ and $R \ge eR_c$ because of the difference in form of the cluster statistics across $R = R_c$; the case $R = R_c$ was treated separately. The contribution from $R \neq R_c$ was shown to yield a contribution to the dc conductivity, $\Delta\sigma_{dc}$,

$$< \Delta\sigma_{dc}(x) > \propto \sigma_{dc}(\infty) \left[\frac{L}{x}\right]^2 \left[1 + \left(\frac{L}{x}\right)^{\frac{1}{\nu}}\right] \tag{9.21}$$

upon ignoring two numerical constants of order unity. The contribution from $R = R_c$ was argued to be of the same form as the first term. The mean conductivity thus diminishes asymptotically with increasing size to its value in the thermodynamic limit, $\sigma_{dc}(\infty)$. The result from Eq. (9.21) is identical to a result for the electrical conductivity of a thin film of thickness x, which can easily be shown to be equivalent to the ensemble mean of the conductivity of a collection of such cubes. The results of Eq. (9.21) were found to be in accord with numerical simulations in Hunt [5], though there was some question as to whether both terms were appropriate.

It was found in Hunt [5] that assuming $R = R_0 \exp\xi$, as above together with the Gaussian form for the cluster statistics, which is more accurate than assuming $q = 1$ leads to the result that the distribution of conductivity values is approximately log-normal, at least in the case where $L \approx x$. Clearly, replacing $\ln(R/R_c)$ by $(R - R_c)$ for the case $R = R_0\xi^k$ ($k = 4$ for Poiseuille flow) will make the result more nearly compatible with Gaussian statistics than with a log-normal distribution. At the time of the original publication on conductivity distributions the coincidence that the log-normal distribution appeared to be consistent with Nielsen's results [6] for the distribution of the steady-state unsaturated hydraulic conductivity values in field soils was considered to be significant, especially since the assumed exponential

dependence of R on a random variable ξ was consistent with Nielsen's [6] observation that K was exponentially dependent on the moisture content. In the meantime we recognize that the exponential dependence on a moisture content is not an obvious result, and this question is rather involved. But this topic is discussed further in Chap. 11 in which heterogeneity on more than one scale is treated.

9.2 Cluster Statistics Treatment of Nonequidimensional Volumes and Anisotropy

An easier means to treat the cluster statistics can be developed, and this treatment is independent of the exact form of the function $f(z)$. Instead of using a particular form for the exponential cut off, replace $f(z)$ by a sharp cut off at $s^{\sigma} \propto (p - p_c)^{-1}$. While such an approximation may seem quite rough, it should capture the scaling behavior properly when resulting distributions are normalized, and it should also lead to accurate results for ensemble means. Treating the exponential cut off as a sharp cut off,

$$n_N = \frac{1}{N^4 l^3} \quad N < \frac{L}{l} \ln^{\nu} \left(\frac{g_c}{g} \right) \tag{9.22}$$

for the case $g < g_c$ and

$$n_N = \frac{1}{N^4 l^3} \quad N < \frac{L}{l} \ln^{\nu} \left(\frac{g}{g_c} \right) \tag{9.23}$$

for the case $g > g_c$. Both Eqs. (9.23) and (9.24) were written here for the case $R = R_0 \exp(\xi)$ again. One can also write the cluster statistics for the case $R = R_0 \xi^k$, with the results

$$n_N = \frac{1}{N^4 l^3} \quad N < \frac{L}{l} |V - V_c|^{-\nu} \tag{9.24}$$

Linearize $V - V_c$ for the Rieu and Sposito model (done in Eq. (4.42)) to get

$$|V - V_c| = \frac{3 - D}{3} \left(\frac{g_c}{g_m} \right)^{\frac{3-D}{3}} \frac{|g - g_c|}{g_c} \tag{9.25}$$

using the additional substitution of $(g_c/g_m)^{(3-D)/3}$ for $(r_c/r_m)^{3-D}$. Note that in Chap. 8 the same problem was considered, but with the assumption that the critical volume fraction $V_c \approx 0$. Under such circumstances, $g_c \approx g_m$, and Eq. (9.24) simplifies to

$$N < \frac{L}{l} |V - V_c|^{-\nu} = \frac{L}{l} \left\{ \frac{g_c}{|g - g_c| \left[1 - (D/3) \right]} \right\}^{\nu} \tag{9.26}$$

It will turn out (in Chap. 10, for example) that a procedure not based on linearization produces much better results. To some degree we continued the linearization

here as a tradition, to some degree we were perhaps lulled by the theoretical arguments that percolation functions and exponents describe behavior precisely only in the asymptotic limit. In any case we present here also an analogous result to Eq. (9.26) that is not based on linearization.

$$N < \frac{L}{l}\left|\frac{1}{1-\left(g/g_c\right)^{1-(D/3)}}\right|^{\nu} \tag{9.27}$$

Equation (9.27) performs better apparently because, under typical conditions in porous media with D on the order of 2.8 or larger, the very small power $1-D/3 = 0.067$ or smaller, makes much wider ranges of g fit close to the percolation threshold.

Consider a system with horizontal dimension x and vertical dimension $\varepsilon^{1/2}x$. The factor, $\varepsilon^{1/2}$, can be regarded as arising from a coordinate transformation corresponding to the transformation from an equidimensional volume in an anisotropic medium to a nonequidimensional volume in an isotropic medium (the discussion of the correspondence of $\varepsilon^{1/2}$ to values of K in the anisotropic case will be discussed after the derivation). Systems with characteristic $g < g_c$ can result from clusters of size x or larger, which serve to block the entire volume, but systems with characteristic $g > g_c$ must be cut from clusters of linear dimension $\varepsilon^{1/2}x$ or larger (see Fig. 9.1). Using these results one can now follow an analogous procedure to Eq. (9.20) to find $W(g)$ by integrating the product of $(Nl)^3$ and an integrand of the form of the right-hand side of Eq. (9.25). The result is the integral

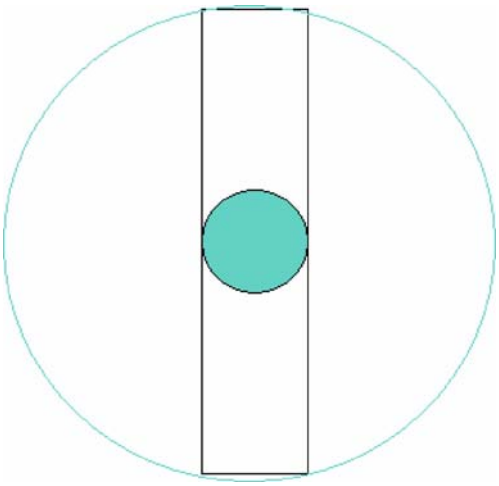

Fig. 9.1 Demonstration that a cluster (*filled*) of $g < g_c$ (not connected to the infinite cluster) of linear dimension equal to the shortest dimension can force a current to flow through a region of lower conductance, while a cluster (*unfilled*) with $g > g_c$ must be as long as the largest dimension of the system

$$W(g) \propto \int \frac{dN}{N} \tag{9.28}$$

The question is what are the limits of such an integral? For either case, $g > g_c$ or $g < g_c$ the upper limit is given by Eq. (9.27). For $g < g_c$, the lower limit is $(x+l)/l$, while for $g > g_c$, the lower limit is $(x\varepsilon^{1/2}+l)/l$. The reason for adding the term l in both cases is to be consistent with the derivation in Chap. 8 which noted that in the limit of small system size x the discretization of the system through the dimensions of the individual resistors could not be neglected. We cannot have cluster sizes smaller than an individual bond length. The results of these integrations are the (unnormalized) expressions for $W(g)$ below,

$$W(g) \propto \ln\left[\left(\frac{L}{l+x\varepsilon^{1/2}}\right)^{\frac{1}{\nu}} \frac{1}{\left(g/g_c\right)^{1-(D/3)}-1}\right] \quad g > g_c \tag{9.29}$$

and

$$W(g) \propto \ln\left[\left(\frac{L}{l+x}\right)^{\frac{1}{\nu}} \frac{1}{\left(g/g_c\right)^{1-(D/3)}-1}\right] \quad g < g_c \tag{9.30}$$

It is possible to use linearized versions of Eqs. (9.29) and (9.30) to calculate a mean value of the distribution as well as a distribution width in terms of the fundamental formula in terms of the difference of the mean value squared and the square of the mean value. Let

$$A = \left(\frac{L}{l+\varepsilon^{1/2}x}\right)^{\frac{1}{\nu}} \frac{1}{1-\left(D/3\right)} \tag{9.31}$$

and

$$A' = \left(\frac{L}{x+l}\right)^{\frac{1}{\nu}} \frac{1}{1-\left(D/3\right)} \tag{9.32}$$

Then it is possible using the linearized versions of Eqs. (9.29) and (9.30) to express an ensemble mean $< g >$ as

$$< g >= \lim\ (\delta \to 0) \frac{\int_{g_c+\delta}^{g_c+Ag_c} g dg \ln\left[Ag_c/(g-g_c)\right] + \int_{g_c-A'g_c}^{g_c-\delta} g dg \ln\left[A'g_c/(g_c-g)\right]}{\int_{g_c+\delta}^{g_c+Ag_c} dg \ln\left[Ag_c/(g-g_c)\right] + \int_{g_c-A'g_c}^{g_c-\delta} dg \ln\left[A'g_c/(g_c-g)\right]} \tag{9.33}$$

The upper (lower) limit of the first (second) integral is determined by the condition that the upper limit of integral (9.28) be larger than the lower limit. The results were obtained without accounting for any special contribution from $g = g_c$. Evaluation of the integrals leads to

$$< g >= g_c \frac{A + A' + (1/4)A^2 - (1/4)A'^2}{A + A'} = g_c \left[1 + \frac{\left[L \Big/ \left(\varepsilon^{1/2} x + l \right) \right]^{\frac{1}{\nu}} - \left[L/(x+l) \right]^{\frac{1}{\nu}}}{4\left[1 - (D/3) \right]} \right] \tag{9.34}$$

For large values of x it is possible to rewrite this expression as

$$< g_v >= \left[1 + \left(\frac{L}{\varepsilon^{1/2} x + l} \right)^{\frac{1}{\nu}} - \left(\frac{L}{x+l} \right)^{\frac{1}{\nu}} \right]^{\frac{3/4}{3-D}} \tag{9.35}$$

where the subscript v has been added to denote vertical flow. The logic of this particular recombination is that it is, in a sense, an inverse of the expansion of $g^{1-D/3} - g_c^{1-D/3}$; thus it is plausible that a more detailed treatment that did not utilize the linearization in the first place would lead to precisely the same result as Eq. (9.35). Of course this recombination is not unique, but this is a particular case where the recombination is a direct reversal of the linearization of Eq. (4.42). In any case, Eqs. (9.34) and (9.35) are equivalent to the lowest order. Further, the results from Eq. (9.35) are very nearly identical to the results from Chap. 8 over a wide range of system sizes x. The only purpose is to compare with the calculations of Chap. 8, for which such a linearization was not necessary. Now Eq. (9.35) can be rewritten in the form

$$< g_v >= g_c \left\{ 1 - \left[1 - \left(\frac{1 + x/L}{1 + \varepsilon^{1/2} x/L} \right) \right]^{\frac{1}{\nu}} \left[\frac{1}{1 + x/L} \right]^{\frac{1}{\nu}} \right\}^{\frac{3/4}{3-D}} \tag{9.36}$$

which clarifies the scaling of $< g_v >$ with length x as a ratio of x/L.

A similar calculation can be made for an ensemble mean bottleneck conductance for horizontal flow through the system. In this case, however, a cluster of size x is large enough to facilitate flow with a larger g than g_c, but it takes a cluster of size $\varepsilon^{1/2} x$ with maximum $g < g_c$ to block flow. The result is easily deduced from Eq. (9.33) to be

$$< g_h >= g_c \frac{A + A' + (1/4)A'^2 - (1/4)A^2}{A + A'} = g_c \left\{ 1 + \frac{\left[L/(x+l) \right]^{\frac{1}{\nu}} - \left[L \Big/ \left(\varepsilon^{1/2} x + l \right) \right]^{\frac{1}{\nu}}}{4\left[1 - (D/3) \right]} \right\} \tag{9.37}$$

where now the subscript h denotes horizontal flow. Equation (9.37) can then also be rewritten in the following form (by the same reversal of linearization as in Eq. (9.34))

$$< g_h >= g_c \left\{ 1 + \left[1 - \left(\frac{1 + x/L}{1 + \varepsilon^{1/2} x/L} \right) \right]^{\frac{1}{\nu}} \left[\frac{1}{1 + x/L} \right]^{\frac{1}{\nu}} \right\}^{\frac{3/4}{3-D}} \tag{9.38}$$

Note that $< g_h > / < g_v >$ is 1 in both the limits of $x \to \infty$ and $x \to 0$. In the limit of an infinite system a critical path may be found equally easily in either the horizontal or the vertical direction and $< g_h > / < g_v >$ should be 1. However the fact that the ratio of g_h (and g_v) in the limit $x \to \infty$ is equal to its value in the limit $x \to 0$ is also 1 is an artifact of the assumption that, $V_c \approx 0$. In the limit $x \to 0$ the present calculation is consistent with the fact that an ensemble mean of systems so small that they are composed of a single element must give the arithmetic mean in either the horizontal or the vertical direction but the effective hydraulic conductivity of an infinite system is only the arithmetic mean if V_c can be argued or chosen to be zero.

Now how do we actually relate ε to the horizontal and vertical measurements of K? ε is assumed to give a ratio of the characteristic values of horizontal and vertical K measurements. If $V_c = 0$, then it must often be possible to find horizontal paths that connect a system from one side to the other that never have to use any smaller pore (or fracture) radii than r_m. So $K_h \propto r_m^2$ (by the results for the saturated hydraulic conductivity, Chap. 4). On the other hand, vertical paths in a system small enough to be 1D must sample every r value. Thus, effectively, a vertical path has $V_c = 1$ and $K_v = r_0^2$. This means that $\varepsilon^{1/2} \propto (r_m/r_0)$, which is identical to the ratio, R, in Chap. 8. As a consequence, since K_v was shown in Chap. 8 to sweep out the values from r_0^2 through r_m^2, the result for K_h cannot involve a very large enhancement, being at most related to the density of flow path inputs rather than maximally valued resistances to flow. And indeed the maximum enhancement is only about an order of magnitude rather than the 6 orders of magnitude reduction in K_v at the same x value.

After this discussion it is now appropriate to consider how well our results fare in comparison with experiment. We choose the same anisotropic fracture system in a carbonate aquifer [7] as was chosen in Chap. 8. In Fig. 9.2 the result (Eq. (9.36)) for $K_v(x)$ is compared with experiment and found to reproduce experiment approximately equally well as the results from Chap. 8 (and using the same parameters) over a wide range of system sizes. This equivalence was also intended, once again, to demonstrate the redundancy of percolation theory, which allows more than one starting point to calculate the same quantity. Additionally we show the results of Eq. (9.38) for $K_h(x)$. Note that, while K_v is an increasing function of x, K_h is a decreasing function. In these representations L was set equal to 1, making the units of the horizontal scale arbitrary.

In Fig. 9.3 we show a 3D plot of the results of Eqs. (9.29) and (9.30) for the pdf for measuring conductance value g as function of size, x.

We have [8] developed a scheme to generate a width of a distribution of conductance values that is highly asymmetric, as in Eqs. (9.29) and (9.30). This scheme can be described most easily in geometric terms. Emplace a horizontal line of variable height on the graph of $W(g)$. This line will normally intersect $W(g)$ in two points. Choose the height so that the area under $W(g)$ between the two intersection points is 68% of the total area under $W(g)$, equal to the fractional area within one standard deviation of the mean of a Gaussian distribution. The range of g values between these two intersection points can then serve as a measure of the distribution width. When we calculate this distribution width again for the same parameters as found in Chap. 8, the results can be represented graphically in Fig. 9.4. While

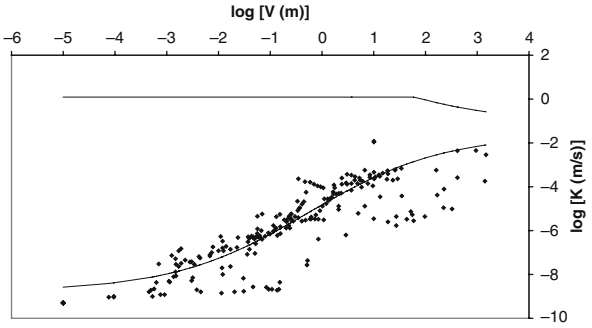

Fig. 9.2 Comparison of the result of Eq. (9.36) for K_v obtained by cluster statistics of percolation with experimental data obtained by Schulze-Makuch [7]. The same values of the parameters, $D = 2.98$, and $r_m/r_0 = \varepsilon^{1/2} = 2,500$ were used as in Eq. (8.8) from Chap. 8. Here we show $K_h > K_v$ from Eq. (9.38) for comparison

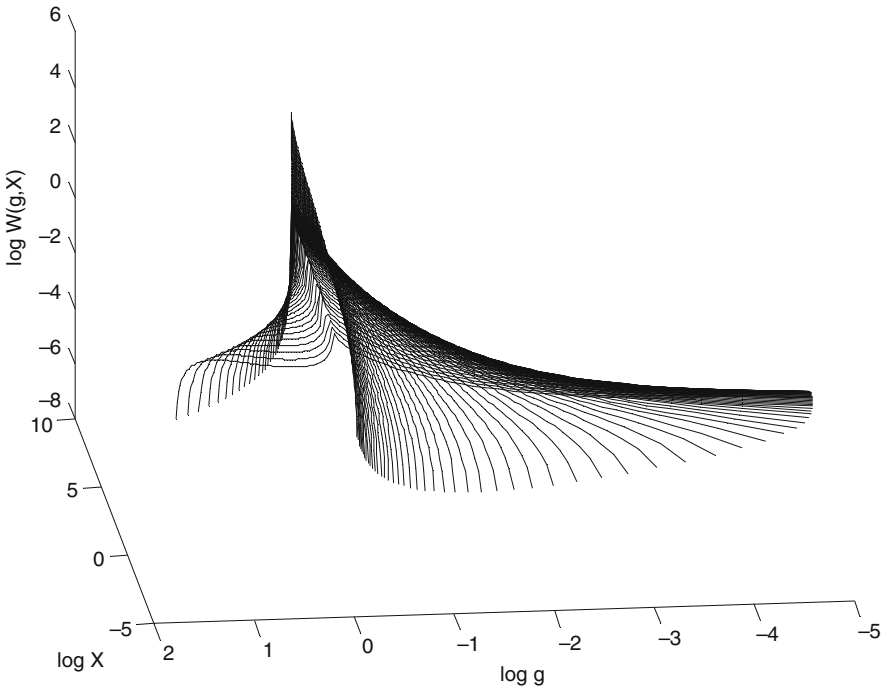

Fig. 9.3 Family of curves describing the distribution of conductance values, $W(g,x)$ as given by the approximation in Eqs. (9.29) and (9.30)

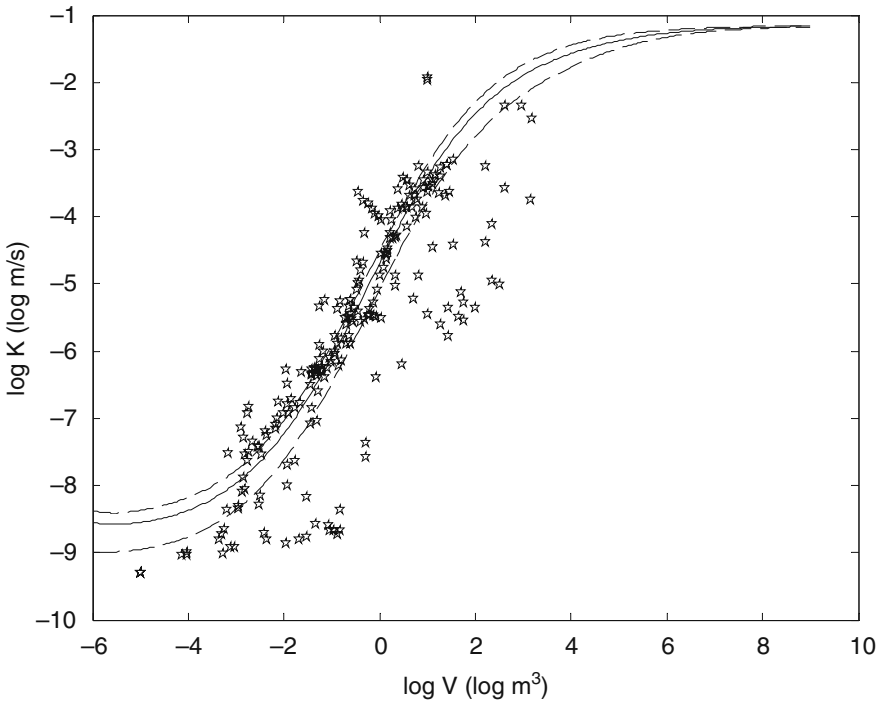

Fig. 9.4 Comparison of the width of the distribution of $W(g)$ values as a function of x with experimental data from Schulze-Makuch [7]. The geometric procedure to calculate the width of the distribution from the approximation given in Eqs. (9.29) and (9.30) is given in the text. The parameters, $D = 2.98$, and $r_m/r_0 = \varepsilon^{1/2} = 2,500$ used were again the same values as those chosen in Chap. 8, though in Chap. 9 only the expected value of the conductivity was treated

the comparisons in Chap. 8 were essentially fits, since the parameters were chosen to fit the data, use of the same parameters here gives Fig. 9.4 at least some of the characteristics of a prediction.

It should be mentioned that the results of this chapter have a potential relevance also to a radioactive waste problem at the Hanford site. Technetium in solution was discharged at the BC Crib site and was expected to drain straight down to the water table. The evidence is that it did not, having encountered a horizontal layer with a large anisotropy in K and spread laterally instead. With increasing time, however, the effective experimental scale will increase, producing an increase in the expected value of K_v and a decrease in the expected value of K_h. Using the application of the cluster statistics that led to Eqs. (9.36) and (9.38) it should be possible to make a prediction of the length, and thus the time scale, before the probabilities of vertical and horizontal advection are similar and thus evaluate the potential danger of contamination of the water supply in a quantitative way. This question is now addressed in Chap. 11 as it is effectively a problem of multiple scales of heterogeneity.

9.3 Semivariograms and Cross-Covariance

The semivariogram for the hydraulic conductivity is defined as

$$\Gamma_{\mathrm{K}}(h) = \frac{1}{2N(h)} \sum_{j=1}^{N(h)} [K(x_j) - K(x_j + h)]^2 \tag{9.39}$$

$K(x_j)$ is the value of the hydraulic conductivity at $x = x_j$, $K(x_j + h)$ is its value at distance h from x_j, and $N(h)$ is the number of pairs of points at which measurements are made a distance h apart. For stationary random functions, the semivariogram is related to the covariance, $C_{\mathrm{K}}(h)$, by $\Gamma_{\mathrm{K}}(h) = C_{\mathrm{K}}(0) - C_{\mathrm{K}}(h)$. In practice the semivariogram (often simply called the variogram) is the product of the variance of K and the difference between 1 and the correlation function of K. The range of the variogram is defined in terms of the length scale which governs the decay of the correlation function.

There are many possible reasons why a random field, such as the hydraulic conductivity, can be correlated from point to point in a geologic porous medium. These include depositional correlations, fractures, folding, etc. There are also reasons that relate to the random combination of highly conducting elements into a larger region of high conductivity. In particular, given the context of this chapter, suppose that a large cluster of resistances of maximum value $R < R_{\mathrm{c}}$ is present in a system of size x. Then a measurement of K in a region of space that covers one part of the cluster will be correlated with a measurement that is made over another part of the cluster. Otherwise, there is no discernible correlation. We can define that probability in terms of conditional probabilities as follows: start from Eq. (9.17) and write [1],

$$J = \int_{x/l}^{\infty} K dN \tag{9.40}$$

where K is the integrand of Eq. (9.17). Equation (9.40) once again gives a (relative) probability that a system of size x has controlling resistance R. The probability that the same cluster determines the resistance after translation at distance h is the (conditional) probability that the cluster that is known to be of minimum size x is actually of size at least $x + h$. This probability is easy to write as [1]

$$P(h) = \frac{\int_{(x+h)/l}^{\infty} K dN}{\int_{x/l}^{\infty} K dN} \tag{9.41}$$

The variogram, since it measures the lack of correlation, is proportional to the complementary probability, $1 - P(h)$. Using Eq. (9.19a and 9.19b) the quantity $1 - P(h)$ can be expressed as [1]

$$1 - P(h) = 1 - \left(\frac{x}{x+h}\right) \exp\left[-\left(\frac{x}{l}\right) |\ln\left(\frac{R}{R_{\mathrm{c}}}\right)|\right] \tag{9.42}$$

Note that Eq. (9.42) is approximate in three respects: one, the cluster statistics of percolation theory are not accurately described by the exponential "Fisher droplet" form used, and two, the approximation for the exponential integral used is an asymptotic limit, and three, cluster statistics far from percolation should be used for R values far from R_c. Again, the main purpose here is instructive. Now the variogram must be obtained by an integral of Eq. (9.42) over the probability density for the cluster resistance, R, since clusters of all resistances can occur. Thus [1],

$$\Gamma_K(h) \propto 1 - \int_0^\infty \frac{x}{x+h} \exp\left[-\left(\frac{x}{l}\right)\left|\ln\left(\frac{R}{R_c}\right)\right|\right] W(R,x)\, dR \tag{9.43}$$

where

$$W(R,x) = \frac{(L/x)\,(R/R_c)^{\frac{x}{L}}/|\ln(R/R_c)}{\int_0^\infty dR\,(L/x)\,(R/R_c)^{\frac{x}{L}}/|\ln(R/R_c)} \tag{9.44}$$

The first term in Eq. (9.43) integrates easily to 1, while the second integrates to $[x/(x+h)]^2$. Thus,

$$\Gamma_K(h) \propto 1 - \left(\frac{x}{x+h}\right)^2 \tag{9.45}$$

Using the representation of the variogram as the product of a spatial dependence and the variance of R yields thus [1],

$$\Gamma_K(h) = R_c^2 \left(\frac{L}{x}\right)^2 \left[1 - \left(\frac{x}{x+h}\right)\right]^2 \tag{9.46}$$

It is easily determined [5] that Eq. (9.46) for the variogram cannot be precisely correct because its Fourier transform can take on negative values, as can thus the Fourier transform of the correlation function, or the characteristic function. The wiggles in the Fourier transform arise from the lack of continuity of the slope of $\Gamma_K(h)$ in the limit $h \to 0$. Owing to the various approximations, including using an asymptotic expansion for large h in the limit of $h \to 0$, the defect of the derived function in this limit is not really unexpected. Nevertheless Eq. (9.45) clearly shows that the range of the variogram is proportional to x, the linear dimension of the measurement. In strongly heterogeneous media, "a quantitative measure of the range of correlation of a random spatial structure may be calculated from the autocorrelation function. In general the integral scale [this range] is not an intrinsic property of the field, but depends on the scale over which it is measured." In other words, the range is a function only of x. Moreover, Neuman and di Federico [2] present experimental results that demonstrate that the range of the variogram for the hydraulic conductivity is linearly proportional to the measurement length scale over many orders of magnitude of x. So, even in the present approximation, this aspect of experiment is achieved. Further, it was shown in Hunt [1] that Eq. (9.45) resembles the spherical approximation for the variogram.

The cross-covariance is given in terms of the probability that a second volume x at a distance h from a first volume has $R \geq R_2$ if volume 1 has $R \geq R_1$. To write down an expression in terms of cluster statistics, one must make some assumptions regarding the magnitudes of R_1 and R_2. In Hunt [1] it is shown that the cross-covariance is given by

$$\frac{\int_{R_1}^{\infty} W(R,x)\,dR \int_{\frac{x+h}{l}}^{\infty} K(R,N)\,dN}{\int_{R_1}^{\infty} W(R,x)\,dR \int_{\frac{x}{l}}^{\infty} K(R,N)\,dN} + \left[\frac{\int_{R_2}^{R_1} W(R,x)\,dR \int_{\frac{x}{l}}^{\frac{x+h}{l}} K(R,N)\,dN}{\int_{0}^{\infty} W(R,x)\,dR \int_{\frac{x}{l}}^{\frac{x+h}{l}} K(R,N)\,dN}\right] \times \left[1 - \frac{\int_{R_1}^{\infty} W(R,x)\,dR \int_{\frac{x+h}{l}}^{\infty} K(R,N)\,dN}{\int_{0}^{\infty} W(R,x)\,dR \int_{\frac{x+h}{l}}^{\infty} K(R,N)\,dN}\right] \tag{9.47}$$

in the case that $R_1 > R_2 > R_c$. The first term gives, as in the calculation of the variogram above, the probability that the second volume is located on the same cluster of linear dimension $x+h$. In that case $R > R_1$ in the second volume certainly guarantees $R > R_2$. But it is also possible that the second volume is not located on the same cluster (the second factor of the second term); then, however, it may still be located on a cluster of size between x and $x+h$ with controlling resistance somewhere between R_2 and R_1. The cluster must be at least size x in order to control the measurement of volume 2, but cannot be as large as $x+h$, or it will control the measurement of volume 1 as well. If it controlled the measurement of volume 1 as well, then volume 1 would have $R < R_1$. Since the choice of volume 1 and volume 2 is arbitrary, this expression can always serve for cases when both R_1 and R_2 are greater than R_c. The other two cases may be written down analogously (when both resistances are smaller than the critical resistance and when one is larger and one is smaller).

Note that in Hunt [1] the expression corresponding to Eq. (9.47) has several typos, but more importantly the limits on the interior integrals of the first factor of the second term are incorrect.

Problems

9.1. Write analogous expressions for the cross-covariance when both controlling resistance values are smaller than R_c and for the case when they are on opposite sides of R_c.

9.2. Use the cluster statistics of percolation theory to predict the variance of the distribution of K_h and K_v as functions of system size. There are two ways to do this calculation. One is to use the full cluster statistics distribution (with its attendant unknowns). The second way, recommended here, is to use the approximation in the text.

References

1. Hunt, A. G., 2000, Percolation cluster statistics and conductivity semi-variograms, *Transp. Porous Media* **39**: 131–141. 247, 261, 262, 263
2. Neuman, S. P., and V. Di Federico, 2003, Multifaceted nature of hydrogeologic scaling and its interpretation, *Rev. Geophys*. **41**: Art. No. 1014. 247, 262
3. Stauffer, D., 1979, Scaling theory of percolation clusters, *Phys. Rep*. **54**: 1–74. 248, 250
4. Hunt, A. G., 1998, Upscaling in subsurface transport using cluster statistics of percolation, *Transp. Porous Media* **30**(2): 177–198. 249, 250, 251, 252, 253
5. Hunt, A. G., 2001, Applications of percolation theory to porous media with distributed local conductances, *Adv. Water Resour*. **24**(3,4): 279–307. 253, 262
6. Nielsen, D. R., 1973, Spatial variability of field-measured soil-water properties, *Hilgardia*, **42**: 215–259. 253, 254
7. Schulze-Makuch, D., 1996, Dissertation, Facies dependent scale behavior of hydraulic conductivity and longitudinal dispersivity in the carbonate aquifer of southeastern Wisconsin, University of Wisconsin, Milwaukee. 258, 259, 260
8. Hunt, A., Blank, L., and Skinner, T., (2006), Distribution of hydraulic conductivity in single scale anisotropy. *Philos. Mag*. **86**(16): 2407–2428. 258

Chapter 10
Properties Based on Tortuosity

10.1 Longitudinal Dispersion of Solutes in Porous Media

Dispersion in porous media is a phenomenon, which is incompletely understood. Dispersion is a term which describes the spatial spreading of solutes in porous media under the action of flowing water. This dispersion can be either in the direction of flow (longitudinal) or perpendicular to it (transverse). We focus our attention here on longitudinal dispersion. Solutes treated can be adsorbed on to surfaces or nonsorbing. We do not address the problem of sorbing solutes here. Compounds dissolved in water in the subsurface are transported by molecular diffusion and advection (motion of the fluid). We address the effects on dispersion from advective flow but omit effects of diffusion. Effects on dispersion from a single capillary tube velocity distribution, known to produce long-tailed arrival time distributions, are also neglected. Solutes treated can be contaminant plumes from any source or radioactive tracers both experimentally and naturally generated.

In order to generate predictive relationships for longitudinal dispersion of solutes we calculate first the distribution of arrival times, $W(t)$, of solute transported in steady flow. This calculation has a close relationship to that of finding the distribution of hydraulic conductivity values in finite-sized systems [1]. In particular, both are based on the relevance of the cluster statistics of percolation theory to a distribution of water fluxes in terms of the critical flow from critical path analysis. Since the critical flow paths are also tortuous, we must also appeal to scaling arguments of percolation regarding the fractal characteristics of such paths. Such an application leads directly to a formulation of solute transport in terms of both critical path analysis and percolation scaling. We calculate a distribution of arrival times, $W(t)$, for a specific random fractal model of the pore space [2]. The present calculations yield asymmetric peaks of $W(t)$ with a long tail. It was possible to compare the results of the present calculations with numerical simulations (Liu et al., [3]) that omit the process of diffusion. The results are in quantitative agreement with the simulations and generally in accord with experiment. Accordingly it appears that the structure of our calculations, limited as they are, may be able to describe many of the properties of experiment that have been considered puzzling. In fact, we believe that we have the first ever reliable calculations of the entire distribution of arrival times, $W(t)$, in advective flow in strongly disordered porous media.

Hunt, A., Ewing, R.: *Properties Based on Tortuosity.* Lect. Notes Phys. **771**, 265–285 (2009)
DOI 10.1007/978-3-540-89790-3_10

10.1.1 Quantifying Limitations of the Neglect of Diffusion

It is important first to define the conditions under which we can expect that it is acceptable to neglect molecular diffusion. Under the action of advection, the effects of diffusion appear to be enhanced. The resulting phenomenon is termed hydrodynamic dispersion, but is typically treated mathematically simply as diffusion with a velocity-dependent diffusion constant. In natural settings it may be legitimate to neglect the effects of either advection or of molecular diffusion. The relevance of advection relative to diffusion may be estimated [4] by use of the Peclet number, $P_e = Lu/D_s$, where L is a relevant spatial scale, u is the fluid velocity, and D_s is the diffusion constant of the solute. Typically it is assumed that for $P_e > 100$ diffusion may be neglected, while for $P_e < 1$ advection may be neglected. In a study related to the present work, Sahimi and Imdakm [5] gave $P_e = 300$ as a lower bound.

10.1.2 Conventional Modeling

A differential equation, commonly called the advection-diffusion equation (or convection-diffusion equation) describing effects of both advection and diffusive processes on the spatio-temporal behavior of dissolved solutes is (e.g., Bear [6])

$$\frac{\partial C}{\partial t} = \nabla \cdot D_h \nabla C - \boldsymbol{u} \cdot \nabla C \tag{10.1}$$

Here, $C(x,t)$ is the concentration of the solute, D_h is the hydrodynamic dispersion coefficient, and $\boldsymbol{u}$ is the velocity of the flow. In case $\boldsymbol{u} = 0$, the only influence on $C(x,t)$ is molecular diffusion, and $D_h = D_s$. Usually, however, D_h is found to exceed D_s. Further, results of experiments typically require that D_h be dependent on spatial and time scales. This suggests that description of the relationship between the microscopic process of advection and the macroscopic description of dispersion as simply analogous to microscopic diffusion is not adequate.

The velocity $\boldsymbol{u}$ is a random field, generated by solution of

$$\nabla \cdot \boldsymbol{u} \propto \nabla \cdot K \nabla P = 0 \tag{10.2}$$

Here K is the hydraulic conductivity (a random scalar field in isotropic media) and P is the pressure. D_h may also be assumed to vary from point to point. Thus, one means to investigate the behavior of solutes in natural porous media is simply to solve numerically Eqs. (10.1) and (10.2) using assumed stochastic variability of the coefficients [7, 8]. A reason for using critical path analysis and percolation theory rather than a stochastic approach to model fluid flow (and thus ultimately particle transport) is the conclusion of Bernabe and Bruderer [9] regarding pore-scale upscaling of the hydraulic conductivity: “At high [relative variance], owing to flow localization, extreme values of [pressure drop squared] occurred at deterministic positions. The flow pattern is so strongly controlled by these huge values

[at bottleneck conductances quantified by percolation theory] that a stochastic description becomes inadequate." So, if the flow itself cannot be described by stochastic methods, it would not be possible to describe the distribution of particle velocities and path lengths either. The conclusion of Bernabe and Bruderer [9] at pore scales is consistent also with Shah and Yortsos' [10] conclusion that the critical path analysis framework was best suited to explain flow channeling in heterogeneous media at geologic scales such as observed by Moreno and Tsang [11]. Our basic method can be applied at either scale.

10.1.3 Experimental Overview

Solution of Eq. (10.1) for steady flow in a homogeneous medium leads to Gaussian spreading superimposed in the direction of flow. Natural porous media of interest (rocks, soils, fracture networks) are never homogeneous and, in fact, such Gaussian behavior of C is seldom inferred or observed [12–22]. A quantity developed, in the Lagrangian representation, to quantify the discrepancy between experiment and the Gaussian solution, is the longitudinal dispersion coefficient [23, 24]

$$D_{\mathrm{l}}(t) = \frac{1}{2}\frac{d}{dt}\sigma^2(t) \propto \frac{\sigma^2(t)}{t} \tag{10.3}$$

where the proportionality follows if $\sigma^2(t)$, *the variance of the spatial solute distribution*, is a power of the time, t. For Gaussian dispersion, the linear proportionality $\sigma^2(t) \propto t$ makes $D_{\mathrm{l}}(t)$ time independent. Since field experiments are pinned to an Eulerian representation, $D_{\mathrm{l}}(t)$ may also be reported as the ratio of the variance to the mean *travel length*, l. The two representations of $D_{\mathrm{l}}(t)$ are not always equivalent, since the mean solute velocity, $v_{\mathrm{s}} \equiv l/t$ is not, in general, scale-independent (e.g., Margolin and Berkowitz [21]; Lee et al. [25]). In fact, D_{l} typically increases as a power of system size [16, 17, 20],

$$D_l(t) \propto t^{\alpha} \tag{10.4}$$

with $0 < \alpha < 1$.

Such behavior is often considered to be a difficult point to explain.

Other experiments also reveal discrepancies with Gaussian spreading. In particular Cortis and Berkowitz [22] point out that several "classical" experiments [12, 26–28] in solute dispersion show breakthrough curves (BTC), for which Gaussian spreading overestimates the arriving solute flux at both short and long times. A long-tailed arrival time distribution (for which the variance or even the mean arrival time may not exist) such as predicted here will produce a longitudinal dispersion coefficient which increases with system size and is consistent with the deviations from Gaussian scaling of the BTCs listed by Cortis and Berkowitz [22]. Both kinds of experimental results point to the importance of being able to predict the entire arrival time distribution, or a spatial distribution of solutes at a given time.

10.1.4 Theoretical Descriptions

There are several avenues of approach to such problems. One can seek a mathematical framework, which produces solutions of the type observed. To this class of approaches belong the Continuous-Time Random Walk (CTRW) formulation and fractional differential equations. Thus such power-law tails may be described accurately with a fractional advection-dispersion equation, in which integer order derivatives in Eq. (10.1) may be replaced by fractional derivatives [29–37]. While such a formulation can model the long-time behavior, it cannot be used to predict it, unless the order of the derivative can be determined in advance. Further, a fractional differential equation does not necessarily generate the appropriate short-time behavior [21]. Additionally if, as derived here, the long-time tail is not a true power law, then such a method will not quite describe the asymptotic behavior either.

CTRW [38–40] appears to generate the entire arrival time distribution (e.g., Margolin and Berkowitz [21], Cortis and Berkowitz [22], Bijeljic and Blunt [41], Berkowitz et al. [42]) in agreement with experiment (except perhaps at very long times), but is also only descriptive. Nevertheless, the CTRW can provide guidance on how to predict large-scale behavior from small-scale observations. But we wish to predict the entire behavior of $C(x,t)$. We believe that this restricts the available options to percolation theory.

Percolation theory has been used before to calculate dispersion-related quantities in porous media [5, 25, 43–49]. While we are not the first to propose a percolation-based approach, our framework is quite distinct from those already in existence because we disentangle the influences of pore-size distributions from the topological complications of the flow paths described in percolation theory. In contrast to, e.g., the saturation dependence of K, for which different aspects of percolation theory dominate at different saturations, here we will show that these different aspects dominate in distinct time periods. In particular, the pore-size distribution, as expressed through a combination of critical path analysis and cluster statistics of percolation, is important near the peak in the arrival time distribution, while the tortuosity becomes relevant to the long-time asymptotic behavior, and thus to the spatial structure of the dispersion coefficient. Even our conclusion regarding the relevance of tortuosity to dispersion on account of the dominance of the critical paths has been anticipated in past discussions, at least qualitatively; consider the following quote from Rivard and Delay [50]:

Moreover, the critical path analysis [51] indicates that transport in a well-connected system in which the hydraulic conductivity distribution is broad, is actually dominated by a small subset of the system in which the magnitude of the conductivities is larger than a certain threshold. Heterogeneous porous media can therefore be mapped onto equivalent percolation networks.

This evaluation of Rivard and Delay [50] is consistent with decades of publications by Sahimi, including Sahimi [52–54]. However, we do not quite agree with the quantitative implications of this statement, that a direct mapping is sufficient. In particular, if the most permeable portion of the system that just percolates is chosen, the paths of flow are infinitely tortuous; following paths with slightly lower hydraulic

conductances would allow solutes to arrive at a much earlier time. Nevertheless, we agree with the general message of Rivard and Delay [50].

10.1.5 General Comments Regarding Experiments

Consider experiments with wetting fronts in natural media. When the medium itself is not too inhomogeneous (such as relatively uniform sand in a sand dune), such wetting fronts are often relatively regular. An interesting result from a particular experiment is that, even though the wetting front was fairly regular, paths of solutes following the fluid could be very irregular [55] (Fig. 10.1). Thus, experiments already suggest that it is appropriate, as in critical path-based calculations of the saturated hydraulic conductivity, K, to find K by an optimization between fluid connectivity and pore-size variability, while solute dispersion may better be determined through an enumeration of all the paths including effects of both pore-size distributions and the connectivity of percolation theory. It is suggested here, moreover, that it is the tendency for flow to emphasize the paths of least resistance which makes the cluster statistics of percolation near the percolation threshold relevant to both the distribution of measured K values and dispersion of solutes. We have found [56, 57] that indeed the distribution of K values in anisotropic fracture networks [58, 59] can be predicted using the cluster statistics of percolation. We now apply the same results to find the distribution of global fluxes. We do not seek a distribution of streamline velocities. Note that, in the simplified version of the problem we are considering, solutes are released at one instant in time, even though in experiments solutes are typically released with equal concentration starting at one particular time. We can relate these two procedures using a simple integral, while in our picture, the concentration, C, arriving at any position can be normalized to

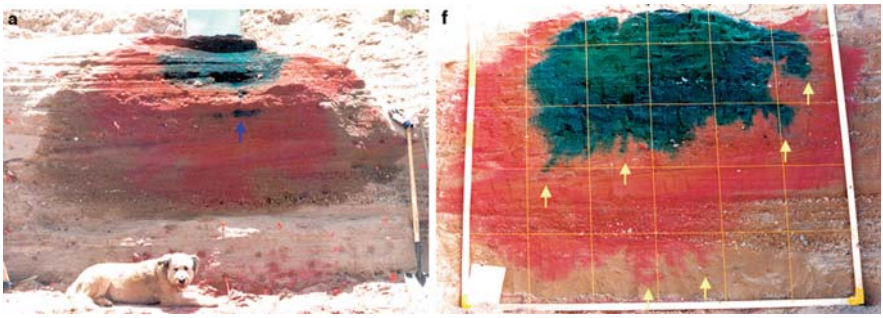

Fig. 10.1 Field experiments [55] reveal a wetting front that is much more regular than solute paths, broadly consistent with calculations of solute transport in terms of an enumeration of all paths, but of the hydraulic conductivity in terms of an optimal path (figure reprinted with permission from the authors). As pointed out by the authors, these characteristics can be identified much more easily with a color image. The two photographs are taken at different vertical slices in the medium

its original value, making C equivalent to a probability, W. This furthers use of the basic probabilistic transformations, on which the derivation is based.

The cluster statistics of percolation theory have been applied [1, 57] to the problem of deriving the distribution of controlling resistances (expressed as conductances, $g = R^{-1}$), of clusters of arbitrary length, N. Here N is a number (equal to the number of controlling resistances along one dimension of the cluster); the linear extent of the cluster must be expressed as the product of N and a typical spatial separation, l, of controlling resistances. The volume concentration of clusters of length Nl is then derived from n_s by using $n_s ds = n_N dN$, and the scaling relationship [60] $(\tau - 1)/\sigma\nu = d$, where d is the dimensionality of the space. The result is [1] (and using the above result for $p - p_c$).

$$n_N = \frac{1}{N^{d+1}} \exp\left\{ -\left[\left(\frac{Nl}{L} \right)^{\frac{1}{\nu}} \left| 1 - \left(\frac{g}{g_c} \right)^{\frac{3-D}{3}} \right| \right]^2 \right\} \tag{10.5}$$

The probability that a given system of Euclidean length, Nl, is spanned by a cluster with controlling conductance g is then proportional to the integral of $N^d n_N$ over clusters of all sizes larger than or equal to the volume in question. The result may be expressed in terms of the exponential integral,

$$\mathrm{Ei}[z] = \int_z^\infty \exp[-y] dy \tag{10.6}$$

as

$$W(g) \propto \frac{1}{\beta} \mathrm{Ei}\left[\alpha \left(\frac{x}{L} \right)^\beta \right] \tag{10.7}$$

where the parameters α and β are given by

$$\alpha = \left| 1 - \left(\frac{g}{g_c} \right)^{\frac{3-D}{3}} \right| \text{ and } \beta = \frac{2}{\nu} \tag{10.8}$$

Here x is the linear dimension of the system concerned, L^3 is a REV, which represents the smallest volume for which statistical arguments, such as percolation theory, apply, and l is a typical distance between critical resistances, which can be taken to be approximately equal to L. One can then set $L = 1$, meaning that $x = 1$ corresponds to the REV scale. In the limit that the pore-size distribution approaches a delta function (no width), the REV scale reduces to the separation of the pores. The result, Eq. (10.7), for $W(g)$ is shown graphically in Fig. 10.2.

An approximation to $W(g)$ is given by

$$W(g) \propto \ln\left\{ \left(\frac{L}{l+x} \right)^{\frac{1}{\nu}} \frac{1}{\left| \left[1 - \left(g/g_c \right)^{1-(D/3)} \right] \right|} \right\} \tag{10.9}$$

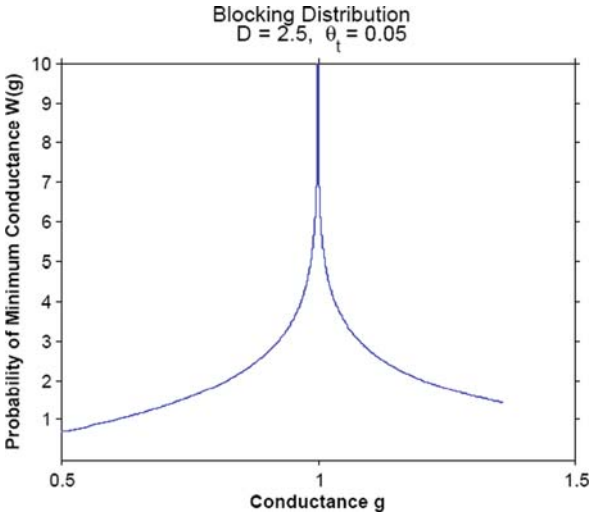

Fig. 10.2 An example of the pdf, $W(g)$, that the controlling (bottleneck) conductance in a system of size x has value g. Horizontal axis is in units of g_c. Fractal dimensionality of the pore space is given

Note that $W(g)$ is a function of system size, and thus $W(g)$ can be explicitly represented as $W(g, x)$. Equation (10.9) shows that the asymptotic behavior of the exponential integral involves a logarithmic divergence in $W(g)$ at $g = g_c = 1$ as can be seen in Fig. 10.2. Such a logarithmic divergence is integrable, meaning that $W(g)$ is normalizable. This same result may be obtained (as in Hunt et al. [57]) by replacing the exponential cut off (of the power-law decay) in Eq. (10.5) by a sharp cut off obtained by setting the argument of the exponential function equal to an arbitrary constant (as implied in Stauffer [60]).

The solute concentration of the water can be assumed to be uniform. Thus, although the probability that a given isotropic system is spanned by a cluster of minimum conductance g is given by Eqs. (10.7) and (10.8), the mass of solute transported through such clusters characterized by minimum conductance g must be proportional to the water flux, thus proportional to $gW(g)$. Since $W(g)$ is such a sharply peaked function, the effects on a distribution of arrival times, $W(t)$, due to the difference between $W(g)$ and $gW(g)$ is, in most cases, undetectable. Nevertheless, the probability that solute reaches the other end of a system at time t is clearly proportional to the volume of advecting fluid arriving at that time, and the solute arrival time distribution, $W(t)$, is thus proportional to $gW(g)$. The proportionality constant is defined next.

In order to use $W(g)$ to give information on arrival times, we must be able to relate the controlling conductance, g, of a path to the time, t, solute takes to travel along that path, $t(g)$. Here, x may be regarded simply as a parameter, independent of t. Thus the notation suppresses the x-dependence. Then one may use the result

$$gW(g)dg = W(t)dt \quad \text{or} \quad W(t) = \frac{gW(g(t))}{dt/dg} \tag{10.10}$$

In the absence of diffusion, the solution for $t(g)$ is deterministic. Note, however, that since $gW(g)$ is not directly normalized, $W(t)$ must be normalized separately. First we consider the effects of the distribution of pore sizes on $t(g)$, then the effects of connectivity and tortuosity.

In the following, the treatment of a percolation path as quasi-1D is not in contradiction to the tortuosity-based arguments; it is merely a first step in finding the influence of the pore-size distribution on the time of transit of a large cluster. Thus we decouple the effects of pore sizes and connectivity. As in an effective resistance, which is the sum of individual resistances along the path, the total *time* of travel is equal to the sum of the travel times through the individual pores along such a quasi-1D path. This means that it is necessary to find the transit times of individual pores on a path for which the mass flux is defined through the largest resistance on that path.

The time that a solute requires to traverse one pore is proportional to $1/v$, where v is the typical velocity in that pore. Then vA, where A is the cross-sectional area of the pore, must (aside from numerical factors) be proportional to Q, where Q is the volume flux of water through the pore. Thus $t \propto r/v \propto rA/Q$, where rA is proportional to r^3, or the volume of the pore. Q for all pores along a quasi-1D critical percolation path is identical and equal to Q_c, which is proportional to g_c. Similarly Q for all pores along a quasi-1D path near critical percolation is proportional to g, where g is the controlling (smallest) conductance on such a path. The probability that a given pore has radius r is proportional to [61] r^{-D-1} (though the fractional volume in such pores is proportional to $r^3 r^{-D-1} = r^{2-D}$). Q is a volume per unit time, but the time factor is explicitly removed (and called t_0) below so that Q is effectively only a volume. Under those stipulations, Q is r^3 and t_0 is a fundamental pore time scale. The value of t_0 is not required as only functional dependences are relevant below. Using these inputs it is possible to write the following expression of proportionality,

$$t(r) \propto t_0 \int_{\mathrm{r}}^{r_\mathrm{m}} dr' \frac{r'^3}{Q} \frac{r'^{-D-1}}{r^{-D}} = t_0 \left[\int_{\mathrm{r}}^{r_\mathrm{c}} dr' \frac{r'^3}{Q} \frac{r'^{-D-1}}{r^{-D}} + \int_{r_\mathrm{c}}^{r_\mathrm{m}} dr' \frac{r'^3}{Q} \frac{r'^{-D-1}}{r^{-D}} \right] \tag{10.11}$$

The division of the integral into two terms is useful for expressing the time in terms of the critical time for percolation. The input into Eq. (10.11) is consistent with the assumption that the paths followed by the solute are straight. Clearly Eq. (10.11) must now be modified to account for the effects of the tortuosity on the transit time. The tortuosity was noted to follow

$$\frac{\Lambda}{\chi} \propto |V - V_\mathrm{c}|^{-(\eta - \nu)} = |V - V_\mathrm{c}|^{-\left(\nu D_\mathrm{opt} - \nu\right)} \tag{10.12}$$

But we cite Lee et al. [25] to support our substitution of the exponent D_b for D_{opt} in Eq. (10.12). In Eq. (10.12) V is an arbitrary volume fraction and V_c its critical value for percolation. In the present context V and V_c may be considered to correspond to the volumetric moisture content, θ, and its critical value for percolation, θ_t, even though the specific problem to be addressed here involves saturated conditions. The effect due to the tortuosity is to lengthen each individual time by the factor represented in Eq. (10.12); thus the combined effects of streamline fluxes and tortuosity are given by the product of Eqs. (10.11) and (10.12). An additional factor of $\left(x/L_0\right)^{D_b}$ enters to give the explicit dependence on the Euclidean measure of the system size, x, in terms of the correlation length, L. Evaluating the integrals in Eq. (10.11) and combining with Eq. (10.12) then yields

$$t = \left(\frac{x}{L}\right)^{D_b} \frac{t_0}{3-D} \left[\frac{1}{r^{3-D}}\right] \left[\left(r_m^{3-D} - r_c^{3-D}\right) + \left(r_c^{3-D} - r^{3-D}\right)\right] \left[\frac{1}{\theta - \theta_t}\right]^{(D_b-1)v} \tag{10.13}$$

Equation (10.13) may be further manipulated to yield

$$t = \left(\frac{x}{L}\right)^{D_b} \frac{t_0}{3-D} \frac{g_c}{g} \frac{1}{(1-\theta_t)^{A-v}} \left[\left(1 + \frac{\theta_t}{1-\theta_t}\right)\left(\frac{g_c}{g}\right)^{1-\frac{D}{3}} - 1\right] \left[\frac{1}{(g/g_c)^{1-(D/3)} - 1}\right]^{(D_b-1)v} \equiv \left(\tfrac{x}{L}\right)^{D_b} t_g \tag{10.14}$$

where t_g, a cluster transit time, is defined by Eq. (10.14). We have performed an analogous derivation for $t(S)$ as a function of saturation, S, but the results may be expressed in the same form as in Eq. (10.14), as long as none of the required conditions are violated. One condition that should be further addressed is the lower limit on g values allowed; as the saturation is reduced the range of possible r-values in $r_c^{3-D} - r^{3-D}$ is reduced since r cannot be less than r_0. Note that, for example, the smallest value of $(r_c/r)^{3-D}$ possible, if the moisture content is the critical moisture content, is $(r_0/r_m)^{3-D} = 1 - \phi$. In this case Eq. (10.14) can be shown to yield a negative value of t if θ_t is not large enough. However, larger values of θ_t also tend to depress r_c toward r_0. Thus we might anticipate that comparison of results for $W(t)$ based on Eq. (10.14) with experiment for unsaturated conditions could lead to unreliable values of θ_t as a fitting parameter, and this is indeed what we observe.

The dependence of $t(g)$ in Eq. (10.14), which contains a power-law divergence at $g = g_c$, is depicted in Fig. 10.3. Note that the vicinity of the percolation threshold occurs here in the limit of infinite time. For g near g_c, but somewhat less than g_c, there occurs a minimum in $t(g)$. This minimum, broadly speaking, corresponds to the optimal conductance which defines the hydraulic conductivity of an infinite system. How can this be understood?

A nonvanishing K cannot be calculated from a subnetwork of the system, which is just at the percolation threshold. Even though this condition certainly defines the most conductive pathways in the system, their spatial separation is equal to χ, which diverges at the percolation threshold, producing an effective conductivity of zero. Thus the network for calculating K must also include a few $g < g_c$ reducing

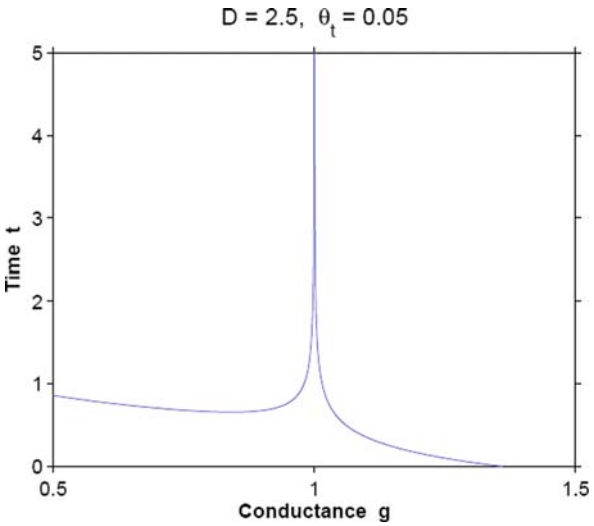

Fig. 10.3 An example of the time, t, of transit through a cluster of minimum conductance, g, for specific values of the fractal dimensionality of the pore space and critical volume fraction for percolation. Horizontal axis is in units of g_c

the conductance of each path but greatly increasing the number of effective paths. The conductivity is then calculated using an optimization procedure [62–64]. This optimization procedure winds up pinning the controlling g near g_c, similarly to the way the minimum in $t(g)$ is tied to g_c.

Under extreme circumstances of very high disorder in very small systems, this minimum can create a spike in $W(t)$; however we do not expect that such a spike (which is a result of $dt/dg = 0$, i.e., many paths with the same arrival time, t) would survive if our calculations would take into account the spreading in $W(t)$ due to the varying velocities in, e.g., a single cylindrical pore. Note as well that in the immediate vicinity of the peak in $t(g)$ the contribution from the variability of the flux (the first factor in square brackets) is negligible in comparison with the tortuosity (the second factor in square brackets), except in the limit of vanishing θ_t. As a consequence one may quickly find the effects of $t(g)$ on the asymptotic, large time behavior of $W(t)$ to be,

$$W(t) \propto \left[\frac{\mathrm{A}}{t}\right]^{\frac{1+(\eta-v)}{\eta-v}} \tag{10.15}$$

with A is a constant. Note, however, that in the cases we have checked heretofore the absolute value of the power predicted by Eq. (10.15) has, in each case, exceeded by ca. 0.5 the result generated by numerical analysis of the full distribution.

A full numerical solution for $W(t)$ from Eq. (10.10) using Eq. (10.14) for $t(g)$ gives the results shown in Figs. 10.4a and 10.4b, for various combinations of fractal dimensionality and critical values of the moisture content in a 2D random percolation system.

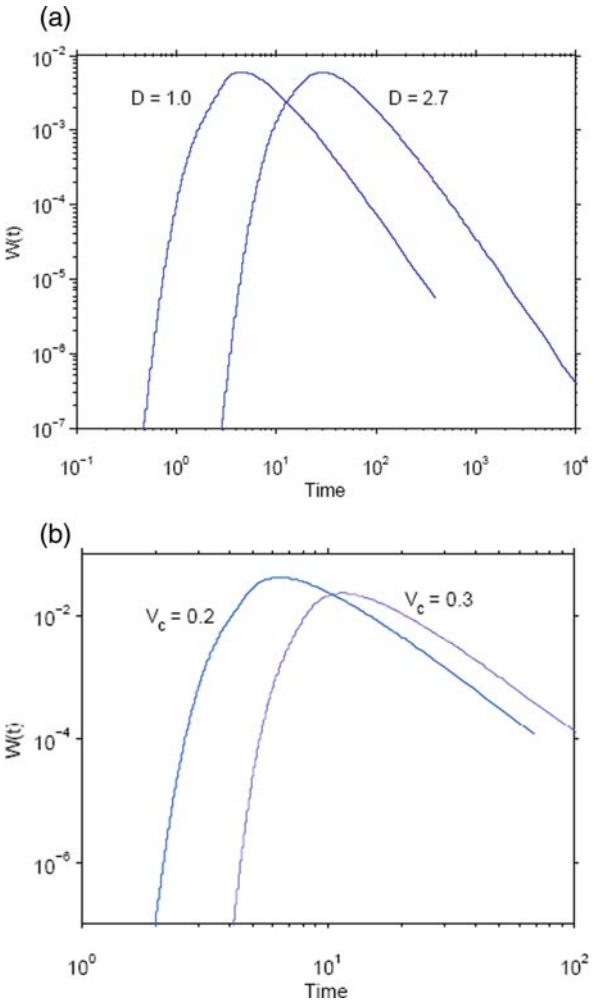

Fig. 10.4 Comparison of the results for the arrival time distribution, $W(t)$, for two different values of the fractal dimensionality of the pore space (10.4a) and two different values of the critical volume fraction for percolation (10.4b)

10.1.6 Spatial Distribution at an Instant in Time

The calculation of the spatial distribution, $W(x)$, of solutes at a given time clearly has some relationship with the calculation of the distribution of arrival times at a given point in space. However, we cannot simply integrate over all g holding x constant, since each g value is associated with its own particular velocity, and only one value of g produces a given value of x. On account of the logarithmic dependence of $W(g, x)$, it is not possible to use simple relationships between spatial and temporal scales as implied in the publication by Margolin and Berkowitz (2004) and the references cited therein.

Consider again the statistics, $W(g, x)$, of clusters of size at least x dominated by minimum conductances, g. $W(g, x)$ represents once again the probability that an arbitrary particle will initiate its motion on such a cluster and can also travel a Euclidean distance at least x on that cluster. If the solute is on a cluster described by $W(g, x)$, its distance of travel, x, and mean velocity, $< v >$, will be related by $x =< v > t$, where t is the time since the solute was initially introduced, and $< v >$ is dependent on scale x as well as g. For consistency we require this distance x to be identical to x in $W(g, x)$. The pore-size dependence of the mean velocity is independent of the distance of travel, and can be roughly estimated using the framework already introduced above as being inversely proportional to $t(g)$ [in particular as $t_0/t(g)$]. Now, $x \propto t^{1/D_b}$, so that $< v >= x/t \propto t^{(1/D_b-1)} \propto x^{1-D_b}$. Using these inputs we find that

$$\langle v \rangle \propto \left(\frac{t_0}{t_g}\right)\left(\frac{L}{x}\right)^{D_b-1} v_0 \tag{10.16}$$

where v_0 is a pore scale velocity. Then one can write for the distance traveled,

$$x = \langle v \rangle t = \left(\frac{L}{t_g}\right)\left(\frac{L}{x}\right)^{D_b-1} t \tag{10.17}$$

where $L \approx v_0 t_0$. Solution of this equation for x/L_0 gives

$$x = L\left(\frac{t}{t_g}\right)^{\left(\frac{1}{D_b}\right)} \tag{10.18}$$

Note that Eq. (10.18) could have been obtained more easily by solving Eq. (10.14) for x, but now we have an expression (Eq. (10.16)) for an average solute velocity too, useful for calculation of the dispersivity. The probability that the particle has actually gone this distance x (at time t) is then given by the probability distribution $W(g, x)$ given in Eqs. (10.7) and (10.8), but with the value of $x(t)$ inserted from Eq. (10.18). Then the logarithmic approximation of $W(g, x)$ (Eq. (10.9)) would look like

$$W(g) \propto \ln\left[\left[\frac{L}{l + L\left(t/t_g\right)^{1/D_b}}\right]^{\frac{1}{\nu}} \frac{1}{\left|\left[1 - \left(g/g_c\right)^{1-(D/3)}\right]\right|}\right] \tag{10.19}$$

Now that $W(g)$ is developed in a form in which both factors are expressed consistently in terms of the same g value, it is possible to make a direct translation between $W(g)$ and $W(x)$ in the same fashion as in Eq. (10.10)

$$W(x) = \frac{W(g, x(t, g))}{dx/dg} \tag{10.20}$$

where dx/dg is obtained from Eq. (10.18) in terms of dt_g/dg from Eq. (10.14), and where the final step involves solving for g in terms of x and t using Eq. (10.17). Thus the results will include the value of the time as a parameter, just as Eq. (10.10) included the value of the spatial coordinate as a parameter. Using Eq. (10.20) it will be possible to calculate the second moment of the spatial solute distribution $\sigma^2(x)$ with the time as a parameter, and the dispersivity as the ratio of $\sigma^2(x(t))/v(t)$ using Eq. (10.16).

10.1.7 Hydraulic Conductivity

While prior calculations have generated the hydraulic conductivity, K, through an optimization of the effects of pore-size distributions and the connectivity/tortuosity factor, it should also be possible to find K directly by summing the contributions over all g of $gW(g)t_0/t(g)$. The fact that there is a local minimum in the arrival time at a g near g_c and that the distribution of g values is sharply peaked at $g = g_c$ should clearly lead to a hydraulic conductivity whose value is controlled by g_c, in accord with the optimization procedure. This is an important project that needs to be addressed in the future.

10.2 Comparison with Simulations

Liu et al. [65] report on simulations of flow and transport on a 2D percolation structure (at the percolation threshold). They do not incorporate any effects of diffusion, nor do they include any effects that would be equivalent to a pore-size variability. The solve the Navier–Stokes equations for flow, and then use particle-tracking methods to determine $W(t)$ (Fig. 10.5). Such a model lends itself to comparison with our predictions. In order to fit the curve with our result for $W(t)$ we employed three parameters: an absolute time scale, t_0, the critical volume fraction for percolation, and the fractal dimensionality of the pore space. These parameters were found by comparison with the curve for $L = 10$, and then our prediction for $L = 50$ was compared with simulation. The parameters $D_b = 1.6432$ and $\nu = 4/3$ were dictated by percolation theoretical arguments made above, and could not be adjusted.

Above we demonstrated that the variability of $W(t)$ with parameters such as D and V_c for the pore space is relatively modest; nevertheless larger values of D appropriate for disordered natural media do produce a noticeable downward curvature at larger times, distinct from the numerical simulations. We find that $D = 1$, which, for $\phi = 0.5$, would be consistent with $r_0 = r_m/\sqrt{2}$, i.e., a very narrow pore-size distribution gives a reasonably good shape fit with simulations. Note that in the absence of disorder, the REV length scale is a single pore length, so that a simulation length scale of 1 [65] corresponds exactly to our system length of 1. Finally, larger values of V_c tended to produce a narrower peak; we found that a rather large value

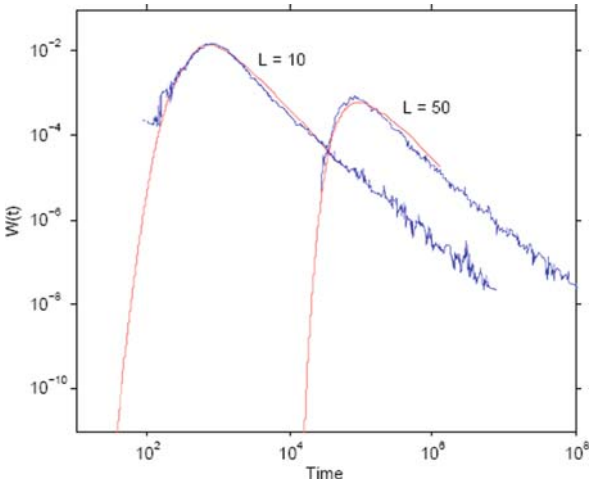

Fig. 10.5 Comparison of the predicted distribution of arrival times with results of numerical simulations by Lee et al. [25]. Both calculation and simulation were done in two dimensions and without accounting for diffusion. Note that three adjustable parameters were used to generate the agreement with spatial system size 10, but the same parameters were used for system size 50. Further, the fractal dimensionality of the pore space used, $D = 1$, corresponds to a system with almost no range of pore sizes, generally consistent with the constraints of the simulations, which include no such range

$V_c = 0.25$ produced the closest fit. In retrospect, we may have preferred to see an even larger value (such as 0.5, p_c for a square lattice in 2D), but we have left out numerical constants throughout the derivation, so we find that for an effectively two-parameter fit (the chosen D at very nearly the "ordered" limit of the Rieu and Sposito model) we have relatively good results. More impressive is that, for exactly the same parameters generated by comparing the $L = 10$ curve with our functional form, we generate almost precisely the correct form for $W(t)$ at $L = 50$, including the appropriate narrowing of the peak on the short-time side.

We emphasize that no publications in the ISI Web of Science to date have given any theoretical explanation for the results of the simulations of Liu et al. [65].

10.3 Comparison with Experiment

Comparison with experiment brings in additional uncertainties. These are (1) experimenters typically report a quantity different from $W(t)$, (2) experimental results include the effects of experimental error, and (3) experiments cannot turn off the effects of molecular diffusion, though they may be small enough to be negligible. Experimentalists typically measure what is called a breakthrough curve (BTC). An experiment, in which solute is transported through a medium by flowing water, can be performed in a column of centimeter scale radius and decimeter scale height (in

other words $10^3 - 10^5$ pore separation). Water flow through a system is allowed to reach steady state, i.e., it is uniform in time and nominally uniform in space. Then, starting at time $t = 0$, solute is released at a steady rate into the water flux. The experimenter then measures $1 - C$ as a function of time at the bottom of the column. Note the difference between the typical experimental procedure and a delta-function introduction of solute, for which the measured $C(t)$ at some particular x value corresponds to $W(t)$. The result of the experimental procedure described is a solute flux, which steadily rises to a value of 1. Since rate of solute release is typically constant, the functional form of the release corresponds to a Heaviside step function, and the temporal dependence of the measured C represents the indefinite integral of $W(t)$. The negative of the time derivative of the measured $1 - C$ thus corresponds to our $W(t)$.

Cortis and Berkowitz [22] summarize results of three "classic" experiments in solute transport [12, 26–28]. We will use two means to check whether our theoretical procedure is compatible with these experiments. First we calculate a predicted local power, $\alpha(t) = d(\log[W(t)])/d(\log[t])$ for all times subsequent to the peak. In Fig. 10.6 we see that α at first drops rapidly from zero, then it tends to level off, although it continues to diminish slowly. This slope can be compared with values of β + 1 [Margolin and Berkowitz [21] refer to Shlesinger [38] who showed that if the asymptotic behavior of $W(t)$ is a power law with power α, the power β that appears in the CTRW is given by $\beta = \alpha - 1$]. In Fig. 10.6 we see that the slopes of the two most distinct predictions in three dimensions, random percolation and invasion percolation (on account of the significantly different values of $D_b = 1.87$ and 1.46, respectively), enclose the values of $\beta + 1$ reported. The smaller value of D_b [and steeper slope of $W(t)$] results when there is residual water, which cannot easily be removed from a medium on account of the lack of continuously connected paths through water-filled pores. Such a moisture configuration corresponds to that

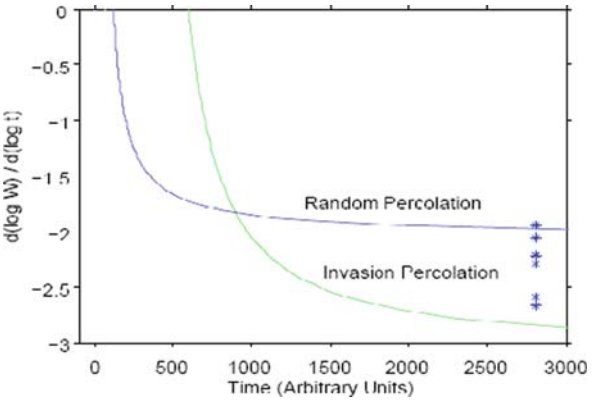

Fig. 10.6 Prediction of local slope of $\log[W(t)]$ vs. $\log[t]$ compared with experimental values for an average slope reported by Cortis and Berkowitz [22]. Predictions are for both random percolation and for bond invasion percolation with trapping (relevant to an approach to the critical moisture content for percolation in unsaturated soils) and in 3D systems

in invasion, bond, percolation with trapping (bond TIP). For $\theta \approx \theta_t$ and 3D systems this value (1.46) is likely the relevant choice of D_b.

Our second check was to determine whether the predicted curve has a shape, which is generally compatible with experiment. For this purpose we digitized the data from Cortis and Berkowitz' [22] Fig. 5 [an Oakley Sand, with data originally from Nielsen and Biggar [27]]. This comparison is shown in Fig. 10.7. Note that the medium considered is not saturated ($\theta = 0.27$), but we have shown that our results, derived for saturated conditions, are relevant also for unsaturated conditions (as long as certain inequalities are not violated). The experimental quantity reported is $1 - \int W(t)dt$, so in order to observe the tail of $W(t)$ at large values of the time, the normalization constant of $W(t)$ must be very accurately known. The reason is that the magnitudes of both terms, 1 and the integral, are nearly equal. We do not yet have such accuracy, so we chose instead to compare our expression for $W(t)$ with the negative of the time derivative of $1 - \int W(t)dt$. Differentiating experimental data, however, introduces its own complications, in particular rather large fluctuations in the value of the experimentally inferred $W(t)$. We used a 9-point running average to smooth out these fluctuations, though some fluctuations remain, and this excludes the first and last five experimental points from our figure. Our results from this process still contain some fluctuations. Then we sought values of D and θ_t, which would provide the best fit to the data. We had to use such a large value of $\theta_t = 0.75$ that it was not consistent to use a random percolation value for D_b, forcing us to use $D_b = 1.46$ for bond Trapping Invasion Percolation (TIP). Then we rescaled

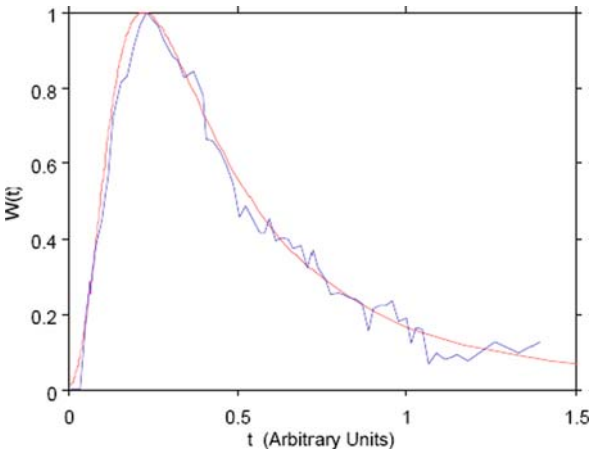

Fig. 10.7 Comparison of an arrival time distribution digitized from Fig. 5 in Cortis and Berkowitz [22] with our prediction of $W(t)$. Since the arrival time distribution in Cortis and Berkowitz [22] clearly rises discontinuously from zero, in contrast to the theoretical result here (which rises through more than 100 orders of magnitude over a short time scale), it was necessary to shift our arrival time distribution as well as to use t_0 as a fit parameter. On the other hand, it is here only our intention to demonstrate that our formulation produces generally the right shape of the experimental arrival time distribution. Note that the linear scale shows that neither experiment nor prediction resembles a Gaussian distribution

the time in the theory by a constant factor. This made the curves almost identical, but it was necessary also to require a uniform translation of our points to smaller times, in order to produce the close agreement that seems to result (Fig. 10.7). We consider that this result should be approached with some caution, on account of the translation in time, whose physical significance we are not sure of, but whose mathematical effect is to narrow the peak. A second uncertainty results from the fact that we used results derived for a saturated medium, presumably leading to the unlikely value of θ_t.

10.4 Discussion

The first point that is important in our discussion is that, on account of the asymptotic logarithmic behavior of the exponential integral in $W(g)$ (Eq. (10.9)), the true behavior of $W(t)$ at long times is not strictly a power law, though it may appear to be so. This logarithmic correction factor involves the system length as well, meaning that it may be important for a wide range of comparisons. Although this may have significant consequences, we could only speculate as to their specific implications, since we do not yet have numerical results for the spatial distribution of solute at a particular time.

While the comparison of our predicted $W(t)$ with simulation was fairly straightforward, the corresponding comparison with experiment was less so. We find certainly that a qualitative description of experimental results is possible, but are less certain regarding the use of the theory at this point to make quantitative predictions. Further, there are several points that may hinder prediction, including (1) predicted peak widths are frequently a little too large, even though the wings of the distribution are well predicted, (2) we do not know, a priori, what pore-size distribution may be most applicable, and the pore size distribution does have an effect on $W(t)$ near the peak, and (3) we are not yet sure whether the variability in experiment will be appropriately accounted for by the variability in theory.

With only our limited perspective at this time it does seem that the narrow width of the peaks may require unrealistic choices of parameters ($\theta_t = 0.75$) to fit experiment. Although we have shown that Eqs. (10.8) and (10.14) apply equally to unsaturated as well as to saturated media, using these equations for unsaturated media is only valid for narrower ranges of parameter values and it is possible that we tried to force these equations into a parameter regime in which the full variability of $W(t)$ cannot logically be invoked when we generated $\theta_t = 0.75$. The answer to this question is not yet known.

Since the peak region is model dependent and not universal, it may be important to add flexibility in choosing different pore-scale models. In order to make a comparison with simulations we had to choose a pore-size distribution which was practically a delta function in form. In that case such a choice was not too worrisome since we knew that the simulations included no variation in pore sizes, although a true delta function pore-size distribution cannot be obtained from the Rieu and Sposito [2] model. In general, however, we do not know a priori what the appropriate soil models for a given experiment may be.

Our theoretical powers in three dimensions for random percolation and invasion percolation with trapping (bond percolation) have values that contain the range of values of $\beta + 1$ reported by Cortis and Berkowitz, but two questions arise in that context. Is the variability of these values accounted for by a reasonable combination of variation in parameters and relevant spatial scale? At first glance it appears so, since the Oakley sand which we actually compared in detail produced a value of $\beta = 1.05$ [22], which should have corresponded more closely to random percolation with a slope near -2 (see Fig. 10.6), but which was apparently adequately accounted for by invasion percolation, with a slope nearer -3. The second related question that comes up refers to other experiments. Will we be able to account for them as well, possibly by including also the 2D parameters (if appropriate)? We have only directly considered models which exclude correlations in the local bond probabilities. It is known (e.g., Araujo et al. [46]) that such correlations can affect D_b, the principal influence on the long-time asymptotic behavior of $W(t)$. Will it be necessary, or even appropriate, to try to account for the potential influences of correlations between pores on experimental results?

Finally, can we also expect Gaussian dispersion from the present theory? Margolin and Berkowitz [21] note that Gaussian dispersion should result when the first and second moments of the arrival distribution time exist ($\beta > 2$) The slope of $W(t)$ for $D_b = 1.46$ is already very nearly $-3 = -(\beta + 1)$; for smaller values of $D_{opt} = 1.217$, such as appropriate for the chemical path length, we should then expect Gaussian dispersion. However, the conditions for which such a choice of fractal dimensionality might be appropriate are not known. We hypothesize that D_{opt} may be appropriate under conditions when the medium is fairly homogeneous both from the standpoint of the pore-size distribution and from the relevance of any percolation structures. This hypothesis is somewhat aligned with the arguments of Bruderer-Weng et al. [66], who argue that flow channeling is relevant to long-tailed arrival time distributions, though in our case the actual cause of the long-tailed distributions remains the relevance of the tortuosity of the pathways and the fractal dimensionality of the backbone cluster, while the flow-channeling along such structures arises from a wide range of pore sizes.

References

1. Hunt, A. G., 1998, Upscaling in subsurface transport using cluster statistics of percolation, *Transp. Porous Media* **30**(2): 177–198. 265, 270
2. Rieu, M., and G. Sposito, 1991, Fractal fragmentation, soil porosity, and soil water properties I. Theory, *Soil Sci. Soc. Am. J.* **55**: 1231. 265, 281
3. Liu, Z-F., X.-H. Wang, P. Mao, and Q.-S. Wu, 2003, Tracer dispersion between two lines in two-dimensional percolation porous media, *Chin. Phys. Lett.* **20**: 1969–1972. 265
4. Pfannkuch, H., 1963, Contribution à l'étude des déplacements de fluides miscibles dans un milieu poreux. Contribution to the study of the displacement of miscible fluids in a porous medium, *Rev. Inst. Fr. Pét.* **2**: 18. 266
5. Sahimi, M., and A. O. Imdakm, 1988, The effect of morphological disorder on hydrodynamic dispersion in flow through porous media, *J. Phys. A: Math Gen.* **21**: 3833–3870. 266, 268

6. Bear, J., 1972, *Dynamics of Fluids in Porous Media*, American Elsevier Publishing Co. Inc., New York. 266
7. Dagan, G., and S. P. Neuman, eds., 1997, *Subsurface Flow and Transport: A Stochastic Approach*, Cambridge University Press: Cambridge, U.K. 266
8. Winter C. L., D. M. Tartakovsky, and A. Guadagnini, 2003, Moment differential equations for flow in highly heterogeneous porous media, *Surv. Geophys.* **24**(1): 81–106. 266
9. Bernabe, Y., and C. Bruderer, 1998, Effect of the variance of pore size distribution on the transport properties of heterogeneous networks, *J. Geophys. Res*., **103**: 513. 266, 267
10. Shah, C. B., and Yortsos, Y, C., 1996, The permeability of strongly disordered systems, *Phys. Fluids* **8**: 280–282. 267
11. Moreno, L., and C. F. Tsang, 1994, Flow channeling in strongly heterogeneous porous media: A numerical study, *Water Resour. Res*. **30:** 1421. 267
12. Scheidegger, A. E., 1959, An evaluation of the accuracy of the diffusivity equation for describing miscible displacement in porous media, in: *Proc. Theory of Fluid Flow in Porous Media* Conf., Univ Oklahoma, 101–116. 267, 279
13. Aronofsky, J. S., and J. P. Heller, 1957, A diffusion model to explain mixing of flowing miscible fluids in porous media, *Trans. AIME*: **210**: 345–349. 267
14. Lallemand-Barres, A., and P. Peaudecerf, 1978, Recherche des relations entre la valeur de la dispersivite macroscpique d 'un milieu aaquifere, ses autres chaacteristiques et les conditions de mesure [Search for relations between the macroscopic dispersivity value of an aquifer, its other characteristics and measurement conditions], Bulletin du B. R. G. M. (deuxieme serie), section III, (4), pp 227–284. 267
15. Silliman, S. E., and E. S. Simpson, 1987, Laboratory evidence of the scale effect in dispersion of solutes in porous media. *Water Resour. Res*. **23**: 1667–1673. 267
16. Arya, A., T. A. Hewett, R. G. Larson, and L. W. Lake, 1988, Dispersion and reservoir heterogeneity, *SPE Reserv. Eng.* **3**: 139–148. 267
17. Neuman, S. P., 1990, Universal scaling of hydraulic conductivities and dispersivities in geologic media, *Water Resour. Res*., **26**: 1749–1758. 267
18. Gelhar, L. W., C. Welty, and K. R. Rehfeldt, 1992, A critical review of data on field-scale dispersion in aquifers. *Water Resour Res*. **28**: 1955–1974. 267
19. Berkowitz, B., and H. Scher, 1995, On characterization of anomalous dispersion in porous and fractured media, *Water Resour. Res*. **31**: 161–2466. 267
20. Xu, M., and Y. Eckstein, 1995, Use of weighted least-squares method in evaluation of the relationship between dispersivity and field scale, *Ground Water* **33**: 905–908. 267
21. Margolin, G., and B. Berkowitz, 2000, Application of continuous time random walks to transport in porous media, *J. Phys. Chem. B* **104**: 3942–3947. 267, 268, 279, 282
22. Cortis, A. and B. Berkowitz, 2004, Anomalous transport in "classical" soil and sand columns, *Soil Sci. Soc. Am. J*. **68**: 1539–1548. 267, 268, 279, 280, 282
23. Dagan, G., 1987, Theory of solute transport by groundwater, *Annual Rev. Fluid Mechanics*, **19**: 183–215. 267
24. Dagan, G., 1991, Dispersion of a passive solute in nonergodic transport by steady velocity-fields in heterogeneous formations, *J. Fluid Mech*., **233**: 197–210. 267
25. Lee, Y, J. S. Andrade, S. V. Buldyrev, N. V. Dokholoyan, S. Havlin, P. R. King, G. Paul, and H. E. Stanley, 1999, Traveling time and traveling length in critical percolation clusters, *Phys. Rev. E* **60**(3): 3425–3428. 267, 268, 273, 278
26. Nielsen, D. R., and J. W. Biggar, 1961, Miscible displacement in soils I Experimental information, *Soil Sci. Soc. Am. Proc*. **25**: 1–5. 267, 279
27. Nielsen, D. R., and J. W. Biggar, 1962, Miscible displacement in soils III Theoretical considerations, *Soil Sci. Soc. Am. Proc*. **26**: 216–221. 267, 279, 280
28. Jardine, P. M., G. K. Jacobs, and G. V. Wilson, 1993, Unsaturated transport processes in undisturbed heterogeneous porous media: 1. Inorganic contaminants, *Soil Sci. Soc. Am. J.* **57**: 945–953. 267, 279
29. Meerschaert, M. M., D. A. Benson, and B. Baumer, 1999, Multidimensional advection and fractional dispersion, *Phys. Rev. E* **59**: 5026–5028. 268

30. Meerschaert, M. M., D. A. Benson, H. P. Scheffler, and P. Becker-Kern, 2002, Governing equations and solutions of anomalous random walk limits *Phy. Rev. E* **66**(6): Art. No. 060102 Part 1. 268
31. Meerschaert M. M., J. Mortensen, and S. W. Wheatcraft, 2006, Fractional vector calculus for fractional advection-diffusion, *Physica A* **367**: 181–190. 268
32. Sanchez, R., B. A. Carreras, and B. P. van Milligen, 2005, Fluid limit of nonintegrable continuous-time random walks in terms of fractional differential equations, *Phys. Rev. E* **71**(1): Art. No. 011111 Part 1. 268
33. Park, M., N. Kleinfelter and J. H. Cushman, 2005, Scaling laws and Fokker-Planck equations for 3-dimensional porous media with fractal mesoscale**,** *Multiscale Model. Simul.* **4**(4): 1233–1244 268
34. Kohlbecker, M. V., S. W. Wheatcraft, and M. W. Meerschaert , 2006, Heavy-tailed log hydraulic conductivity distributions imply heavy-tailed log velocity distributions, *Water Resour. Res*. **42**(4): Art. No. W04411 APR 19 2006. 268
35. Krepysheva, N., L. Di Pietro, and M. C. Neel, 2006, Space-fractional advection diffusion and reflective boundary condition, *Phys. Rev. E* **73** 2): Art. No. 021104 Part 1. 268
36. Zhang X. X., J. W. Crawford, and L. K. Deeks et al., 2005, A mass balance based numerical method for the fractional advection-diffusion equation: theory and application, *Water Resour. Res*. **41**(7): Art. No. W07029 JUL 27 2005. 268
37. Zhang, Y, D. A. Benson, and M. M. Meerschaert et al., 2007, Space-fractional advection-dispersion equations with variable parameters: diverse formulas, numerical solutions, and application to the macrodispersion experiment site data, *Water Resour. Res*. **43**(5): Art. No. W05439. 268
38. Shlesinger, M. F., 1974. Asymptotic solutions of continuous-time random walks, *J. Stat. Phys*. **10**: 421–434. 268, 279
39. Scher, H., and E. W. Montroll, 1975, Anomalous transit-time dispersion in amorphous solids, *Phys. Rev. B* **12**(6): 2455–2477. 268
40. Klafter, J., and R. Silbey, 1980, Derivation of the continuous-time random walk equation, *Phys. Rev. Lett*. **44**: 55–58. 268
41. Bijeljic, B., and M. J. Blunt, 2006, Pore-scale modeling and continuous time random walk analysis of dispersion in porous media, *Water Resour Res.* **42** (1): Art. No. W01202 JAN 31. 268
42. Berkowitz, B., A. Cortis, M. Dentz et al., 2006, Modeling non-Fickian transport in geological formations as a continuous time random walk *Rev. Geophys.* **44**(2): Art. No. RG2003 . 268
43. Koplik, J., S. Redner, and D. Wilkinson, 1988, Transport and dispersion in random networks with percolation disorder, *Phys. Rev. A* **37**: 2619–2636. 268
44. Porto, M., S. Havlin, H. E. Roman, and A. Bunde, 1998, Probability distribution of the shortest path on the percolation cluster, its backbone, and skeleton, *Phys. Rev. E* **58**(5): R5205–R5208. 268
45. Paul, G., S. Havlin, and H. E. Stanley, 2002, Fractal behavior of the shortest path between two lines in percolation systems, *Phys. Rev. E* **65**, 066105–1, 066105–8. 268
46. Araujo, A. D., A. A. Moreira, R. N. Costa Filho, and J. S. Andrade, Jr., 2003, Statistics of the critical percolation backbone with spatial long-range correlations, *Phys. Rev. E* **67**: 027102–1 to 027102–4. 268, 282
47. Barthelemy, M., S. V. Buldyrev, S. Havlin, and H. E. Stanley, 2003, Scaling and finite-size effects for the critical backbone, *Fractals 11* (supplement): 19–27. 268
48. Lopez, E., S. V. Buldyrev, L. A. Barunstein, S. Havlin, and H. E. Stanley, 2005, Possible connection between the optimal path and flow in percolation clusters, *Phys. Rev. E* **72**: 056131–1 056131–6. 268
49. Havlin, S., L. A. Braunstein, S. V. Buldyrev, R. Cohen, T. Kalisky, S. Sreenivasan, and H. E. Stanley, 2005, Optimal path in random networks with disorder: a mini review, *Physica A* **346**: 82–92. 268
50. Rivard, C., and F. Delay, 2004, Simulations of solute transport in fractured porous media using 2D percolation networks with uncorrelated hydraulic conductivity fields, *Hydrogeology J.* **12**: 613–627. 268, 269

51. Ambegaokar, V. N., B. I. Halperin, and J. S. Langer, 1971, Hopping conductivity in disordered systems. *Phys. Rev. B* **4**: 2612–2621. 268
52. Sahimi, M., 1993, Fractal and superdiffusive transport and hydrodynamic dispersion in heterogeneous porous media, *Transp. Porous Media* **13**: 3–40. 268
53. Sahimi, M., 1993, Flow phenomena in rocks − from continuum models to fractals, percolation, cellular automata, and simulated annealing, *Rev. Mod. Phys.* **65**(4): 1393–1534. 268
54. Sahimi, M., 1995, *Flow and Transport in Porous Media and Fractured Rock from Classical Methods to Modern Approaches*, Wiley VCH Weinheim, Germany, 500 pp. 268
55. Glass, R. J., J. R. Brainard, and T-C. J. Yeh, 2005, Infiltration in unsaturated layered fluvial deposits at Rio Bravo: macroscopic anisotropy and heterogeneous transport, *Vadose Zone J.* **4**(1): 22–31. 269
56. Hunt, A. G., 2005, Percolation theory and the future of hydrogeology, *Hydrogeology J.* **13**: 202–205 269
57. Hunt, A. G., and T. E. Skinner, 2008. Longitudinal dispersion of solutes in porous media solely by advection. *Philos. Mag*. **88**(22): 2921–2944. 269, 270, 271
58. Schulze-Makuch, D., 1996, Dissertation, Facies dependent scale behavior of hydraulic conductivity and longitudinal dispersivity in the carbonate aquifer of southeastern Wisconsin, University of Wisconsin, Milwaukee. 269
59. Schulze-Makuch, D., D. A. Carlson, D. S. Cherkauer, and P. Malik, 1999, Scale dependency of hydraulic conductivity in heterogeneous media, *Ground Water* **37**: 904–919. 269
60. Stauffer, D., 1979, Scaling theory of percolation clusters, *Phys. Rep.* **54**: 1–74. 270, 271
61. Hunt, A. G., and G. W. Gee, 2002, Water retention of fractal soil models using continuum percolation theory: tests of Hanford site soils, *Vadose Zone J*, **1:** 252–260. 272
62. Friedman, L., and M. Pollak, 1981, The hall effect in the variable-range hopping system, *Philos. Mag. B* **44**: 487–507. 274
63. Hunt, A. G., 2001, AC hopping conduction: perspective from percolation theory, *Philos. Mag. B* **81**: 875–913. 274
64. Hunt, A. G., 2001, Applications of percolation theory to porous media with distributed local conductances, *Adv. Water Resour.* **24**(3,4): 279–307. 274
65. Liu, Z-F., X.-H. Wang, P. Mao, and Q.-S. Wu, 2003, Tracer dispersion between two lines in two-dimensional percolation porous media, *Chin. Phys. Lett*. **20**, 1969–1972. 277, 278
66. Bruderer-Weng, C., P. Cowie, and Y. Bernabe, et al., 2004, Relating flow channeling to tracer dispersion in heterogeneous networks, *Adv. Water Resour*. **27**(8): 843–855. 282

Chapter 11
Effects of Multiscale Heterogeneity

It is generally agreed that problems with multiscale heterogeneity present the biggest challenge to computation and understanding. A few such problems may be easily understood using percolation theory. It is not clear at this time whether such treatments will prove particularly useful in the general case; however, as always, they will be superior to simple averaging techniques. Four problems will be dealt with, one at the pore scale, in which the effects of soil structure on hydraulic properties are discussed, the second treats a two-scale upscaling problem, where the percolation variable is different at the two scales, the third was only meant to be a schematic treatment of a geologic scale hierarchical problem, but appears to have captured the essence of a "scale effect" on the hydraulic conductivity. The fourth is an attempt to address a problem of saturation-dependent anisotropy at the US Department of Energy Hanford site in Richland, WA.

11.1 Soil Structure

To a physicist without agricultural background the easiest way to imagine a soil with structure is to call back memories of throwing dirt clods. The relatively large spaces between the dirt clods would represent the "structural" pores, while the interior of the dirt clod contains "textural" pores. The soil structure refers to the existence of clods, called "aggregates," and the space between them, and knowledge of the structure implies knowledge of the statistics of the occurrence of aggregates of a given size, structural pores as a function of size, and any spatial correlations in their location. Realistically, however, one is fortunate indeed if one has a measurement of the distribution of structural pore sizes, even though soil structure has been a consistent subject of agricultural and soil physics research for at least 40 years (e.g., Sharma [1]).

In any discussion of transport properties of such media one runs immediately into a conceptual problem. Imagine that the structural pores are relatively ordered and that they may be connected on a multicentimeter gridlike random resistors. Clearly one can represent the textural pores as shorter resistors (with larger resistance values) inside each grid cell and allow them to connect to the structural resistances at

Hunt, A., Ewing, R.: *Effects of Multiscale Heterogeneity.* Lect. Notes Phys. **771**, 287–306 (2009)
DOI 10.1007/978-3-540-89790-3_11

the boundaries of each grid cell. But can one allow the resistances representing the textural pores in one grid cell to connect to those representing the textural pores in a neighboring grid cell without connecting to the structural pores that divide the cells? This is a critical conceptual problem, and to our knowledge there is no general answer. If one allows such connections, one has what is called a "dual porosity" model [2, 3], if one does not, one has a hierarchical model. Since both types of model are used, there is clearly no general consensus as to what is physically allowed. The difference in transport is as follows: In the hierarchical model, when the saturation drops to the extent that water no longer occupies the structural pores, all processes which require a continuous water phase cease. Since this is clearly not the case in agricultural soils, dual porosity models are more common in the soil science literature. However, in geological applications with different contexts hierarchical models tend to be the rule.

When a dual porosity model is used for soil structure Nimmo [2, 4, 5], the percolation treatment is relatively easy; the two contributions to the pore space are simply treated as though they exist in parallel to each other, and there are no additional limitations considered to transferring water between the structural and the textural pores. As a consequence the total porosity of the medium is obtained using a sum of the contributions from the structural and textural pores. If both can be treated as fractals, for example, one has

$$\phi_{\mathrm{s}} = \frac{3-D_{\mathrm{s}}}{r_{s_{\mathrm{m}}}^{3-D_{\mathrm{s}}}} \int_{r_{\mathrm{s}_0}}^{r_{\mathrm{s}_{\mathrm{m}}}} r_{\mathrm{s}}^{2-D_{\mathrm{s}}} dr_{\mathrm{s}}; \quad \phi_{\mathrm{t}} = \frac{3-D_{\mathrm{t}}}{r_{\mathrm{t}_{\mathrm{m}}}^{3-D_{\mathrm{t}}}} \int_{r_{t_0}}^{r_{\mathrm{t}_{\mathrm{m}}}} r_{\mathrm{t}}^{2-D_{\mathrm{t}}} dr_{\mathrm{t}} \tag{11.1}$$

and

$$\phi = \phi_{\mathrm{s}} + \phi_{\mathrm{t}} \tag{11.2}$$

Here the subscripts s and t stand for structural and textural respectively. As long as the smallest structural pore radius is larger than the largest textural pore, a general procedure can be formulated, which does not make any particular distinction between the two types of pores, except as regards critical volume fractions for percolation. Such values must be treated separately.

For simplicity it will be assumed here that the largest textural pore is smaller than the smallest structural pore. The data, with which the theoretical predictions are compared, will conform to that constraint. Then, as water drains from the medium, it will drain first from the structural pores, before it can begin to drain from the interior of the aggregates; this is simply another consequence of the Young–Laplace relationship between the tension and the pore radius. It is typical for researchers in the field of soil physics to assume that the effects of soil structure are limited to large moisture contents (e.g., Nimmo [2]). Since we will use the same type model for the structural pores as for the textural pores, we will assume that the critical volume fraction for percolation of the structural pores is approximately $\phi_{\mathrm{s}}/10$, exactly as assumed for textural pores *when the specific surface area is small*. For structural pores, with radii much larger than textural pores, this assumption is realistic. Since structural pores typically account for only about 10% of the total porosity, $\phi_{\mathrm{s}}/10$ is

actually only about $\phi/100$, and can probably be set to zero without serious difficulty. Furthermore, setting the critical volume fraction for the structural pores equal to zero is consistent with the assumption that they do not provide a barrier to water flow at any water content (dual porosity) and with the assumption that they can drain completely. These characteristics also appear to be in accord with experiments generally.

Under the above conditions, the derivation of water-retention curves is also brief. For $\theta > \phi_t$, one has

$$\theta = \frac{3-D_t}{r_{t_m}^{3-D_t}} \int_{r_{t_0}}^{r_{t_m}} dr_t r_t^{2-D_t} + \frac{3-D_s}{r_{s_m}^{3-D_s}} \int_{r_{t_0}}^{r_{s>}} dr_s r_s^{2-D_s} \tag{11.3}$$

In Eq. (11.3) $r_{s>}$ refers to the largest structural pore that contains water, and it is given through the usual constraint, $r_{s>} = A/h$, where A is, also as usual, unknown in value. For $\theta < \phi_t$, the result of Chap. 3 applies, using the subscript t for textural pores. The fractal dimensionality of the textural pores is found exactly as already shown in Chap. 3. The fractal dimensionality of the structural pores is found by an analogous procedure, although in this case one often has direct data for the pores themselves, and not for a surrogate, such as the particle size. Since the ratio of smallest to largest particle size is typically assumed to be the same as that for the smallest to the largest pore size, there is no difference in the calculations. However, the scaling formulation for water retention will require the use of a parameter inversely proportional to the largest pore size, h_A, and knowledge of the largest structural pore size.

The hydraulic conductivity is calculated as follows: For moisture contents $\theta \leq \phi_t$, such that the structural pores are empty, the result for K is exactly as in Chap. 4, but with all quantities (fractal dimensionality, critical moisture content, and porosity) referred to the textural pore space. For moisture contents $\theta > \phi_t$, such that some fraction of the structural pores is also wetted, the result for K is a sum of a constant term, corresponding to full saturation of the textural pores, and again a term of the same form as in Chap. 4, but written in terms of the structural quantities. In principle, the hydraulic conductivity for the structural pores should also undergo a crossover from pore size dominated to connectivity-dominated forms, but in actual comparison with experiment such a crossover is not included for five reasons: (1) the porosity associated with structural pores is so small (in the case to be considered, 0.04) that division into multiple ranges appears overambitious, (2) the crossover moisture content depends on the critical volume fraction for percolation, which, though likely very small, is merely assumed to be zero, (3) the connectivity may not be completely percolation dominated, since plant roots (particularly in agricultural soils) may introduce a spatial scale (some regularity in separation), (4) in the range of lowest saturations of the structural pores, where the discrepancy between theory and experiment will be largest, the hydraulic conductivity due to the textural pores will dominate in many cases, and (5) in most cases measurements of the hydraulic

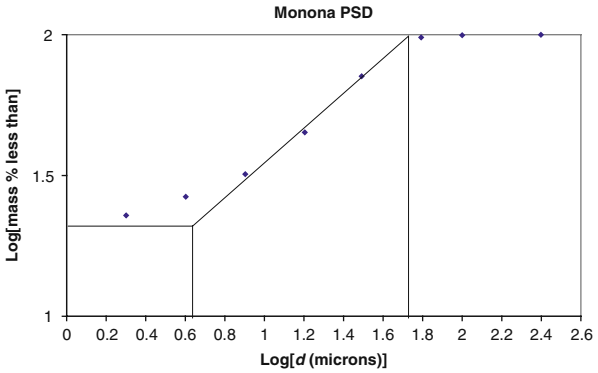

Fig. 11.1 Particle size data for the Monona soil (data unpublished, S. Logsdon)

conductivity will never be accurate and detailed enough to discover the precise form of K in this range of moisture contents.

The particular case considered for comparison with experiment has $\phi_s = 0.04$, $\phi_t = 0.376$. The particle size data (given in Fig. 11.1) yield $D_t = 2.81$. The optical pore-size data (given in Fig. 11.2) yield $D_s = 2.979$. The particle size data is nearly identical to the McGee Ranch soil, with $D = 2.81$, $r_m = 54\,\mu m$, and $r_0 = 4.3\,\mu m$, so we use the same θ_t value, 0.11. Figure 11.3 shows the comparison between theory and experiment for the water-retention curve. In order to obtain the agreement shown, the air entry pressures for the textural and structural pores had to be chosen

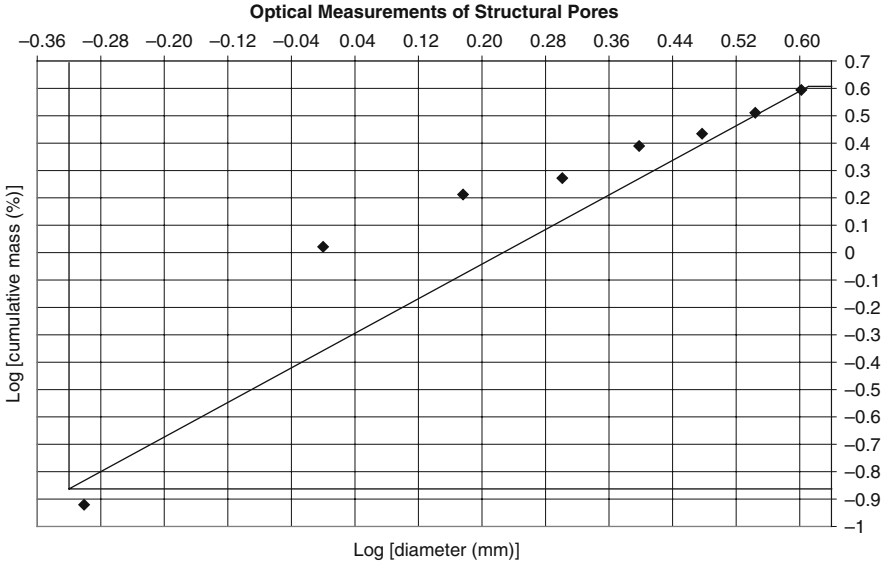

Fig. 11.2 Optical data for structural pores of a soil adjacent to the Monona soil

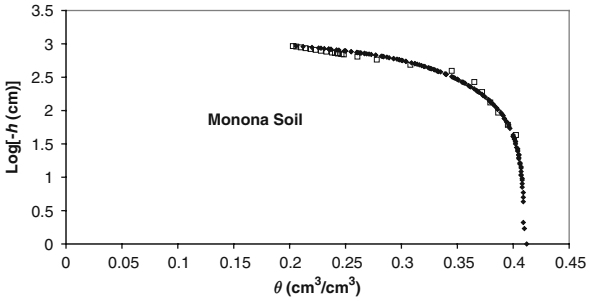

Fig. 11.3 Experimental data for the water-retention function of the Monona soil together with the predictions of Eq. (3.22) for both the structural and the textural pores separately. Two adjustable parameters, the equivalent air entry pressures for each pore size range, are used

to be 340 and 26 cm, respectively. Thus the ratio of saturated hydraulic conductivities for the structural and textural pores must be assumed to be (from eq. (4.40), (4.41), and (4.46))

$$\frac{K_{S_s}}{K_{S_t}} = \left(\frac{340}{26}\right)^2 \frac{(1-0)^{\frac{3}{3-2.979}}}{(1-0.11)^{\frac{3}{3-2.81}}} = 1077 \tag{11.4}$$

Using these parameters, the hydraulic conductivity may be predicted using one adjustable parameter, K_{S_s}, and the comparison of that prediction with experiment is given in Fig. 11.4. This comparison appears reasonable for a one-parameter prediction

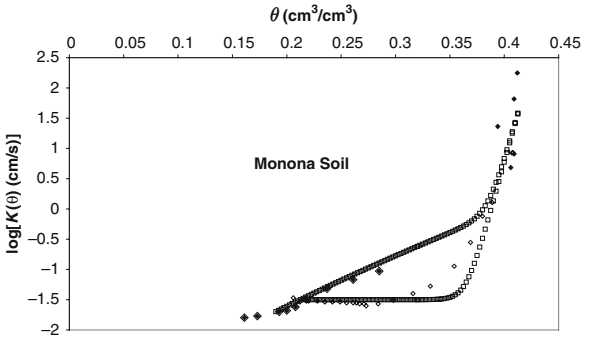

Fig. 11.4 Data for the hydraulic conductivity for several depths of the Monona soil. The predicted hydraulic conductivity from Eq. (5.14) using two parallel contributions, one from the textural pores and one from the structural pores. The porosities and fractal dimensionalities of each are known, and the ratio of the values of K_S is given by Eq. (11.4), so there is only one adjustable parameter in the comparison, the value of K_S for the structural pores. For the soil at the surface the theoretical prediction agrees. However, the experimental data at one depth drop more rapidly than predicted with declining moisture content and then remain constant, even though the moisture content continues to drop

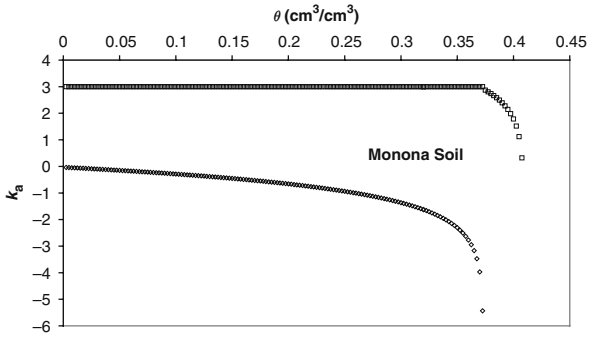

Fig. 11.5 Predictions of the air permeability for the Monona soil. The *open diamonds* describe the result of using Eq. (6.1) for the textural pores only. The *open squares* give the additional contribution from the structural pores

In another exercise consider the effects of the structural pores on the air permeability. In this case, the dual porosity treatment leads to a constant contribution to the air permeability from the structural pores for all water contents less than, ϕ_t. This contribution masks the singular behavior of the contribution of the air permeability from the textural pores, and the air permeability appears nearly flat over most of the range of air-filled porosities. Then, for $\theta > \phi_t$, the singular behavior of the air permeability due to the structural pores causes a very rapid drop in air permeability as saturation is approached. The general effects of soil structure on the air permeability and hydraulic conductivity (as functions of saturation) are shown in Fig. 11.5. This result explains the general tendency for the minimal dependence of the air permeability on air-filled porosity for highly structured soils, as well as the perception that the air permeability may be nonzero at full saturation (since it is so difficult to achieve 100% saturation, particularly with the large hydraulic conductivity associated with such large structural pores).

Note that, as expected with a small range of porosity associated with much larger pores, drainage of these larger pores causes the hydraulic conductivity to fall precipitously over a very small range of moisture contents before it drops more slowly over a wider range of moisture contents associated with the textural pores. This feature is very common among soils; in fact it is so common that the van Genuchten parameterization introduced in Chap. 3 was developed to predict such a change in curvature from positive to negative with diminishing moisture content. However, the van Genuchten parameterization attempts to unite all the ranges of moisture content into one function. It seems obvious that the structural pores need have no specific relationship with the textural pores, while at the dry end complications from incomplete equilibration may be introduced. This leads to major difficulties with the identification of the parameters of the van Genuchten function (see Hunt [6] for further comparisons).

Thus it is seen that when two scales of heterogeneity exists, one possible avenue of approach is to use a dual porosity model and apply critical path analysis and

percolation scaling to both components of the porosity separately. While this sort of approach may be applicable to three or more scales of heterogeneity as well, the appeal of an approach, which is, (a) simple, (b) physically based, and (c) parsimonious, diminishes with increasing complexity because of the diminution in parsimony. On the other hand, use of a van Genuchten-type argument, which tacitly assumes a correspondence between the parameters of two different types of pores, also becomes less appealing with increasing levels of complexity, because its performance tends to worsen. Clearly any approach to problems with such an increase in complexity is going to suffer from some defect.

11.2 Variable Moisture Content

A significant problem in the soil science community arises from the understanding of the distributions of the saturated and unsaturated hydraulic conductivity. It is frequently assumed that the distribution of the saturated hydraulic conductivity is log-normal, but that the distribution of the unsaturated hydraulic conductivity values is normal. However, we have seen in Chap. 7 that narrow distributions of measured K values (Khaleel and Relyea [7], for example) at low saturations may be more a product of the time limits of the experimenter than of the medium.[1] The often quoted results of Nielsen [8] appear to show that the values of K for steady flow under unsaturated conditions are log-normally distributed, but doubt has been cast on his results for the distribution of K values in the context of the doubt generated by his result that K is exponentially dependent on the moisture content. Most people in the soil science community believe that K is more nearly a power of saturation than an exponential function [as indeed expected from the Rieu and Sposito [9] model considered here in depth]. So the question of how K is distributed for saturated and unsaturated conditions is of considerable interest to the soil sciences community.

Since hydraulic conductivity values in *geologic* media are typically spread out over many orders of magnitude, one of the goals of that community for a long time has been to try to "derive" a log-normal distribution for K. Formulations using separation of variables in the macroscopic equations (Laplace's equation), though simple, are clearly unfounded, since such equations tell us nothing about the microscopic details of conduction. We will consider only the soil science problems here.

The results of Chap. 9 appear to imply that, because K_S is determined through Poiseuille flow, it should be (approximately) normally distributed. We believe that the large spread in experimental results for "saturated" conditions is tied to the lack of control over the saturated moisture content (which, as noted, can generate measurements of the saturated water content of the same sample at different US Department of Energy laboratories which differ by as much as 20%). Given the huge

[1] The fact that these authors tended to replace equilibrium K values less than $5 \times 10^{-8}\,\mathrm{cm\,s^{-1}}$ with approximately this value (which represented a maximum experimental time) narrowed the widths of their K distributions drastically in the limit of small θ.

effect of structural pores (with only 10% of the porosity) on K discussed in the previous section, it is easy to comprehend that failure to saturate these pores could lead to huge underestimations of K_S. But, although we believe that complications due to saturation are very likely the cause of these results, first consider the following potential explanation for Nielsen's experiments.

Below is presented a brief description of a compound upscaling procedure, which yields a distribution of unsaturated K values which is (approximately) log-normal for local values of the $K(S)$, which are exponential functions of the moisture content [10]. This result would then be compatible with the conditions of Nielsen's experiments [8].

Rewrite Eq. (5.14) as

$$K(S) = K_S \left[1 - \phi \frac{1-S}{1-\theta_t}\right]^{\frac{3}{3-D_p}} \tag{11.5}$$

In the limit $D_p \to 3$ (with the consequent condition that $\phi \to 0$, Eq. (11.5) yields

$$K(S) = K_S \exp\left[-3\left(\frac{1-S}{1-\theta_t}\right)\ln\left(\frac{r_m}{r_0}\right)\right] \tag{11.6}$$

Although Rieu and Sposito [9] state explicitly that $D_p < 3$ for their discrete fractal model, there is no reason in a continuum model why $r^3 W(r) = r^{2-D_p}$ cannot be proportional to r^{-1}. In fact using $D_p = 3$ explicitly leads precisely to the result that $K(S)$ is an exponential function of saturation [11], though of not quite the same form as Eq. (11.6).

If one considers the possibility that the moisture content can vary over length scales much smaller than a field measurement (such as Nielsen's), then Eq. (11.6) could describe the local variability of K due to variable saturation. In the case of steady flow, the local moisture contents would not be changed by definition, and one could apply an upscaling procedure to Eq. (11.6). If the local saturations were normally distributed with mean S_m and standard deviation σ_S, then applying critical path analysis [10] to Eq. (11.6) would yield

$$K(S) = K_S \exp\left[-3\left(\frac{1-S_m-c\sigma_s}{1-\theta_t}\right)\ln\left(\frac{r_m}{r_0}\right)\right] \tag{11.7}$$

where c is a numerical constant [σ_S was mistakenly referred to in Hunt [10] as the variance of S]. The value of c would be larger for smaller critical volume fractions. Such values of the critical volume fraction for percolation would not be correlated with θ_t for the critical moisture content at the pore scale. Thus Nielsen's [8] measurements of an (approximately) exponential form for $K(S)$ on a large scale (Eq. (11.7)) could be consistent with an exponential form on a smaller scale as well, and application of cluster statistics of percolation theory to Eq. (11.6) would yield a distribution of K values that was approximately log-normal (an approximation for at least two reasons, clearly).

But actually Eq. (11.5) can be approximated (to first order) by an exponential dependence of K on S in another limit as well, namely that $S \to 1$ for arbitrary D_p. If the soil is not structured, the fractal dimensionality is likely to be more nearly 2.8 (occasionally as high as 2.9). For the case $D = 2.9$, a variation of the moisture content of 20%, for $\phi = 0.4$ and $\theta_t = 0.04$, would produce a variation in K of only a factor 50. But in the case of structural pores we found that the fractal dimensionality can be very near 3 (2.98) on account of the small associated porosities. With D so near 3 the exponential approximation is quite accurate. Further, variation of the moisture content of only 10% (0.04 for a total porosity of 0.4) can cause a variability in K over a factor 500 because of the large power $[3/(3-D) = 150]$. This range of variability in K is also roughly compatible with a log-normal distribution, and ultimately for much the same reasons as might explain the Nielsen [8] experiments.

Thus it is suggested that measurements of both the saturated and the unsaturated hydraulic conductivity distributions can be strongly affected by experimental error: In the first case a relatively narrow distribution can be perceived to be very wide if the moisture content is not controlled carefully, and in the second case a very wide distribution can be perceived as very narrow because of the influence of the time constraints of the experiment.

11.3 A Schematic Hierarchical Problem

Media with geological complexity are difficult even to describe. If the description of a medium is too complex, an analytical application of concepts from percolation theory is not likely to exist. The purpose here is not to address such complications seriously; in fact, we would claim that attributing what seem to be exotic behaviors of the hydraulic conductivity to exotic descriptions of porous media may be misleading. If these "exotic" media appear to produce an increase in K with increasing scale of the medium, then there appears to be a problem of conceptualization. Thus we seek for simpler causes of such apparent scale effects using known physics and idealized, but easily verifiable, models. In Chaps. 8 and 9 the examples of nonequidimensional support volumes and anisotropic hydraulic conductivity fields were treated, and shown to lead to apparent scale effects. In this chapter it will be shown that multiple scales of heterogeneity can also lead to a (mistaken) conclusion that hydraulic conduction becomes easier with increasing length scales.

Consider the following idealized medium [12] composed of seven different types of material, each of which has seven subunits. Let the hydraulic conductivity have a log-uniform distribution in each of the 49 subunits. Make these individual distributions overlap in the following way: The most highly conductive unit has hydraulic conductivities from 2^0 to 2^{-6}, in equal proportions, while the next most conductive unit has hydraulic conductivities from 2^{-3} to 2^{-9}, the third from 2^{-6} to 2^{-12}, etc., as shown in Fig. 11.6. No assumption is made regarding the shapes of the individual volumes, which means that this problem is best treated using continuum percolation theory. If one approaches the upscaling of this medium with a "coarse graining"

procedure, then the effective conductivity of each subunit is first found, and then the heterogeneous subunits are replaced with a homogeneous material characterized by the effective subunit conductivity. Since the critical volume fraction for percolation in 3D will be less than 0.5, if repeated often, such a procedure will tend to overestimate the hydraulic conductivity at the largest scales, since most of the volume of any given subunit will have a smaller conductivity than the effective value.

A common value of the critical volume fraction for such continuum problems is ca. 15% (see Chap. 2 as well), though, as has been seen for problems at the pore scale, even much smaller values can occur. A point of the coarse-graining of such a self-similar medium is that V_c must remain the same at every scale. Applying continuum percolation theory to each of the subunits individually leads to effective K values of 2^{-1}, 2^{-4}, 2^{-7}, 2^{-10}, 2^{-13}, 2^{-16}, and 2^{-19}, as indicated in Fig. 11.6. In each case the quoted value of K is the second largest in the subunit because the volume associated with the largest value of K is only $1/7 \approx 0.143 < 0.15$, and is thus insufficient to "percolate." The median (geometric mean) values of K in each of these units are, however, 2^{-3}, 2^{-6}, 2^{-9}, 2^{-12}, 2^{-15}, 2^{-18}, and 2^{-21}, each a factor 2^2 smaller than the effective K value. If continuum percolation is again applied to the seven units with the above seven K values, the effective K value for the entire medium is 10^{-4}, again the second largest of seven values. Further, if continuum percolation theory is applied to the composite distribution of all 49 subunits simultaneously, the effective K value obtained for the entire medium is also 2^{-4}, provided that the same value, 0.15, is used for V_c. The median or geometric mean value of the geometric means of the subunits is 2^{-12}, which is too small by a factor of 2^8. Clearly the value of V_c in the latter case may not be quite 0.15. On the other hand, the

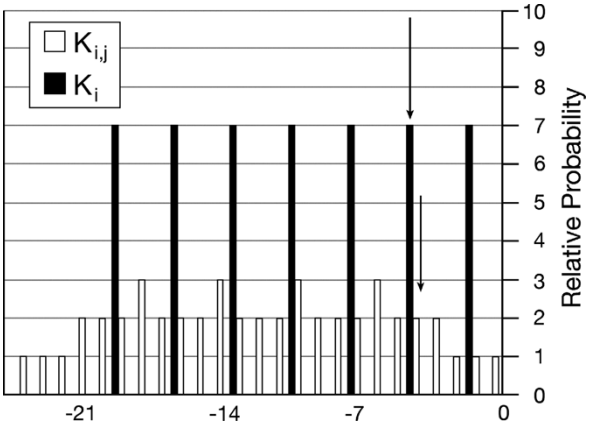

Fig. 11.6 Discrete hydraulic conductivity distributions for two-scale medium as described in text. The *open bars* are the composite distribution of the seven overlapping subunits, each with log-uniform distributions. The *solid bars* are the effective conductivities of each of the subunits, each of which has an equal chance of being encountered. The *arrows* point to the effective conductivity of the system, upscaled from the subunit scale and from the unit scale. The two values are identical (from Hunt [12])

coarse-graining procedure is also slightly inaccurate. Nevertheless each of these uncertainties is small compared with the error incurred by assuming that the upscaled value of K is closely related to the geometric mean value of K. Further, relating the effective K to the geometric mean value tends to produce an underestimation of K, which grows with increasing scales. The point of this exercise, however, is that the existence of multiple scales of heterogeneity does not lead to an increase in an effective K value with increasing scale, even though certain quantities often taken as predictors of the effective K value do increase with increasing scale.

To make this exercise a little more quantitative we make a specific comparison of the predicted upscaled values of K with the Matheron [13] conjecture, often regarded as a standard means of upscaling K. It was derived specifically for Gaussian random fields in one and two dimensions, and has been generalized to three dimensions, although it has been proved that it cannot be general in 3D. In any case the Matheron conjecture is expressed as follows:

$$K_{\text{eff}} = K_{\text{g}} \exp\left[\sigma^2 \left(\frac{1}{2} - \frac{1}{d}\right)\right] \tag{11.8}$$

In this expression K_{g} is the geometric mean, d is the dimensionality of the medium, and σ^2 is the variance of the (log) conductivity distribution. Note that for $d = 2$ the Matheron result yields $K_{\text{eff}} = K_{\text{g}}$, which itself cannot be general as already seen in Chap. 3, as the effective conductivity depends very sensitively on the local connectivity. One can calculate the variance of the conductivity distributions given here very easily and then compare the results of an "enhancement factor," $K_{\text{eff}}/K_{\text{g}}$ for both the Matheron conjecture and the continuum percolation. This comparison is given in Table 11.1, where the variance in the distribution was calculated in Excel. This calculation for the Matheron conjecture is not strictly valid, of course, since the distributions chosen were log-uniform rather than log-normal. The result is that the Matheron conjecture also tends to underestimate the value of K_{eff}, especially in media with multiple scales of heterogeneity. Furthermore, these underestimations already become noticeable in the case of $V_{\text{c}} = 0.15$. As has been seen, however, at the pore scale V_{c} can be much smaller than 0.15, and this is likely the case in some geological problems as well, though for some, V_{c} may also be larger than 0.15. In fact, the point of a small, but growing body of literature is to answer the question of why critical site percolation probabilities are so low in geologic media (most of

Table 11.1 Factors representing enhancement of K relative to geometric mean value. Percolation values are calculated using assumed V_{c} of 0.15. Values in parentheses calculated from $V_{\text{c}} = 0.06$. Subunit scale is upscaled from the subunit values. Unit scale is upscaled from the unit values. Composite means the entire distribution. Product is the product of the enhancements at the subunit and the unit scales

Method	Subunit scale	Unit scale	Composite	Product
Percolation	$2^2(2^3)$	2^6 (2^9)	2^8 (2^{11})	2^8 (2^{12})
Stochastic	$2^{0.53}$	2^7	$2^{6.8}$	$2^{7.53}$

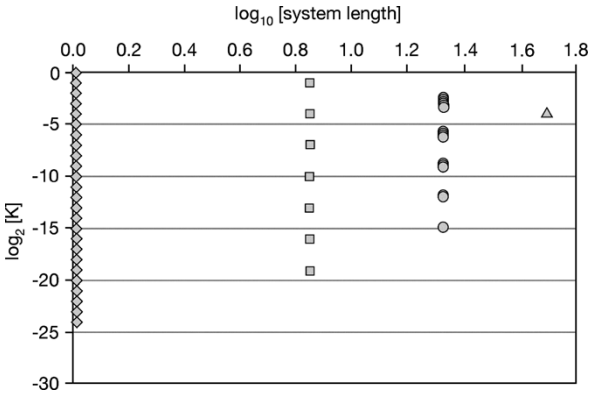

Fig. 11.7 For the system of Fig. 11.6 the distribution of K values as a function of linear scale

these works, e.g., Silliman [14]; Shah and Yortsos [15]; Proce et al. [16], divide the medium up into blocks of uniform size and look to correlations in the block conductivities to explain critical percolation probabilities much lower than 0.3116 for a cubic lattice, rather than comparing such probabilities with continuum values, starting from Scher and Zallen [17]). For $V_c = 0.06$, the Matheron conjecture underestimates the hydraulic conductivity by more than four orders of 2, or more than two-thirds the width of an individual subunit distribution.

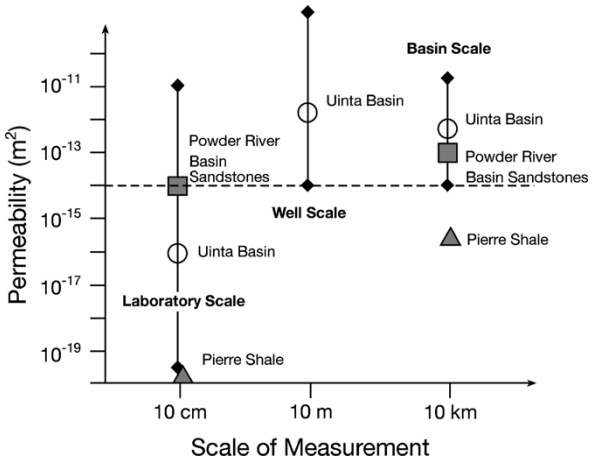

Fig. 11.8 Effect of scale on permeability of rocks in 3 different sedimentary basins in the United States including the Uinta Basin of Utah [35], the Powder River Basin, Wyoming, and the Pierre shale in South Dakota [36]. Dashed line at 10^{-14} m^2 indicates average crustal permeability inferred by Brace [37]. Error bars associated with Uinta Basin data reflect the full range of permeability evaluated at each scale (reprinted by permission from McPherson, 2003)

Note that the value of K at any scale is contained within the distribution of K values at all smaller scales. However, especially for V_c very small, it may be located well into the tail of the distribution. Under such circumstances (if $V_c = 0.05$) limitations in sampling (significantly less than $20 = 1/0.05$ samples) might suggest that the value of K at a larger scale was not represented at all at the smaller scale. So the general implications of continuum percolation theory are that inference of an increase in K with increasing scale may be due to inadequate sampling (in the case of very small V_c) as well as inappropriate inferences due to established methods of inferring K_{eff}.

Figure 11.7 gives a schematic representation of the predicted dependence of measured values of K as a function of scale. This representation is schematic because the representation in terms of system size does not follow automatically from the representation in terms of hierarchical rank (Fig. 11.6). Figure 11.8, from McPherson [18], gives actual K measurements as a function of scale. Note the general similarity.

11.4 A More Realistic Hierarchical Problem

This subsection combines pore scale modeling with geologic scale modeling. In particular, results of pore scale predictions are then used as inputs into geologic scale predictions. The results may have practical relevance.

The effective hydraulic conductivity in the subsurface at the US Department of Energy Hanford site under unsaturated conditions shows evidence of anisotropy [19–21]. This anisotropy is expressed in the predominantly horizontal transport of moisture. Underlying the predominantly horizontal is its dependence on anisotropic sedimentary structures on many spatial scales [22, 23]. Any tendency to lateral flow can be logically assumed to lead to predominantly lateral of contaminants, which appears to have been observed in the case of Technetium [24].

$^{43}Tc_{99}$ is spreading mostly laterally through the US Department of Energy Hanford site sediments. An important question to try to answer is: over what length scale can the transport remain horizontal before the $^{43}Tc_{99}$ is likely to be transported vertically to the water table. In a medium with sufficient randomness to be treated within the framework of percolation theory, even if anisotropy exists, it must be possible mathematically to transform the medium so as to make it isotropic. In that case, percolation in the vertical and horizontal dimensions must coexist. Practically speaking this means that at some large-enough length scale, vertical flow must be as easy as horizontal flow and the Technetium will be transported vertically to the water table. Of course there are many potential vertical transport paths, which might not be treatable in percolation theory, such as vertical conduits known as clastic dikes [25]. If the Technetium transport is controlled by such features (because it occurs at smaller horizontal length scales than what we would predict), our proposed procedure will not be relevant.

An area of the US Department of Energy Hanford called the Vadose Zone Transport Field Study (VZTFS) (Ward et al., 2000) [26] was selected for study based

partly on its earlier study by Sisson and Lu [27] and partly on its potential relevance to the subsurface of the BC Crib area, where the cited Technetium discharge was located. The sediments in the vicinity of the VZTFS consist principally of sand with interstitial silt and silt beds [22, 23]. The hydraulic conductivity is a strongly varying function of moisture content, as we have seen. The Hanford subsurface, located in a semiarid region, typically has fairly high tensions, h. Thus, at higher tensions in the unsaturated zone, the hydraulic conductivity may be strongly anisotropic as a consequence of the tendency of finer soils to retain more water than coarser ones, and for these soils to have been deposited primarily in horizontal structures. This apparent anisotropy may have some important consequences for the Tc transport.

We proposed the following procedure to address this question:

(1) Use critical path analysis from percolation theory [28, 29] to predict the unsaturated hydraulic conductivity [30, 31] at the sample scale using soil physical information [32] from relevant soils at the US Department of Energy Hanford site, (2) find the relevant parameters regarding the statistical occurrence and physical extent of such soils [25, 32], (3) use critical path analysis again together with cluster statistics of percolation theory to predict the distribution of hydraulic conductivity, K, values at geologic scales and with geologic complications such as anisotropy [33, 34], (4) use sample scale information to generate the appropriate input parameters for the geologic scale treatment, and (5) use the predicted K distribution at geologic scales to estimate the risk involved in a particular solute spill.

Since all the theoretical work is already described in this book, the present discussion can be restricted to finding the necessary input parameters to develop the appropriate output for analysis.

One important input that should be mentioned is that of a quasiequilibrium assumption; namely that the tension h is constant at a given elevation across soils of different type. This does not mean that we assume no lateral gradients in h, rather that we can calculate a relevant distribution of K values without taking local variablity in h into account.

We hypothesized that one could find a distribution of hydraulic conductivity values at a given tension and force that distribution of conductivity values into the form of the Rieu and Sposito [9] distribution.

Specifically we used Eqs. (10.7) and (10.8) to predict the distribution of vertical K values (referenced to the typical horizontal hydraulic conductivity) that one would expect to find at a given spatial scale. These equations require several parameters as input, namely an effective porosity, and effective fractal dimensionality, a ratio of a maximum to minimum K, and a relevant length scale. The first three parameters are, as noted previously, not independent as formulated in the Rieu and Sposito model. The next paragraphs will explain how we estimated appropriate parameters, and then we will present the results.

Schaap et al. [32] give particle size data, water-retention curves, and the saturated hydraulic conductivity for 53 of 60 soils investigated at the VZTFS site. We took our methods from Chap. 5 [31] to predict the hydraulic conductivity as a function of tension for 39 of these soils. The soils discarded were eliminated due to data prob-

lems (cumulative mass fractions with negative slopes, missing saturated values of the hydraulic conductivity, etc.). The reader will note that the following discussion is very practically based, partly because we force data to be compatible with a given subsurface model. Yet we know that the universal aspects of percolation theory tend to make most model characteristics nearly irrelevant, except for the magnitude of r_m/r_o in the Rieu and Sposito model.

We predicted $K(\theta)$ in terms of K_S using the particle size data as a proxy for the pore-size data. We matched predicted and observed water-retention curves in order to extract h_A, the air entry pressure, and then used the predicted $\theta(h)$ curve together with the predicted $K(\theta)$ and the observed K_S in order to generate K as a function of h without any unknown parameters. We then used summaries of the data to generate our distributions of K values. In fact, we used parameters from these data in order to generate parameters for the K distributions.

Specifically, we produced regressions of $K(h)$ on total silt + clay content for each of three values of h (50, 100, and 200 cm, the latter two in Figs. 11.9 and 11.10). We used the regression equation to generate typical values of K for relatively fine-rich, K_{loam}, and fine-poor, K_{sand}, soils (at two specific values of fine content, 7.6 and 20.1%. These two values were identified by taking (arbitrarily) half the maximum fine content (26.8%) as the value (13.4%), which distinguishes between fine-rich and fine-poor soils, and then taking the average values of fine content in each range separately. When fine-rich soils had appreciably higher K than fine-poor soils (at $h = 100$ and $h = 200$ cm) we used the ratio K_{loam}/K_{sand} in each case to represent the square of the ratio of largest to smallest pore size in the Rieu and Sposito model. The results were $K_{loam}/K_{sand} = 54,800$ at $h = 200$ cm, and $K_{loam}/K_{sand} = 25.8$ at $h = 100$ cm. Clearly the anisotropy at $h = 100$ cm was too small to be relevant. While $h = 200$ cm is too large a tension to be relevant in the field (Rockhold, personal communication, 2008), we also know [30] that the procedures associated with

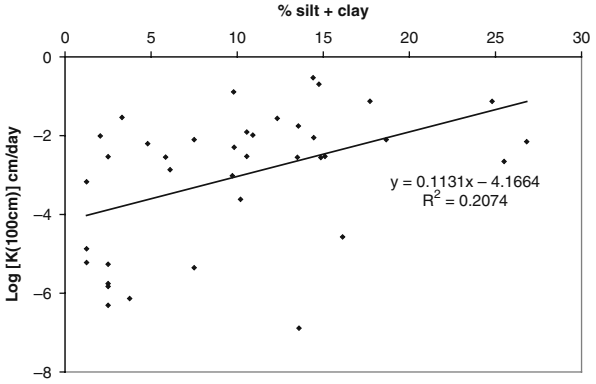

Fig. 11.9 Predicted $K(h = 100\,\text{cm})$ for 39 VZTFS soils (source, Schaap et al. [32]) as a function of fine content percentage (silt + clay). Note that the relationship is very similar if plotted against silt content (not shown). Note also that the R^2 value is lower than if $K(h = 100\,\text{cm}/K_S)$ is correlated with fine content since the absolute $K(h = 100\,\text{cm})$ depends on K_S as well, and K_S has a slight negative correlation with fine content

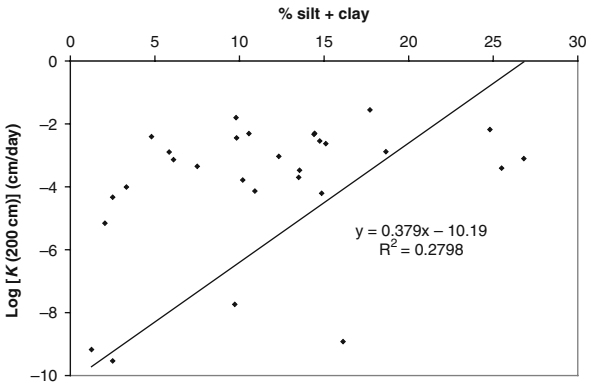

Fig. 11.10 Predicted $K(h = 200\,\text{cm})$ for 39 VZTFS soils (source, Schaap et al. [32]) as a function of fine content percentage (silt + clay)

laboratory measurements produce h_A values about twice what is usually found in the field. This means that, in fact, the anisotropy that we found for $h = 200$ cm should be relevant for field conditions with $h = 100$ cm. Then we took the fraction of the fine-rich soils as an analogue to the porosity, completing the analogy. In our case 14 out of 39 of these soils had fine content greater than 13.4%, so we had an effective porosity of 14/39. We then used the relationship $\phi = 1 - (r_0/r_m)^{3-D}$ to find the effective fractal dimensionality, D. From this we could use Eqs. (10.7) and (10.8) to produce the final two Figs. 11.11 and 11.12. Note that there is a volume scale in this figure, and that volume scale is relevant. Nevertheless, the amount of work needed

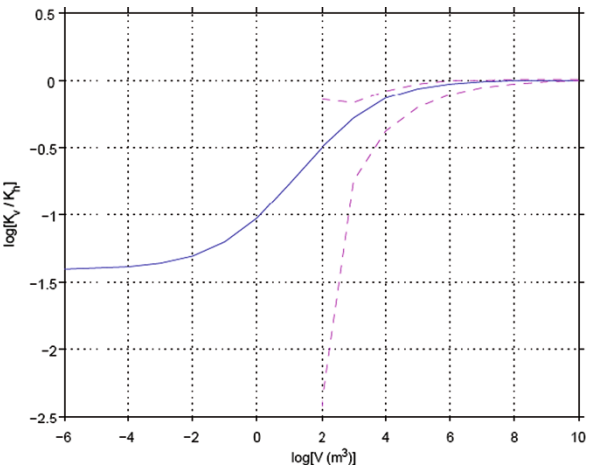

Fig. 11.11 Predicted distribution of K_v values as a function of plume volume for the case that typical conditions favor $h = 100$ cm. In this case $D = 2.72$ and $R = 5.08$. Note that the expected K_v/K_h is ca. 1/5 at a volume of about $43\,\text{m}^3 = 6 \times 6 \times 1.2$ m, whereas the expected ratio is ca. 1/3 at a volume of about $1,000\,\text{m}^3$. Both of these values would be too small to account for significant anisotropy in spreading

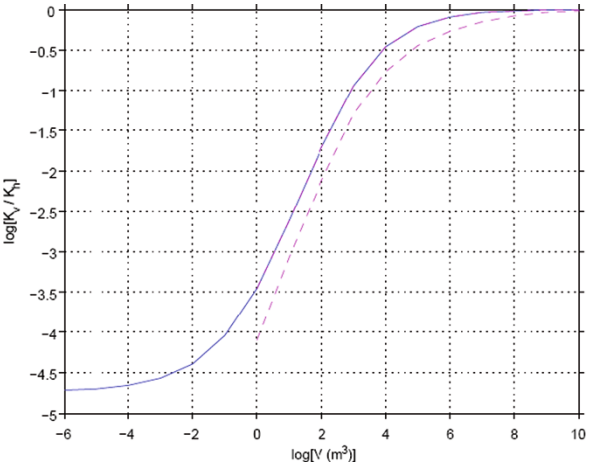

Fig. 11.12 Predicted distribution of K_v values as a function of plume volume for the case that typical conditions favor $h = 200$ cm. In this case $D = 2.918$ and $R = 234$. Note that the expected K_v/K_h is ca. 1/200 at a volume of about $43\,m^3 = 6 \times 6 \times 1.2$ m, whereas the expected ratio is ca. 1/2 at a volume of about $10,000\,m^3$. At volumes $10,000\,m^3$ it is thus relatively common to find K_v values as high as 1/2 the expected K_h. This implies that a plume spreading through individual soil units of volume $43\,m^3$ (and length 6 m) can spread to a distance of roughly $(10,000/43)^{1/2}6\,m \approx 100$ m in length before it is likely to begin spreading vertically

to fix that scale using semivariograms for the hydraulic conductivity (given in Ward [25]) is too great to reproduce here. However, there were at least three distinct spatial scales present in those variograms. We related the smallest scale to the support volume, rather than to relevant structures in the subsurface. When we chose the intermediate volume scale of ca. $40\,m^3$ as potentially most suitable to a compound upscaling based on pore-scale results we generated a prediction [38] that when the Tc plume spreads to about $10{,}000\,m^3$, we should expect vertical transport to become about a factor $10^{-1/2} \approx 1/3$ as rapid as horizontal transport. The horizontal scale that we deduced from this was about 70 m. This value appears to be two orders of magnitude too small when compared with field data [24] which appear to show nearly 10 km of predominantly horizontal migration. When we used the largest spatial scale present in the variograms, we found that a transition to vertical transport should occur at closer to 1 km.

In addition to the uncertainty of which spatial scale to use as the input scale (or even a compound process), we had two additional uncertainties: (1) Our only information presently is a 2D map from Cole et al. [24], so although we know that transport has been primarily horizontal, we do not know if it has a relevant vertical component, and (2) we do not know whether the VZTFS site is truly appropriate to develop accurate parameters for application to another location. For these reasons we wish to close with the following remark: We have been able to demonstrate how one could use our theoretical framework to address realistic transport problems with a hierarchy of scales, but we do not know how successful the application to the anisotropy of the Tc transport at the US DOE Hanford site will ultimately turn out to be.

Problems

11.1. Repeat the calculations of K for nested heterogeneity that led to the entries of Table 11.1, but using a critical volume fraction of 0.10.

11.2. Allow K to follow a log-uniform distribution with a prescribed width equal to that of the example in Sect. 11.3, and discretize the distribution as in the procedure there. Find the upscaled K as a function of an arbitrary critical volume fraction. Find the value of the critical volume fraction which yields the Matheron conjecture (Eq. (2.25)). How does this critical volume fraction compare with the typical value of about 0.16 quoted in the literature? Is it possible for the Matheron conjecture to be accurate for all values of the width parameter using the same critical volume fraction?

11.3. Consider problem 11.2 again, but allow nested heterogeneity analogously to the procedure of this chapter. Thus the critical volume fraction is, to a good approximation, independent of scale. Investigate the performance of the Matheron conjecture for the upscaling at both scales; does choice of the critical volume fraction of problem 11.2, which guarantees equivalence to the Matheron conjecture at the lowest length scale, also guarantee equivalence to the Matheron conjecture at the next higher length scale?

References

1. Sharma, M. L., 1966, Influence of soil structure on water retention, water movement, and thermodynamic properties of absorbed water, Ph. D. Thesis, Univ. Hawaii, 190 pp. Univ. Microfilms, Ann Arbor, Mich. [Diss. Abst. 28 17600B (1966)]. 287
2. Nimmo, J. R., 1997, Modeling structural influences on soil water retention, *Soil Sci. Soc. Am. J.* **61**: 712–719. 288
3. Barenblatt, G. I., lu. P. Zheltov, and I. N. Kochina, 1960, Basic concepts in the theory of seepage of homogenous liquids in fissured rocks, *J Appl. Math. Mekh.* **24**: 1225–1303. 288
4. Gerke, H. H., and M. T. van Genuchten, 1993, A dual-porositymodel for simulating the preferential movements of water and solutes in structured porous media. *Water Resour. Res.* **29**: 305–319. 288
5. Ross, P. J., and K. R. J. Smettem, 1999, Simple characterization of non-equilibrium water flow in structured solis, in: *haracterization and Measurement of the Hydraulic Properties of Unsaturated Porous Media,* ed. M. Th. van Genuchten, F. J. Leij, and L. Wu, U.S. Salinity Laboratory, Agriculture Reserch Services, U.S. Department of Agriculture, Riverside, CA, pp. 851–854. 288
6. Hunt, A. G., 2004b, A note comparing van Genuchten and percolation theoretical formulations of the hydraulic properties of unsaturated media, *Vadose Zone J.* **3**: 1483–1488. 292
7. Khaleel, R., and J. F. Relyea, 2001. Variability of Gardner's alpha for coarse-textured sediments. *Water Resour. Res.* **37**: 1567–1575. 293
8. Nielsen, D. R., 1973, Spatial variability of field-measured soil-water properties, *Hilgardia*, **42**: 215–259. 293, 294, 295
9. Rieu, M., and G. Sposito, 1991, Fractal fragmentation, soil porosity, and soil water properties I. Theory, *Soil Sci. Soc. Am. J.* **55**: 1231. 293, 294, 300

10. Hunt, A. G., 2001, Applications of percolation theory to porous media with distributed local conductances, *Adv. Water Resour.* **24**(3,4): 279–307. 294
11. Hunt, A, G., 2004, An explicit derivation of an exponential dependence of the hydraulic conductivity on saturation, *Adv. Water Resour.* **27**: 197–201. 294
12. Hunt, A. G., 2003, Some comments on the scale dependence of the hydraulic conductivity in the presence of nested heterogeneity, *Adv. Water Resour.*, **26**: 71–77. 295, 296
13. Matheron, G., 1967 *Elements pour une Theorie des Milieux Poreux*, Masson et Cie, Paris. 297
14. Silliman, S. E., 1990, The influence of grid discretization on the percolation probability within discrete random fields, *J. Hydrol*. **113**: 177–191. 298
15. Shah, C. B., and Yortsos, Y, C., 1996, The permeability of strongly disaordered systems, *Phys. Fluids* **8**: 280–282. 298
16. Proce C. J., R. W. Ritzi, D. F. Dominic, and Z. X. Dai, 2004, Modeling multiscale heterogeneity and aquifer interconnectivity, *Ground Water* **42**: 658–670 298
17. Scher, H., and R. Zallen, 1970, Critical density in percolation processes, *J. Chem. Phys*. **53:** 3759. 298
18. McPherson, B.J., and the EarthLab Steering Committee, 2003, *EarthLab: A Subterranean Laboratory and Observatory to Study Microbial Life, Fluid Flow, and Rock Deformation*, Geosciences Professional Services, Inc., Bethesda, MD, 60 pp. 299
19. Ward, A. L., Z. G. Zhang, and G. W. Gee, 2006, Upscaling unsaturated hydraulic parameters for flow through heterogeneous anisotropic sediments, *Adv. Water Resour.* **29**: 268–280. 299
20. Yeh, T.-C., M. Ye, and R. Khaleel, 2005, Estimation of effective unsaturated hydraulic conductivity tensor using spatial moments of observed moisture plume, *Water Resour. Res.* **41**: doi 10.1029/2004 WRR003736. 299
21. Ye, M., R. Khaleel, and T.-C. Yeh, 2005, Stochastic analysis of moisture plume dynamics of a field injection experiment, *Water Resour. Res.*, **41**: doi 10.1029/2004WR003735. 299
22. Last, G. V., and T. G. Caldwell, 2001, Core sampling in support of the vadose zone transport field study, PNNL-13454, Pacific Northwest National Laboratory, Richland, WA 99352. 299, 300
23. Last, G. V., T. G. Caldwell, and A. T. Owen, 2001, Sampling of boreholes WL-3A through -12 in support of the vadose zone transport field study, PNNL-13631, Pacific Northwest National Laboratory, Richland, WA 99352. 299, 300
24. Cole, C. R., S. K. Wurstner, M. P. Bergeron, M. D. Williams, and P. D. Thorne, 1997, Three-dimensional analysis of future groundwater flow conditions and contaminant plume transport in the Hanford site unconfined aquifer system, FY 1996 and 1997 status report, PNNL 11801, Pacific Northwest National Laboratory, Richland, WA 99352. 299, 303
25. Ward, A. L., 2006 ,Vadose zone transport field study: Summary report, PNNL Report 15443, Pacific Northwest National Laboratory, Richland, WA 99352. 299, 300, 303
26. Ward, A. L., T. G. Caldwell, and G. W. Gee, 2000, Vadose Zone transport field study: soil water content distributions by neutron moderation, PNNL Report 13795, Pacific Northwest National Laboratory, Richland, WA 99352. 299
27. Sisson, J. B., and A. H. Lu, 1984, Field calibration of computer models for application to buried liquid discharges: a status report. RHO-ST-46 P. Rockwell Hanford Operations, Richland, WA 99352. 300
28. Ambegaokar, V. N., B. I. Halperin, and J. S. Langer, 1971, Hopping conductivity in disordered systems. *Phys. Rev. B* **4**: 2612–2621. 300
29. Pollak, M., 1972, A percolation treatment of dc hopping conduction. *J. Non-Cryst. Solids* **11**: 1–24. 300
30. Hunt, A. G., and G. W. Gee, 2002, Water retention of fractal soil models using continuum percolation theory: tests of Hanford site soils, *Vadose Zone J*, **1**: 252–260. 300, 301
31. Blank, L. A., A. G. Hunt, and T. E. Skinner, 2008, A numerical procedure to calculate hydraulic conductivity for an arbitrary pore size distribution, *Vadose Zone J.* **7**: 461–472. 300
32. Schaap, M. G., P. J. Shouse, and P. D. Meyer, 2003, Laboratory measurements of the unsaturated hydraulic properties at the vadose zone transport field study site, PNNL Report, 14284, Pacific Northwest National Laboratory, Richland, WA 99352. 300, 301, 302

33. Hunt, A., Blank, L., & Skinner, T. (2006). Distribution of hydraulic conductivity in single scale anisotropy, *Philos. Mag.* **86**(16): 2407–2428. 300
34. Hunt, A., 2006, Scale-dependent hydraulic conductivity in anisotropic media from dimensional cross-over, *Hydrogeology J.* **14**(4): 499–507. 300
35. Willett**,** S. D., and D. S. Chapman**,** 1987, *Temperatures, fluid flow and the thermal history of the Uinta Basin*, *Collection Colloques et Seminaires - Institut Francais du Petrole* Vol. 45. Paris : Technip. 298
36. Bredehoeft, J. D., 1983, Groundwater – a review, *Rev. Geophys*. **21**: 760765. 298
37. Brace, W. F., 1980, Permeability of crystalline and argillaceous rocks, *Int. J. Rock Mech. Min*. **17**: 242–251. 298
38. Hunt. A., and Skinner, T., 2009, A Proposed Analysis of Saturation-Dependent Anisotropy for U.S. DOE Hanford Sites Soils, accepted to Hydrogeology Journal. 303

Summary

It seems a useful addition to include a table summarizing the uses of percolation variables in calculating the transport properties of porous media. This table is constructed with the purpose of describing media with continuous distributions of local properties, rather than for media which have only two local conditions, conducting vs. nonconducting. But it is likely that there is considerable overlap in the two; remember that the Representative Elementary Volume is given by the cube of the correlation length in both cases. This table is taken from Hunt [1].

Percolation variable	Pore-scale K	Geologic scale K	Dispersion/solute transport
p_c	Effective K, residual moisture, solute diffusion, dc electrical conductivity	Effective K	Most likely arrival time
Cluster statistics	K distributions	K distributions, spatial statistics (variograms), finite-size corrections, anisotropy, residuals	Distribution of times
P (accessibility)	Hysteresis	Oil or DNAPL residuals	Fate of contaminants

Percolation variable	Pore-scale K	Geologic scale K	Dispersion/solute transport
Correlation length	Interruptions in water entry, such as produced by hydrophobic particles, REV	Dimensionality of conduction, anisotropy, REV	
Cluster density profile			Fate of contaminants
Tortuosity	Effective K		Distribution of times
Fractal dimensionality			Distribution of times

Reference

1. Hunt, A. G., 2005c, Percolation theory and the future of hydrogeology, *Hydrogeology J.* **13**: 202–205. 307

Index